OPG's DEEP GEOLOGIC

REPOSITORY

FOR LOW & INTERMEDIATE LEVEL WASTE

Descriptive Geosphere Site Model

March 2011

Prepared by: Intera Engineering Ltd.

NWMO DGR-TR-2011-24

INTERA

OPG's DEEP GEOLOGIC
REPOSITORY
FOR LOW & INTERMEDIATE LEVEL WASTE

Descriptive Geosphere Site Model

March 2011

Prepared by: Intera Engineering Ltd.

NWMO DGR-TR-2011-24

THIS PAGE HAS BEEN LEFT BLANK INTENTIONALLY

Document History

Title:	Descriptive Geosphere Site Model		
Report Number:	NWMO DGR-TR-2011-24		
Revision:	R000	**Date:**	March 2011
Intera Engineering Ltd.[1]			
Prepared by:	K. Raven, D. McCreath (Laurentian University), R. Jackson, I. Clark (University of Ottawa), D. Heagle, S. Sterling, M. Melaney		
Reviewed by:	J. Avis		
Approved by:	J. Avis		
Nuclear Waste Management Organization			
Reviewed by:	B. Semec, A. Parmenter, L. Kennell, T. Lam, D. Luhowy, J. McLay, R. Crowe, R. Beauheim (Consultant)		
Accepted by:	M. Jensen		

[1] Currently known as Geofirma Engineering Ltd.

THIS PAGE HAS BEEN LEFT BLANK INTENTIONALLY

EXECUTIVE SUMMARY

Ontario Power Generation (OPG) is proposing the development of a Deep Geologic Repository (DGR) at the Bruce nuclear site, situated in the Municipality of Kincardine, Ontario, for the long-term management of Low and Intermediate Level Waste (L&ILW) generated by OPG-owned or operated nuclear reactors. The DGR will be constructed as an engineered facility comprising a series of underground emplacement rooms at a depth of about 680 m below ground surface within the Paleozoic argillaceous limestone of the Cobourg Formation. This report presents the Descriptive Geosphere Site Model (DGSM), developed based on the results of a three-phase geoscientific investigation of the Bruce nuclear site. The geoscientific activities of Phase 1, 2A and 2B, described in a Geoscientific Site Characterization Plan (GSCP), were completed during August 2006 - June 2010.

This document provides a summary compilation, description, assessment and interpretation of geoscientific data collected as part of a series of investigations which are described in a set of 69 technical reports. All technical reports were completed in accordance with approved test plans. All technical reports and test plans were prepared following the requirements of the Intera DGR Project Quality Plan (INTERA 2009), which meets the requirements of NWMO's DGR Project Quality Plan (NWMO 2009).

The DGSM described in this document summarizes the current understanding of underground geological, hydrogeological and geomechanical conditions of the Bruce nuclear site relevant to DGR repository engineering and safety assessment functions. The geological, hydrogeological and geomechanical site conditions are presented through the development of individual descriptive geological, hydrogeological and geomechanical models of the Bruce nuclear site.

Most of the geoscientific data presented and discussed in this report were obtained from four deep vertical boreholes, DGR-1, DGR-2, DGR-3 and DGR-4 and two deep inclined boreholes DGR-5 and DGR-6, as well as from three shallow boreholes US-3, US-7 and US-8 completed within the upper 200 m of the site. With the exception of borehole US-8, boreholes were continuously cored, core logged and subject to borehole geophysical logging. Extensive straddle-packer hydraulic testing was conducted on all DGR boreholes. With the exception of boreholes DGR-5 and DGR-6, all boreholes were completed with Westbay MP38 and MP55 multi-level groundwater monitoring systems to allow for long-term pressure monitoring and groundwater sampling. As part of the GSCP, 4,962 m of boreholes were drilled, 3,804 m of continuous core was collected and logged, 6,276 m of borehole was geophysically logged, and 2,425 m of borehole was subject to detailed hydraulic testing in 89 straddle-packer tests.

2,019 samples of recovered core were subject to an extensive program of field and laboratory testing. 707 core samples were subject to field geomechanical testing, including point load tests, slake durability tests and P- and S-wave velocity tests. 1,213 core samples were preserved and submitted to commercial and university research laboratories for geomechanical, geological, petrophysical and hydrogeochemical testing.

The results of the geological investigations, including completion of 19.7 km of 2-D seismic reflection surveys are summarized in the descriptive geological model of the Bruce nuclear site. The geological site model describes the occurrence and the lithological and structural characteristics of 34 distinct sedimentary bedrock formations, members or units (excluding the overburden and Precambrian basement), extending from near ground surface to a depth of about 860 metres below ground surface (mBGS). In general, the thickness and orientation of these 34 sedimentary strata are remarkably uniform between the DGR boreholes separated by

up to 1318 m. The thickness and orientation of formations are somewhat variable above the Salina B Unit due to collapse and minor rotation of the overlying bedrock following paleo-dissolution of the Salina B and D Unit salt beds. Below the B Unit the average strike and dip of the deeper Silurian and the Ordovician formations at the Bruce nuclear site (N20°W/0.6°SW) are consistent with regional geological mapping of Armstrong and Carter (2006) and with site predictions developed based on the drilling and logging records of the Texaco No. 6 oil and gas exploration well located 2.9 km southeast of the Bruce nuclear site.

Detailed core logging and borehole geophysical logging of DGR and US-series boreholes show that that Devonian and Upper Silurian dolostones are moderately to highly fractured and of poor to fair rock quality designation (RQD), whereas the deeper Silurian formations below the Salina G Unit, the Ordovician shales that overlie the DGR host formation (Cobourg Formation), the host Cobourg Formation and the argillaceous limestones below the host formation are very sparsely fractured to unfractured with excellent RQD. In summary, the DGSM shows that the bedrock formations at the Bruce site are laterally extensive and of uniform and predictable lithological and structural properties. The Ordovician limestone and shale formations that will host, overlie and underlie the proposed DGR are of uniform and excellent rock quality.

The results of the hydrogeological investigations are summarized in the descriptive hydrogeological model of the Bruce nuclear site. The descriptive hydrogeological site model provides representative values of key hydrogeological properties of the 39 layers that represent the Bruce nuclear site, and then groups these model layers into nine hydrostratigraphic units that have similar hydrogeological properties, and into three hydrogeological systems. Estimates of vertical and horizontal hydraulic conductivity, specific storage, total porosity, hydraulic gradients, vertical and horizontal effective diffusion coefficients, diffusion porosity and groundwater/porewater major ion and isotope chemistry for model layers and hydrostratigraphic units are summarized in this report.

The results of hydrogeological investigations are conveniently summarized through description of the three major hydrogeologic systems at the Bruce nuclear site – shallow, intermediate and deep. The shallow hydrogeological system consists mostly of permeable Devonian dolostones, extends from ground surface to reference depths of 169.3 mBGS in DGR-1, and contains fresh to brackish water with evidence of glacial meltwater. Solute migration within this permeable groundwater system is principally by advection. The intermediate system, consists of Silurian dolostones, shales and anhydrites and extends to reference depths of 447.7 mBGS in DGR-1. Groundwater and porewater within this predominately low-permeability system, transitions from saline Ca-SO_4 water near the top of the system to a Na-Cl brine at the bottom of the system. Tracer profiles indicate solute transport within most of the intermediate system is by diffusion with advective transport likely occurring laterally within the two thin permeable Salina Upper A1 Unit and Guelph Formation non-potable aquifers. The deep system occurs at reference depths of 447.7 to 860.7 mBGS and includes Ordovician shale and limestone and Cambrian sandstone. It comprises an exceptionally low permeability Ordovician shale and Trenton Group limestone aquiclude ($K_h = 10^{-15}$ to 10^{-14} m/s), a low permeability Black River Group aquitard ($K_h = 10^{-12}$ to 10^{-11} m/s) and a non-potable Cambrian aquifer ($K_h = 10^{-9}$ to 10^{-6} m/s). Groundwater and porewater within the deep system is Na-Cl to Na:Ca-Cl brine. Tracer profiles suggest diffusion-controlled solute transport within the bulk of the deep system, with the exception of the Cambrian aquifer that suggests lateral advective transport to the east.

The results of the geomechanical investigations are summarized in the descriptive geomechanical model of the Bruce nuclear site. The geomechanical site model describes and summarizes the current understanding of the principal geomechanical properties of the rock

materials and rock mass beneath the Bruce nuclear site, and also summarizes local seismicity and estimates of in situ stress. The geomechanical site model focuses on presentation of quantitative estimated physical properties that will control the geomechanical behaviour of the rock mass beneath the site during and after construction of the subsurface infrastructure required for development of the DGR. The descriptive geomechanical site model provides representative values of key geomechanical properties of the 34 layers that represent the Bruce site, and then groups these model layers into five mechano-stratigraphic units that have similar geomechanical properties. Representative values are based on combining the specific quantitative values of various parameters derived from field and laboratory testing with expert judgement, where appropriate.

The geomechanical site model describes both the rock material geomechanical characteristics and the rock mass geomechanical characteristics for each of the five mechano-stratigraphic units based on and testing of DGR-1 to DGR-6. Rock material geomechanical characteristics include, where available, information on short and long-term uniaxial compression strengths, triaxial compression strength, indirect tensile strength, direct shear strength, slake durability, free swell behaviour, abrasiveness, and dynamic properties (elastic and shear moduli, Poisson's ratio) based on the testing of intact cores. Rock mass geomechanical characteristics include, where available, information on rock quality designation, natural fracture frequency, and bulk properties from borehole geophysical logging (dynamic elastic and shear moduli). The available data on rock material and rock mass geomechanical characteristics generated from Phase 1, 2A and 2B site characterization work demonstrate that the geomechanical properties of the proposed DGR rocks are better than expected based on precedent projects and regional data summaries.

THIS PAGE HAS BEEN LEFT BLANK INTENTIONALLY

TABLE OF CONTENTS

LIST OF TABLES

Page

LIST OF FIGURES

Page

1. INTRODUCTION

Intera Engineering Ltd. under contract to Nuclear Waste Management Organization (NWMO), has undertaken geoscientific site characterization work at the Bruce nuclear site located in the municipality of Kincardine, Ontario. The purpose of this site characterization work is to assess the suitability of the Bruce nuclear site to implement a Deep Geologic Repository (DGR) for the long-term management of Low and Intermediate Level Waste (L&ILW) generated at Ontario Power Generation-owned or operated facilities. The proposed DGR would be constructed within low-permeability limestone at depths of about 680 m and overlain by at least 200 m of regionally extensive low-permeability shale. The geoscientific site characterization work has been implemented in accordance with the Geoscientific Site Characterization Plan (GSCP) (INTERA 2006, 2008).

This report summarizes the results of the geoscientific site characterization work completed as part of Phase 1, 2A and 2B of the GSCP in the period August 2006 to June 2010. In accordance with the GSCP, geoscientific data collected in Phase 1, 2A and 2B are summarized based on the development of a descriptive geosphere site model (DGSM) of the Bruce nuclear site. The DGSM for the Bruce nuclear site includes descriptive geological, hydrogeological and geomechanical site models.

This report provides a summary compilation, description, assessment and interpretation of geoscientific data collected as part of a series of investigations, which are described in a set of technical reports. Technical reports generally provide limited interpretation and are intended as summaries of collected data. All technical reports were completed in accordance with approved test plans. All technical reports and test plans were prepared following the requirements of the Intera DGR Project Quality Plan (INTERA 2009), which meets the requirements of NWMO's DGR Project Quality Plan (NWMO 2009).

1.1 Report Organization

This document consists of the following sections.

- Chapter 1: Introduction – the remaining parts of Chapter 1 describe organization of this report, the DGR concept, geoscientific site characterization plans, the strategy for development of the DGSM, the pre-existing DGSM and project quality planning.
- Chapter 2: Primary Data Sources – a summary of the technical reports, test plans and other sources of data used to develop the specific descriptive site models given in Chapters 3, 4 and 5.
- Chapter 3: Descriptive Geological Site Model – a summary of the elements, scope, data sources, detailed description and confidence assessment of the geological site model for the Bruce DGR based on Phase 1, 2A and 2B investigations.
- Chapter 4: Descriptive Hydrogeological Site Model – a summary of the elements, scope, data sources, detailed description and confidence assessment of the hydrogeological site model for the Bruce DGR based on Phase 1, 2A and 2B investigations.
- Chapter 5: Descriptive Geomechanical Site Model – a summary of the elements, scope, data sources, detailed description and confidence assessment of the geomechanical site model for the Bruce DGR based on Phase 1, 2A and 2B investigations.
- Chapter 6: Summary – an overview summary of the characteristics of the descriptive geological, hydrogeological and geomechanical site models.
- Chapter 7: References.
- Chapter 8: Units.

- Chapter 9: Abbreviations and Acronyms.
- Appendix A: Comparison of Hydrogeological Parameters Used in Modeling and in the DGSM.
- Appendix B: Composite Geophysical Logs for all DGR boreholes.

1.2 DGR Concept

The DGR is proposed to be constructed at a depth of about 680 m below ground surface within the argillaceous limestone of the Cobourg Formation. Figure 1.1 shows the proposed layout of the DGR below the Bruce nuclear site. The approximate plan location and extent of the proposed DGR is shown on Figure 1.2. The DGR will require construction of a general access shaft and a ventilation shaft.

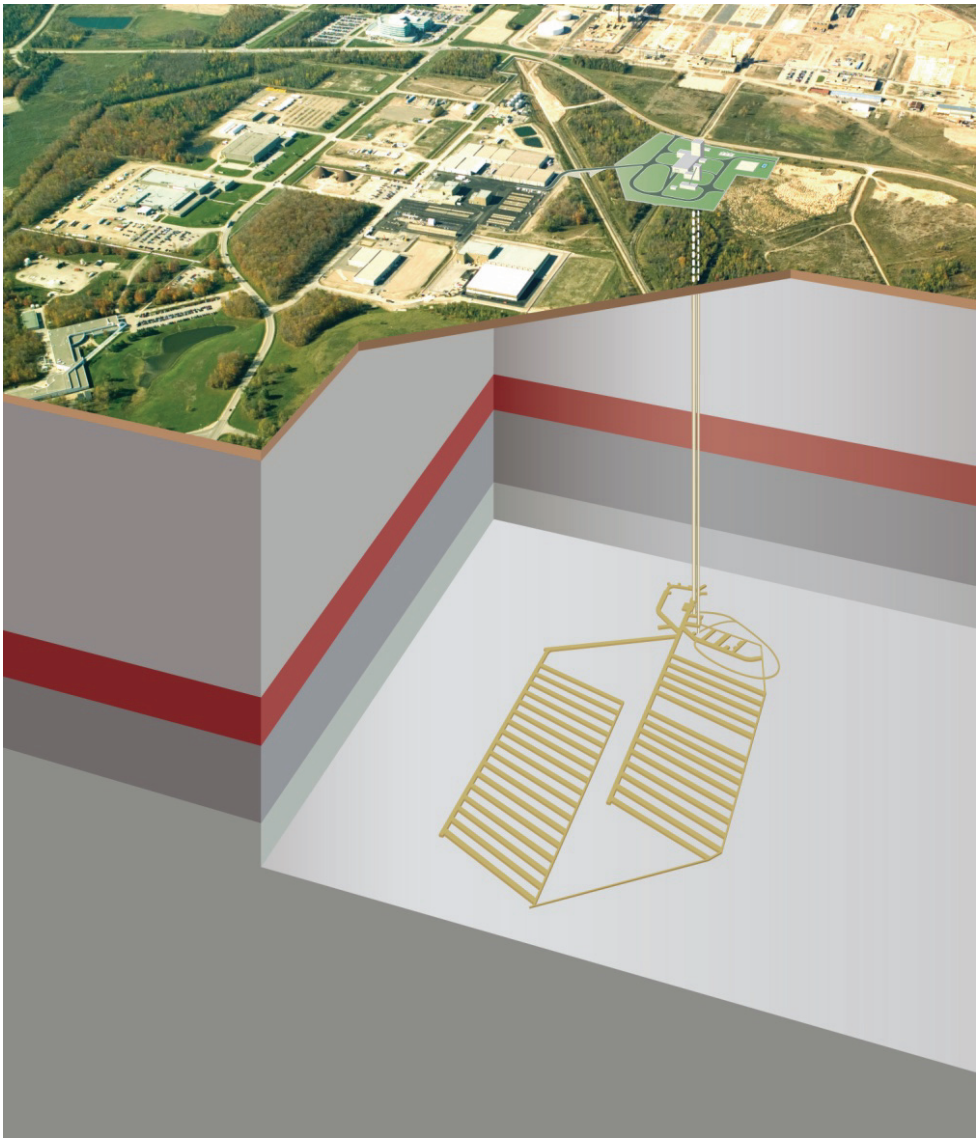

Figure 1.1: Conceptual Layout of the DGR below the Bruce Nuclear Site

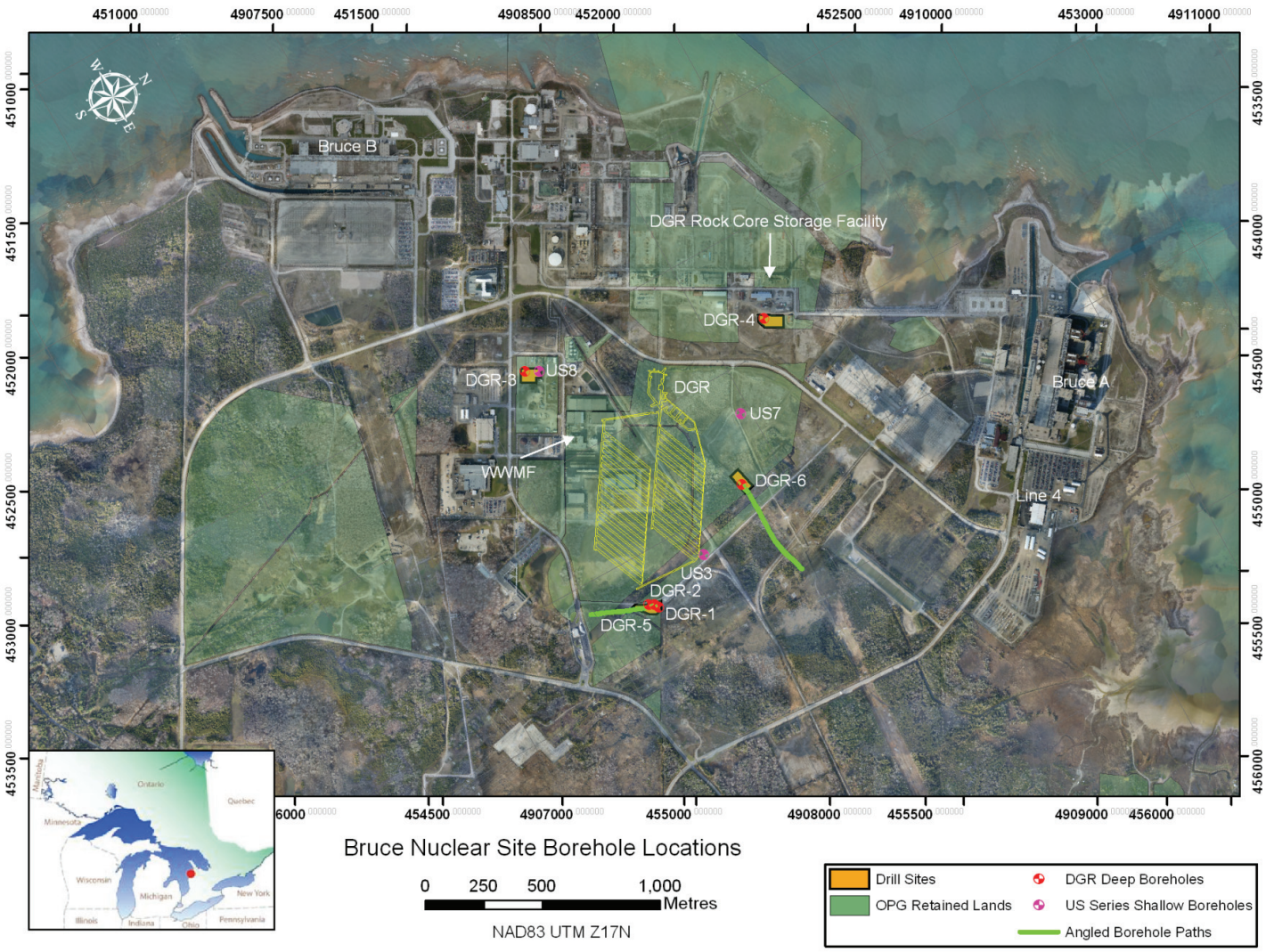

Figure 1.2: DGR Boreholes, US Boreholes and the Proposed DGR Layout at the Bruce Nuclear Site

The DGR will be designed to receive low- and intermediate-level wastes currently in interim storage at the Bruce nuclear site and similar wastes produced at Ontario Power Generation (OPG)-owned or operated nuclear generating stations.

1.3 Geoscientific Site Characterization Plan

The GSCP provides a technical description of the selection and proposed application of preferred tools and methods for site-specific geoscientific characterization of the deep sedimentary bedrock formations found at the Bruce nuclear site. These tools and methods were identified based on assessment of geoscience data needs and collection methods, review of the results of detailed geoscientific studies completed in the same bedrock formations found off the Bruce nuclear site, within Ontario, and recent international experience in geoscientific characterization of similar sedimentary rocks for long-term radioactivewaste management purposes.

The GSCP is a multiple-year, three-phase (1, 2A, 2B) program designed for iterative development, testing and refinement of site-specific descriptive geosphere models, including geological, hydrogeological and geomechanical models. The GSCP is structured into three principal work components: a series of initiation activities necessary to start the site characterization work; three investigative phases; and a geosynthesis or analysis and interpretation task.

The primary focus of the GSCP is subsurface characterization through borehole drilling and testing and surface seismic reflection surveys. Furthermore, this subsurface characterization is to be completed through surface-based investigations only and therefore the GSCP does not include underground-based investigations. The overall GSCP and the detailed investigative activities for Phase 1 work are described by INTERA (2006).

The Phase 1 GSCP provides a detailed description of initiation requirements; Phase 1 work elements for geologic, hydrogeologic and geomechanical site characterization plans; and of geosynthesis, project quality and data management plans. Phase 2A and Phase 2B GSCP activities are necessarily described in general terms in the Phase 1 GSCP.

The majority of Phase 1 GSCP investigations are based on drilling and testing of two deep boreholes, DGR-1 and DGR-2, completed to depths of 462.87 and 862.25 metres below ground surface (mBGS) into the top of the Queenston Formation shale and the Precambrian basement, respectively. Additional shallow to intermediate depth site characterization work included drilling and testing of borehole US-8 to a depth of 200.40 mBGS into the Salina Formation F Unit shale and testing and sampling in existing boreholes US-3 and US-7 completed to depths of 74.31 and 90.56 mBGS, respectively.

The detailed Phase 2 GSCP (INTERA 2008) was prepared to guide Phase 2 geoscientific site characterization work at the Bruce nuclear site in 2008 to 2010. The Phase 2A site characterization involved core drilling and testing of two deep vertical boreholes, DGR-3 and DGR-4, completed to depths of 869.17 and 856.98 mBGS, respectively, into the Cambrian sandstone in 2008. Phase 2B site characterization focused on completion of two boreholes, DGR-5 and DGR-6, inclined at 60° to 65° from the horizontal, to investigate potential deep sub-vertical structural features in the Silurian and Ordovician formations in 2009 and 2010. Phase 2A and Phase 2B activities were originally described as Phase 2 and Phase 3 activities in the Phase 1 GSCP.

Figure 1.2 shows the location of boreholes DGR-1 to DGR-6, US-3, US-7, US-8, and other US-series boreholes relative to the proposed DGR footprint at the Bruce nuclear site.

1.4 Strategy for Development of the DGSM

The DGSM described in this report is based on the following strategic considerations.

- A three-phase site characterization program designed for iterative development, testing and refinement of site-specific descriptive geosphere models. This approach allows for adaptive management of the GSCP to respond to acquired geoscientific knowledge and emerging information requirements for development of the DGSM and DGR Safety Case development.
- An assessment of internationally accepted site-specific geoscience attributes relevant to understanding technical site acceptability.
- Peer review of the DGSM plans by OPG/NWMO stakeholders, regulatory agencies and the independent Geoscience Review Group.
- Integration of the DGSM with on-going regional geologic, hydrogeologic and geomechanical geosynthesis studies in southwestern Ontario relevant to assessing concepts of long-term DGR safety.
- Direct inclusion of international geoscience site characterization experience in investigating deep sedimentary formations for long-term radioactive waste management purposes.
- Participation in various international forums focused on development of geoscience approaches and methods for demonstrating safety of geological disposal in sedimentary formations.
- Preparation of the DGSM under an appropriate Project Quality Plan.

1.5 Pre-Existing Descriptive Geosphere Site Model

The DGR concept for the Bruce nuclear site is largely premised on a pre-existing descriptive geosphere site model developed based on compilation and review of previous geoscience investigations completed at, near and distant from the Bruce nuclear site (GOLDER 2003, Mazurek 2004, NWMO and ITASCA CANADA 2011). This pre-existing site model includes several geoscientific attributes and features judged favourable for the long-term isolation and containment of low- and intermediate-level radioactive waste. The favourable geoscience attributes and features of the pre-existing geosphere site model for the Bruce nuclear site relevant to demonstrating repository safety are listed below.

- The deep horizontally layered shale and argillaceous limestone sedimentary sequence that will overlie and host the DGR is geologically stable, geometrically simple and predictable, relatively undeformed and of large lateral extent.
- There is no evidence of active faulting or seismicity at or near to the site.
- The deep argillaceous formations that will host the DGR will provide stable and practically dry openings.
- The regional stress regime (horizontally compressive) is favourable with respect to sealing of any vertical fractures and faults.
- The deep shale and argillaceous limestones are thick and of very low permeability, providing a very tight bedrock horizon for the DGR, and a very tight 200-m-thick barrier to upward migration from the facility.
- Mass transport in the deep shales and limestones is diffusion dominated. The deep groundwater system in the shales and limestones is saline, stagnant, stable and ancient, not

showing evidence of either glacial perturbations or cross-formational flow or mixing.
- The shallow water supply aquifer in the upper carbonate bedrock is hydrogeologically isolated and protected from the sluggish deep saline groundwater system.
- There is low probability of economic hydrocarbon or mineral deposits in the sedimentary formations in the local area of the Bruce nuclear site and the DGR.

1.6 Project Quality Plan

Intera Engineering Ltd. is an ISO 9001:2008 registered company (BSI Management Systems registration certificate FS 51197) with a specific scope of "provision of environmental consulting services". The company operates under a Quality Management System (QMS), which prescribes procedures and protocols for conducting technical work.

For the Site Characterization project, the QMS has been augmented by a Project Quality Plan (PQP) (INTERA 2009), which describes project-specific procedures and documents how the QMS and additional procedures comply with the NWMO PQP (NWMO 2009). The project-specific procedures address unique requirements of the SC project and the NWMO PQP and are intended to insure that: all project deliverables are of uniformly high quality; that all project work is well documented; and that all testing results and interpretations are traceable. A total of seven project-specific procedures have been defined, and are briefly described below.

- **DGR P1 Organization and QA Program** – Defines the project organization and project staff and management responsibilities. Describes management of subcontractor quality. Prescribes records retention requirements and provides an overview of other project-specific procedures.
- **DGR P2 Document and Activity Record Control** – Describes categories of project documents to be produced and associated review requirements. Activity records are data produced during the execution of a test plan. The procedure prescribes approaches for managing these records.
- **DGR P3 Test Plans** – Plans for all technical activities must be developed before work on the activities commences. Work planning also includes description of verification approaches, where appropriate. This procedure describes the required content for test plans.
- **DGR P4 Sample and Standard Control** – Requirements for the identification of core, surface water, drill water, and groundwater samples acquired from proposed boreholes. Chain-of-custody requirements for sample shipments to laboratories are described.
- **DGR P5 Measurement and Test Equipment Control** – Measurement equipment is used for field analyses of various groundwater and drill-water parameters, for geomechanical tests on core, and for measurement of pressures and flow rates during hydraulic testing. This procedure describes the requirements for equipment calibration and the records to be produced for each calibration event.
- **DGR P6 Scientific Notebooks** - Field and laboratory staff will document daily technical activities in Scientific Notebooks. The format of notebook entries and content guidelines are described in this procedure. Records requirements specific to scientific notebooks are also addressed.
- **DGR P7 Corrective Action** – Identification and documentation of nonconformances and corrective actions to address nonconformances are described in this procedure.

The PQP also describes an audit regime consisting of bi-annual internal audits and annual external audits.

2. PRIMARY DATA SOURCES

2.1 Technical Reports

The primary sources of data that support the descriptive geosphere site models given in Sections 3, 4 and 5 are a series of technical reports. Technical reports principally present and summarize data collected as part of the Phase 1 and 2 geoscientific investigations of the Bruce nuclear site. In some instances, technical reports provide some interpretation of collected data, but most interpretations of collected data are presented in this DGSM Report.

Technical reports are prepared in accordance with approved test plans. Test plans are documents that describe the purpose and scope, activity process, training and health and safety requirements for all data collection activities within the DGR site characterization program. Test lan activity processes include description of overall strategy, specific implementation activities, as well as procedures for sample control, data quality control, data identification and test plan verification.

Table 2.1 summarizes the 69 technical reports that serve as primary data sources in this DGSM Report. Table 2.1 identifies the technical report number, title and report reference. Reference to technical reports in this DGSM Report is by report number. Complete references for technical reports as listed in Table 2.1 are provided in Chapter 9.

Table 2.1: Summary of Bruce Nuclear Site Characterization Technical Reports

Report No.	Report Title	Reference
TR-07-02	Summary of Surrogate Core Analyses	Jackson and Sterling (2008)
TR-07-03	Laboratory Geomechanical Strength Testing of DGR-1 & DGR-2 Core	Gorski et al. (2009a)
TR-07-04	CERCHAR Abrasivity Testing of Argillaceous Limestone of the Cobourg Formation	Maloney (2010)
TR-07-05	Bedrock Formations in DGR-1 and DGR-2	Sterling (2010a)
TR-07-06	Drilling, Logging and Sampling of DGR-1 and DGR-2	Sterling (2010b)
TR-07-07	Field Geomechanical Testing of DGR-1 and DGR-2 Core	Gaines and Sterling (2009a)
TR-07-08	Borehole Geophysical Logging in DGR-1 and DGR-2	Pehme and Melaney (2010a)
TR-07-09	Drilling Fluid Management and Testing in DGR-1 and DGR-2	Raven and Sterling (2009)
TR-07-10	Westbay MP55 Casing Completions in DGR-1 and DGR-2	Raven and Gaines (2010)
TR-07-11	Opportunistic Groundwater Sampling in DGR-1 and DGR-2	Jackson and Heagle (2010)
TR-07-12	Petrographic and Mineralogic Analyses of DGR-1 and DGR-2 Core	Schandl (2009)
TR-07-14	Fluid Electrical Conductivity Logging in Borehole DGR-1	Beauheim and Pedler (2009)
TR-07-15	2D Surface Seismic Survey of the Bruce Site	Watts et al. (2009)
TR-07-16	Laboratory Swell Testing of DGR-2 Core	Micic and Lo (2010)
TR-07-17	Measurement of Diffusion Properties by XRay Radiography and by Through-Diffusion Techniques Using Iodide and Tritium Tracers: Core Samples from OS-1 and DGR-2	Al et al. (2010a)
TR-07-18	Laboratory Petrophysical Testing of DGR-2 Core	Whitney and Lee (2010)

Report No.	Report Title	Reference
TR-07-19	Drilling and Logging of US-8	Briscoe (2009)
TR-07-20	Westbay MP38 Casing Completions in US-3, US-7 and US-8	Raven and Sterling (2010)
TR-07-21	Pore Water And Gas Analysis in DGR-1 and DGR-2 Core	Clark et al. (2010a)
TR-07-22	Diffusion of ^{125}I in Limestone and Red Shale Samples from DGR-2 Core	Van Loon (2010)
TR-08-01	XRD Mineralogical Analysis of DGR-1 and DGR-2 Core	Skowron and Hoffman (2009a)
TR-08-02	Geochemical and SEM/EDS Analysis of DGR-1 and DGR-2 Core	Skowron and Hoffman (2009b)
TR-08-03	Borehole Geophysical Logging of US-3 and US-7	Melaney (2009)
TR-08-04	Analysis of DGR-1 and DGR-2 Borehole Images for Stress Characterization	Valley and Maloney (2009)
TR-08-06	Borehole DGR-2: Pore-Water Investigations	Koroleva et al. (2009)
TR-08-07	Evaluation of Possible Hydraulic Communication Between DGR-1 and DGR-2 at the Brue Site	Beauheim (2009)
TR-08-08	Initial Groundwater Monitoring, US-3, US-7 and US-8	Heagle (2010)
TR-08-10	Compilation and Consolidation of Field and Laboratory Data for Hydrogeological Properties	Walsh (2011)
TR-08-11	DGR-2 Long-Term Strength Degradation Tests	Gorski et al. (2009b)
TR-08-12	Bedrock Formations in DGR-1, DGR-2, DGR-3 and DGR-4	Wigston and Heagle (2009)
TR-08-13	Drilling, Logging and Sampling of DGR-3 and DGR-4	Briscoe et al. (2010)
TR-08-14	Field Geomechanical Testing of DGR-3 and DGR-4 Core	Gaines and Sterling (2009b)
TR-08-15	Borehole Geophysical Logging in DGR-3 and DGR-4	Pehme and Melaney (2010b)
TR-08-16	Drilling Fluid Management and Testing in DGR-3 and DGR-4	Pinder (2009)
TR-08-17	Westbay MP55 Casing Completions in DGR-2, DGR-3 and DGR-4	Sterling et al. (2011a)
TR-08-18	Opportunistic Groundwater Sampling in DGR-3 and DGR-4	Heagle and Pinder (2010)
TR-08-19	Pore Water and Gas Analysis in DGR-3 and DGR-4 Core	Clark et al. (2010b)
TR-08-20	Petrographic Analysis of DGR-3 Core	Schandl (2010a)
TR-08-21	Petrographic Analysis of DGR-4 Core	Schandl (2010b)
TR-08-22	Mineralogy and Geochemistry of DGR-3 Core	Wigston and Jackson (2010a)
TR-08-23	Mineralogy and Geochemistry of DGR-4 Core	Wigston and Jackson (2010b)
TR-08-24	Laboratory Geomechanical Strength Testing of DGR-3 & DGR-4 Core	Gorski et al. (2010a)
TR-08-25	CERCHAR Abrasivity Testing of Argillaceous Limestone of the Cobourg Formation from DGR-3 and DGR-4	Maloney and Bahrani (2009)
TR-08-26	Laboratory Free Swell Testing of DGR-3 and DGR-4 Core	Micic and Lo (2009)
TR-08-27	Measurement of Diffusion Properties by X-Ray Radiography and by Through-Diffusion Techniques Using Iodide and Tritium Tracers: Core Samples from DGR-3 and DGR-4	Al et al. (2010b)
TR-08-28	Laboratory Petrophysical Testing of DGR-3 and DGR-4 Core	Jackson and Wigston (2010)

Report No.	Report Title	Reference
TR-08-29	Organic Geochemistry and Clay Mineralogy of DGR-3 and DGR-4 Core	Jackson (2009)
TR-08-30	Phase 2 Groundwater Monitoring: US-3, US-7 and US-8	Murphy and Heagle (2011)
TR-08-31	Pressure and Head Monitoring in MP55 Casing Systems Installed in DGR-1 to DGR-4	Sterling and Raven (2011)
TR-08-32	Analysis of Borehole Straddle-Packer Tests in DGR Boreholes	Roberts et al. (2011)
TR-08-33	Two-Phase Flow Parameters from DGR-2, DGR-3 and DGR-4 Petrophysics Data	Calder (2011)
TR-08-34	Assessment of Porosity Data and Gas Phase Presence in DGR Cores	Sterling et al. (2011b)
TR-08-35	Analysis of DGR-1, DGR-2, DGR-3 and DGR-4 Borehole Images for Stress Characterization	Valley and Maloney (2010)
TR-08-36	Long-Term Strength Degradation Testing of DGR-3 and DGR-4 Core	Gorski et al. (2010b)
TR-08-37	Vacuum Distillation Experiments on DGR Core	Clark et al. (2010c)
TR-08-38	Radioisotopes in DGR Groundwater and Porewater	Clark and Herod (2011)
TR-08-39	Supplementary Uniaxial Compressive Strength Testing of DGR-3 and DGR-4 Core	Gorski et al. (2010c)
TR-08-40	Boreholes DGR-3 and DGR-4 Porewater Investigations	Hobbs et al. (2011a)
TR-09-01	Drilling, Logging and Sampling of DGR-5 and DGR-6	Sterling et al. (2011c)
TR-09-02	Drilling Fluid Management and Testing in DGR-5 and DGR-6	Raven and Sterling (2011)
TR-09-03	Borehole Geophysical Logging of DGR-5 and DGR-6	Pehme and Melaney (2011)
TR-09-04	Pore Water Analysis in DGR-5 and DGR-6 Core	Clark et al. (2011)
TR-09-05	Petrographic Analyses of DGR-5 and DGR-6 Core	Schandl (2011)
TR-09-06	Mineralogical and Lithogeochemical Analyses of DGR-5 and DGR-6 Core	Jackson and Murphy (2011)
TR-09-07	Laboratory Geomechanical Strength Testing of DGR-2 to DGR-6 Core	Gorski et al. (2011)
TR-09-08	Laboratory Petrophysical Testing of DGR-5 and DGR-6 Core	Raven and Jackson (2011)
TR-09-09	Oriented Core Logging of DGR-5 and DGR-6 Core	Gaines et al. (2011a)
TR-09-10	Temporary Sealing of Boreholes DGR-5 and DGR-6	Gaines et al. (2011b)
TR-09-11	Bedrock Formations in DGR-1 to DGR-6	Sterling and Melaney (2011)

Several technical reports describe in-situ stress analyses (TR-08-04, TR-08-35) and bedrock formations in DGR boreholes (TR-07-05, TR-08-12, TR-09-11). For these reports, the latter report is the report relied upon in this DGSM report. Earlier versions of these technical reports reflect reporting using data that was available at the time of report preparation. Additional data collected subsequent to preparation of the earlier reports, has resulted in replacement of these earlier reports with more recent versions. These earlier technical reports are reported in Table 2.1 for completeness.

2.2 Other Data Sources

In addition to geoscientific site characterization technical reports, other sources of data were used in development of the descriptive geosphere site models. These other sources of data, which are referenced in Chapter 9, are listed below.

- Compilation of available geological, hydrogeological and geotechnical/geomechanical information for the proposed Bruce DGR as part of a geotechnical feasibility study (GOLDER 2003).
- Geoscientific data compilation, international review and geosynthesis assessment of the Paleozoic sedimentary rock in southern Ontario for radioactivewaste disposal (Mazurek 2004).
- Laboratory and field data collection, review and compilation reports prepared as part of the Ontario Hydro Sedimentary Sequence Study looking at radioactive waste disposal within sedimentary rock formations in Ontario.
- Reports on core drilling, logging and testing of the shallow bedrock (US-series holes) to depths of about 100 m as part of an earlier investigation of the Bruce nuclear site for radioactive waste storage (Lukajic 1988, Lee et al. 1995).
- Reports on geologic, hydrogeologic and geomechanical conditions of the overburden and shallow bedrock to 60 m depth at the Bruce nuclear site from generating station/intake tunnel construction and operation and monitoring of radioactive waste operations areas and conventional construction landfills (Lukajic et al. 1986, Lukajic and Dupak 1986, Intera Technologies Ltd. 1988, McKay 1989).
- Deep Geologic Repository: Geosynthesis Report (NWMO 2011) summarizing the regional geoscientific studies conducted to understand the predictability, stability and geologic isolation provided by the geologic setting at the Bruce nuclear site.
- Geosynthesis Supporting Technical Reports. Noteworthy supporting studies include technical reports on regional geology (AECOM and ITASCA CANADA 2011), regional geomechanics (NWMO and AECOM 2011), regional and site hydrogeologic modeling (Sykes et al. 2011) and regional hydrogeochemical synthesis (Hobbs et al. 2011b).

2.3 DGR Borehole Investigation Program

Most of the geoscientific data presented and discussed in this report were obtained from four deep diamond-cored vertical boreholes, DGR-1, DGR-2, DGR-3 and DGR-4 and two deep inclined boreholes DGR-5 and DGR-6.

Boreholes DGR-1 and DGR-2, drilled about 40 m apart, were designed to provide two separate boreholes with open bedrock intervals through the relatively shallow dolostone and limestone formations of Silurian and Devonian age (DGR-1) and through the relatively deeper shale and limestone formations of Ordovician age (DGR-2).

DGR-1 was continuously diamond cored, with the upper 182.9 m reamed to accommodate installation of intermediate steel casing. DGR-1 was completed with an open bedrock interval from near the top of the Salina Formation F Unit shale (182.9 mBGS) to approximately 15 m into the top of the Queenston Formation (462.87 mBGS).

DGR-2 was rotary drilled to a depth of 450.7 mBGS to accommodate installation of two intermediate steel casings. DGR-2 was then diamond cored and completed with an open bedrock interval from near the top of the Queenston Formation (450.88 mBGS) to approximately 1 m into the Precambrian basement (862.25 mBGS).

Two separate boreholes for DGR-1 and DGR-2 were designed to minimize vertical cross-connection and cross-contamination of groundwater between the shallow and deep hydrogeologic environments with suspected distinctly different groundwater chemistry and to minimize risk of borehole loss should caving or other poor drilling conditions be encountered. TR-07-06 describes the rationale and completion of the drilling and casing of boreholes DGR-1 and DGR-2.

Boreholes DGR-3 and DGR-4 were continuously diamond cored from about 22 m below bedrock surface (approximately 30 mBGS) to depths of 869.17 and 856.98 mBGS, respectively, into the Cambrian sandstone. The upper 208.5 m of DGR-3 and the upper 188.7 m of DGR-4 were reamed to accommodate installation of intermediate steel casing. Together, boreholes DGR-1/2, DGR-3 and DGR-4, which are spaced approximately 1047 to 1318 m from each other, triangulate the proposed DGR and allow for assessment of the uniformity of bedrock formation thickness, orientation and properties in the vicinity of the DGR. TR-08-13 describes the drilling and casing installation in boreholes DGR-3 and DGR-4.

Boreholes DGR-5 and DGR-6 were inclined boreholes drilled to investigate possible faults identified from seismic surveys, and general vertical structure and permeability within the DGR bedrock. To ensure adequate sampling of possible vertical structure, boreholes DGR-5 and DGR-6 were drilled in approximate orthogonal directions away from the proposed DGR footprint. Borehole DGR-5 was rotary drilled to 188.2 metres length below ground surface (mLBGS) to allow for installation of intermediate steel casing, and then continuously cored to a target depth of 807.15 mLBGS within the bottom of the Kirkfield Formation. Starting and final azimuth/plunge of DGR-5 were 190°/65° and 201°/78°, respectively. Borehole DGR-6 was rotary drilled to 214.8 mLBGS to allow for installation of intermediate steel casing, and then continuously cored to a target depth of 903.16 mLBGS within the top of the Gull River Formation. Starting and final azimuth/plunge of DGR-6 were 80°/60° and 73°/57°, respectively. TR-09-01 describes the drilling and casing installation in boreholes DGR-5 and DGR-6.

A major source of geological, hydrogeological and geomechanical data described in this report is derived from laboratory testing of preserved core samples collected from DGR boreholes. TR-07-06, TR-08-13 and TR-09-01 describe the collection and preservation of core samples for laboratory testing from boreholes DGR-1 and DGR-2, boreholes DGR-3 and DGR-4, and boreholes DGR-5 and DGR-6, respectively. In general, core samples were selected to be representative of material for which laboratory testing was to be performed. 1213 core samples were collected from DGR boreholes and submitted for laboratory testing.

3. DESCRIPTIVE GEOLOGICAL SITE MODEL

3.1 Model Elements and Scope

The geologic site model describes the 3-D spatial distribution of all important geologic formations and the occurrence of all important geologic structural features within the Paleozoic (Devonian to Cambrian) and Precambrian bedrock units. The descriptive geologic model provides a basis for geoscientific understanding of the current condition of the Bruce nuclear site, its past evolution and likely future natural evolution over the period of interest for the safety assessment of the proposed DGR. The descriptive geologic site model also provides the basic framework for the development of descriptive hydrogeological and geomechanical site models that are described in Chapters 4 and 5 of this report.

3.2 Data Sources

Primary data sources for the descriptive geological site model are listed below.

- Drilling and core logging of boreholes DGR-1 and DGR-2 (TR-07-05, TR-07-06), boreholes DGR-3 and DGR-4 (TR-08-12, TR-08-13) and boreholes DGR-5 and DGR-6 (TR-09-01, TR-09-09, TR-09-11).
- Borehole geophysical logging of boreholes DGR-1 and DGR-2 (TR-07-08), boreholes DGR-3 and DGR-4 (TR-08-15), and boreholes DGR-5 and DGR-6 (TR-09-03). Note the complete borehole geophysical logs for all DGR boreholes are provided on a CD in Appendix B to this report.
- Laboratory geochemical, mineralogical and petrographic analyses of DGR-1 and DGR-2 core (TR-07-12, TR-08-01, TR-08-02, TR-08-06), DGR-3 and DGR-4 core (TR-08-20, TR-08-21, TR-08-22, TR-08-23, TR-08-29, TR-08-40) and DGR-5 and DGR-6 core (TR-09-05, TR-0-06).
- Drilling and core logging of boreholes US-1 and US-3 to US-7 (Lukajic 1988).
- Drilling, chip sampling and borehole geophysical logging of borehole US-8 (TR-07-19).
- Borehole geophysical logging of US-3 and US-7 (TR-08-03).
- 2-D seismic reflection surveys (TR-07-15).
- Regional geological framework developed from related geosynthesis studies (NWMO 2011, NWMO and AECOM 2011).

3.3 Paleozoic Stratigraphy and Depositional History of Southern Ontario

The Paleozoic stratigraphy of southern Ontario is summarized by Armstrong and Carter (2006, 2010) and in the context of the Bruce DGR project by AECOM and ITASCA CANADA (2011). The bedrock map of southern Ontario illustrating the location of the Bruce nuclear site and the regional geological framework study area surrounding the site is shown in Figure 3.1. The following description of the Paleozoic stratigraphy of southern Ontario are from AECOM and ITASCA CANADA (2011).

During the Paleozoic Era, eastern North America was mainly located in tropical latitudes and intermittently covered by basin-centred inland seas. Consequently, the Paleozoic bedrock in southern Ontario consists largely of marine sediments from Cambrian to Mississippian age (Armstrong and Carter 2010). The Paleozoic stratigraphy and depositional history of southern Ontario and the Bruce site is conveniently discussed according the following main stratigraphic sequences:

- Cambrian sandstones and carbonates;
- Ordovician carbonates;
- Ordovician shales;
- Silurian carbonates and shale;
- Silurian Salina Group and Bass Islands Formation; and
- Devonian carbonates.

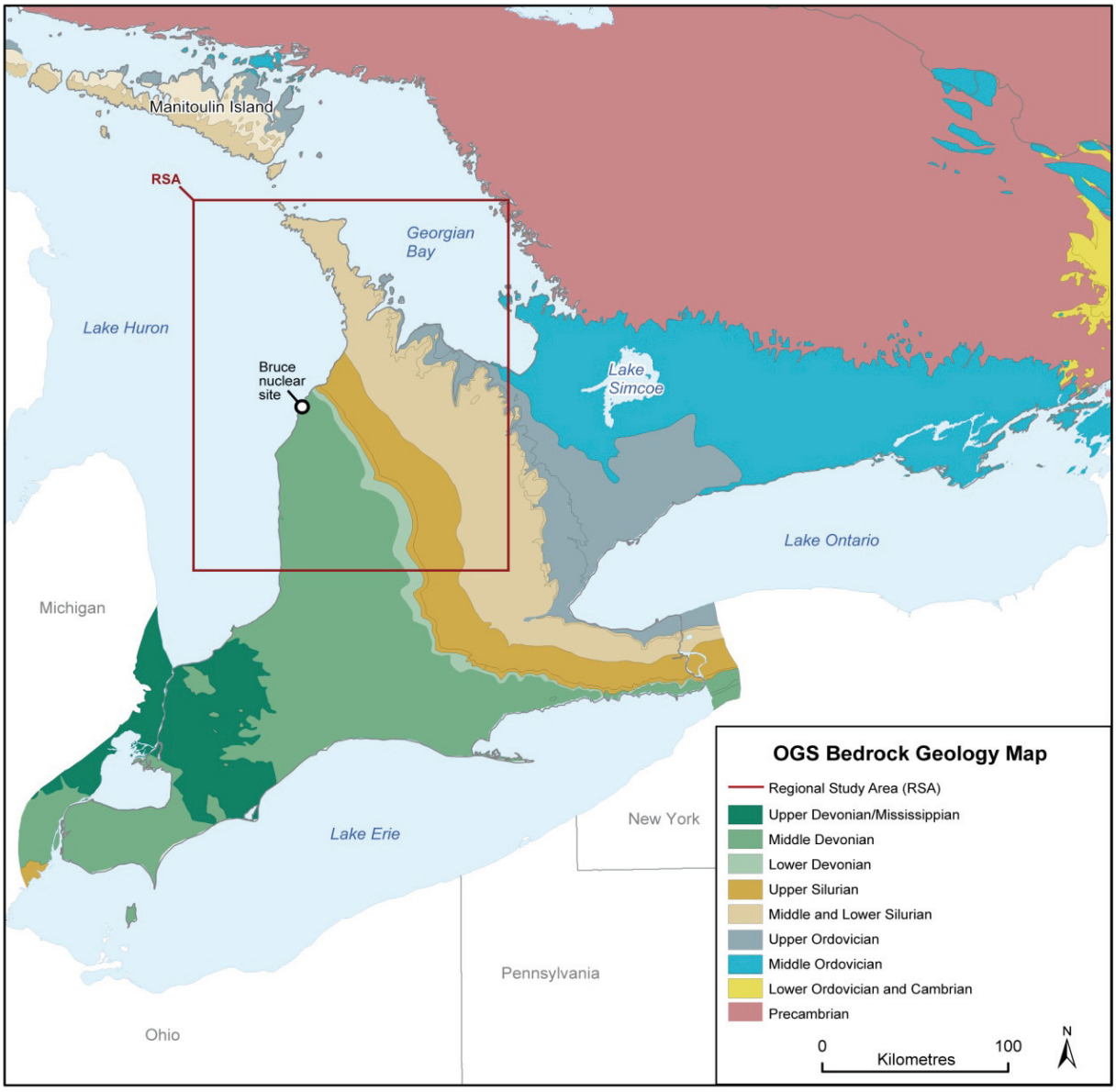

Note: After Ontario Geological Survey (1991).

Figure 3.1: Bedrock Geology of Southern Ontario Showing Bruce Nuclear Site and Boundary of Regional Geological Framework Study Area

Cambrian rocks of Ontario were deposited over the irregular and altered Precambrian surface and extend from the Appalachian Basin to the Michigan Basin but have largely been eroded over the Algonquin Arch. The lithology of the Cambrian deposits ranges from fine to medium crystalline dolostone, sandy dolostone, argillaceous dolostone to fine and coarse sandstone.

The Middle Ordovician carbonates of southern Ontario are divided into two groups, the Black River Group (Shadow Lake, Gull River and Coboconk formations) and the Trenton Group (Kirkfield, Sherman Fall and Cobourg formations). These carbonate rocks were deposited in a major marine transgression that followed the uplift and erosion of Cambrian rocks. This transgression was responsible for the sequence of Black River and Trenton facies assemblages that characterize a succession from supratidal and tidal flat clastics/carbonates to lagoonal carbonates and offshore shallow water and deep shelf carbonates.

Onset of the Taconic Orogeny in the Early to Middle Ordovician resulted in the collapse of platform carbonates of the Trenton Group and the westward inundation of these rocks with orogen-derived marine clastic (shale) sediments resulting in deposition of the Blue Mountain, Georgian Bay and Queenston formations. The quantity of clastics decreases over the Algonquin Arch and into the Michigan Basin.

The top of the Queenston Formation is a discontinuity associated with a global eustatic/sea level drop and marks the return to carbonate-forming conditions during the marine transgressions that followed the Queenston disconformity. The Manitoulin, Cabot Head, Fossil Hill, Lions Head, Gasport, Goat Island and Guelph formations were deposited during these marine transgressions.

The change from the Guelph Formation deposition to the Salina deposition marks a significant change in sedimentary environments that was the result of arch uplift and rapid basin subsidence caused by the late Silurian Acadian Orogeny. Increasingly restricted marine conditions in the Michigan Basin led to evaporative brine concentration and precipitation of carbonate, gypsum/anhydrite, halite and sylvite. Periodic intrusion of fresh marine water returned the Basin to carbonate-forming conditions. As a result of these processes, a repeating pattern of deposition of carbonates, evaporites and argillaceous sediments characterize the Salina Group. The Bass Islands Formation represents a change back to marine carbonate conditions away from the cyclic evaporite and carbonate-forming conditions of the Salina Group.

At the end of the Silurian, there was a long period of sediment exposure resulting in the formation of an erosional disconformity. Subsequent to this erosion, Devonian limestones and dolostones of the Bois Blanc, Amherstburg and Lucas formations were deposited in a major marine transgression.

3.4 DGR Reference Stratigraphic Sequence

The DGR reference overburden and bedrock stratigraphic sequence at the Bruce nuclear site, based on the results of DGR-1 to DGR-6 borehole drilling, logging and testing, is schematically illustrated in Figure 3.2. Reference stratigraphy is defined in this report as the stratigraphy present at boreholes DGR-1 and DGR-2 and is required for data presentation purposes due to the slight dip of the bedrock formations at the site (see Section 3.5).

Figure 3.2 and the detailed bedrock formation descriptions that follow in Sections 3.5 and 3.8 are primarily based on the subsurface stratigraphic nomenclature of Armstrong and Carter (2006), lithologic and discontinuity logging of DGR-1 to DGR-6 and US-series boreholes, and the results of three geological core workshops attended by senior geologists from the Ministry of

Natural Resources, the Ontario Geological Survey, the Geological Survey of Canada and the University of Waterloo (TR-07-05, TR-08-12, TR-09-11).

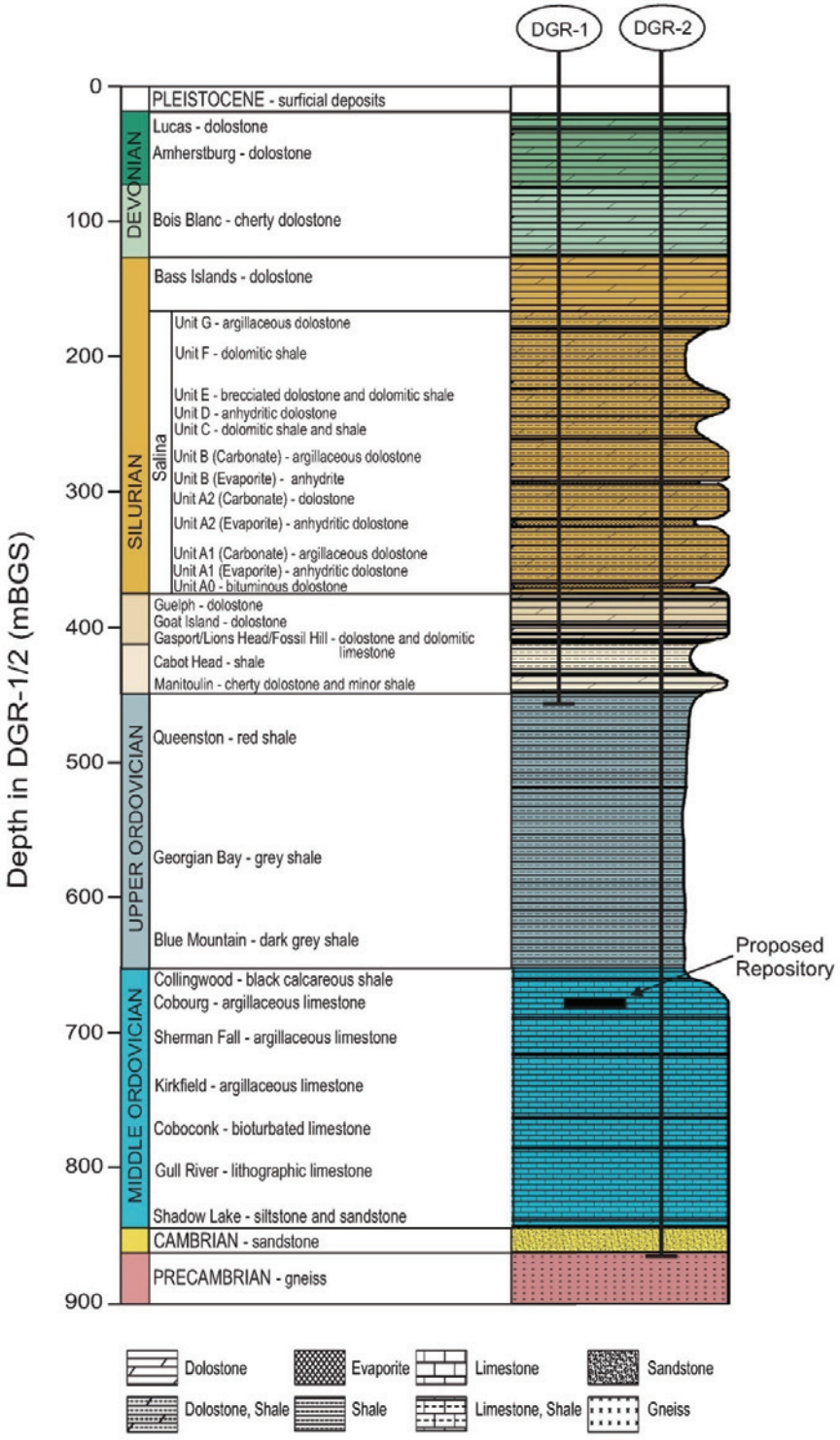

Figure 3.2: Reference Stratigraphic Column at the Bruce Nuclear Site Based on DGR-1 and DGR-2 Borehole Data

The geological core workshops were convened to seek expert consensus on the identification and naming of the bedrock formations and members/units present in DGR-series and US-series boreholes as well as identification of contacts between formations and units present in these boreholes.

The reference stratigraphic sequence presented here differs slightly from Armstrong and Carter (2006) in that the Silurian Gasport and Goat Island Members of the Lockport Formation are considered to have formation status, as per Brett et al. (1995), as does the Lions Head unit.

The paperback Ontario Geological Survey open file report of Armstrong and Carter (2006) has recently been released as an updated and reformatted hard-cover Special Volume publication (Armstrong and Carter 2010). The subsurface bedrock stratigraphic nomenclature is generally the same in both of these publications, although Armstrong and Carter (2010) include an updated stratigraphic chart that removes the Middle Silurian and re-assigns the Middle Ordovician limestone units to the lower portion of the Upper Ordovician. The stratigraphic nomenclature of Armstrong and Carter (2006) is used in this DGSM Report and in supporting technical reports, except as noted above.

3.5 Formation Depth, Thickness and Orientation

Logging of boreholes DGR-1 to DGR-6 identified the presence of 35 distinguishable bedrock formations, members, units or subunits at the Bruce DGR site (TR-08-12, TR-09-11) consisting of 34 sedimentary bedrock layers and the Precambrian basement. Table 3.1 summarizes the true depth to top and thickness of each bedrock formation, member, unit or subunit in the DGR boreholes based on calculated true vertical depths and elevations, and considering the measured orientation of both inclined and vertical boreholes (TR-09-11). TR-08-12 reported on top depth and thickness of formations for DGR-1/DGR-2, DGR-3 and DGR-4 assuming these boreholes were vertical with zero tilt. Comparison of formation thicknesses presented in TR-08-12 and TR-09-11 shows that the assumption of verticality in boreholes DGR-1/DGR-2, DGR-3 and DGR-4 has negligible influence on calculated formation thicknesses (maximum error of 0.1 m).

Table 3.2 lists the strike and dip of the top of each of these bedrock layers based on solution of a simple three-point elevation problem (TR-09-11) for true top of formation elevations in DGR-1/DGR-2, DGR-3 and DGR-4. Comparison of formation strikes and dips in TR-08-12 and TR-09-11 shows that the assumption of verticality in boreholes DGR-1/DGR-2, DGR-3 and DGR-4 has very minor influence on calculated formation strikes (maximum error of 0.5°) and dips (maximum error of 0.03°). The calculated formation orientations in Table 3.2 are representative of expected values in the area of the proposed DGR, and consistent with the regional geometric framework for this part of the Michigan Basin.

Tables 3.1 and 3.2 show the formation thicknesses and orientations in DGR boreholes are remarkably uniform over the DGR borehole collar separation distances of up to 1318 m (DGR-2 to DGR-4). The thickness and orientation of formations are somewhat more variable above the Salina B Unit and more uniform below the B Unit. This is most likely due to collapse and minor rotation of the overlying bedrock following paleo-dissolution of the Salina B and D Unit salt beds and the difficulty of making formation picks based on geophysical logs, especially in DGR-6 between the Salina B Unit and E Unit. In DGR-6 the thickness of the Salina C Unit and the Salina B Unit carbonate are noticeably different than in other DGR boreholes. The reasons for these differences are further discussed in Section 3.13.2.

Below the Salina B Unit, formation thicknesses in DGR boreholes are typically within a few metres of each other in different holes, and the formation strikes are within 5-10° and formation dips are within 0.10° for each formation. The average strike and dip of the deeper Silurian and the Ordovician formations of N20°W/0.6°SW at the Bruce nuclear site is consistent with results of the regional 3-D geological framework model (AECOM and ITASCA CANADA 2011). Noteworthy minor excursions of uniformity of thickness and orientation for formations below the Salina B Unit at the Bruce nuclear site include the Queenston Formation whose upper contact is a regional erosional unconformity.

Additional discussion of formation orientation is given in Section 3.9. Section 3.9 describes the identification of distinct thin marker beds in the DGR Paleozoic bedrock sequence at the Bruce nuclear site that provide very accurate strike and dip information.

Table 3.1: Summary of True Top Vertical Depth and Thickness of Bedrock Formations, Members and Units in DGR-1/DGR-2, DGR-3, DGR-4, DGR-5 and DGR-6

Formation, Member, Unit	True Top Vertical Depth (mBGS)					Thickness (m)				
	DGR-1/2	DGR-3	DGR-4	DGR-5	DGR-6	DGR-1/2	DGR-3	DGR-4	DGR-5	DGR-6
Lucas	20.0	7.9	7.5	20.0	14.4	10.4	46.6	30.1	10.4	16.9
Amherstburg	30.4	54.5	37.6	30.4	31.3	44.6	39.4	38.6	44.6	42.5
Bois Blanc	75.0	93.8	76.2	75.0	73.9	49.0	49.3	49.8	47.3	48.0
Bass Islands	124.0	143.1	126.0	122.2	121.9	45.3	44.0	44.1	44.6	44.2
Salina G Unit	169.3	187.1	170.1	166.8	166.1	9.3	9.2	7.3	7.6	8.6
Salina F Unit	178.6	196.3	177.4	174.3	174.7	44.4	43.0	43.6	38.7	40.0
Salina E Unit	223.0	239.3	220.9	213.1	214.7	20.0	23.8	24.4	19.4	20.1
Salina D Unit	243.0	263.1	245.4	232.4	231.9	1.6	2.6	1.8	1.0	1.0
Salina C Unit	244.6	265.6	247.2	233.5	232.8	15.7	11.9	14.7	12.8	33.1
Salina B Unit-Carb	260.3	277.5	261.9	246.3	266.2	30.9	25.1	28.8	40.8	21.2
Salina B Unit-Evap	291.2	302.6	290.7	287.1	287.4	1.9	1.6	1.7	3.2	4.0
Salina A2 Unit - Carb	293.1	304.2	292.4	290.3	291.4	26.6	28.8	28.4	27.9	25.8
Salina A2 Unit-Evap	319.7	333.0	320.8	318.2	317.2	5.8	5.1	5.2	5.6	3.7
Salina A1 Unit - Carb	325.5	338.1	326.0	323.7	320.9	41.5	41.1	40.7	41.5	40.4
Salina A1 Unit -Evap	367.0	379.2	366.7	365.2	361.2	3.5	4.4	5.0	4.4	4.4
Salina A0 Unit	370.5	383.6	371.7	369.6	365.7	4.0	2.6	3.8	2.8	3.9
Guelph	374.5	386.2	375.5	372.3	369.6	4.1	5.4	4.9	5.4	3.7
Goat Island	378.6	391.6	380.4	377.7	373.3	18.8	18.3	18.6	18.1	18.5
Gasport	397.4	409.9	399.0	395.8	391.8	6.8	6.5	6.5	9.2	7.9
Lions Head	404.2	416.4	405.5	405.0	399.7	4.4	4.5	4.4	2.3	3.6
Fossil Hill	408.7	420.9	409.9	407.3	403.3	2.3	1.3	1.5	2.4	2.6
Cabot Head	411.0	422.2	411.4	409.7	405.9	23.8	24.7	24.2	23.7	23.4
Manitoulin	434.8	446.9	435.6	433.4	429.3	12.8	9.5	10.6	12.9	13.2

Formation, Member, Unit	True Top Vertical Depth (mBGS)					Thickness (m)				
	DGR-1/2	DGR-3	DGR-4	DGR-5	DGR-6	DGR-1/2	DGR-3	DGR-4	DGR-5	DGR-6
Queenston	447.6	456.4	446.2	446.2	442.6	70.3	74.4	73.0	70.3	69.3
Georgian Bay	518.0	530.7	519.2	516.6	511.9	90.9	88.7	88.7	88.6	88.2
Blue Mountain	608.9	619.4	607.9	605.2	600.1	42.7	44.1	45.1	45.1	45.0
Collingwood Member	651.6	663.6	653.0	650.3	645.1	7.9	8.7	8.4	8.6	6.5
Cobourg	659.5	672.3	661.4	658.9	651.6	28.6	27.8	27.5	27.1	28.5
Sherman Fall	688.1	700.1	688.8	686.0	680.2	28.0	28.9	28.3	29.3	28.8
Kirkfield	716.1	729.0	717.1	715.3	709.0	45.9	45.8	45.7	--	46.8
Coboconk	762.0	774.9	762.8	-	755.8	23.0	23.7	23.8	--	22.4
Gull River	785.0	798.6	786.6	-	778.1	53.6	51.7	52.2	--	--
Shadow Lake	838.6	850.3	838.8	-	-	5.2	4.5	5.1	--	--
Cambrian	843.8	854.8	843.9	-	-	16.9	>13.7	>12.9	--	--
Precambrian	860.7	-	-	-	-	--	--	--	--	--

Table 3.2: Summary of True Strike and Dip of Bedrock Formations, Members and Units as Defined by Intersections in DGR-1/DGR-2, DGR-3 and DGR-4

Formation, Member, Unit	Strike	Dip
Lucas	-	-
Amherstburg	N16°W	1.15°SW
Bois Blanc	N27°W	0.95°SW
Bass Islands	N25°W	0.95°SW
Salina G Unit	N17°W	0.90°SW
Salina F Unit	N33°W	0.95°SW
Salina E Unit	N35°W	0.89°SW
Salina D Unit	N25°W	1.01°SW
Salina C Unit	N25°W	1.07°SW
Salina B Unit -Carb	N24°W	0.85°SW
Salina B Unit-Evap	N24°W	0.53°SW
Salina A2 Unit - Carb	N20°W	0.52°SW
Salina A2 Unit-Evap	N28°W	0.62°SW
Salina A1 Unit - Carb	N21°W	0.59°SW
Salina A1 Unit -Evap	N25°W	0.58°SW
Salina A0 Unit	N19°W	0.61°SW
Guelph	N16°W	0.53°SW
Goat Island	N16°W	0.59°SW

Formation, Member, Unit	Strike	Dip
Gasport	N15°W	0.57°SW
Lions Head	N16°W	0.55°SW
Fossil Hill	N17°W	0.55°SW
Cabot Head	N19°W	0.51°SW
Manitoulin	N19°W	0.55°SW
Queenston	N24°W	0.41°SW
Georgian Bay	N17°W	0.61°SW
Blue Mountain	N23°W	0.51°SW
Collingwood Member	N14°W	0.56°SW
Cobourg	N14°W	0.60°SW
Sherman Fall	N17°W	0.57°SW
Kirkfield	N18°W	0.63°SW
Coboconk	N19°W	0.63°SW
Gull River	N16°W	0.66°SW
Shadow Lake	N19°W	0.56°SW
Cambrian	N18°W	0.52°SW
Precambrian	-	-

3.6 Core Quality and Natural Fracture Frequency

Table 3.3 lists the rock quality descriptions for core and bedrock formations, including RQD (Rock Quality Designation), used in this report that are determined from core logging data based on International Society for Rock Mechanics (1977) guidance. RQD values determined for the 75-mm-diameter core from DGR boreholes were calculated as the sum of lengths of core greater than 15 cm length (i.e., twice the core diameter) excluding drilling-induced breaks, divided by length of hole drilled per core run. Core recovery is defined as the length of core recovered per length of hole drilled per core run. Core runs were typically 3.05 m in length. Natural fracture frequency was calculated as the total number of identified natural fractures divided by the length of recovered core.

Figures 3.3 and 3.4 summarize the RQD and natural fracture frequency data determined from core logging of DGR-1 to DGR-6 as described in TR-07-06, TR-08-13 and TR-09-01 with calculated parameter values plotted at the mid-depth of each core run in each borehole. Data from boreholes DGR-1 and DGR-2 are combined in these figures to create a combined data set for comparison against DGR-3, DGR-4, DGR-5 and DGR-6 results. Data from inclined boreholes DGR-5 and DGR-6 are calculated based on borehole length and then scaled to plot against vertical borehole reference stratigraphy of DGR-1 and DGR-2. As coring was not completed above the Salina F Unit in DGR-5 and DGR-6, RQD and natural fracture frequency data are not available for these boreholes above that depth.

Table 3.3: Summary of Rock Quality Descriptions and Fracture Frequency

RQD (%)	Core Quality Description	Natural Fracture Frequency (/m)	Formation Fracture Description
0-25	Very Poor	>10	Highly Fractured
25-50	Poor	>1.0-10	Moderately Fractured
50-75	Fair	0.5-1.0	Sparsely Fractured
75-90	Good	<0.5	Very Sparsely Fractured
90-100	Excellent	0	Unfractured

Figures 3.3 and 3.4 show that Devonian and Upper Silurian dolostones are very sparsely to highly fractured and of poor to fair RQD, whereas the deeper Silurian formations below the Salina G Unit and the Ordovician shales and argillaceous limestones are very sparsely fractured to unfractured with excellent RQD. Many of the low core recoveries and RQDs recorded for the Bois Blanc and Bass Islands formations were attributed to difficult drilling conditions created in part by alternating hard and soft beds within these formations. Occasional joints/natural fractures were also identified within the deeper Silurian and Ordovician formations from core logging (TR-07-06, TR-08-13, TR-09-01) and borehole geophysical logging (TR-07-08, TR-08-15, TR-09-03). These core quality and natural fracture frequency characteristics are very similar in all DGR boreholes. More detailed discussion of these natural fractures is given in Section 3.12.

Figure 3.4 also illustrates that natural fracture frequency increases in the Cambrian sandstone. Results of hydraulic testing of this bedrock sequence (TR-08-32), demonstrate that many of these Cambrian natural fractures are open and permeable.

Table 3.4 provides an overall summary of core recovery, RQD and natural fracture frequency in boreholes DGR-1 to DGR-6 from logging of recovered core given in TR-07-06, TR-08-13 and TR-09-01. Table 3.4 lists the minimum, maximum and arithmetic mean values for these parameters grouped by formation and unit from all borehole data. Some low core recovery and RQD values (<10%) in the Ordovician shales and limestones are due to core grinding during drilling. Spatial variability in natural fracture frequency in DGR cored boreholes is summarized in Table 3.5. Table 3.5 lists the average natural fracture frequency of formations for individual boreholes and for all boreholes. Table 3.5 and Figure 3.4 show that the spatial variability of natural fracture frequency in DGR boreholes is limited. The Ordovician limestones in DGR-4 appear to be more fractured than in other DGR boreholes. Notably the natural fracture frequency of Silurian formations and Ordovician shales in inclined boreholes DGR-5 and DGR-6 is not noticeably different than in the vertical boreholes DGR-1 to DGR-4. This suggests the frequency of sub-vertical or inclined fractures in DGR boreholes is not significantly greater than the frequency of sub-horizontal fractures.

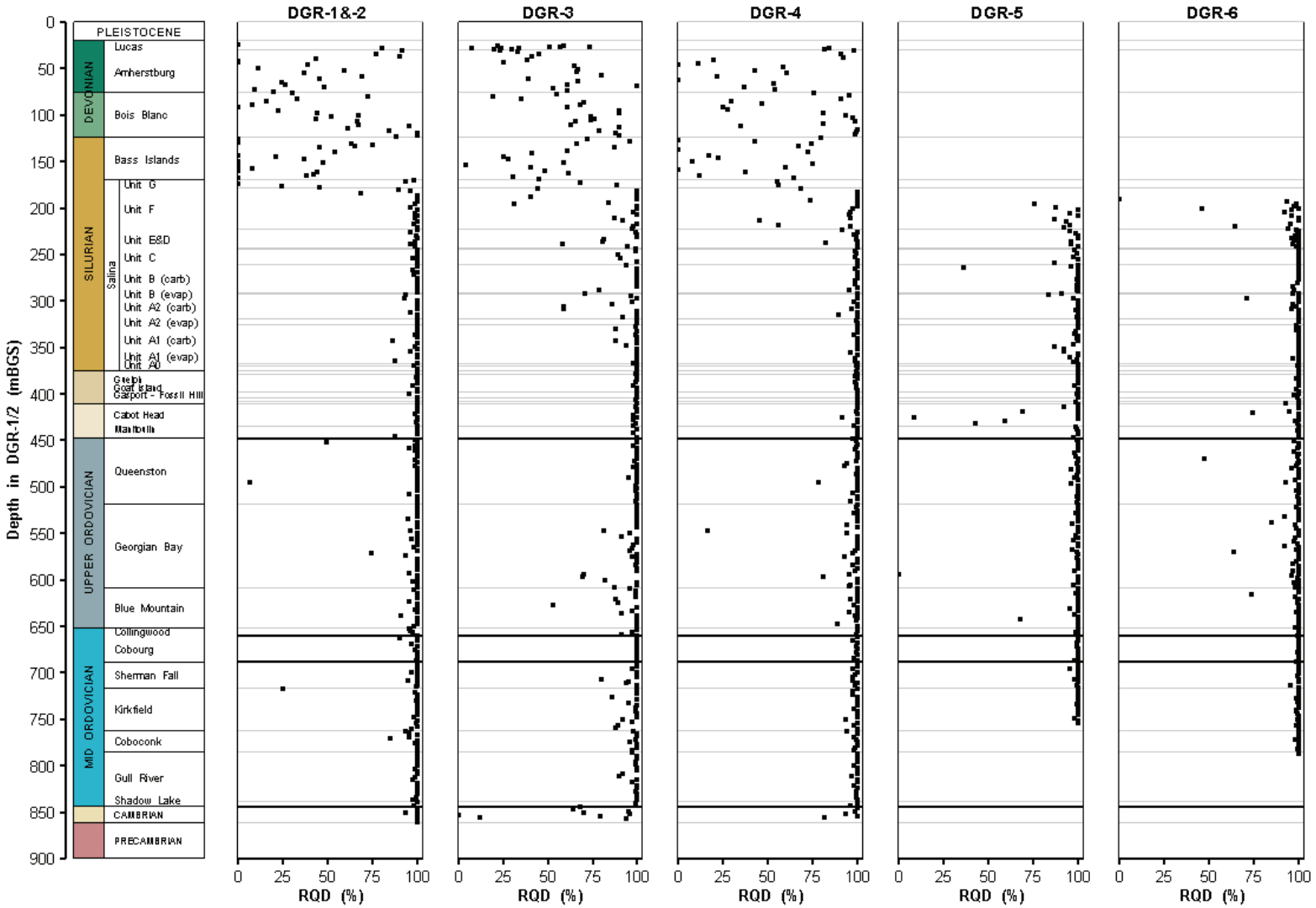

Note: Occasional low RQD values in the Ordovician shale and limestones are due to core grinding during drilling.

Figure 3.3: Profiles of Core RQD in DGR Boreholes

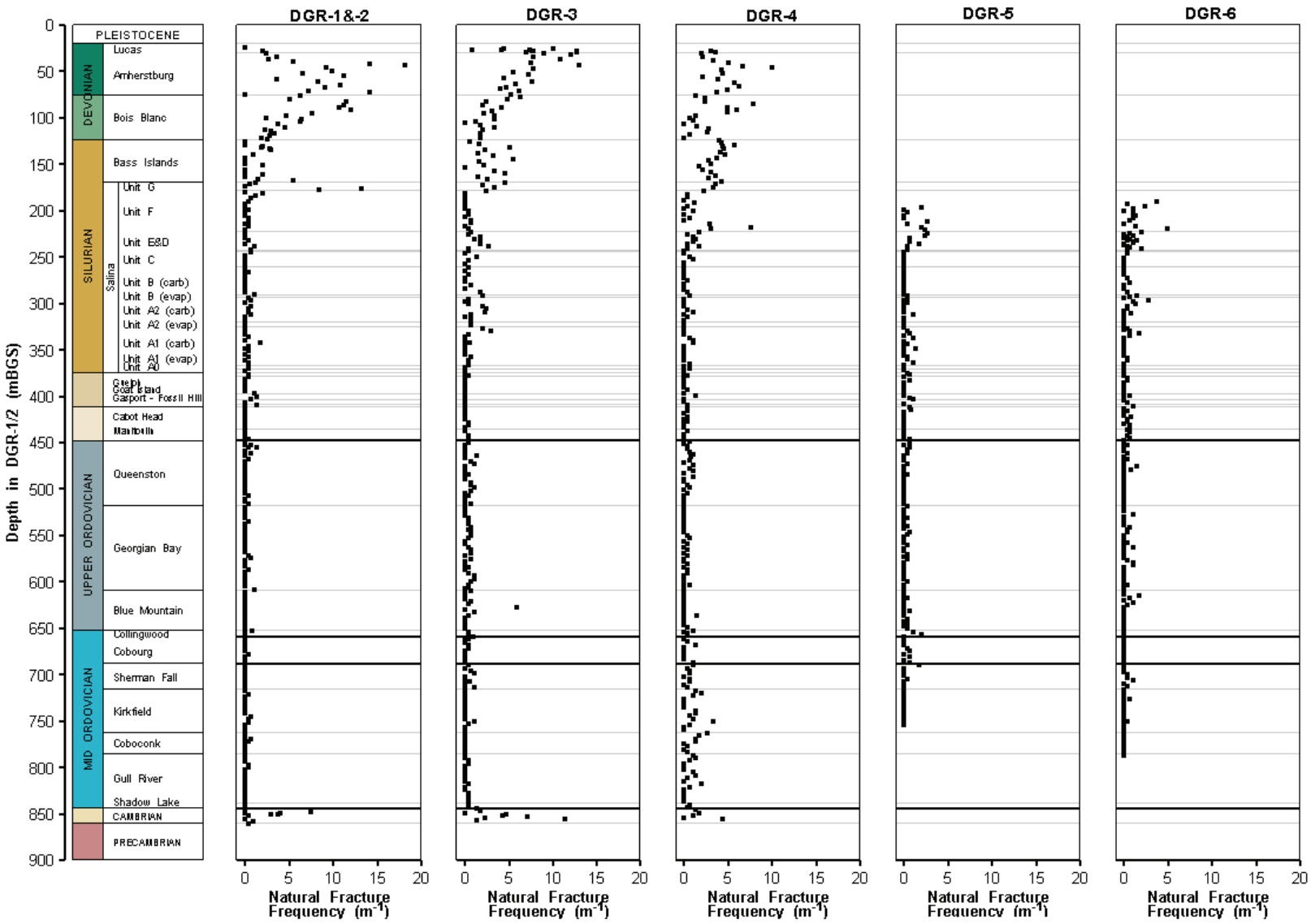

Figure 3.4: Profiles of Core Natural Fracture Frequency in DGR Boreholes

Table 3.4: Summary of Core Recovery, RQD and Natural Fracture Frequency Logged in DGR Boreholes

Formation	% Recovery			% RQD			Natural Fracture Frequency (1/m)		
	Min	Max	Mean	Min	Max	Mean	Min	Max	Mean
Lucas + Amherstburg Formations	20%	100%	91%	0%	100%	47%	0.00	18.06	5.36
Bois Blanc Formation	24%	100%	92%	0%	100%	68%	0.00	12.00	3.61
Bass Islands Formation	0%	100%	77%	0%	96%	34%	0.00	5.71	2.75
Salina Formation - G Unit	33%	100%	72%	0%	98%	54%	0.00	13.11	3.79
Salina Formation - F Unit	0%	100%	94%	0%	100%	90%	0.00	7.50	0.88
Salina Formation - E Unit	97%	100%	100%	58%	100%	96%	0.00	2.62	0.77
Salina Formation - D Unit + C Unit	89%	100%	99%	87%	100%	98%	0.00	1.97	0.33
Salina Formation - B Unit	98%	100%	100%	71%	100%	97%	0.00	2.62	0.53
Salina Formation - A2 Unit	88%	100%	100%	59%	100%	96%	0.00	2.77	0.41
Salina Formation - A1 Unit + A0 Unit	78%	100%	100%	87%	100%	99%	0.00	2.95	0.21
Guelph, Goat Island, Gasport, Lions Head, Fossil Hill Formations	100%	100%	100%	95%	100%	99%	0.00	1.31	0.20
Cabot Head Formation	19%	100%	96%	8%	100%	94%	0.00	0.98	0.14
Manitoulin Formation	96%	100%	100%	87%	100%	99%	0.00	0.66	0.21
Queenston Formation	7%	100%	99%	7%	100%	98%	0.00	1.38	0.22
Georgian Bay Formation	7%	100%	99%	0%	100%	97%	0.00	1.00	0.16
Blue Mountain Formation	98%	100%	100%	53%	100%	97%	0.00	5.90	0.21
Cobourg Formation - Collingwood Member	93%	100%	100%	90%	100%	99%	0.00	1.97	0.45
Cobourg Formation - Lower Member	0%	100%	98%	90%	100%	99%	0.00	1.31	0.14
Sherman Fall Formation	81%	100%	100%	80%	100%	99%	0.00	1.64	0.24
Kirkfield Formation	28%	100%	99%	25%	100%	98%	0.00	3.28	0.22

Formation	% Recovery			% RQD			Natural Fracture Frequency (1/m)		
	Min	Max	Mean	Min	Max	Mean	Min	Max	Mean
Coboconk Formation	85%	100%	99%	85%	100%	98%	0.00	2.62	0.26
Gull River Formation	98%	100%	100%	90%	100%	99%	0.00	1.97	0.16
Shadow Lake Formation	79%	100%	100%	68%	100%	98%	0.00	1.25	0.43
Cambrian Sandstone	98%	100%	100%	0%	100%	96%	0.00	11.33	2.44
Precambrian	100%	100%	100%	100%	100%	100%	0.33	0.33	0.33

Table 3.5: Summary of Mean Natural Fracture Frequency in DGR Cored Boreholes in Fractures/m

Formation, Member, Unit	DGR-1/2	DGR-3	DGR-4	DGR-5	DGR-6	All
Lucas + Amherstburg Formations	7.25	7.41	4.42	n/a	n/a	5.36
Bois Blanc Formation	5.65	2.49	2.59	n/a	n/a	3.61
Bass Islands Formation	1.05	2.77	3.60	n/a	n/a	2.75
Salina Formation - G Unit	4.61	2.55	3.38	n/a	n/a	3.79
Salina Formation - F Unit	0.35	0.20	1.40	1.05	1.39	0.88
Salina Formation - E Unit	0.28	1.19	0.74	1.22	0.42	0.77
Salina Formation - D Unit + C Unit	0.11	0.41	0.33	0.00	0.79	0.33
Salina Formation - B Unit	0.13	0.55	0.07	1.50	0.29	0.53
Salina Formation - A2 Unit	0.27	0.98	0.19	0.14	0.50	0.41
Salina Formation - A1 Unit + A0 Unit	0.25	0.34	0.25	0.29	0.20	0.21
Guelph, Goat Island, Gasport, Lions Head, Fossil Hill Formations	0.41	0.03	0.19	0.25	0.13	0.20
Cabot Head Formation	0.00	0.09	0.15	0.14	0.32	0.14
Manitoulin Formation	0.09	0.22	0.11	0.13	0.52	0.21
Queenston Formation	0.12	0.31	0.38	0.11	0.11	0.22
Georgian Bay Formation	0.09	0.33	0.11	0.11	0.17	0.16
Blue Mountain Formation	0.00	0.59	0.12	0.12	0.20	0.21
Cobourg Formation - Collingwood Member	0.08	0.38	0.33	1.48	0.00	0.45
Cobourg Formation - Lower Member	0.03	0.11	0.33	0.23	0.00	0.14
Sherman Fall Formation	0.00	0.34	0.48	0.20	0.18	0.24
Kirkfield Formation	0.11	0.09	0.83	0.00	0.05	0.22
Coboconk Formation	0.09	0.00	0.94	n/a	0.00	0.26
Gull River Formation	0.04	0.14	0.48	n/a	0.00	0.16
Shadow Lake Formation	0.00	0.79	0.49	n/a	n/a	0.43
Cambrian Sandstone	1.60	4.07	1.66	n/a	n/a	2.44
Precambrian	0.33	n/a	n/a	n/a	n/a	0.33

Although not reflected in the RQD or natural fracture frequency plots, the degree and extent of brecciation of the Salina B to E Units due to paleo-dissolution of the B and D Unit salts was observed to be greater in DGR-6 core than in other DGR cores. This increased brecciation resulted in decreased confidence in the top of formation picks in DGR-6 for the Salina B, C, D and E Units.

3.7 Rock Mineralogy and Geochemistry

Samples of core recovered from DGR-1 through DGR-6 were analyzed for a full suite of laboratory tests intended to determine intact rock mineralogy and lithogeochemistry, i.e., total rock chemistry including porewater, as well as to confirm or modify the stratigraphy and lithology of the bedrock sequence as described by Armstrong and Carter (2006).

All core samples are identified in this report by borehole name and mid-sample depth in mBGS or mLBGS. For example, core sample DGR2-606.62 describes a core sample collected from borehole DGR-2 with the middle of the core sample collected from a depth of 606.62 mBGS.

Laboratory testing included thin section petrography with electron microscope analyses to confirm optical identifications, whole rock and clay fraction XRD testing, SEM/EDS analyses, trace element ICP analyses, elemental oxide analyses by ICP optical emission spectrometry, carbon and sulphur infrared spectroscopy analyses, and chloride by instrumental neutron activation analyses.

This laboratory work was completed by GeoConsult (TR-07-12) and Activation Laboratories (TR-08-01, TR-08-02) for core samples collected from DGR-1 and DGR-2; and by University of Bern for core samples collected from DGR-2 (TR-08-06, TR-08-40). For DGR-3 and DGR-4, similar analyses were conducted but clay mineral analysis was only conducted on the Upper Ordovician shales; this study also included the organic geochemical analysis of these shales by Core Laboratories (TR-08-29). Otherwise, DGR-3 and DGR-4 cores were tested in a similar manner as were DGR-1 and DGR-2 cores, i.e., thin section petrography with electron microprobe analysis by GeoConsult (TR-08-20,TR-08-21) and XRD, SEM/EDS and lithogeochemistry by SGS Laboratories (TR-08-22, TR-08-23) and by University of Bern (TR-08-40). Core samples from DGR-5 and DGR-6 were also tested by GeoConsult (TR-09-05) using thin section petrography and electron microprobe analyses, and by SGS Laboratories (TR-09-06) using XRD, SEM/EDS and lithogeochemical analyses.

The similar rock mineralogy and geochemistry analyses performed for core from DGR boreholes by different laboratories allow for corroboration of laboratory test results.

3.7.1 Whole Rock Mineralogy

3.7.1.1 Major Minerals

Figures 3.5 and 3.6 show the individual core measurements and arithmetic formation averages of major minerals identified in DGR-1 to DGR-6 core. Figure 3.5 shows calcite and dolomite (including ankerite or Fe dolomite) in weight percent. Figure 3.6 shows quartz and total sheet silicates or clay mineral contents. Clay minerals also include minor amounts of several dioctahedral micas (i.e., muscovite, hydromuscovite, glauconite) which are typically not distinguishable from common clay minerals such as illite in XRD analyses. Throughout this report, the term illite refers to illite and other related indistinguishable micas. Although not shown on plots in this section, other noteworthy minerals identified in DGR cores include anhydrite, gypsum, pyrite, hematite, halite and feldspar.

As shown on these figures, no significant mineralogical differences are apparent between the Phase 1 cores (DGR-1 and DGR-2) and those from Phase 2A (DGR-3 and DGR-4) and Phase 2B (DGR-5 and DGR-6).

Figures 3.5 and 3.6 show that Devonian and Upper Silurian carbonate sequences are predominately dolostone with some minor limestone-rich layers and minor occurrence of sheet silicates as illite and mica. The quartz identified in these Devonian carbonate rocks is mostly chert. Increasing quartz content is also evident with depth in the Ordovician shales. Quartz content is minimal in the Ordovician limestones with maximum values of about 85% detected in the middle to lower sections of the Cambrian sandstone. Figure 3.5 also shows that parts of the Cabot Head Formation shale are locally calcareous and dolomitized and that the Queenston Formation shale is both calcareous and dolomitized particularly in upper parts of the formation. The Georgian Bay, Blue Mountain and Collingwood shales also show dolomite presence. The deeper Ordovician sequence including the Cambrian and overlying Shadow Lake Formation and the lower parts of the Gull River Formation also show the presence of significant amounts of dolomite, whereas the Middle Ordovician carbonates are predominately calcite.

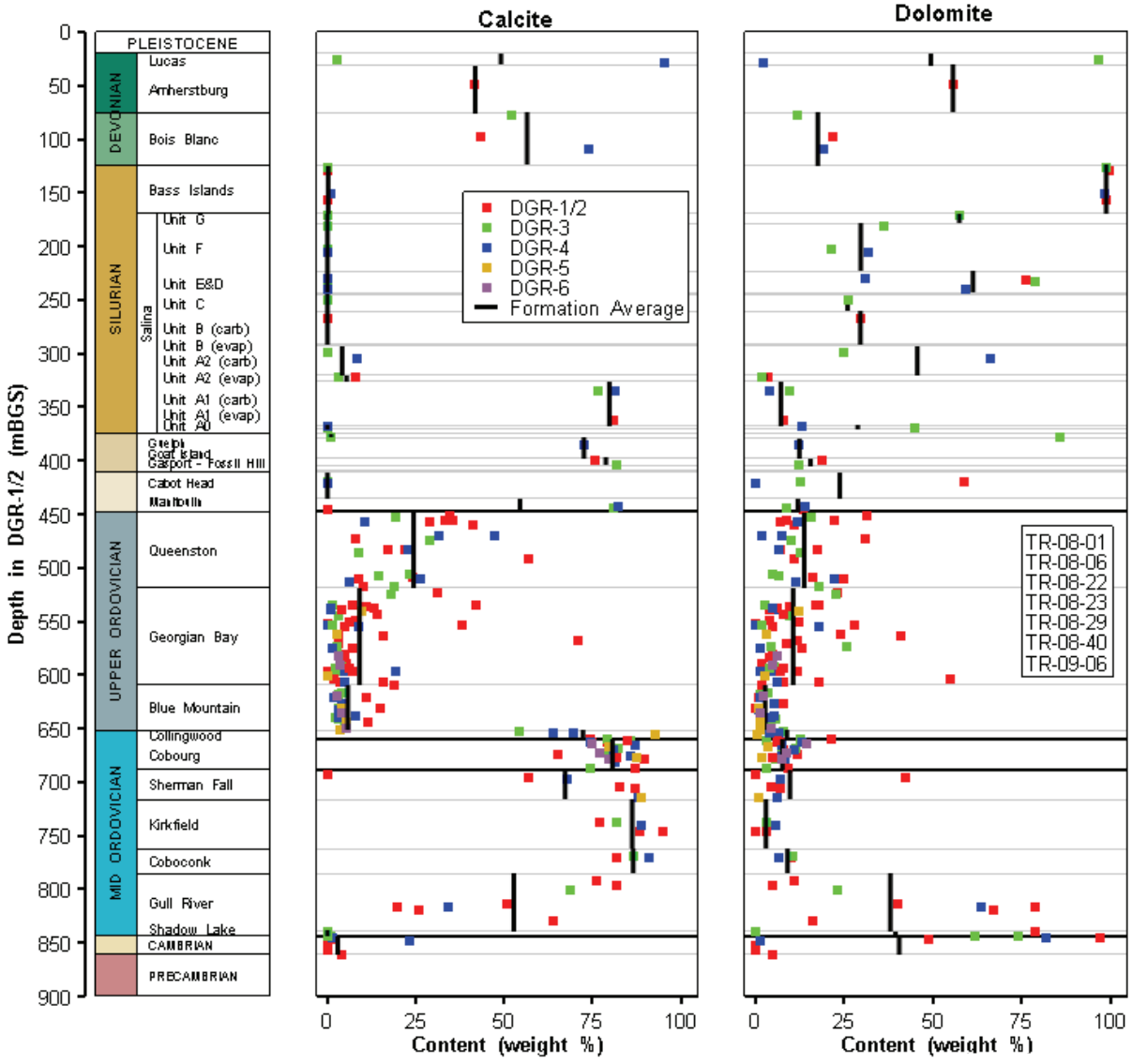

Figure 3.5: Profiles of Calcite and Dolomite in DGR Cores Showing Point Data and Arithmetic Formation Averages

The clay content of the Paleozoic sequence, as reported by total sheet silicates based on XRD analyses, ranges from zero for the Devonian and Upper Silurian dolostones to 15 to 70% within the Silurian Cabot Head and Ordovician shales of the Queenston, Georgian Bay and Blue Mountain formations. The clay content of the Ordovician limestones is typically less than 20%. The total sheet silicates within the Precambrian basement are not clays, but are micaceous minerals including biotite and muscovite.

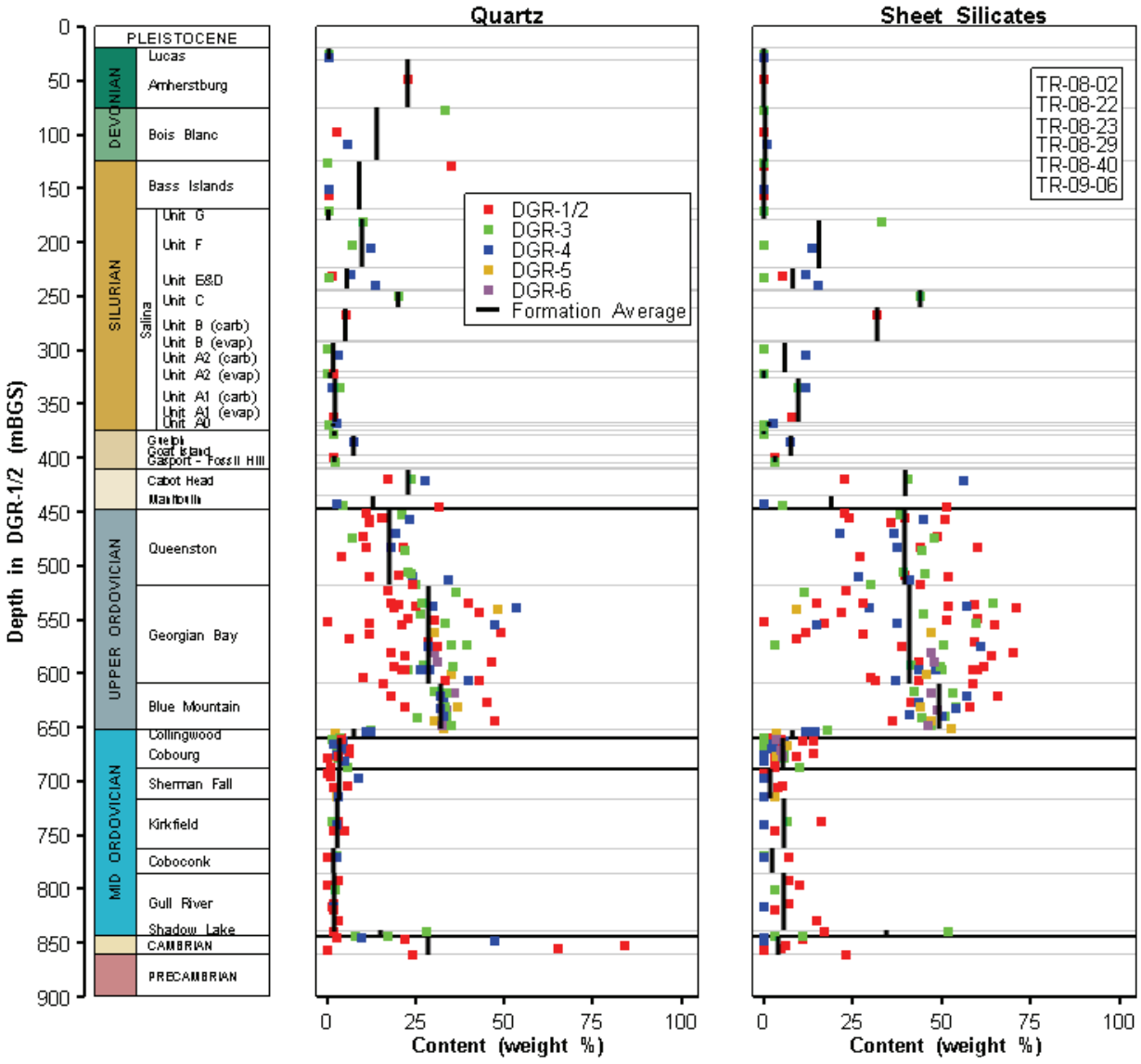

Figure 3.6: Profiles of Quartz and Total Sheet Silicates in DGR Cores Showing Point Data and Arithmetic Formation Averages

Figure 3.7 shows the composition of the sheet silicates is primarily illite and related indistinguishable micas with lesser amounts of chlorite. Illite is also present within the Salina E Unit dolomitic shale, B Unit argillaceous dolostone and A1 Unit argillaceous dolostone. In the Salina above the B Unit, the illite is frequently associated with a clay-rich matrix that encompasses the brecciated dolostone created by dissolution of the former B Unit salt and collapse of overlying formations. Illite and chlorite dominate the Ordovician shale mineralogy. Only trace levels (2%) of chlorite are evident in the Ordovician limestones and the Shadow Lake Formation. Illite+mica content of the Ordovician limestones is variable ranging from about 12% in the Cobourg Formation to zero in parts of the underlying formations.

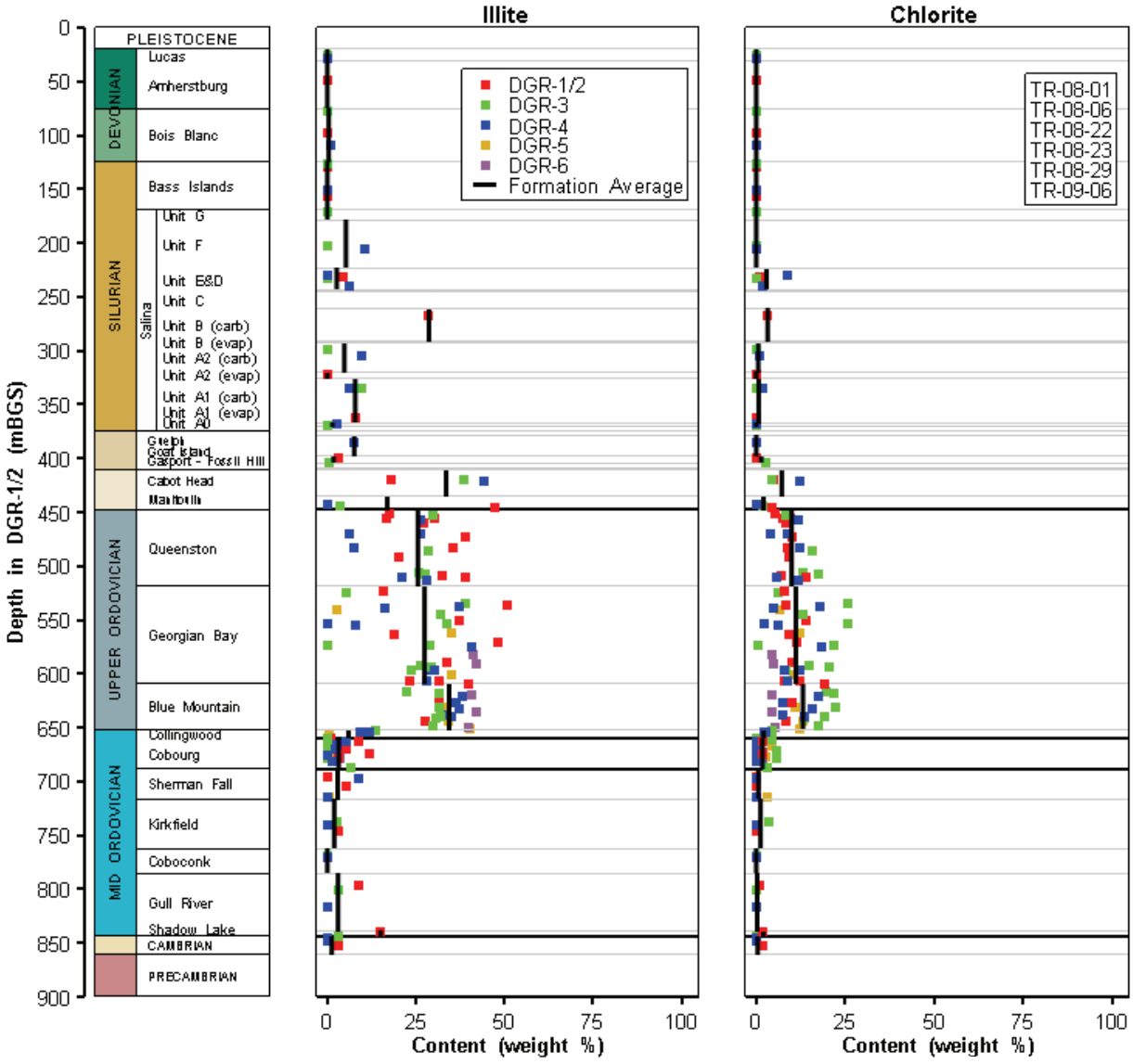

Figure 3.7: Profiles of Illite and Chlorite Clay Mineral Content in DGR Cores Showing Point Data and Arithmetic Formation Averages

Figure 3.7 also shows that the illite content of the Ordovician shales is variable ranging from about 15 to 50%. The magnitude and range of chlorite content in the Ordovician shales is less, ranging from 5 to 25%. These variations in clay content are due to heterogeneity in layering within these formations. Only trace levels (2%) of chlorite are evident in the Ordovician limestones and the Shadow Lake Formation. Illite content of the Ordovician limestones appears to decrease with depth from about 12% in the Cobourg Formation to zero in the bottom of the Gull River Formation.

The clay fraction of the DGR-3 and DGR-4 Ordovician shale cores was investigated (TR-08-29) during Phase 2A as part of a larger study involving the organic geochemistry of these shales. The clay minerals identified (Figure 3.8) are predominantly illite and mica – typically > 50% of all clay minerals – chlorite (20-45%) with minor kaolinite and interstratified illite-smectite. The interstratified illite-smectite is predominantly illite, with only 5-10% smectite layers, which therefore comprise only about one percent of all clay minerals. Typically these Ordovician shales contained about 20-30% quartz and highly variable amounts of carbonate minerals. The major iron mineral changes from hematite in the Queenston to pyrite in the Georgian Bay and Blue Mountain, in which iron concentrations reached 4-6 wt%.

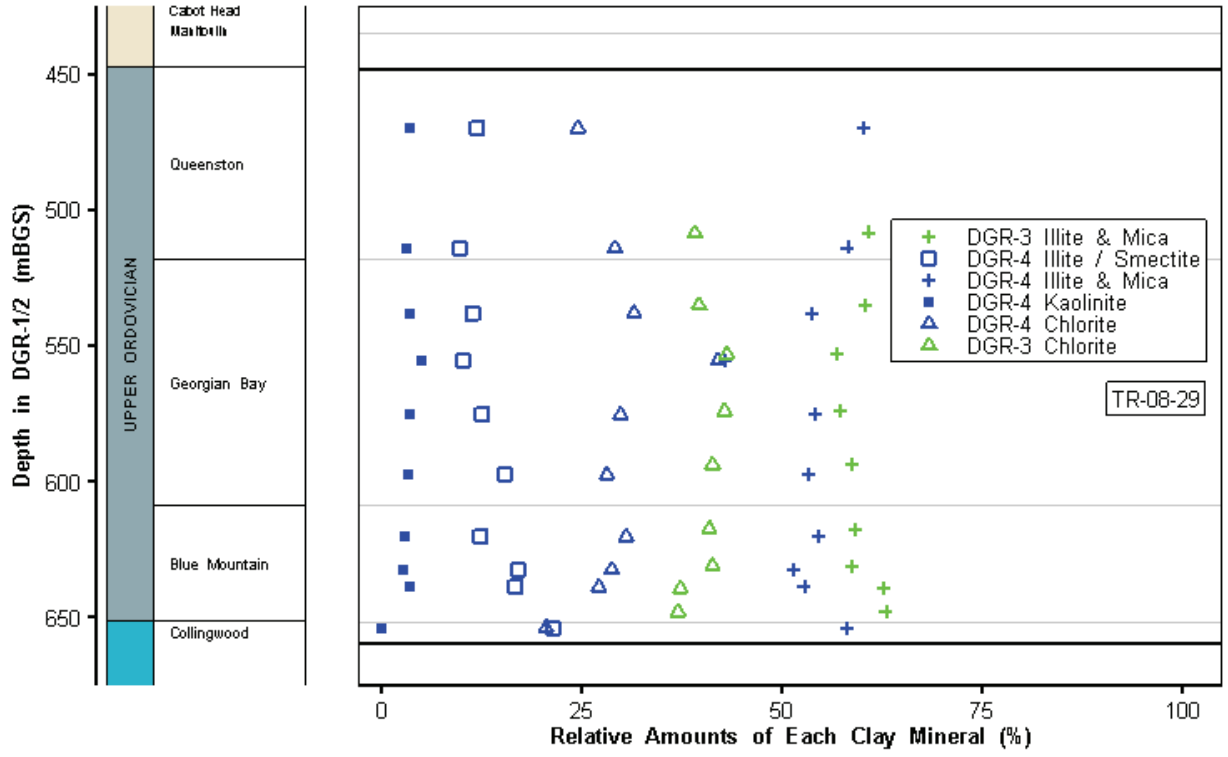

Figure 3.8: Composition of Clay Fraction Present in Ordovician Shales of DGR-3 and DGR-4 Cores

Comparison of the major mineralogy identified by the different analytical laboratories (i.e., GeoConsult, Activation Laboratories, University of Bern, SGS Laboratories and Core Laboratories) shows comparable results, although the range of results within individual formations and groups of formations is large and suggests that heterogeneity of mineralogy at core scale is significant in these formations.

3.7.1.2 Geochemically Important Minor Minerals

Particular attention has been paid throughout the DGR project to the occurrence of geochemically important minor minerals, such as (1) the soluble sulphate minerals gypsum, anhydrite and celestite, (2) soluble halite and (3) pyrite and other iron sulphides. These minerals are common in minor or trace concentrations – i.e., <10% – which for the soluble minerals indicates that fluids undersaturated with respect to the minerals have not recently advected through these core sections and presumably through adjacent sections of these formations unless discontinuities indicate otherwise. Pyrite is geochemically important because it is a redox indicator and may be a source of sulphate reported in porewater characterization studies. Table 3.6 summarizes the reported detections of gypsum, anhydrite, pyrite and halite in DGR cores from core logging, XRD or optical microscopy. In addition, halite detection is divided into visual/XRD detection and SEM/EDS detection.

Some Silurian formations are predominately composed of sulphate minerals, e.g., the Salina A1 Evaporite and A2 Unit anhydrite units (Table 3.6). Gypsum and anhydrite were frequently logged in core or identified by XRD in the Salina units. Anhydrite was also observed within the Manitoulin, Queenston and Georgian Bay formations. Pyrite or other iron sulphide minerals are also frequently detected, particularly below the Cabot Head Formation.

Table 3.6: Mineral Detection in DGR Cores by Core Logging, XRD, Optical Microscopy or SEM/EDS

Formation, Member, Unit	Gypsum	Anhydrite	Pyrite	Halite Visual/XRD	Halite SEM/EDS
Lucas Formation					
Amherstburg Formation					
Bois Blanc Formation			✓		
Bass Islands Formation	✓		✓		
Salina Group - G Unit	✓	✓			
Salina Group - F Unit	✓	✓			
Salina Group - E Unit	✓	✓	✓		✓
Salina Group - D Unit		✓			
Salina Group - C Unit	✓	✓		✓	✓
Salina Group - B Unit Carbonate	✓	✓		✓	✓
Salina Group - B Unit Evaporite		✓			
Salina Group - A2 Unit Carbonate	✓	✓	✓		
Salina Group - A2 Unit Evaporite		✓			

Formation, Member, Unit	Gypsum	Anhydrite	Pyrite	Halite Visual/XRD	Halite SEM/EDS
Salina Group - A1 Unit Carbonate	✓	✓	✓		✓
Salina Group - A1 Unit Evaporite		✓	✓		
Salina Group - A0 Unit		✓			
Guelph Formation				✓	✓
Goat Island Formation			✓		
Gasport Formation		✓	✓	✓	
Lions Head Formation		✓			
Fossil Hill Formation		✓			
Cabot Head Formation	✓	✓	✓	✓	✓
Manitoulin Formation	✓	✓	✓	✓	✓
Queenston Formation	✓	✓	✓	✓	✓
Georgian Bay Formation	✓	✓	✓	✓	✓
Blue Mountain Formation			✓	✓	✓
Cobourg Formation - Collingwood Member			✓		✓
Cobourg Formation - Lower Member		✓	✓		✓
Sherman Fall Formation	✓	✓	✓		✓
Kirkfield Formation			✓		
Coboconk Formation	✓	✓	✓		
Gull River Formation		✓	✓		✓
Shadow Lake Formation					
Cambrian Sandstone		✓	✓		✓
Precambrian basement					

Halite was specifically targeted for mineral identification because of its high solubility (~6000 mmol/kgw) and its role as a groundwater tracer. The presence of halite within a formation or group of formations is a strong indicator that there has been no flow of halite-undersaturated, water through that rock sequence since the halite was precipitated.

Halite was detected visually during core logging, and via optical microscope, XRD, and SEM/EDS analyses (Figure 3.9, Table 3.7). Halite occurrences include: mineral infilling of subhorizontal and steeply-dipping fractures; voids and cavities; a grain-boundary mineral phase within a matrix dominated by gypsum, dolomite, calcite, or silicate minerals; and, as disseminated grains and irregular, discontinuous stringers. Halite was found within several Silurian units, in abundance throughout the Upper Ordovician shales, as a minor mineral phase in the Cobourg and Sherman Fall and Gull River Formations, and within the Cambrian (Table 3.6 and Figure 3.9). Whole-rock and clay-mineral XRD analyses of Ordovician shales

yielded average halite concentrations of 0.7 wt % and 0.6 wt % in DGR-3 and DGR-4, respectively. Maximum halite concentrations were recorded in the Blue Mountain Formation with concentrations ranging from 0.5 to 1.4 wt %.

Halite was most commonly observed infilling mm-scale to hairline thickness fractures throughout the Upper Ordovician shales (e.g., Figure 3.9 top and middle core photos). There is visual evidence that drilling fluids locally dissolved some of the vein halite (e.g., Figure 3.9 top photo), but where this occurred there was generally enough preserved for positive identification. In the deeper limestones, including the Cobourg Formation, a lack of open fractures is consistent with halite only being recognized as a mineral phase at the micron scale. In these instances it was commonly observed as the dominant mineral phase within networks of irregular cavities between larger calcite grains (e.g., Table 3.7, Figure 3.9, SEM backscatter image of DGR3-699.62).

Table 3.7: Semi-Quantitative Spot Analysis of Halite, Calcite, Pyrite, Sheet Silicate and Feldspar in the Cobourg Formation Sample Shown in Figure 3.9

Sample: DGR3 – 699. 62		Elements (in Wt.%)									
Spots	**Mineralogy**	**O**	**Na**	**Mg**	**Al**	**Si**	**S**	**Cl**	**K**	**Ca**	**Fe**
1-Py	Pyrite						55.78				44.22
2-Ca	Calcite	56.01		0.50	0.34	2.64				40.52	
3-Fd	Feldspar	47.69	8.44	0.61	1.16	6.57		17.72	0.79	16.41	0.61
4-Ca	Calcite	56.16				0.30				43.54	
5-Ha	Halite	7.02	36.28		0.58	1.31		53.82		0.98	
6-Ha	Halite	5.40	35.98		0.74	3.11		53.59	0.43	0.76	
7-Ha	Halite	8.11	35.17	0.39	1.54	5.18		47.24	0.85	1.05	0.47
8-Ha	Halite	10.03	32.67		1.16	2.58	1.00	50.04	0.59	1.02	0.89
9-Ha	Halite	15.08	33.54	0.38	1.44	3.15		45.35	0.74	0.31	
10-Si	Silicate (Clay)	33.26	15.43		3.64	11.15		21.19	4.23	11.09	

Halite saturation index calculations, using porewater chemistry results for the Silurian, Ordovician and Cambrian DGR cores as summarized in Section 4.6, provide indirect information on the occurrence of halite in DGR cores. Eight core samples from the Silurian dolostones (DGR3-417.60, DGR5-426.96, DGR5-440.13, DGR6-428.53, DGR6-431.76, DGR6-460.10, DGR6-465.67 and DGR6-502.30) and five core samples from the Ordovician limestones (DGR3-702.54, DGR4-669.18, DGR4-772.19, DGR6-686.14 and DGR6-822.76) had calculated halite saturation or supersaturation based on PHREEQC modeling. With the exception of three samples (DGR2-523.08, DGR3-539.46 and DGR6-659.17) core samples of Silurian and Ordovician shales are uniformly undersaturated (see Section 4.6.3). Given the obvious evidence for halite presence within these shales, these lower than saturation porewater concentration estimates may be due to release of clay-bound water during laboratory heating (Section 4.6.3) and/or anion exclusion processes (Section 4.6.4).

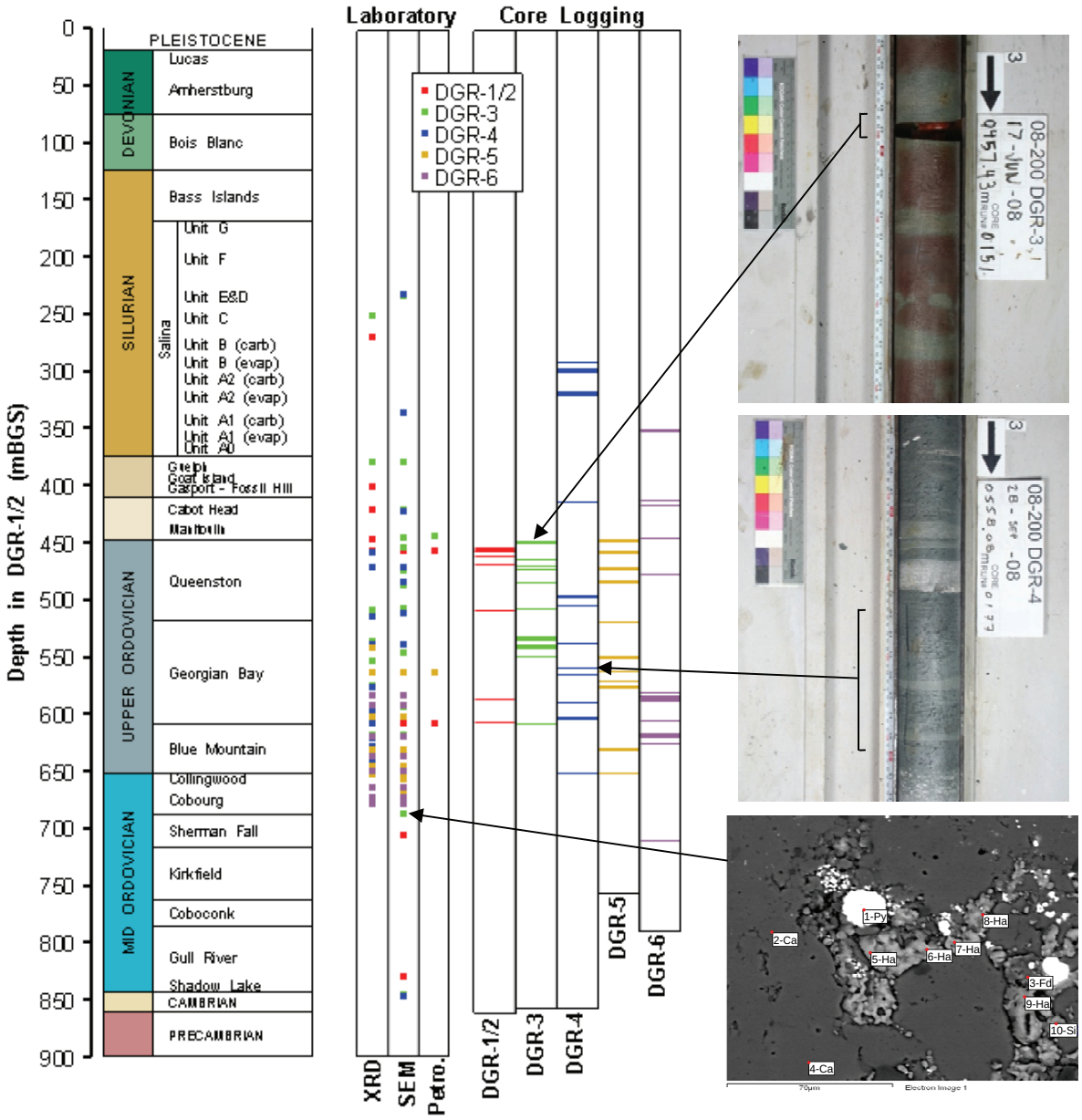

Figure 3.9: Halite Occurrences in DGR Boreholes Noted from Core Logging and Laboratory Testing

Similar calculations, and the opportunistic groundwater analyses, indicated that the Cambrian sandstone samples were also undersaturated with respect to halite. These results, which suggest that halite should not be present in the Cambrian, are inconsistent with its identification in one Cambrian sample (DGR-3-856.28) using SEM/EDS (Figure 3.10, Table 3.8). A SEM feasibility study (Herwegh and Mazurek 2008) exposed a sample from the Cambrian sandstone (DGR2-852.39) to air and examined the minerals formed on the surface of the core. Halite and

Ca-sulphate minerals (gypsum and anhydrite) formed on the core due to the evaporative concentration of the porewater.

These results suggest that a small amount of halite and Ca-sulphate may be produced by the evaporation of cores during sample preparation for mineral identification, and this may explain the halite presence in the Gull River and Cambrian. This is clearly not the case in the DGR-3 Cobourg sample where the SEM backscatter image (Figure 3.9) shows halite grains completely surrounding pyrite grains within the irregular voids between larger calcite crystals, indicative of a primary halite occurrence. This interpretation is consistent with the observed distribution of chloride, sodium and TDS in porewater with depth in the vertical DGR boreholes (Figures 4.53 and 4.54 in Section 4.6.5). The results indicate that the highest concentrations are measured in the Middle and Lower Silurian formations through the Upper Ordovician shales and into the Sherman Fall Formation with concentrations decreasing below the Coboconk Formation.

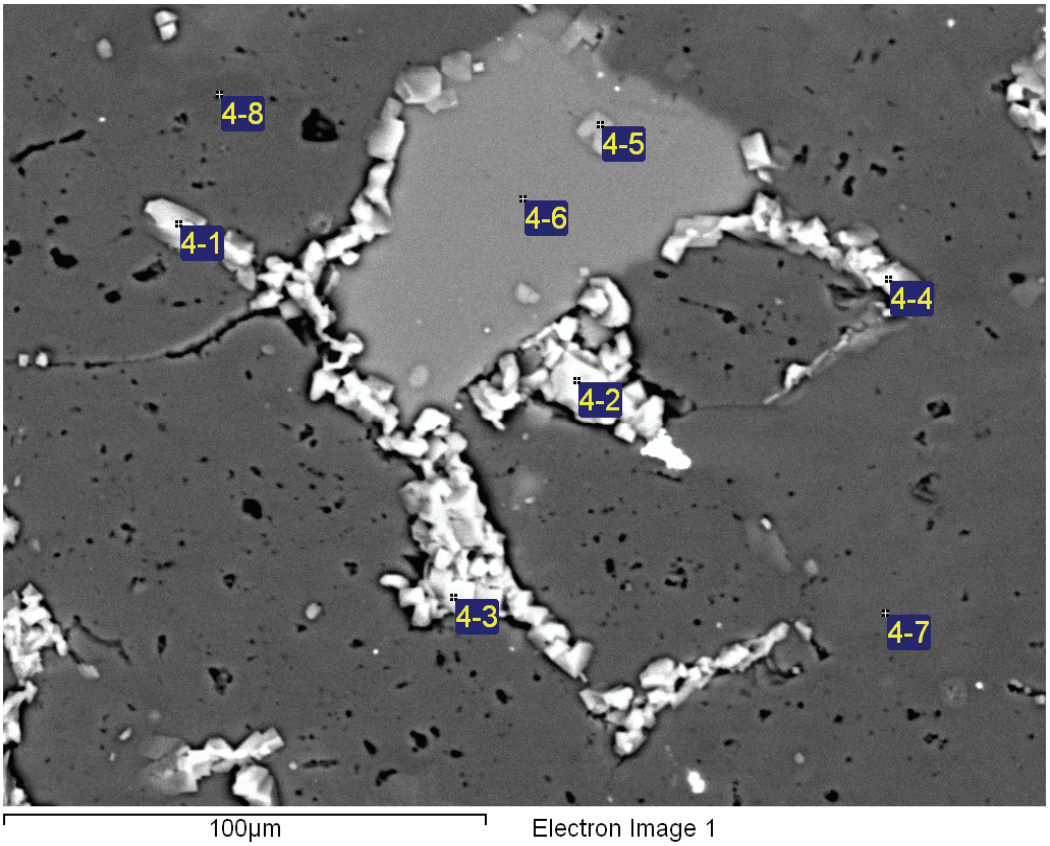

Figure 3.10: Halite in DGR3-856.28 (Cambrian Formation)

Table 3.8: Semi-quantitative Spot Analysis of Halite, Dolomite and Feldspar in Cambrian Formation

Sample: DGR3 – 856.2	Elements (in Weight %)									
Spots	**O**	**Na**	**Mg**	**Al**	**Si**	**S**	**Cl**	**K**	**Ca**	**Ba**
4-1	3.62	37.75	1.91	0.29	0.71	0.46	48.68	0.26	6.31	
4-2		40.31					59.33		0.36	
4-3		34.95		0.28	0.60		63.34	0.27	0.56	
4-4	5.70	33.45	0.54				58.40		1.90	
4-5	21.97	15.25		7.88	26.43		17.18	11.29		
4-6	49.11	0.40		8.91	29.03			11.90		0.65
4-7	59.48		15.34						25.19	
4-8	59.38		15.68						24.94	

3.7.2 Lithogeochemistry

Figures 3.11, 3.12 and 3.13 show the results of lithogeochemical analyses of DGR core samples for major elemental oxides including CaO, MgO, SiO_2, Al_2O_3, and Fe_2O_3 as well as chloride. Figures 3.11, 3.12 and 3.13 also show the calculated arithmetic formation averages for these major oxides. These compounds and other elemental oxide contents including SO_4, K_2O, MnO_2, Na_2O, P_2O_5 and CO_2 are also reported in TR-08-02, TR-08-22, TR-08-23 and TR-09-06. Table 3.9 lists the major elemental geochemistry for DGR-1 and DGR-2 from TR-08-02 that are of use in identification of major rock mineralogy. Review of Figures 3.11 to 3.13 and of Table 3.9 shows that no significant variations were detected between the oxide geochemistry of Phase 1 (DGR-1 and DGR-2) samples and those from Phase 2A (DGR-3 and DGR-4) and Phase 2B (DGR-5 and DGR-6).

The major elemental oxide data provide confirmation of the mineralogy presented in Figures 3.5 and 3.6 and discussed in Section 3.8. The CaO and MgO data (Figure 3.11) show that most of the Devonian and Silurian carbonates are dolomitic (with the exception of the Salina A1 Unit Carbonate that is limestone), that the Queenston shale is calcareous, and that there is dolomitization of the minor carbonate content of the Cabot Head shale and of the Georgian Bay and Blue Mountain shales and of the lower Gull River Formation and upper Cambrian rocks. These data further show that most of the Ordovician limestones are indeed limestone with very minor dolomite present, and that there is a clear correlation between an increase in dolomite and decrease in calcite with depth through the Gull River Formation (Figure 3.11).

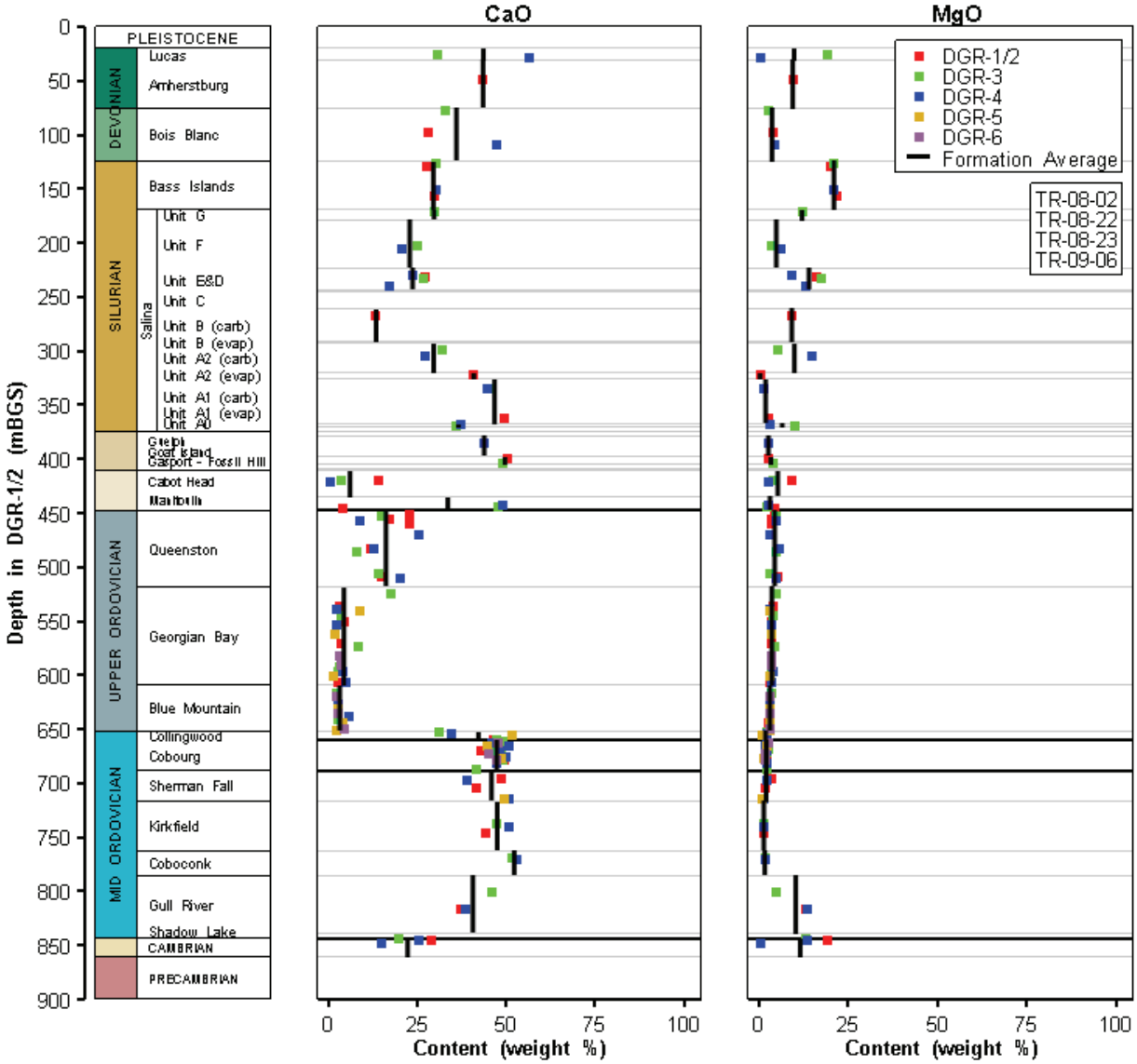

Figure 3.11: Profile of Calcium and Magnesium Oxide Content in DGR Cores Showing Point Data and Arithmetic Formation Averages

Table 3.9: Summary of Elemental Geochemical Analyses of DGR-1 and DGR-2 Cores (weight %)

Sample	Formation	CaO	MgO	SiO_2	Al_2O_3	SO_4	Fe_2O_3	K_2O	Cl
DGR1-049.16	Amherstburg	43.49	9.48	1.46	0.35	0.4	0.22	0.05	0.05
DGR1-097.08	Bois Blanc	27.99	4.00	39.2	0.83	0.6	0.40	0.33	0.04
DGR1-130.03	Bass Islands	27.73	20.02	5.52	1.16	0.3	0.33	0.66	0.04
DGR1-156.63	Bass Islands	29.97	21.98	0.33	0.08	<0.3	0.07	0.05	0.05
DGR1-231.49	Salina E Unit	27.26	16.12	14.58	3.66	10.6	1.65	0.98	0.13
DGR1-267.78	Salina B Unit	13.38	9.21	36.51	9.20	6.8	3.75	2.37	0.63
DGR1-322.19	Salina A2 Unit-Evap.	40.86	0.36	1.49	0.08	69.8	0.03	<0.01	0.04
DGR1-361.76	Salina A1 Unit	49.64	2.61	4.31	1.45	2.7	0.57	0.47	0.12
DGR1-399.85	Gasport	50.29	2.77	2.07	0.35	<0.3	0.58	0.21	0.10
DGR1-419.99	Cabot Head	14.10	9.13	33.58	9.61	0.5	3.91	3.21	0.61
DGR1-446.25	Manitoulin	4.00	4.28	49.31	15.42	<0.3	8.21	5.05	0.81
DGR1-455.45	Queenston	16.98	3.74	36.44	11.72	<0.3	5.48	3.69	0.63
DGR1-456.01	Queenston	17.02	3.89	35.68	11.36	<0.3	5.24	3.57	1.38
DGR1-460.77	Queenston	22.95	3.64	21.42	9.89	<0.3	3.64	3.09	0.51
DGR2-451.33	Queenston	22.83	4.37	29.96	9.47	<0.3	3.67	3.04	0.45
DGR2-482.45	Queenston	11.77	5.16	42.09	13.26	0.4	5.04	4.27	0.58
DGR2-508.93	Queenston	14.75	5.10	39.74	11.48	<0.3	5.18	3.50	0.57
DGR2-535.56	Georgian Bay	2.97	4.09	51.25	16.31	<0.3	7.09	5.13	0.62
DGR2-550.28	Georgian Bay	4.29	3.60	53.54	15.19	0.4	6.59	4.90	0.56
DGR2-570.73	Georgian Bay	3.48	3.74	51.53	15.61	0.4	7.01	4.92	0.60
DGR2-590.10	Georgian Bay	3.35	3.41	53.94	15.38	0.6	6.77	4.57	0.61
DGR2-606.62	Georgian Bay	2.84	3.34	55.47	15.62	1.8	6.62	4.67	0.57
DGR2-606.96	Georgian Bay	2.76	3.16	55.57	16.28	0.8	6.96	4.94	0.57
DGR2-626.29	Blue Mountain	2.79	3.15	54.83	16.49	0.9	6.95	4.80	0.51
DGR2-644.49	Blue Mountain	4.14	2.87	53.13	15.76	1.4	6.49	4.62	0.45
DGR2-659.31	Collingwood Member	46.60	2.08	8.37	2.32	0.4	0.89	0.92	0.10
DGR2-669.27	Cobourg	42.90	2.19	11.98	3.31	0.5	1.01	1.42	0.14
DGR2-677.93	Cobourg	49.67	2.04	5.03	1.25	0.4	0.68	0.55	0.08
DGR2-695.51	Sherman Fall	48.56	3.34	4.17	1.01	0.4	0.74	0.39	0.08
DGR2-704.87	Sherman Fall	41.48	1.91	14.00	3.86	1.2	1.40	1.64	0.18
DGR2-745.97	Kirkfield	44.30	1.54	11.81	2.83	0.7	0.91	1.19	0.11
DGR2-816.85	Gull River	37.42	12.92	2.46	0.32	<0.3	0.38	0.15	0.24
DGR2-844.95	Cambrian	29.11	19.39	7.04	0.45	<0.3	0.64	0.39	0.26

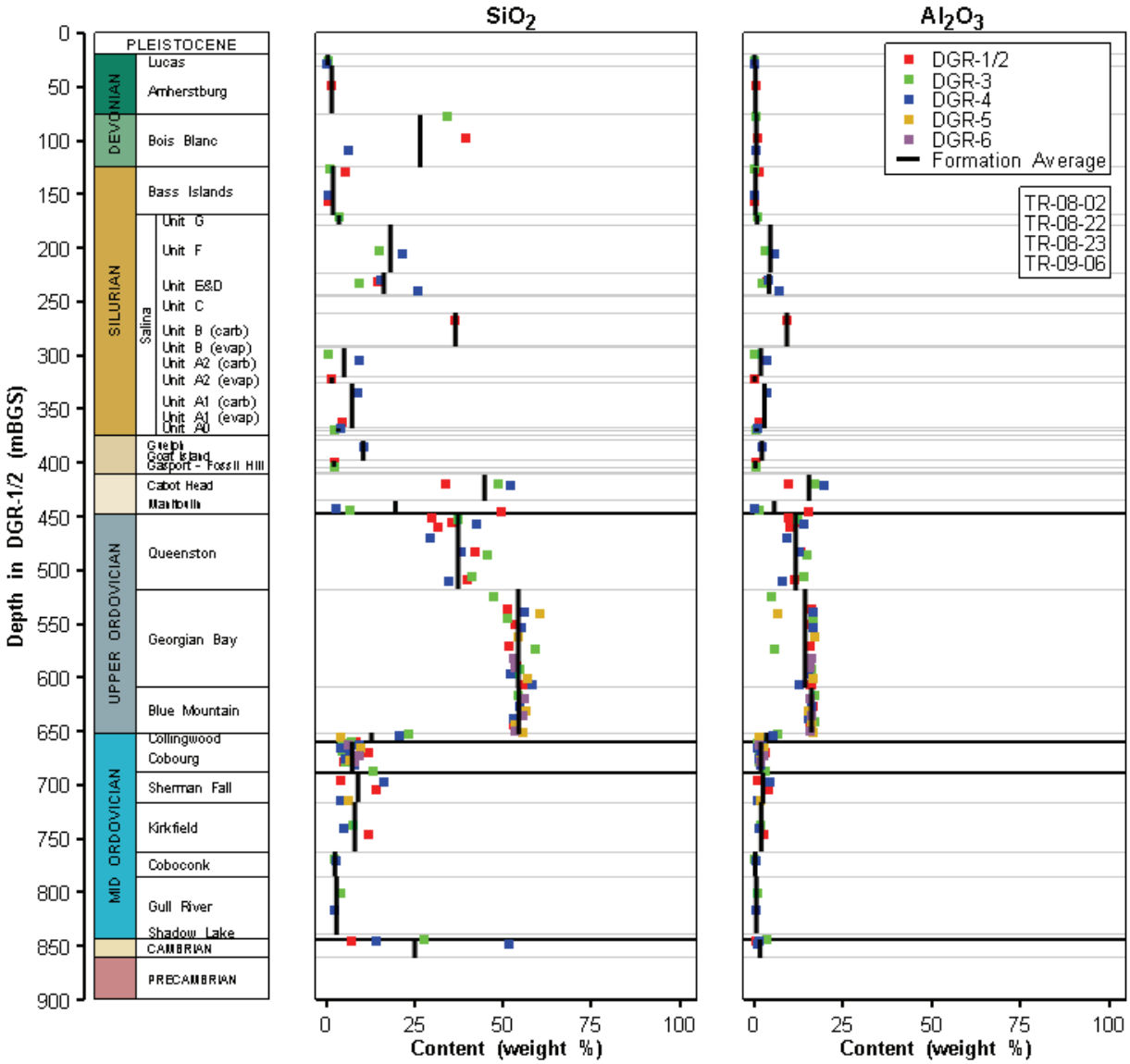

Figure 3.12: Profile of Silica and Aluminum Oxide Content in DGR Cores Showing Point Data and Arithmetic Formation Averages

The elevated SiO_2 and Al_2O_3 contents (Figure 3.12) confirm the presence of clay minerals as alumina-silicates sporadically in the Silurian formations and throughout the Ordovician shales. The Fe_2O_3 content (Figure 3.13) is generally depleted (<1.5%) in the Devonian and Silurian formations relatively, uniform at about 4 to 8% in the Cabot Head, Queenston, Georgian Bay and Blue Mountain formation shales, and depleted again in the Ordovician limestones. Most of the detected Fe_2O_3 , especially in the deeper Ordovician formations, is present as a sulphide phase, e.g., pyrite.

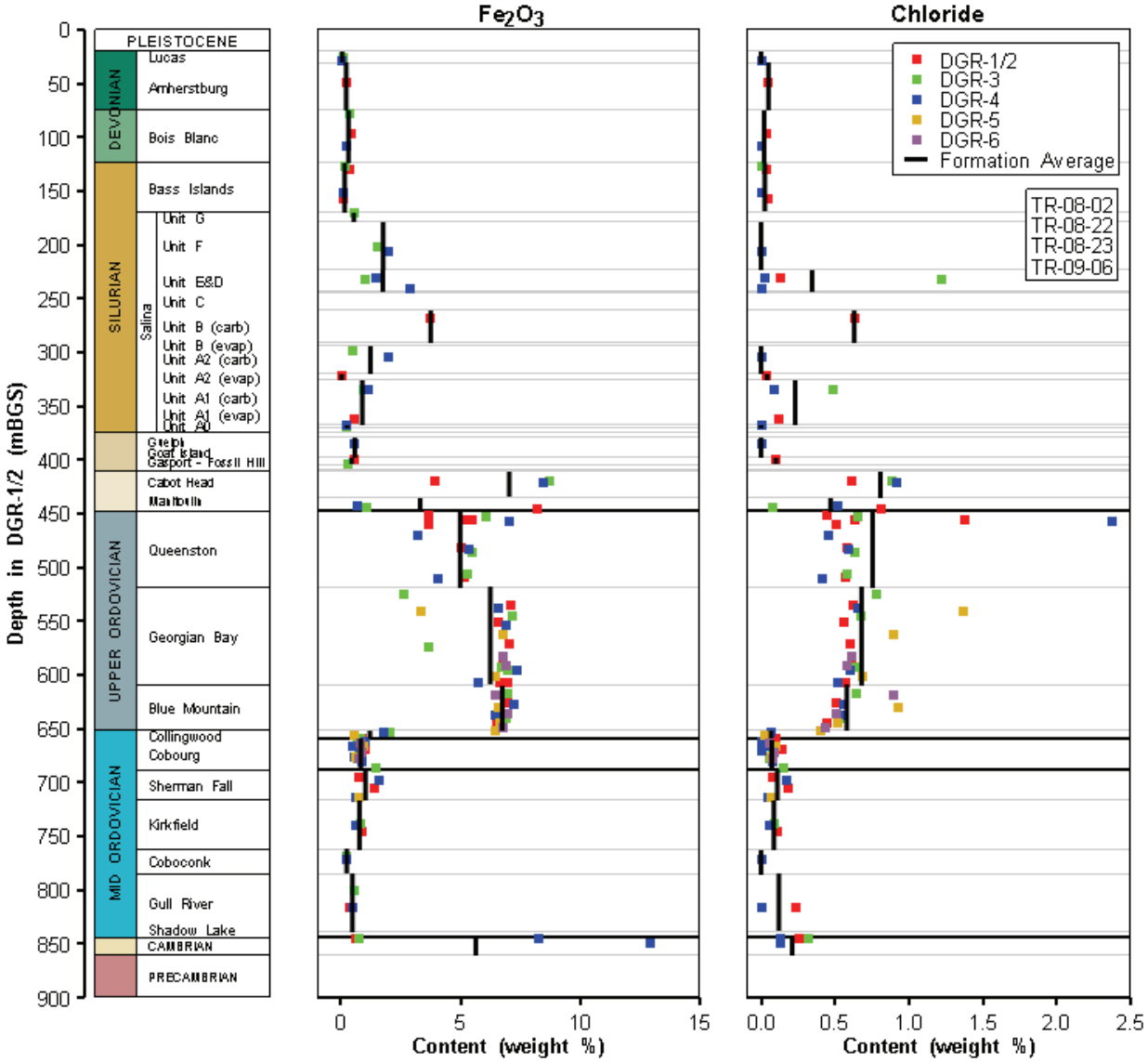

Figure 3.13: Profile of Iron Oxide and Chloride Content in DGR Cores Showing Point Data and Arithmetic Formation Averages

Figure 3.13 also illustrates the chloride content of DGR core samples determined by instrumental neutron activation analyses (INAA) in DGR-1 and DGR-2 and wet chemistry and ion chromatography in DGR-3, DGR-4, DGR-5 and DGR-6. Reported total chloride reflects presence of halite or other chloride-bearing minerals, as well as chloride present in porewater in rock porosity. If halite and other chloride-bearing minerals are not present, the chloride content will simply reflect the mass of chloride present in core sample porewater.

Figure 3.13 shows that the chloride content is typically low (<0.06%) in the Devonian and Upper Silurian dolostones, except in three halite-containing samples from the Salina E, B and A1 Units. The chloride content increases to greater than 0.5% in the Cabot Head Formation shale and remains uniform at about 0.5 to 0.6% through the Queenston, Georgian Bay and Blue Mountain formation shales. The elevated chloride contents of 0.7 to 2.4% were measured at the top of the Queenston and Georgian Bay formations where halite has been observed in core samples and petrography. Chloride contents in the low porosity Ordovician limestones range from about 0.10 to 0.25% with the higher values associated with the Gull River Formation and similar concentrations in the Cambrian rocks.

Comparison of elemental oxide and chloride results identified by different analytical laboratories (i.e., Activation Laboratories for DGR-1 and DGR-2, SGS Laboratories for DGR-3 to DGR-6) shows comparable results, which provides confidence in these analytical results.

3.7.3 Dolomitization

Figure 3.14 also shows the calculated dolomitization of DGR core. Dolomitization of carbonates detected within core samples is calculated (TR-08-06) as:

$$\text{Dolomitization (\%)} = 100 \times \text{Dolomite (\%)}/[\text{Dolomite (\%)} + \text{Calcite (\%)}] \qquad (3.1)$$

The significance of the dolomitization plot of Figure 3.14 should be interpreted jointly with the major mineralogy (Figures 3.5 and 3.6) and major elemental oxides (Figures 3.11, 3.12 and 3.13) plots. For example, although the dolomitization calculated for the Ordovician shales appears large at 25 to 75%, the significance of this result is mitigated by the low carbonate content of these rocks as apparent in Figures 3.5 and 3.11. Conversely, the dolomitization values of 25 to 100% for the Devonian and Silurian formations are more significant due to the much higher carbonate content of these rocks. Dolomitization of the bottom half of the Gull River Formation and of the Shadow Lake Formation and upper Cambrian is significant also at about 50 to 100%.

3.7.4 Organic and Sulphur Geochemistry

3.7.4.1 Organic Carbon and Sulphur

Figure 3.15 illustrates the profile of organic carbon and total sulphur in DGR core. These plots show that many of the formations are quite low in organic carbon (<0.3%). Notable exceptions are middle and lower parts of the Georgian Bay Formation (0.4 to 0.7%), the Blue Mountain Formation and Collingwood Member (0.4 to 2.5%). The organic carbon content of the Ordovician limestones and underlying Shadow Lake and Cambrian rocks are variable (0.1 to 2.0%) likely reflecting the sporadic occurrences of bituminous laminae and oil observed in recovered core.

Total sulphur contents of DGR core reflect the presence of sulphur-bearing minerals including sulphate minerals of gypsum and anhydrite and sulphide minerals of pyrite and to a lesser extent sphalerite, marcasite and chalcopyrite. Not shown on Figure 3.15 due to scale compatibility are the elevated sulphur contents of 23.2% from the Salina A2 Unit anhydritic dolostone and 23.4% from the Salina A2 Unit Evaporite that suggest about 70% sulphate from gypsum and/or anhydrite. The other detected sulphur contents in the Silurian rocks (0.44 to 7.23%) are reflective of anhydrite and/or gypsum in the Salina and Cabot Head formations. The

detected sulphur contents in the Ordovician shale and limestone (0.1 to 1.4%) likely reflect the presence of sulphide-bearing minerals (pyrite in shales) and traces of anhydrite (limestones).

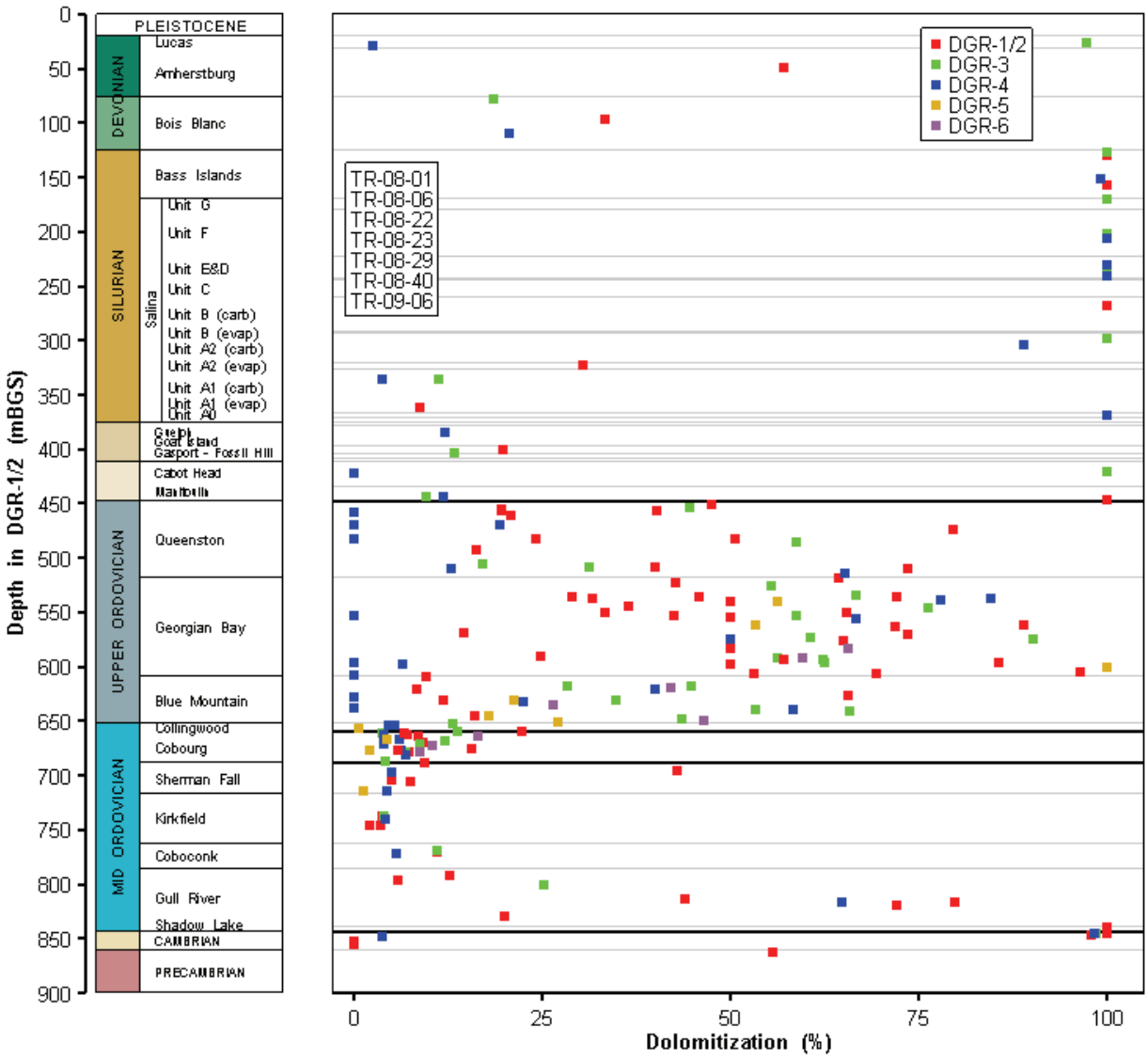

Figure 3.14: Dolomitization in DGR Cores

Figure 3.15 shows that both the total sulphur and organic carbon contents in DGR core peak in the Blue Mountain Formation and Collingwood Member as compared to the other formations. These trends correlate well with occurrences of petroleum and bitumen in the cores that are discussed in the next section.

Although the data in Figure 3.15 is not discriminated by laboratory, comparable organic carbon and total sulphur results are reported for DGR core by the different laboratories (Activation

Laboratories, SGS Laboratories, University of Bern, Core Laboratories) that completed these analyses. This provides increased confidence in the results.

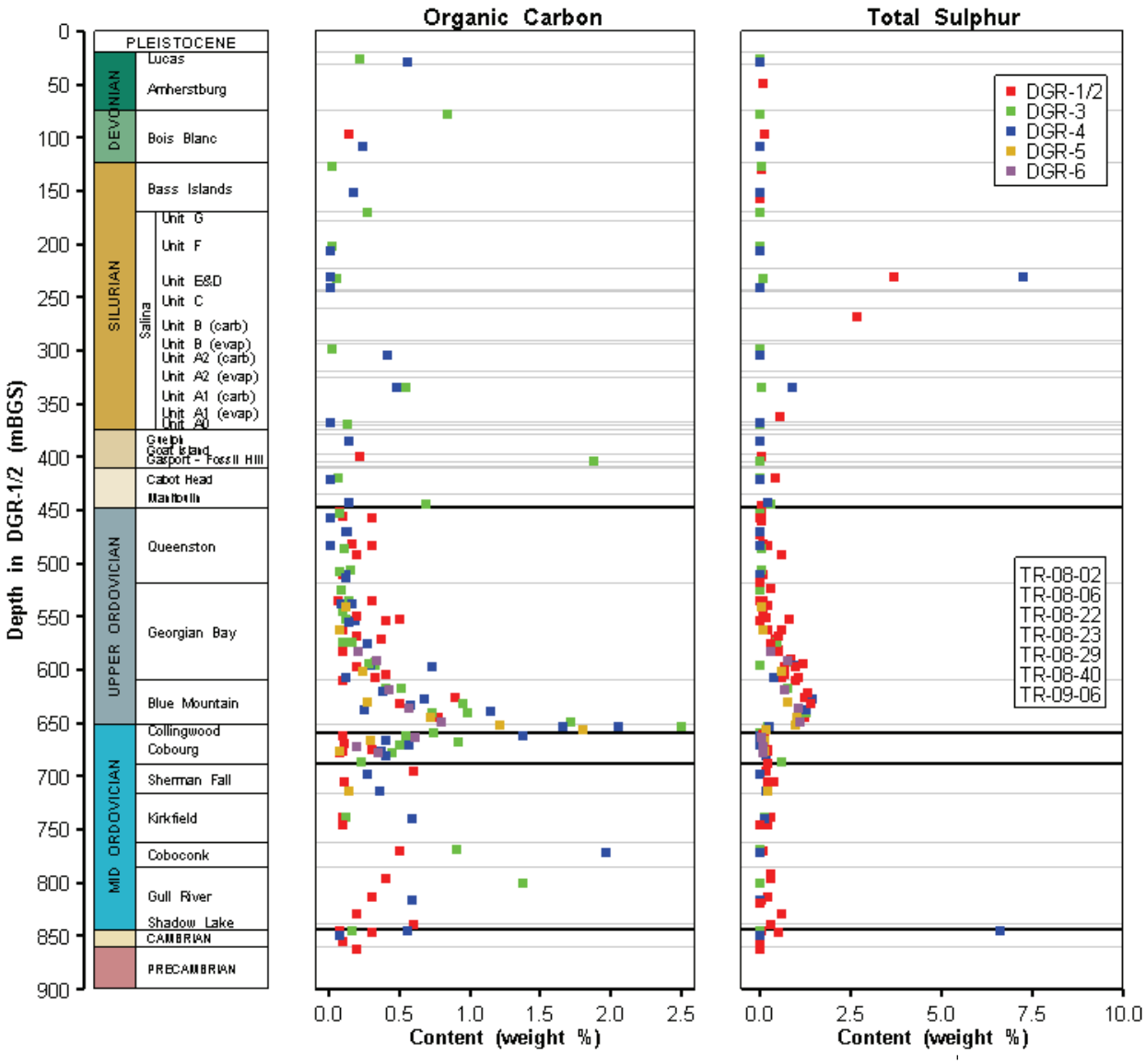

Figure 3.15: Organic Carbon and Sulphur Contents of DGR Cores

3.7.4.2 Hydrocarbons

In the part of the Michigan Basin that underlies Ontario, the focus of previous studies of the organic geochemistry of the Paleozoic sequence has been on the properties of hydrocarbons in the producing areas around Chatham (Carter 2002), approximately 250 km south of the Bruce nuclear site. Obermajer et al. (1996, 1999 and 2002) identified two 'petroleum systems' existing

in those Silurian and Ordovician rocks of southwestern Ontario that are present in the DGR. The Ordovician petroleum system is considered to have its origin within the Ordovician rocks themselves such that the petroleum was generated in "thin organic rich shaly Trenton laminae" from which the oil has migrated to stratigraphically proximate Cambrian and Silurian reservoirs. The Trenton Group consists of the Cobourg, Sherman Fall and Kirkfield formations. Secondly, the Middle Silurian formations, such as the Guelph and Salina reef carbonate rocks, are distinctly different "suggesting a carbonate source rock deposited under hypersaline conditions" (Obermajer et al. 2002).

During the drilling of the Phase 1 DGR boreholes, there were observations of hydrocarbons in cores recovered from the Devonian, Silurian and Ordovician formations that are summarized in Table 3.10.

Table 3.10: Observations of Hydrocarbon Occurrences Made in DGR-1 and DGR-2 Cores

Depth in DGR-1/2 (mBGS)	Formation	Hydrocarbon Occurrence
94-106	Bois Blanc	Dense, bituminous laminations every metre
341-366	Salina A1 Unit Carbonate	Thin lamina of bitumen, hydrocarbon odour, visible oil over 0.4 m vuggy section at bottom of Unit.
384-394	Goat Island	Bituminous laminations throughout
585-591	Georgian Bay	Petroliferous shale with hydrocarbon odour, suspected gas-containing fracture at 585.7 mBGS (see Figure 3.61)
616-653	Blue Mountain & Collingwood Member	Petroliferous shale with hydrocarbon odour
665-677	Cobourg	Bituminous laminations throughout
768-777	Coboconk	Vuggy petroliferous zone with oil weeping from core, strong hydrocarbon odour
814-830	Gull River	Light brown oil seeping from pores and styolites (see Figure 3.45)
840	Shadow Lake	Oil oozing from sandstone

Figure 3.16 summarizes the occurrences of hydrocarbons in DGR boreholes noted during core-logging as bituminous laminations/layers, petroliferous odours and minor (trace) oil seeps. Figure 3.16 shows there is some variability of hydrocarbon occurrences in DGR boreholes that in part may be attributed to heterogeneity in hydrocarbon distribution and in part to the subjective observational nature of the identification of hydrocarbon presence during logging.

There is no evidence in the DGR cores of commercially attractive oil and gas occurrences that might pose a risk of future intrusion into a closed DGR by those seeking to extract oil or gas, nor does there appear to be a risk to repository construction from these observations.

The observations of hydrocarbon occurrence made in DGR-1 and DGR-2, which were corroborated in DGR-3 to DGR-6, identified the need for a Phase 2A program to examine the organic geochemistry of the Ordovician shales (see TR-08-29) that form the caprock above the

proposed repository. This work included studies of clay mineralogy (see Section 3.7.1.1) and the testing of 19 DGR-3 and DGR-4 cores for total organic carbon (TOC) and by Rock-Eval pyrolysis, a standard test method to determine the basic organic geochemical parameters that characterize the thermal maturity of the sedimentary organic carbon or kerogen within the shales.

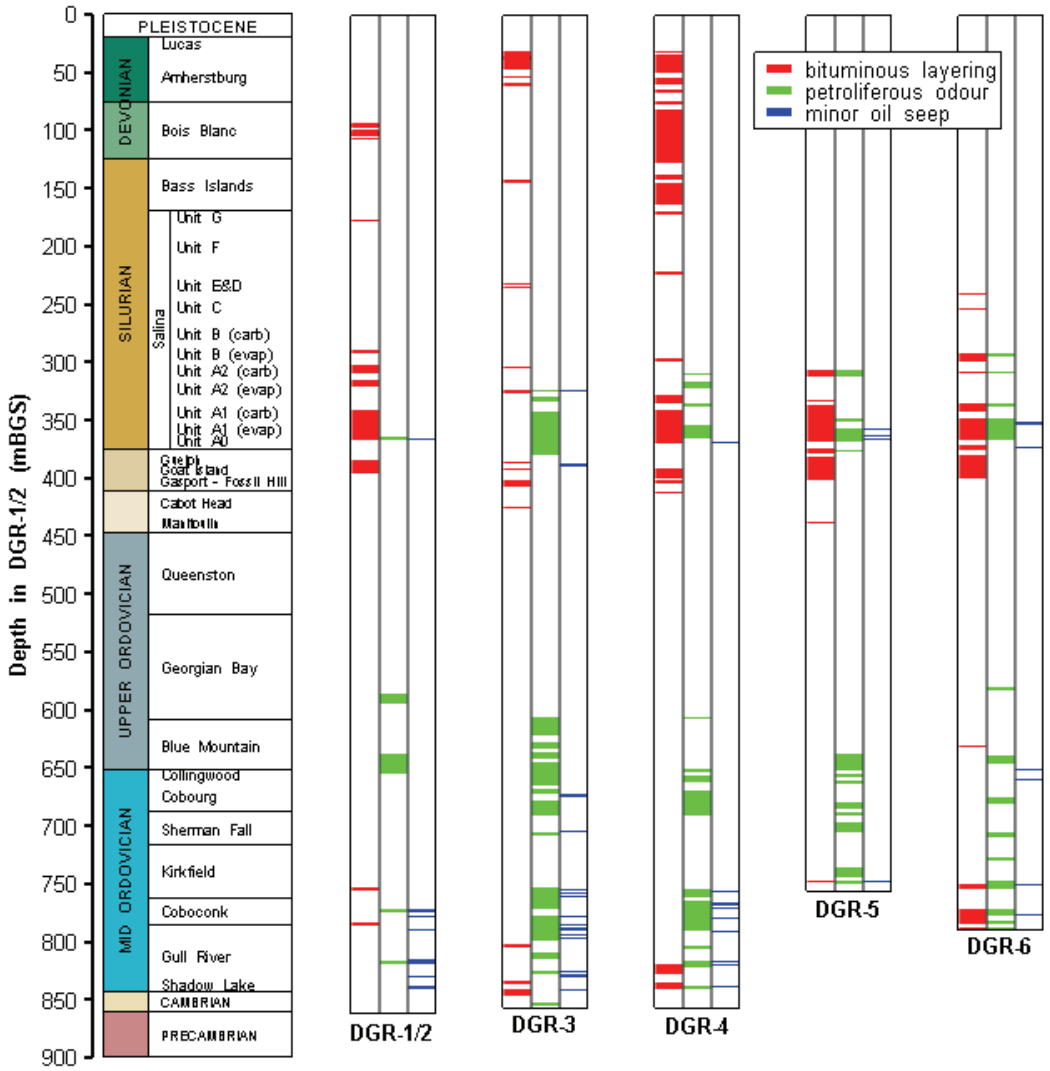

Figure 3.16: Summary of Observations of Hydrocarbon Presence in DGR Cores

The average TOC values for the Ordovician shales increase with depth from 0.11% in the Queenston, to 0.25% in the Georgian Bay to 0.90% in the Blue Mountain, and up to 2.5% in the Collingwood Member of the Cobourg Formation (Figure 3.15). The degree of thermal maturity of the kerogen correlates with this TOC trend. Figure 3.17 indicates that the peak pyrolysis

temperatures at which the kerogen produces hydrocarbon gas – T_{max} – increase with depth through the shales towards the lower Blue Mountain Formation and the Collingwood Member of the Cobourg Formation. The distribution of the Hydrogen Index (HI) – a measure of the amount of kerogen that can still produce oil and gas hydrocarbons normalised to its TOC concentration – versus T_{max} indicates the 'oil window' in which the kerogen of the core samples is presumed 'mature'.

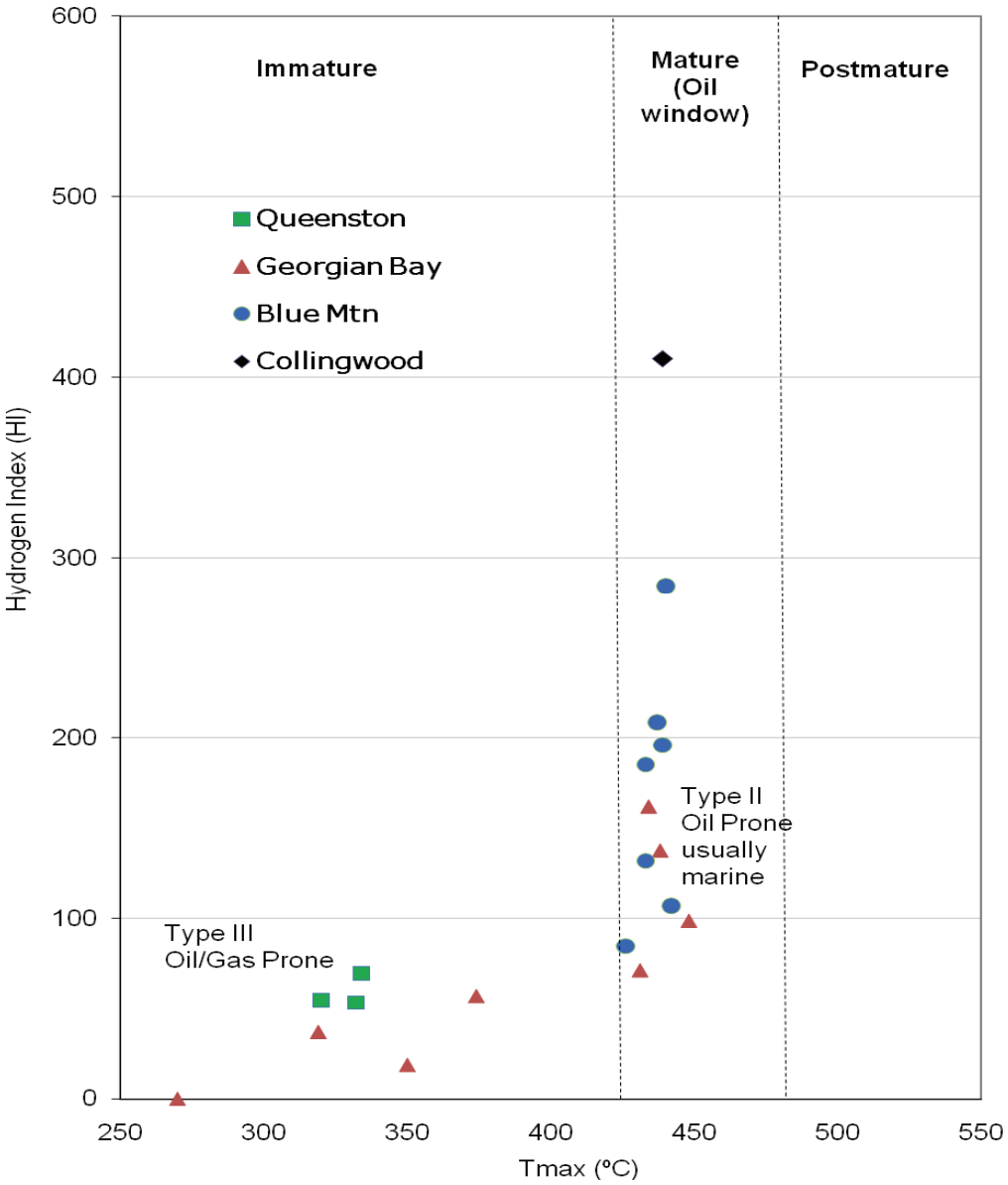

Figure 3.17: Plot of Peak Pyrolysis Temperature, T_{max}, vs. Hydrogen Index Indicating Kerogen Types

On this basis, the Collingwood sample and all Blue Mountain cores are considered as being thermally mature. Their kerogen is Type II, i.e., that common to marine basins and which tends to form oil rather than gas. Most Georgian Bay and all Queenston cores contain Type III

kerogen, which is derived from terrestrial organic matter, e.g., lignin and cellulose, and is more gas prone than Type II kerogen. These conclusions are consistent with what is known about the sedimentary provenance of these shales, i.e., the Queenston is associated with a coastal environment while the Georgian Bay and Blue Mountain are considered to be of marine origin. Thermal maturity values for this kerogen indicate in situ temperatures during maturation of between 70 and 130°C. Based on understanding of the burial history of this part of the Michigan Basin (Coniglio and Williams-Jones 1992), the actual in situ temperatures experienced were likely towards the lower end of this range. Thus, in terms of petroleum geology, the Ordovician shales that constitute the immediate caprock to the proposed repository horizon – the lower Blue Mountain and Collingwood members – constitute a 'self-sourcing' petroleum system, albeit a non-commercial one, that explains the occasional observation of oil seeping from the DGR cores.

3.8 Formation Stratigraphic Descriptions

Descriptions of mineralogical compositions of the tested core samples are provided in this section using a variety of adjectives. The meaning of these compositional descriptors, as defined in the mineralogical technical reports (TR-08-01, TR-08-22, TR-08-23, TR-09-06), are as follows: major - >30% weight or volume, moderate – 10-30%, minor – 2-10% and trace - <2%. Accessory minerals are minerals identified but not quantified, and are present in quantities less than trace amounts.

3.8.1 Quaternary Deposits

The overburden at the Bruce nuclear site is of variable thickness ranging from a thin veneer in the western part of the site near Lake Huron to upwards of 25 m in the eastern and northeastern part of the site (Figure 1.2). The increase in overburden thickness to the east and northeast reflects both a rising ground surface and a deepening bedrock surface.

The overburden stratigraphy typically comprises a surficial fill and sand and gravel unit overlying clayey silt to sandy silt glacial till, which is frequently underlain by a basal gravel deposit at the weathered bedrock surface. The surficial sand and gravels are former beach deposits and the till has been mapped as the Elma-Catfish Creek Till by the Ontario Geological Survey (Sharpe and Edwards 1979). Several reports (Jensen and Heystee 1987, Jensen and Heystee 1989, Jensen and Sykes 1993, INTERA 2004) provide database listings of the types and thicknesses of overburden deposits in selected areas of the Bruce nuclear site based on historical and recent borehole and test pit investigations.

Table 3.11 summarizes the overburden conditions logged during drilling of DGR-1 to DGR-6 and the US-series boreholes.

Data from US-series boreholes (Lukajic 1988) and DGR-1 to DGR-6 (TR-07-06, TR-08-13, TR-09-11) show the overburden thickness ranges from 7.41 m at US-5 to 22.6 m at US-6, with an average thickness of about 10.4 m at US-7 near the proposed DGR footprint. The overburden stratigraphy at these drilling locations is typically 1.0 to 3.0 m of granular fill overlying 5.0 to 21.0 m of grey sandy silt till, overlying 0 to 2.0 m of basal gravel and weathered bedrock.

3.8.2 Middle and Lower Devonian Formations

Middle and Lower Devonian age bedrock formations identified in DGR- and US-series boreholes include Lucas Formation dolostone, Amhertsburg Formation limestone and dolostone and Bois Blanc Formation dolostone.

Table 3.11: Summary of Overburden Conditions at DGR-Series and US-Series Boreholes

Borehole No.	Ground Surface Elevations (mASL)	Bedrock Surface Elevation (mASL)	Overburden Thickness (m)	Overburden Stratigraphy
US-1	192.12	173.59	18.53	Not logged
US-2	190.92	173.44	17.48	Very dense brown to grey sandy silt till
US-3	184.56	166.27	18.29	Till
US-4	191.18	175.04	16.14	Till
US-5	186.60	179.19	7.41	Not logged
US-6	191.90	169.30	22.60	Not logged
US-7	182.98	172.55	10.43	Not logged
US-8	187.20	178.67	8.53	Gravel fill over grey clay till
DGR-1	185.71	165.71	20.00	Gravel fill over brown/grey sandy silt till with basal gravel
DGR-2	185.84	162.44	20.00	Gravel fill over brown/grey sandy silt till with basal gravel
DGR-3	187.36	179.46	7.90	Gravelly fill over brown/grey sandy silt till
DGR-4	181.60	174.07	7.53	Gravelly fill over brown/grey sandy silt till
DGR-5	185.70	165.70	20.00	Gravel fill over brown/grey sandy silt till with basal gravel
DGR-6	183.50	168.60	14.42	Not logged

3.8.2.1 Lucas Formation Dolostone

The Lucas Formation dolostone is the upper bedrock unit over the western half of the Bruce nuclear site including DGR-1 to DGR-6, US-8 and likely other US boreholes and is thought to extend north to the vicinity of the Bruce A Generating Station. Regionally, the undifferentiated Lucas Formation is a thin- to medium-bedded, light to grey brown, fine-crystalline, lightly fossiliferous dolostone and limestone with stromatolitic laminations (Armstrong and Carter 2006).

The Lucas Formation is identified in boreholes DGR-1 to DGR-6 and in US-8 based on the occurrence of predominately grey to light brown dolostone core and chip samples, the inferred maximum thickness of the Lucas Formation of about 99 m at Sarnia (Armstrong and Carter 2006) and the regional bedrock mapping of the Geological Survey of Canada (1981) that shows the presence of the formation at the Bruce nuclear site. The contact with the underlying Amherstburg Formation is identified as the transition from greyish tan dolostone to brown dolostone.

The erosional surface is found in DGR-1 to DGR-6 at true vertical depths of 7.5 to 20.0 mBGS (TR-09-11), indicating an eroded formation thickness of 10.4 to 46.6 m. Based on the occurrence in all DGR boreholes, it is likely that the Lucas Formation is also present in all US-series boreholes. However, the upper bedrock in the US-series boreholes was logged (Lukajic 1988) including the Lucas as part of the Amherstburg Formation dolostone.

Petrographic analysis of core collected from DGR-3 and DGR-4 (TR-08-20, TR-08-21) shows the formation to be predominately calcareous mudstone/dolostone and recrystallized wackestone. The cores are very fine grained to microcrystalline with <20% fossil fragments, calcite inclusions in the dolomitic matrix and traces of quartz. Quantitative XRD analyses of the same core samples (Figures 3.5 and 3.6) identified the major minerals as dolomite and calcite with minor quartz and sphalerite. This indicates the rock is a form of dolostone or limestone. These XRD analyses are confirmed by the lithogeochemical analyses (Figures 3.11, 3.12 and 3.13) which show the dominant elemental oxides are CaO, MgO and minor SiO_2.

Because of the limited opportunity for coring through the Lucas Formation in DGR holes, RQD and natural fracture frequency data for this formation are grouped with the Amherstburg Formation in Table 3.4. The available RQD and natural fracture frequency data (Figures 3.3 and 3.4) and US-series boreholes indicate poor to fair core quality and moderately to highly fractured conditions characterize the Lucas Formation. Video logging of this formation in US-8 (TR-07-19) confirms these characteristics with the presence of moderately fractured conditions with several broken zones at depths of 20.1, 28.3, and 49.1 mBGS.

3.8.2.2 Amhertsburg Formation Dolostone

Regionally, the Amhertsburg Formation is a tan to grey-brown, fine- to coarse-grained, bituminous, bioclastic, fossiliferous limestone and dolostone with vuggy horizons and frequent open weathered fractures and brecciated zones (Armstrong and Carter 2006). At the Bruce nuclear site, the Amherstburg Formation is a dolostone characterized by the presence of abundant rugose and tabulate corals, especially in the bottom 5 to 10 m of the formation. Armstrong and Carter (2006) indicate up to 60 m thickness for the Amherstburg Formation that conformably overlies the cherty fossiliferous dolostones of the Bois Blanc Formation.

In DGR and US boreholes, the formation top is found at true vertical depths of 30.4 to 54.5 mBGS with thickness of 38.6 m to 44.6 m. The contact with the underlying Bois Blanc Formation dolostone is very difficult to identify in core, but generally correlates with the dominating presence of chert in the Bois Blanc Formation.

Petrographic analysis of core collected from DGR boreholes (TR-07-12) shows the formation to be predominately fossiliferous carbonates, recrystallized carbonates and void-filling carbonates of various grain sizes. Minor pyrite was noted with the very fine grained ferrous-calcareous mud that is interstitial to the fragmented fossils. Quantitative XRD analyses of the same core samples (Figures 3.5 and 3.6) identified the major minerals as dolomite and calcite with minor

quartz, confirming the field identification of the Amherstburg as predominately dolostone. These XRD analyses are confirmed by the lithogeochemical analyses (Table 3.9, Figures 3.11, 3.12 and 3.13) which show the dominant elemental oxides are CaO, MgO and minor SiO_2.

Based on logged core recovery, RQD and natural fracture frequency recorded in DGR boreholes (Table 3.4 and Figures 3.3 and 3.4), the Amherstburg Formation dolostone is moderately to highly fractured with core of very poor to fair quality. Video inspections of US-8 (TR-07-19) confirm these formation discontinuity characteristics with zones of borehole enlargement and intense fracturing evident.

RQD values for the seven cored US boreholes that intersected the Amherstburg Formation dolostone were higher (0 to 100%, mean 65%) than those recorded in DGR-1, DGR-3 and DGR-4, indicating fair core quality. Tunnelling and other construction and investigation experience associated with the Bruce A and B generating stations (Lucajic et al. 1986, Lucajic and Dupak 1986) suggest the formation rock quality may be locally poor. Considering the difficulties encountered with coring in the upper parts of DGR boreholes, the analysis of the US series borehole data and tunnelling experiences at the Bruce nuclear site that provide an assessment of fair core quality, is considered to be representative for the Amherstburg Formation dolostone.

3.8.2.3 Bois Blanc Formation Cherty Dolostone

Based on regional data, the Bois Blanc Formation is a greenish grey to brown, thin- to medium-bedded, fine- to medium-grained, fossiliferous, cherty dolostone, with a high natural fracture frequency, local dense bituminous laminations and occasional broken and rubble zones (Armstrong and Carter 2006). Figure 3.18 shows a core sample of the Bois Blanc Formation collected from DGR-1. The Bois Blanc Formation dolostone at the Bruce nuclear site is characterized by the presence of white to grey to black chert nodules and layers that locally constitute up to 90% of the rock volume. Armstrong and Carter (2006) indicate a 50 m thickness in the area of the Bruce nuclear site for the Bois Blanc Formation that disconformably overlies Silurian strata.

In DGR boreholes and US-8 the formation top is found at true vertical depths of 73.9 to 93.8 mBGS with thickness of 47.3 m to 49.3 m. A major discontinuity at the Devonian-Silurian boundary occurs at the base of the Bois Blanc Formation.

Petrographic analysis of core collected from DGR boreholes (TR-07-12, TR-08-20, TR-08-21) shows the formation to be predominately a fragmented and silicified fossiliferous carbonate packstone (dolostone) with cherty domains. Part of the rock consists of very fine-grained featureless oxidized and fragmented dark shale intercalated with chert and chalcedony fragments, and the other part consists of fossiliferous packstone with fine-grained dolomite matrix. Petrographically, the core mineralogy is estimated at 65-80% carbonate, trace-30% quartz (chert) with minor accessory minerals of disseminated pyrite, chalcopyrite and hematite. Quantitative XRD analyses of the same core samples (Figures 3.5 and 3.6) identified similar mineralogy with the major minerals as calcite, quartz and dolomite with trace of illite. These petrographic and XRD analyses are consistent with the lithogeochemical analyses (Table 3.9, Figures 3.11, 3.12 and 3.13) which show the dominant elemental oxides are SiO_2, and CaO with minor MgO.

Figure 3.18: Core Sample of Bois Blanc Formation Cherty Dolostone with Bituminous Laminations, 102.3 mBGS, DGR-1

Based on core logging of DGR boreholes (Table 3.4, Figures 3.3 and 3.4), the Bois Blanc Formation dolostone is moderately to highly fractured with fair core quality. Video inspections of US-8 (TR-07-19) confirm these formation discontinuity characteristics with zones of major borehole enlargement and intense fracturing evident at depths of 113.7, 131.1 and 132.3 mBGS, as well as the frequent occurrence of vertical and horizontal fracturing and minor enlargements.

RQD values for the six US-series cored boreholes that intersected the upper to middle parts of the formation were higher (64 to 100%, mean 94%) than those recorded in DGR boreholes (0 to 100%, mean 68%) indicating excellent core quality. Considering the difficulties encountered with coring in the upper to middle parts of the formation in DGR boreholes, US-8 data and the broader coverage afforded by US boreholes, the assessment of fair core quality based on US-series borehole data is considered representative for the Bois Blanc Formation dolostone.

3.8.3 Upper Silurian Formations

The Upper Silurian age formations encountered in DGR boreholes include Bass Islands Formation dolostone and Salina Formation Units G to A0 dolostones, evaporites and shales. Borehole US-8 intersects Upper Silurian Bass Islands Formation and Salina Formation Units G and F.

3.8.3.1 Bass Islands Formation Dolostone

The Bass Islands Formation has not been excavated or previously investigated at the Bruce nuclear site. Regionally, it is a brown to tan-grey, variably laminated, very fine- to fine-grained, argillaceous dolostone, with a high natural fracture frequency and occasional broken and rubble zones, particularly in the upper sections of the formation. Armstrong and Carter (2006) indicate a 10 to 90 m thickness for the combined Bass Islands and Bertie formations in southern Ontario. The Bass Islands Formation dolostone at the Bruce nuclear site is characterized by the very fine-grained dolostone lacking chert and fossils.

In DGR boreholes and US-8, the formation top is found at true vertical depths of 121.9 to 143.1 mBGS with thickness of 44.0 m to 45.3 m. The upper surface of the Bass Islands Formation is a major regional unconformity caused by paleo-erosion between the older Silurian rocks and the younger overlying Devonian rocks. The characteristics of this regional unconformity are discussed in Section 3.11.1 of this report.

Petrographic analysis of core samples collected from DGR boreholes (TR-07-12, TR-08-20, TR-08-21) shows the formation as microcrystalline aphanitic dolostone with minor amounts of gypsum and celestite and trace amounts of quartz (chert), and pyrite. Some samples also show oolitic dolostone, with intergranular pore space at about 0.5 to 1%. Petrographically, the core mineralogy is estimated at 85-95% carbonate (principally dolostone) with 8-10% gypsum or celestite. Quantitative XRD analyses of the same core samples (Figure 3.5 and 3.6) identified similar mineralogy with the major mineral as dolomite with trace quartz (chert) and calcite. These petrographic and XRD analyses are confirmed by the lithogeochemical analyses (Table 3.9, Figures 3.11, 3.12 and 3.13) which show the dominant elemental oxides are CaO and MgO and some SiO_2.

Based on core logging of DGR boreholes (Table 3.4, Figures 3.3 and 3.4), the Bass Islands Formation dolostone is moderately to highly fractured with poor core quality. The low mean core recovery of 77% and low mean RQD of 34% are attributed to difficult drilling conditions and to zones of intense fracturing and weathering due to presence of the regional erosional discontinuity. Similar to better formation discontinuity characteristics are also present in US-8 based on borehole video inspection (TR-07-19) that showed zones of highly broken rock and intense fracturing at depths of 170.7 mBGS, as well as the frequent occurrence of minor borehole enlargements and fracturing. Based on available DGR-1 and US-8 data, poor to fair core quality is considered representative of the Bass Island Formation dolostone.

3.8.3.2 Salina Formation, G Unit Argillaceous Dolostone

The Salina Formation is a succession of evaporites and evaporite-related carbonate sediments that is subdivided into lettered units A through G based on subsurface stratigraphic characteristics. All of the units within the Salina Formation were deposited conformably, although small-scale disconformities occur due to post-depositional dissolution of evaporite beds in the Bruce area (e.g., D Unit and B Unit salts) (Armstrong and Carter 2006).

Regionally, the G Unit is a tan to grey, argillaceous dolostone, with shale and anhydrite layers. Armstrong and Carter (2006) indicate a 12 m thickness of the G Unit in the Michigan Basin. The G Unit dolostone at the Bruce nuclear site is identified by the first presence of white, orange and pink anhydrite layers and nodules.

Based on core logging in DGR boreholes, the G Unit is 7.3 to 9.3 m thick and the top of the unit is found at true vertical depths of 166.1 to 187.1 mBGS. It is logged as medium grey argillaceous dolostone with intermittent layers of medium grey fine-grained dolostone and grey dolomitic shale. White, orange and pink anhydrite/gypsum veins and layers are present through the Unit as secondary infilling of healed fractures.

Petrographic analysis of core collected from borehole DGR-3 (TR-08-20) shows the unit to be predominately very fine-grained, fragmented dolostone and coarse-grained gypsum with anhydrite inclusions. The presence of large anhedral grains of gypsum within the dolomite-rich domains and the abundance of fine-grained inclusions of dolostone in the gypsum indicate the dissolution of dolomite and replacement by gypsum. Petrographically, the core mineralogy is estimated at 50% dolomite and 48% gypsum with trace anhydrite with minor accessory minerals of disseminated pyrite and quartz. Quantitative XRD analyses of the same core samples (Figures 3.5 and 3.6) identified similar mineralogy with the major minerals as dolomite and gypsum with traces of sanidine (K feldspar) and quartz. These petrographic and XRD analyses are confirmed by the lithogeochemical analyses (Table 3.9, Figures 3.11, 3.12 and 3.13) which show the dominant elemental oxides are CaO and MgO with minor SiO_2.

Based on core logging of DGR boreholes (Table 3.4, Figures 3.3 and 3.4), the G Unit dolostone is moderately fractured with fair core quality. These general unit discontinuity characteristics are also present in US-8 based on borehole video inspection that showed good quality borehole wall conditions with occasional horizontal fractures within the G Unit.

3.8.3.3 Salina Formation, F Unit Dolomitic Shale

Based on regional data, the F Unit is a grey/green to grey/blue dolomitic shale with shale and anhydrite. Armstrong and Carter (2006) indicate the F Unit is typically comprised of dark green shales with anhydrite in the upper half and mixed dolostones, shales and anhydrite in the lower half, with an estimated unit thickness of 30 m. The F Unit shale at the Bruce nuclear site is identified by the presence of predominately grey-blue shale and a gamma high on the borehole geophysical logs.

Based on core logging in DGR boreholes, the F Unit is 38.7 to 44.4 m thick and the top of the unit is found at true vertical depths of 174.4 to 196.3 mBGS. The upper part of the unit is grey to green fine-grained dolomitic shale with white and orange anhydrite/gypsum veins throughout (Figure 3.19).

A 0.2-m-thick layer of tan massive dolostone found at depths of 181.5 to 200.5 mBGS in DGR-1 to DGR-4 is a DGR formation marker bed that can be used to accurately estimate formation orientation (TR-08-12, TR-09-11). Below this marker bed, the unit is often stained reddish-brown with increasing content of anhydrite as veins, layers and large nodules that infill and surround brecciated shale and dolostone fragments. The bottom 6.0 m of the F Unit shale is composed of tan brown brecciated dolostone with abundant veins and layers. The brecciation of the F Unit is likely related to the collapse of the formation caused by paleo-dissolution of the underlying Salina D Unit salt.

Petrographic analysis of core collected from boreholes DGR-3 and DGR-4 (TR-08-20, TR-08-21, TR-08-40) shows the formation to be predominately very fine-grained, fragmented dolostone to calcareous shale with coarse- and fine-grained aggregates (veins, interstitial and anhedral grains) of gypsum with anhydrite inclusions. The presence of fragments of dolomitic matrix rock within gypsum veins indicate the gypsum veins post-date the matrix gypsum

interstitial to dolomitic shale host rock. Petrographically, the core mineralogy is estimated at 36 to 60% dolomite, up to 33% sheet silicates and 18-50% gypsum with trace anhydrite and minor accessory minerals of orthoclase, disseminated pyrite and quartz. Quantitative XRD analyses of the same core samples (Figures 3.5 and 3.6) identified similar mineralogy with the major minerals as dolomite and gypsum with minor amounts of orthoclase, undifferentiated clays and quartz. These petrographic and XRD analyses are confirmed by the lithogeochemical analyses (Table 3.9, Figures 3.11, 3.12 and 3.13) which show the dominant elemental oxides are CaO and SiO_2 with minor MgO and Al_2O_3.

Figure 3.19: Orange Anhydrite Veins Cut by White Gypsum Veins in Salina F Unit Dolomitic Shale, 222.6 mBGS in DGR-3

Based on core logging of DGR boreholes (Table 3.4, Figures 3.3 and 3.4), the F Unit shale is sparsely to moderately fractured with excellent core quality. These general unit discontinuity characteristics are also present in US-8 based on borehole video inspection that showed good quality borehole wall conditions with occasional horizontal fractures within the F Unit below 196.5 mBGS.

3.8.3.4 Salina Formation, E Unit Brecciated Dolostone and Dolomitic Shale

Regionally, the E Unit is a brown/grey brecciated dolostone and dolomitic shale with anhydrite. Armstrong and Carter (2006) indicate the E Unit is typically 30 m thick. The E Unit shale at the Bruce nuclear site is identified by the presence of a distinctive upper 2-m-thick bed of grey-green dolomitic shale as suggested by Armstrong and Carter (2006).

Based on core logging in DGR-1 to DGR-6 boreholes, the E Unit is 19.3 to 24.4 m thick and the top of the unit is found at true vertical depths of 213.1 to 239.3 mBGS. In descending order, the E Unit typically consists of about 2.3 m of grey-green dolomitic shale and brecciated dolostone, 10.9 m of brecciated dolostone with anhydrite, and 6.8 m of tan-grey dolomitic shale with anhydrite and gypsum. The middle horizon contains angular fragments of tan and brown dolostone and grey shale within a grey anhydritic dolomudstone matrix. The brecciation is greater in DGR-6 than in other DGR boreholes. The anhydrite/gypsum content of the lower horizon as veins, layers and nodules increases with depth.

Petrographic analysis of core collected from DGR boreholes (TR-07-12, TR-08-20, TR-08-21, TR-08-40, TR-09-05) shows the E Unit to be predominately fragmented and re-cemented dolomite to dolomitic shale with fibrous gypsum veinlets, pods and aggregates interstitial to the dolomite, and traces of fine-grained anhydrite, quartz and pyrite disseminated throughout the carbonate-rich matrix. Petrographically, the core mineralogy is estimated at 40-99% carbonate, 1-60% gypsum, and 0-2% quartz with trace pyrite and anhydrite. Quantitative XRD analyses of the same core sample (Figures 3.5 and 3.6) identified similar mineralogy with the major minerals as dolomite and gypsum, with minor illite, chlorite, quartz, orthoclase and sanidine. These petrographic and XRD analyses are confirmed by the lithogeochemical analyses (Table 3.9, Figures 3.11, 3.12 and 3.13) which show the dominant elemental oxides are CaO, MgO, SiO_2 and SO_4.

Based on logging of DGR boreholes (Table 3.4, Figures 3.3 and 3.4), the E Unit dolostone and shale is very sparsely to sparsely fractured with excellent core quality.

3.8.3.5 Salina Formation, D Unit Anhydritic Dolostone and C Unit Dolomitic Shale and Shale

The D Unit at the Bruce nuclear site is a thin blue-grey to brown anhydritic dolostone that represents the less soluble or non-salt constituents of the D Unit salt bed that has been dissolved in the geologic past (see Figure 3.20). Armstrong and Carter (2006) indicate the D Unit salt is up to 16 m thick elsewhere in Ontario, where the salt is preserved and that the C Unit is an inter-layered red and green-grey shale with anhydrite veins and nodules that grades into a dolomitic shale or dolomite with depth.

Based on core logging in DGR boreholes, the D Unit is 1.0 to 2.6 m thick and the top of the D Unit is found at true vertical depths of 231.9 to 263.1 mBGS. The C Unit is 11.9 to 33.3 m thick and is found at true vertical depths of 232.8 to 265.6 mBGS. The D Unit is a blue-grey to brown fragmented tan to brown dolostone within a white to bluish grey anhydrite/gypsum matrix. The C Unit typically consists of an upper 6.4 m of red and green shale and a lower 7.9 m of dolomitic shale. Anhydrite veins and nodules are common throughout the C Unit. The lower section of the C Unit includes broken shale and dolostone infilled and healed with white to blue anhydrite as a secondary mineral. The fragmentation or brecciation of the D and C Units is greatest in DGR-6.

No core samples of the D Unit anhydritic dolostone were submitted for geochemical, mineralogical or petrographic analyses.

Petrographic analysis of core collected from the C Unit in DGR-3 (TR-08-40) shows the unit to be predominately red oxidized silty calcareous shale consisting of detrital quartz, feldspar and muscovite (illite) cemented by dolomite. Quantitative XRD analyses of the core sample

(Figures 3.5 and 3.6) identified similar mineralogy with the major minerals as sheet silicates (44%) and dolomite (26%), quartz (20%), with minor albite, K-feldspar and trace halite.

Figure 3.20: Core Sample of Salina D Unit Anhydritic Dolostone from 243.14 mBGS in DGR-1

Based on core logging of DGR boreholes (Table 3.4, Figures 3.3 and 3.4), the combined D and C Units are unfractured to very sparsely fractured with excellent core quality.

3.8.3.6 Salina Formation, B Unit Argillaceous Dolostone and Evaporite

Regionally, the B Unit comprises a grey-green argillaceous dolostone, a salt horizon and an underlying thin evaporite (i.e., anhydrite) and dolostone layer. Armstrong and Carter (2006) indicate the B Unit is up to 90 m thick where it contains salt. The brecciation of the upper dolostone of the B Unit, which is most intense in DGR-6, reflects the dissolution of the formerly underlying B Unit salt, which is the thickest salt bed in Ontario (Armstrong and Carter 2006). The B Unit evaporite layer is the less soluble or non-salt constituents of the B Unit at the Bruce nuclear site that may also contain dolostone and shale.

Based on core logging in DGR boreholes, the B Unit overall is 25.2 to 44.0 m thick and the top of the B Unit is found at true vertical depths of 246.3 to 277.5 mBGS. Because the salt has been entirely removed, this unit is referred to as the B equivalent. In descending order, the B Unit typically consists of 21.2 to 40.8 m of grey-green brecciated argillaceous dolostone and a basal bed of 1.6 to 4.0 m thick grey anhydrite with brown dolostone layers. The upper brecciated unit consists of angular tan to grey dolomitic mudstone and dolostone clasts within a grey dolomitic shale matrix that is infilled with secondary white to bluish-grey anhydrite/gypsum veins, layers and nodules. The lower evaporite bed is grey with brown dolostone layers.

Petrographic analysis of cores collected from DGR boreholes (TR-07-12, TR-08-40) shows the sample to be very fine-grained, aphanitic calcareous shale to argillaceous dolostone with alternating light and dark domains. Petrographically, the core mineralogy is qualitatively estimated in order of decreasing abundance as illite, carbonate, quartz and traces of anhydrite, pyrite, hematite, zircon and oxyhydroxide. Quantitative XRD analyses of the same core sample (Figures 3.5 and 3.6) identified similar mineralogy with the major minerals as dolomite, illite, quartz and gypsum with minor chlorite and trace of halite. These petrographic and XRD analyses are confirmed by the lithogeochemical analyses (Table 3.9, Figures 3.11, 3.12 and 3.13) which show the dominant elemental oxides are SiO_2, CaO, MgO, Al_2O_3 and SO_4 with minor Fe_2O_3.

Based on core logging of DGR boreholes (Table 3.4, Figures 3.3 and 3.4), the B Unit argillaceous dolostone and anhydrite is unfractured to sparsely fractured with excellent core quality.

3.8.3.7 Salina Formation, A2 Unit Dolostone and Anhydritic Dolostone

The A2 Unit is regionally recognized as a tan-grey argillaceous, laminated to thin-bedded dolostone and an underlying anhydritic dolostone. The A2 Unit is subdivided into the A2 Unit Carbonate and the A2 Unit Evaporite. The A2 Unit Carbonate has been mapped as argillaceous dolostone and the A2 Unit Evaporite as anhydritic dolostone as defined by Armstrong and Carter (2006).

Based on core logging in DGR boreholes, the A2 Unit is 29.5 to 33.9 m thick and the top of the unit is found at true vertical depths of 290.3 to 304.2 mBGS. In descending order, the A2 Unit Carbonate typically consists of about 13-14 m of grey fine-grained dolomite with black shale layers, 2.0 m of dark grey dolomitic shale, 4.0 m of tan-grey argillaceous dolostone, 2.0 m of anhydritic dolostone and 5-6 m of tan-grey argillaceous dolostone with bituminous laminations. The underlying A2 Unit Evaporite is a 3.7- to 5.8-m-thick bed of light grey-blue anhydritic dolostone to dolomitic anhydrite (Figure 3.21).

Petrographic analysis of core collected from the A2 Unit Carbonate in DGR boreholes (TR-08-20, TR-08-21, TR-08-40) shows the unit to be very fine-grained to fine-grained equigranular dolomite and calcite with minor gypsum. Petrographically, the core mineralogy is estimated at 80-100% carbonate, 0-20% gypsum with trace pyrite, quartz and celestite. Quantitative XRD analyses of the same core samples (Figures 3.5 and 3.6) identified similar mineralogy with the major minerals as dolomite and gypsum with minor calcite and illite and trace of quartz, pyrite and orthoclase. These petrographic and XRD analyses are confirmed by the lithogeochemical analyses (Table 3.9, Figures 3.11, 3.12 and 3.13) which show the dominant elemental oxides are CaO, MgO and SiO_2 (note SO_4 was not quantified in these samples).

Petrographic analysis of core collected from the A2 Unit Evaporite (TR-07-12, TR-08-40) shows the samples to be massive to fibrous radiating anhydrite, porphyroblasts of gypsum and minor disseminated dolomite. Petrographically, the core mineralogy is estimated at 85-90% anhydrite, 3-10% gypsum and 3-5% carbonate which defines it as mainly anhydrite. Quantitative XRD analyses of the same core sample identified similar mineralogy with the major mineral as anhydrite, with minor calcite, dolomite, gypsum and quartz and trace of feldspar. These petrographic and XRD analyses are confirmed by the lithogeochemical analyses (Table 3.9, Figures 3.11, 3.12 and 3.13) which show the dominant elemental oxides are SO_4 and CaO.

Figure 3.21: Dolomitic Anhydrite of Salina A2 Unit Evaporite, 322.75 mBGS in DGR-4

Based on core logging of DGR boreholes (Table 3.4, Figures 3.3 and 3.4), the A2 Unit argillaceous dolostone and anhydritic dolostone is unfractured to very sparsely fractured with excellent core quality.

3.8.3.8 Salina Formation, A1 Unit Argillaceous Dolostone and Anhydritic Dolostone, A0 Unit Bituminous Dolostone

Regionally, the A1 Unit is similar to the A2 Unit in that it is divided into an upper A1 Unit Carbonate and a lower A1 Unit Evaporite. The A1 Unit is comprised of a grey-brown, argillaceous, bituminously laminated dolostone and an underlying anhydritic dolostone. The A0 Unit is a thin bituminous dolostone that is not well mapped in Ontario and historically has been grouped with the underlying Guelph Formation dolostone (Armstrong and Carter 2006).

Based on core logging in DGR boreholes, the A1 Unit is 44.8 to 45.9 m thick and the top of the unit is found at true vertical depths of 320.9 to 338.1 mBGS. The A1 Unit Carbonate logged in DGR boreholes is a thinly laminated, grey-brown dolostone with black bituminous layers and minor anhydrite layering. The upper 3.2 to 3.7 m of the A1 Unit Carbonate has open vuggy porosity and permeability (Figure 3.22). A thin (0.2 to 0.4 m thick) show of hydrocarbon as crude oil was observed in the bottom of the A1 Unit Carbonate in several DGR boreholes (e.g., Figure 3.16). The underlying A1 Unit Evaporite is a 3.5- to 5.0-m-thick bed of light grey-blue anhydritic dolostone.

Figure 3.22: Open Vuggy Porosity of Upper A1 Unit Carbonate at 326.2 mBGS in DGR-4

The A0 Unit dolostone at the DGR site is a 2.6- to 4.0-m-thick bed with the top of the unit found at true vertical depths of 365.7 to 383.6 mBGS. It is a massive, intact, dark brown-black, thinly laminated, fine-grained bituminous dolostone. Notably, the bituminous laminations of the A0 Unit in DGR-1 dip at about 5 to 30° increasing with depth in the unit. The dips of these bituminous laminations are much greater than the expected regional dip of about 1° or less and may be indicative of sedimentation on the flank of a minor local reef that would be in the underlying Guelph Formation, although there is no evidence in the core that the Guelph Formation is reefal. There is insufficient resolution of the laminations within the A0 Unit in DGR boreholes to allow identification of dip direction of these laminations using borehole acoustic televiewer logs. Figure 3.23 shows the intact core collected from the A0 Unit dolostone during coring of DGR-1.

Petrographic analysis of core collected from the A1 Unit Carbonate in DGR boreholes (TR-07-12, TR-08-20, TR-08-21, TR-08-40) shows the unit to be laminated, very fine-grained calcareous shale to dolostone or limestone with alternating light and dark bands. Petrographically, the core mineralogy is estimated in order of decreasing abundance as carbonate, illite, pyrite and trace of quartz and gypsum. Quantitative XRD analyses of the core samples (Figures 3.5 and 3.6) identified the major minerals as 76-82% calcite, 7.9-11.6% illite, 4.1-10.7% dolomite and traces of quartz, orthoclase and anhydrite. The XRD analyses are confirmed by the lithogeochemical analyses (Table 3.9, Figures 3.11, 3.12 and 3.13), which show the dominant elemental oxide is CaO, with minor amounts of SiO_2, SO_4, Al_2O_3 and MgO. Based on XRD and lithogeochemical analyses the A1 Carbonate Unit is predominately limestone, not dolostone.

Figure 3.23: Intact 3.0-m-length Core of the Salina A0 Unit Dolostone at 371-374 mBGS in DGR-1

Petrographic analysis of core collected from the A1 Unit Evaporite in DGR boreholes (TR-08-20, TR-08-21, TR-08-40) shows the unit to be laminated alternating bands of fine-grained dolomite and recrystallized saddle dolomite and anhydrite (Figure 3.24), to fine-grained anhydrite and illite, to massive anhydrite. Petrographically, the core mineralogy is qualitatively estimated in order of decreasing abundance as up to 60% carbonate, 40-66% anhydrite, up to 33% illite and trace of pyrite and quartz. Quantitative XRD analyses of the core samples identified the major minerals as 50-81% anhydrite, 13-45% dolomite, with minor amounts of illite, quartz and sanidine.

Based on core logging of DGR boreholes (Table 3.4, Figures 3.3 and 3.4), the A1 and A0 Units dolostone and anhydritic dolostone are unfractured to sparsely fractured with excellent core quality.

3.8.4 Middle and Lower Silurian Formations

The Middle and Lower Silurian age formations encountered in DGR boreholes include the Guelph, Goat Island, Gasport, Lions Head and Fossil Hill Formation dolostones (Middle Silurian), and the Cabot Head Formation shale, and Manitoulin Formation dolostone and shale (Lower Silurian)

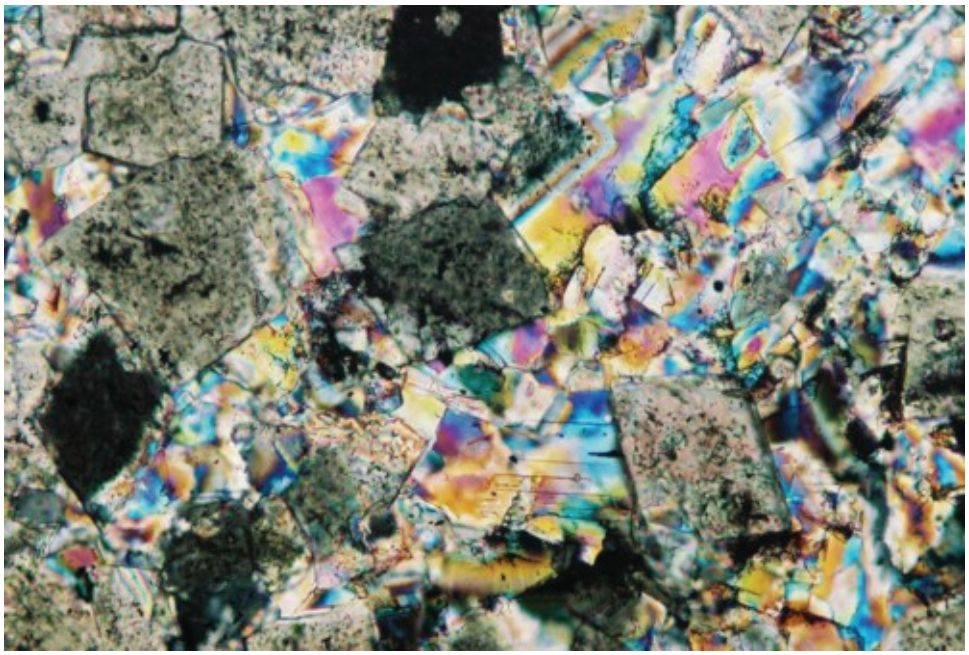

Note: Width of photo 0.45 mm, crossed nicols, anhydrite displays 3rd order birefringence colours. Saddle dolomite displays a tan colour.

Figure 3.24: Saddle Dolomite within Anhydrite Matrix at 382.29 mBGS in Salina A1 Unit Evaporite in DGR-3

3.8.4.1 Guelph, Goat Island, Gasport, Lions Head and Fossil Hill Formation Dolostones

Based on limited thickness and lithologic similarity, the dolostone sequence comprising the Guelph Formation, Goat Island Member of the Lockport Formation, Gasport Member of the Lockport Formation, Lions Head Member of the Amabel Formation and Fossil Hill Formation are grouped together, but individually described here.

The Guelph Formation dolostone in DGR boreholes is a 3.7- to 5.4-m-thick bed of brown vuggy sucrosic dolostone with the formation top at true vertical depths of 369.6 to 386.2 mBGS. It is a thin, porous and permeable formation (Figure 3.25). Although Armstrong and Goodman (1990) and Johnson et al. (1992) have shown the Bruce nuclear site to be located on the edge of the pinnacle reef belt, Carter et al. (1994) and Armstrong and Carter (2006) have interpreted the small thickness of the Guelph, as evident at the Bruce nuclear site, to be indicative of non-reefal, inter-pinnacle facies on the basin slope. This interpretation is confirmed by the DGR core that shows no evidence of reefal facies.

Petrographic analysis of a core sample collected from DGR-3 (TR-08-40) show the Guelph Formation as veined brown sucrosic dolostone composed of dolomite with minor fine-grained disseminated pyrite. The veins are partially infilled with hydrothermal dolomite (ankerite) with minor quartz and abundant halite. Quantitative XRD analyses of the core sample (Figures 3.5 and 3.6) identified similar mineralogy with 86% dolomite, 10% halite, and traces of quartz, calcite and pyrite.

Figure 3.25: Core Photograph of Guelph Formation Porous Dolostone at 376 mBGS in DGR-1

The Goat Island Member of the Lockport Formation dolostone in DGR boreholes is an 18.1- to 18.8-m-thick bed of light to dark brown-grey, very fine-grained, thin to medium bedded, dolostone with the formation top found at true vertical depths of 373.3 to 391.6 mBGS. Chert and microstylolites are present. It is sparsely to moderately fossiliferous (Armstrong and Carter 2006). Petrographic analysis of a core sample collected from DGR-4 (TR-08-21) shows the Goat Island to be a partly recrystallized fossiliferous packstone with traces of illite and quartz. Quantitative XRD analyses of the core sample (Figures 3.5 and 3.6) identified similar mineralogy with 73% calcite, 11.4% dolomite and ankerite, 7.6% illite and 7.4% quartz. The XRD analyses are confirmed by the lithogeochemical analyses (Figures 3.11, 3.12 and 3.13) which show the dominant elemental oxides are CaO and SiO_2, with minor amounts of Al_2O_3 and MgO.

The Gasport Member of the Lockport Formation dolostone in the DGR boreholes is a 6.5- to 9.2-m-thick bed of blue-grey to white, fine- to coarse-grained, dolomitic limestone with the formation top found at true vertical depths of 391.8 to 409.9 mBGS. It has bituminous laminations and microstylolites throughout. Petrographic analysis of cores collected from the Gasport (TR-07-12, TR-08-20) shows the formation to consist of mostly calcareous fossils comprised of mostly calcite with some dolomite within a carbonate-rich matrix. Petrographically, the core mineralogy is estimated at 90-99% carbonate, 0-10% illite, with accessory minerals of pyrite, anhydrite and quartz. Quantitative XRD analyses of the same core samples (Figures 3.5 and 3.6) identified major minerals as calcite and dolomite with minor illite and quartz. The lithogeochemical analyses (Table 3.9, Figures 3.11, 3.12 and 3.13) show

the dominant elemental oxides are CaO with minor MgO and SiO_2 indicating the tested core sample is a dolomitic limestone.

The Lions Head Member of the Amabel Formation dolostone in DGR boreholes is a 2.3- to 4.5-m-thick bed of light grey to grey-brown, fine- to crystalline-grained, dolostone found with the top of formation at true vertical depths of 399.7 to 416.4 mBGS. According to Armstrong and Carter (2006), it is sparsely fossiliferous with locally abundant chert nodules. No core samples of the Lions Head dolostone were submitted for geochemical, mineralogical or petrographic analyses.

The Fossil Hill Formation dolostone in the DGR boreholes is a 1.3- to 2.6-m-thick bed of light- to medium-brownish grey, coarse-grained, thin- to medium-bedded, fossiliferous dolostone with the top of formation found at true vertical depths of 403.3 to 420.9 mBGS. According to Armstrong and Carter (2006), it is very fossiliferous, which is consistent with the logging in DGR boreholes. No core samples of the Fossil Hill Formation dolostone were submitted for geochemical, mineralogical or petrographic analyses.

Based on core logging of DGR boreholes (Table 3.4, Figures 3.3 and 3.4), the dolostone sequence comprising the Guelph, Goat Island, Gasport, Lions Head and Fossil Hill formations is unfractured to very sparsely fractured with excellent core quality.

3.8.4.2 Cabot Head Formation Shale

Regionally, the Cabot Head Formation is a grey to green to red-maroon noncalcareous shale with subordinate sandstone and carbonate interbeds (Armstrong and Carter 2006).

Based on core logging in DGR boreholes, the Cabot Head Formation is 23.4 to 24.7 m thick with the formation top found at depths of 405.9 to 422.2 mBGS. In DGR boreholes, the Cabot Head Formation is a green-grey and red massive shale grading to interbedded grey carbonate and black fossiliferous shale at the bottom of the unit. Figure 3.26 shows the upper section of the Cabot Head Formation.

Petrographic analysis of cores collected from the Cabot Head Formation shale (TR-07-12, TR-08-20, TR-08-21) show the samples to be a featureless Fe-stained, very fine-grained oxidized shale. Petrographically, the core mineralogy is estimated as Fe-stained illite (40-80%), Fe-hydroxide (10-20%), minute angular quartz clasts (10-35%), very fine-grained carbonates (5-10%) and trace of anhydrite (<1%). Quantitative XRD analyses of the same core samples (Figures 3.5 and 3.6) identified the major minerals as illite and quartz with minor dolomite, chlorite, orthoclase, goethite and trace halite, gypsum and pyrite. Lithogeochemical analyses (Table 3.9, Figures 3.11, 3.12 and 3.13) show the dominant elemental oxides are SiO_2, Al_2O_3, and Fe_2O_3 with minor MgO and CaO. These laboratory analyses show the cores range from non-calcareous to calcareous shale.

Based on core logging of DGR boreholes (Table 3.4, Figures 3.3 and 3.4), the Cabot Head Formation shale is unfractured to very sparsely fractured with excellent core quality. Based on review of the borehole acoustic televiewer logs, an inclined fracture (50°dip) is evident at a depth of 414.3 mBGS in DGR-1, indicating that the top of the Cabot Head Formation is sparsely fractured.

Figure 3.26: Top of Cabot Head Formation Shale, 411.02 to 414.07 mBGS in DGR-1

3.8.4.3 Manitoulin Formation Cherty Dolostone and Minor Shale

Based on regional data, the Manitoulin Formation is recognized as a bed of cherty dolostone, argillaceous dolostone and minor grey-green shale. According to Armstrong and Carter (2006), the dolostone is typically grey, thin- to medium-bedded, moderately fossiliferous, fine- to medium-grained and commonly contains chert nodules or lenses and silicified fossils.

Based on core logging in DGR boreholes, the Manitoulin Formation is 9.5 to 13.2 m thick with the formation top found at true vertical depths of 429.3 to 446.9 mBGS. It is a grey, fine- to medium-grained dolostone with minor grey-green noncalcareous shale. The upper ~9.5 m is cherty dolostone with silicified shell fragments, and the bottom ~3.4 m is fine-grained crystalline dolostone with increasing shale content below 445.0 mBGS in DGR-1.

Petrographic analysis of cores collected from the middle to bottom part of the Manitoulin Formation dolostone and shale in the DGR boreholes (TR-07-12, TR-08-20, TR-08-21) show the samples to be fossiliferous calcareous grainstone to very fine-grained laminated dolomitic shale with alternating bands of fine-grained dolomite and illite. Petrographically, the core mineralogy is estimated as carbonates (39 to 99%), illite (0-60%), anhydrite (2%) (Figure 3.27), traces of quartz (<1%) and pyrite (1%), and a few minute grains of gypsum.

Quantitative XRD analyses of the same core samples (Figures 3.5 and 3.6) identified the major minerals as calcite (0-82%), illite (5-60%), quartz (0-32%), dolomite and ankerite (8.6-14%) with minor chlorite (0-4.3%) and hematite (0-3.1%) and trace of halite and gypsum. The identified higher percentage of quartz in the XRD analyses of one sample is likely attributable to the presence of chert. The petrographic and XRD analyses are supported by the lithogeochemical

analyses (Table 3.9, Figures 3.11, 3.12 and 3.13) which show the dominant elemental oxides are CaO and SiO_2, with minor Al_2O_3, MgO and Fe_2O_3.

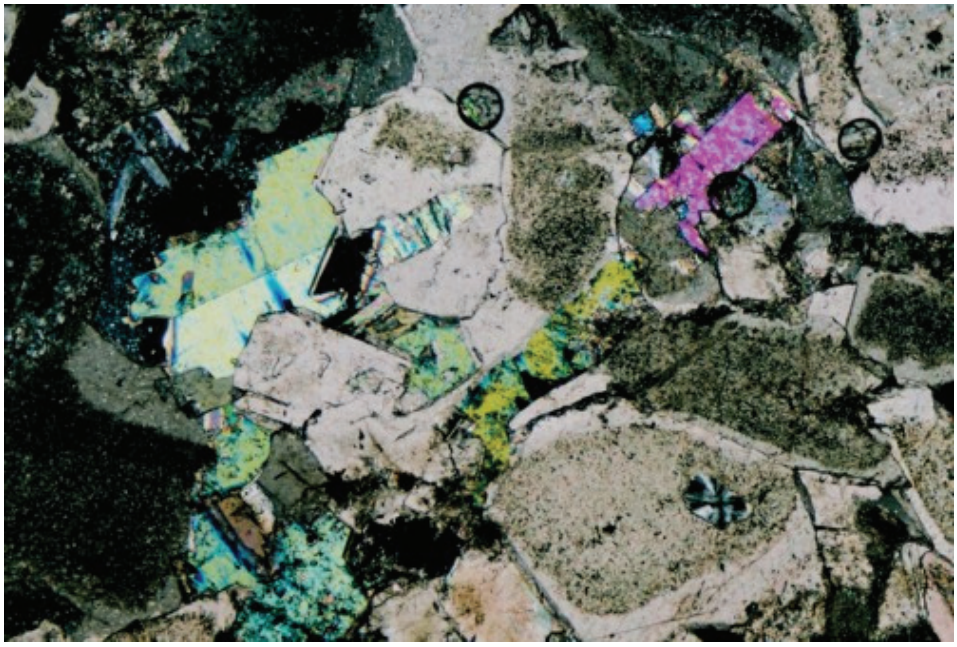

Note: Width of photo 2.3 mm, crossed nicols, anhydrite displays 3rd order birefringence colours.

Figure 3.27: Anhydrite Grains and Interstitial to Recrystallized Calcite at 442.74 mBGS in Manitoulin Formation in DGR-4

Based on core logging of DGR boreholes (Table 3.4, Figures 3.3 and 3.4), the Manitoulin Formation cherty dolostone and shale is unfractured to very sparsely fractured with excellent core quality.

3.8.5 Upper Ordovician Formations

The Upper Ordovician age formations encountered in DGR boreholes include Queenston Formation shale, Georgian Bay Formation shale and limestone, and the Blue Mountain Formation shale.

Petrography and XRD mineralogical analyses of cores from DGR boreholes are available from independent testing completed by Activation Laboratories Ltd. (TR-08-01), SGS Laboratories (TR-08-22, TR-08-23), and Geoconsult (TR-07-12, TR-08-20, TR-08-21), as well as from Rock Water Interaction, University of Bern (TR-08-06, TR-08-40).

3.8.5.1 Queenston Formation Red Shale

Regionally, the Queenston Formation is a bed of brick red to maroon, noncalcareous to calcareous shale with subordinate amounts of green shale, siltstone, sandstone and limestone (Armstrong and Carter 2006). Gypsum occurs as locally abundant nodules and thin,

subhorizontal fracture infillings. Carbonate content, both of the shale and in terms of abundance and thickness of limestone beds, tends to increase regionally to the northwest. On the Bruce peninsula, the middle part of the formation consists of green shale interbedded with fossiliferous limestone (Armstrong and Carter 2006). The top of the Queenston Formation is an erosional unconformity with the overlying Silurian strata.

Based on core logging of DGR boreholes, the Queenston Formation is 69.3 to 74.4 m thick with the top of the formation found at true vertical depths of 442.6 to 456.4 mBGS. The upper 35-36 m of the formation is massive red-maroon calcareous shale with grey-green calcareous shale layers and lenses. Orange fracture infilling minerals (halite with some bounding calcite) were logged in the upper 10 to 30 m of the formation (Figure 3.28) as well as deeper in the formation. Figures 3.28, 3.29 and 3.30 show typical core samples and a thin section for the upper part of the Queenston Formation red shale.

Figure 3.28: Halite-infilled Horizontal Fracture at 458.6 mBGS in Upper Queenston Formation in DGR-3

Figure 3.29: Core Sample of Green and Red Shale, Upper Queenston Formation, 454.82 mBGS, DGR-1

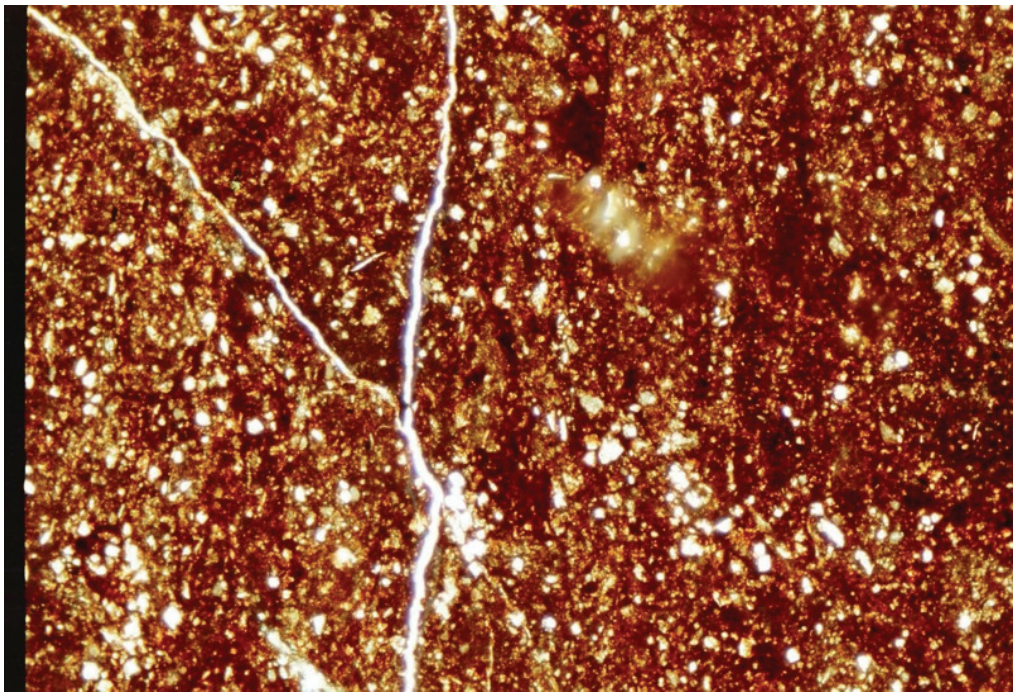

Figure 3.30: Carbonate Veinlets in Ferruginous Shale, Upper Queenston Formation, 455.45 mBGS in DGR-1, Width of Photo: 2.3 mm, Plane Polarized Light

The middle ~26 m of the formation is green shale interbedded with medium to light grey, medium- to coarse-grained fossiliferous limestone layers (Figure 3.31). The limestone layers represent about 25 to 50% of the middle part of the Queenston Formation. The bottom 10-11 m of the formation is red-maroon shale interbedded with grey-green shale layers and minor limestone beds.

Figure 3.31: Interbedded Green Shale and Grey Fossiliferous Limestone, Middle Queenston Formation at 496 mBGS in DGR-3

Core disking was first observed in DGR boreholes at depths of 511 mBGS within the lower red-maroon shale of the Queenston Formation. Core disking in this report refers to the regular breaking of intact core into centimetre-length pieces upon retrieval to ground surface. Although this term is often used in the geotechnical literature as an indicator of high ground stress conditions, its use in this report does not imply such conditions. It is recognized in argillaceous rocks that core disking can also be due to other physio-chemical causes as deep core is equilibrated with atmospheric conditions.

Figure 3.32 shows the variation of stratigraphy evident within the Queenston Formation in DGR-3 from core logging and from selected borehole geophysical logs. Complete geophysical logs for all DGR boreholes are given in Appendix B to this report. Figure 3.32 illustrates the three dominant lithologies of shale, interbedded shale and limestone, and shale as evident from gamma and neutron logs. The interbedded shale and limestone is apparent as a decreased natural gamma response and increased neutron response compared to the more massive, clay-rich and higher porosity shales. Also evident in Figure 3.32 is an anomaly in the

temperature variability log suggesting some permeability at the top of the Queenston Formation, and the sharp contact with the overlying Manitoulin Formation shown on the gamma log. The fossiliferous limestone marker bed for the Queenston Formation at 517.7 to 518.1 mBGS is apparent as a natural gamma decrease and neutron increase reflecting the decreased shale content and decreased porosity. Several halite-infilled fractures and minor borehole enlargements are also highlighted in Figure 3.32 as kicks in the bed resolution density log and the caliper log. Based on temperature variability logs, these fracture and enlargement features are tight.

A total of 24 core samples from the Queenston Formation in DGR boreholes were subject to geochemical, mineralogical and/or petrographic analyses (TR-07-12, TR-08-01, TR-08-06, TR-08-20, TR-08-21, TR-08-22, TR-08-23, TR-08-29, TR-08-40).

Petrographic analysis of core collected from the upper part of the Queenston Formation shale shows all the samples to be similar as iron-stained, fine-grained calcareous shale with some fossiliferous layers and minor anhydrite-gypsum and halite veins. Petrographically, the mineralogy in these cores is estimated as carbonates (40 to 85%), clays (trace to 50%), calcite fossils (0 to 40%), dolomite (7-10%), halite (0 to 10%), quartz (0 to 12%), gypsum/anhydrite (0 to 2.5%) and traces of pyrite, hematite, goethite, and Fe-oxyhydroxide. Quantitative XRD analyses of the same core samples (Figures 3.5 and 3.6) identified similar mineralogy with the major minerals as calcite, illite, dolomite, quartz and chlorite with minor to trace amounts of pyrite, hematite, halite, anhydrite and gypsum. These petrographic and XRD analyses are confirmed by the lithogeochemical analyses (Table 3.9, Figures 3.11, 3.12 and 3.13) which show the dominant elemental oxides are SiO_2, CaO and Al_2O_3 with minor amounts of Fe_2O_3, K_2O and MgO.

Petrographic analysis of vein material collected from the upper part of the Queenston Formation at 456.01 mBGS in DGR-1 shows the sample to be predominately halite with minor amounts of calcite. Quantitative XRD and SEM/EDS analyses of the same vein sample identified similar mineralogy with the halite as predominant, calcite as a medium amount, dolomite and quartz present in small to trace amounts and illite and chlorite present in trace amounts.

Petrographic analysis of core collected from the middle part of the Queenston Formation shale and interbedded limestone shows this formation to be fossiliferous argillaceous limestone and shale. Petrographically, the core mineralogy is estimated as carbonates (25-85%), fossiliferous carbonates (0-25%), quartz (0-40%) and biotite/dark clays (10-35%) with accessory minerals of pyrite, chalcopyrite, anhydrite and celestite. Quantitative XRD analyses of the same core samples (Figures 3.5 and 3.6) identified similar mineralogy with the major minerals as illite, quartz, dolomite, calcite and chlorite. These petrographic and XRD analyses are confirmed by the lithogeochemical analyses (Table 3.9, Figures 3.11, 3.12 and 3.13) which show the dominant elemental oxides are SiO_2, Al_2O_3 and CaO with minor MgO, Fe_2O_3 and K_2O.

Petrographic analysis of cores collected from the lower part of the Queenston Formation shale shows this part of the formation to be iron-stained, very fine-grained dolomitized calcareous shale. Petrographically, the core mineralogy is estimated as carbonates (30-53%), Fe-oxide/hydroxides (0-50%), illite (15-20%), and quartz (5%) with accessory minerals of pyrite and anhydrite. Quantitative XRD analyses of the core samples (Figures 3.5 and 3.6) identified the major minerals as illite, quartz, calcite, dolomite and chlorite. These XRD analyses are supported by the lithogeochemical analyses (Table 3.9, Figures 3.11, 3.12 and 3.13) which show the dominant elemental oxides are SiO_2, CaO and Al_2O_3 with minor Fe_2O_3, MgO and K_2O.

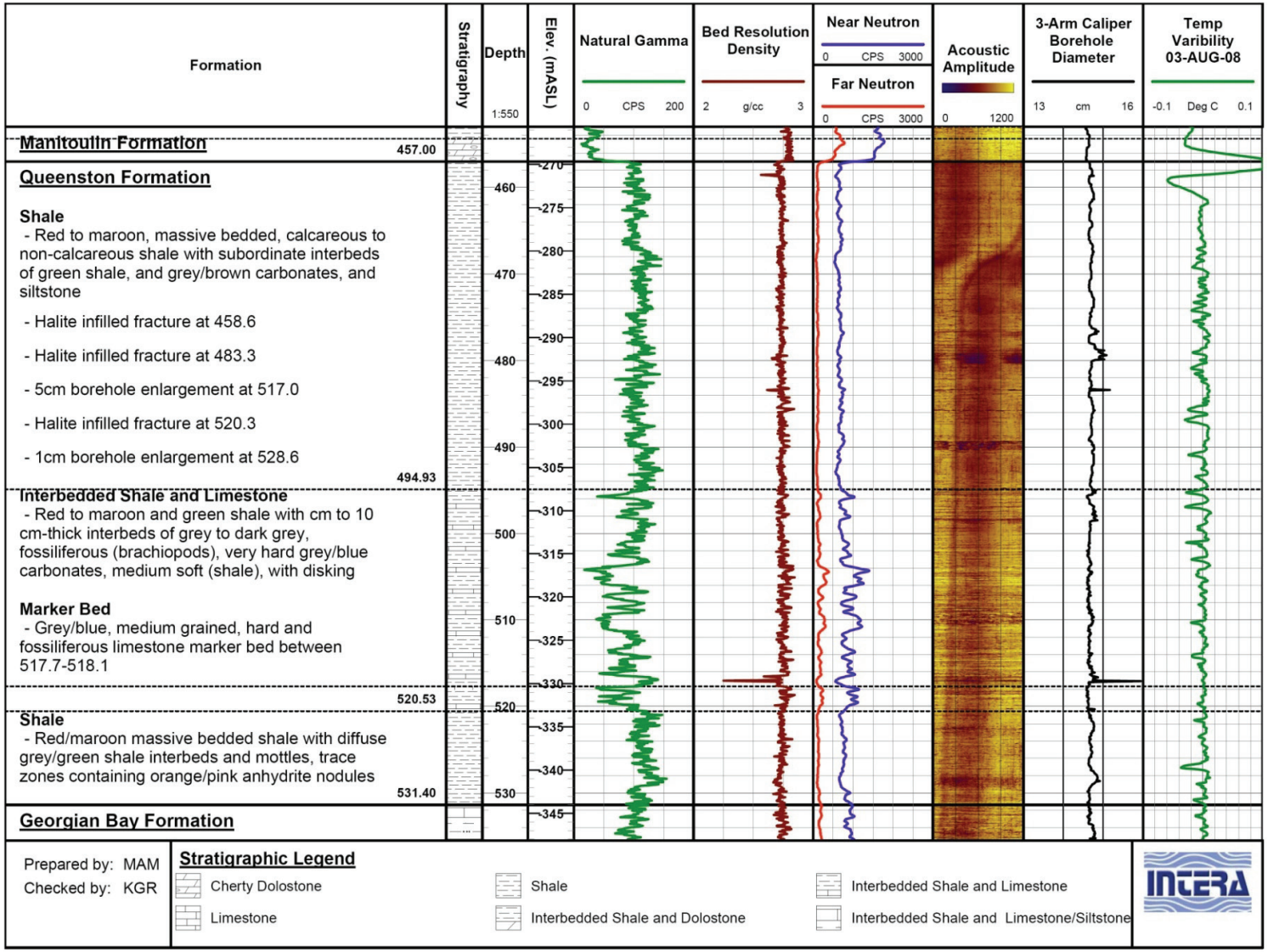

Figure 3.32: Stratigraphy of the Queenston Formation in DGR-3 from Core Logging and Selected Borehole Geophysical Logs

Based on core logging (Table 3.4, Figures 3.3 and 3.4), the Queenston Formation is unfractured to sparsely fractured with excellent core quality (Figure 3.33 - left). Core logging identified the sporadic occurrence of several smooth natural fractures in the Queenston Formation in DGR boreholes most of which were sealed and infilled with halite, calcite and/or gypsum. Some of these fractures were inclined (i.e., dip greater than 35°). Borehole acoustic televiewer logging identified a similar number and orientation of natural fractures in the Queenston Formation with several of these found in the upper 15 m of the formation and an equal number of inclined and subhorizontal natural fractures present throughout the formation. Fracture surfaces occasionally showed the presence of discontinuous slickensided surfaces. These surfaces were most likely formed during consolidation and induration.

Figure 3.33: Intact Core Runs: Left - Queenston Formation, 475.73-478.78 mBGS in DGR-3, Right - Blue Mountain Formation, 619.08-622.13 mBGS in DGR-4

3.8.5.2 Georgian Bay Formation Grey Shale

Regional data show that the Georgian Bay Formation is a bed of greenish to bluish grey shale, interbedded with limestone, siltstone and sandstone (Armstrong and Carter 2006). Generally, the abundance and thickness of non-shale constituents (i.e., limestone, siltstone and sandstone or “hard beds”) and overall carbonate content decreases with depth (Armstrong and Carter 2006).

Based on core logging, the Georgian Bay Formation at the DGR site is 88.2 to 90.9 m thick and the top of the formation is found at true vertical depths of 511.9 to 530.7 mBGS. The upper 30 m of the formation is dark grey-green shale with grey, fine- to medium-grained, occasionally fossiliferous limestone, siltstone and sandstone layers or hardbeds (see Figure 3.34). The lower 60 m of the formation is dark grey-green shale with occasional layers and laminations of fossiliferous limestone, siltstone and sandstone, the frequency of which decreases with depth. Core disking was prevalent in the Georgian Bay Formation 10 m below the top of the formation (see Figure 3.35). A possible gas-bearing and normally pressured feature was logged in core and by borehole acoustic televiewer at 585.9 mBGS in DGR-2 as a halite-infilled fracture with sulphurous and petroliferous odours. A similar subhorizontal normally pressured fracture was identified at 594.4 mBGS in the lower Georgian Bay in DGR-4.

Figure 3.34: Core Sample of Upper Georgian Bay Formation Interbedded Shale and Limestone, 542.25 mBGS, DGR-2

Figure 3.35: Core Disking in Upper Georgian Bay Formation Shale, 569.90 mBGS, DGR-2

Figure 3.36 shows the variation of stratigraphy evident within the Georgian Bay Formation in DGR-4 from core logging and from selected borehole geophysical logs. Due to the presence of carbonate hardbeds, the natural gamma and neutron logs exhibit a spikey appearance. This pattern decreases with depth as the frequency of hardbed occurrence decreases. Distinctive limestone hardbeds are evident as natural gamma lows and neutron highs at depths of 529.8 and 577.9 mLBGS. The lowest hardbed comprises fossiliferous limestone and is an identified marker bed for the Georgian Bay Formation (see Figure 3.48, Section 3.9). The normally pressured fracture at 594.4 mBGS is evident as a minor kick on the bed resolution density log and caliper log. The temperature variability log shows several minor kicks that appear to be related to halite-infilled fractures from which the halite has washed out or to siltstone/limestone beds.

A total of 43 core samples from the Georgian Bay Formation in DGR boreholes were subject to geochemical, mineralogical and/or petrographic analyses (TR-07-12, TR-08-01, TR-08-06, TR-08-20, TR-08-21, TR-08-22, TR-08-23, TR-08-29, TR-08-40, TR-09-05, TR-09-06).

Petrographic analysis of cores collected from the upper part of the Georgian Bay Formation shale shows the samples to be calcareous shale, calcareous siltstone and fossiliferous limestone. Petrographically, the core mineralogy in these cores is estimated as carbonates (20 to 75%), fossil fragments (10 to 35%), clays (20 to 40%), quartz (10 to 40%), anhydrite and halite (0 to 2.0%), and traces of pyrite, biotite, sericite and celestite.

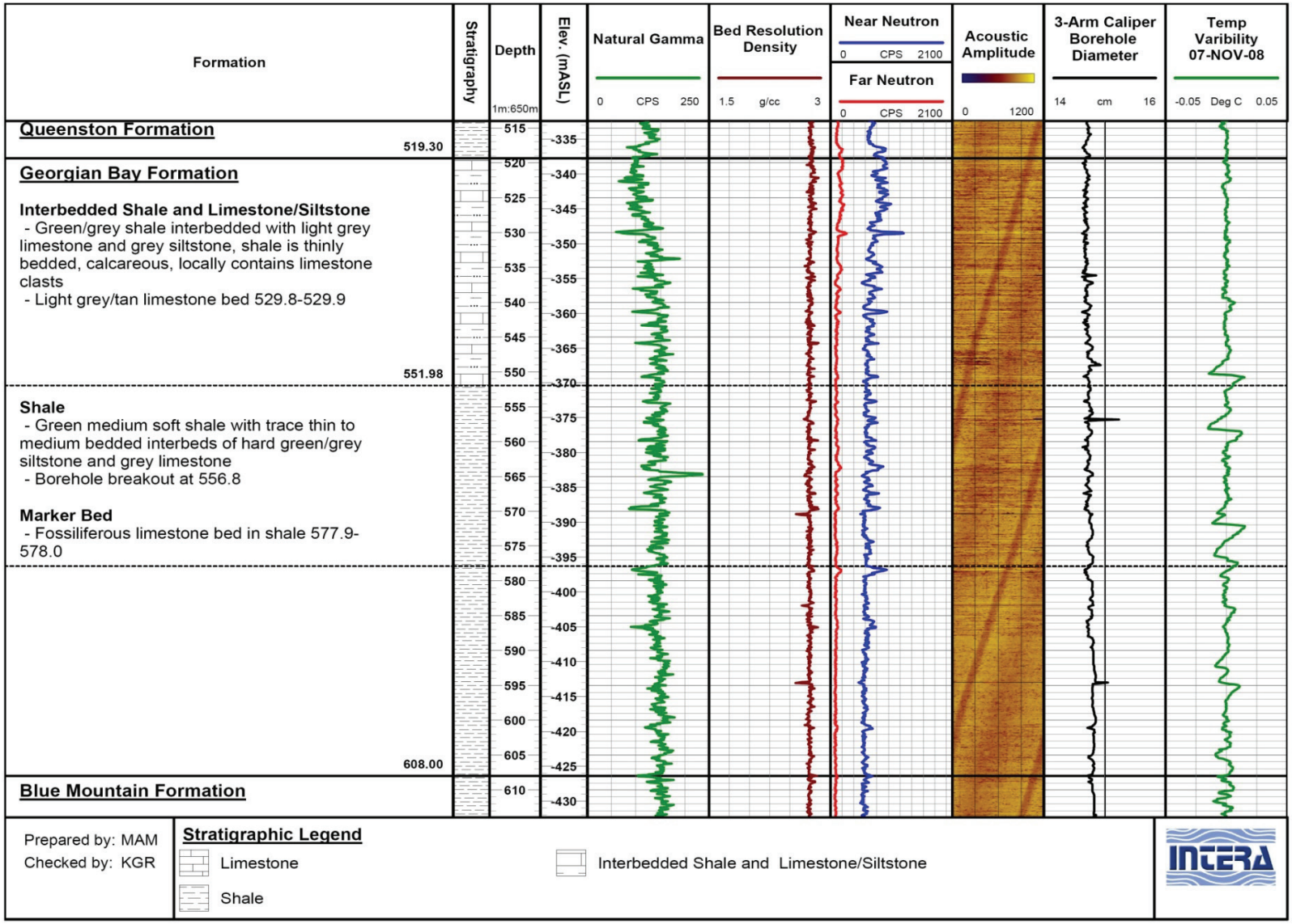

Figure 3.36: Stratigraphy of the Georgian Bay Formation in DGR-4 from Core Logging and Selected Borehole Geophysical Logs

Quantitative XRD analyses of the same core samples (Figures 3.5 and 3.6) identified similar mineralogy with the major minerals as illite (10 to 35%), quartz (16 to 53%), orthoclase (9 to 23%), dolomite (2 to 23%), chlorite (0.4 to 25%), calcite (1 to 19%) and pyrite (1.4 to 4.5%). These petrographic and XRD analyses are confirmed by the lithogeochemical analyses (Table 3.9, Figures 3.11, 3.12 and 3.13) which show the dominant elemental oxides are SiO_2 and Al_2O_3 with minor Fe_2O_3, K_2O, MgO and CaO and trace SO_4.

Petrographic analysis of cores collected from the lower part of the Georgian Bay Formation shale shows the samples to be fossiliferous dolostone/limestone and calcareous shale. Petrographically, the core mineralogy in these cores is estimated as carbonates (5 to 40%), fossil fragments (0 to 35%), clays (25 to 70%), quartz (0 to 10%), anhydrite and halite (0 to 2.0%), and traces of pyrite, sericite and celestite. Quantitative XRD analyses of the same core samples (Figures 3.5 and 3.6) identified generally similar mineralogy with the major minerals as quartz (16 to 43%), illite (23 to 40%), dolomite (1.3 to 55%), chlorite (4.6 to 19%), orthoclase (5 to 19%), calcite (2.4 to 19%) and pyrite (1.2 to 4.7%). These petrographic and XRD analyses are confirmed by the lithogeochemical analyses (Table 3.7, Figures 3.10 and 3.11) which show the dominant elemental oxides are SiO_2 and Al_2O_3 with minor Fe_2O_3, K_2O, MgO and CaO and trace SO_4.

Based on core logging of DGR boreholes (Table 3.3, Figures 3.3 and 3.4), the Georgian Bay Formation shale is unfractured to sparsely fractured with excellent core quality.

3.8.5.3 Blue Mountain Formation Dark Grey Shale

Regionally, the Blue Mountain Formation is a bed of dark grey-green to black, soft, non-calcareous shale with decreasing abundance of carbonate content and interbeds of limestone, siltstone and sandstone with depth (Armstrong and Carter 2006).

Based on core logging in DGR boreholes, the Blue Mountain Formation is 42.7 to 45.1 m thick with the top of the formation at true vertical depths of 600.1 to 619.4 mBGS. It was initially subdivided into an upper and lower member (TR-07-05, TR-08-12), based on Armstrong and Carter (2006). The upper member is typically a 38.1- to 41.1-m-thick sequence of dark greenish-grey shale interbedded with grey siliceous siltstone and sandstone layers and fossiliferous limestone layers. The lower member is a 4.0- to 4.6-m-thick bed of hard dark grey calcareous shale. Core disking was prevalent throughout the Blue Mountain Formation, particularly in the lower member (see Figure 3.37) although core quality observed immediately after core recovery to ground surface was excellent (Figure 3.33 – right). Sulphurous and petroliferous odours were also present throughout the formation. Because of the difficulty of the distinguishing the upper and lower members, the Blue Mountain Formation is considered a single lithological unit throught the remainder of the DGSM and for the presentation of data for the Blue Mountain Formation.

Petrographic analysis of cores collected from DGR boreholes from the upper member of the Blue Mountain Formation shows the samples to be very fine-grained, weakly laminated calcareous shale and calcareous siltstone. Petrographically, the mineralogy in these cores is estimated as illite and other clays (15 to 83%), carbonate (5 to 60%), quartz (1 to 10%), Fe-hydroxide (0 to 25%) and pyrite (0 to 3%). Quantitative XRD analyses of the same core samples (Figures 3.5 and 3.6) identified similar mineralogy with the major minerals as illite and chlorite, quartz with minor dolomite, calcite, feldspar pyrite and halite. These petrographic and XRD analyses are supported by the lithogeochemical analyses (Table 3.9, Figures 3.11, 3.12

and 3.13) which show the dominant elemental oxides are SiO_2 and Al_2O_3 with minor Fe_2O_3, K_2O, MgO and CaO and trace SO_4.

Figure 3.37: Core Disking of Lower Member, Blue Mountain Formation Shale, 652 mBGS, DGR-2

Petrographic analysis of cores collected from DGR boreholes from the lower member of the Blue Mountain Formation shows the samples to be very fine-grained, calcareous shale and siltstone. Petrographically, the mineralogy in the cores is estimated in order of decreasing abundance as illite and other clays, carbonates, quartz, K–feldspar, and Fe-hydroxide with traces of hematite and pyrite. Quantitative XRD analyses of the core samples (Figures 3.5 and 3.6) identified similar mineralogy with the major minerals as illite (29-40%), chlorite (5-17%), and quartz (25-35%) with minor dolomite (1.3-5.8%), calcite (3.0-5.3%), feldspar (2.0-16.1%) and pyrite (3.7-6.2%) with traces of halite (0.3-0.5%). These petrographic and XRD analyses are supported by the lithogeochemical analyses (Table 3.9, Figures 3.11, 3.12 and 3.13) which show the dominant elemental oxides are SiO_2 and Al_2O_3 with minor Fe_2O_3, K_2O, MgO and CaO and trace SO_4.

Based on core logging (Table 3.4, Figures 3.3 and 3.4), the Blue Mountain Formation shale with limestone interbeds in the DGR boreholes is unfractured to very sparsely fractured with excellent core quality. However, this formation is subject to rapid and extensive core disking upon recovery of core at ground surface (Figure 3.37).

3.8.6 Middle Ordovician Formations

The Middle Ordovician age formations encountered at the DGR site include the Cobourg (including the Collingwood Member), Sherman Fall and Kirkfield formations of the Trenton Group, and the Coboconk, Gull River and Shadow Lake formations of the Black River Group.

3.8.6.1 Cobourg Formation Black Shale and Argillaceous Limestone

Based on regional data, the Cobourg Formation is subdivided into upper and lower members. The upper or Collingwood Member, consists of dark grey to black, organic-rich, calcareous shale with very thin fossiliferous limestone interbeds. The Lower Member consists of very- fine- to coarse-grained, fossiliferous, bluish-grey to grey-brown argillaceous limestone (Armstrong and Carter 2006). The Lower Member of the Cobourg Formation is the proposed host rock for the DGR at the Bruce nuclear site. Unless otherwise indicated, reference to the Cobourg Formation in this report implies reference to the Lower Member of the Cobourg Formation.

Armstrong and Carter (2006) note that the Collingwood Member pinches out west of Port Elgin, implying this part of the formation may not be present at the Bruce nuclear site and that in southwestern Ontario the uppermost few metres of the Lower Member are dolomitized. Neither of these geologic conditions is evident in DGR boreholes. Armstrong and Carter (2010) also note that where the Collingwood is absent, a phosphatic lag is observed in the form of a thin phosphate horizon, unconformably separating the Cobourg and Blue Mountain Formations. At the Bruce nuclear site, both the Collingwood Member and a thin ~10 cm phosphatic lag are observed. Since both features are observed at the Bruce nuclear site it is presumed that several metres of the organic - rich upper portion of the Collingwood Member have been eroded at the Bruce nuclear site and the phosphates deposited unconformably on top.

Based on core logging in DGR boreholes, the entire Cobourg Formation is 35.0 to 36.5 m thick with the top of the formation at true vertical depths of 645.1 to 663.6 mBGS. The Collingwood Member is a 6.6- to 8.7-m-thick sequence of dark-grey to black calcareous shale interbedded with argillaceous limestone layers. The Lower Member is a 27.1- to 28.6-m-thick bed of light to dark brownish-grey, hard, mottled, very fine-grained to crystalline, fossiliferous, argillaceous limestone. Core disking was prevalent throughout the Collingwood Member, but was absent in the Lower Member. The contact between the Blue Mountain Formation and the Collingwood Member is shown in Figure 3.38. Figure 3.39 shows a typical intact core run of the Cobourg Formation approximately from the proposed repository depth of 677-680 mBGS in DGR-3.

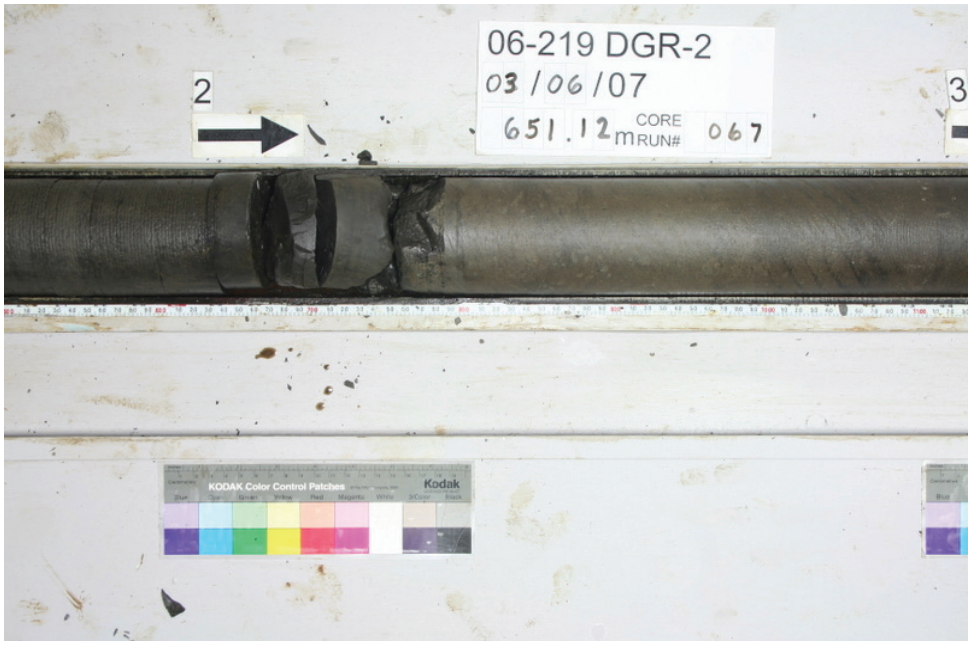

Figure 3.38: Contact between Dark Grey Blue Mountain Formation (Left) and Brownish-Grey Collingwood Member of the Cobourg Formation (Right), 651.6 mBGS in DGR-2

Figure 3.39: Intact Core Run from the Approximate Repository Depth in the Cobourg Formation, 677.04 - 680.08 mBGS in DGR-3

Figure 3.40 shows the variation of stratigraphy evident within the Collingwood Member and the Cobourg Formation in DGR-4 from core logging and from selected borehole geophysical logs. The natural gamma and neutron logs are informative showing the sharp contact between the Blue Mountain shale and calcareous shale of the Collingwood Member (see Figure 3.38 for core photo), the gradational contact between the Collingwood and the underlying Cobourg Formation, and the sharp contact with the underlying Sherman Fall Formation. The natural gamma, bed resolution density, neutron and caliper logs are relatively uneventful with the exception of highlighting two fractures associated with thin shaley beds at depths of 665.0 and 688.6 mBGS. Both of these features show gamma increases and neutron decreases reflecting the increased clay content and porosity of the shale bed. The lower fracture and shale bed which is shown in core in Figure 3.64, also shows a pronounced signature on the bed resolution log and the caliper logs. Based on the temperature variability log, both of these identified fractures appear to be tight.

Petrographic analysis of core collected from the Collingwood Member shows the samples to be fossiliferous limestone with minor mudstone domains. Petrographically, the core mineralogy is estimated as fossil fragments and carbonates (80-99%), and illite clays (0-20%) with accessory minerals of pyrite and quartz disseminated through the rock. Quantitative XRD analyses of the core samples (Figures 3.5 and 3.6) identified major minerals as calcite with minor dolomite, illite, chlorite and quartz and trace of pyrite and feldspar. The lithogeochemical analyses (Table 3.9, Figures 3.11, 3.12 and 3.13) support the XRD analyses showing the dominant elemental oxides are CaO and occasionally SiO_2, with minor Al_2O_3, MgO and Fe_2O_3. The laboratory petrographic, XRD and lithogeochemical analyses indicate that the tested cores include samples of the thin fossiliferous limestone interbeds, rather than the organic-rich calcareous shales.

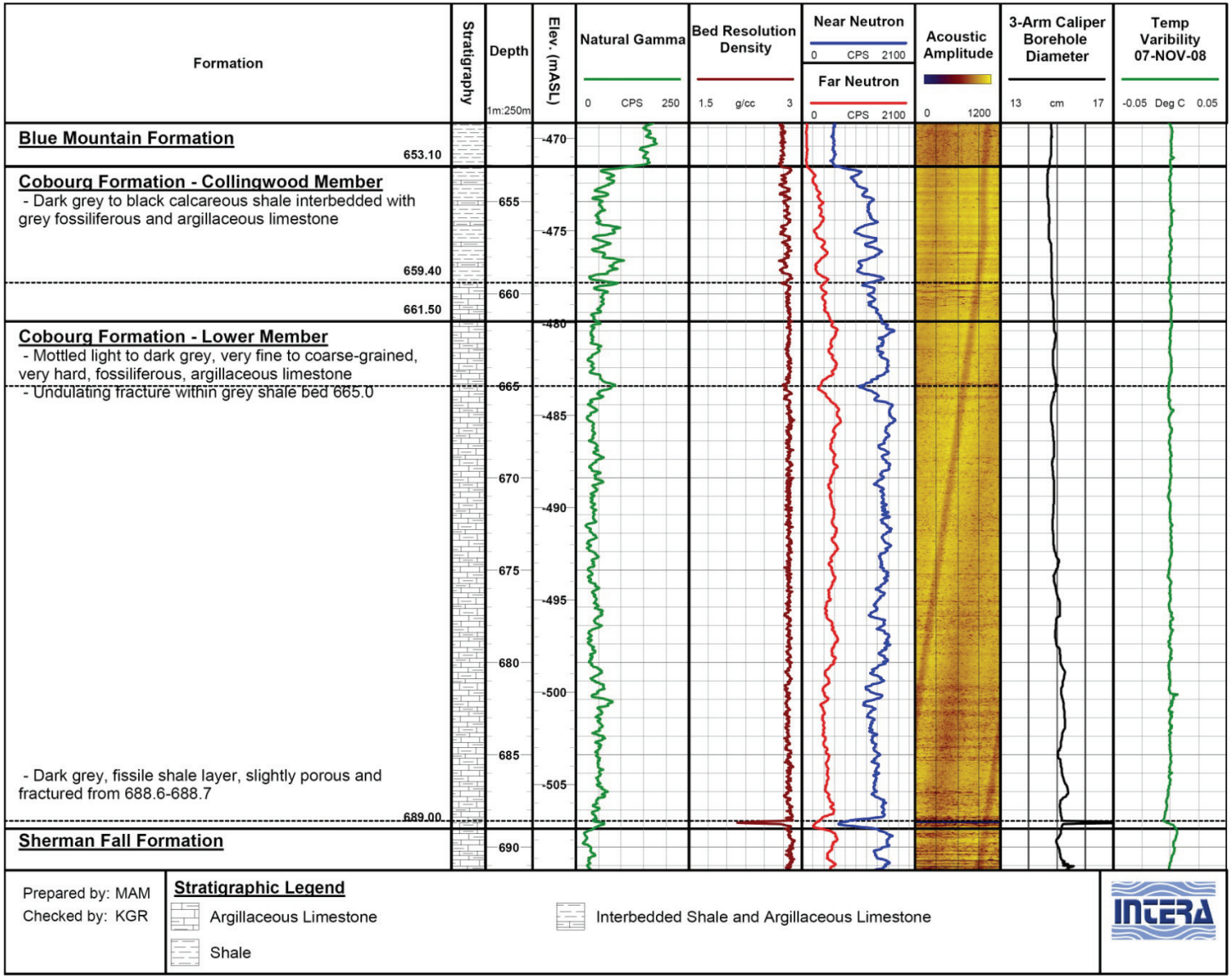

Figure 3.40: Stratigraphy of the Collingwood Member and Lower Member of the Cobourg Formation in DGR-4 Evident from Core Logging and Selected Borehole Geophysical Logs

Petrographic analysis of 20 cores collected from the Cobourg Formation (e.g., Figure 3.41) shows the samples to be fossiliferous argillaceous limestone – packstone/wackestone where the abundant recrystallized calcareous fossil fragments are contained in a fine-grained calcareous, Fe-stained clay matrix (micrite). Petrographically, the core mineralogies in these cores are similar, estimated as carbonates (10-50%), calcareous fossil fragments (35-60%), clays (5-20%) and pyrite (0-3%, see Figure 3.42), with accessory minerals of quartz and occasionally anhydrite. Quantitative XRD analyses of the core samples (Figures 3.6 and 3.7) identified similar mineralogy with the major minerals as calcite with minor dolomite, quartz and illite with traces of chlorite, pyrite and feldspar. These petrographic and XRD analyses are supported by the lithogeochemical analyses (Table 3.9, Figures 3.11, 3.12 and 3.13) which show the dominant elemental oxide is CaO with minor SiO_2, Al_2O_3, MgO, and K_2O and trace Fe_2O_3.

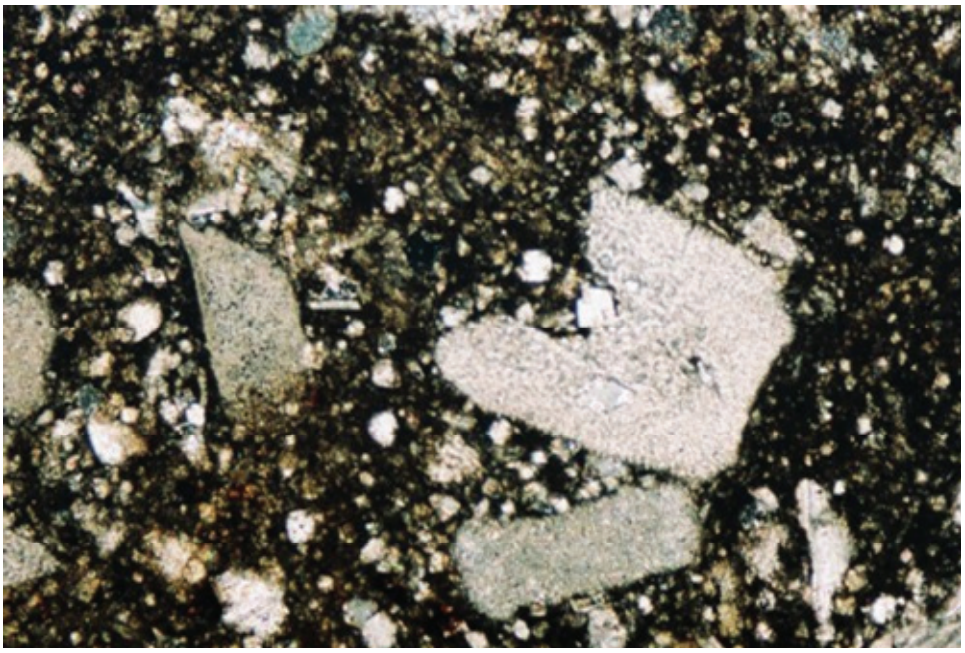

Figure 3.41: Calcareous Fossil Fragments within Illite- and Dolomite-Rich Clay Matrix, Cobourg Formation, 664.26 mBGS in DGR-4, Width of Photo 2.3 mm, Crossed Nicols

Based on core logging of DGR boreholes (Table 3.4, Figures 3.3 and 3.4), the Cobourg Formation shale and argillaceous limestone consisting of the Collingwood Member and the Lower Member, is unfractured to very sparsely fractured with excellent core quality.

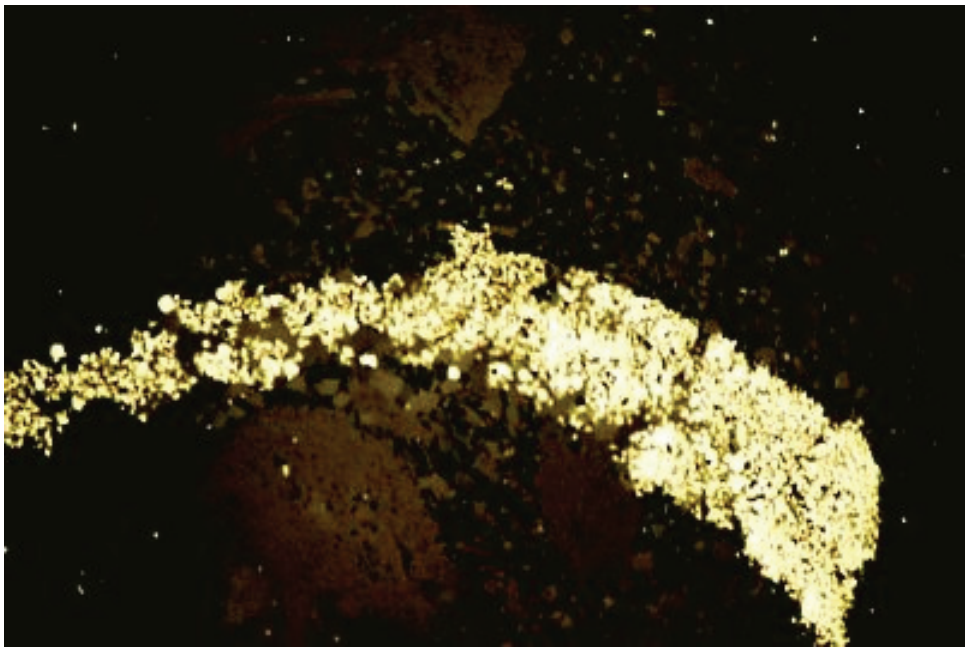

Figure 3.42: Very Fine-Grained Aggregates of Pyrite as a Vein or Fossil Replacement, Cobourg Formation, 768.58 mLBGS in DGR-6, Width of Photo 2.3 mm, Crossed Nicols

3.8.6.2 Sherman Fall Formation Argillaceous Limestone

Regionally, the Sherman Fall Formation consists of two members: a thinner upper member consisting of coarser-grained bioclastic or fragmental limestone and a thicker lower member of argillaceous fossiliferous limestone and shale (Armstrong and Carter 2006).

In DGR boreholes, the Sherman Fall Formation is 28.0 to 29.3 m thick with the top of the formation at true vertical depths of 680.2 to 700.1 mBGS. Although the upper and lower members are discussed in TR-07-05, they are not formally distinguished (i.e., see TR-08-12, TR-09-11) due to the difficulty in defining the contact between these two members in both core and borehole geophysical logs. The upper member is logged as a coarse-grained, grey-brown shaley limestone. The lower member is logged as an interbedded grey argillaceous limestone and dark grey calcareous shale (Figure 3.43). Overall, the Sherman Fall Formation is logged as an argillaceous limestone.

Petrographic analysis of core collected from the Sherman Fall Formation shows the samples to be similar as fine-grained fossiliferous limestone with varying amounts of fossil fragments, pyrite and Fe-staining of the calcareous clay matrix. Petrographically, the mineralogies in the cores are similar, estimated as carbonates (45 to 70%), calcareous fossil fragments (20 to 30%), clays (10 to 35%) and pyrite (trace to 5%), with accessory minerals of quartz, rutile and chalcedony. Quantitative XRD analyses of these core samples (Figures 3.5 and 3.6) identified similar mineralogy with the major minerals as calcite with minor dolomite, illite, chlorite and quartz, and trace pyrite and anhydrite. The petrographic and XRD analyses are supported by the lithogeochemical analyses (Table 3.9, Figures 3.11, 3.12 and 3.13) which show the dominant elemental oxide is CaO with minor SiO_2, Al_2O_3, and MgO, and trace K_2O, SO_4 and Fe_2O_3.

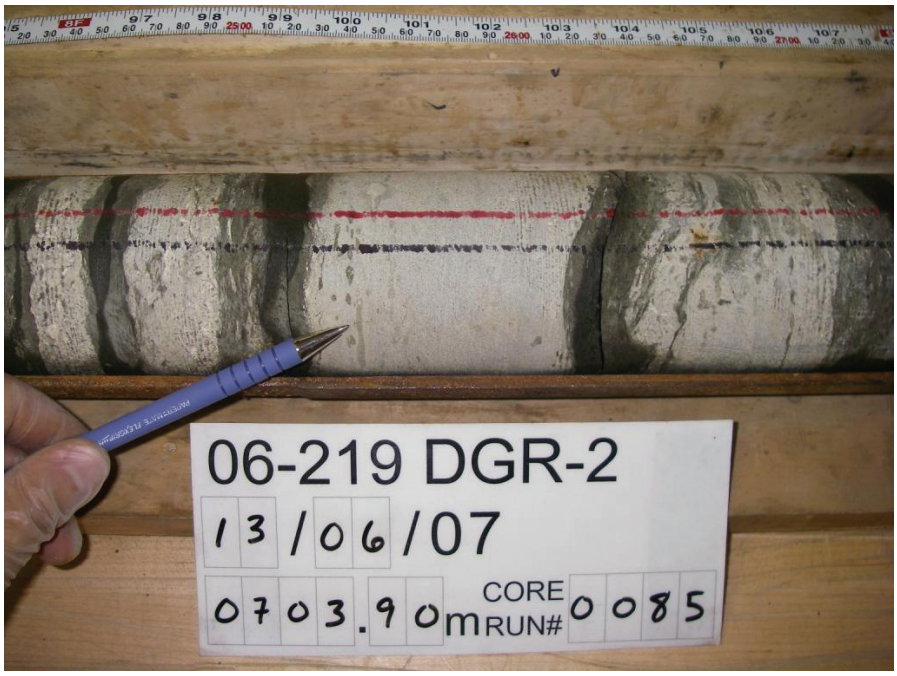

Figure 3.43: Core Sample of Lower Member of Sherman Fall Argillaceous Limestone, 703.90 mBGS, DGR-2

Based on core logging (Table 3.4, Figures 3.3 and 3.4), the Sherman Fall Formation argillaceous limestone is unfractured to very sparsely fractured with excellent core quality.

3.8.6.3 Kirkfield Formation Argillaceous Limestone

Based on regional information, the Kirkfield Formation is thin- to thick-bedded, fossiliferous limestone with shaley partings and locally significant thin shale interbeds (Armstrong and Carter 2006). Based on core logging in DGR boreholes, the Kirkfield Formation is 45.7 to 46.8 m thick with the top of the formation at true vertical depths of 709.0 to 729.0 mBGS. It is logged as a tan to dark grey, fine-grained, irregularly bedded, fossiliferous and argillaceous limestone with dark grey/green shale interbeds. It is distinguished from the overlying Sherman Fall Formation by a minor decrease in natural gamma response on the borehole geophysical logs. Some of the shale interbeds near the base of the formation exhibit petroliferous odours (Figure 3.16).

Petrographic analysis of core collected from the Kirkfield Formation shows the samples to be fossiliferous shale and bioclastic argillaceous limestone comprised of large fossil fragments with carbonate-rich and clay–rich domains. The clay domains contain dolomite grains. Petrographically, the core mineralogy is estimated as carbonates (25-65%), fossil fragments (30-50%), and Fe-stained clays with illite (4-25%) with accessory minerals of pyrite, pyrrhotite, and quartz disseminated through the rock. Veins are noticeably absent in all samples analysed. Quantitative XRD analyses of the same core samples (Figures 3.5 and 3.6) identified similar mineralogical composition from the petrography with the major mineral as calcite with minor dolomite, quartz and illite and trace feldspar and pyrite. The lithogeochemical analyses (Table 3.9, Figures 3.11, 3.12 and 3.13) support the XRD analyses showing limited amounts of SiO_2 and Al_2O_3 (i.e., aluminosilicates or clays). The dominant elemental oxide is CaO, with minor SiO_2, Al_2O_3, MgO and K_2O.

Based on core logging of the DGR boreholes (Table 3.4, Figures 3.3 and 3.4), the Kirkfield Formation argillaceous limestone is unfractured to very sparsely fractured with excellent core quality. As evident in Figure 3.4 and Table 3.5, fracturing of the Kirkfield Formation is noticeably higher in DGR-4 than in DGR-2, DGR-3, DGR-5 or DGR-6. The increased fracturing evident in DGR-4 is likely reflective of spatial variability of fracturing in the Kirkfield Formation. The low minimum core recovery and RQD values listed in Table 3.4 are from one core run (DGR-2, CR-90) that experienced difficult drilling conditions resulting in grinding and breaking of the core.

3.8.6.4 Coboconk Formation Bioturbated Limestone

Regionally, the Coboconk Formation consists of light grey-tan to brown-grey, medium- to very thick-bedded, fine- to medium-grained, bioturbated bioclastic limestone (Armstrong and Carter 2006).

The Coboconk Formation at the DGR site is 22.4 to 23.8 m thick with the top of the formation at true vertical depths of 755.8 to 774.9 mBGS. It is logged in DGR boreholes as a light- to medium-grey, very fine-grained, very hard, bioturbated limestone with minor dark grey/green shale interbeds. The bioturbation (stirring or mixing of sediment by organisms, especially burrowing or boring) results in a characteristic mottled texture with frequent stylolites and nodules. The Coboconk Formation is distinguished from the overlying Kirkfield Formation by a significant decrease in natural gamma response on the borehole geophysical logs reflecting a decrease in shale content. This distinction is also very clear in the recovered core.

Parts of the lower half of the Coboconk Formation is petroliferous with minor out-gassing and hydrocarbon bubbling from styolites and some thin vuggy zones (Figure 3.16). A thin volcanic ash bed, which is a DGR formation marker bed used to accurately determine formation strike and dip, was logged in all boreholes (except DGR-5 which was terminated above this ash layer), in the upper third of the formation (see Figure 3.44). Although the mineralogy of the ash layer was not determined in this study, published work by Kolata et al., (1998) indicates the altered ash is primarily K-bentonite associated with volcanism during the Taconic orogeny. A second DGR formation marker bed consisting of a tan dolostone bed is also present within the bottom third of the Coboconk Formation.

Petrographic analysis of cores collected from the middle sections of the Coboconk Formation shows the samples to be partly dolomitized bioclastic limestone to very fine-grained fossiliferous limestone with traces of Fe-stained clays and pyrite. Quantitative XRD analyses of the core samples (Figures 3.5 and 3.6) show major mineralogy as calcite with minor dolomite and clays with trace quartz, pyrite and anhydrite. The petrographic and XRD analyses are supported by the lithogeochemical analyses (Table 3.9, Figures 3.11, 3.12 and 3.13) which show the dominant elemental oxide is CaO with minor SiO_2, MgO and Al_2O_3, and trace SO_4 and Fe_2O_3.

Based on core logging of DGR boreholes (Table 3.4, Figures 3.3 and 3.4), the Coboconk Formation bioturbated limestone is unfractured to sparsely fractured with excellent core quality. As with the overlying Kirkfield Formation, fracturing within the Coboconk Formation is higher in DGR-4 than in DGR-2, DGR-3 or DGR-6.

Figure 3.44: Volcanic Ash Bed, Coboconk Formation, 768.6 mBGS, DGR-2

3.8.6.5 Gull River Formation Lithographic Limestone

Based on regional logging, the Gull River Formation, especially the upper part, is characterized by very fine-grained (lithographic), light grey to dark brown limestone, with lesser amounts of dolostone, shale and argillaceous sandstone (Armstrong and Carter 2006). The abundance of lime mud is noted by Armstrong and Carter (2006) as the distinguishing characteristic of the Gull River Formation as compared to the coarser-grained limestones of the overlying Coboconk Formation. The lower part of the formation is lithologically variable, consisting of fine-grained dolostones, fossiliferous limestones, sandy dolostones and minor shale (Armstrong and Carter 2006).

Based on core logging in DGR boreholes, the Gull River Formation is 51.7 to 53.6 m thick with the formation top at true vertical depths of 778.1 to 798.6 mBGS. It is logged as a medium grey, fine- to very-grained (lithographic), fossiliferous, limestone/mudstone with thin dark grey shale interbeds. It is distinguished from the overlying Coboconk Formation by a minor and spikey increase in natural gamma response on the borehole geophysical logs. Selected thin vuggy and styolitic sections of the Gull River Formation are slightly petroliferous showing out-gassing and traces of liquid hydrocarbons (see Figures 3.16 and 3.45).

Figure 3.46 shows the variation of stratigraphy within the Coboconk and Gull River formations in DGR-3 from core logging and from selected borehole geophysical logs. The natural gamma, bed resolution density, neutron, caliper, acoustic televiewer and temperature variability log are diagnostic of several important stratigraphic and hydrogeologic features. The gradational contact between the Kirkfield and the Coboconk formations is evident in the natural gamma logs as is the contact between the Coboconk and the Gull River formations. The natural gamma and

neutron logs are noticeably spikier in the Gull River Formation than in the Coboconk Formation. Two marker beds (volcanic ash bed at 781.0 mBGS and tan dolostone bed at 790.5 mBGS) are evident within the Coboconk Formation based on geophysical log signatures. The ash bed which is shown in core in Figures 3.44 and 3.49 is evident as a gamma high, bed resolution density low, neutron low and caliper high, reflecting the increased clay content and porosity of the ash. The tan dolostone bed is apparent based primarily on a neutron low reflecting increased porosity. The temperature variability log suggests some minor permeability may be associated with the Coboconk ash marker bed and in the lower part of the Gull River Formation at 839-840 mBGS in DGR-3.

Figure 3.45: Trace of Hydrocarbon Weeping from Stylolites, Gull River Formation, 817.0 mBGS in DGR-2

Petrographic analysis of core collected from the Gull River Formation shows the samples to be bioclastic argillaceous limestone with some fine-grained micritic dolomite with Fe-stained clays. Petrographically, the core mineralogy of the samples was estimated as carbonates (70-100%) and Fe-stained clays (0-30%). Quantitative XRD analyses of the core samples (Figures 3.5 and 3.6) identified similar mineralogical composition with the major minerals as calcite and dolomite with minor feldspar, illite and quartz and trace pyrite and anhydrite. These petrographic and XRD analyses are confirmed by the lithogeochemical analyses (Table 3.9, Figures 3.11, 3.12 and 3.13) which show the dominant elemental oxides are CaO and MgO with minor to trace SiO_2, Fe_2O_3, and Al_2O_3.

Based on core logging of DGR boreholes (Table 3.4, Figure 3.3 and 3.4), the Gull River Formation lithographic limestone is unfractured to sparsely fractured with excellent core quality. As with the overlying Kirkfield and Coboconk formations, fracturing within the Gull River Formation is higher in DGR-4 than in DGR-2 or DGR-3. This increased fracturing is likely reflective of spatial variability of fracturing in DGR-4.

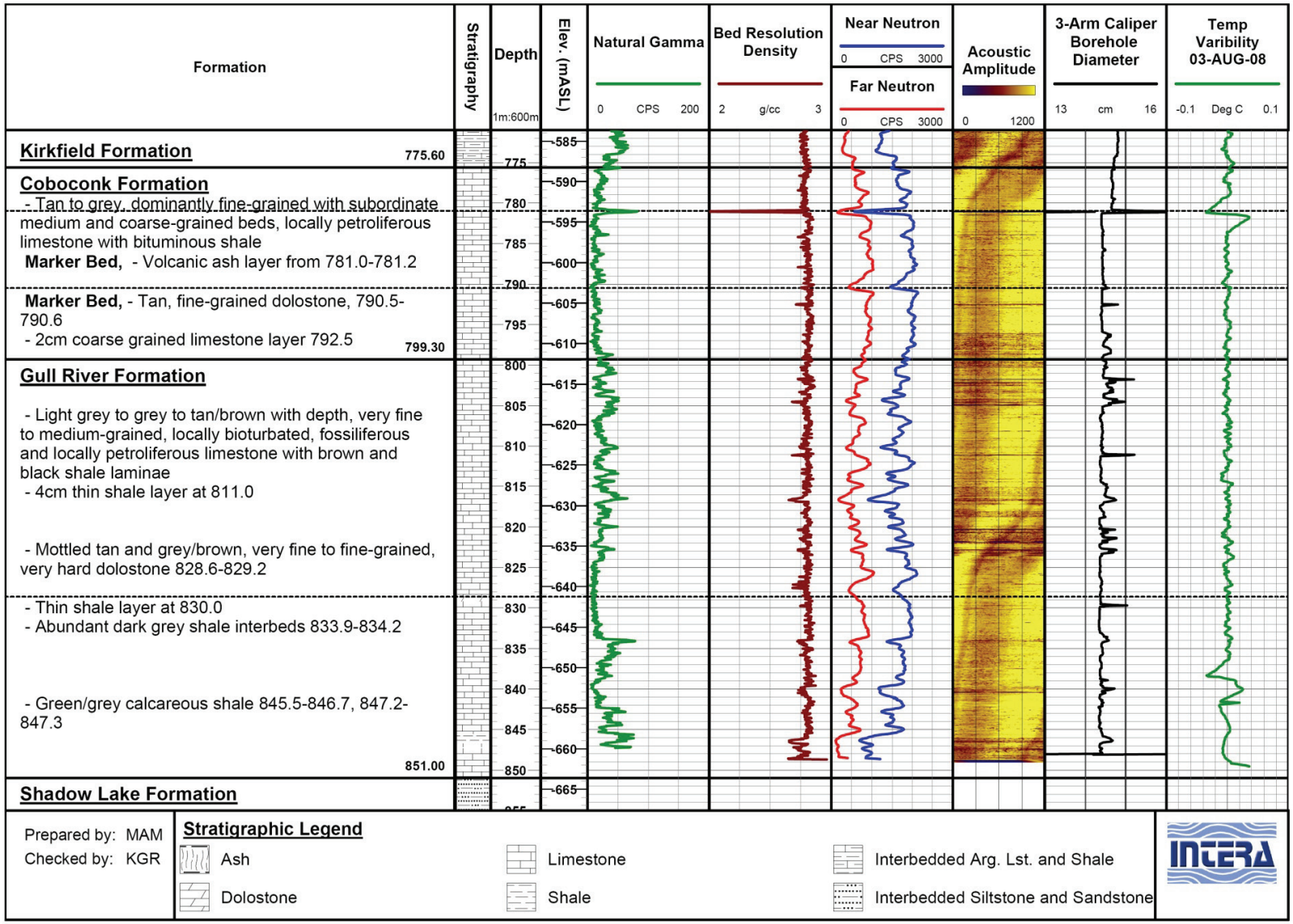

Figure 3.46: Stratigraphy of the Coboconk and Gull River Formations in DGR-3 from Core Logging and Selected Borehole Geophysical Logs

3.8.6.6 Shadow Lake Formation Siltstone and Sandstone

Regionally, the Shadow Lake Formation is recognized as comprising red and green sandy shales, argillaceous and arkosic sandstones and minor sandy argillaceous dolostones (Armstrong and Carter 2006). Green glauconitic sandstone is also recognized as a common lithofacies of the Shadow Lake Formation. The formation has variable thickness due to the irregular paleo-topography of the Precambrian basement, with a maximum reported thickness of 15 m (Armstrong and Carter 2006).

The Shadow Lake Formation at the DGR site is 4.5 to 5.2 m thick with the top of the formation at true vertical depths of 838.6 to 850.3 mBGS. It is logged in DGR boreholes as a poorly sorted mix of grey-green sandy mudstone and green-grey siltstone and sandstone. The top of the Shadow Lake Formation is distinguished from the overlying Gull River Formation by the presence of the first grey-green silty sandstone layer. The sandstone layers have increasing grain size with depth and are glauconitic with pyrite and traces of liquid hydrocarbon.

Petrographic analysis of cores collected from the Shadow Lake Formation shows the samples to be partly dolomitized silty limestone with traces of pyrite to silty sandstone comprised of quartz, K-feldspar, clay and pyrite. Quantitative XRD analyses of one of the core samples (Figures 3.5 and 3.6) shows mineralogy as dolomite with minor clays and quartz and trace pyrite. The petrographic and XRD analyses indicate that the tested core sample is representative of a locally dolomitized layer of siltstone with limited shale or sandstone. No samples of the Shadow Lake Formation were submitted for lithogeochemical (i.e., major oxide) analyses.

Based on core logging of DGR boreholes (Table 3.4, Figures 3.3 and 3.4), the Shadow Lake Formation siltstone and sandstone is unfractured to very sparsely fractured with excellent core quality.

3.8.7 Cambrian Sandstone

Regionally, the Cambrian rocks are dominated by the presence of quartzose sandstones. Lithologically, the Cambrian succession in southwestern Ontario consists of, in descending order, dolostones, interbedded sandstones and dolostones, and quartzose sandstones (Armstrong and Carter 2006). The Cambrian has highly variable thickness due to the irregular paleo-topography of the Precambrian basement.

The top of the Cambrian sandstone was found at true vertical depths of 843.8 to 854.8 mBGS in DGR-2, DGR-3 and DGR-4. However, DGR-2 is the only borehole that drilled completely through this unit, yielding 16.9 m of total thickness. It is logged as a tan to orange-grey, fine- to medium-grained, very hard, silty sandstone/sandy dolostone with clasts of granitic gneiss and calcite veins. The upper part of the formation is tan to grey, sandy siltstone to sandstone interbedded with fine-grained sandy dolostone that grades with depth into cream to orange-brown, coarse-grained quartz sandstone. Dolomitization of the upper parts of the unit are significant ranging up to 100%, and decreasing to about 0% near the bottom of the unit (Figure 3.14). The bottom third of the Cambrian is a coarse-grained, orange-brown stained quartz sandstone with local glauconitic stringers. Figure 3.47 shows a portion of the core collected from the middle of the Cambrian sandstone in DGR-2.

Petrographic analysis of core collected from the upper and middle parts of the Cambrian shows the samples to be medium-grained, recrystallized dense dolostone and limestone with interstitial

detrital quartz and lesser amounts of feldspars and pyrite that grades with depth into quartz sandstone with K-feldspar.

Figure 3.47: Light Brown Cambrian Sandstone, 850.67 mBGS, DGR-2

Petrographically, the mineralogy of the upper cores is estimated as carbonates (90-95%), quartz (3-5%), plagioclase (trace-0.5%), and pyrite (trace-7%) with traces of K-feldspar, marcasite and Fe-stained quartz. Quantitative XRD analyses of these upper cores (Figures 3.5 and 3.6) identified similar mineralogical composition with the major minerals as dolomite and quartz with minor clays and feldspar and trace pyrite. These petrographic and XRD analyses of the upper parts of the Cambrian are confirmed by the lithogeochemical analyses (Table 3.9, Figure 3.11, 3.12 and 3.13) which show the dominant elemental oxides are CaO and MgO with minor SiO_2, and trace Fe_2O_3 and Al_2O_3.

The middle parts of the Cambrian show petrology comprised of microcrystalline to medium-grained quartz/chert/ chalcedony (80%) and pyrite (7%) hosted by quartz- and carbonate-rich sediments. Quantitative XRD analyses of cores collected from the middle section of the Cambrian strata (Figures 3.5 and 3.6) identified major minerals as quartz, calcite and pyrite with minor illite, feldspars and kaolinite clays and traces of dolomite, gypsum and anhydrite. Lithogeochemical analyses (Table 3.9, Figure 3.10, 3.11, 3.12 and 3.13) support these petrographic and mineralogical analyses, showing dominant elemental oxides as SiO_2, CaO and Fe_2O_3 with trace amounts of Al_2O_3 and MgO.

Core logging of DGR boreholes (Table 3.4, Figures 3.3 and 3.4) shows the Cambrian sandstone is moderately fractured with excellent core quality.

3.8.8 Precambrian

The Precambrian in southwestern Ontario is part of the Central Gneiss Belt of the Precambrian Grenville Province. This basement formation consists of a variety of metamorphic rock types ranging from felsic gneisses to mafic metavolcanics to marble (Armstrong and Carter 2006). The rocks are typically gneissic with a well-developed mineral foliation parallel to gneissosity. The upper several metres of the Precambrian basement is often comprised of a weathered alteration zone.

Borehole DGR-2 intersects 1.55 m of the Precambrian basement at the DGR site; no other boreholes went deeper than the middle of the Cambrian. Based on core logging in DGR-2, the top of the Precambrian basement is found at a true vertical depth of 860.7 mBGS. The Precambrian basement is logged as a pink to grey, fine- to medium-grained, felsic granitic gneiss. The core observations indicate some alteration of the Precambrian with extensive red to green and black staining evident in the upper 1.2 m (see Figure 3.56).

Petrographic analysis of core collected from the upper part of the Precambrian at 861.90 mBGS in DGR-2 shows the sample to be granitic gneiss with quartz, K-feldspar and biotite with minor muscovite alteration and traces of rutile and pyrite. Quantitative XRD analyses of the core sample shows mineralogy as K-feldspar (40%), quartz (24%), clays (23.0%), dolomite (5.0%), calcite (4.0%), albite (4.0%) and pyrite (0.2%).

Based on very limited core logging of DGR-2 (Table 3.4, Figures 3.3 and 3.4), the Precambrian granitic gneiss is very sparsely fractured with excellent core quality.

3.9 Marker Beds

For many of the formations identified in DGR boreholes, the contacts are abrupt and easily discernable from inspection of core and review of borehole geophysical logs. For example, selection of the contacts for the Salina F Unit shale, the Guelph Formation vuggy dolostone, the Cabot Head Formation shale, the Cobourg Formation limestone and the Shadow Lake Formation siltstone and sandstone is unambiguous when core is available. However, for many of the other formations, the contacts are gradational and required some judgment on making formation top picks.

To assist in assessment of formation orientation, several thin, laterally continuous, diagnostic marker beds were identified in DGR core (TR-08-12, TR-09-11). These marker beds are typically 10-20 cm thick beds with visually identifiable lithofacies features and/or borehole geophysical logging signatures that are distinct from the surrounding rocks. Noteworthy marker beds identified to date in boreholes DGR-1 to DGR-6 are listed in Table 3.12. Figures 3.48 and 3.49 show the appearance of two of these marker beds (Georgian Bay fossiliferous limestone bed and Coboconk ash layer) in DGR borehole core photographs.

Table 3.12 lists the depth of occurrence of these marker beds along each DGR borehole and the calculated strike and dip of the marker beds based on intersections in the three vertical boreholes DGR-1/DGR-2, DGR-3 and DGR-4. Because the upper parts of DGR-5 and DGR-6 were not cored, and the termination of drilling of these boreholes in the Kirkfield and Gull River formations, respectively, all marker beds were not cored in all DGR boreholes. As shown in Table 3.12, the marker bed orientations are consistent with the conclusions of Section 3.5 and the data in Table 3.2, that indicate the orientations of the Paleozoic formations below the

Salina B Unit are remarkably uniform and consistent with average regional strike/dip estimates of about N20°W/0.6°SW.

Table 3.12: Summary of Marker Bed Descriptions, Depths along Boreholes and Orientations in DGR Boreholes

Formation	Marker Bed or Horizon	Depth (mLBGS)					Orientation	
		DGR-1/2	DGR-3	DGR-4	DGR-5	DGR-6	Strike	Dip
Salina F Unit	brown dolostone bed in grey shale	182.0	200.7	181.5	--	--	N32°W	0.98°SW
Queenston	limestone bed in shale	504.3	517.7	505.6	546.0	568.6	N17°W	0.61°SW
Georgian Bay	fossiliferous limestone bed in grey shale	576.5	589.2	577.9	622.3	649.6	N14°W	0.56°SW
Coboconk	dark grey volcanic ash bed in grey limestone	768.8	781.0	769.0	--	876.7	N19°W	0.55°SW
Coboconk	tan dolostone bed in grey limestone	778.7	790.5	778.3	--	888.0	N22°W	0.54°SW

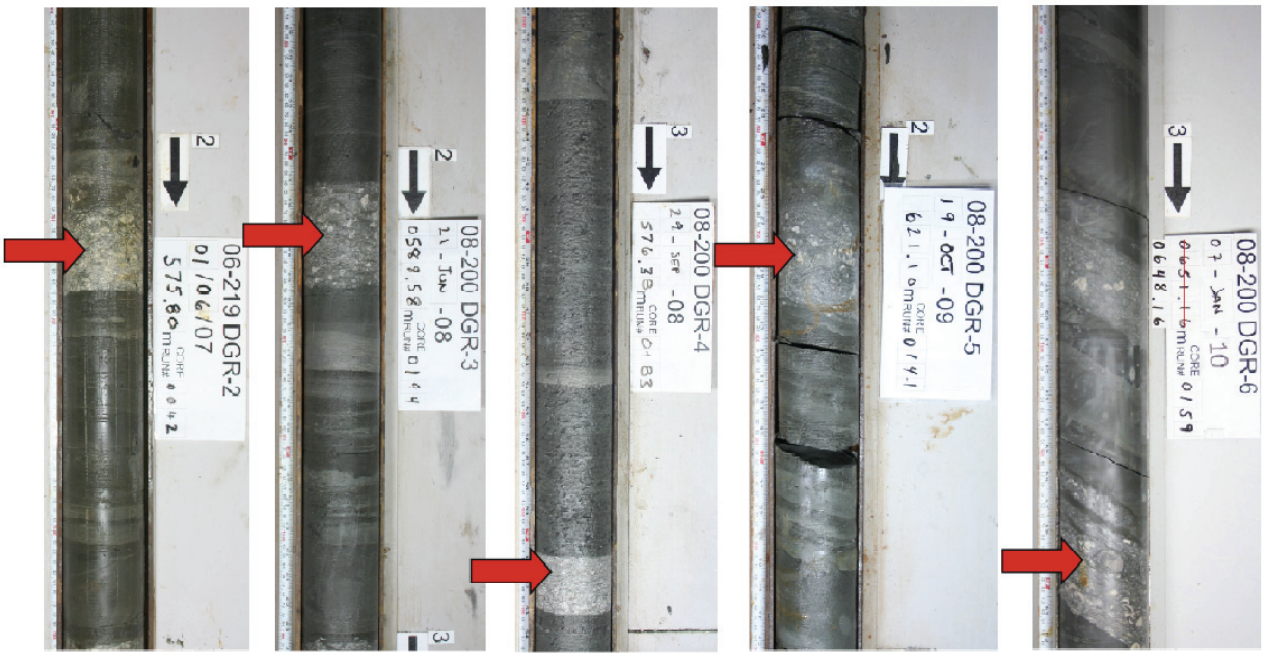

Figure 3.48: Fossiliferous Limestone Marker Bed within Georgian Bay Formation Shale in DGR Boreholes

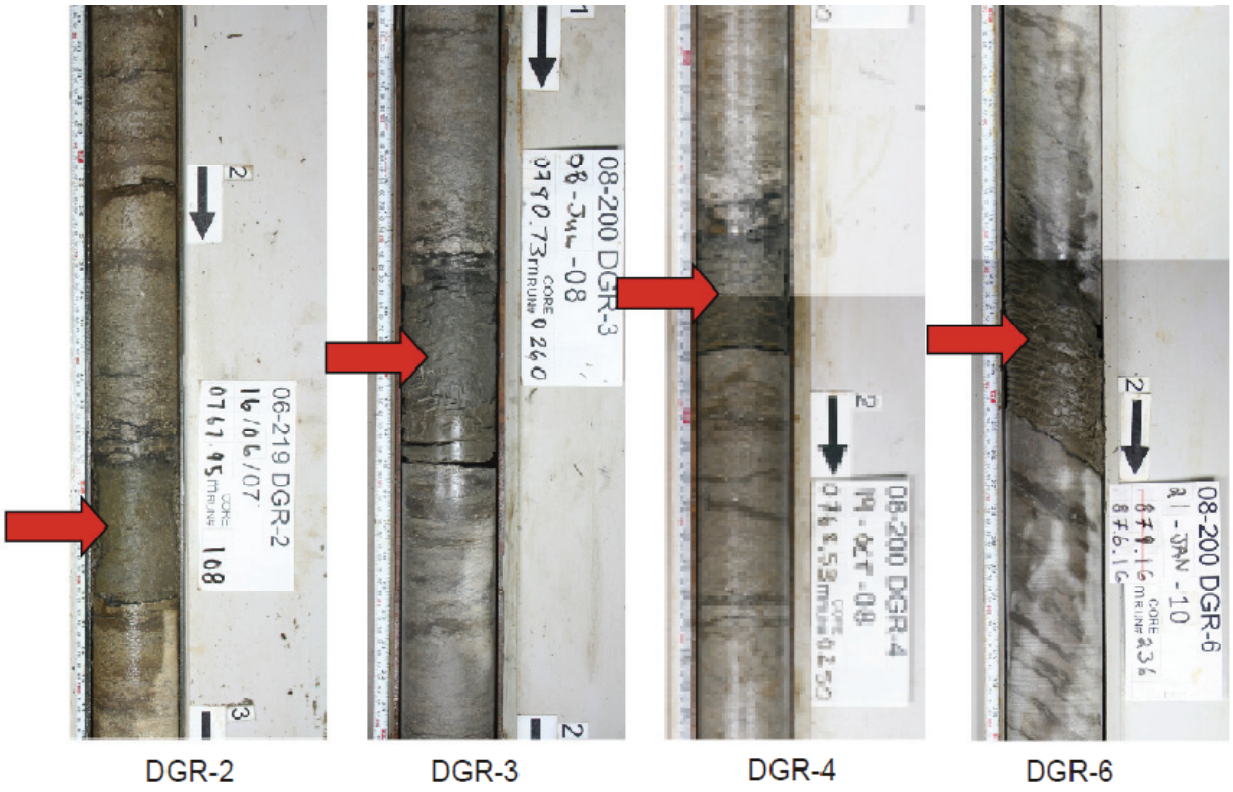

Figure 3.49: Volcanic Ash Marker Bed within Coboconk Formation Bioturbated Limestone in DGR Boreholes

3.10 Fracture Infill, Veins and Other Secondary Mineralogy

Fracture infill, veins and other secondary minerals including nodules were observed during core logging (TR-07-05, TR-07-06, TR-08-13, TR-09-01), laboratory petrographic analyses (TR-07-12, TR-08-06, TR-08-20, TR-08-21, TR-08-40, TR-09-05), and XRD and SEM/EDS mineralogical testing (TR-08-01, TR-08-06, TR-08-22, TR-08-23, TR-08-40, TR-09-06) of DGR-1 to DGR-6 core samples.

3.10.1 Core Logging

Logging of recovered core identified a full suite of fracture infill (see Figures 3.50 and 3.51), vein and other secondary mineral features including nodules. This suite included chert, quartz, calcite, pyrite, halite, anhydrite, gypsum, celestite, Fe oxide/hydroxide and clay. Halite was found in core intermittently in the Salina Formation and commonly from the Guelph Formation through the Ordovician shales and occasionally in the Cobourg and Sherman Fall limestones (Figure 3.9). Anhydrite was frequently observed from the Bass Islands Formation to the Coboconk Formation. Gypsum was observed in the Salina G to A2 Units. Generally, although occasionally ambiguous, differentiation of anhydrite from gypsum was done in the field based on hardness and colour. However, in many samples both anhydrite and gypsum are present (see Figure 3.19). Calcite and pyrite were observed from the Amherstburg Formation to the Shadow Lake Formation.

Figure 3.50: Orange Halite and Calcite Fracture Infill in the Queenston Formation Shale at 456.01 mBGS in DGR-1

Figure 3.51: Partially Washed-out, White Halite Fracture Infill in the Lower Georgian Bay Formation Shale at 680.25 mLBGS in DGR-6

Soluble fracture infill minerals were commonly observed in the Upper Ordovician shales. Samples of the upper Queenston Formation shale in all DGR boreholes contained prominent halite-filled fractures that were bounded by a carbonate mineral lining the fracture wall (see Figures 3.28 and 3.50). Other Queenston samples displayed calcite, anhydrite, celestite and gypsum veins. Within the Georgian Bay Formation shales, illite- and calcite-filled veins were observed as were narrow halite-infilled fractures and veins (see Figure 3.51). Pyrite and illite veins were observed in the Blue Mountain shale.

3.10.2 Petrographic and XRD/SEM Analyses

Petrographic analyses of DGR cores indicated the frequent occurrence of 'vein' minerals. The use of the term 'vein' does not necessarily imply any hydrothermal origin of these infill materials, merely that the minerals appear to be secondary infilling features. Some of the identified vein minerals may be the result of simple secondary precipitation reactions that have occurred at ambient temperatures. The vast majority of observed vein minerals as defined here occur as features within the intact rock and therefore represent sealed or healed discontinuities or fractures.

Devonian cherty dolostones often contained quartz and chert veins within shale interbeds. The Silurian core samples frequently displayed both gypsum and anhydrite veins in dark shales and iron-stained illite veins in fossiliferous dolostone. Many of the vein minerals identified in the brecciated Salina F, E and B Units are related to the healing of fractures following collapse and settlement due to underlying salt bed dissolution.

Soluble minerals (e.g., halite, calcite and to a lesser extent gypsum, anhydrite and celestite) were frequently detected as distinct veins and as interstitial material in the Ordovician shales by petrography and XRD/SEM mineralogical analyses. Figure 3.52 shows the chevron texture remnants of a halite-infilled vein in a thin section of the Georgian Bay Formation in DGR-2. Figure 3.53 shows the thin section occurrence of calcite, celestite and halite within a composite vein in Georgian Bay Formation shale in DGR-5.

Occasionally, these same soluble minerals of halite, celestite and calcite were also detected within the Silurian shales and dolostones (Figure 3.54). Petrographic and XRD/SEM analyses also frequently detected the presence of minor to trace amounts of other secondary minerals including illite, dolomite, feldspars, pyrite, marcasite and sphalerite. However, porewater evaporation during laboratory sample preparation may have caused tertiary minerals to precipitate (Section 3.7.1.2). Minerals detected only by SEM/EDS without supporting visual or XRD evidence should be interpreted with care.

Figure 3.54 shows the SEM/EDS analyses of a sample of Guelph Formation dolostone collected from a depth of 391.34 mBGS in DGR-3 (TR-08-40). Image A shows a vein in dolomitized rock filled by dolomite crystals and paragenetically later halite. Black areas on these photomicrographs correspond to remaining porosity. The host rock contains traces of disseminated pyrite as white dots. Image B shows EDS analysis of the point indicated in image A, corresponding to halite. The small peaks of Ca, Mg and O are due to the matrix effect of the nearby dolomite. Images C to F show analysis of a small (about 50 µm thick) veinlet filled by dolomite and later calcite and halite. Black areas on these images are remaining porosity. Image E shows EDS analysis of the point shown in image F, corresponding to calcite. The small peaks of Mg, Cl and Na are due to the nearby presence of halite and dolomite. All pictures in Figure 3.54 are back-scattered electron views of uncoated thin sections.

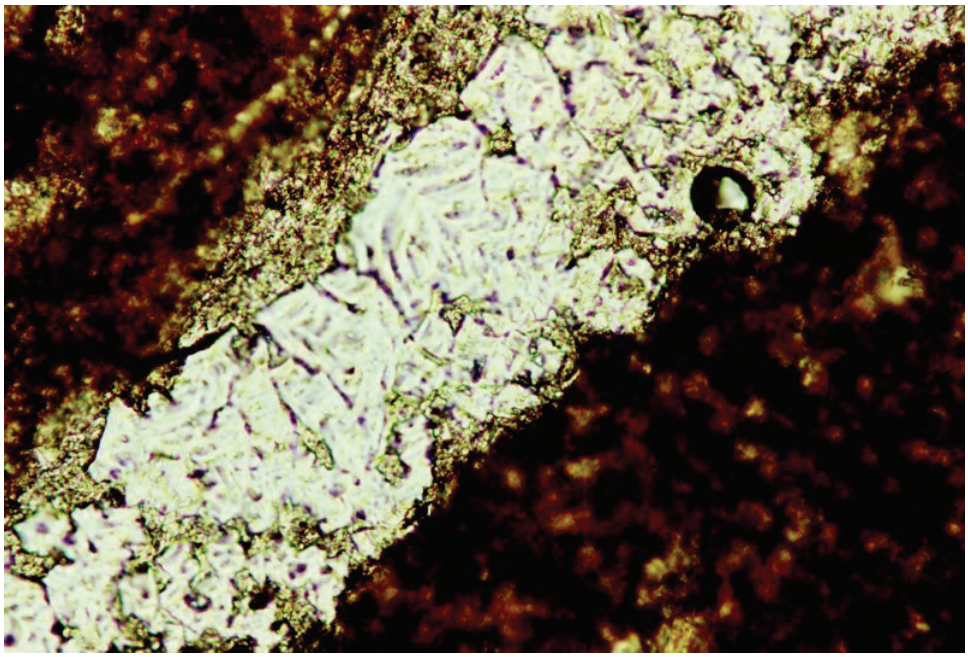

Figure 3.52: Halite Vein in Georgian Bay Formation Shale at 606.96 mBGS in DGR-2, Width of Photo: 0.34 mm, Plane Polarized Light

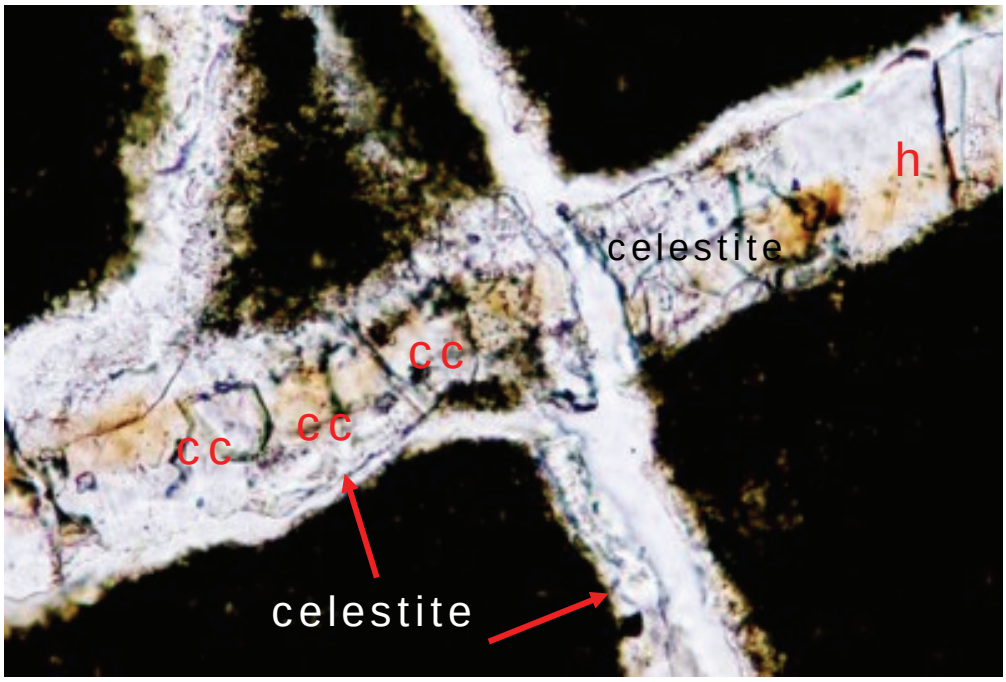

Note. Width of photo: 0.45 mm, plane polarized light.

Figure 3.53: Composite Vein Consisting of Halite (h), Celestite and Calcite (cc) in Georgian Bay Formation Shale at 605.55 mLBGS in DGR-5

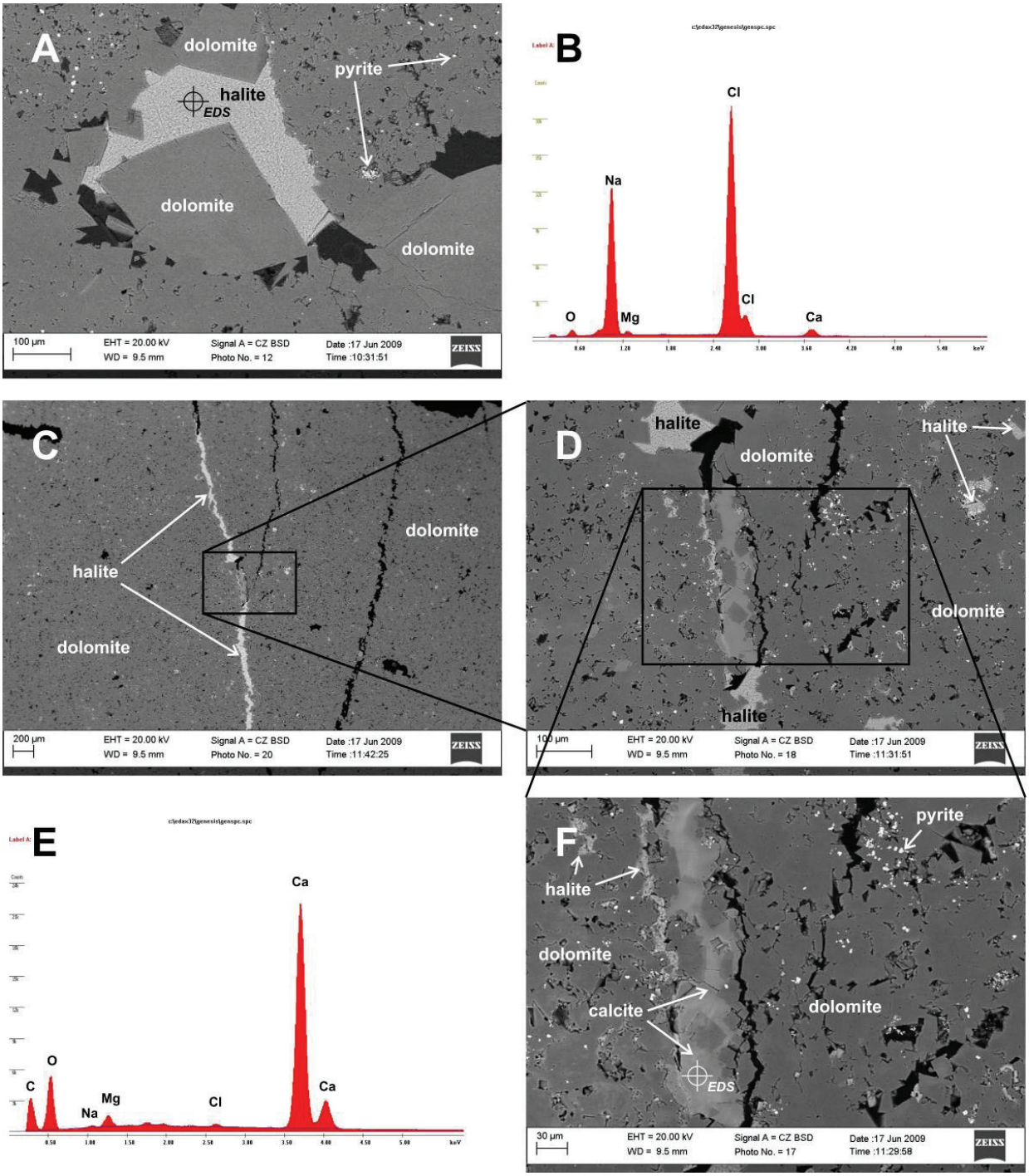

Figure 3.54: SEM/EDS Analyses of Vein and Intact Rock Mineralogy of Guelph Formation Dolostone at 391.34 mBGS in DGR-3

3.10.3 Summary

Table 3.13 summarizes the observed occurrences of fracture infill, vein and secondary mineralogy in DGR core from core logging and laboratory petrography/XRD/SEM work.

Table 3.13: Summary of Occurrences of Fracture Infill, Vein and Other Secondary Mineralogy in DGR Boreholes

Formation	Core Logging	Petrography/XRD/SEM
Lucas + Amherstburg	Calcite, pyrite, Fe staining	Calcite, quartz
Bois Blanc	Calcite, pyrite, chert	Quartz, chert, calcite, pyrite
Bass Islands	Calcite, pyrite, anhydrite, Fe staining	Calcite, gypsum, pyrite, celestite
Salina G+F	Anhydrite, gypsum	Gypsum, anhydrite
Salina E+D	Anhydrite, gypsum	Gypsum, anhydrite, calcite, halite, celestite
Salina C+B	Anhydrite, gypsum, halite	Quartz, chert, halite
Salina A2	Anhydrite, gypsum, clay, halite	Anhydrite, gypsum, calcite
Salina A1+A0	Anhydrite, gypsum, calcite, pyrite	Calcite, pyrite, halite, anhydrite, gypsum
Guelph to Fossil Hill	Calcite, anhydrite, pyrite	Fe-stained illite, halite
Cabot Head + Manitoulin	Chert, quartz, halite, anhydrite	anhydrite, gypsum, quartz, halite, celestite, clays
Queenston	Halite, gypsum, anhydrite, pyrite, Fe staining	Halite, calcite, gypsum, anhydrite, celestite, pyrite
Georgian Bay	Halite, anhydrite, gypsum, pyrite	Illite, calcite, halite, anhydrite, celestite, pyrite, sphalerite
Blue Mountain	Calcite, pyrite, halite, clay	Illite, calcite, pyrite, halite
Cobourg	Anhydrite	Dolomite, Fe-stained illite, pyrite, halite, marcasite, calcite
Sherman Fall	Clay, anhydrite, halite	Calcite, Fe-hydroxide, pyrite, anhydrite, halite, illite
Kirkfield	Calcite	Calcite, pyrite, marcasite
Coboconk	Anhydrite, calcite	Pyrite, calcite
Gull River	Calcite, celestite, aragonite	Fe-staining, pyrite, calcite, dolomite, anhydrite, halite
Shadow Lake	Glauconite, calcite, pyrite, celestite	Pyrite
Cambrian	Calcite, quartz, pyrite, glauconite, Fe staining	Calcite, quartz, pyrite, marcasite, halite, green chlorite
Precambrian	-	Muscovite, rutile, pyrite

There are some minor differences in the listed occurrences of identified minerals in Table 3.13 that are unavoidable and are due in part to differences in the mineralogical detection capabilities of field core logging and laboratory petrography/XRD/SEM work. As noted above, differentiation of gypsum and anhydrite is occasionally difficult in the field and identification of individual clay minerals is similarly limited. Also, halite detected in the Cambrian sandstone may be tertiary

halite formed by the evaporation of porewater during sample preparation (see Section 3.7.1.2 above).

3.11 Major Structural and Stratigraphic Discontinuities

3.11.1 Silurian-Devonian Unconformity

The contact between the Bois Blanc Formation and the underlying Bass Islands Formation at true vertical depths of 121.9 to 143.1 mBGS at the Bruce DGR site is an erosional unconformity that has resulted in enhanced weathering, dissolution, and permeability in the upper parts of the underlying Bass Islands Formation, creating a regional disconformity. This feature is best displayed in core recovered from DGR-4 and is characterized by the change from grey-brown to tan brown dolostone with attendant moderate fracturing (Figure 3.55).

Figure 3.55: Devonian-Silurian Unconformity (Middle of Core Photo) at the Depth of 126.0 mBGS in DGR-4

Observations of drilling fluid loss, core logging, borehole geophysical and video logging and opportunistic groundwater sampling of boreholes that intersect this unconformity (TR-07-06, TR-07-11, TR-07-19, TR-08-13, TR-08-15, TR-09-01), show that the upper 15 to 20 m of the Bass Islands Formation is weathered, open and permeable due to the presence of this erosional unconformity. Rock quality in this weathered zone is fair to very poor with moderately to highly fractured intervals. Drilling fluid losses of up to 8 m^3/hr were recorded during drilling through this weathered and permeable zone in DGR boreholes and in US-8. These observations indicate that weathered bedrock near the Devonian-Silurian boundary will be a zone of significant groundwater inflow. This horizon will require grouting during shaft sinking operations.

GOLDER (2003) provides a regional description of the Silurian-Devonian unconformity based on observations made at the Rockwood Quarry in southeastern Michigan. At this Quarry, the contact undulates several metres over distances of hundreds of metres and the upper 2 to 8 m of the Bass Islands Formation is soft, weathered and permeable compared to the deeper, more competent Bass Islands dolostones.

3.11.2 Silurian-Ordovician Unconformity

The contact between the Manitoulin Formation and the underlying Queenston Formation at true vertical depths of 442.6 to 456.4 mBGS in DGR boreholes is an unconformity that creates variations in thickness of the Queenston Formation of up to 5.1 m and slight changes in the top of formation orientation. However, other than these minor changes in formation geometry, the unconformity is only otherwise marked by a lithology change, and the occurrence of halite-infilled fractures within the Queenston Formation. No significant deterioration in rock quality or enhancement of hydraulic conductivity is associated with the Silurian-Ordovician unconformity.

3.11.3 Cambrian-Precambrian Unconformity

The erosional unconformity between the Cambrian sandstone and the Precambrian granitic gneiss is found at a true vertical depth of 860.7 mBGS in DGR-2. The contact as evident in recovered core (see Figure 3.56) is sharp with some evidence of weathering and no evidence of rubble zones.

Figure 3.56: Contact between Cambrian Formation and Precambrian Basement at 860.70 mBGS in DGR-2, NB Contact Is at Start of Arrow

3.11.4 Inclined Faults

The possible presence of steeply dipping to vertical faults at the Bruce nuclear site was assessed through completion of 2-D seismic surveys (TR-07-15), and from the detailed logging of formation contacts with the understanding that offset contacts may be attributed to faulting (Raven et al. 2009).

The 2-D seismic survey at the Bruce nuclear site included the completion of nine survey lines totalling 19.7 km over and around the proposed DGR footprint (see Figure 3.57). TR-07-15 describes the acquisition, processing, interpretation and limitations to the interpretation of the seismic data considering regional geology and southwestern Ontario structural geological models and local site geological information.

The interpretations of the 2-D seismic data provide a reasoned assessment of possible geologic features and structural trends that might be present beneath the Bruce nuclear site. Uncertainty in these interpretations is influenced by variable data quality resulting, in part, from the poor seismic energy coupling experienced regionally between the low velocity, variably thick and heterogeneous glacial drift and underlying bedrock, and anthropogenic and natural background noise. These uncertainties were, however, mitigated through optimization of field data collection techniques and completion of data processing using two independent companies using different data processing procedures.

Figure 3.58 illustrates a typical processed and interpreted seismic data set (survey line 1) that extends southeast to northwest across the proposed DGR area. Figure 3.58 shows the interpreted tops of several formations that are good seismic reflectors (i.e., Salina A2 Evaporite, Guelph, Manitoulin, Queenston, Cobourg and Gull River formations and the Precambrian) as well as the interpreted occurrence of two steeply east-dipping faults that propagate upward from the Precambrian to near the top of the Queenston Formation shale. Although these formation seismic reflectors were identified on all survey lines, it is possible that the interpreted faults may be artefacts from the sources of uncertainty listed above.

Upward propagation of faulting from the Precambrian is the most likely mode of paleofault formation for the Ordovician sedimentary sequence in southern Ontario (Carter et al. 1996). No faults younger than the Trenton Group limestones have been mapped in this part of southern Ontario (Armstrong and Carter 2010). Evidence from regional geosynthesis studies (AECOM and ITASCA CANADA 2011) suggests that there is no major or active basement faulting within the Bruce area. This is also consistent with the microseismic monitoring activities which have reported no active seismicity proximal to the Bruce nuclear site (see Section 5.3).

Figure 3.57 shows the consolidated interpretation of mapped seismic discontinuities that may represent possible vertical to sub-vertical faults within the Ordovician formations at the Bruce nuclear site. These possible faults trend north-northwest to south-southeast. The presence of these possible fault structures was investigated through inclined oriented core drilling of boreholes DGR-5 and DGR-6 as part of Phase 2B site characterization work (INTERA 2008). Figure 3.59 shows the proposed and final trajectories of DGR-6 and the probable occurrence window for the northwest-trending feature located northeast of the proposed DGR and intersecting seismic lines #5 and #6.

Figure 3.59 shows that borehole DGR-6 fully intersected the fault occurrence window in the Georgian Bay, Blue Mountain, Cobourg, Sherman Fall and Coboconk formations before terminating within the upper part of the Gull River Formation. The results of core logging,

borehole geophysical logging and hydraulic testing of both DGR-5 and DGR-6 show no evidence of fault presence, as characterized by increased fracturing, dolomitization, and increased formation hydraulic conductivity.

Calculations of the depth, thickness and strike and dip of the Paleozoic bedrock formations and marker beds at the Bruce nuclear site (Tables 3.1 and 3.2) show remarkably uniformity particularly below the Salina B Unit which is the deepest unit suspected to have experience settlement due to paleo-dissolution of salt. This uniformity in depth and orientation of DGR strata below the Salina B Unit argues against significant faulting having disturbed formation contacts. The simple planar continuation of formation contacts from the DGR boreholes to those within the Texaco #6 well 2.9 km away to the southeast (see Section 3.13.1 and Figure 3.69) argues strongly against the presence of vertical faults within the Paleozoic bedrock at or near the Bruce nuclear site.

Based on the geological data available as part of DGR site characterization work, there are no data that indicate the presence of inclined or vertical faults in the area surrounding the proposed DGR defined by boreholes DGR-1 to DGR-6.

3.12 Minor Structural Discontinuities

Other minor discontinuities, primarily natural fractures, within the Devonian, Silurian and Ordovician formations are identified on the core logs for DGR boreholes (TR-07-06, TR-08-13, TR-09-01, TR-09-09) and on borehole geophysical logs (TR-07-08, TR-08-15, TR-09-03) as well as in the calculations of natural fracture frequency and RQD that are summarized in Table 3.4 and Figures 3.3 and 3.4. As described in Table 3.4 and Figures 3.3 and 3.4, and the narrative description of each formation given in Section 3.8, there are numerous fractures in the permeable upper dolostones of the Lucas to Bass Islands formations, but there are few discontinuities clearly evident in the deeper borehole core and geophysical logs, such that the deeper Silurian and Ordovician formations are described as unfractured to sparsely fractured.

There is inherent uncertainty in identification of fractures by core logs, with many identified fractures being potentially mechanical breaks. Correlation of core logs and core photographs with borehole geophysical logs, in particular borehole acoustic televiewer (ATV) image logs, provides confirmation of suspected discontinuities identified in recovered core. However, there is similar uncertainty with identification of discontinuities by ATV, as many of the horizontal features evident on ATV logs that may be potential discontinuities are actually thin beds of variable lithology from the host rock (e.g., thin siltstone and limestone beds within host shale formations).

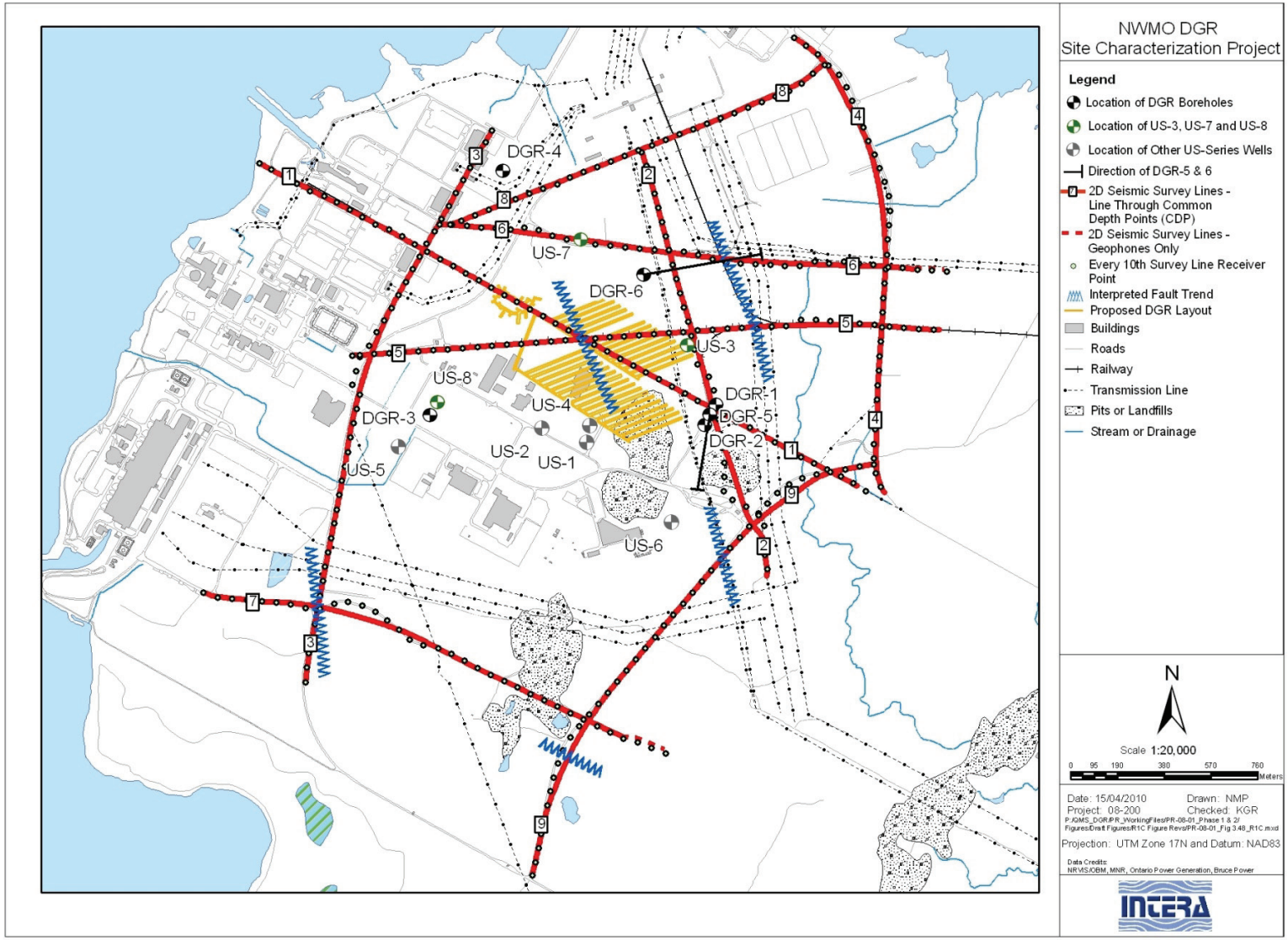

Figure 3.57: 2-D Seismic Survey Lines and Interpreted Occurrence of Possible Subvertical Faulting within the Ordovician Formations at the Bruce Nuclear Site

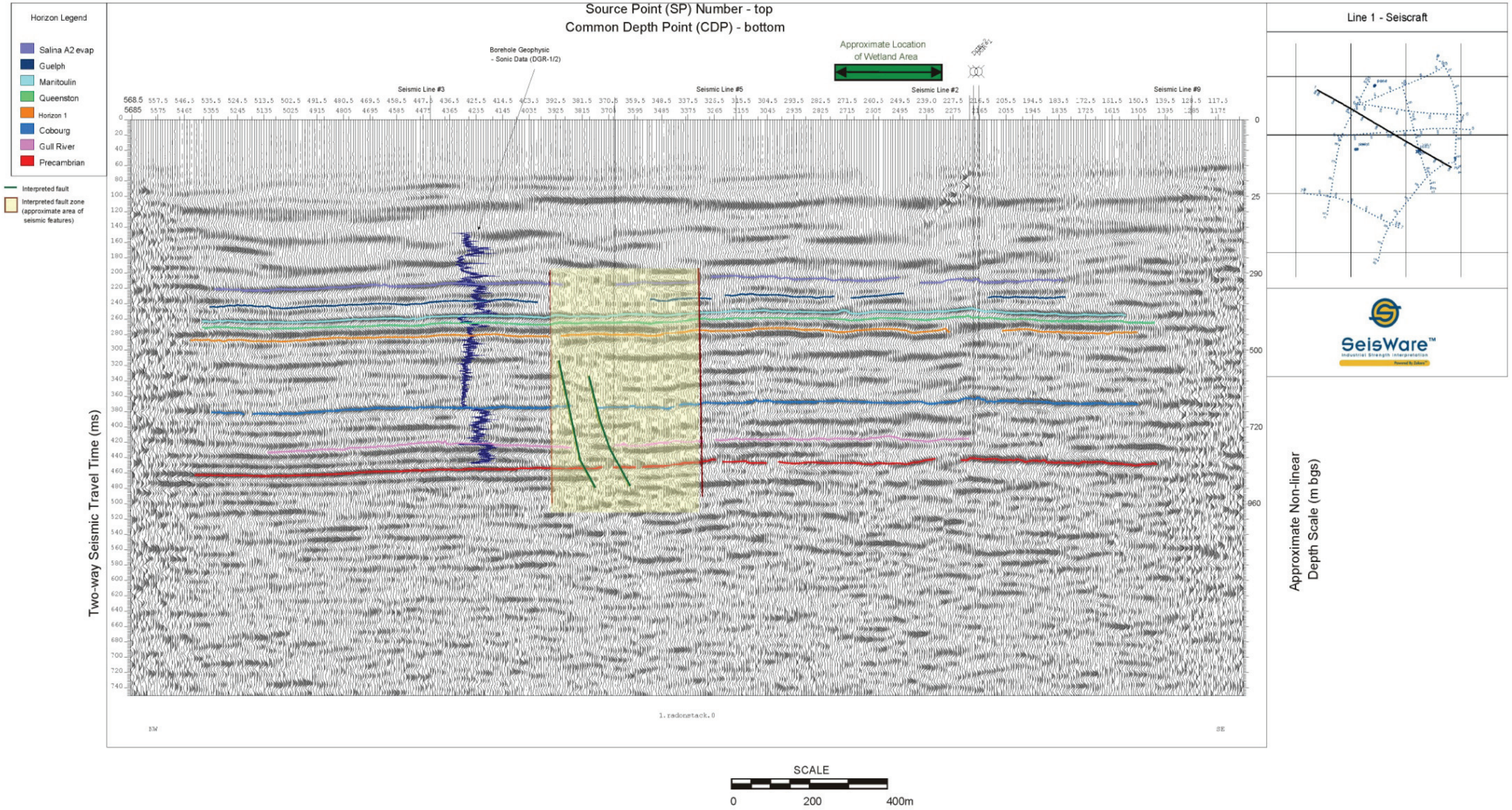

Figure 3.58: Processed and Interpreted Bedrock Stratigraphy and Structure of Seismic Survey Line 1

THIS PAGE HAS BEEN LEFT BLANK INTENTIONALLY

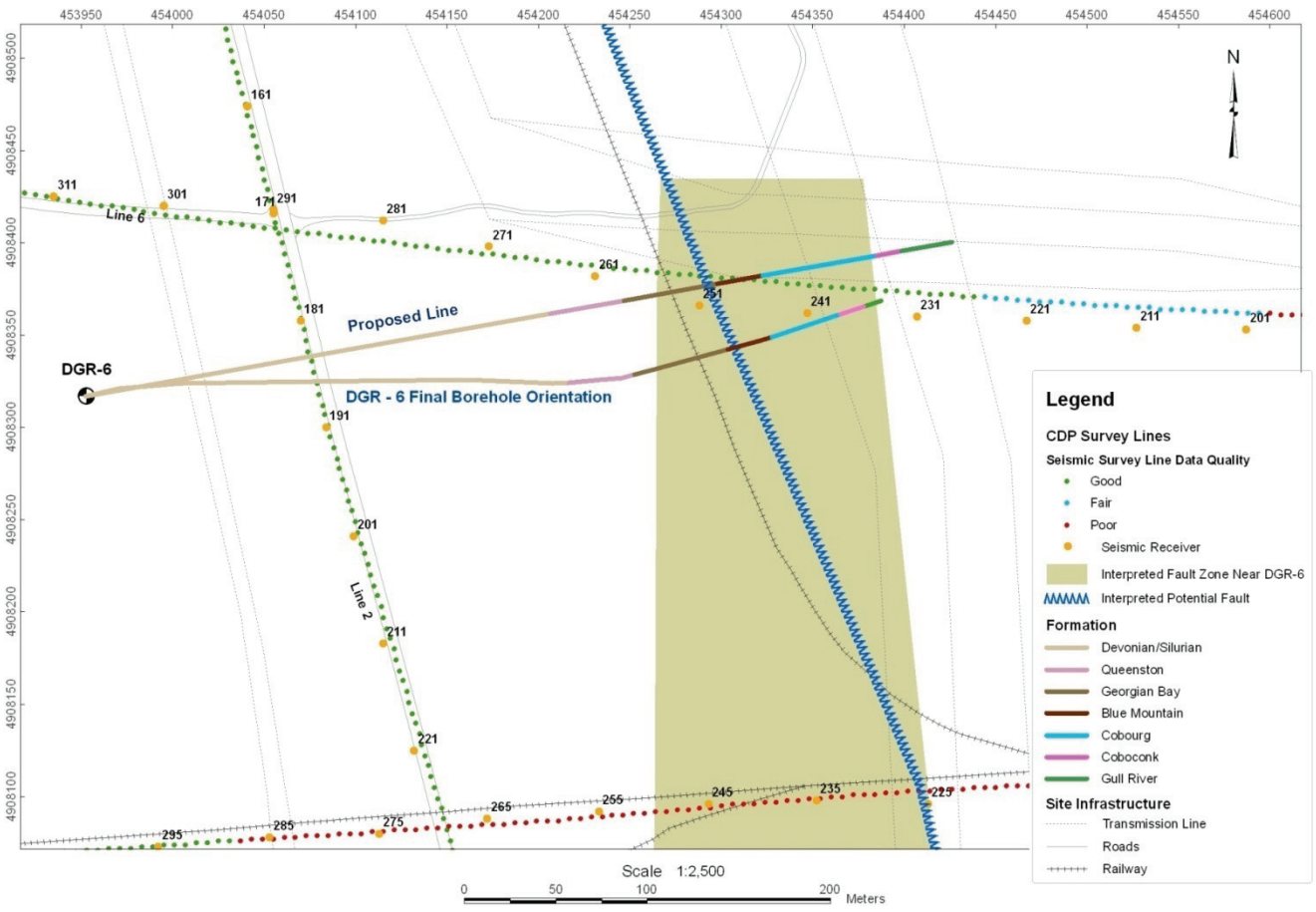

Figure 3.59: Trajectory of Borehole DGR-6 and the Occurrence Window for the Potential Fault Defined by Seismic Surveys and Located Northeast of the Proposed DGR

3.12.1 Example Discontinuities

Figures 3.60, 3.61, 3.62, 3.63 and 3.64 provide examples of some of the more noteworthy discontinuities identified from review of borehole geophysical logs (ATV borehole wall image and ATV caliper), core logs and core photography. It is beyond the scope of this report to present and discuss all identified discontinuities in DGR boreholes. TR-07-06, TR-08-13 and TR-09-01 provide detailed logs of all natural fractures photographed and logged in recovered DGR core, and TR-07-08, TR-08-15 and TR-09-03 provide detailed identification of all natural fractures identified from ATV images of the DGR borehole walls.

Figure 3.60 shows the occurrence of two horizontal discontinuities at 483.35 and 515.70 mBGS in DGR-2 within the Queenston Formation. The ATV logs show both features created 5-cm-wide zones of borehole enlargement due to drilling activities. The core at 483.40 mBGS, however, shows the appearance of a mechanical break that was not logged as a natural fracture, while the core at 515.70 mBGS shows the presence of a natural fracture. Neutron and fluid temperature logs (TR-07-08) show that both of these features create geophysical log anomalies suggestive of an open and relatively permeable feature compared to the surrounding

shale bedrock. Fluid resistivity logs do not show significant changes or anomalies at these fractures. These observations suggest two possible explanations: 1) some of the features logged as mechanical breaks may in fact be fractures, or 2) neutron, temperature and fluid resisitivity anomalies may not always reflect features that are more permeable than the surrounding rock mass. Which, if either, of these two explanations is correct is not yet known.

Figure 3.61 shows the occurrence of an inclined fracture at 585.7 mBGS within the Georgian Bay Formation in DGR-2 and minor borehole enlargements at 616.0 to 616.4 mBGS in DGR-2 within the Blue Mountain Formation. The inclined discontinuity was logged in the core as a closed halite-filled fracture that created a minor zone of borehole enlargement evident on the ATV logs, most likely due to salt washout during drilling. Fluid temperature logs show that this is a permeable fracture, while straddle-packer hydraulic testing (TR-08-32) and Westbay MP55 pressure profiles (TR-08-31) indicate that this fracture is overpressured relative to adjacent rock. The ATV and core photographs show that the minor borehole enlargements are associated with a 5-cm-thick hard bed of fossiliferous siltstone and limestone.

Figure 3.62 shows the ATV logs and core photography images of the contact between the Blue Mountain Formation and the Collingwood Member at a depth of 651.6 mBGS in DGR-2. Figure 3.62 shows that the core is broken and a natural fracture was identified just above the contact, while the ATV image of the borehole wall shows the faint presence of a closed fracture at this depth. Neutron, fluid temperature and resistivity logs confirm the closed nature of this fracture with no evidence of fluid flow.

Figure 3.63 shows the ATV logs, selected geophysical logs and core photography for the 10-cm-thick volcanic ash bed found at a depth of 768.8 to 768.9 mBGS within the Coboconk Formation in DGR-2. This ash bed is a DGR formation marker bed and was washed out during drilling, resulting in the increased borehole diameter shown on the acoustic caliper log of DGR-2. Although this zone was subject to drilling washout, the borehole fluid temperature logs and resistivity logs (TR-07-08) show that it may not be a zone of fluid flow or enhanced permeability in DGR-2. Similar observations are made for the ash layer in DGR-6 and straddle-packer hydraulic testing in DGR-6 also indicated that the ash bed was not a zone of enhanced permeability relative to the rest of the Coboconk Formation (TR-08-32). However, fluid temperature logs from DGR-3 and DGR-4 (TR-08-15, see Figure 3.46) suggest that the volcanic ash bed may be a zone of fluid flow and enhanced permeability in these boreholes. Borehole neutron logging of all DGR boreholes also shows a neutron low at this location confirming the increased porosity of the ash bed and associated washout relative to the surrounding low-porosity limestone. Confirmation of the increased porosity of ash bed was made based on porewater characterization of a sample collected from DGR-6 (Figure 4.2, Section 4.3.2.2).

Figure 3.64 shows the occurrence of a thin (10-cm-thick) subhorizontal fractured fissile shale layer within the core at a depth of 688.6 mBGS in DGR-4 at the bottom of the Cobourg Formation. This feature is evident as a zone of increased borehole diameter on acoustic televiewer and borehole caliper logs indicating washout of the shale during drilling of the borehole. It also shows density and neutron kicks on the borehole geophysical logs indicating a zone of increased porosity or the washout. A minor kick on the temperature variability log is also evident at this depth suggesting potential for increased formation permeability. Similar lithologic and structural features were not detected in the Cobourg Formation in DGR-2, DGR-3, DGR-5 and DGR-6.

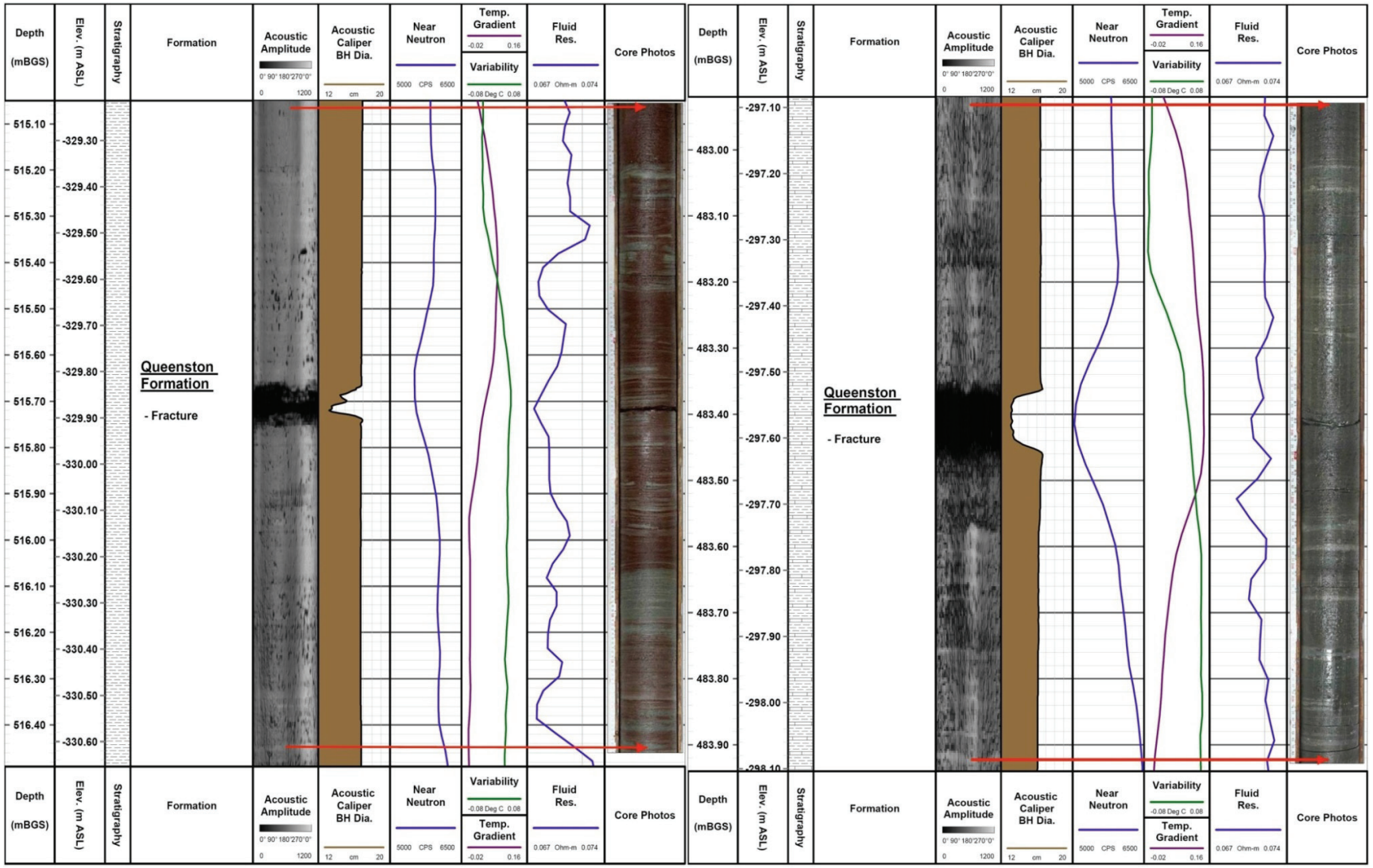

Figure 3.60: ATV Logs, Selected Geophysical Logs and Core Photographs of Two Subhorizontal Fractures in the Queenston Formation, DGR-2

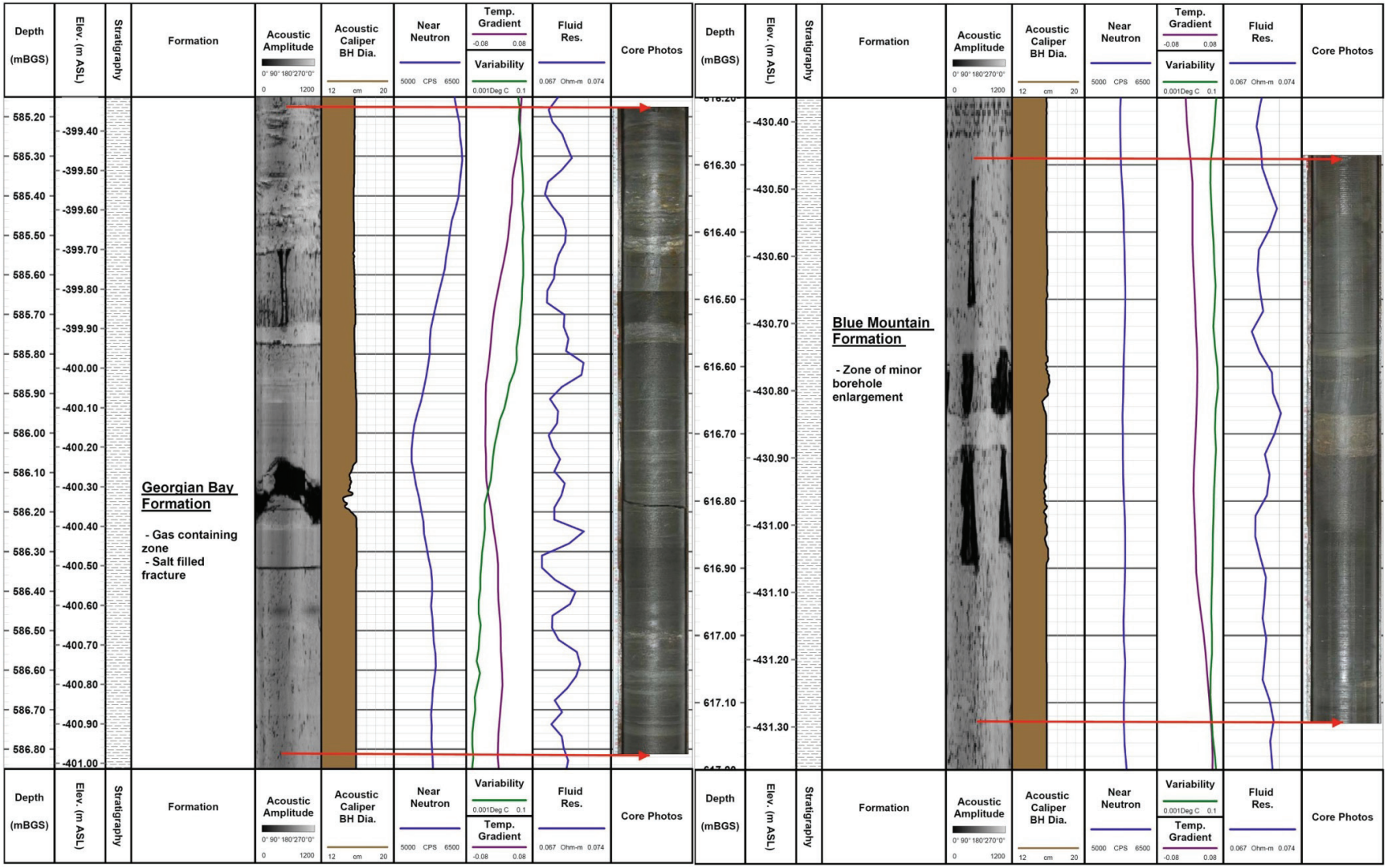

Figure 3.61: ATV Logs, Selected Geophysical Logs and Core Photographs of Possible Gascontaining Fracture (Left) in Georgian Bay Formation in DGR-2 and Zone of Minor Borehole Enlargement (Right) in Blue Mountain Formation in DGR-2

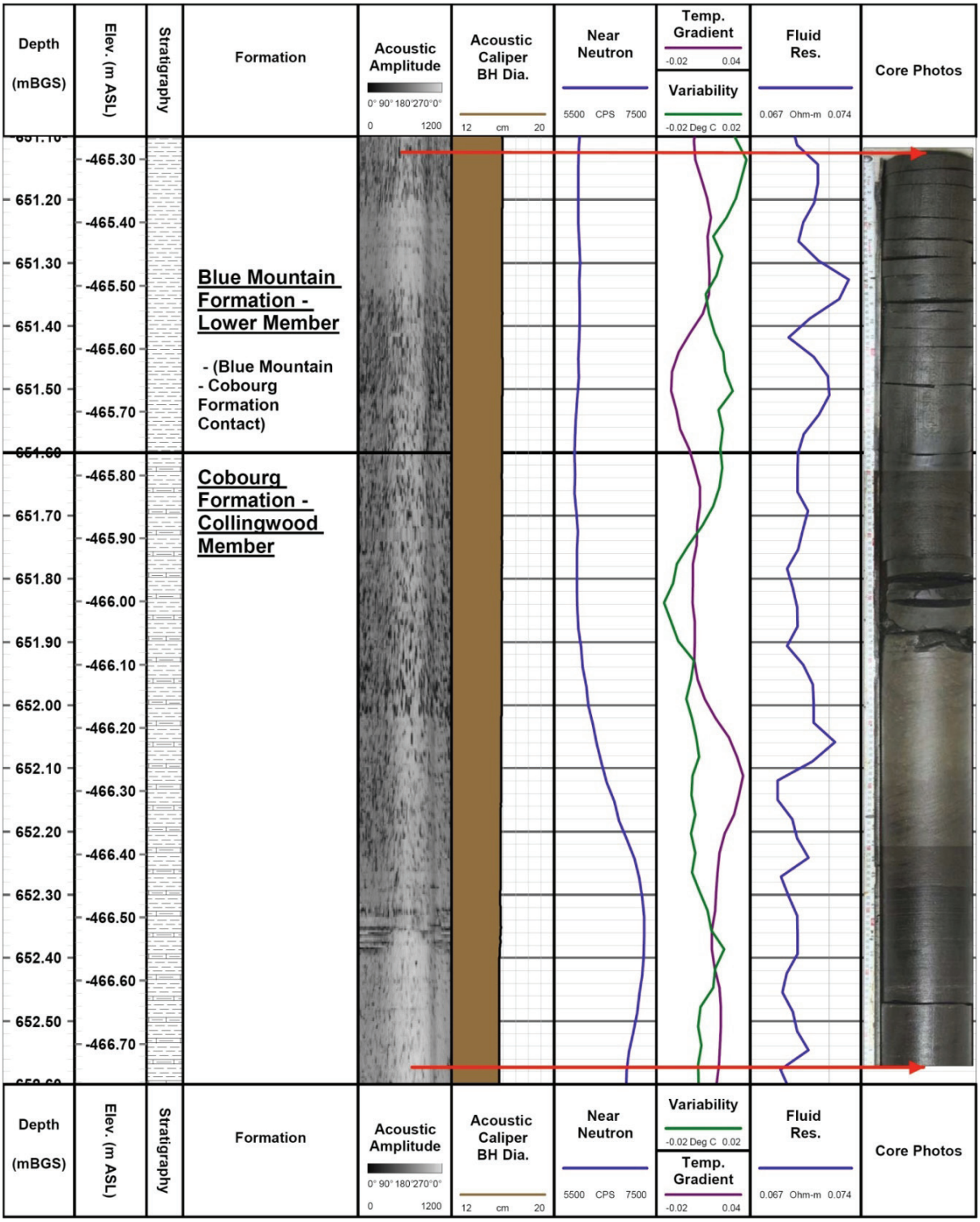

Figure 3.62: ATV Logs, Selected Geophysical Logs and Core Photographs of Contact between Blue Mountain Formation and Collingwood Member of the Cobourg Formation, DGR-2

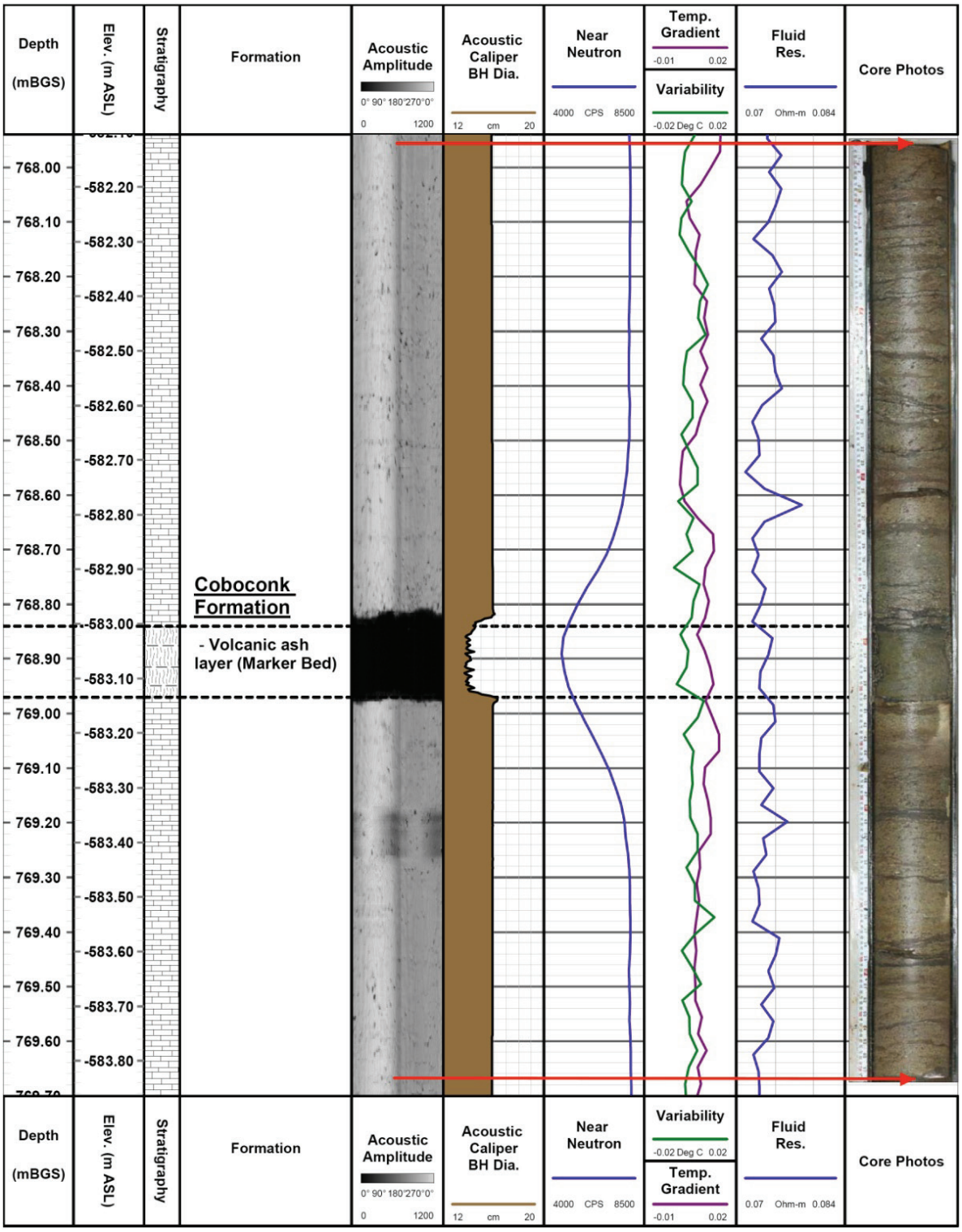

Figure 3.63: ATV Logs, Selected Geophysical Logs and Core Photographs of Volcanic Ash Bed, Coboconk Formation, DGR-2

3.12.2 Fracture Occurrence and Orientation

Identification of fracture occurrence and orientation is an important part of the DGR site characterization program, but such characterization, particularly for inclined fractures using vertical boreholes DGR-1 to DGR-4 is inherently difficult due to limited sampling of such features provided by vertical boreholes. With the inclusion of data from inclined boreholes DGR-5 and DGR-6, logging of core and analysis of ATV images of DGR borehole walls provides information on the occurrence and orientation of fractures in DGR boreholes.

More detailed characterization of fracture set orientation, including spacing, is presented in Sections 5 of this report for mechano-stratigraphic units based on oriented core logging of inclined boreholes DGR-5 and DGR-6 (TR-09-09). The data on fracture set orientation presented here is based on analysis of fracture orientations from ATV logs and core logging of all DGR boreholes. Examples of inclined fractures photographed in DGR-5 and DGR-6 are given in Figures 3.65 and 3.66.

Figure 3.64: Fractured Fissile Shale Layer at a Depth of 688.6 mBGS in the Bottom of the Cobourg Formation, DGR-4

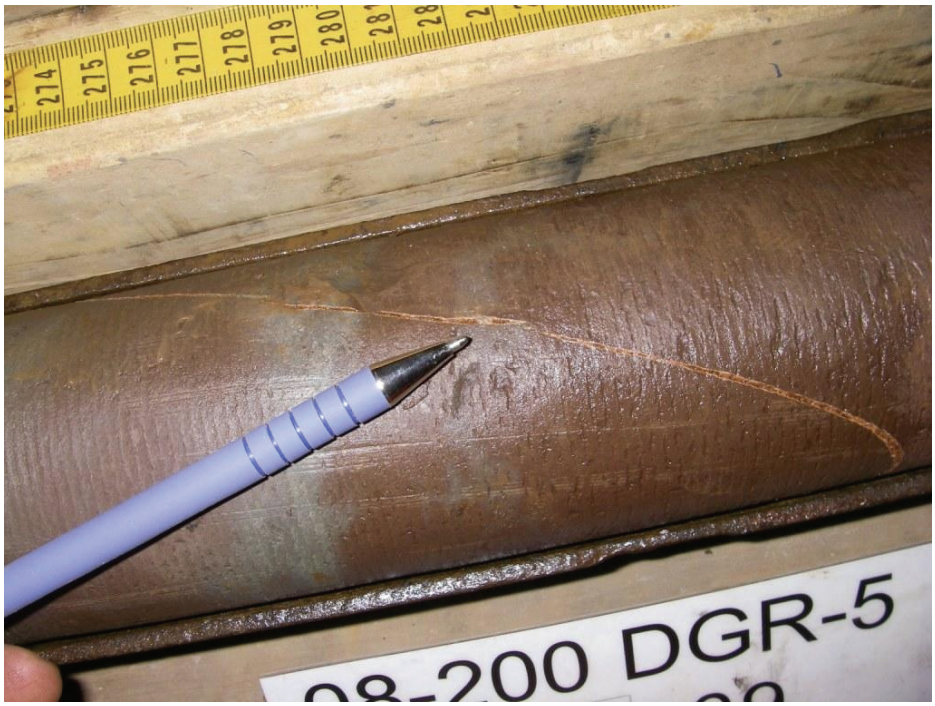

Figure 3.65: Inclined Halite and Calcite-infilled Fracture at Depth of 501.7 mLBGS in Queenston Formation, DGR-5

Figure 3.66: Inclined Halite-infilled Fracture at Depth of 655.3 mLBGS in Georgian Bay Formation, DGR-6

While logging of core from vertical DGR boreholes can identify the occurrence and approximate dip of some inclined to sub-vertical structural features, analysis of ATV images provides information on the occurrence and orientation (strike and dip) of such features though analysis of the depths of the tops and bottoms of the elliptical traces made by such features on the borehole wall. For the purposes of this discussion, inclined features are defined as those features with dip greater than 35° as measured from the horizontal. Features with dips greater than this threshold can be easily distinguished and separated from more flat-lying features that may be associated with bedding planes and other sedimentological features.

3.12.2.1 Mapping of Inclined Fractures by Core Logging and ATV Logging

Table 3.14 summarizes the identification of inclined fractures in DGR boreholes based on core logging and ATV logging of all DGR boreholes. Table 3.14 lists the total number of discontinuities with dip greater than 35° in Silurian and in Ordovician formations. The Devonian and Silurian dolostones above the Salina F Unit are not included in this overall inclined fracture assessment because ATV logging and fracture analysis were not performed in DGR boreholes above the Salina F Unit. ATV-logged inclined fractures include all major open, minor open, continuous and filled single fractures as defined in TR-07-08, TR-08-15 and TR-09-03.

Table 3.14 shows that more inclined fractures are consistently logged in core than with ATV in both the Silurian and Ordovician formation in all DGR boreholes. The reasons for these differences likely relate to the reduced ability of ATV logs over core logs to identify tight and infilled fractures, and the possibility that some core fractures may actually be mechanical breaks. Most importantly, Table 3.14 shows that the occurrence of inclined fractures is very much reduced within the Ordovician formations compared to the Silurian formations.

Table 3.14: Summary of the Number of Inclined Fractures Identified in DGR Boreholes

Borehole	Silurian Formations		Ordovician Formations	
	Core Logging	ATV Logging	Core Logging	ATV Logging
DGR-1 and DGR-2	77	14	13	*4*
DGR-3	201	35	44	*9*
DGR-4	184	54	16	*1*
DGR-5	36	6	28	*8*
DGR-6	41	21	31	*11*
Totals	539	130	132	38

3.12.2.2 Fracture Orientations in Silurian Formations

The orientation of all fractures and inclined fractures in the Silurian formations determined from ATV logging are illustrated in Figures 3.67 and 3.68, respectively. Figures 3.67 and 3.68 show contoured polar equal-area plots of all fractures and inclined fractures generated using Rockscience Inc. DIPS v.5 107 software. These plots are corrected for Terzaghi (1965) sampling bias.

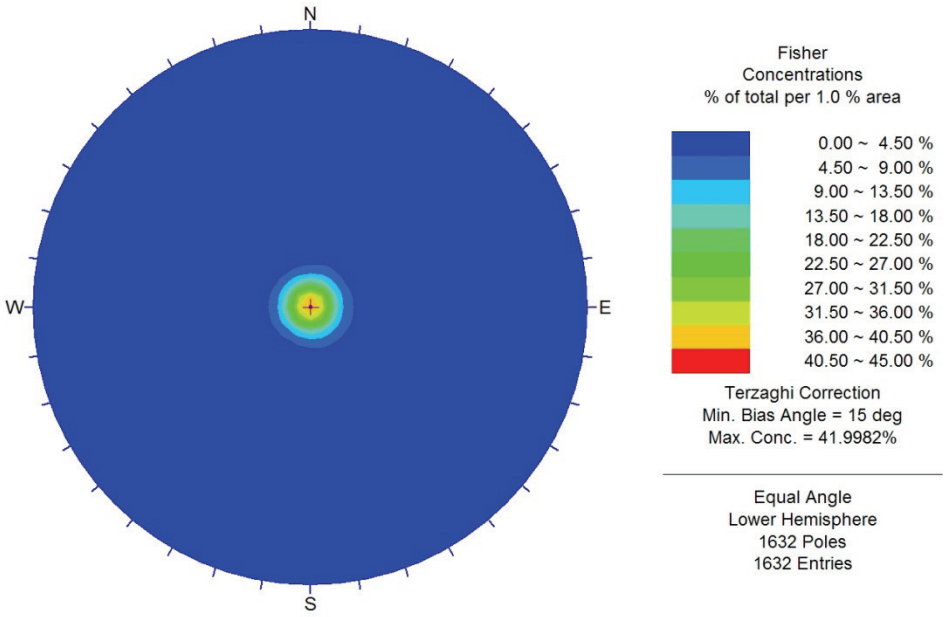

Figure 3.67: Contoured Equal-area Polar Plot of All Fractures in Silurian Formations from ATV Logging of all DGR Boreholes

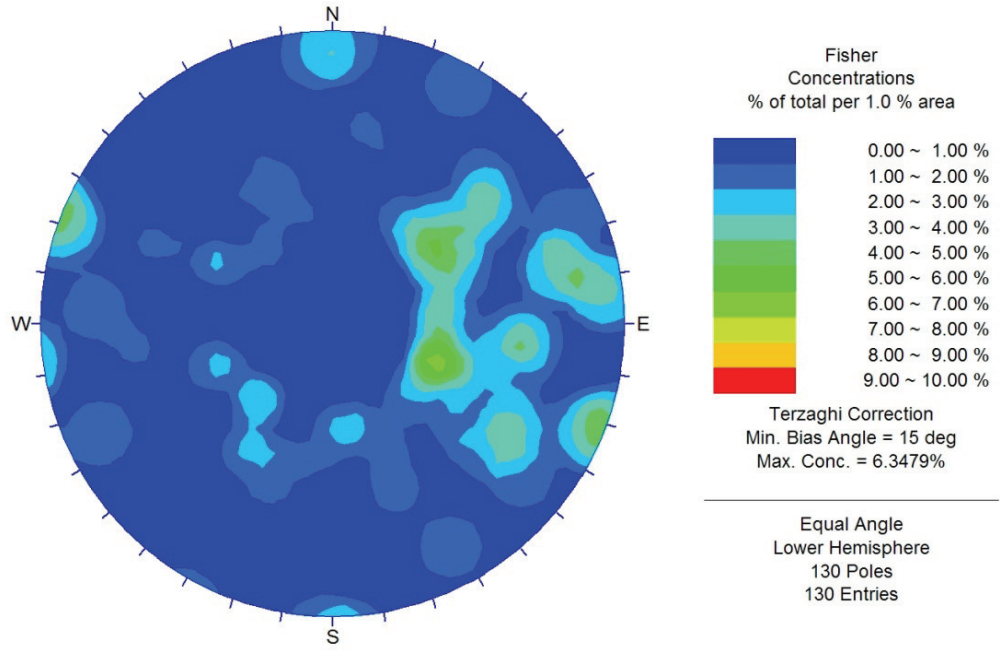

Figure 3.68: Contoured Equal-area Polar Plot of Inclined Fractures in Silurian Formations from ATV Logging of All DGR Boreholes

Figure 3.67 indicates the presence of a single dominant sub-horizontal fracture set. The orientation of subordinate inclined fracture sets are only evident when fractures with dips less 35° are excluded as shown on Figure 3.68. Figure 3.68 indicates the presence of NNE, NW, NNW and E striking fractures that dip vertically, moderately to the W, moderately to the SW and vertically, respectively. These fracture patterns are somewhat comparable to those mapped in nearby Inverhuron Park and southern Bruce peninsula (Cruden 2011, AECOM and ITASCA CANADA 2011). Local mapping of joints in Inverhuron Park showed strikes of ENE and NNW, whereas mapping of the southern Bruce peninsula showed joint strikes of ENE, NNW and N.

3.12.2.3 Fracture Orientations in Ordovician Formations

The orientation of all fractures and inclined fractures in Ordovician formations determined from ATV logging are illustrated in Figures 3.69 and 3.70, respectively. Figures 3.69 and 3.70 show contoured polar equal-area plots of all fractures and inclined fractures corrected for Terzaghi (1965) sampling bias. Figure 3.69, similar to Figure 3.67 indicates the presence of a single dominant sub-horizontal fracture set. Again, the orientation of subordinate inclined fracture sets are only evident when fractures with dips less 35° are excluded as shown on Figure 3.70. Figure 3.70 indicates the presence of WNW and ENE to NE striking fractures that are both steeply dipping. These fracture patterns are again somewhat comparable to those mapped in nearby Inverhuron Park and southern Bruce peninsula (NWMO 2011). Ordovician inclined fracture patterns determined from ATV logging are also very comparable to those determined from oriented core logging of the Ordovician shales in boreholes DGR-5 and DGR-6 that are described in Section 5.7.2.1. Results of oriented core logging (TR-09-09, see Section 5) indicate the inclined fractures within the Silurian and Ordovician formations are widely spaced with minimum average spacings of 6.8 to 11.5 m.

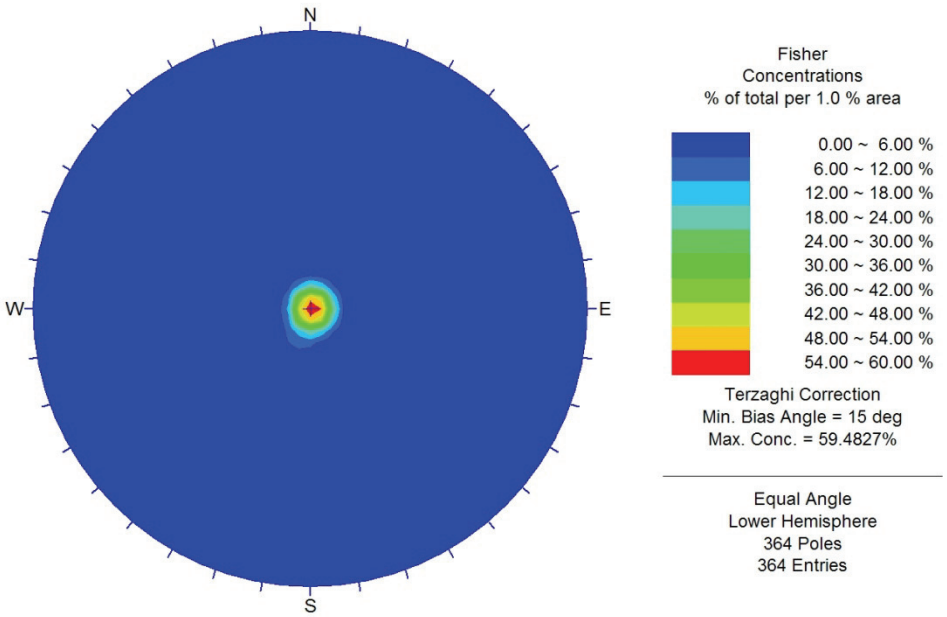

Figure 3.69: Contoured Equal-area Polar Plot of All Fractures in Ordovician Formations from ATV Logging of All DGR Boreholes

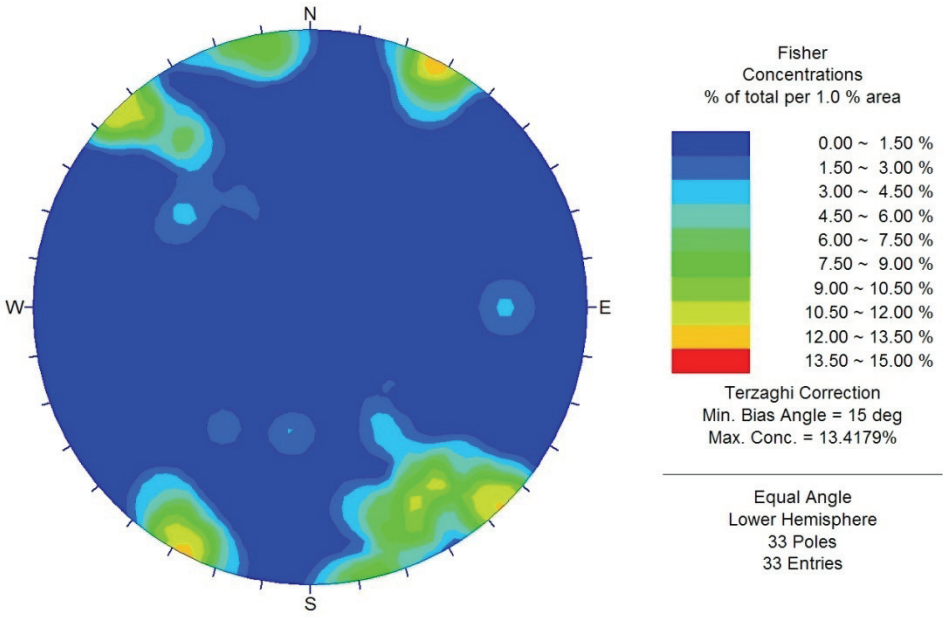

Figure 3.70: Contoured Equal-area Polar Plot of Inclined Fractures in Ordovician Formations from ATV Logging of All DGR Boreholes

3.13 Formation Lateral Predictability

Assessment of the lateral predictability of bedrock formations at the Bruce nuclear site can be made based on assessment of predicted and observed bedrock conditions between the closest oil and gas exploration well and DGR-1/DGR-2, and between DGR-5/DGR-6 and DGR-1 to DGR-4.

3.13.1 Texaco #6 and DGR-1/DGR-2

Prior to the start of DGR drilling, the depth and thickness of bedrock formations at the Bruce nuclear site were estimated (GOLDER 2003) based on the results of chip and geophysical logging of the Texaco #6 oil and gas well (MNR ID: T002636) located approximately 2900 m southeast of boreholes DGR-1 and DGR-2 and identification of the top of the Bois Blanc Formation in US-4. The comparison of estimated and actual formation depths and thicknesses in DGR-1 and DGR-2 are summarized in Table 3.15. The estimated formation depths for DGR-1 and DGR-2 are corrected for the dip of the Bois Blanc Formation as given in Table 3.1 and the distance between US-4 and DGR-1/2. Actual formation depths and thicknesses are for DGR-1 and DGR-2 from TR-09-11.

Several simplifications have been made to make the comparison between predicted and actual formation depths and thicknesses meaningful. Most of the these simplifications include combining formations that were logged differently by GOLDER (2003) and in TR-08-12 due to changes in stratigraphic nomenclature that occurred with release of the updated nomenclature by Armstrong and Carter in 2006 or simply combining formations for ease of presentation. The simplifications and rationale for the simplifications are as follows.

- Combining Salina G+F, E+D, C+B and A1+A0 Units for ease of presentation and because GOLDER (2003) assumed the Salina D and A0 Units were not present.
- Combining all of the Middle Silurian dolostone formations because of the complexity of the many thin formations identified in TR-08-12.
- Combining the Cabot Head and Manitoulin formations for ease of presentation.
- Combining Sherman Fall, Kirkfield and Coboconk formations as these individual formations were defined and identified differently by GOLDER (2003) than in TR-09-11.
- Including the Collingwood in the Cobourg Formation.

Review of Table 3.15 shows that for the vast majority of the formations, the actual depths are about 30 m deeper (i.e., +30 m) than predicted depths and the cause of the under-prediction of depths appears to be derived from two additive errors. This common under-prediction is likely due to an erroneous identification of the top of the Bois Blanc Formation (~20 m offset) in US-4 and underestimation of the thickness of this formation at the Bruce nuclear site by about 10 m. Correcting for this combined 30-m offset brings actual formation depths in DGR-1 and DGR-2 remarkably close to predictions based on Texaco #6 stratigraphy.

This last observation implies that almost all of the formation thicknesses were reasonably well predicted. Review of the last column of Table 3.15 shows this to be the case, with most differences in formation thickness being less than 10 m. Those formations with thickness differences greater than this amount are those formations where combining of formations was necessary to offset different formation nomenclature and identification (e.g., Sherman Fall, Kirkfield, Coboconk and Gull River), or formation thickness was uncertain due to natural variability caused by uncertain lower erosional surfaces (e.g., Cambrian sandstone).

Figure 3.71 shows the cross section constructed between Texaco# 6 well and boreholes DGR-1, DGR-2 and DGR-3. The contacts for the Ordovician shale and limestone formations in the Texaco # 6 well log were adjusted to be consistent with the formation pick rationale developed in TR-09-11 and applied to DGR boreholes. This adjustment, which was made based on borehole geophysical logs (natural gamma), resulted in minor movement of the formation depth contacts for the Queenston, Collingwood, Sherman Fall, Kirkfield and Gull River formations. Figure 3.71 illustrates the continuity of Paleozoic formation thicknesses and attitudes over distances of 3 to 4 km in the vicinity of the proposed Bruce DGR.

Figure 3.71 shows apparent dips of about 0.8 to 1.0° for the Devonian dolostones and about 0.4° for the Ordovician shales and limestones on the Bruce nuclear site. Lower apparent dips are evident from Texaco #6 to DGR-1/2 because these wells are almost along strike of each other. These apparent formation dips are consistent with the regional geological compilation (AECOM and ITASCA CANADA 2011) that concluded regional formation dips in the vicinity of the Bruce nuclear site average 0.5 to 0.6°SW and increase towards the centre of the Michigan Basin.

Table 3.15: Summary of Formation Predictions and Occurrences in DGR-1 and DGR-2

Formation	Predicted Depth to Top (mBGS)	Actual Depth to Top (mBGS)	Vertical Offset (m)	Predicted Fm Thickness (m)	Actual Fm Thickness (m)	Vertical Offset (m)
Amherstburg	7.8	30.4	+22.6	46.2	44.6	-1.6
Bois Blanc	54.0	75.0	+21.0	38.2	49.0	+10.8
Bass Islands	92.4	124.0	+31.6	42.1	45.3	+3.2
Salina G+F	134.5	169.3	+34.8	46.3	53.7	+7.4
Salina E+D	180.8	223.0	+42.2	32.6	21.6	-11.0
Salina C+B	213.4	244.6	+31.2	47.9	46.6	-1.3
Salina A2	261.3	293.1	+31.8	33.5	31.7	-1.8
Salina A1+A0	294.8	325.5	+30.7	44.2	49.0	+4.8
Guelph - Fossil Hill	339.0	374.5	+35.5	42.1	36.5	-5.6
Cabot Head + Manitoulin	381.1	411.0	+29.9	35.6	36.7	+1.1
Queenston	416.7	447.7	+31.0	79.3	70.4	-8.9
Georgian Bay	496.0	518.0	+22.0	95.1	90.9	-4.2
Blue Mountain	591.1	608.9	+17.8	32.6	42.7	+10.1
Cobourg (Lindsay)	623.7	651.6	+27.9	44.5	36.5	-12.0
Sherman Fall+ Kirkfield+ Coboconk (Verulam+ Bobcaygeon)	659.4	688.1	+28.7	107.9	96.9	-11.0
Gull River	767.3	785.0	+17.7	43.9	53.6	+9.7
Shadow Lake	811.2	838.6	+27.4	4.8	5.2	+0.4
Cambrian	816.0	843.8	+27.8	8.0	16.9	+8.9
Precambrian	824.0	860.7	+36.7	--	--	--

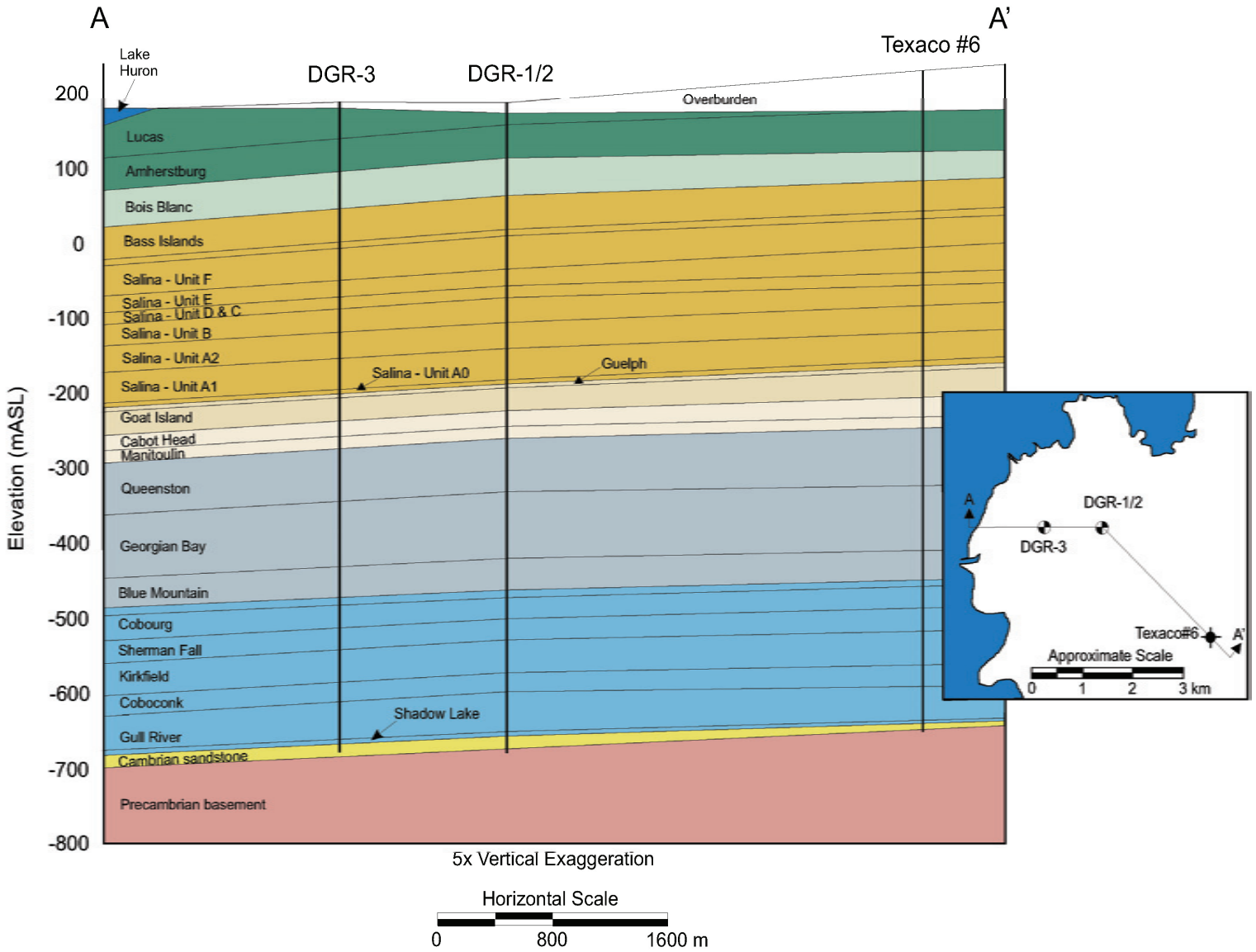

Figure 3.71: Regional Stratigraphic Cross-Section - Texaco # 6 to Bruce Nuclear Site

3.13.2 Predictions of DGR-5 and DGR-6 Formation Tops

An assessment of the predictability of bedrock formations in the vicinity of the DGR was also made based on a comparison of the observed and predicted elevations of formation tops in boreholes DGR-5 and DGR-6 (Table 3.16). Formation contacts found to be deeper or at a lower elevation than prediction are considered positive offsets.

Predictions of the elevations of formation tops in DGR-5 and DGR-6 were made based on the strike and dip of formations defined based on DGR-1/DGR-2, DGR-3 and DGR-4 data (Table 3.2) and the three-dimensional intersection of the equation of the formation plane with the known DGR-5 and DGR-6 borehole positions based on ATV and gyroscopic logging. Details of the calculations are provided in TR-09-11 and the results are summarized in Table 3.16.

For DGR-5, contacts above the Salina Formation B Unit Evaporite are up to 15.4 m above the predicted elevations (Salina Formation B Unit Carbonate), while below the Salina B Unit, bedrock formation elevations range from 0.05 m above (Lions Head Formation) to 5.0 m above (Blue Mountain Formation) but mostly are approximately 2.0 to 3.0 m above the predicted values. DGR-5 is located adjacent to DGR-1 and DGR-2, therefore these minor, yet consistent differences above the predicted bedrock formation elevations suggest a consistent error or bias in the determination of the tops of formations in DGR-5. This error may be due to overestimation of the plunge of DGR-5 as measured by ATV logging. An error of 0.3°-0.4° in borehole plunge measurement would account for the observed difference of 2.0 to 3.0 m in DGR-5.

For DGR-6, contacts above the Salina Formation B Unit Evaporite range between 7.6 m above (Salina Formation C Unit) to 9.7 m below (Salina Formation B Unit Carbonate) their predicted elevations. These variable offsets are most likely due to the difficulty in making formation picks in a section of bedrock with increased brecciation as discussed in Section 3.6. For example, anhydrite and tan dolostone marker beds that have been evident in the Salina B, C and E Units and have been relied on to help establish these formation tops in DGR-1 through DGR-5, are brecciated and absent in DGR-6 (TR-09-11). Therefore, selection of formation contacts for these units in DGR-6 is difficult and may not correspond to more obvious marker beds in other DGR boreholes. Conversely, contacts below the Salina B Unit show bedrock formation elevations that range from 1.7 m below (Salina Formation A2 Unit) to 3.5 m above (Blue Mountain Formation), but mostly are 1.5 to 2.5 m above the predicted values. This consistent under-prediction of the elevation of the top of the formation in DGR-6 may be due to overestimation of the borehole plunge of DGR-6 as measured by gyroscopic surveys.

Table 3.16: Summary of Formation Predictions and Occurrences in DGR-5 and DGR-6

Formation, Member, Unit	DGR-5			DGR-6		
	Predicted Elevation (mASL)	Measured Elevation (mASL)	Vertical offset (m)	Predicted Elevation (mASL)	Measured Elevation (mASL)	Vertical Offset (m)
Lucas	165.98	165.70	+0.28	168.0	169.1	-1.13
Amherstburg	154.77	155.32	-0.55	153.2	152.2	+1.00
Bois Blanc	109.98	110.71	-0.74	111.4	109.6	+1.77
Bass Islands	60.77	63.46	-2.69	62.5	61.6	+0.85
Salina G Unit	15.24	18.90	-3.67	17.9	17.4	+0.50
Salina F Unit	5.72	11.35	-5.64	9.8	8.8	+1.00
Salina E Unit	-38.86	-27.37	-11.49	-34.2	-31.2	-3.00
Salina D Unit	-58.94	-46.72	-12.22	-55.5	-48.4	-7.09
Salina C Unit	-60.65	-47.77	-12.88	-56.9	-49.3	-7.57
Salina B Unit - Carb	-76.03	-60.60	-15.43	-73.0	-82.7	+9.68
Salina B Unit-Evap	-106.52	-101.37	-5.15	-104.3	-103.9	-0.44
Salina A2 Unit - Carb	-108.42	-104.58	-3.84	-106.2	-107.9	+1.72
Salina A2 Unit-Evap	-135.21	-132.46	-2.74	-132.9	-133.7	+0.76
Salina A1 Unit - Carb	-141.00	-138.02	-2.98	-138.6	-137.4	-1.25
Salina A1 Unit -Evap	-182.70	-179.52	-3.18	-179.5	-177.7	-1.79
Salina A0 Unit	-186.13	-183.87	-2.26	-183.5	-182.2	-1.38
Guelph	-189.91	-186.63	-3.28	-187.9	-186.1	-1.85
Goat Island	-194.13	-192.01	-2.13	-192.0	-189.8	-2.19
Gasport	-212.92	-210.08	-2.83	-210.8	-208.3	-2.43
Lions Head	-219.78	-219.33	-0.46	-217.5	-216.2	-1.31
Fossil Hill	-224.26	-221.59	-2.67	-221.9	-219.8	-2.07
Cabot Head	-226.50	-224.02	-2.49	-224.1	-222.4	-1.69
Manitoulin	-250.47	-247.67	-2.80	-247.7	-245.8	-1.88
Queenston	-263.07	-260.54	-2.52	-260.5	-259.1	-1.45
Georgian Bay	-333.38	-330.87	-2.52	-330.0	-328.4	-1.61
Blue Mountain	-424.45	-419.46	-4.99	-420.1	-416.6	-3.54
Collingwood Member	-467.05	-464.56	-2.49	-463.2	-461.6	-1.67
Cobourg	-475.04	-473.19	-1.85	-471.0	-468.1	-2.86
Sherman Fall	-503.74	-500.29	-3.45	-499.1	-496.7	-2.48
Kirkfield	--	-529.57	--	-526.6	-525.5	-1.09
Coboconk	--	--	--	-572.0	-572.3	+0.25
Gull River	--	--	--	--	-594.6	--
Shadow Lake	--	--	--	--	--	--
Cambrian	--	--	--	--	--	--

3.14 Representative Estimates of Descriptive Geological Model Properties

Tables 3.17 and 3.18 summarize the representative estimates of the main structural and mineralogical properties of the 36 layers that comprise the descriptive geological model for the Bruce DGR site. Table 3.17 summarizes the estimates of top depth, thickness, strike/dip, Rock Quality Designation (RQD) and natural fracture frequency (NFF) of the 36 layers that comprise the descriptive geological site model. Table 3.18 summarizes the main mineralogical properties, including major primary mineralogy and trace mineralogy of the 36 model layers.

Table 3.17: Representative Estimates of Structural Properties of Descriptive Geological Model Layers

Model Layer	Top Depth (mBGS)	Thickness (m)	Orientation		RQD (%)	NFF (1/m)
			Strike	Dip		
Clay till overburden	0	20.0	-	-	-	-
Lucas	20.0	10.4	-	-	47	5.4
Amherstburg	30.4	44.6	N16°W	1.15°SW	47	5.4
Bois Blanc	75.0	49.0	N27°W	0.95°SW	68	3.6
Bass Islands	124.0	45.3	N25°W	0.95°SW	34	2.7
Salina G Unit	169.3	9.3	N17°W	0.90°SW	54	3.8
Salina F Unit	178.6	44.4	N33°W	0.95°SW	90	0.9
Salina E Unit	223.0	20.0	N35°W	0.89°SW	96	0.8
Salina D Unit	243.0	1.6	N25°W	1.01°SW	98	0.3
Salina C Unit	244.6	15.7	N25°W	1.07°SW	98	0.3
Salina B Unit – Carb	260.3	30.9	N24°W	0.85°SW	97	0.5
Salina B Unit – Evap	291.2	1.9	N24°W	0.53°SW	97	0.5
Salina A2 Unit – Carb	293.1	26.6	N20°W	0.52°SW	96	0.4
Salina A2 Unit - Evap	319.7	5.8	N28°W	0.62°SW	96	0.4
Salina A1 Unit – Carb	325.5	41.5	N21°W	0.59°SW	99	0.2
Salina A1 Unit - Evap	367.0	3.5	N25°W	0.58°SW	99	0.2
Salina A0 Unit	370.5	4.0	N19°W	0.61°SW	99	0.2
Guelph	374.5	4.1	N16°W	0.53°SW	99	0.2
Goat Island	378.6	18.8	N16°W	0.59°SW	99	0.2
Gasport	397.4	6.9	N15°W	0.57°SW	99	0.2
Lions Head	404.2	4.4	N16°W	0.55°SW	99	0.2
Fossil Hill	408.7	2.3	N17°W	0.55°SW	99	0.2
Cabot Head	411.0	23.8	N19°W	0.51°SW	94	0.1
Manitoulin	434.8	12.9	N19°W	0.55°SW	99	0.2
Queenston	447.7	70.4	N24°W	0.41°SW	98	0.2

Model Layer	Top Depth (mBGS)	Thickness (m)	Orientation		RQD (%)	NFF (1/m)
			Strike	Dip		
Georgian Bay	518.0	90.9	N17°W	0.61°SW	97	0.2
Blue Mountain	608.9	42.7	N23°W	0.51°SW	97	0.2
Cobourg – Collingwood Member	651.6	7.9	N14°W	0.56°SW	99	0.4
Cobourg – Lower	659.5	28.6	N14°W	0.60°SW	99	0.1
Sherman Fall	688.1	28.0	N17°W	0.57°SW	99	0.2
Kirkfield	716.1	45.9	N18°W	0.63°SW	98	0.2
Coboconk	762.0	23.0	N19°W	0.63°SW	98	0.3
Gull River	785.0	53.6	N16°W	0.66°SW	99	0.2
Shadow Lake	838.6	5.2	N19°W	0.56°SW	98	0.4
Cambrian	843.8	16.9	N18°W	0.52°SW	96	2.4
Upper Precambrian	860.7	-	-	-	100	0.3

Table 3.18: Representative Estimates of Mineralogical Composition of Descriptive Geological Model Layers

Model Layer	Major Mineralogy (%)					Trace Mineralogy
	Calcite	Dolomite	Quartz	Sheet Silicates	Other	
Clay till overburden	-	-	-	-	-	-
Lucas	49	49	0.4	0	0	Sp
Amherstburg	42	56	2	0	0	Py
Bois Blanc	56	20	14	1	0	Ch, Py, He
Bass Islands	1	88	6	0	5-Gy	Ce, Py
Salina G Unit	0	57	1	0	42-Gy/An	An, Py, Sa
Salina F Unit	0	30	10	16	44-Gy/An	An, Py, O
Salina E Unit	0	61	6	8	23-Gy	An, Py, O, Sa
Salina D Unit	0	20	0	0	80-An/Gy	An
Salina C Unit	0	26	20	44	0	An, Sa, Ha
Salina B Unit – Carb	10	30	5	32	15-An/Gy	Ha
Salina B Unit – Evap	0	10	0	0	90-An/Gy	-
Salina A2 Unit -	10	60	5	10	10-Gy/An	Ha, Py, Ce, O

Model Layer	Major Mineralogy (%)					Trace Mineralogy
	Calcite	Dolomite	Quartz	Sheet Silicates	Other	
Carb						
Salina A2 Unit - Evap	5	3	1	0	90-An	Gy
Salina A1 Unit - Carb	79	7	2	10	0	Py, O, Gy, An
Salina A1 Unit 0 Evap	0	30	2	2	66-An	Py, Sa
Salina A0 Unit	15	75	2	2	0	Py, An
Guelph	1	86	2	0	10-Ha	Py
Goat Island	73	12	7	8	0	Py
Gasport	79	15	2	3	0	An, He, Py
Lions Head	79	15	2	3	0	An, He
Fossil Hill	79	15	2	3	0	An, Py
Cabot Head	0	25	25	40	6-Go/O	Gy, An, Ha, Py, Ce
Manitoulin	54	12	13	19	0	An, Gy, Ha, Py, He
Queenston	24	14	17	40	0	Gy, An, Ha, He, Go
Georgian Bay	9	11	29	41	9-O	Ha, Gy, An, Py, Ce
Blue Mountain	6	3	32	49	10-O/Mi	Ha, Py
Cobourg – Collingwood Member	73	9	7	10	0	M, O, Py
Cobourg - Lower	81	8	3	6	0	Mi, Py, Ha, An
Sherman Fall	75	10	3	2	6-Mi	An, Ha, Py
Kirkfield	86	3	3	5	3-O/Mi	Py, Ma
Coboconk	86	9	2	2	0	An, Py
Gull River	53	38	2	6	0	An, Py
Shadow Lake	0	40	15	35	9-Kf	Gl, Py, Ce
Cambrian	3	40	30	4	12-O/Mi	Py, Ma, Gy, Ha, An
Upper Precambrian	4	5	24	23	40-Kf	Py

Notes: An = Anhydrite, Ce = Celestite, Ch = Chalcopyrite, Gy = Gypsum, Go = Goethite, Gl = Glauconite, Ha = Halite, He = Hematite, Kf = K Feldspar, O = Orthoclase, Ma = Marcasite, Mi=Microcline, Py = Pyrite, Sa = Sanidine, Sp= Sphalerite

The estimates of the depth of the top and thickness of each model layer are defined based on the reference stratigraphy occurring at DGR-1 and DGR-2, as listed in Figure 3.2 and Table 3.1 (TR-09-11). Strike and dip of the model layers are given in Table 3.17 based on the calculated layer orientations provided in Table 3.2 (TR-09-11) assuming true vertical depths. RQD and natural fracture frequency are calculated as arithmetic averages of these measurements made on all 3.05-m core runs completed within each model layer from boreholes DGR-1 to DGR-6 as summarized in Table 3.4 and presented in Figures 3.3 and 3.4.

Table 3.18 lists the estimates of percent weight composition of major mineralogy for each of the 36 model layers determined principally from semi-quantitative XRD analyses of DGR core (TR-08-01, TR-08-06, TR-08-22, TR-08-23, TR-08-29, TR-08-40, TR-09-06), supplemented by petrographic analyses. Major minerals include calcite, dolomite, quartz, sheet silicates and others (e.g., gypsum/anhydrite, feldspars, where the weight percentage is estimated to be greater than or equal to 5%). As discussed in Section 3.7.1.1, dolomite includes ankerite or Fe dolomite and sheet silicates include all common clay minerals such illite, chlorite, montmorillonite, smectite and minor dioctahedral micas (i.e., muscovite, hydromuscovite, glauconite) which are typically not distinguishable from common clay minerals in XRD analyses.

3.15 Confidence Assessment of Geological Data and Model

Confidence in the descriptive geological site model presented in Chapter 3 is assessed based on an evaluation of the quality and uncertainty in the key data that comprise the model, consistency of the data sets that comprise the model, and consistency of the geological model with other geoscientific models presented in Chapter 4 (descriptive hydrogeological site model) and Chapter 5 (descriptive geomechanical site model).

Data quality is often evaluated based on an assessment of data quality indicators of precision, accuracy, representativeness, comparability and completeness. These so-called PARCC attributes, while developed primarily to assess laboratory environmental quality data (US EPA 2002), have some relevance and application to geological data quality evaluation.

The following key geological data sets are subject to a confidence assessment:

- Depth, thickness and orientation of model layers;
- Major mineralogy of model layers;
- Occurrence of soluble minerals;
- Occurrence of major structural features; and
- Characterization of minor structural features.

3.15.1 Depth, Thickness and Orientation of Model Layers

Confidence in the geometry of the 36 layers that comprise the descriptive geological model is judged to be high. The geometry of the model layers is defined based on identification of formation, member and unit contacts and accuracy in borehole depth and location measurements obtained during drilling and borehole geophysical logging. The collection of continuous core in all DGR boreholes provides a level of confidence in formation identification and depths not usually obtained in deep sedimentary formation drilling in southern Ontario.

The stratigraphic nomenclature and depth of the top of each formation, member and unit contact in DGR boreholes were defined based on consensus opinion of expert geologists assembled in three core workshops held at the Bruce Core Storage Facility following the completion of drilling

and borehole geophysical logging of DGR-1 and DGR-2 (September 5 and 6, 2007), DGR-3 and DGR-4 (November 25 and 26, 2008) and DGR-5 and DGR-6 (May 26 and 27, 2010) Senior geologists from the Ministry of Natural Resources – Petroleum Resources Centre, Ontario Geological Survey and Geological Survey of Canada, as well as NWMO and Intera geologists attended these core workshops. TR-08-12 and TR-09-11 describe the methodology and results of these workshops in defining the stratigraphic nomenclature and formation contact depths in each DGR borehole. The stratigraphic nomenclature adopted at these workshops and throughout this report are those of Armstrong and Carter (2006), except where previously noted.

Formation contacts are defined in DGR boreholes based on logging of recovered core and borehole geophysical logging. Accuracy of core depths in DGR boreholes is estimated to be in the range of 0.1 to 0.5 m, decreasing with depth, although core logging is undertaken to a precision of 0.01 m. Accuracy of borehole geophysical logs is assumed to be similar to that of the core logging as the borehole geophysical logs are adjusted to core log depths to overcome any cable stretch and slippage in the borehole geophysical depth counter.

Formation contacts in DGR boreholes range from abrupt, easily discernable features in core (e.g., top of the Salina F Unit shale, Guelph dolostone, Cabot Head shale, Cobourg limestone and Shadow Lake siltstone and sandstone) to gradational, subjective features requiring judgment and reliance on borehole geophysical logs that provide signals averaged over borehole lengths that are greater than the depth accuracy of core logs. TR-08-12 and TR-09-11 assess the relative difficulty of the identification of the tops of formations in DGR boreholes and note that the tops of the Amherstburg dolostone, the Bois Blanc dolostone, Gasport dolostone, Lions Head dolostone, Blue Mountain shale, Sherman Fall limestone and Kirkfield limestone are all difficult picks for both core logging and borehole geophysics. For these gradational contacts, the actual contact depths may be off by +/- 1 to 2 m. To improve the depth estimates of DGR formations, thin unambiguous marker beds have been identified in selected formations ranging from the F Unit shale to the Coboconk Formation (Section 3.9, Raven et al. 2009, NWMO 2011).

As described in Section 3.5, the thickness and orientation of the 36 model layers in DGR boreholes are remarkably uniform over the DGR borehole separation distances of up to 1318 m, particularly below the Salina B Unit, considering the potential uncertainty in several formation picks. The variability in formation depths and thicknesses above the Salina B Unit is most likely due to collapse and minor rotation of the overlying bedrock following paleo-dissolution of the Salina B and D Unit salt beds. Below the Salina B Unit, formation thicknesses in DGR boreholes are within 1-2 m of each other in different holes, and the formation strikes are within 5-10° and formation dips are within 0.10° for each formation. The average strike and dip of the deeper Silurian and the Ordovician formations of N20°W/0.6°SW at the Bruce nuclear site are consistent with results of the regional 3-D geological framework model (AECOM and ITASCA CANADA 2011) and the stratigraphy in the nearby Texaco #6 well (see Figure 3.71). Noteworthy minor excursions of uniformity of thickness and orientation for formations below the Salina B Unit at the Bruce nuclear site include the Queenston Formation whose upper contact is a recognized erosional unconformity. This general consistency in thickness and orientation of formations between DGR boreholes and regional data provides confidence in the depth, thickness and orientation of the model layers in the descriptive geological site model.

Depths, thicknesses and orientations of bedrock formations in DGR boreholes are determined considering the known tilt of boreholes DGR-1 to DGR-4. Borehole geophysical logging of DGR boreholes provides continuous information on the exact azimuth and plunge of the boreholes and this information (TR-07-08, TR-08-15) shows that the assumed vertical boreholes are

slightly non-vertical with tilts ranging up to maximums of 1.8°, 1.4°, 5.4° and 3.8° from vertical for boreholes DGR-1, DGR-2, DGR-3 and DGR-4, respectively. Integrating the continuous borehole azimuth and tilt angles along the length of each borehole determines the correct depth and lateral position of each formation contact in each borehole. Using these correct contact positions in boreholes DGR-1 to DGR-4, a perturbation analysis was also undertaken to determine the effect of uncertainty in formation contact depth to calculated strike and dip of DGR bedrock formations. Uncertainties in contact depths of +/- 0.1, 0.5 and 1.0 m were considered for two representative formations – the Cabot Head shale and the Coboconk limestone as represented by the volcanic ash marker bed. In the perturbation analysis, true vertical depth contacts are raised and lowered by the defined uncertainty level in each well and in combinations of wells (total of 18 combinations for each uncertainty level) such that the complete range of strikes and dips are determined. Table 3.19 summarizes the results of the perturbation analyses as strikes and dips, compared against the strike and dip determined assuming borehole verticality as reported in TR-08-12, and the strike and dip based on the exact borehole positions as listed in Table 3.2.

Table 3.19 shows that the error in formation strike and dip associated with the assumption of borehole verticality is insignificantly small and within strike and dip measurement error. For the Cabot Head and Coboconk formations, the strike varies by 0.6° and 0.3° and the dip varies by 0.02° and 0.03°, respectively. The perturbation analyses show that uncertainty of +/- 0.1 m in true vertical depths of formation contacts results in strike and dip errors of about +/- 1.4° and +/- 0.02° for the Cabot Head Formation, and +/- 0.9° and +/- 0.01° for the Coboconk Formation. Increasing the uncertainty to +/- 0.5 m increases potential errors in strike and dip to about +/- 5° and +/- 0.06° for the Cabot Head Formation, and about +/- 5° and +/- 0.06° for the Coboconk Formation. With uncertainty of +/- 1 m in formation contacts, the potential errors in strike and dip increase to large values of about +/- 10° and +/- 0.1° for the Cabot Head Formation, and +/- 8° and +/- 0.1° for the Coboconk Formation.

Table 3.19: Summary of Effects of Borehole and Formation Contact Assumptions on Calculated Strikes and Dips of Cabot Head and Coboconk Formations in DGR Boreholes

Formation and Contact Assumption	Strike	Dip
Cabot Head Shale		
Assumed Borehole Verticality	N18.6°W	0.53°SW
True Borehole Positions	N18.0°W	0.51°SW
0.1 m Uncertainty	N16.6°W to N18.5°W	0.49° to 0.51°SW
0.5 m Uncertainty	N12.8°W to N22.5°W	0.44° to 0.55°SW
1.0 m Uncertainty	N6.7°W to N27.7°W	0.39° to 0.60°SW
Coboconk Formation – Ash Marker Bed		
Assumed Borehole Verticality	N19.6°W	0.58°SW
True Borehole Positions	N19.3°W	0.55°SW
0.1 m Uncertainty	N18.5°W to N20.2°W	0.54° to 0.56°SW
0.5 m Uncertainty	N15.1°W to N23.8°W	0.50° to 0.61°SW
1.0 m Uncertainty	N11.1°W to N28.3°W	0.45° to 0.66°SW

Assuming that the strata below the Salina B Unit should have relatively uniform orientation, the ranges of potential errors in strike and dip listed in Table 3.19, when compared to the range of strikes and dips recorded in Table 3.2, suggest that errors in identified formation contacts are likely between 0.1 and 0.5 m, which is essentially the potential error in depth determination within DGR boreholes.

The descriptive geological site model confirms that a total thickness of 212 m of tight shale and argillaceous limestone of Ordovician age overlies the proposed DGR repository host Cobourg Formation. Additional barrier rocks also exist within the overlying 278-m-thick Silurian formations that contain similar tight shales, evaporites and dolostones.

3.15.2 Major Mineralogy of Model Layers

Confidence in the reported major mineralogy of the 35 bedrock layers that comprise the descriptive geological model is judged to be high. Major mineralogy is determined from a wide range of methods including core logging by field geologists, and laboratory testing using thin section petrography, whole rock and clay fraction XRD, SEM/EDS analyses and elemental oxide analyses undertaken by several different laboratories. Interpretation of these different data sets on a formation or model layer basis, as described in Section 3.8, yields a generally coherent identification of the major mineralogy of the model layers that is consistent with the stratigraphic descriptions provided for these rocks by Armstrong and Carter (2006). Consequently, it is reasonable to extrapolate and assume the major mineralogy defined by data at DGR boreholes is representative of mineralogy across the entire DGR site.

Examples of the similar identification of major minerals by different testing laboratories is provided in Figures 3.72 and 3.73.

Figure 3.72 shows the percent weight content of calcite and dolomite in whole rock for all DGR boreholes determined from XRD analyses differentiated on the basis of analytical laboratory. Figure 3.73 shows the same information for quartz and total sheet silicate contents. Figures 3.72 and 3.73 are similar to Figures 3.5 and 3.6, except that the data are differentiated based on analytical laboratory rather than based on DGR borehole.

Figures 3.72 and 3.73 show that the four different laboratories engaged in quantitative to semi-quantitative analyses of major mineralogy by XRD (Activation Laboratories, SGS Laboratories, Core Laboratories and UniBern) generally reported similar contents of calcite, dolomite, quartz and sheet silicates in DGR cores. There is clearly some variability in reported major mineral percentages, but this variability is most likely due to mineralogical heterogeneity in the analysed core samples, not to bias or error in laboratory analyses.

3.15.3 Occurrence of Soluble Minerals

Confidence in the reported occurrence of soluble minerals in the layers that comprise the descriptive geological model is judged to be moderate to high depending upon the mineral and the model layer considered. For the major evaporite layers (e.g., B Unit anhydrite, A2 Unit evaporite and A1 Unit evaporite), soluble minerals are present in major percentages and their detection is not an issue. However, identification of soluble minerals such as gypsum, anhydrite, celestite and halite, when present in minor or trace amounts, is difficult but nonetheless important because their presence is an indicator of a lack of recent advection through the formations and understanding their presence or absence is essential to accurate interpretation of porewater chemistries. Dissolution of trace soluble minerals during crush and

leach experiments (see Section 4.6) can significantly influence the resultant estimates of Ca, Sr, Na and Cl concentrations in porewater. Furthermore, release of mineralogically bound

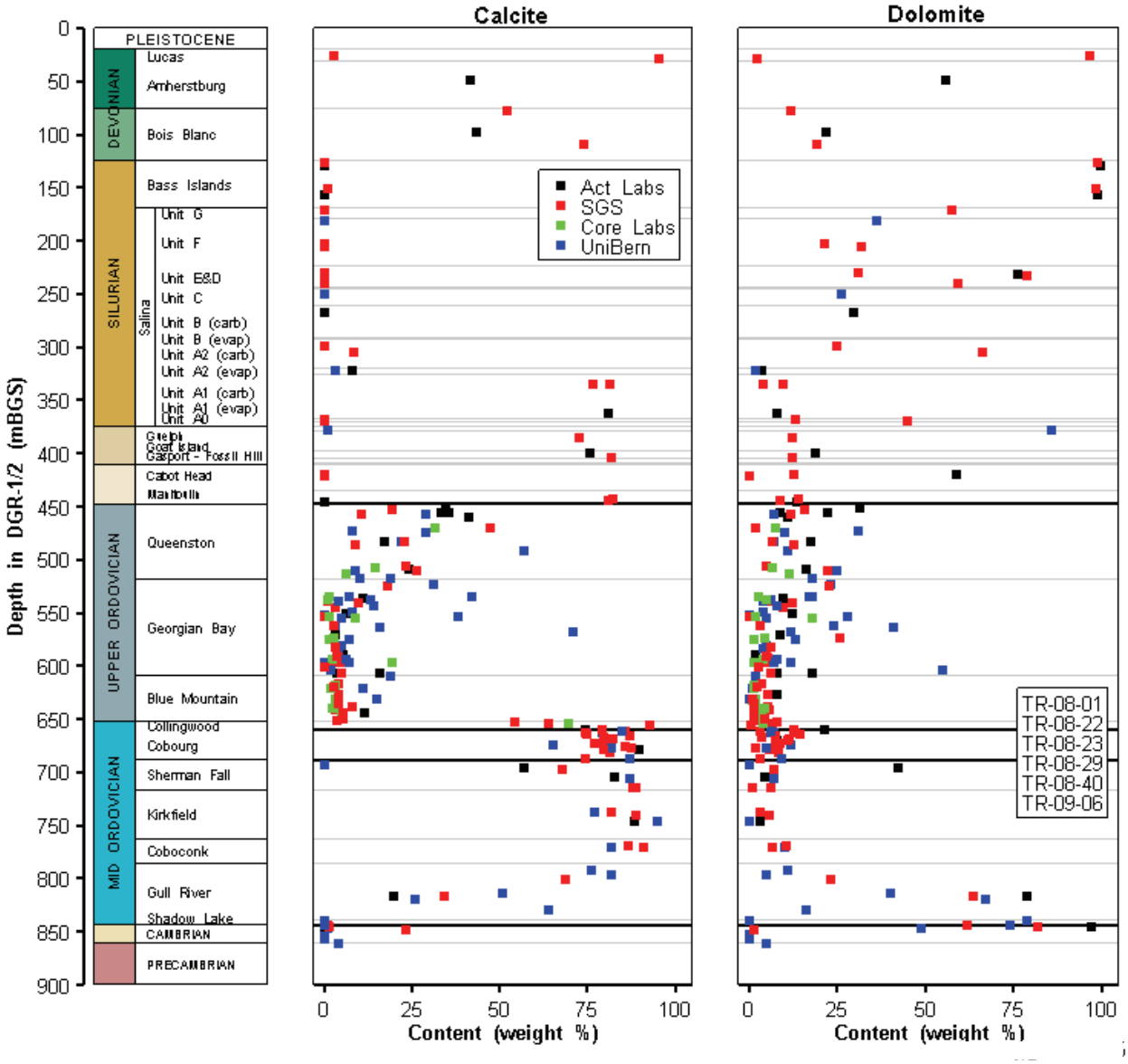

Figure 3.72: Profiles of Calcite and Dolomite in DGR Cores Differentiated by Analytical Laboratory

water from gypsum during heating and vacuum distillation can result in overestimation of water loss and liquid porosity.

Because soluble minerals are often present in trace amounts, their reliable detection in core and on fracture surfaces during core logging is often difficult and frequently not possible. This is especially true for highly soluble minerals such as halite, which are subject to dissolution by

drilling fluids, despite the use of Na:Ca-Cl brine drilling fluids with TDS averaging about 150,000 mg/L for drilling of the Silurian and Ordovician formations. Figure 3.28 is an example of such dissolution of halite as a fracture-infilling mineral within the Queenston shale, where the estimated original thickness of halite (~ 1 cm) was sufficiently large that even with dissolution, halite remnants were observed. For thinner halite fracture infillings, dissolution would likely remove all visual evidence of halite on the fracture surfaces. For anhydrite, gypsum and celestite, which are moderately soluble, detection in core is possible. These mineral phases have been observed during core logging activities, although distinguishing between anhydrite and gypsum in the field is problematic.

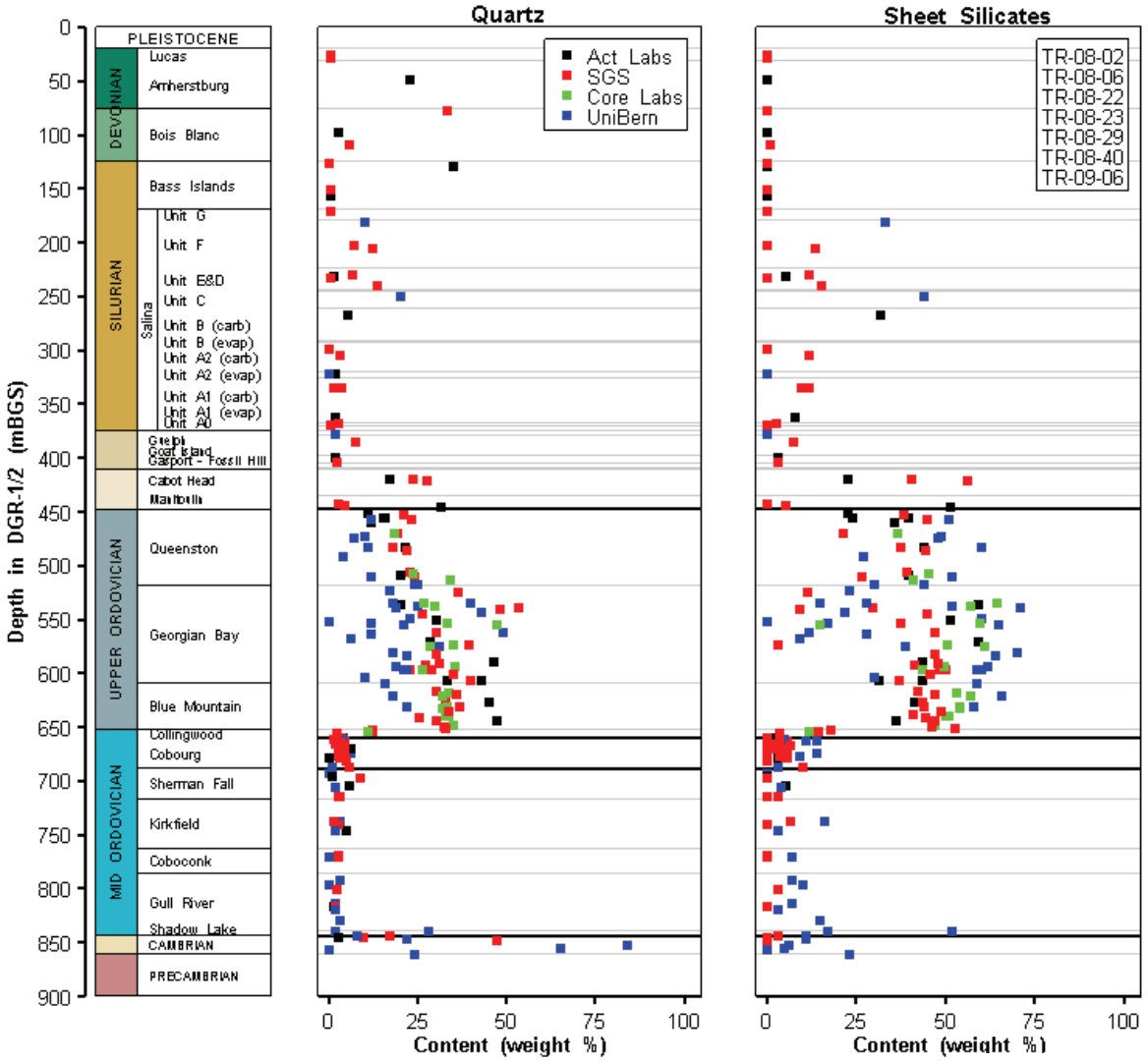

Figure 3.73: Profiles of Quartz and Total Sheet Silicates in DGR Core Differentiated by Analytical Laboratory

Recognizing these field limitations to identification of soluble minerals, laboratory methods were utilized to provide more reliable identification. Thin section petrography, XRD and SEM/EDS

methods were used to directly identify the presence or absence of trace levels of soluble minerals. Anhydrite, gypsum and celestite were routinely detected by thin section petrography, as well as by XRD and SEM/EDS. Lithogeochemical analyses including elemental oxides, as well as sulphate and total sulphur analyses provided support for detection of these soluble sulphate minerals.

However, for halite, detection by thin section petrography was unreliable due to mineral dissolution during thin section preparation despite precautions, including use of oil during cutting and polishing, taken to minimize such effects. XRD and SEM/EDS were much more reliable in detecting halite occurrence as interstitial veins, grain boundary minerals and as mineralogical rims or coatings. Based on frequency of detection, SEM/EDS methods were the most effective at identification of halite in Silurian and Ordovician model layers. However, there is also some uncertainty associated with halite detection by SEM/EDS analyses as some of the reported spot detections may simply be halite precipitation from porewater caused by sample desiccation and drying (Herwegh and Mazurek 2008). Mineral identification by visual inspection, optical microscopy and XRD methods are not likely affected by sample desiccation since these methods are only applicable for relatively large mineral weight percents, which cannot be created by porewater evaporation.

Based on the comparability of soluble minerals identified in different DGR boreholes and by different laboratories and laboratory analytical methods, it is reasonable to assume that occurrence of soluble minerals defined based on DGR borehole data is representative of occurrences across the entire DGR site.

3.15.4 Occurrence of Major Structural Features

Confidence in the ability to recognize the occurrence of major structural features, such as erosional unconformities and faults, and other structures other than simple fractures in the descriptive geological model for the immediate vicinity of the DGR is judged to be high for subhorizontal features and moderate for inclined features.

The occurrence of major subhorizontal features is reliably defined based on detections in DGR boreholes. The uniformity and predictably of the bedrock formations at the Bruce nuclear site shows that geological conditions that would identify the presence or absence of subhorizontal structural features can be confidently assessed from DGR borehole data. For example, the presence of subhorizontal structures as erosional unconformities associated with the Devonian-Silurian unconformity and the Cambrian-Precambrian unconformity are reliably identified in DGR boreholes. Similarly, the lack of subhorizontal structure associated with the Silurian-Ordovician unconformity is also evident in all DGR boreholes.

Confidence in the occurrence of major inclined structural features is always low when drilling investigations are based on vertical boreholes, because of the negligible horizontal coverage and potential for intersection of subvertical structure afforded by vertical boreholes. This low confidence in the occurrence of major inclined structures is improved through the completion of 2-D seismic reflection surveys, inclined borehole drilling of identified potential seismic features, and the recognized lack of vertical offsets in formation contacts that would be indicative of subvertical faults. As discussed in Section 3.11.4, the available data from Phase 2 investigations, in particular the drilling of DGR-5 and DGR-6, indicate the absence of major inclined structural features in the vicinity of the DGR site. As well, the simple planar geometry and consistent thickness of the stratigraphic units between the DGR boreholes and the Texaco #6 well argues strongly against any major fault offsets in the vicinity of the Bruce nuclear site.

Confidence in the assessment of the presence or absence of inclined major structural features at the DGR site is in part linked to confidence in the results of the 2-D seismic reflection surveys and the identification of seismic anomalies investigated by directional drilling of DGR-5 and DGR-6. There are clearly limitations and uncertainties in the 2-D seismic surveys which are fully described in TR-07-15. These limitations and uncertainties are due to poor seismic energy coupling between the overburden and bedrock, anthropogenic and natural background noise, and constraints on seismic sources and line coverage inherent in completing the surveys in a developed area of a nuclear site. As discussed in Section 3.11.4, these limitations and uncertainties were mitigated by optimization of data collection techniques and additional effort in data processing. The potential 2-D seismic features identified and targeted for drilling were judged to be those with the strong signatures identified on multiple survey lines and hence most likely to be representative of potential vertical structure at the Bruce nuclear site. As these potential structures with the strong seismic signatures have been shown to be absent based on drilling of DGR-5 and DGR-6, it is unlikely that other sub-vertical structures associated with weaker seismic features would be present at the site.

3.15.5 Characterization of Minor Structural Features

Confidence in the characterization of minor structural features, such as simple fractures (e.g., joints) in the 35 bedrock layers that comprise the descriptive geological model is judged to be high for subhorizontal features and moderate for inclined and subvertical features based on current borehole data.

As described above, the sampling of subhorizontal fractures is very good with vertical boreholes and the available data on their occurrence and characteristics is given in TR-07-06 and TR-08-13 from core logging and in TR-07-08 and TR-08-15 from borehole geophysical logging, in particular borehole acoustic televiewer logs. As discussed in Section 3.12, there are biases in the identification of fractures from both core logging and from interpretation of borehole geophysical logging. However, judicious comparison of the results of these two data sets considering these biases allows for a reasonable interpretation of the characterization of fractures in the layers that comprise the descriptive geological model of the DGR site.

Fracture occurrence as evident from RQD and natural fracture frequency plots (Figures 3.3 and 3.4) from core logging is comparable on a formation or model layer basis in all DGR boreholes. This comparability suggests that subhorizontal fracture characterization defined based on DGR borehole data is representative of occurrences across the entire DGR site. For the vertical boreholes of Phase 1 and 2A site characterization, orientation of fractures was only quantifiable from interpretation of borehole acoustic televiewer logs, which likely underestimates fracture occurrence compared to core logging. Because core logs of borehole DGR-1 to DGR-4 are not oriented they cannot be used to determine strike and dip of logged fractures.

Although inclined to vertical fractures have been logged in DGR boreholes (see Section 3.12.2), the sampling of such fractures in vertical boreholes is very limited and subject to significant bias and underestimation of frequency of occurrence. However, even the limited sampling from DGR-1 to DGR-4 does indicate that inclined to vertical fractures are present in the DGR strata. This initial assessment of inclined fracture occurrence in DGR boreholes was confirmed with oriented core logging and borehole acoustic televiewer logging of inclined boreholes DGR-5 and DGR-6. Because boreholes DGR-5 and DGR-6 have been drilled approximately orthogonal to each other, there is limited overall sampling bias of inclined to vertical fractures from these holes.

There is general similarity of inclined fracture occurrence determined from both oriented core logging and borehole acoustic televiewer logging. However, the similarity between the orientation of inclined fractures determined from oriented core logging/ATV logging of the Silurian and Ordovician formations in DGR boreholes with detailed surface mapping near the Bruce nuclear site and regional datasets is judged to be fair, with some but not all fracture sets evident in the two data sets. This partial comparability is not entirely unexpected as surface data are primarily from Devonian formations and subsurface DGR data are presented for Silurian and Ordovician formations. Some variation in fracture set characteristics should be expected between Devonian, Silurian and Ordovician groups of formations.

4. DESCRIPTIVE HYDROGEOLOGICAL SITE MODEL

4.1 Model Elements and Scope

The hydrogeological site model describes the hydrogeologic properties and 3-D spatial distribution of all important hydrogeologic units and features within the Paleozoic bedrock units at the Bruce nuclear site. The descriptive hydrogeological model provides a basis for understanding the groundwater flow and solute transport properties of the Paleozoic bedrock that will contain and isolate the proposed Bruce DGR, based on detailed field and laboratory testing. The hydrogeological site model focuses on description of the physical properties (rock density, porosity, fluid saturations, gas-brine flow properties, permeability/hydraulic conductivity, specific storage, pressure/hydraulic head and diffusivity) of the bedrock, and geochemical/isotopic properties of the groundwater and porewater of the Bruce nuclear site.

4.2 Data Sources

Primary data sources for the descriptive hydrogeological site model include:

- The descriptive geological site model given in Chapter 3 of this report;
- Observations during drilling, logging and sampling of boreholes DGR-1 and DGR-2 (TR-07-05, TR-07-06), DGR-3 and DGR-4 (TR-08-12, TR-08-13), DGR-5 and DGR-6 (TR-09-01, TR-09-11) and US-8 (TR-07-19);
- Borehole geophysical logging of DGR-1 and DGR-2 (TR-07-08), DGR-3 and DGR-4 (TR-08-15), DGR-5 and DGR-6 (TR-09-03) and US-3, US-7 and US-8 (TR-07-19);
- Borehole fluid electrical conductivity logging of DGR-1 (TR-07-14) and straddle-packer hydraulic testing of DGR boreholes (TR-08-32);
- Evaluation of hydraulic communication between DGR-1 and DGR-2 (TR-08-07);
- Opportunistic groundwater sampling of DGR-1 and DGR-2 (TR-07-11) and of DGR-3 and DGR-4 (TR-08-18);
- Pressure monitoring of DGR boreholes completed with MP55 multi-level monitoring casings (TR-08-31);
- Groundwater monitoring of US-3, US-7 and US-8 boreholes completed with MP38 multi-level monitoring casings (TR-08-08, TR-08-30);
- Laboratory petrophysical testing of DGR-2 core (TR-07-18, TR-08-06), of DGR-3 and DGR-4 core (TR-08-28, TR-08-40), and of DGR-5 and DGR-6 core (TR-09-08);
- Laboratory diffusion testing of DGR-2 core (TR-07-17, TR-07-22) and of DGR-3 and DGR-4 core (TR-08-27);
- Laboratory porewater characterization of DGR-1 and DGR-2 core (TR-07-17, TR-07-21, TR-08-06), of DGR-3 and DGR-4 core (TR-08-19, TR-08-27, TR-08-37, TR-08-40), and of DGR-5 and DGR-6 core (TR-09-04);
- Characterization of groundwater and porewater for radioisotopes (TR-08-38);
- Compilation and consolidation of field and laboratory data for hydrogeological properties (TR-08-10);
- A comparative and critical evaluation of porosity and fluid saturation data generated for DGR cores by different testing laboratories (TR-08-34);
- Geotechnical investigations and cooling water intake tunnelling experience (GOLDER 2003) and straddle-packer hydraulic testing of boreholes US-1 and US-3 to US-7 (Lukajic 1988); and

- Regional hydrogeological modeling (Sykes et al. 2011) and regional hydrogeochemical (Hobbs et al. 2011b) geosynthesis studies and geosynthesis updates to these studies (NWMO 2011).

4.3 Petrophysical Properties

4.3.1 Rock Density

Wet and dry bulk densities and grain density were measured on DGR core samples by Core Laboratories, University of New Brunswick, and the University of Bern as part of petrophysical, diffusion and porewater characterization programs. All of these density parameters can be determined from basic lab measurements of wet and dry rock sample weights and volumes and assumptions of porewater salinity and density. However, not all laboratories reported all three density values and the densities reported here are only those reported in technical reports by each laboratory.

Core Laboratories (Core Labs) completed single tests of wet bulk density on "as received" calipered sub-cores and of grain density using Boyle's Law of gas expansion on "cleaned and dried" sub-cores subject to depth-specific hydrostatic confining stress of 17 kPa/m (for DGR-2 cores – TR-07-18) and 34 kPa/m (for DGR-3 and DGR-4 cores – TR-08-28) that approximates the effective stress due to the overlying rock mass. DGR-5 and DGR-6 cores tested by Core Labs (TR-09-08) were not subject to confining stress. Core Labs density measurements were completed on small plugs of core weighing approximately 150 g.

University of New Brunswick (UNB) reported (TR-07-17, TR-08-27) mean grain density for triple to quadruple subsamples of DGR-2, DGR-3 and DGR- 4 core subject to oven drying considering the density of the brine porewater. UNB density measurements were completed on small discs of core weighing approximately 140 g.

University of Bern (UniBern) reported mean bulk wet density, mean dry densities and mean grain density on subsamples of DGR-2, DGR-3 and DGR-4 core (TR-08-06, TR-08-40). Bulk wet densities were measured in duplicate on 4-6 g samples using the paraffin displacement method. Grain densities were measured in duplicate on 15-g samples using the kerosene-pycnometry method. Dry bulk densities were both measured in duplicate using the paraffin displacement method (DGR-2 and DGR-4 cores) and calculated from bulk wet density and porewater content measured on different sized samples (DGR-2, DGR-3 and DGR-4 cores).

Table 4.1: Summary of Wet Bulk Density, Dry Bulk Density and Grain Density of DGR Cores in g/cm^3

Formation	Wet Bulk Density			Dry Bulk Density			Grain Density		
	Mean	Std Dev	N	Mean	Std Dev	N	Mean	Std Dev	N
Silurian formations	2.63	0.12	69	2.57	0.17	18	2.80	0.11	104
Ordovician shales	2.65	0.04	69	2.59	0.06	40	2.76	0.04	126
Ordovician limestones	2.69	0.04	65	2.66	0.02	38	2.71	0.03	109
Shadow Lake and Cambrian sandstone	2.60	0.17	9	2.54	0.24	10	2.72	0.10	9

The University of Ottawa (UofO) reported (TR-07-21, TR-08-19) mean grain densities for samples of crushed rock chips used in porewater analyses that weighed approximately 30 g.

In total, approximately 106 measurements of dry bulk density, 212 measurements of "as received" bulk wet density and 348 measurements of grain density were made. Table 4.1 summarizes the mean, standard deviation and number (N) of density samples grouped by Silurian formations, Ordovician shales, Ordovician limestones and the Shadow Lake sandstone/siltstone and Cambrian sandstone.

The mean wet bulk density of the Ordovician shales of Table 4.1 is 2.65 g/cm^3. This can be compared to a mean of 2.69 g/cm^3 for the argillaceous limestones. The difference is a reflection of the porosity distribution and mineralogy of the two rock types. The mean wet bulk density for the Shadow Lake and Cambrian rocks was 2.60 g/cm^3. As expected, the dry bulk densities are less than the wet bulk densities due to the loss of porewater. The mean bulk dry density of the Shadow Lake and Cambrian sandstone is much lower at 2.54 g/cm^3, reflecting its higher porosity of about 15%.

Table 4.1 also presents grain densities of the 348 core samples tested by the three laboratories. Results are similar between laboratories and are in accordance with expectations based on formation mineralogy. The formations with the highest grain densities are the Queenston, Georgian Bay and Gull River formations, in which certain zones have densities of or approaching 2.8 g/cm^3. Such relatively high grain densities appear to be correlated with the presence of relatively heavy iron minerals such as pyrite (5.0 g/cm^3) and hematite (5.25 g/cm^3). By contrast, limestones, which are composed of calcite (2.71 g/cm^3) and dolomite (2.90 g/cm^3), or iron-poor shales, in which illite (~2.8 g/cm^3) and chlorite (2.6-2.8 g/cm^3) are the predominant minerals, yield lower grain densities. The mean grain density of the Ordovician shales is 2.76 g/cm^3 that may be compared to a mean of 2.71 g/cm^3 for the argillaceous limestones. The mean grain density of the Shadow Lake and Cambrian sandstone is 2.72 g/cm^3 reflecting the dominant presence of quartz and carbonate minerals in the strata.

Figure 4.1 illustrates the wet bulk, dry bulk and grain density data plotted against depth and DGR-1/2 reference formation stratigraphy. Figure 4.1 shows the individual core measurements and the arithmetic formation averages. Replicate analyses from the same core samples were averaged and plotted as single values in Figure 4.1. The Core Labs and UniBern data are "as received" wet bulk densities that reflect the presence of porewater in the samples. The grain densities are from the Boyle's Law measurements on "cleaned and dried" samples by Core Labs and on oven-dried samples from UNB and UniBern.

Figure 4.1 shows that there is considerable scatter in the Silurian and Cambrian wet bulk and grain densities, but that the densities within the Ordovician shales and limestones are typically more uniform. The scatter in the Silurian samples is likely due to variations in grain density reflecting the porosity variations and the relative abundances of gypsum (2.3 g/cm^3) versus heavier minerals such as dolomite (2.9 g/cm^3) and anhydrite (2.9 g/ cm^3). The scatter in the Cambrian data is similarly likely due to porosity and mineralogical variations evident in the dolomitic and quartzose sandstone facies that comprise the Cambrian rocks.

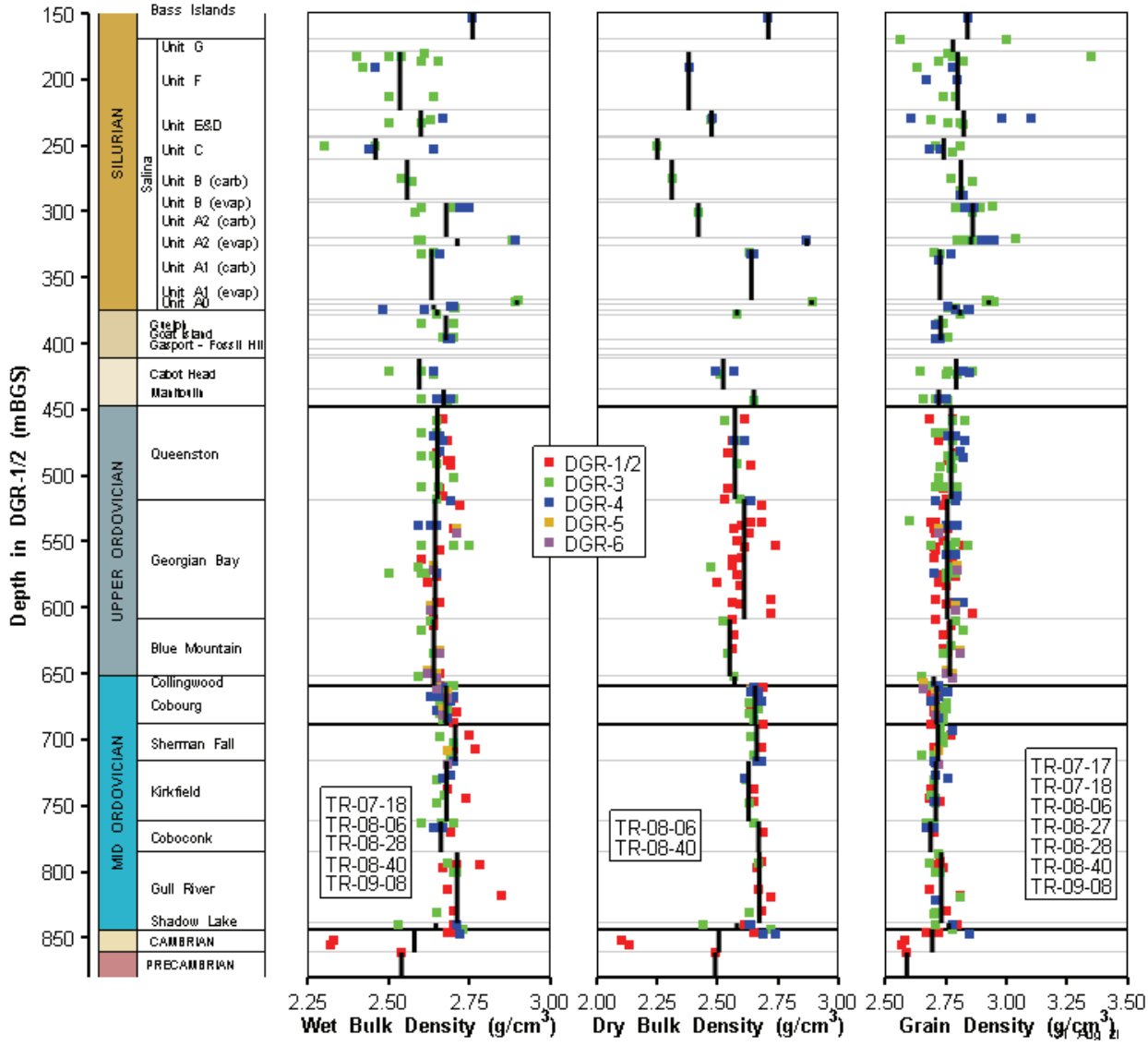

Figure 4.1: Wet Bulk Density, Dry Bulk Density and Grain Density Data Profiles from DGR Cores Showing Point Data and Arithmetic Formation Averages

4.3.2 Porosity

4.3.2.1 Definitions and Experimental Methods

Porosity is a general term used to describe the fraction of the volume of voids over the total rock volume. Three types of porosity are defined in this DGSM to differentiate the type of fluid occupying the void space and the measurements made by different testing laboratories - total porosity, liquid porosity and water-loss porosity. Total porosity, also known as physical porosity, is the sample volume not occupied by mineral grains (i.e., total volume of voids) divided by the volume of the sample. Liquid porosity is the volume of the voids occupied by liquid (i.e., pure

water plus dissolved solutes and oil) divided by the total volume of the sample. Water-loss porosity is the volume of the voids occupied by pure water divided by the total volume of the sample. Total porosity should equal liquid porosity plus porosity occupied by any gas (e.g., methane). The equations and data used to calculate water-loss porosity and liquid porosity may be found in TR-08-34. TR-08-10 provides a discussion on the selection of total porosity for each hydrogeological model layer from available data.

Total porosity and/or water-loss porosity was measured on DGR rock cores by Core Laboratories, University of Ottawa, University of New Brunswick and University of Bern as part of petrophysical, diffusion and porewater testing programs. Several of these laboratories also reported liquid porosities by correcting the water-loss porosities for an assumed brine density, individually selected by each lab. In order to compare liquid porosity measurements between the different laboratories, a consistent density correction needs to be applied. Therefore, all lab data were reduced to water-loss porosity values and were converted to liquid porosity values by assuming a mass of salts for each sample based on average brine densities and total dissolved solids (TDS) concentrations for each formation. TR-08-34 describes the process of this standardization and conversion of porosity data.

Individual laboratory methods are described and sample measurements are included in the following technical reports:

- Core Labs - DGR-2 core (27 samples, TR-07-18), DGR-3 and DGR-4 core (37 samples, TR-08-28) and DGR-5 and DGR-6 core (19 samples, TR-09-08);
- University of Ottawa – DGR-2 core (50 samples, TR-07-21), DGR-3 and DGR-4 core (78 samples, TR-08-19) and DGR-5 and DGR-6 (104 samples, TR-09-04);
- University of New Brunswick – DGR-2 core (14 samples, TR-07-17) and DGR-3 and DGR-4 core (58 samples, TR-08-27); and
- UniBern – DGR-2 core (48 samples, TR-08-02) and DGR-3 and DGR-4 core (50 samples, TR-08-40).

Table 4.2 summarizes the various approaches taken by individual laboratories to determine DGR core porosity as well as additional calculations undertaken in this report to provide a common basis for comparison of different porosity data.

Total porosity was typically determined from bulk dry and grain density data on confined and unconfined core samples. Water-loss porosity was typically determined gravimetrically through heating and drying of unconfined core samples.

Core Labs measured total porosity on horizontal and vertical subsamples of core (~150-g plug) by the Boyle's Law gas (He) expansion method on cores that had pore fluids removed (i.e., "cleaned and dried") and were then brought to a depth-specific hydrostatic confining stress (17 kPa/m for DGR-2 cores, 34 kPa/m for DGR-3 and DGR-4 cores). Water-loss porosity values were calculated using lab data from Dean Stark fluid saturation measurements. For DGR-3 and DGR-4 cores, Core Labs also measured total porosity on unconfined cores, such that a direct estimate of the magnitude of porosity increase due to core relaxation could be determined. For DGR-5 and DGR-6 cores, Core Labs measured total porosity and liquid porosity using Dean Stark methods and using Nuclear Magnetic Resonance (NMR)/He gas expansion methods on the same cores. These DGR-5 and DGR-6 tests were done on unconfined cores, as core confinement was not possible during NMR testing.

UniBern reported total porosity data for core subsamples (~4-5 g plug) based on the average of two replicate measurements of bulk dry and grain densities for each core subsample. UniBern also analysed larger subsamples (~60-500 g) for liquid porosity measurements on DGR-2 core (assuming the density of pore fluid was at halite saturation) and water-loss porosity values on DGR-3 core. All UniBern liquid porosity data were reduced to water-loss porosity values for comparison to similar data from other labs.

University of Ottawa reported volumetric water content for subsamples of crushed cores (~30 g) based on the average of four to five replicate measurements using vacuum distillation methods (150°C) to remove porewater. All University of Ottawa volumetric water content values were converted to water-loss porosity values for comparison to similar data from other labs.

Table 4.2: Summary of Porosity Measurements for DGR Core by Different Testing Laboratories

Test Element	UniBern	UofO	UNB	Core Labs
Reported measurements	98 total porosity 21 liquid porosity	232 water content	72 liquid porosity	83 total porosity and water saturation
Methods	Bulk dry/grain density calculation using Archimedes Principle (paraffin displacement)	Bulk dry/grain density calculation using Vacuum Distillation	Bulk dry/grain density calculation using Archimedes Principle (brine displacement)	Boyles Law gas expansion on confined & unconfined samples, Dean Stark & NMR/He gas fluid saturations
Sample size	~4-5 g plug (total) ~60-420 g (water-loss)	~30 g crushed	~40-100 g disc	~150 g plug
Drying temperature	40°C and 105°C	150°C	105°C	105°C
Drying time in days, range (mean)	48-135 (99) @ 40°C 12-174 (92) @ 105°C	0.25 by vacuum distillation	7 to 89 (21)	2 to 7 vacuum oven
Correction for brine density	1.3 g/cm^3 (< 830 mBGS) 1.2 g/cm^3 (> 830 mBGS)	DGR-1/2 (not corrected); DGR-3/4 (sample specific TDS)	variable	1.187 g/cc (TDS=250 g/kg)
Additional Intera calculations	Reduced to water-loss porosity and then converted to liquid porosity based on formation average TDS	Converted water content to water-loss porosity and then to liquid porosity based on formation average TDS	Reduced to water-loss porosity and then converted to liquid porosity based on formation average TDS	Calculated water-loss porosity from S_w and then converted to liquid porosity based on formation average TDS

University of New Brunswick reported liquid porosity values for small discs of core (~40-100 g) based on the average of three or four replicate measurements using oven heating methods and assuming various brine densities based on depth. All University of New Brunswick liquid porosity data were reduced to water-loss porosity values for comparison to similar data from other labs.

4.3.2.2 Porosity Values

Figures 4.2 and 4.3 show the liquid and total porosity data including arithmetic formation averages, respectively, from DGR cores plotted against depth and bedrock formations. Replicate analyses from the same core sample were averaged and plotted as a single value in this figure. Figures 4.2 and 4.3 also show the arithmetic mean values of the porosity data calculated on a formation, member and unit basis. Table 4.3 summarizes the overall mean and standard deviation of all of the porosity data including the standardized water-loss porosity by formation and groups of formations.

Table 4.3: Summary of Water-loss, Liquid and Total Porosities of DGR Cores in %

Formation	Water-Loss Porosity			Liquid Porosity			Total Porosity		
	Mean	Std Dev	N	Mean	Std Dev	N	Mean	Std Dev	N
Silurian and Devonian	7.5	6.3	145	8.2	6.7	145	8.9	6.8	31
Ordovician shales	7.0	1.5	104	8.0	1.7	104	7.4	1.7	41
Ordovician shale hard beds	1.5	0.9	22	1.7	1.1	22	2.5	1.8	17
Ordovician limestones	1.6	1.5	167	1.8	1.6	167	1.9	1.3	43
Shadow Lake and Cambrian sandstone	6.9	5.3	16	7.5	5.8	16	9.5	7.1	6

To allow for a common basis for comparison with other laboratory test results, only the total porosity values determined from Core Labs for unconfined cores are included in the summary Table 4.3 and Figure 4.3, and in subsequent figures that compare liquid and total porosities. This is because none of the other testing laboratories applied confining stress in the determination of total or liquid porosities. For DGR-5 and DGR-6 cores tested by Core Labs, the total and liquid porosity data set includes data from both Dean Stark and NMR/He testing. Where available, the total porosity values for confined cores determined by Core Labs are used in the calculation of fluid saturations (Section 4.3.3), in the plotting of fluid saturation against total porosity data, and in the assessment of total porosity changes due to core relaxation that occurs from in situ confined conditions to unconfined lab testing conditions.

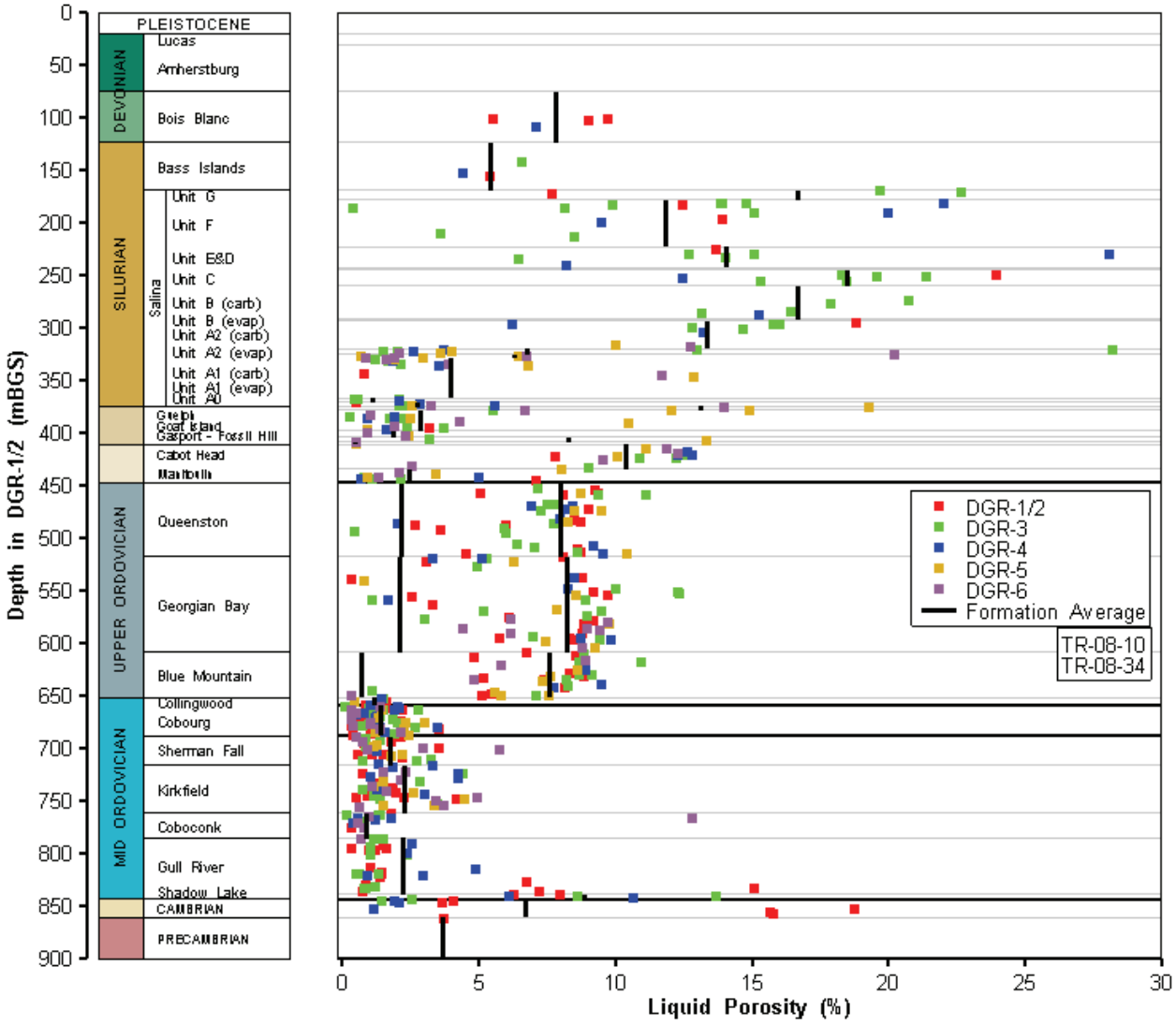

Figure 4.2: Liquid Porosity Profile for DGR Cores Showing Point Data and Arithmetic Formation Averages

The total and liquid porosity measurements in the uppermost Silurian Salina F through A2 Units, as shown in Figures 4.2 and 4.3, range from 5 to 25%, often exceeding 10%. The highest measurements of liquid porosity occur in the Salina C Unit dolomitic shale and a shaly dolostone sample found in the Salina B Unit Carbonate with values of 14-25%. The mean liquid porosities reported for the Devonian and Silurian Units and formations range from 1.1% for the Salina A1 Unit Evaporite to 18.5% for the Salina C Unit dolostone. Silurian argillaceous dolostone and shale sequences as represented by the Salina G and F Units and Cabot Head Formation show mean liquid porosities of 16.7%, 10.7% and 10.4%, respectively. Other Devonian and Silurian dolostone sequences including the Bois Blanc, Bass Islands, Goat Island, Gasport, Lions Head, Fossil Hill and Manitoulin formations and Salina Lower A1 Unit show variable liquid porosity ranging from 0.5 to 8.3%. The permeable Silurian aquifers of the

Salina Upper A1 Unit and the Guelph Formation have mean liquid porosity of 6.3% and 13.1%, respectively. For many of the core samples collected from the Salina Formation where gypsum ($CaSO_4 \cdot 2H_2O$) may be present as secondary mineralogy (e.g., G Unit to A2 Unit Carbonate), the liquid porosities are likely overestimations due to release of the hydration water during heating.

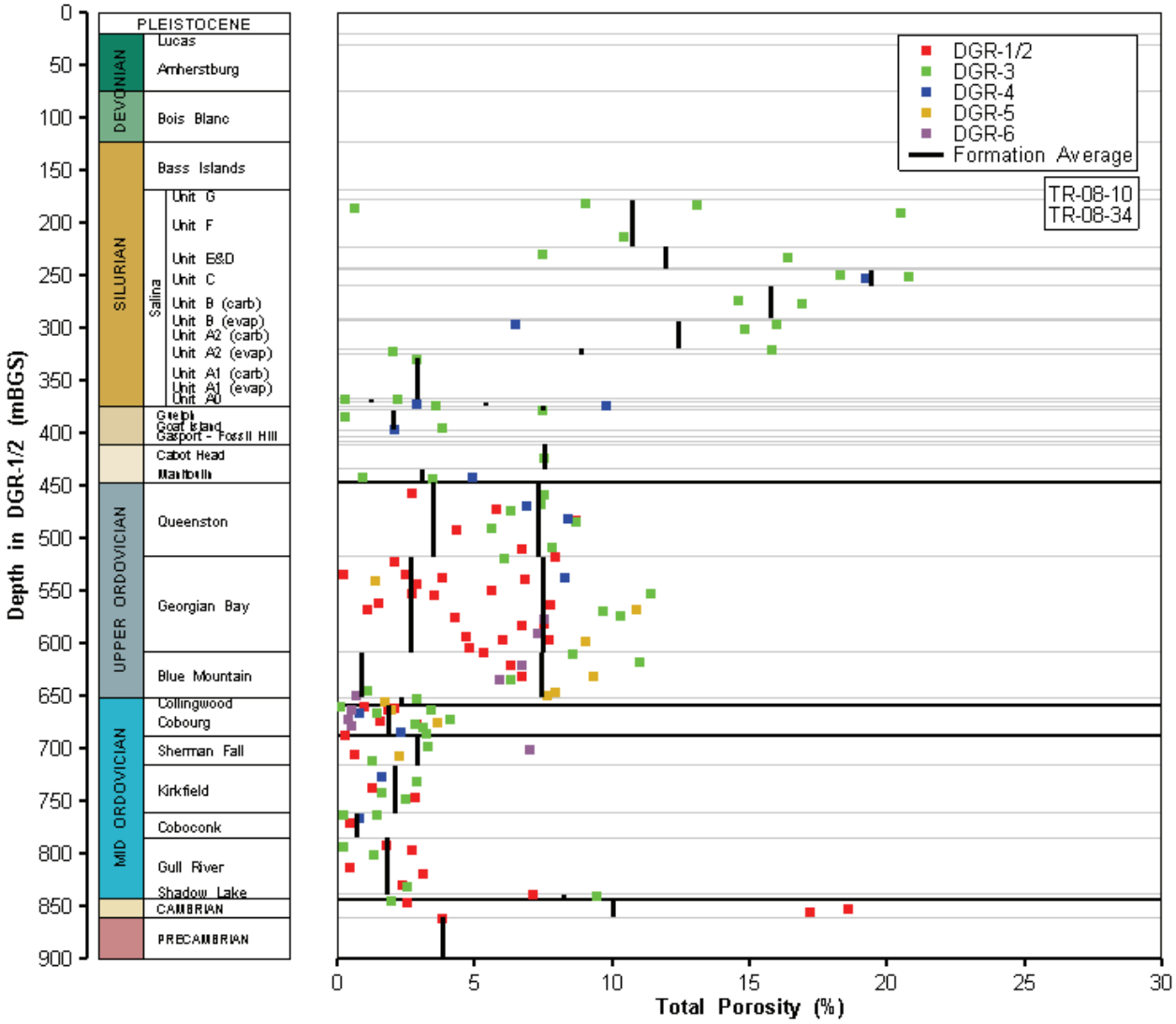

Figure 4.3: Total Porosity Profile for DGR Cores Showing Point Data and Arithmetic Formation Averages

The total and liquid porosity profiles display a very pronounced reduction in porosity in the Lower Silurian formations and immediately above the Ordovician shales. This reduction in porosity is generally to below 5% and is consistent with the porosity values observed in the

Ordovician limestones and also the limestone/siltstone “hard beds” found in the Ordovician shales.

Figures 4.2 and 4.3 show that the total and liquid porosities for the Ordovician shale formations are clustered by two groupings and that the liquid porosities are slightly larger than the total porosities. The two groupings of porosity data reflect the different mineralogy of samples tested within the Ordovician shale formations. The more massive shale samples show formation mean total porosity of 7.3 to 7.5% and liquid porosity of 7.6 to 8.2%. The lower porosity data (mean formation total porosity 0.9 to 3.5%, mean formation liquid porosity 0.7 to 2.2%) are for ‘hard beds’ within these shale formations that are primarily limestone and/or siltstone.

Figures 4.2 and 4.3 present two formation average values for the Upper Ordovician shales representing the shales themselves and the limestone/siltstone hardbeds that exhibit a much lower porosity range that is similar to the underlying Middle Ordovician limestones. Section 4.6.3 discusses the potential role of clay-bound water on the water chemistry. It is assumed that the clay-bound water is accounted for by the water-loss porosity, and since liquid porosity values were based on water-loss porosity, any clay-bound water is also accounted for in the liquid porosity data.

The total and liquid porosity data for the Ordovician limestones are very similar with overall mean values of 1.9% and 1.8%, although the University of Ottawa reported high values (6 to 15%) at the base of the Ordovician limestones (i.e., bottom of Gull River Formation). The single high liquid porosity result of 12.8% from the Coboconk Formation in DGR-6 shown on Figure 4.2 is a sample of the volcanic ash layer. The porosity data for the Shadow Lake and Cambrian sandstone are elevated compared to the overlying limestones with mean total porosity of 9.5% and mean liquid porosity 7.5%.

4.3.2.3 Assessment of Porosity Data

In most hard rocks, total porosity can be similar to or greater than liquid porosity because there are isolated water-filled pores which do not have a physical pathway that allows the water to escape upon heating or solvent extraction. In sedimentary rocks where a separate gas phase may be present, total porosity must also include the gas-filled porosity as well as the liquid porosity.

Figure 4.4 shows the cross plot of liquid porosity and total porosity (unconfined cores) with a 1:1 equivalence or trend line for all data (72 samples) for which total and liquid porosities are measured on the same core sample. Such testing was completed by UniBern and Core Labs. Core Labs total porosity data measured on unconfined core plugs are plotted in Figure 4.4. Figure 4.4 shows the variability in total and liquid porosities discriminated based on major strata groups of Silurian formations, Ordovician shales and Ordovician limestones.

Figure 4.4 shows that 42% of the samples have liquid porosity greater than total porosity and that liquid porosity is more often greater than total porosity for porosities greater than 5%. For total porosities less than 5%, liquid porosity is more comparable to and frequently less than total porosity. Figure 4.4 shows that almost all of the samples with liquid porosity greater than total porosity are Ordovician shales or Silurian formations. The Ordovician limestones plot much closer to the 1:1 trend line and the Cambrian sandstone samples plot very close to the 1:1 trend line. Because many of the units, members or formations with porosity greater than 5% contain clays and gypsum, Figure 4.4 suggests that the exceedences of liquid porosity over total porosity may have a mineralogical explanation.

Therefore, the liquid porosity values of the higher porosity shales and most of the Salina units may be inflated by the presence of gypsum that may lose its hydration waters or clays that might lose their bound waters upon heating (see Section 4.6.3 for detailed description and quantification of this effect). This potential mineralogical explanation for elevated liquid porosities is supported by Lucia (1999) who identifies "(1) incomplete removal of all fluids and (2) alteration of rock fabrics that contain minerals with bound water such as gypsum and clay minerals" as two sources of inaccuracies in laboratory porosity measurements of carbonate rocks.

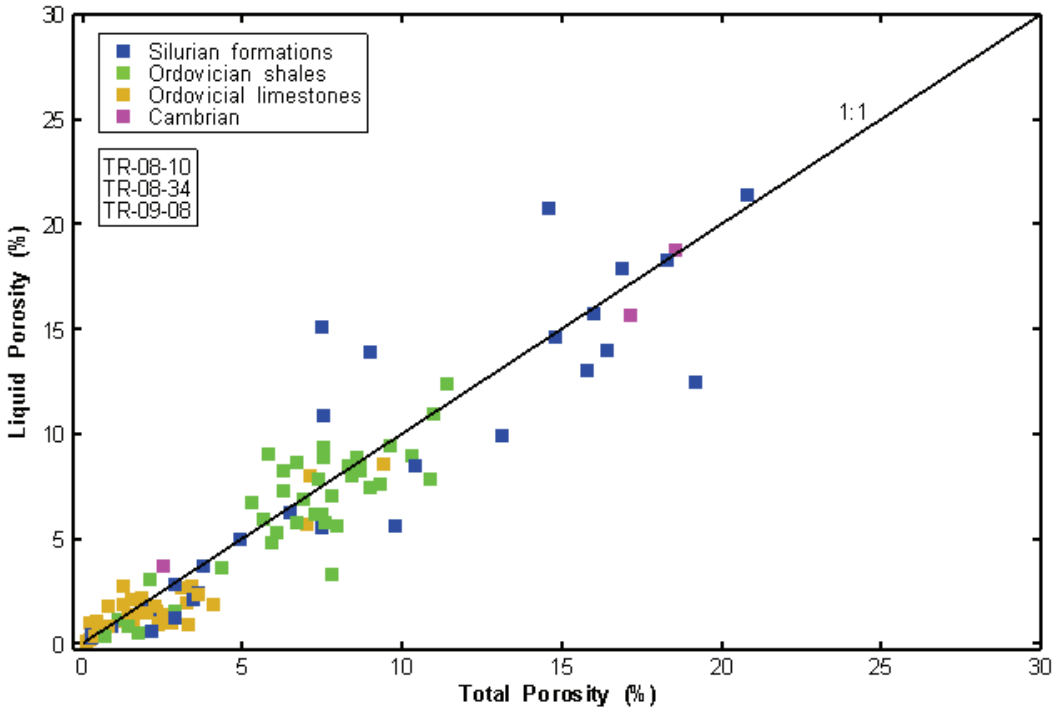

Figure 4.4: Comparison of Liquid and Total Porosities on the Same DGR Core Samples by UniBern and Core Labs, 1:1 Trend Line Is Shown

An additional explanation to account for the higher liquid porosity measurements, although not quantifiable, is that total porosity and liquid porosity are measured by some labs using different methods and on different subsamples of core that are subject to different handling and sample preparation techniques. For example, UniBern measures total porosity on a 4-5 g plug of core while measuring liquid porosity on a different 40-500 g subsample of core. The tested volume in the liquid porosity sample is much greater compared to the total porosity sample and given heterogeneity in mineralogy and porosity which is evident in DGR cores at the cm scale and larger, the equivalence of both porosity values is unlikely due to probable sample size effects, sample heterogeneity, and possibly anisotropy effects.

Anisotropy in porosity at the cm scale is also evident from comparison of the total porosity measurements (unconfined samples) made by Core Labs on 2- to 5-cm-length core plugs that were drilled out of adjacent sections of the same 20-cm-length core sample but in different

directions, i.e., horizontally parallel to the bedding plane or vertically normal to the bedding plane (see Figure 4.5). Figure 4.5 shows the variability of horizontal and vertical total porosities discriminated based on major strata groups of Silurian formations, Ordovician shales and Ordovician limestones. Figure 4.5 shows that there is variability between the total porosity of horizontal and vertical core plugs with horizontal porosity being greater than vertical for the Ordovician limestones and the Ordovician shales by factors of less than 2. For the Silurian rocks tested, the anisotropy is less clear with horizontal:vertical total porosity ratios ranging from 0.5 to 2. The Core Labs error in estimating the porosity by Boyle's Law gas expansion is ~0.3%.

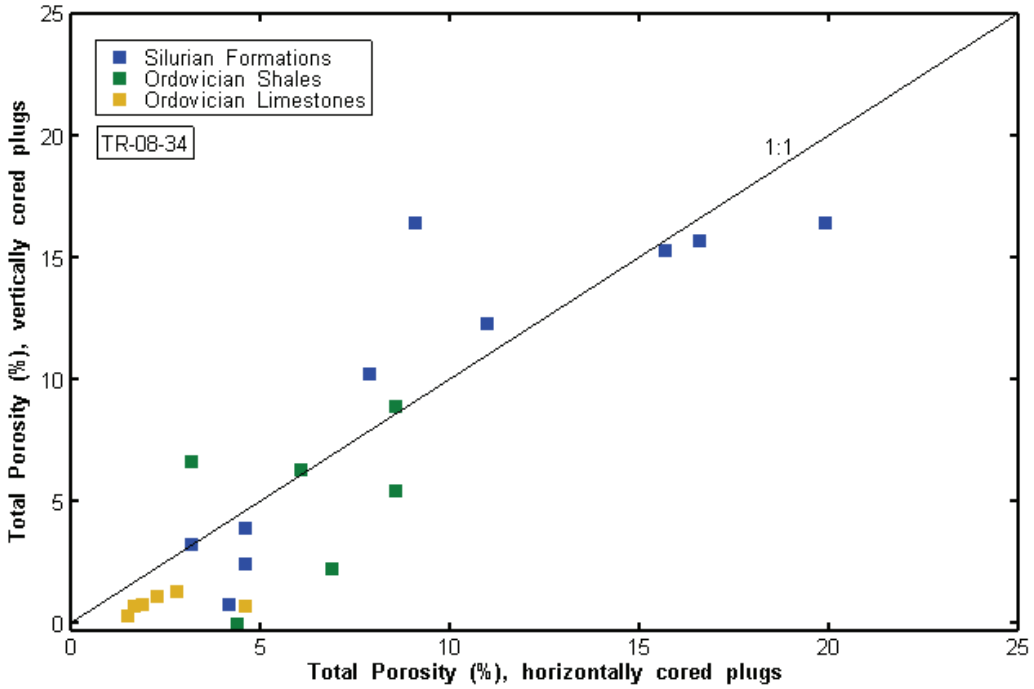

Figure 4.5: Measurements of Horizontal and Vertical Total Porosity on Core Plugs from Adjacent Sections of the same Core Sample, 1:1 Linear Trend Line Is Shown

Based on the above discussion, it is clear that the most reliable comparison between total and liquid porosity needs to be made based on testing of the same subsample or plug of core. The only lab that completes both measurements on the same plug of core is Core Labs. Figure 4.6 shows the Core Labs total porosity and liquid porosity data generated from sequential testing of the same core plugs under unconfined conditions. Figure 4.6 shows that almost all of the measured total porosities exceed liquid porosities when testing is completed on the same core plug. This suggests that sample size may be a factor in understanding the differences in total and liquid porosities reported by some labs.

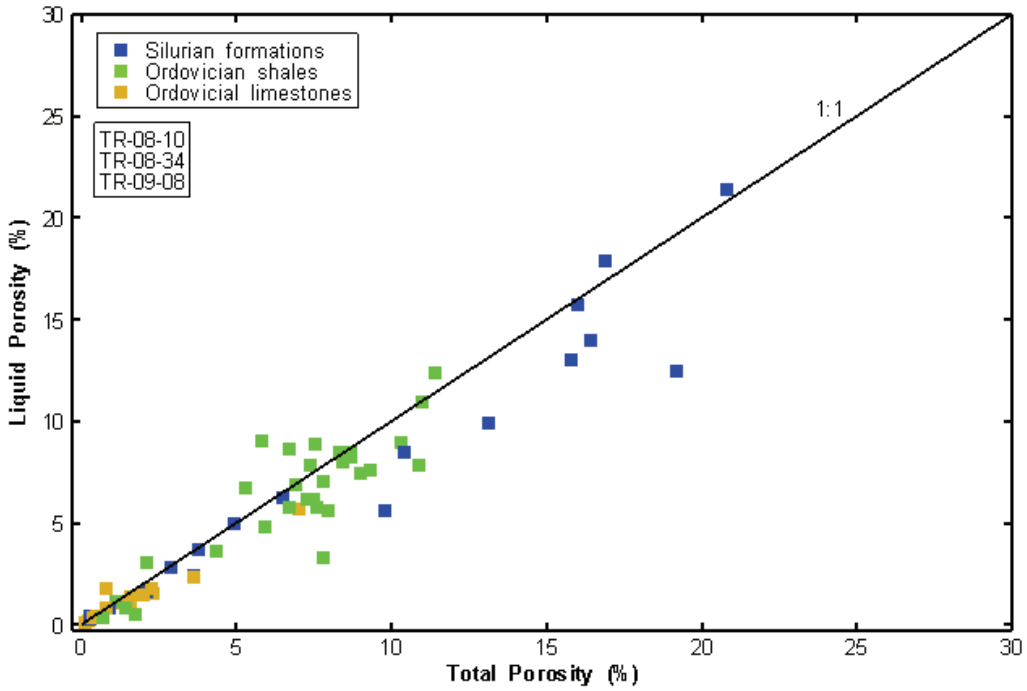

Figure 4.6: Comparison of Liquid and Total Porosity on the Same Core Plugs Tested by Core Labs, 1:1 Linear Trend Line Is Shown

Some of the observed differences in total porosity between different testing labs may also be due to the effects of imposing a confining stress during the testing of total porosity by Core Labs, which may result in a lower total porosity value due to microcrack closure. The Core Labs testing of total porosity for confined and unconfined DGR-3 and DGR-4 samples allows quantitative assessment of this effect. Figure 4.7 shows the ratio of unconfined to confined total porosity plotted by major formation groupings versus confined total porosity. This figure, which also shows mean ratio values for major groups of formations, indicates that core relaxation results in total porosity increases of about 17%, 31% and 39% for Silurian formations, Ordovician shales and Ordovician limestones, respectively, with the percentage change increasing with decreasing total porosity.

In addition, for the very low porosity Ordovician limestones, small errors in measurement procedures may significantly affect calculations of total and liquid porosities (i.e., such that the actual difference between total and liquid porosity may be smaller than the typical measurement error). Measurement error will be different for each analytical method and may include loss or gain of water during handling and testing due to evaporation and condensation, transfer of a droplet of water from a previous sample in the Dean Stark apparatus that could be falsely attributed to the distillate from the current sample being measured, and the sensitivity and accuracy of measurements of water volumes and weights (see Figure 4.14 in Section 4.3.3).

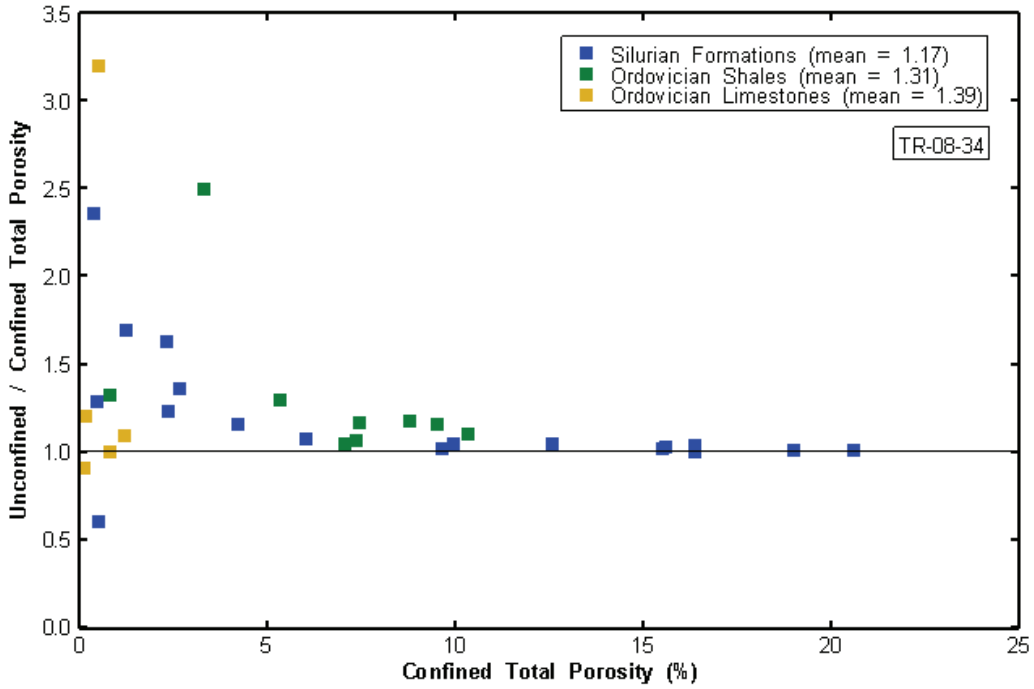

Note: Arithmetic mean ratios for major groups of formations are also shown.

Figure 4.7: Comparison of Ratio of Unconfined to Confined Total Porosity Versus Confined Total Porosity Measured by Core Labs on DGR-3 and DGR-4 Core Plugs

In summary, the available data show that calculated liquid porosities that exceed total porosity measurements can be attributed to a combination of factors including mineralogical effects, sample size effects, sample heterogeneity and anisotropy, application of different testing methods and test measurement errors. Given these differences and complications in interpreting porosity data, the use of total porosity data are recommended for most DGR hydrogeologic assessment purposes. Lacking comparable data sets for total porosity, liquid porosity data can be used for these purposes.

4.3.3 Residual Fluid Saturations

The fraction (or percentage) of brine, oil and gas in the pore volume of a core plug drilled from the core sample is the 'saturation' or S. This was estimated by Core Laboratories on 83 samples of DGR core by the Dean Stark method and using total porosity measured on confined core plugs (DGR-2, DGR-3 and DGR-4), as well as by NMR/He methods on 23 unconfined cores (DGR-4, DGR-5 and DGR-6).

For these fluid saturation analyses $S_W + S_O + S_G = 1.0$ (or 100%), where the subscripts refer to saline or brine water (W), oil (O) and gas (G). For Dean Stark testing, the water content was determined directly by boiling toluene and using the vapour as the solvent to extract the water from the core plugs. After water extraction, the toluene was condensed and used to remove any oil from the core plugs. These two steps determine S_W and S_O. By measuring the total porosity on this "clean and dry" sample by the Boyle's Law method of gas expansion under

confining pressure, the residual pore volume not accounted for by water and oil is attributed by difference to the presence of gas, yielding an estimate of the gas saturation, S_G. Thus, the estimate of S_G incorporates the errors accumulated in estimating both S_W and S_O. Figure 4.8 presents the measured brine (S_W) and estimated gas (S_G) saturations for the Core Labs core plugs plotted by depth and formation as well as the arithmetic averages of brine and gas saturations for each formation, member or unit.

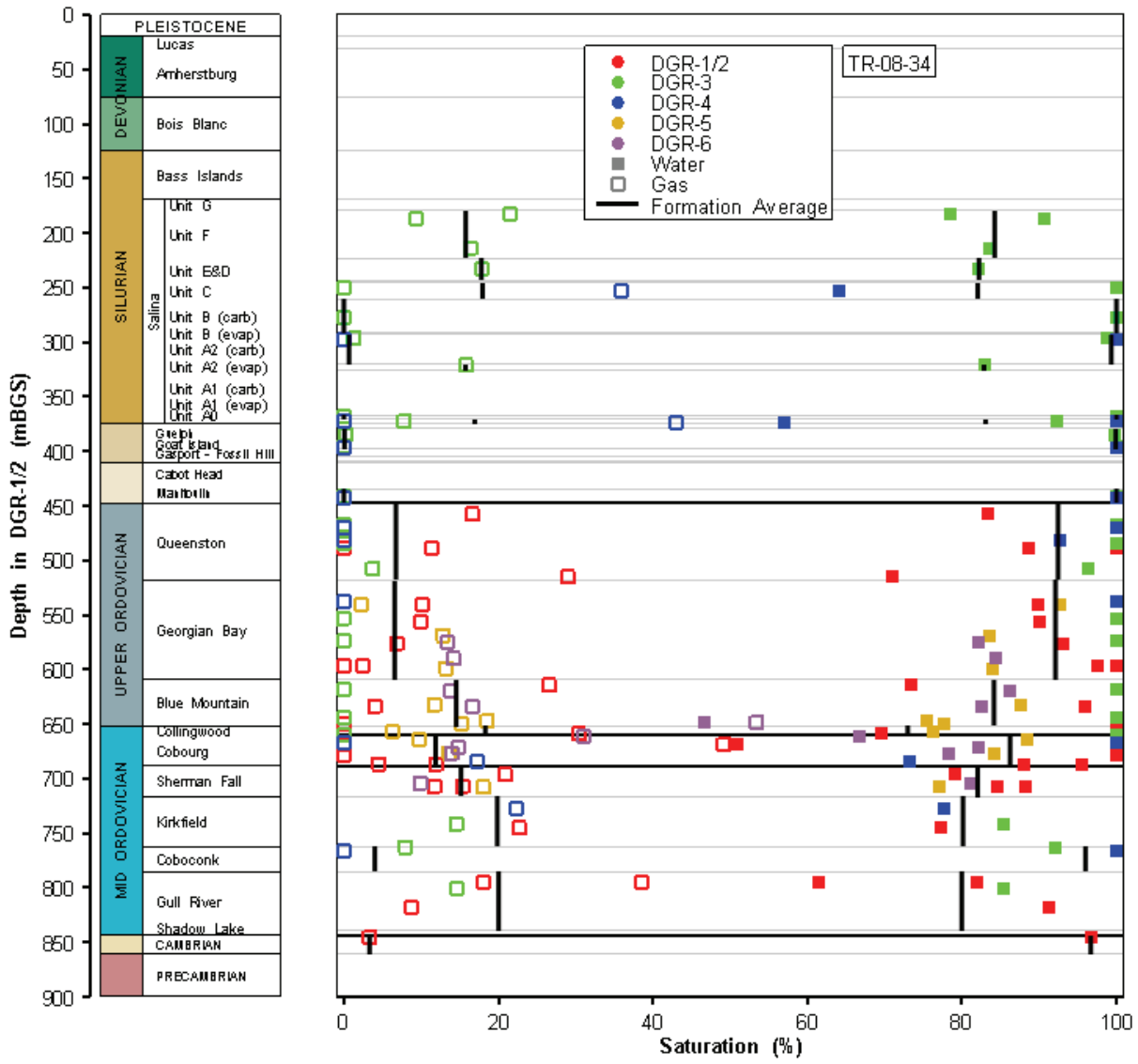

Figure 4.8: Pore Water (Brine) and Gas Saturation Profiles in Confined (DGR-2, DGR-3 and DGR-4) and Unconfined (DGR-5 and DGR-6) Cores Showing Point Data and Arithmetic Formation Averages

In these calculations, the oil density is assumed to be similar to that of other oils in southwestern Ontario and was therefore assigned a value of 0.83 kg/L. The brine salinity was assigned a

value in mg/kg equal to the arithmetic average for the formation, member or unit based on porewater and groundwater geochemical characterization (see Section 4.6.5 and TR-08-34). This resulted in the estimated oil saturations as zero in 63 of the 83 core plugs (see Figure 4.9). The range of reported oil saturations is 0 to 17.4%. The limited and sporadic occurrence of oil saturation in DGR cores is supported by core observations. There is sporadic evidence of oil presence in some core sections – notably a thin section of the Salina A1 Unit carbonate and parts of the Coboconk and Gull River formation limestones as well as petroliferous odours in several Ordovician shale and limestone formations (Table 3.10, Figure 3.16). However, because the petrophysical testing program primarily focused on characterization of the properties of the Ordovician and other low permeability barrier rocks and oil presence was limited in these formations, direct comparison of oil saturations determined from fluid saturation testing and core observations was not possible with available core data.

The Dean Stark results provide a measure of fluid saturations that is available by no other method except that of measuring the total liquid saturation ($S_W + S_O$) by Nuclear Magnetic Resonance (NMR) and the gas saturation by the Boyle's Law method using He gas expansion (TR-08-34). The results of a comparison of the traditional Dean Stark method with this NRM/He method are shown in Figure 4.10. For the 24 DGR cores that were tested under unconfined conditions, the correlation coefficient (r^2) between values (shown as a linear trend in the figure) is 0.94.

The range of brine saturations is 60-100%. These values are shown in Figure 4.11 plotted against total porosity measured on confined samples. The confined Ordovician argillaceous limestone samples have an overall average S_W of 86% (std. deviation = 13%), while the Ordovician shales above the repository horizon have an overall average S_W of 93% (std. deviation = 10%). The Silurian formations tested show similar brine saturations (average S_W of 91%, standard deviation = 13%).

The gas saturations that have been measured for confined DGR cores are shown in Figure 4.12 plotted against total porosity. The S_G values range from 0% to 46%, which is at the lower end of the range for dense, crystalline carbonate reservoir rocks of low porosity (i.e., <10%) reported by Keelan and Pugh (1975). Their data indicate that such limestones might well have residual gas saturations of up to 40%. Consequently, the range of gas saturations for the DGR rocks is well within reported values in the technical literature. These values and the strong likelihood of the presence of a gas phase in the DGR rock column are discussed in TR-08-34. Figure 4.13 shows a histogram of estimated gas saturations for the grouped Silurian, Ordovician shales and Ordovician limestone samples with median values indicated.

In considering sources of error in fluid saturation analysis, two issues are of particular interest: (1) errors due to limitations on the volumetric water contents of cores and (2) errors due to the irrecoverable geomechanical relaxation of the core during in situ recovery, on-site handling, shipping and laboratory handling and testing.

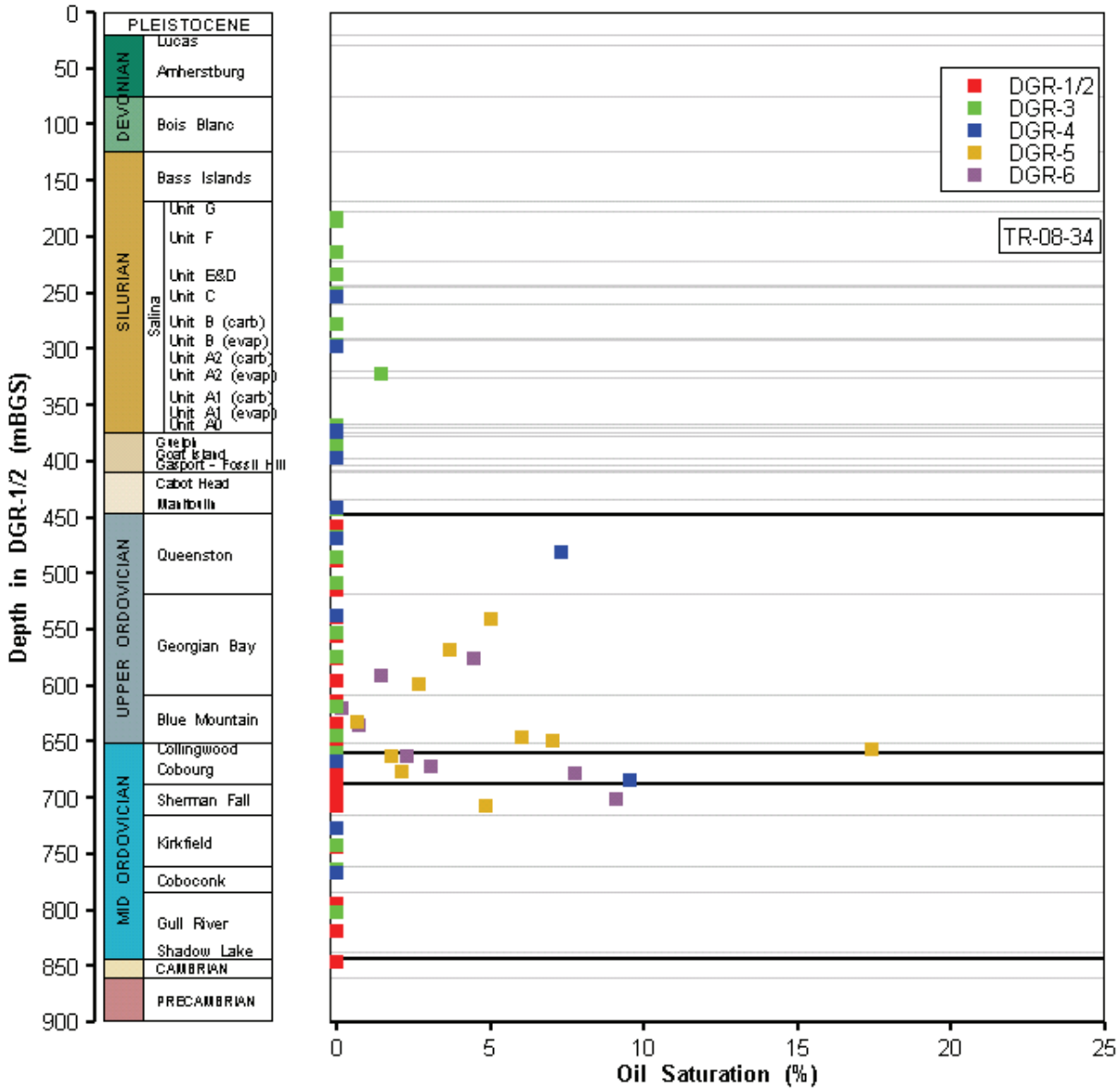

Figure 4.9: Oil Saturation Profile in Confined and Unconfined DGR Cores Determined from Dean Stark Analyses

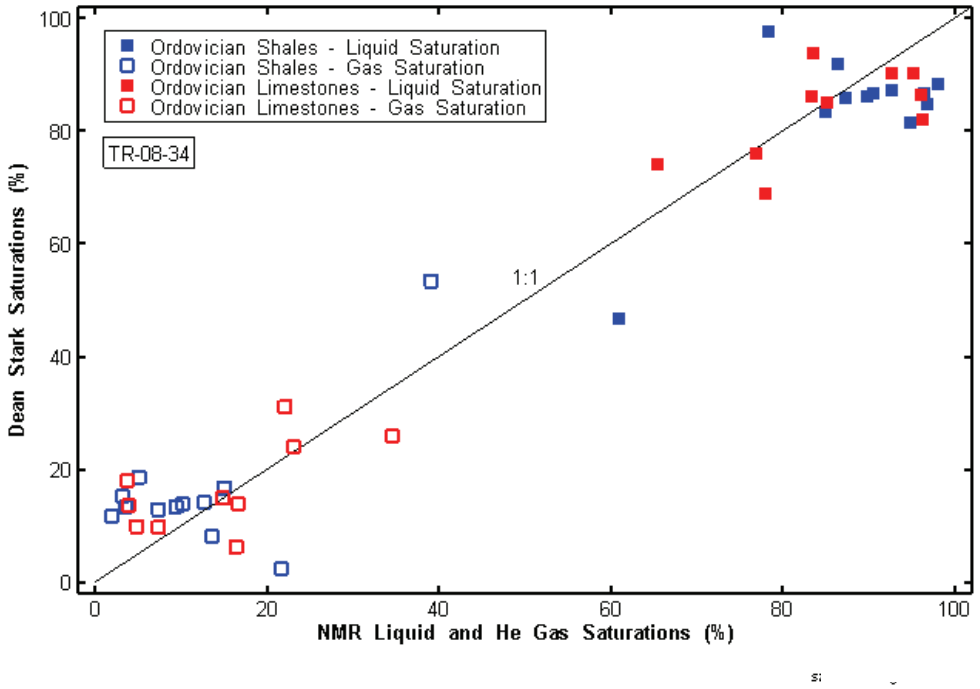

Figure 4.10: Comparison of Methods for Fluid Saturation Measurement in Unconfined DGR Cores

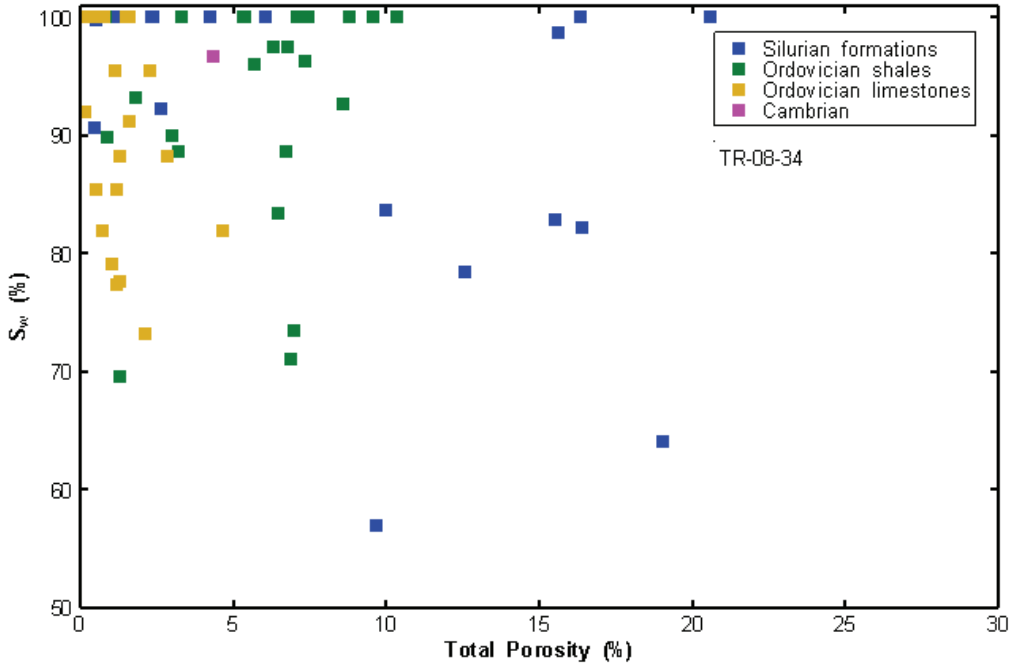

Figure 4.11: Water Saturations as a Function of Total Porosity in Confined DGR Cores

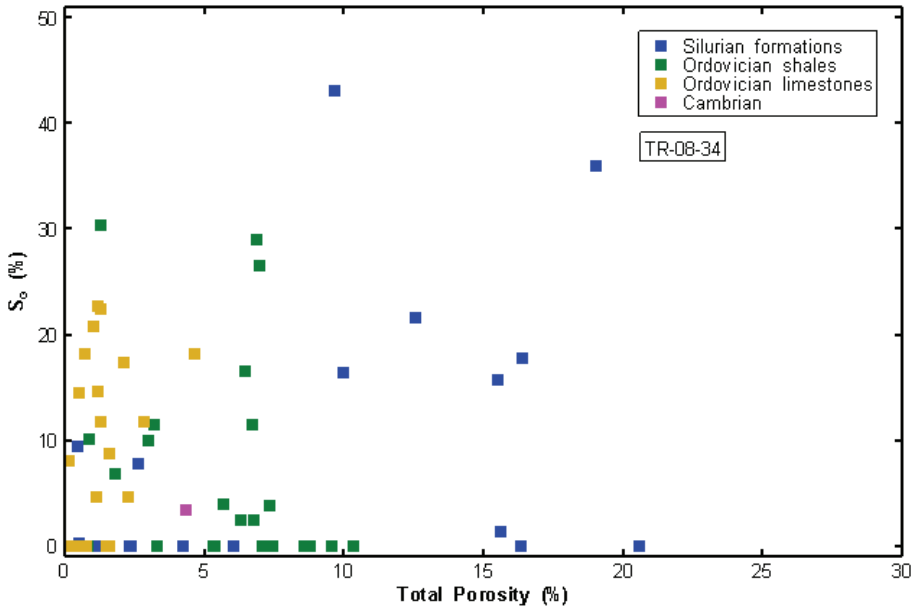

Figure 4.12: Estimated Gas Saturations as a Function of Total Porosity in Confined DGR Cores

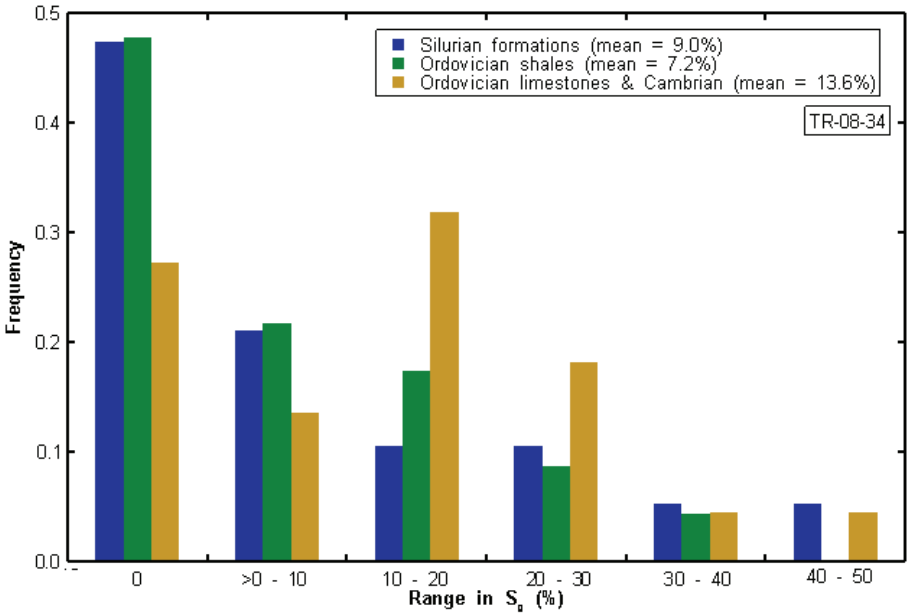

Note: Arithmetic values for major groups of formations are shown in the legend.

Figure 4.13: Distribution of Gas Saturations (S_G as % of Pore Volume) in Confined DGR Cores inferred from Dean Stark Fluid Saturation Analysis and Boyle's Law (He gas) Total Porosity Measurements

Figure 4.14 shows the fractional uncertainty in S_w *vs.* total porosity for DGR core samples based upon error propagation theory:

$$\frac{dSw}{Sw} = \sqrt{\left(\frac{dVw}{Vw}\right)^2 + \left(\frac{dVp}{Vp}\right)^2} \tag{4.1}$$

where V_W is the water yield from the core plug and V_P is the pore volume or total porosity.

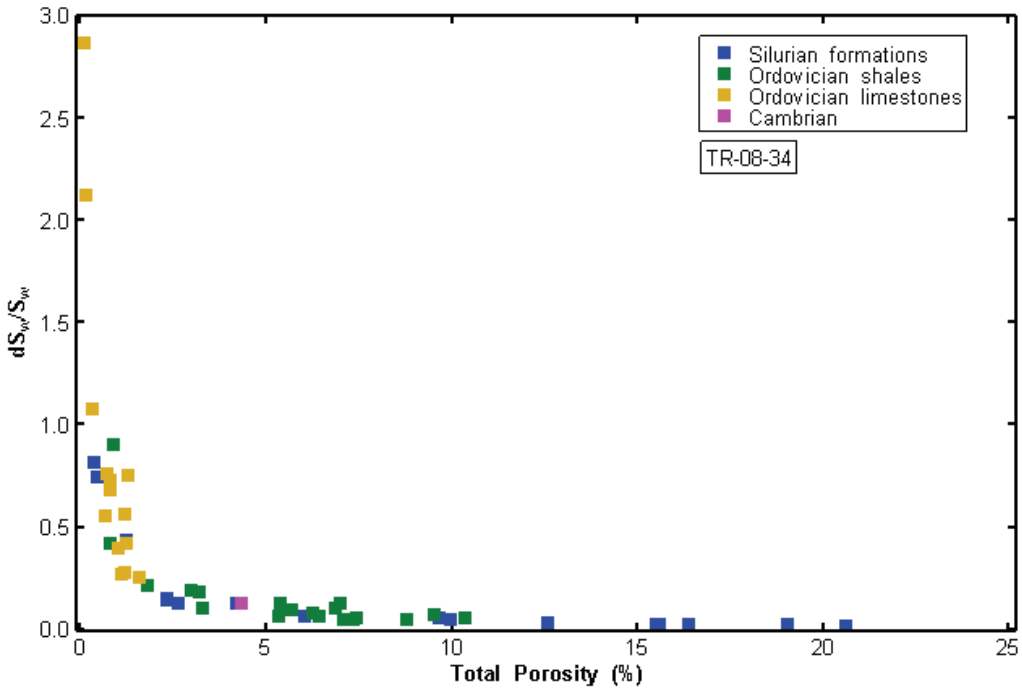

Figure 4.14: Fractional Uncertainty in the Water (Brine) Saturation (dS_w/S_w) Plotted against Total Porosity from Dean Stark Analysis of Confined DGR Cores

Figure 4.14 shows that for porosities < 2%, there is a significant error. Because the error in estimating the water yield from the Dean Stark method is ~50 µL, the low water yields associated with the limestones and shale hardbeds produce large uncertainties. These uncertainties affect the measured brine saturations and hence the estimated gas saturations. The convergence of data from the Dean Stark and the NMR/He(g) methods indicates that this source of error is limited in its effect.

Another potential source of error in estimating the gas saturation can arise when the in situ stresses on the core are relaxed (i.e., producing dilational strain) creating new pore space measured by the petrophysical testing in the form of new microcracks that cannot completely close upon sample reloading. Such irrecoverable strains can become filled by a gas phase exsolving from the brine and any oil present in the pore. In addition to cracking due to core relaxation, irrecoverable microcrack-based strains could form due to damage during coring or

sample handling and preparation. Calculations (see Section 4.6.3) indicate that the brine in the Ordovician rocks is at saturation with methane, therefore degassing is a possible effect on the measured values. As indicated in Figure 4.7, the amount of core relaxation is potentially significant resulting in average porosity increases of 15 to 40%.

However, as fluid saturation testing of DGR cores is primarily based on total porosity measured under confined conditions, the amount of porosity increase that may affect gas saturations would be restricted to irrecoverable strains attributed to creation of new microcracks during sample drilling and recovery and laboratory preparation and testing, that cannot be completely closed upon sample reloading. Such anelastic porosity increases cannot be reliably quantified from available data including geomechanical stress-strain data from uniaxial and triaxial strength testing (Chapter 5 of this report, TR-07-03, TR-08-24, TR-08-39, TR-09-07) because such data measure largely elastic strains during sample loading. The available geomechanical stress-strain data can only be used to bracket the possible range of anelastic porosity increases by assuming that a percentage of the calculated elastic relaxation porosity is due to anelastic microcrack behaviour.

Thus, to estimate the potential scale of this phenomenon, the microcrack relaxation porosity is estimated by analyzing the volumetric strain curves measured by CANMET during uniaxial and triaxial compression testing as part of the DGR geomechanical strength testing program. Therefore, this analysis, which is presented in TR-08-34, quantifies (a) the total amount of core relaxation that can be attributed to elastic microcrack behaviour, (b) estimates a likely range of anelastic porosity assuming it is a percentage of elastic relaxation porosity, and (c) assesses whether it is likely that the finite gas saturations measured during petrophysical testing of DGR cores are laboratory artefacts or are representative of in situ conditions.

Figure 4.15 shows this analysis for representative samples of the Georgian Bay Formation shale (DGR3-589.61) and Cobourg Formation limestone (DGR3-675.06) that were subject to triaxial compression testing. Data from triaxial compression testing are used in this example analysis as such data are likely to provide more representative estimates of volumetric strains than similar data from uniaxial compression testing, which are also given in TR-08-34. It is noteworthy that the microcrack relaxation porosity determined from the geomechanical analyses (e.g., Cobourg - 0.10%) is similar to that determined from petrophysical testing of total porosity of unconfined and confined cores. This later porosity for the Cobourg is determined as unconfined total porosity [1.9% - Table 4.3] – 1.9%/average ratio of unconfined/confined total porosity [1.04 – Figure 4.7 excluding anomalous value of 3.2] = 0.07%. Given the uncertainty in the ratio of unconfined/confined total porosity evident in Figure 4.7 due to limited data for Ordovician limestones, the two estimates of microcrack relaxation porosity are considered comparable.

The calculated theoretical porosity change due to elastic microcrack formation and expansion during core relaxation is shown in Figure 4.15 as 0.18% for Georgian Bay Formation shale and 0.10% for Cobourg Formation limestone. Assuming that the anelastic porosity created by new microcracks that cannot completely close on reloading is 10% of the elastic porosity, the resultant anelastic porosities are 0.018% for the Georgian Bay shale and 0.01% for the Cobourg limestone. These calculated anelastic porosity increases, based on average total porosity of 7.6% and 1.8% for these formations (Figure 4.3), would create equivalent gas saturations of 0.24% (Georgian Bay shale) and 0.5% (Cobourg limestone). Since these calculated gas saturations for the Georgian Bay shale are less than the reported average Dean Stark gas saturations of the Georgian Bay shales of 6.6%, it is unlikely that anelastic pore volume expansion caused by irrecoverable core relaxation can solely explain the occurrence of the

reported gas saturations in the Ordovician shales. For the Cobourg limestones, which have average gas saturation of 12.1%, the calculated anelastic gas saturations are also much smaller suggesting that the reported gas saturations are not solely artefacts of irrecoverable core relaxation. However, these conclusions for the Cobourg limestones are tempered by the fact that the Cobourg limestone with average porosity of 1.9% has greater fractional uncertainty in fluid saturation estimates (see Figure 4.14).

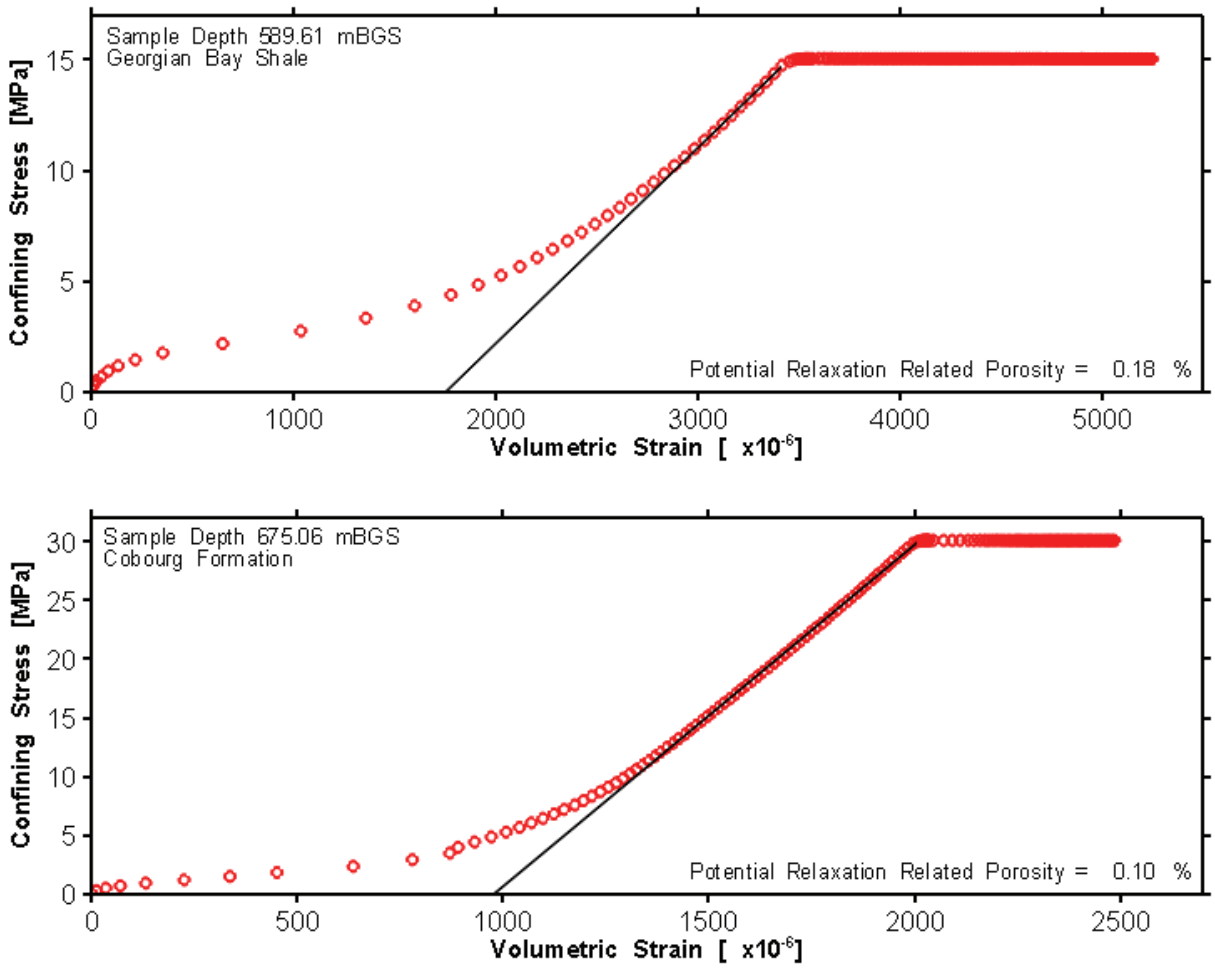

Figure 4.15: Determination of Relaxation Porosity from Volumetric Strain Data – Above Georgian Bay Formation Shale (589.61 mBGS), Below Cobourg Formation Limestone (675.06 mBGS) in DGR-3

4.3.4 Rock Permeability to Gas and Brine

Pulse-decay permeability (PDP) tests were used to measure the permeability of DGR rock cores to gas and brine. Tests were performed on “as received” core that contained porewater, on “clean and dry” cores that had porewater and salts removed, and on brine-saturated cores (TR-07-18, TR-08-28). The PDP method was originally developed by Brace et al. (1968) for measurement of permeability of intact granites under high pressure and has been adopted for

use in rock mechanics (Hart and Wang 2001), hydrogeology (Finsterle and Persoff 1997) and petrophysics (Jones 1997).

The response of a core plug to a gas or brine pulse was measured as a result of a quickly pressurized upstream reservoir discharging through the core plug into a downstream reservoir, while maintaining a very low differential pressure across the entire length of the sample (Jones 1997). The core plug was hydrostatically loaded to a depth-specific net confining stress (17 kPa/m for DGR-2 cores; 34 kPa/m for DGR-3 and DGR-4 cores), which approximates the effective stress considering the overlying weight and compressive forces of the bedrock. Following this loading, the initial pressure in the core and reservoirs was brought to 7 MPa. The Klinkenberg effect – molecular slippage of the gas in the pore – was only minimized by the use of the high pore pressure and not eliminated by it, which requires multiple runs at different pressures. Jones (1997) indicates that at a mean pore pressure of 7 MPa, the measured permeability to gas is 10% higher than the slip-corrected gas permeability. The range of permeability measurements with Core Labs' test instrument is typically from 10^{-21} m^2 to 10^{-16} m^2.

Figure 4.16 shows the variation in vertical and horizontal permeability (k) with depth throughout the Silurian, Ordovician and Cambrian sequence of rocks for both "as received" and "clean and dry" tests determined from gas permeability testing. "As received" core plugs contain variable brine contents that are likely to influence the gas permeability measurement because the gas saturations are small compared to the brine saturations. However, the PDP testing of 'as received' cores provides a measure of the effective gas permeability of the sample in the presence of brine. After Dean Stark fluid extraction and convection drying, the pore volume is identified as "clean and dry" so that the measured permeability is now that permeability measured in the absence of any other fluid present in the pore space, i.e., the absolute or intrinsic permeability. Consequently, each test produces one point on a relative gas permeability curve. Section 4.3.9 and TR-08-33 discuss the determination of two-phase (gas, brine) flow properties from the Core Labs petrophysical data.

The lowest 'as received" permeabilities – approximately 10^{-21} to 10^{-20} m^2 – were measured in the Salina F, C, B, A2 and A0 Units, and the Goat Island, Gasport, Manitoulin, Queenston, Georgian Bay, Cobourg, Sherman Fall, Kirkfield and upper Coboconk formations, although higher values of up to 10^{-16} m^2 were frequently measured in the Ordovician shales. The lowest "clean and dry" or intrinsic permeabilities – again approximately 10^{-21} to 10^{-20} m^2 – were measured in the Salina A1 Unit, and Goat Island, Gasport, Manitoulin, Georgian Bay, Collingwood, Cobourg, Kirkfield and upper Coboconk formations, although higher values of up to 10^{-15} m^2 were again frequently measured in the Ordovician shales. The cores from the dolomitic upper Cambrian, and from the Gull River Formation below 800 mBGS, were of similar high vertical intrinsic permeability (~10^{-16} m^2). The clustering of k values at $5x10^{-21}$ m^2 in Figure 4.16 represents tests with estimated k below the lower testing limit, which are plotted at the lower testing limit of $5x10^{-21}$ m^2.

Horizontal k data from gas permeability testing were only obtained on a limited number of DGR-2 cores. These limited data show that intrinsic ("clean and dry") permeability of horizontal sub-cores is generally greater than that of vertical sub-cores. Additional discussion of core k anisotropy is given below with reference to both air and brine permeability testing.

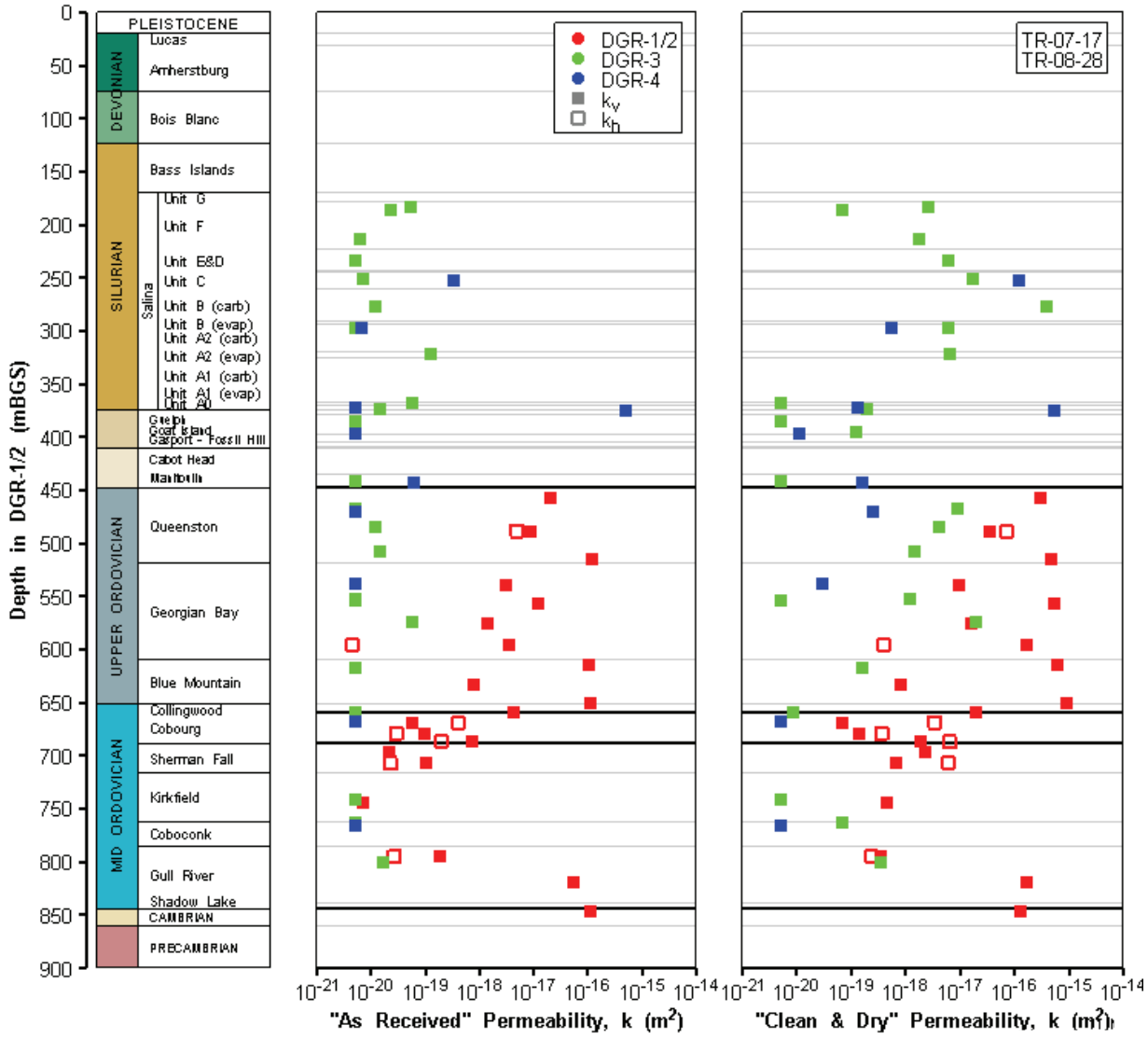

Figure 4.16: Vertical and Horizontal Permeability Profile Measured by Gas Pulse Pressure Decay Testing on DGR Cores

Figure 4.17 is a cross plot of brine-saturated permeability versus “clean and dry” gas permeability following fluid extraction and convection drying of DGR-3 and DGR-4 cores. Both vertically oriented and horizontally oriented cores are shown in Figure 4.17 without distinction. The data in Figure 4.17 show the calculated gas intrinsic permeabilities are up to four orders of magnitude higher than the brine permeabilities for different sub-cores of each sample. These data suggest that the Core Lab processes of cleaning and drying cores results in physical/chemical disturbance and damage of the core and enhancement of core permeability. This disturbance appears to be greater for Silurian formations and the Ordovician shales than for the Ordovician limestones.

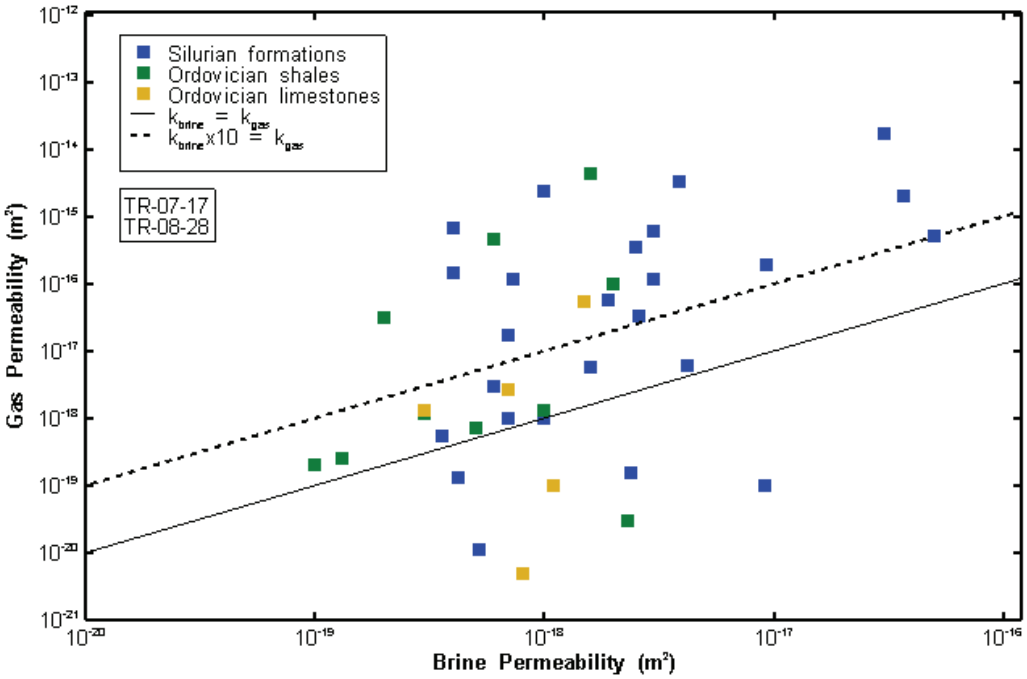

Figure 4.17: Brine-saturated Core Permeability Plotted Against Gas Intrinsic Permeability in DGR-3 and DGR-4

In addition to physical/chemical damage to core during cleaning and drying, core may also be subject to mechanical disturbance and damage (Martin and Stimpson 1994, Santarelli and Dusseault 1991). As was shown in the previous section (see Figures 4.7 and 4.15), sample disturbance in tight rocks results in microcrack formation that is likely caused by stress concentration during drilling and by core and pore fluid expansion during sample unloading as core is recovered and brought to surface. Visual inspection of core plugs (Figure 4.18) that had anomalously high measured permeabilities did not show any evidence of damage, suggesting that the core damage is occurring at the micro-scale and not at the macro or visible scale of the core samples.

Thus, despite the sophistication of the PDP measurement technique and the application of the confining stress, petrophysical testing is likely to result in much higher measured permeabilities than those measured by in situ hydraulic testing (see Section 4.9.3 for further discussion of the comparison of field and lab permeability data). The lab k data are considered to be unrealistically high values due to irrecoverable damage of core during drilling, recovery and shipment to the lab for testing and handling, and sample preparation in the lab. Based on geomechanical strength considerations and observations of core disking during core recovery, this mechanical damage is likely to be greater in the weaker Ordovician shales than in the stronger Ordovician limestones.

Note: Hydraulic testing of these intervals yielded in situ values of horizontal permeability of ~1x10^{-21} m^2.

Figure 4.18: Core Plugs from DGR2-613.93 (Left) and DGR2-650.12 (Right) in Blue Mountain Formation had Measured Vertical Permeabilities of 6x10^{-16} and 9x10^{-16} m^2.

Quantitative bounds on the amount of permeability overestimation due to mechanical core damage can be inferred from international experience (Martin and Stimpson 1994, Martin and Lanyon 2003, Neuzil 1993). The minimum amount of overestimation is likely to be similar to the tenfold amount reported by Martin and Stimpson for competent Lac du Bonnet granite at similar depths of 400 to 800 mBGS at the AECL Underground Research Laboratory. This minimum overestimation is likely to be more applicable to the more competent Silurian dolostones and Ordovician limestones than to Silurian and Ordovician shales. The maximum amount can be indirectly inferred assuming that the properties of the relaxed and disturbed cores are similar to the properties of the stress-relieved excavation damaged zone (EDZ) that surrounds deep underground openings. Martin and Lanyon (2003) reported that hydraulic properties of the EDZ in Opalinus Clay at the Mount Terri Rock Laboratory were 100 to 10,000 times higher than undisturbed clay shales with permeability of about 10^{-20} m^2. These maximum overestimations are likely to be more applicable to the less competent Ordovician shales.

Applying these mechanical and physical/chemical overestimation factors to the Core Labs test results (i.e., “clean and dry” values) for disturbed cores suggests the in situ vertical permeability of undisturbed Ordovician shales and limestones (excluding the lower Gull River rocks) approximate 10^{-21} m^2 or less. These estimated undisturbed in situ permeabilities are supported by published data of Neuzil (1994, 1993) who also noted up to 100-fold overestimation by laboratory testing due to sample disturbance.

Neuzil’s compilations of porosity and permeability data for argillaceous formations indicates that shale and limestone rocks of similar porosity to those measured in DGR Ordovician formations are likely to have permeability of less than 10^{-20} m^2. This observation is supported by recent work of Waber et al. (2007) who reported that shallow samples of Cobourg limestone collected from a borehole depth of 62 m at the St. Marys Cement quarry near Bowmanville Ontario had

vertical permeability of about 10^{-20} m^2 based on initial flow rates measured during advective displacement testing. Vilks and Miller (2007) also reported similar average values of intact rock vertical permeability under triaxial confining pressures of 4-15 MPa of $9.4x10^{-22}$ m^2 for Cobourg limestone core collected near the St. Mary's Quarry, and $4.5x10^{-21}$ m^2 for Queenston shale core collected at Niagara Falls. Based on the shallow depth of all of these samples, core disturbance is likely to be minimal and these samples provide reasonable estimates of intact in situ permeability of these formations at depth at the DGR site.

The anisotropy in the measured intrinsic permeability data is illustrated in Figure 4.19. The k data presented in Figure 4.19 are based upon gas permeability testing of DGR-2 core and brine permeability testing of DGR-3 and DGR-4 core.

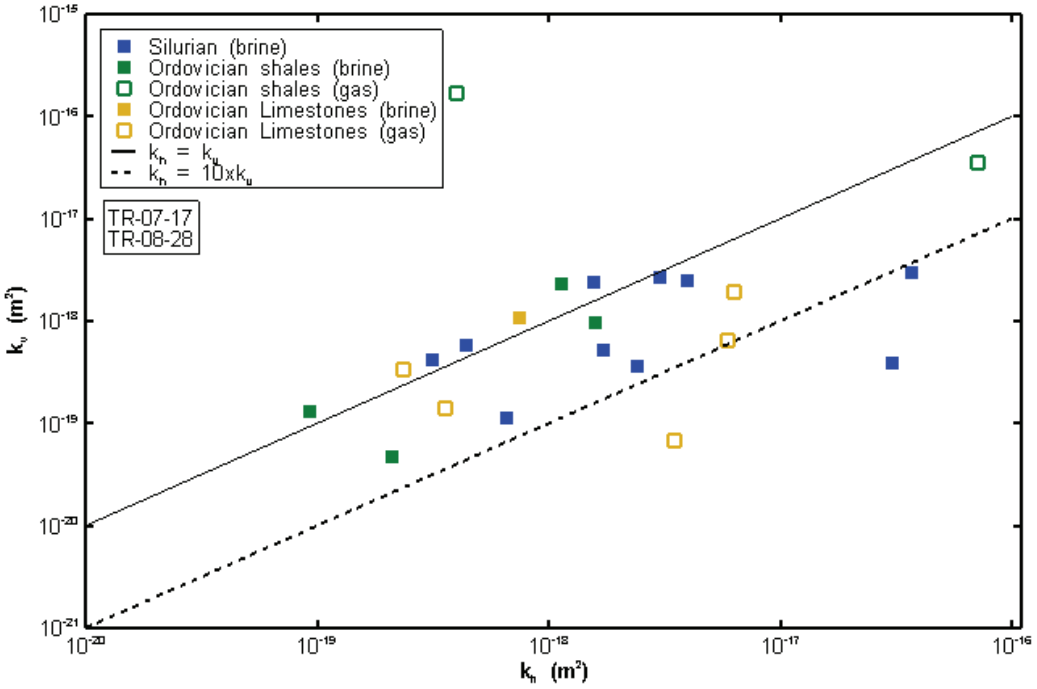

Figure 4.19: Anisotropy in Core Permeability from Gas Permeability Testing of DGR-2 Cores and Brine Permeability Testing of DGR-3 and DGR-4 Cores

Generally, the horizontal permeability exceeds the vertical by a ratio of between 1:1 and 10:1. One limestone core (DGR2-669.10) has an extreme k_h:k_v anisotropy ratio of 50:1 that is reflected in the different total porosities (ϕ) of the two core plugs (i.e., ϕ = 0.007 for the vertical core plug and ϕ = 0.017 for the horizontal core plug). One shale sample (DGR2-596.09) that indicates k_v>>k_h, likely fractured during sample handling and testing. The DGR-3 and DGR-4 brine permeability samples show a similar pattern of anisotropy with two outliers, both from the Salina F Unit shale. The small number of DGR-3 and DGR-4 pairs shown in Figure 4.19 was due to a high rate of core plug failure during testing (35%) such that both plugs in only 15 of 25 pairs were tested successfully.

Lucia (1999) developed a series of petrophysical models of carbonate rocks based upon their gas permeability and porosity. The models are based upon the regression analysis of petrophysical data from many carbonate formations in the USA and the Middle East, particularly those from West Texas. Lucia defined three classes of carbonates of which Class 3 is that of mud-dominated fabrics that have a permeability field controlled by the predominance of carbonate grains in the < 20 µm range, (i.e., packstone, wackestone and mudstone and fine crystalline, mud-dominated dolostones). This description best fits the petrographic observations of Schandl, who has described the DGR cores, i.e., TR-07-12 (DGR-1 and DGR-2), TR-08-20 (DGR-3),TR-08-21 (DGR-4) and TR-09-05 (DGR-5 and DGR-6).

Figure 4.20 shows the plot of available vertical gas permeability and porosity data for carbonate rocks intersected by DGR boreholes compared to Lucia's Class 3 carbonate model. DGR carbonate rocks included in Figure 4.20 include Silurian dolostones and limestones (carbonates), limestone and siltstone hard beds within the Ordovician shales, Ordovician limestones, and the dolostone-rich upper part of the Cambrian strata.

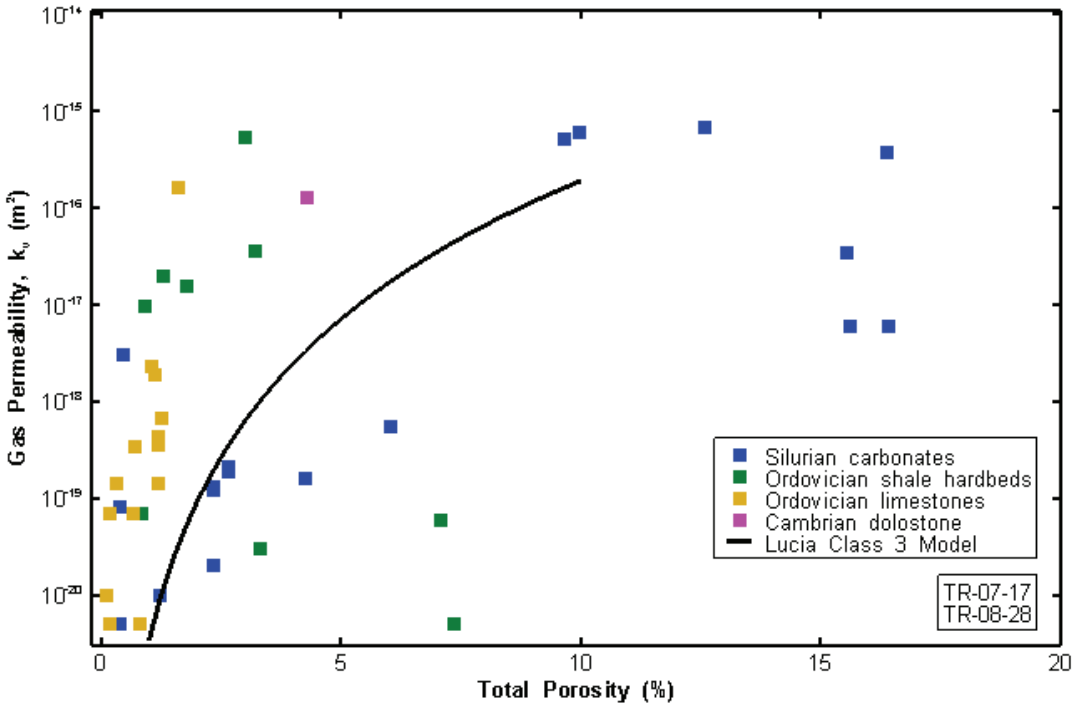

Note: Points plotting one or more orders of magnitude above the power curve are suspect due to core disturbance and damage. Lucia's class 3 carbonate permeability-porosity model is described by the 'power' curve fit shown.

Figure 4.20: Gas Permeability Plotted against Total Porosity for DGR Cores

Figure 4.20 shows that the vertical gas permeability is roughly correlated with porosity using Lucia's petrophysical model of a Class 3 carbonate model. The plot of gas permeability versus porosity shown in Figure 4.20 reveals that most of the Ordovician limestones (and many of the

Ordovician shale hard beds) are two or more orders of magnitude higher in gas permeability than the model predicts. The departure of the data from the Lucia model is very minor at permeability of about 10^{-21} m^2 suggesting that this may be the representative value of in -situ permeability for the Ordovician limestones. The overestimation of lab permeability for the Ordovician carbonate cores relative to Lucia's model is likely due to core relaxation and damage effects in these gas permeability measurements. A number of samples are very well predicted by the model line; these are Salina A0 Unit and Goat Island Formation dolostones. The good fit by these Lower Silurian formations indicates that these rocks should be considered as the uppermost part of the caprock overlying the proposed repository formation. The underestimation of lab permeability for the Salina carbonates relative to Lucia's model is likely due to the presence of abundant evaporite minerals (i.e., gypsum, anhydrite) in these formations.

The lower extremity of the permeability-porosity space relationship shown in Figure 4.20 – i.e., $k<1x10^{-20}$ m^2 and $\phi < 0.1$ – is referred to by Neuzil (1994) as "a highly lithified, low porosity unit that one would expect to be prone to fracturing". This rock description is appropriate for the majority of the DGR Silurian and Ordovician rocks.

4.3.5 Mercury Injection Pore-Size Distribution

High-pressure mercury porosimetry testing was used to determine:

1) The capillary-pressure/fluid saturation curve for a non-wetting fluid (i.e., mercury);
2) The pore-size distribution of the core sample;
3) The entry pressure required for a non-wetting fluid to penetrate the pore space; and
4) The Leverett J function for averaging capillary pressure curves.

Figure 4.21 shows example mercury intrusion profiles for four groups of core samples in terms of the injection pressure versus mercury saturation. These are: (a) Silurian formations; (b) Upper Ordovician shales immediately above the proposed repository horizon; (c) the Cobourg Formation; and (d) carbonate formations beneath the Cobourg Formation. In high-pressure mercury injection following fluid extraction by the Dean Stark process, mercury is injected into the core plugs under increasing pressure, causing air to 'drain' from the pores as mercury intrudes. Pittman (1992) reported that a saturation of 10% (i.e., $S_{Hg} = 0.1$), might represent a continuous zone of mercury present across the core plug, (i.e., in the most permeable set of interconnected pores).

The Silurian formations, shown in Figure 4.21a, display two styles of capillary behaviour. The flatness of the capillary pressure that occurs after penetration in the Goat Island Formation – DGR3-398.05 sample reflects the homogeneity of the pore-size distribution in this dolostone. This slope indicates that very little incremental injection pressure is needed to significantly increase S_{Hg}, whereas a steep slope indicates a large injection pressure requirement (e.g., Salina A2 Unit – DGR3-308.53 ($k_v=4.2x10^{-18}$ m^2) and Salina A0 Unit – DGR4-375.40, ($k_v>5.0x10^{-17}$ m^2)). The deeper formations display a much higher threshold injection pressure (~ 100 MPa) for full penetration by mercury and a somewhat lower brine permeability (e.g., the Goat Island dolostone – DGR3-398.05 ($k_h = 9.7x10^{-19}$ m^2), the Cabot Head shale – DGR3-432.57 ($k_v=2.5x10^{-18}$ m^2) and the Manitoulin dolostone - DGR4-441.78 ($k_V = 2.4x10^{-18}$ m^2)). The Lower and Middle Silurian rocks comprising the Manitoulin, Cabot Head and Goat Island formations (and the smaller stratigraphic units between them) may be considered the upper extension of the repository caprock formed by the Ordovician shales.

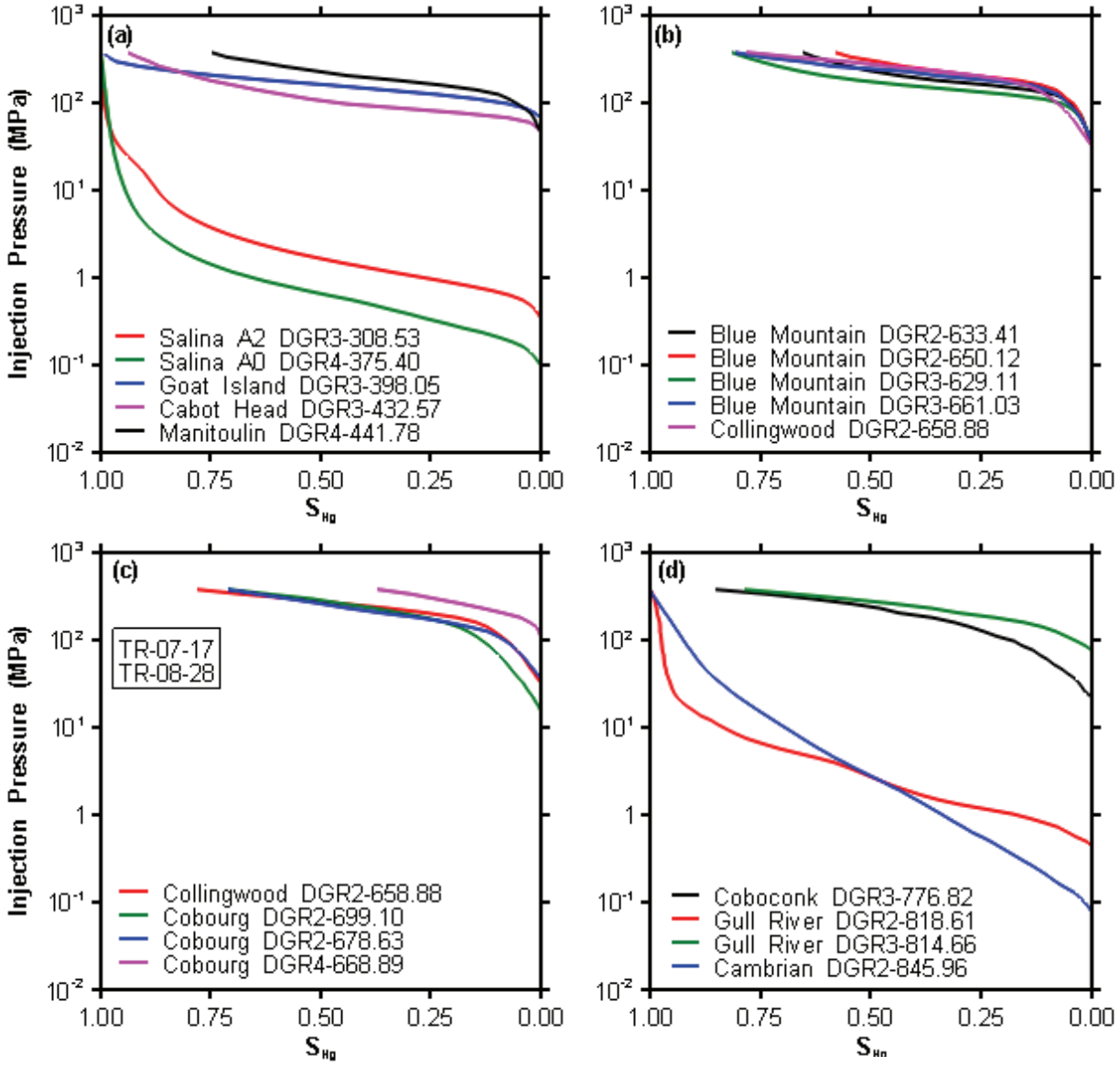

Figure 4.21: Mercury Injection Profiles (S_{Hg} or Mercury Saturation vs. Injection Pressure in MPa) for the Silurian Formations (a), the Ordovician Shales Immediately above the Repository Horizon (b), the Cobourg Formation (c) and the Black River Limestones and Cambrian Sandstone (d)

The tight shales that immediately overlie the proposed repository formation, which are shown in Figure 4.21b, are not fully penetrated by the mercury until the injection pressure exceeds 40 MPa for the Collingwood – DGR2-658.88 sample. The equivalent values for the four Blue Mountain cores (DGR2-633.41, DGR2-650.12, DGR3-629.11, and DGR3-661.03) shown exceed 100 MPa, indicating an extremely tight caprock. This very tight zone is associated with biogenic methane, discussed later.

Figure 4.21c shows the capillary pressure curves for the Cobourg Formation. Both the Collingwood Member (DGR2-658.88) and the Cobourg Lower Member (DGR2-669.10, DGR2-678.63, DGR4-668.89) core samples are shown to be of relatively uniform pore size. Although it only reaches 40% mercury saturation, one of the lower Cobourg cores (DGR4-668.89) displays the tightest capillary response of any of the 54 DGR cores tested by high-pressure mercury intrusion (i.e., > 200 MPa for S_{Hg} = 0.1).

Figure 4.21d shows the capillary pressure curves for the Coboconk, Gull River, and Cambrian. The Coboconk curve (DGR3-776.82) and one of the Gull River curves (DGR3-814.66) are very similar to those of the Cobourg (Figure 4.21c). The other Gull River curve (DGR2-818.61) and the Cambrian curve (DGR2-845.96) show that mercury fully penetrates the samples at relatively low pressures. The two Gull River cores were visually similar.

4.3.6 Gas Entry Pressure

The capillary pressure curves shown for the shales in Figure 4.21 indicate that penetration by gas – a non-wetting fluid like mercury – must overcome significant capillary resistance from the wetting fluid present in the pores. Here it is assumed that brine is the wetting fluid occupying the pore throats, although it may be more reasonable to assume that the carbonate formations are mixed wet, i.e., some pores are oil wet while others are water wet as noted by Lucia (1999). The entry pressure required by gas to penetrate a water-wet pore throat is given by the Washburn equation (Dullien 1979, Pittman 1992) which is a form of the Laplace equation for a cylindrical or capillary-tube model of pore structure (Guéguen and Palciauskas 1994):

$$P_C = \frac{2\sigma\cos\theta}{r} \tag{4.2}$$

where P_C is the capillary pressure (in Pa) required to cause entry of the non-wetting fluid into the water-wet porous medium, σ is the interfacial tension between wetting and non-wetting fluids (in N/m), θ is the contact angle formed by the water with the pore surface and r is the radius of the capillary pore throat (in m) - with a detection limit of ~2 nm (0.002 µm) by mercury injection porosimetry. The Washburn equation can be solved for the pore throat radius, r, if all other parameter values in the equation are known or can be independently estimated. In this context, pore throats represent constrictions that control formation permeability.

The capillary pressure (P_c) curves for mercury/air that are shown in Figure 4.21 can be converted to capillary pressure curves for gas/brine by correcting the P_c for mercury/air by the ratio of the σ·cosθ for methane/brine to that for mercury/air, i.e.,

$$P_{c(Gas/Brine)} = P_{C(Hg/Air)} \cdot \frac{\sigma \cdot \cos\theta_{(Gas/Brine)}}{\sigma \cdot \cos\theta_{(Hg/Air)}} \tag{4.3}$$

Values for the independent variables in this equation are readily available (e.g., Vavra et al. 1992, Guéguen and Palciauskas 1994) and a capillary curve for methane/brine can be computed. Such curves will be identical in shape to those in Figure 4.21. For methane/brine, the ratio is:

$$P_{c(Gas/Brine)} = P_{C(Hg/Air)} \cdot \frac{72mN/m \cdot \cos 0^{\circ}_{(Gas/Brine)}}{485mN/m \cdot \cos 140^{\circ}_{(Hg/Air)}} \tag{4.4}$$

Thus, the P_c value for a gas/brine system is a factor of 0.194 that of the Hg/air capillary pressure profile. The entry pressure for gas into a brine-filled pore volume can thus be computed for a methane/brine system for which the gas entry pressure (P_d) is estimated as the P_c when S_{Hg} = 0.1 or 10% of mercury saturation (Pittman 1992). Despite the negative value of cos 140°, capillary pressures are reported as positive values by convention.

Figure 4.22 shows the median pore throat radius (r_{50}) plotted against the calculated gas entry pressure (P_d) into a brine-filled pore throat distinguished by formation. Figure 4.23 shows the depth profiles of both of these parameters. Most samples of limestone and all shales have similar median pore throat radii of 2 – 7 nm. However, the lower Gull River and Cambrian samples have median pore throat radii of ~270 nm. Figures 4.22 and 4.23 show that the calculated gas entry pressures to brine-filled pores for the DGR formations range from less than 200 kPa for the Cambrian sandstone (40 kPa), lower Gull River (150 kPa), Salina A2 Unit (130 kPa) and parts of the A0 Unit (40 kPa), to 13 - 21 MPa for the Cobourg Formation, to 10 – 30 MPa for Ordovician shales. The Middle and Lower Silurian formations also have high gas entry pressures (Manitoulin – 20-24 MPa, Cabot Head – 13.5 MPa, Goat Island – 12.5 MPa).

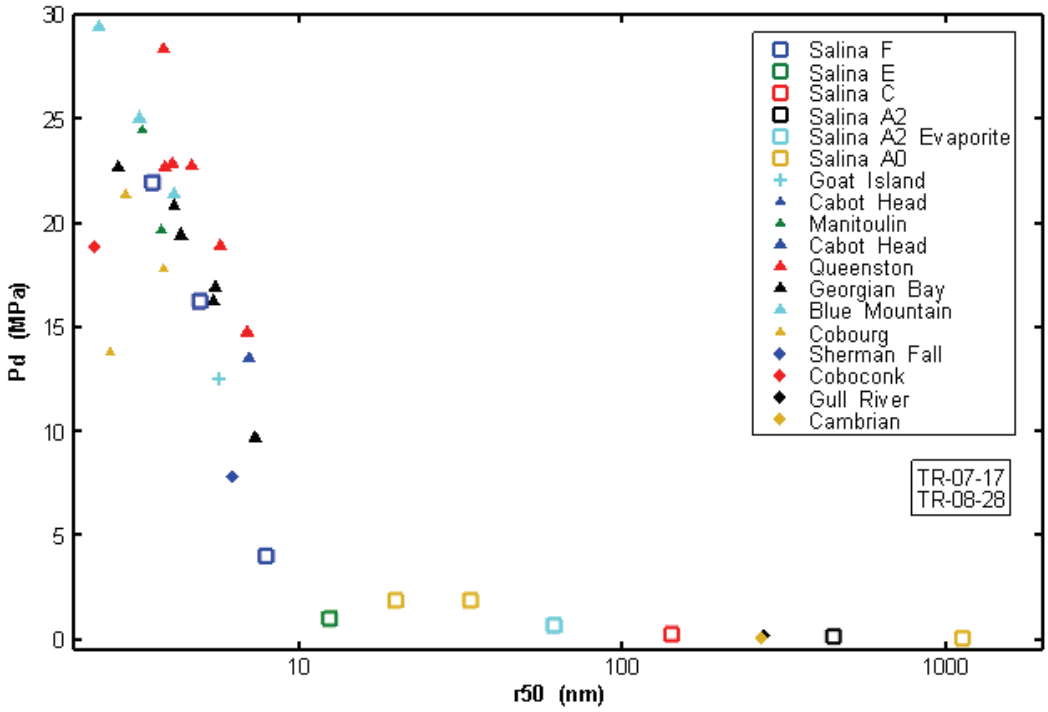

Figure 4.22: Relationship between Median Pore Throat Radius, r_{50} in Nanometres and Gas Entry Pressure into a Brine-Filled Pore, P_d in MPa for DGR Cores

It is noteworthy that for any particular pore throat radius value (evident for r_{50} values in the size range <10 nm), the gas entry pressure for the shales is higher than that of the limestones (see Figure 4.22). The median pore throat radius (r_{50}) is shown varying with depth in

Figure 4.23 with an increasing trend in pore-throat size above the proposed repository horizon (i.e., from the Cobourg Formation through the Blue Mountain to the Georgian Bay shales). Figure 4.23 also shows the existence of a gas entry barrier near the contact between the Blue Mountain and Collingwood shales.

Given the observations of oil presence in some core sections (Section 4.3.3), the gas entry pressure of oil-wet pores is also of interest. Lake (1989) reported that 28% of carbonate rocks were determined to be oil wet, 8% were water wet and the rest of an intermediate state (i.e., a contact angle of 75° – 105° as measured through the wetting phase). In the case of an oil-wet pore throat, the mercury would still be the non-wetting phase and would displace the oil as if it were brine; thus, the gas entry pressures reported here should also be appropriate for use with an oil-wet system.

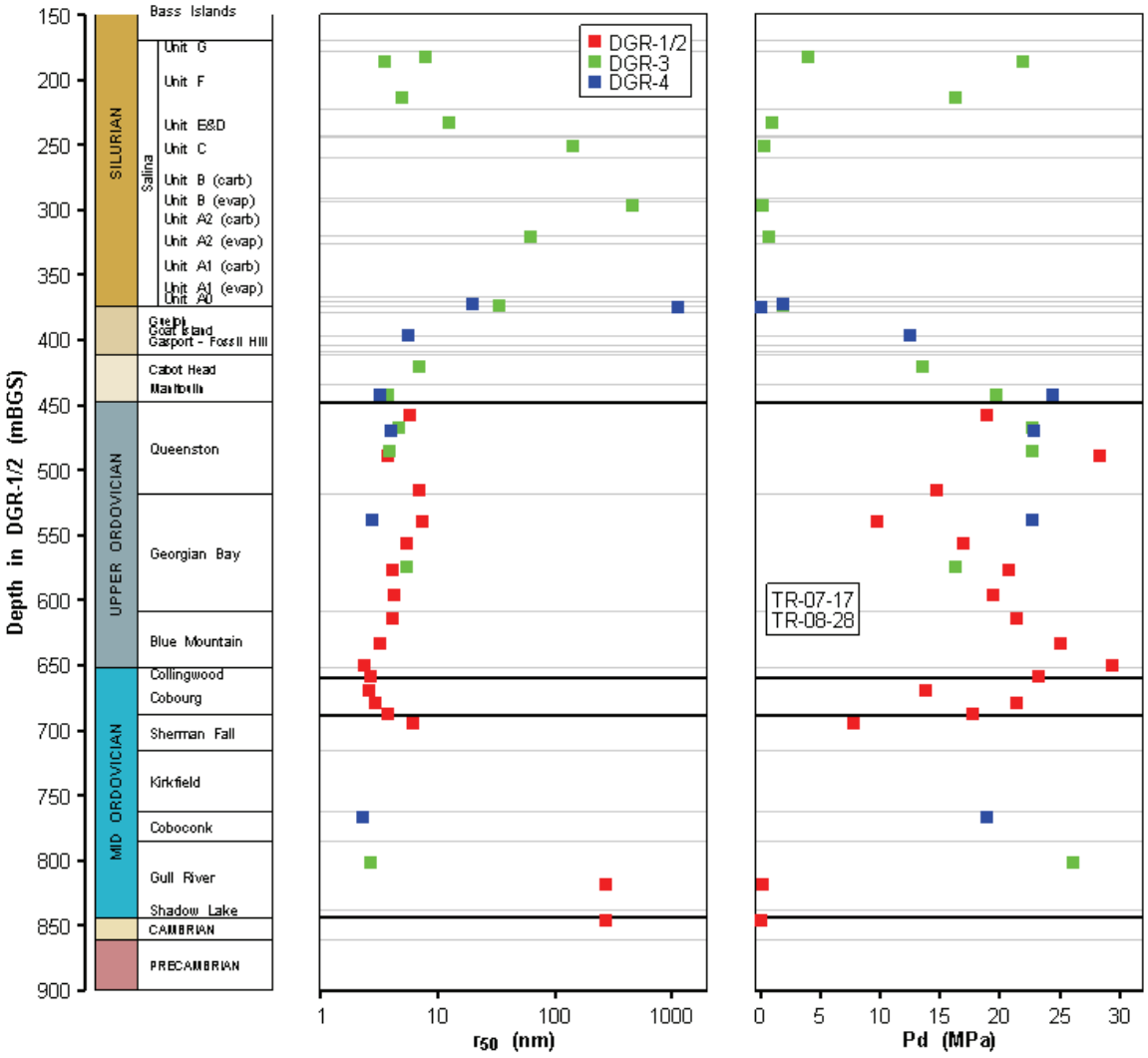

Figure 4.23: Profile of Median of Pore-Throat Radii (r_{50}) and Gas Entry Pressure (P_d) of Silurian and Ordovician DGR Cores determined from Mercury Injection Porosimetry

Figure 4.24 shows the depth distribution of pore-throat radii and gas entry pressure for the formations that occur in the 280 m of Ordovician shale and Silurian shale and dolostone that form the low-permeability barrier above the proposed repository horizon. That is, the figures in this section suggest that the Middle and Lower Silurian formations – consisting of the Goat Island dolostone, the Cabot Head shale, the Manitoulin dolostone (and the smaller formations between them) – constitute the upper part of the low-permeability barrier overlying the Cobourg Formation. The Upper Ordovician shales constitute the lower part of this caprock above the Cobourg Formation.

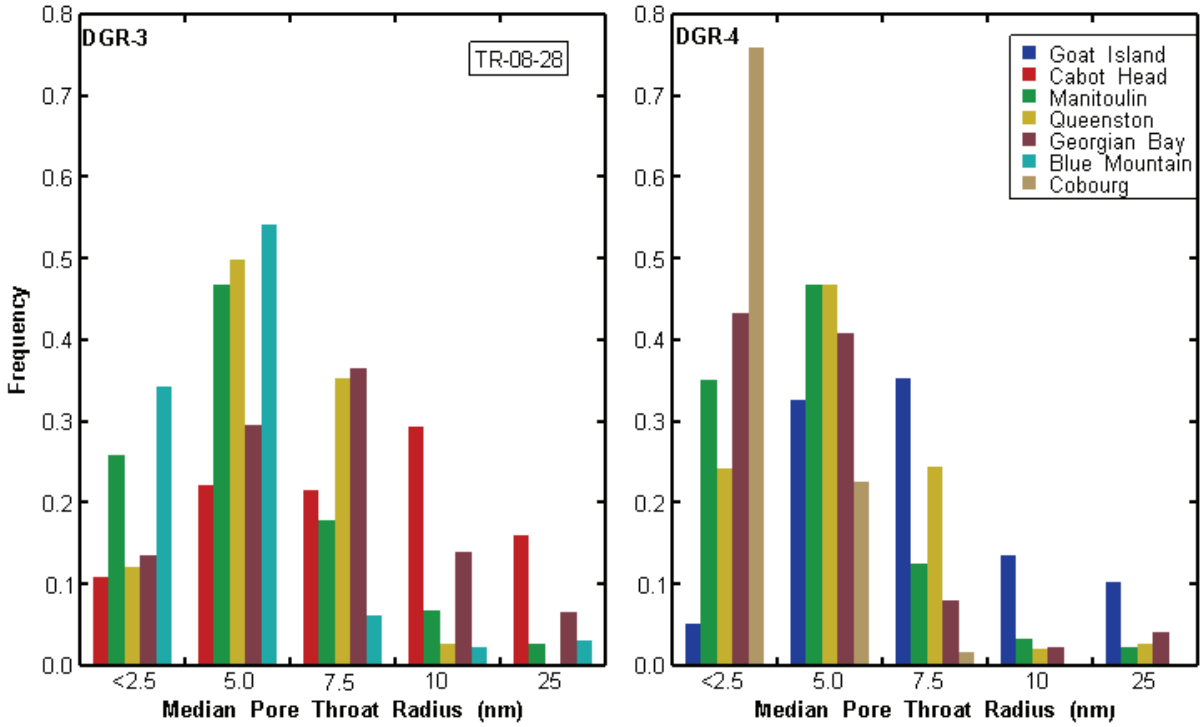

Figure 4.24: Histograms of the Distribution of Median Pore-Throat Radii (r_{50}) for Lower and Middle Silurian Shales and Dolostones and Ordovician Shales and Limestones in DGR-3 and DGR-4 Cores

4.3.7 Leverett's J Function

As noted above, there is strong evidence of overestimation in the measured permeabilities of the Ordovician cores that is most likely due to microcracking during coring, shipping and lab testing. However, porosity and mercury intrusion results appear to be correct or at least not subject to the same magnitude of overestimation seen in the permeability data. Leverett's J function is used in reservoir engineering to correlate permeability and porosity characteristics in a single parameter. The J function hypothesizes that the pore geometries of the various core plugs being compared are similar and accounts for changes in permeability, porosity and wetability (Tiab and Donaldson 2004):

$$J = P_c \frac{\sqrt{k/\phi}}{\sigma \cos\theta} \tag{4.5}$$

where P_c is the capillary pressure (Hg/air), k is the permeability, ϕ is the total porosity, σ is the interfacial tension and θ is the contact angle. Should the pore geometries differ, then the capillary pressure curves will not overlap. Tiab and Donaldson (2004) show how the (dimensionless) J function may be derived by substituting the capillary pressure into the Carman-Kozeny equation. Based upon this reasoning, the J function provides a means of comparing average rock properties in terms of permeability, porosity and wetability (Lucia 1999).

Figure 4.25 shows the J function plotted against mercury saturation for six DGR cores from the Ordovician shale sequence. Five samples from the three Ordovician shale formations (Queenston, Georgian Bay, Blue Mountain) follow a similar pattern that can be identified as diagnostic of these shales with an abrupt breakthrough prior to 10% mercury saturation and a smooth, flat curve indicating homogeneity in pore geometry before increasing in slope again. However, DGR2-650.12, a core from the Blue Mountain Formation, departs from the pattern. Because the J function is computed using a permeability measurement from a permeameter and not from the mercury porosimeter, the J function plot identifies this particular permeability measurement (k_v = 9.0x10^{-16} m^2) as an overestimate. This conclusion is supported by the similarity of the DGR2-650.12 porosimetry to the other Blue Mountain porosimetries shown on Figure 4.21b as well as similar porosity values. Thus, it is possible to identify a more accurate estimate of the permeability of DGR2-650.12 – and of DGR3-661.03 that failed during testing – by comparison with the other shales in the figure (i.e., $k_v \approx$ 1x10^{-19} m^2 or $K_v \approx$ 1x10^{-12} m/s).

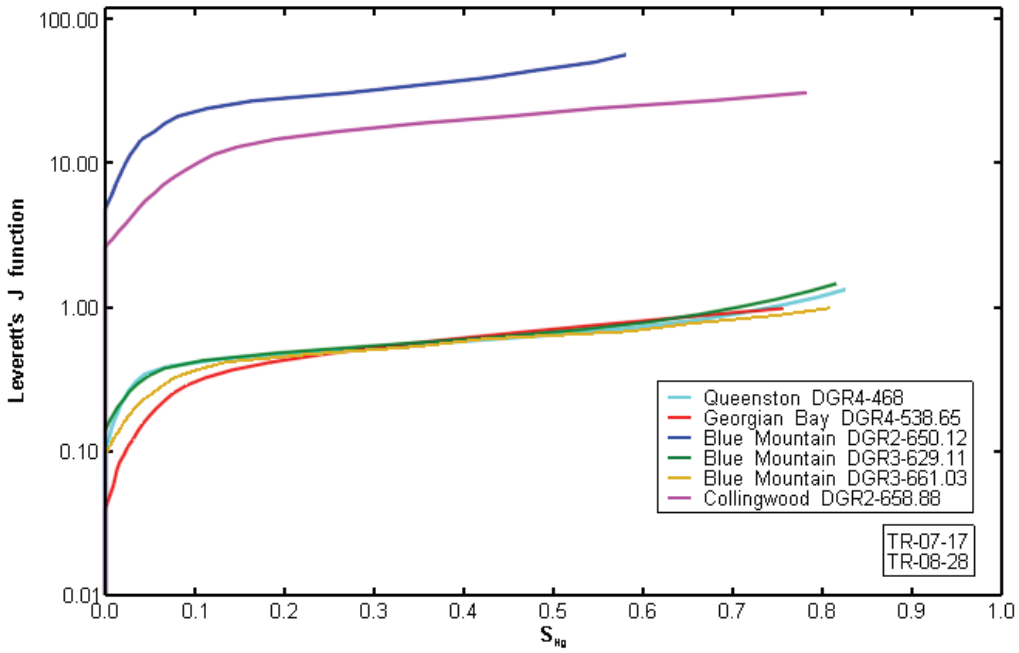

Figure 4.25: Leverett J Function Curves for DGR Ordovician Shale Cores

Similarly, Figure 4.26 identifies a diagnostic pattern for the Ordovician limestones shown at the bottom of the figure that exhibits a smoother breakthrough curve. Two limestone cores from the Cobourg Formation – DGR2-669.10 and DGR2-678.63 – also appear to have measured permeabilities that are overestimates, however in this case the measurements are already of the order of $k_v \approx 1x10^{-19}$ m^2, therefore the true value appears to be $<1x10^{-20}$ m^2. But the patterns displayed by these two cores during mercury intrusion otherwise mimic the diagnostic pattern below. A core from the Gull River Formation – DGR2-818.61 – initially follows the diagnostic pattern of the other limestones but then departs from this pattern and appears to be developing microcracks at approximately 1 MPa applied mercury pressure (see Figure 4.21d).

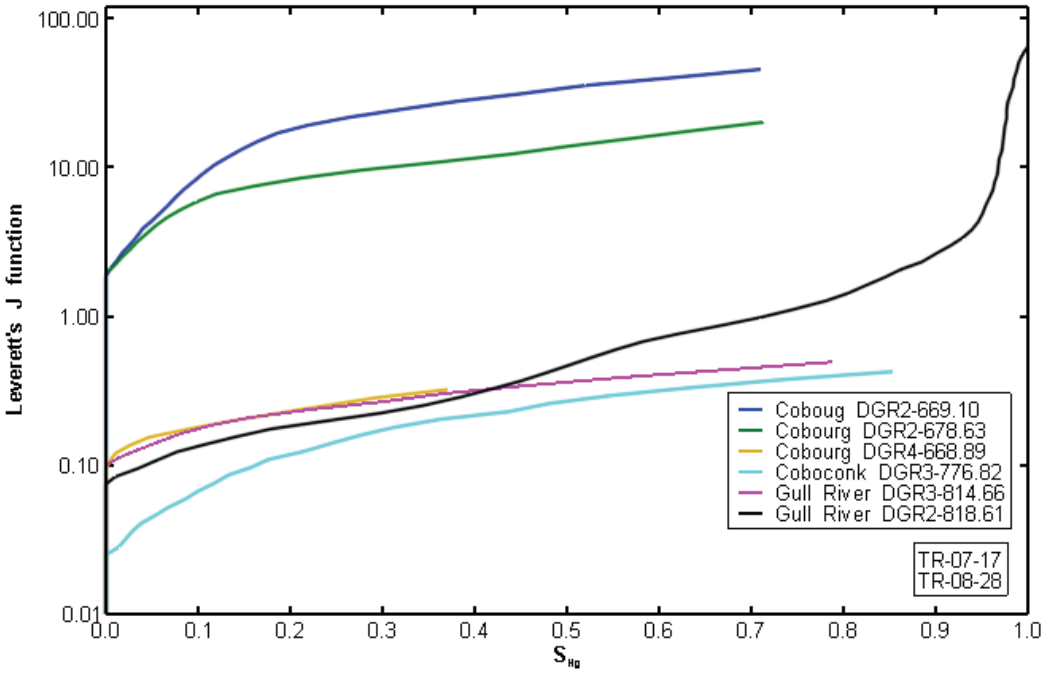

Figure 4.26: Leverett J Function Curves for DGR Ordovician Limestone Cores

Therefore, the Leverett J function plots can be used to identify (1) overestimates in the measurement of permeability – or underestimates in the measurement of total porosity – and (2) diagnostic patterns for permeability-porosity correlation in both the Ordovician shales and limestones. Because of the perceived reliability of the total porosity measurements by gas expansion and Boyle's Law (Lucia 1999, p.2), the anomalies detected in the J function figures are ascribed to microfracturing during permeability measurement and not to errors during the measurement of total porosity.

4.3.8 Surface Area Measurements

The external specific surface areas of DGR-2 core samples were measured by UniBern (TR-08-06, TR-08-40) using the Brunauer, Emmett, Teller (BET) method (Brunauer et al. 1938) and are presented in Figures 4.27 and 4.28 as a function of total porosity and total sheet silicate

(clay) content, respectively. Specific surface area was quantified as part of characterization of potential sorption properties of DGR cores to aid in reconstruction of porewater chemistries from crush and leach experiments (TR-08-06) and to assist in interpretation of core diffusion experiments (TR-07-17, TR-08-27). In addition, for 11 samples that were selected to cover a wide range of clay contents, the complete N_2-adsorption isotherms in the relative nitrogen pressure (P/P_0) range from 0 to 1.0 were obtained (TR-08-06).

Figure 4.27 shows the variation in BET surface area with total porosity. Both the Ordovician shales and limestones show a rather scattered increase in surface area with increasing porosity. While it is possible that a few of the Georgian Bay samples may in fact be carbonate hard beds, there is a clear indication of the very high specific surface area in the Ordovician limestones (e.g., Cobourg Formation).

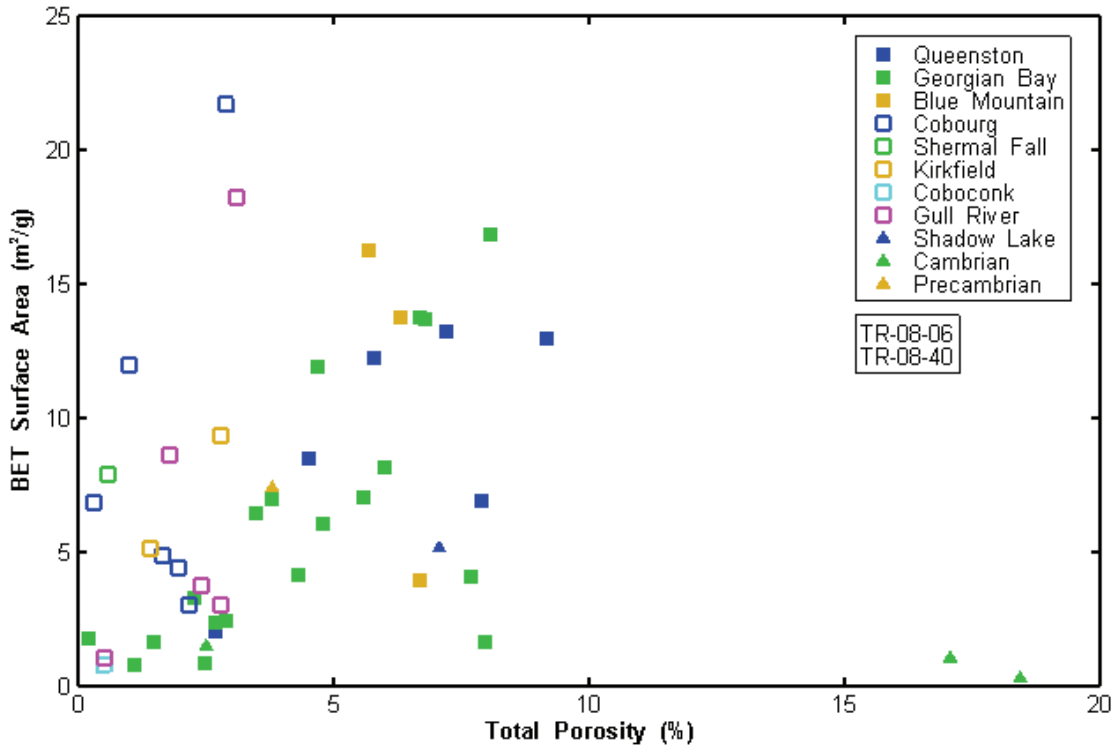

Figure 4.27: Specific Surface Area as a Function of Total Porosity in DGR-2 Cores

Figure 4.28 shows the BET surface area versus clay mineral content for these same DGR-2 cores. This figure shows that the surface areas are positively correlated with the clay mineral content of the Ordovician shales, but less so for the Ordovician limestones. Figure 4.28 indicates that despite their low porosity, the argillaceous limestones of the Cobourg, Sherman Fall and Kirkfield formations can have very substantial surface area, often equivalent to that of the shales.

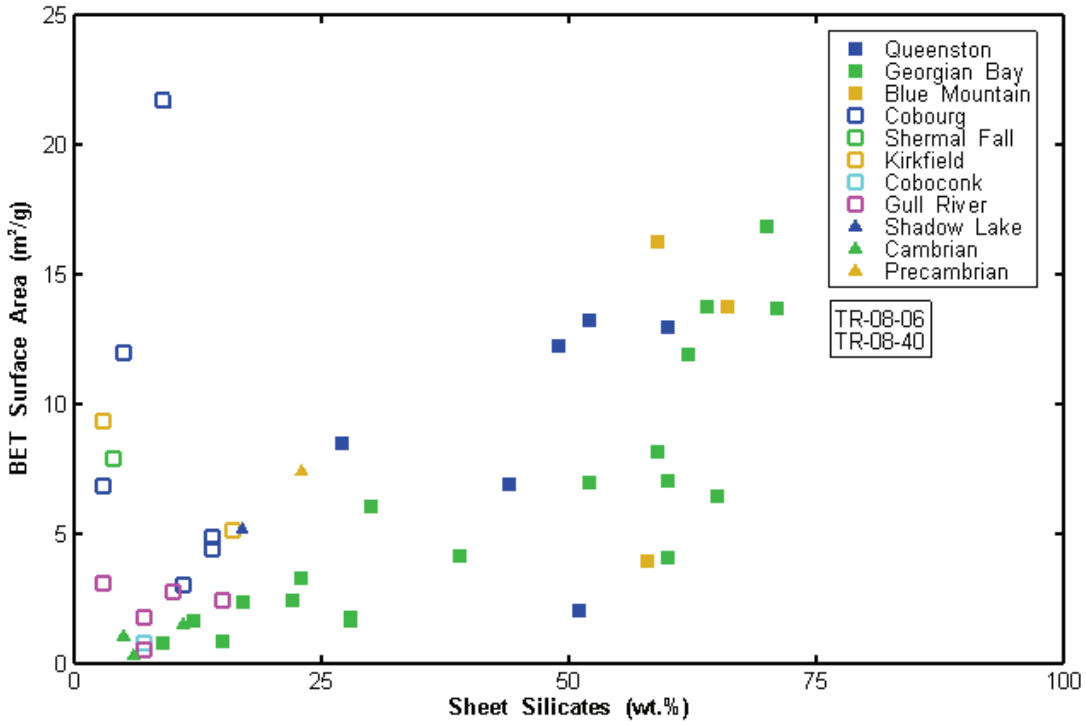

Figure 4.28: Specific Surface Area as a Function of Total Sheet Silicates in DGR-2 Cores

Full adsorption isotherms obtained for a subset of all DGR-2 samples are shown in Figure 4.29. All samples have typical S-shaped profiles, which characterises monolayer adsorption at low P/P_0 and multilayer adsorption at intermediate P/P_0. The BET surface is measured at a sample-specific P/P_0 where the monolayer is saturated, (i.e., at the onset of multilayer adsorption).

The break in slope at high P/P_0 corresponds to the onset of capillary condensation, (i.e., multi-layer sorption). There is an excellent correlation between clay content and the shape of the adsorption curve. The flattest curve is observed for Cambrian sandstone (DGR2-855.89), whereas clay-rich samples from the Georgian Bay Formation (DGR2-581.32 and DGR2-609.39) indicate a much higher adsorption (and therefore surface area) over the entire pressure range. Capillary condensation starts at lower P/P_0 in clay-rich samples when compared to the almost clay-free Cambrian sandstone, indicative of smaller pore apertures in these rocks (see TR-07-18, Table 4).

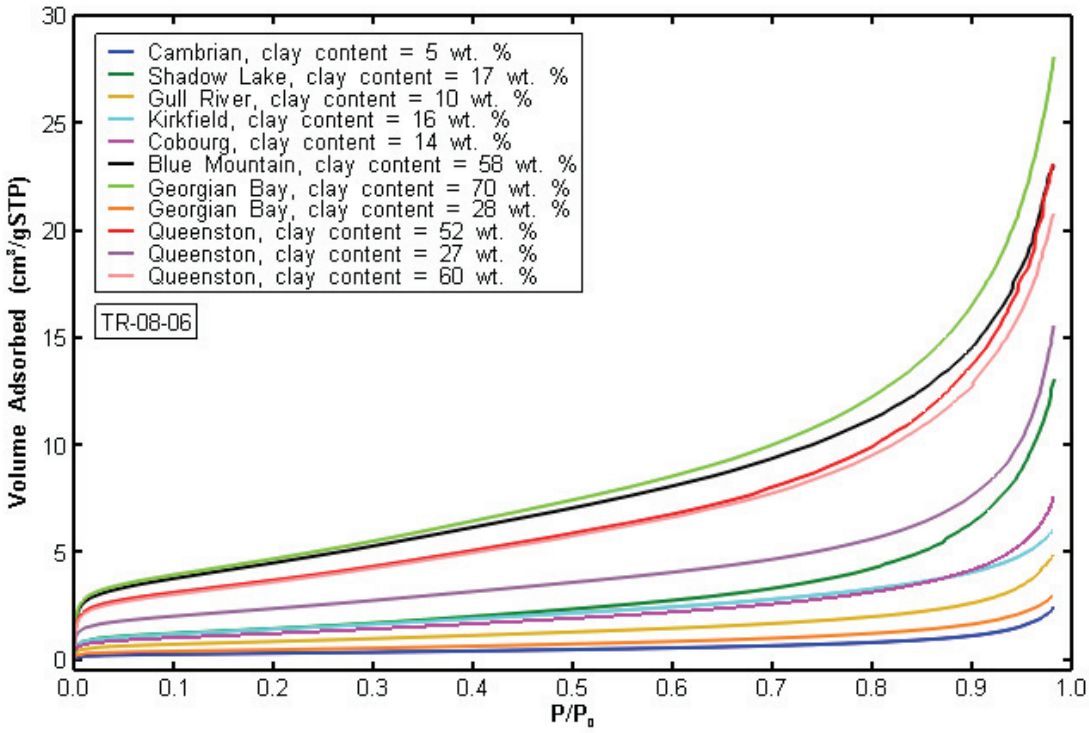

Figure 4.29: Full N_2 Adsorption Isotherms for DGR-2 Cores

4.3.9 Gas-Brine Flow Properties

Mercury injection porosimetry data, fluid saturation data and gas pulse permeability data for "as received" and "clean and dry" core samples were used to calculate van Genuchten characteristic two-phase (gas-brine) flow parameters for DGR cores (TR-08-33) that may be required to simulate multi-phase flow of gas and brine following repository closure. Mercury injection porosimetry data were used to generate van Genuchten fitting parameters for capillary pressure – liquid saturation curves. "As received" permeability data with defined fluid saturations were used with the "clean and dry" permeability data to calculate a relative gas permeability. The relative gas permeability and associated liquid and gas saturations were used to determine van Genuchten fitting parameters for relative permeability – liquid saturation curves.

Figures 4.30, 4.31, 4.32 and 4.33 show the fitted van Genuchten capillary pressure-saturation curves for gas-brine in DGR cores generated in TR-08-33. Consistent with Figure 4.21, the highest capillary pressures are associated with the Ordovician limestones (Figure 4.33) and the lowest with the Salina Formation Units (Figure 4.30). For the estimated gas saturations of ~10 to 20%, the resultant capillary pressures of 10 to 50 MPa are calculated for the Ordovician shales and limestones.

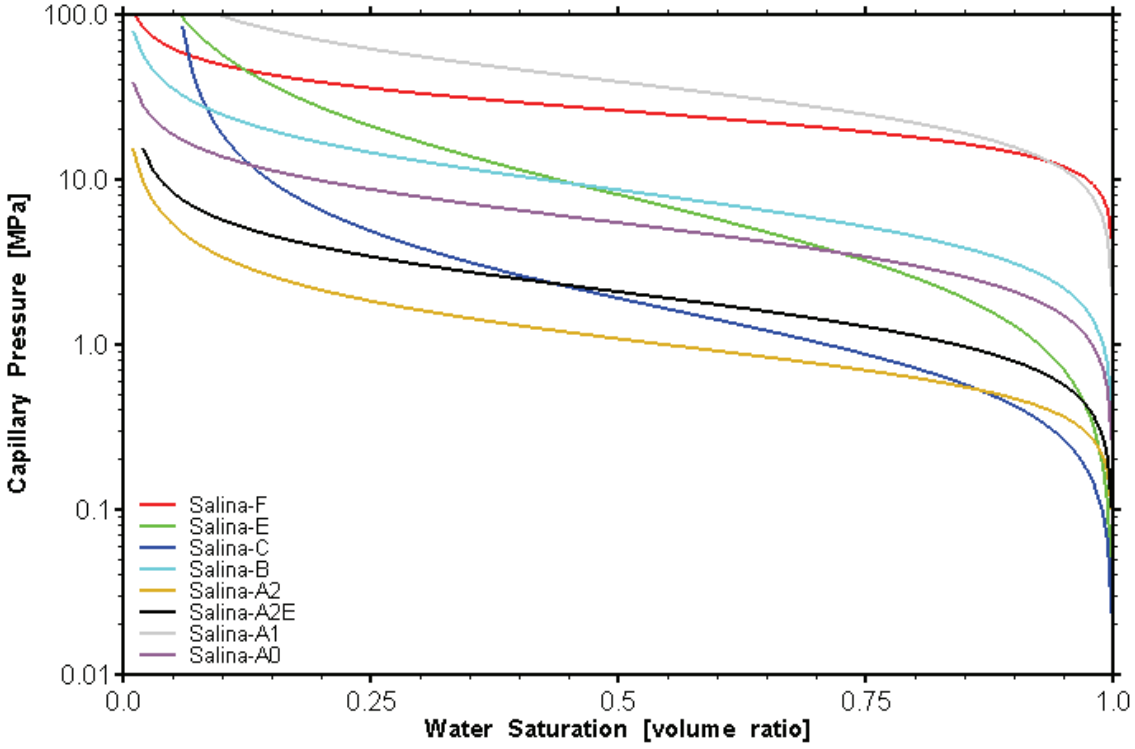

Figure 4.30: Fitted Capillary Pressure - Brine Saturation Curves for DGR Cores from the Salina Formation

Each capillary pressure curve is paired with a set of relative permeability-saturation curves shown in Figures 4.34 through 4.37. These figures show that the estimated gas saturations of ~10 to 20% result in reductions of brine permeability by 5-50%. These same gas saturations inhibit gas migration due to this relative permeability effect and the likelihood that pore throats are wetted by brine or even oil. That is, high in situ gas pressures would be required to cause gas migration. The most likely formations in which this might occur would be in the lower Blue Mountain and Collingwood formations where the methane solubility limit is exceeded by the largest margin (see Section 4.6.7.3).

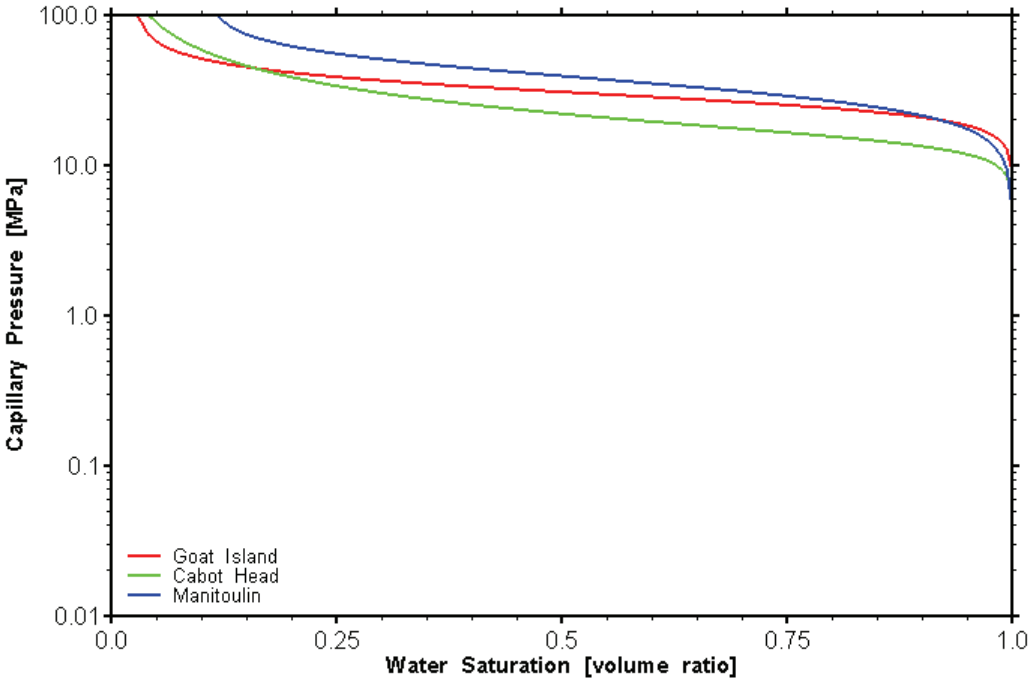

Figure 4.31: Fitted Capillary Pressure - Brine Saturation Curves for DGR Core from Lower Silurian Formations

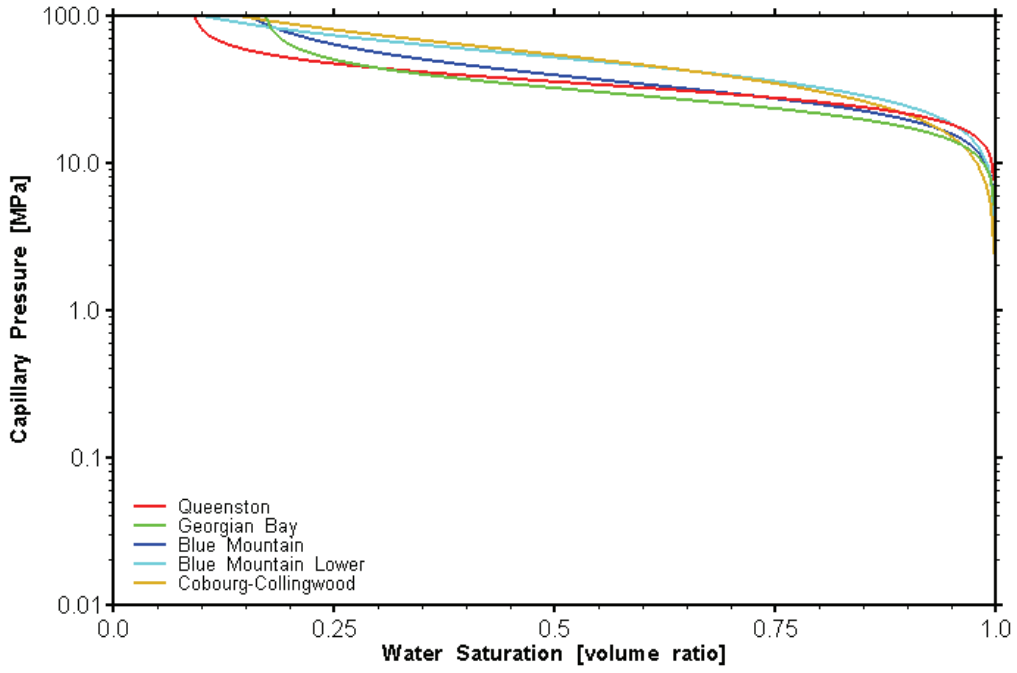

Figure 4.32: Fitted Capillary Pressure - Brine Saturation Curves for DGR Core from Ordovician Shale Formations

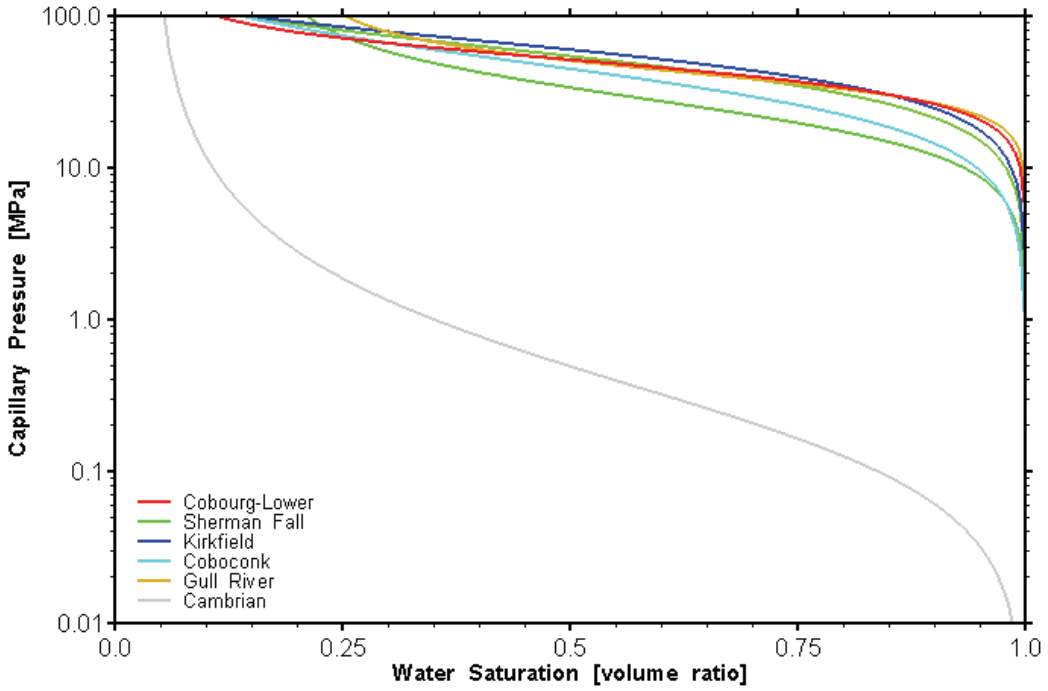

Figure 4.33: Fitted Capillary Pressure - Brine Saturation Curves for DGR Core from Ordovician Limestone Formations and Cambrian Strata

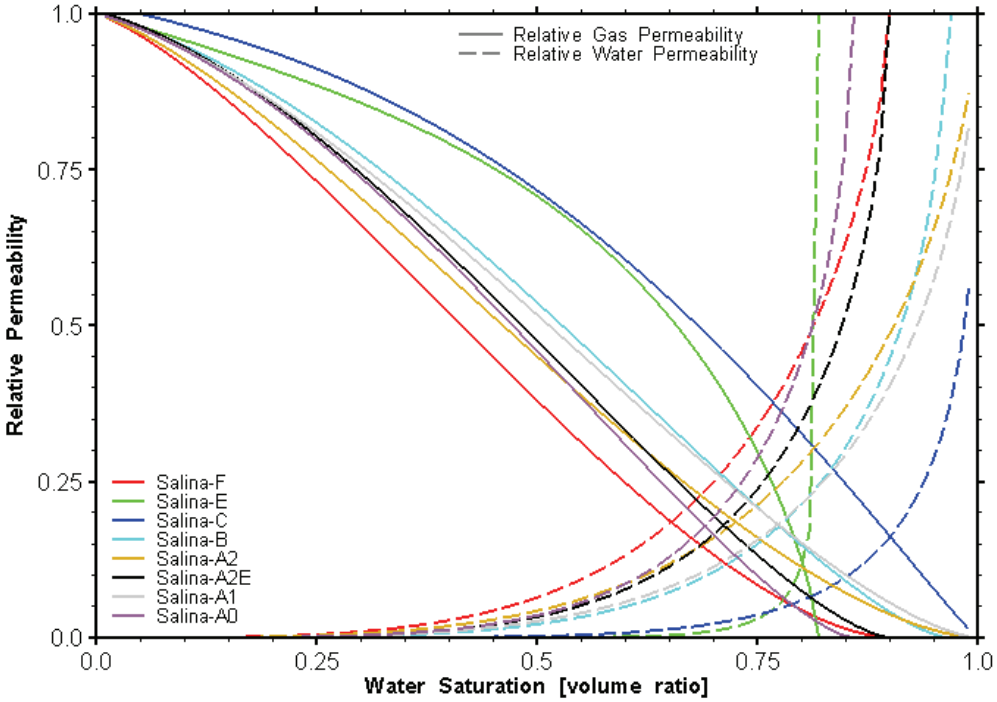

Figure 4.34: Fitted Relative Permeability – Brine Saturation Curves for DGR Cores from the Salina Formation

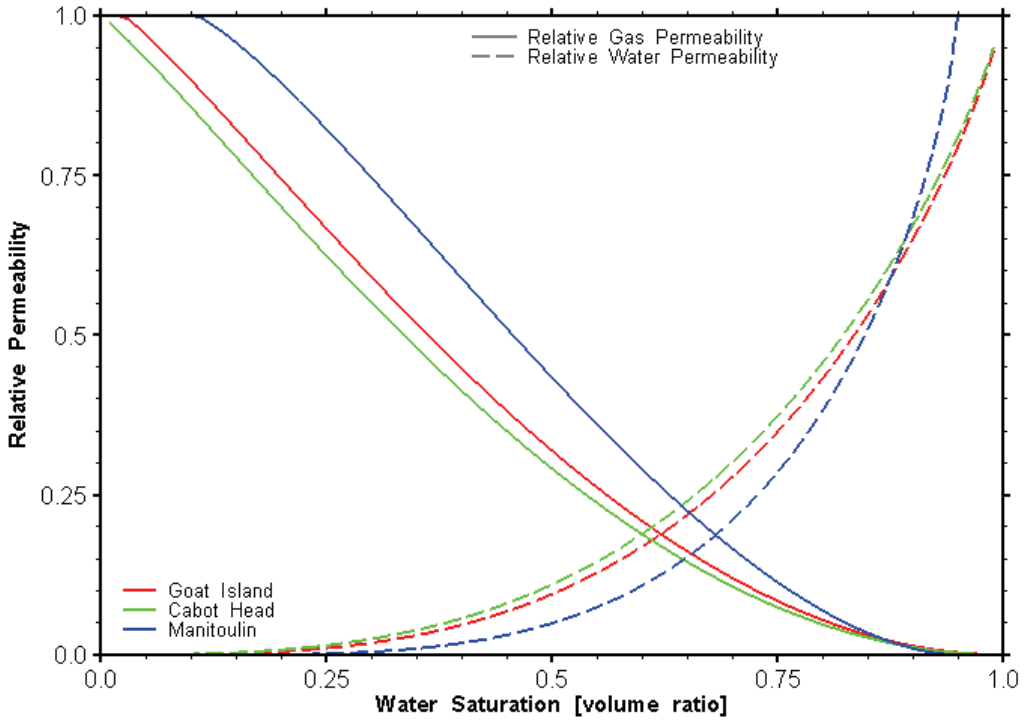

Figure 4.35: Fitted Relative Permeability – Brine Saturation Curves for DGR Cores from Lower Silurian Formations

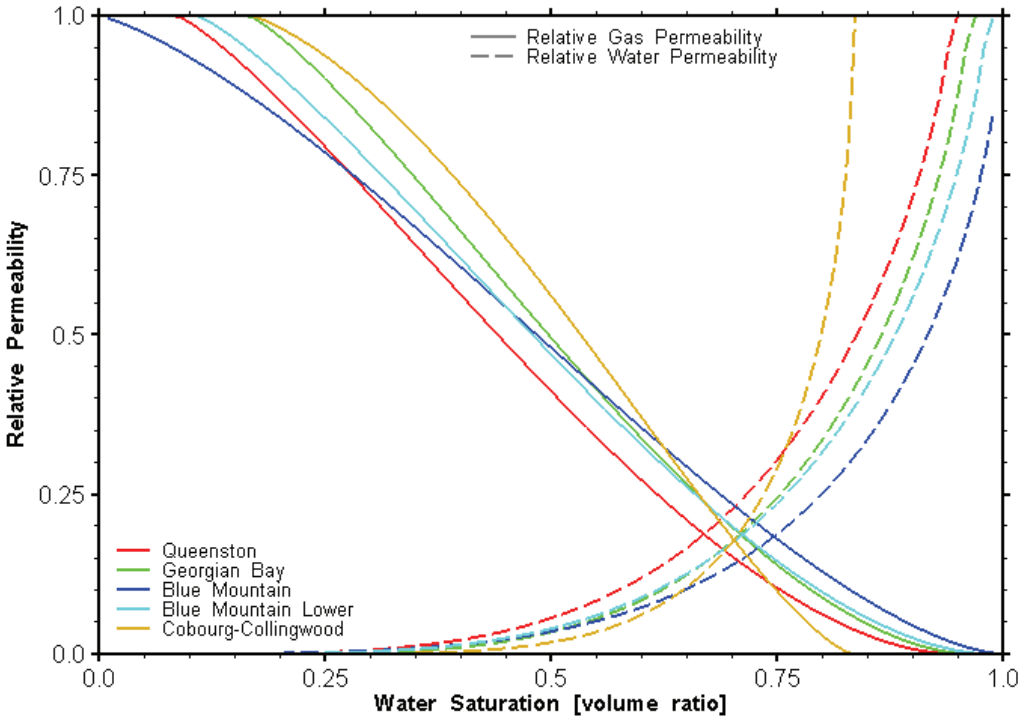

Figure 4.36: Fitted Relative Permeability – Brine Saturation Curves for DGR Cores from Ordovician Shale Formations

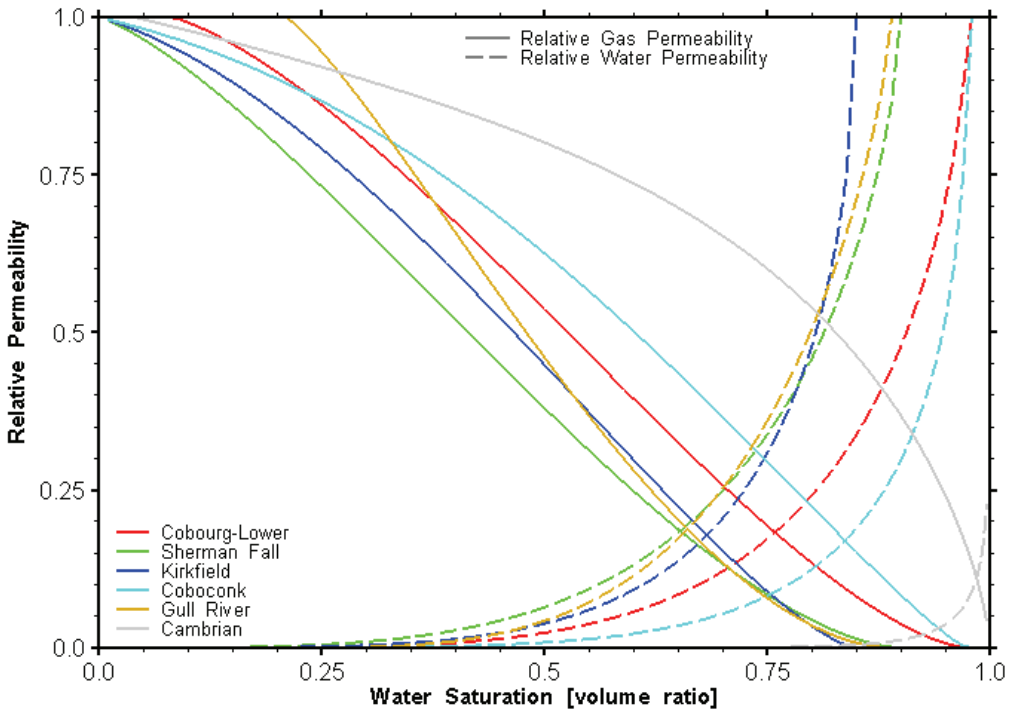

Figure 4.37: Fitted Relative Permeability – Brine Saturation Curves for DGR Cores from Ordovician Limestone Formations and Cambrian Strata

4.4 Diffusion Properties

The very low hydraulic conductivities that are reported above in Section 4.3.4 and later in Section 4.9.2 indicate the likelihood that diffusion will drive solute transport in the Ordovician shales and limestones. Two methods of measurement were employed by the University of New Brunswick (UNB) to determine the effective diffusion coefficient and the diffusion porosity of DGR core samples: an X-ray radiographic technique for measuring normal (vertical) and parallel (horizontal) to bedding and one based upon a conventional through-diffusion cell approach for measuring vertical properties (TR-07-17 and TR-08-27). The use of two methods was originally thought necessary in order to check the results of the UNB X-ray radiographic method (Tidwell et al. 2000) against the more widely used through-diffusion method (Boving and Grathwohl 2001, Van Loon et al. 2003). The paper of Cavé et al. (2009) provides a benchmark of the two methods.

As it developed, the poor signal-to-noise ratio measured by the radiographic technique in the low-porosity (<0.03) argillaceous limestones required the use of the through-diffusion method for these samples. Irrespective of the method used, the core plugs tested were saturated with a synthetic brine porewater and then the diffusion measurements were made with either a sodium iodide (NaI) tracer solution (radiographic method) or with a tritiated-water (HTO) or NaI tracer solution (diffusion cell). A comparison of the two techniques (TR-07-17, Cavé et al. 2009) indicated that they provide comparable results, differing by no more than a factor of 2.25 for paired sets of samples.

A further comparison of UNB iodide test results was provided through duplicate, normal to bedding, through-diffusion testing of DGR-2 core samples of Cobourg Formation argillaceous limestone and Queenston Formation red shale completed by the Paul Scherrer Institute (PSI), Switzerland using ^{125}I as a tracer (TR-07-22). Comparative results are presented in Table 4.4 and demonstrate good agreement between laboratories.

Table 4.4: Inter-Laboratory Comparison of the Effective Diffusion Coefficients (D_e) and Tracer-Accessible Porosity (ϕ) Determined from Though-diffusion Testing of Queenston Shale and Cobourg Limestone Cores from DGR-2

Diffusion Parameter	PSI DGR2-466.38		UNB DGR2-456.97	PSI DGR2-675.48		UNB DGR2-677.11
	Queenston Sample 1	Queenston Sample 2	Queenston Sample	Cobourg Sample 1	Cobourg Sample 2	Cobourg Sample
D_e (m^2/s)	3.63×10^{-12}	3.05×10^{-12}	2.60×10^{-12}	6.74×10^{-13}	6.26×10^{-13}	4.50×10^{-13}
ϕ (%)	13.4	9.6	9.4	2.4	2.4	1.2

4.4.1 Effective Diffusion Coefficients

The results of all effective diffusion coefficient testing completed by UNB are presented in Figure 4.38 versus DGR-1/2 reference depth and formation, discriminated by borehole, tracer type (NaI or HTO) and testing direction (normal and parallel to bedding). One hundred and thirteen estimates of effective diffusion coefficient (D_e) were measured by UNB using through-diffusion and X-ray radiography testing techniques. Testing was completed on preserved cores collected from Silurian and Ordovician formations in boreholes DGR-2, DGR-3 and DGR-4. For iodide diffusion testing normal to bedding, Figure 4.38 also shows the geometric mean D_e for each formation member or unit. A cursory review of Figure 4.38 shows that there are no systematic differences in D_e values between individual DGR boreholes.

As shown in Figure 4.38, with the exception of a few samples from the Upper Silurian, the D_e values measured from DGR cores all fall in the range of 10^{-12} m^2/s or lower. The few highest values closest to or exceeding 10^{-11} m^2/s occur in the high-porosity (>10%) Salina B, C, E and F Units and the Cabot Head shale as expected based on the known correlation of diffusion coefficients with porosity (Lerman 1979). The lowest D_e values, on the order of 3 to 5 x 10^{-14} m^2/s, were measured on gypsum-anhydrite layers of the Salina A2 and A1 Unit evaporites and dolostones, in the carbonate hard beds within the lower Queenston and upper Georgian Bay formations, and on several limestone samples from the lower Gull River Formation. These extremely low values may be the lowest ever measured on sedimentary rocks to date, and all of the diffusion data measured as part of the DGR program fall below or near the lower range of reported international data (Section 4.4.3). The majority of the D_e values are in the range of 10^{-13} to 10^{-11} m^2/s, with the Lower Silurian and Upper Ordovician shale samples representing the higher end of this range due to their relatively high porosity (~10%). Fifteen diffusion measurements have been made on samples of the Lower Member of the Cobourg Formation, which is the proposed DGR host rock; the results indicate consistently low D_e values of 10^{-13} to 10^{-12} m^2/s.

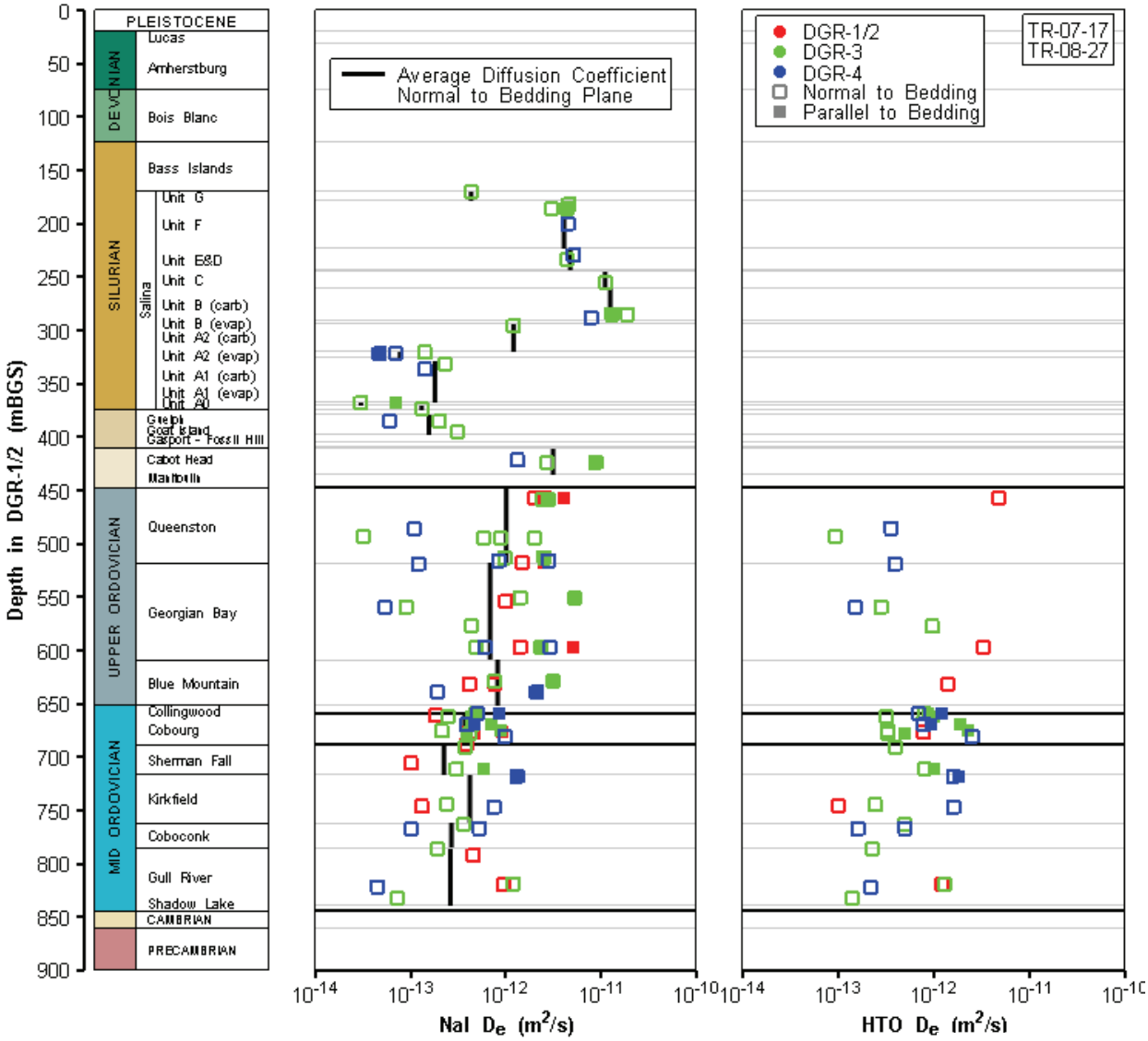

Figure 4.38: Effective Diffusion Coefficient (D_e) Profile as Determined by X-ray Radiography and Through-Diffusion Testing of DGR Cores Showing Point Data and Formation Averages

The D_e data display systematic variability as a function of the tracer used to make the measurements. D_e values obtained from through-diffusion testing with HTO tracer are on average 1.9 times greater (range 0.8 to 4.9) than D_e values measured with the iodide tracer. Figure 4.39 provides a cross plot of all of the D_e data measured by through-diffusion for HTO and iodide tracers. This difference is primarily attributed by UNB (TR-08-27) to anion exclusion in lowering the tracer-accessible porosity, although 20% of the differences in D_e values are due to a 20% larger value of free-water diffusion coefficient for iodide over HTO. Anion exclusion effects in porous media are commonly attributed to charge interactions between ions in solution and the electric double layer (EDL) present in clay-rich media. Some simple calculations of EDL

thickness and comparison to pore throat sizes determined from high-pressure mercury injection testing provide insight to this exclusion process.

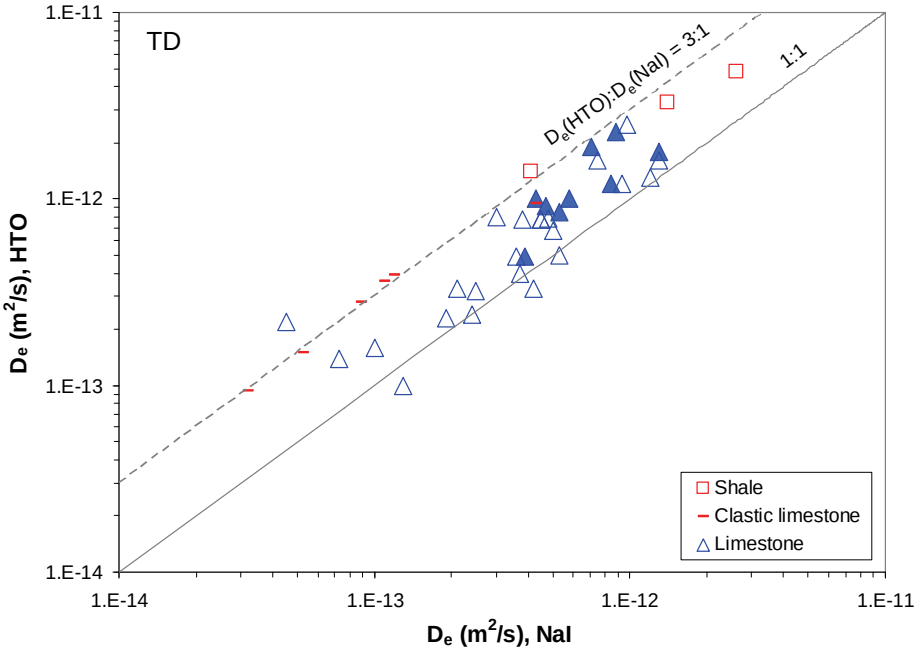

Note: Open symbols are normal to bedding; filled symbols are parallel to bedding.

Figure 4.39: Relationship between D_e Determined with Iodide Tracer and D_e Determined with HTO Tracer on DGR Cores Measured by Through-diffusion

The thickness of the electrical double layer (EDL) for a 5M NaCl brine is ~0.14 nm (Stumm 1992, p.49); that is an order of magnitude smaller than the smallest of the pore throat radii in Figure 4.22. The EDL associated with a negatively charged clay colloid such as an illite surface may be estimated by the general equation for the EDL (Stumm 1992, p.47-49). The inverse of the thickness of the EDL, κ, is given by Stumm as:

$$\kappa = \sqrt{\left\{ \frac{2F^2 \cdot I \cdot 10^3}{\varepsilon \varepsilon_0 RT} \right\}} \qquad (4.6)$$

Where F is the Faraday constant (9685 Coulombs per mole), I is the ionic strength (M) of the solution associated with the charged surface, ε is the dielectric constant of water (ε = 78.5 at 25ºC), ε_0 is the permittivity of free space (8.854×10^{-12} C^2 J/m), R is the molar gas constant (8.314 J mol/K) and T is the absolute temperature (K). For a brine with a TDS ~300 g NaCl/L, (i.e., 5M NaCl), κ^{-1} is ~ 0.14 nm. By comparison with the method detection limit (MDL) for mercury injection shown in Figure 4.24, the EDL thickness is much smaller than this MDL, which is approximately 2.5 nm. Therefore, pore throats with the median radii shown in Figure 4.24 would exhibit only a limited ability to inhibit anion (and cation) migration because most throats

appear >> $2\kappa^{-1}$ or 0.3 nm, which is the projection of EDLs by both grain walls into a pore throat. However, experimental evidence presented in Section 4.4.2 (Figure 4.41 - i.e., the marked difference between average tracer-accessible porosity and water-loss porosity), indicates that ion exclusion is likely occurring. Results from porewater chemistry extractions suggest that must be due to ion exclusion occurring in numerous very small pores with pore throat diameters < 2.5 nm and that this halite-undersaturated porewater is released during crush and leach extraction.

Thus, anion exclusion does not appear to be the only cause of the difference in De values obtained using different tracers. Lerman (1979, p.93) indicates that the diffusion of dissolved species in small pore throats of the sizes shown in Figure 4.22 is also retarded by a combination of geometric and hydrodynamic effects (hindrance of pore walls) through an increased drag force. Because the hydrated iodide ion is larger than the HTO molecule (~1.4 nm) and the pore throats are of the order of 1-10 nm, it may be that 'hindrance of pore walls' in addition to anion exclusion is responsible for the differences shown in Figure 4.39. "Clastic limestones" in Figure 4.39 are the limestone hard beds within the Ordovician shales.

There is also a systematic difference in the D_e values based on the orientation of the measurements with respect to bedding direction. With only two exceptions (in the Salina B Unit anhydrite and A2 Unit evaporite, Figure 4.38), the D_e values determined from paired samples are greatest for diffusion in the direction parallel to bedding. The anisotropy ratio (D_e parallel/D_e normal) ranges from 1 to 4 for measurements made with iodide tracer, and from 1 to 7 for measurements made with HTO tracer (TR-08-27). Figure 4.40 shows the relationship between D_e values measured parallel and normal to bedding in all DGR cores tested by X-ray radiography and through-diffusion using iodide and HTO tracers.

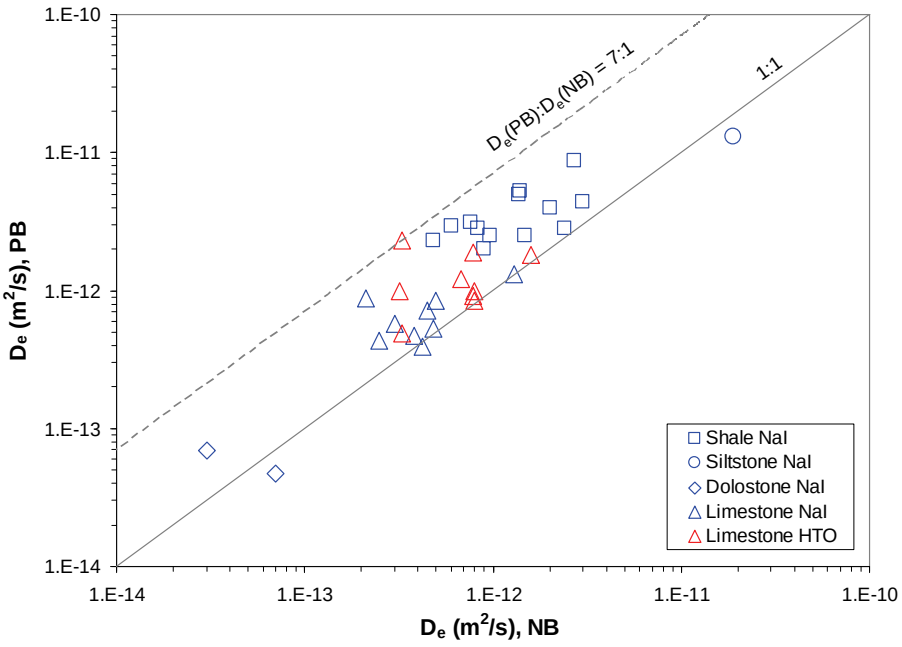

Figure 4.40: Relationship between D_e Determined Normal to Bedding (NB) and Parallel to Bedding (PB) in DGR Cores

Cavé et al. (2010) developed formation-scale estimates of iodide De and anisotropy for the Georgian Bay Formation in DGR-2 considering the thickness of shale and carbonate hard beds within individual core runs and average normal to bedding De values for shale ($1.2x10^{-12}$ m^2/s) and hardbeds ($1.3x10^{-13}$ m^2/s) and average parallel to bedding De values for shale ($3.9x10^{-12}$ m^2/s) and hardbeds ($1.9x10^{-13}$ m^2/s). A formation scale anisotropy for De (parallel:normal to bedding) of 7.2 was determined by calculating the ratio of weighted arithmetic mean formation De to the weighted harmonic mean formation De for the entire Georgian Bay Formation.

4.4.2 Diffusion Porosity

The diffusion (tracer-accessible) porosity values determined from all diffusion testing on DGR core are presented in Figure 4.41 versus DGR-1/2 reference depth and formation, discriminated by testing method (X-ray radiography and through-diffusion [TD]), tracer type (NaI or HTO) and testing direction (normal and parallel to bedding). Liquid porosities determined by UNB for the same DGR samples subject to diffusion testing are also shown on Figure 4.41.

Figure 4.41 shows that liquid porosity values exceed the tracer-accessible porosities by a large margin in some of the Silurian shales (F Unit, C Unit, and Cabot Head) and the Ordovician shales but are similar in many of the Silurian dolostones and the Ordovician limestones, which is likely the result of the very low water yields that obscure the differences in the measurements. Some of the large differences in the Silurian formations are also likely due to overestimation of liquid porosity due to incorporation of gypsum-bound water in the liquid porosity estimate. As discussed in Section 4.4.1, the differences in tracer-accessible porosity from diffusion testing and liquid porosity from oven heating are primarily attributed to anion exclusion and hydrodynamic hindrance effects.

Figure 4.42 shows cross plots of tracer-accessible porosity determined by X-ray radiography versus liquid porosity (a – upper plot) and the same plot based on through-diffusion measurements (b – lower plot). The through-diffusion data indicate that some of the low-porosity Ordovician limestones have higher tracer-accessible porosity than liquid porosity, which is physically impossible. This illustrates the uncertainty associated with the porosity values obtained from through-diffusion experiments in the low-porosity limestones and, for this reason, further discussion of tracer-accessible porosity is limited to the results from the radiography testing.

Figure 4.42a shows that values of iodide-accessible porosity for the Silurian and Ordovician shales are consistently lower than liquid porosity, on average being 50% of the liquid porosity values consistent with expectations based on anion exclusion theory. For the dolostone and limestone samples, with little to no clay and gypsum, tracer-specific difference in porosity is not as evident. The ratio of iodide-accessible to liquid porosity for the limestones and dolostones ranges from 0.5 to 1.0. Outliers shown on Figure 4.42a include Silurian dolostone and limestone samples that likely contain gypsum and samples with low porosity (<1%) which approaches the detection limit for the radiography method.

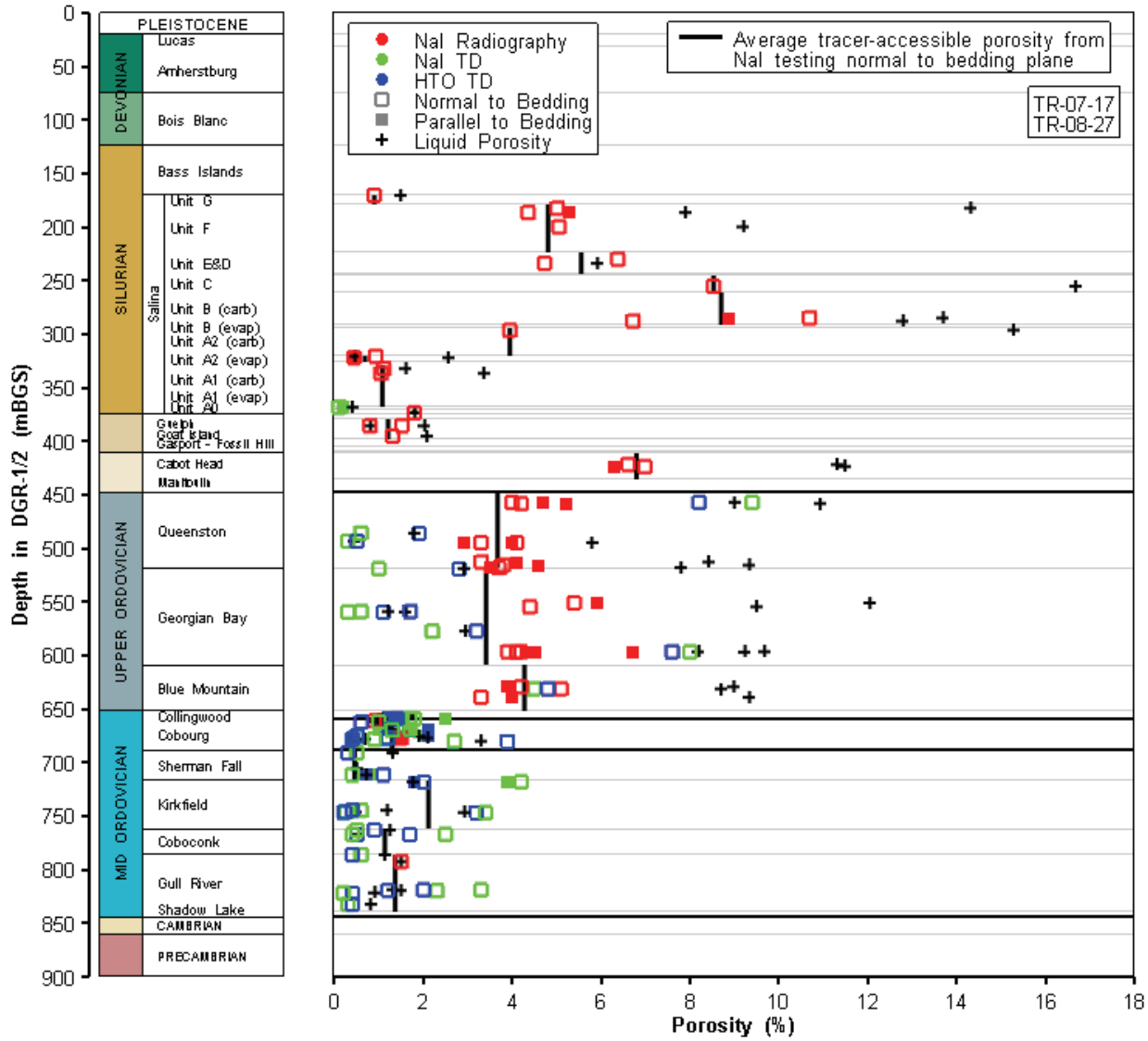

Note: Formation averages of tracer-accessible porosity from NaI testing normal to bedding planes are also shown.

Figure 4.41: Profile of Liquid Porosity and Tracer-Accessible Porosity Determined from Diffusion Testing of DGR Cores

4.4.3 Comparison with International Data

In order to obtain an international perspective, the diffusion coefficient data from the DGR cores can be compared to diffusion coefficient data obtained from argillaceous rocks by researchers involved with radioactive waste programs in other countries. The Claytrac Project is sponsored by the Nuclear Energy Agency of the Organization for Economic Co-operation and Development (OECD/NEA) and it included a review of diffusion studies conducted at nine different European sites (Mazurek et al. 2009).

Comparison of the results from diffusion measurements of DGR cores with international data collected from these nine study sites shows that the DGR formations within the Michigan Basin exhibit relatively low D_e and porosity values (Figure 4.43). Figure 4.43 shows the comparison of DGR data and international data for water-accessible porosity versus D_e for tritium tracers and anion-accessible porosity versus D_e for chloride and/or iodide tracers.

The international data were critically reviewed and compiled by Mazurek et al. (2009) and represent the most appropriate site-specific data from Belgium, France, Switzerland and the United Kingdom available to date. For the UNB data, water-accessible porosity is represented by the measured water-loss porosity and the anion-accessible porosity is represented by the iodide-accessible porosity measured using either radiography or through-diffusion.

Included in Figure 4.43 are curves derived from Archie's Law (Boving and Grathwohl 2001) which relate D_e to porosity by:

$$D_e = D_0 \phi^m \tag{4.7}$$

where D_0 is the value of the ionic diffusion coefficient in free water, m is an empirical exponent and ϕ is considered to be the total or physical porosity. Lerman (1979, p. 92) indicated the value of m should be about 2.0. Diffusion testing of DGR core by Paul Scherrer Institute (TR-07-22) indicates an m value of 2.3. Figure 4.43 shows that most of the DGR diffusion data are consistent with an m value of 2.0 +/- 0.5. Figure 4.43 shows curves representing Equation 4.7 for m values of 1.5, 2.0, 2.5 and 3.0.

The diffusion data, both international and from this report, fall within the expected relationships for geologic materials, with the exception of two outliners in the international $D_{e\text{-}HTO}$ data, both of which are from unlithified clay strata, and one outlier in the $D_{e\text{-}anion}$ data, a porous limestone sample.

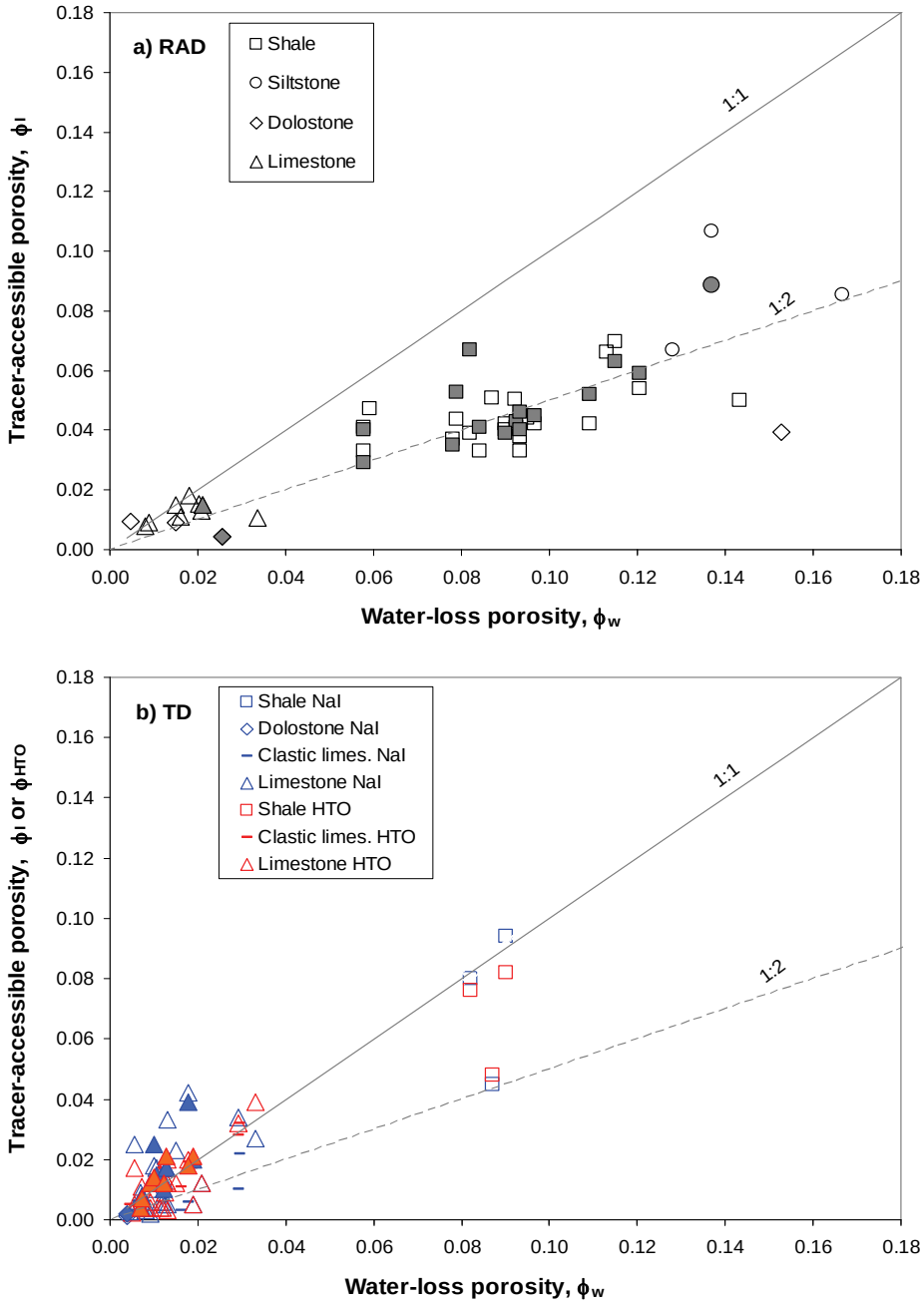

Note. Open symbols are normal to Bedding; Filled Symbols are Parallel to Bedding.

Figure 4.42: Relationship of Tracer-Accessible Porosity to Liquid (Water-Loss) Porosity for DGR Cores – a) Radiography Testing and b) Through-diffusion Testing

Note that there are very limited international data from limestone formations. The Ordovician limestones, in which the proposed DGR is expected to be hosted, and the Silurian dolostone/ limestones represent the lowest measured D_e values by 1 to 2 orders of magnitude. The Ordovician shales of the Michigan Basin fall within and towards the lower end of the range of the international clay and shale D_e values. The four international data points with the highest D_e and porosity values in Figure 4.43 represent unconsolidated clay while the remainder of the data within that group represent shales and claystones. The Silurian shale values are higher than the Ordovician shales, but still fall within the mid-range of the international data, while the Silurian siltstones fall close to the high range of D_e values measured in the international lithified sequences. In comparison with the data collected from DGR samples, the D_e values obtained from the European site characterization programs are generally higher by a factor of approximately 10.

4.5 Groundwater Characterization

The water in the fractures and pore spaces at the site is divided into two categories, groundwater and porewater. The term groundwater refers to free flowing groundwater and porewater refers to water from low-permeability zones (Gimmi and Waber 2004). Groundwater samples were collected following completion of shallow boreholes US-3, US-7 and US-8 with MP38 multi-level monitoring casing (TR-08-08, TR-08-30) and during drilling of deep DGR boreholes (TR-07-11, TR-08-18). Porewater was sampled by sub-sampling cores and removing the porewater from the rock in laboratories at the Universities of Ottawa (TR-07-21, TR-08-19, TR-09-04), New Brunswick (TR-07-17, TR-08-27) and Bern (TR-08-06, TR-08-40), and calculating porewater concentrations.

4.5.1 Shallow Groundwater Chemistry – US Wells

The three boreholes US-3, US-7 and US-8 (Figure 1.2) were instrumented with MP38 multi-level casings manufactured by Westbay Instruments Inc. (TR-07-20). These casings allow groundwater pressures to be monitored and groundwater samples to be obtained from packer-isolated intervals. The location of the boreholes was selected to enable three-dimensional analysis of groundwater flow direction as well as to determine the spatial variability of shallow (<200 mBGS) bedrock groundwater chemistry.

US-3 and US-7 were completed in the upper 90 m of bedrock, which includes the Amherstburg Formation (dolostone) that overlies the Bois Blanc Formation (cherty dolostone). US-8 was completed into the top of the Salina F Unit (dolomitic shale), at a depth of approximately 200 mBGS as described in TR-07-19.

Groundwater samples were obtained in the spring and fall of 2008 and 2009 from all three boreholes. However, the only sampling event that sampled all of the intervals was in spring 2008. The subsequent sampling events only obtained groundwater samples from approximately one third of the sample intervals in the boreholes. Therefore, the results presented in the figures are for the 2008 spring sampling event that occurred from the end of May to the beginning of June.

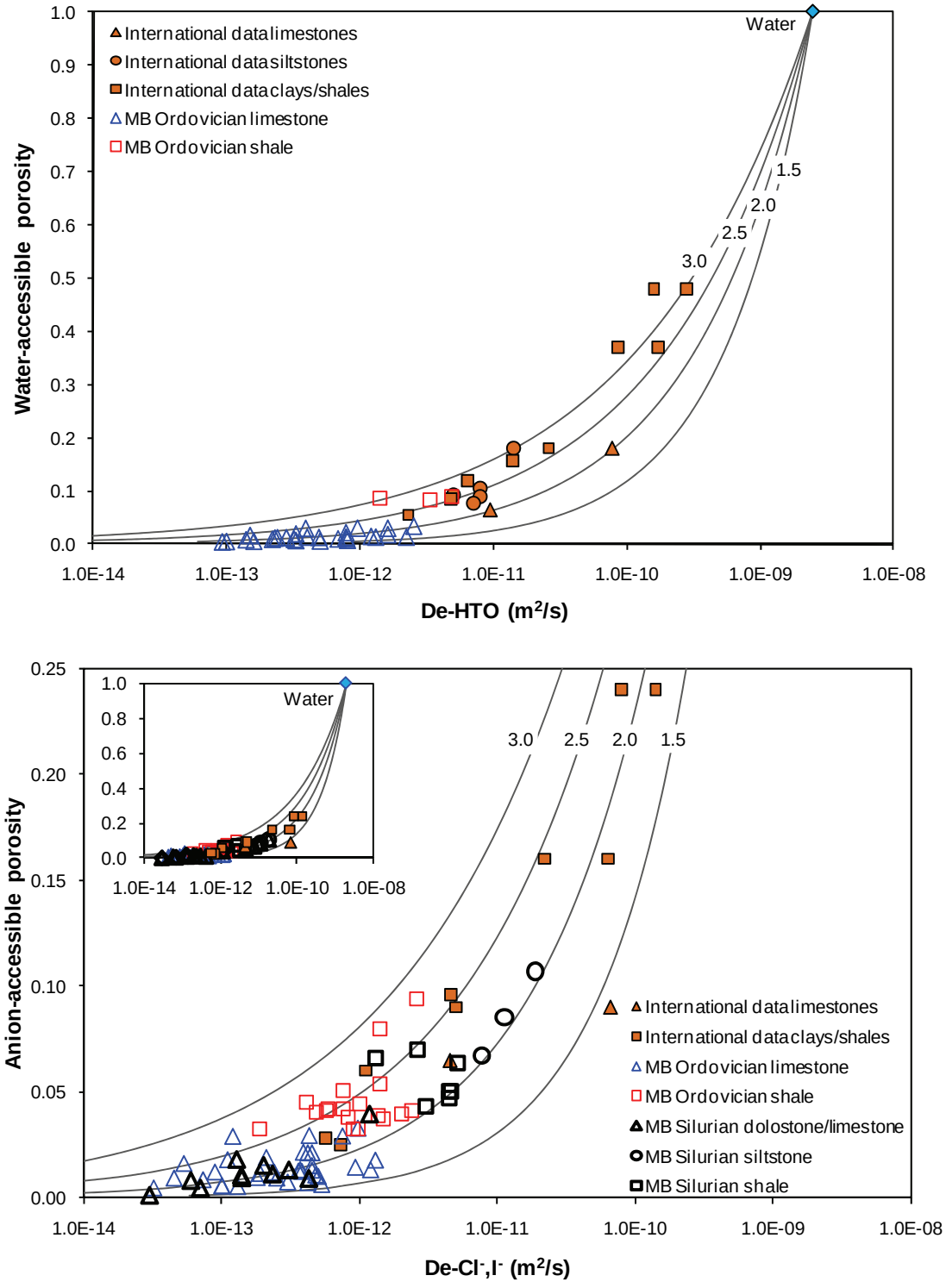

Note: The data represent diffusion coefficients normal to bedding. Plots include D0 for tracers in free water. Upper plot – water accessible porosity vs De from tritium tracers; lower plot – anion-accessible porosity versus De from chloride and/or iodide tracers

Figure 4.43: DGR Diffusion Data (Michigan Basin, MB) Compared with International Data from Geologic Repository Studies

Sampling was performed following interval purging and was completed using the Westbay MOSDAX system, which involved lowering stainless steel sample containers to the desired port to retrieve groundwater samples. The sample water was returned to surface where field parameters (electrical conductivity[EC], pH, Eh, and dissolved oxygen [DO]) were measured in a closed flow cell. After the measurements were conducted, sample water was conveyed into bottles for major ions, tritium, and deuterium and ^{18}O in water analyses.

4.5.1.1 Field Parameters and Major Ions

Colourimetric and potentiometric measurement of DO showed concentrations were below 2 mg/L, except for one measurement of 6.3 mg/L. The measured DO concentrations in groundwater were similar to the concentrations measured by Lee et al. (1995) in US-series boreholes. These low oxygen levels indicate dissolved oxygen is limited in the shallow groundwater. Iron staining in the Amherstburg and Bois Blanc formations however was likely due to ferric iron, or oxidized iron (Fe^{3+}), which is commonly associated with relatively oxidizing conditions. The presence of ferric iron suggests oxidizing conditions were present in isolated zones of the upper two hundred metres.

Ferrous iron, or reduced iron (Fe^{2+}), concentrations in US-series samples were between 0 and 1.3 mg/L. Where there was dissolved ferrous iron in the groundwater, the reduction-oxidation state may be classified as iron reducing. This classification is supported by the core logging, which noted pyrite in the DGR-1 core near the base of the Amherstburg Formation and inconsistently observed pyrite through the Bois Blanc and Bass Islands formations in all DGR boreholes (TR-07-06, TR-08-13). Although pyrite was identified in the core, sulphide was not detected in the groundwater samples.

The observed low oxygen and ferrous iron concentrations in the groundwater, combined with the iron and pyrite evidence in the cores, suggests oxygen is almost absent in the shallow groundwater, and the redox conditions are in a transition from near-anaerobic to iron reducing. The Eh results in US-3 and US-7 support a low-oxygen, or iron-reducing environment, which is also indicated by low dissolved oxygen readings (TR-08-08, TR-08-30). The Eh results in US-8 suggest oxidizing conditions are present down to approximately 70 mBGS, which is supported by dissolved oxygen readings in groundwater samples (TR-08-08, TR-08-30). Below 70 mBGS, Eh decreases and iron was detected colourimetrically in the field (TR-08-30), which is indicative of reducing conditions.

The concentration of total dissolved solids (TDS) in solution may be used to classify the salinity of water into four categories (pg. 84 in Freeze and Cherry 1979) as shown in Table 4.5.

Table 4.5: Classification of Groundwater Salinity

Water Category	Total Dissolved Solids (mg/L)
Fresh Water	0 – 1,000
Brackish Water	1,000 – 10,000
Saline Water	10,000 – 100,000
Brine Water	>100,000

The TDS of the groundwater samples from the US-series wells indicated groundwater in the Lucas and Amherstburg formations was fresh to brackish water, and groundwater from the Bois Blanc to the top of the Salina G Unit was brackish (up to 5,700 mg/L TDS). These TDS concentrations were relatively low compared to the deeper groundwater and porewater at the site (Sections 4.5 and 4.6).

Groundwater solute concentrations (mg/L) were converted to units of molarity (mol/L). Molar concentrations of the major ions were used to calculate molar ratios. In turn, the molar ratios were used to determine the dominant ions in the groundwater and to classify groundwaters.

Groundwater in the overburden aquifer was classified as a Ca:Na-HCO_3 type water (INTERA 2007). Below the overburden the groundwater chemistry transitions from the low TDS Ca:Na-HCO_3 type water to a brackish Ca-SO_4 water near 178 mBGS, and is a Ca-SO_4 water down to 193 mBGS. However, four sampling intervals between 150 and 178 mBGS were a Na-Cl type water. The concentration of each of the major ions is presented with depth for US-8 in Figure 4.44.

Only US-8 data are shown in these figures because it is the deepest of the three US-series boreholes, and to avoid presenting duplicate results. Concentrations are reported as molality (mmol/kg water) to remain consistent with the presentation of major ion concentrations for the deeper groundwater and porewater (see Section 4.6). Generally, groundwater solute concentrations in US-3 were greater than in US-7 and US-8, but the molar ratios were similar in each borehole and groundwater solute concentrations increased with depth in each borehole (TR-08-08, TR-08-30).

Groundwater alkalinity ranged from approximately 1 to 3 mmol/kgw as $CaCO_3$. The pH of the samples was commonly near 7.5, but was between 6.7 and 8.5. The distribution of carbonate species with pH indicates alkalinity was dominantly in the form of HCO_3 (pg. 51 in Drever 1988); assuming all of the alkalinity in the samples was derived from carbonate species, i.e., the alkalinity from silicate, boron, and organic carbon compounds was negligible.

The major ion concentrations and pH were input to PHREEQC (Parkhurst and Appelo 1999) to calculate the mineral saturation indices. Minerals were considered to be saturated if the calculated saturation index (SI) was equal to 0 ± 0.1. All PHREEQC calculations were carried out using the USGS Pitzer activity coefficient database for PHREEQC. Calcite was saturated in all of the groundwater samples except for one sample at depth of 93 mBGS in US-8. Calcite was also observed in core samples analyzed by XRD (TR-08-01, TR-08-22, TR-08-23). Gypsum and celestite were near saturation below 135 mBGS, consistent with the observation of the occasional presence of gypsum, anhydrite and celestite in the Bass Islands Formation by visual inspection and/or XRD analyses of the recovered core (Tables 3.6, 3.13 and 3.18).

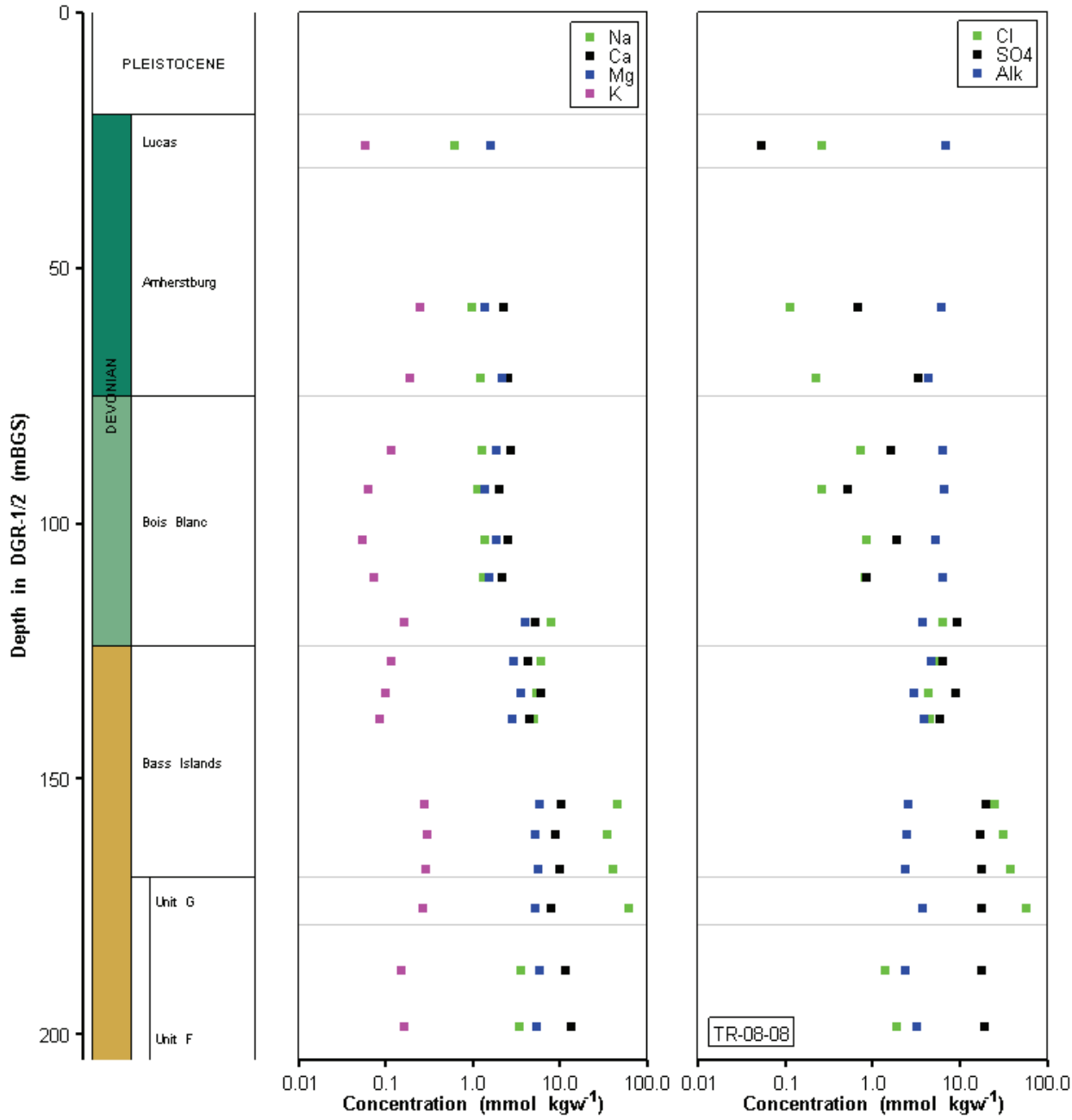

Figure 4.44: Major Ion Chemistry Profile of Shallow Bedrock Groundwater: Left Cations, Right Anions - US-8

4.5.1.2 Environmental Isotopes

The environmental isotope data, $\delta^{18}O$ and δD, for shallow bedrock groundwater collected from US-3, US-7, US-8 and DGR-2, as well as drill waters and Westbay casing installation waters are plotted in Figure 4.45 and compared to the Global Meteoric Water Line (GMWL). Figure 4.45

shows the shallow bedrock groundwater grouped by Middle-Lower Devonian dolostones (Lucas, Amherstburg and Bois Blanc formations) and Upper Silurian dolostones (Bass Islands and Salina G Unit). For comparison purposes, the groundwater samples collected from the Cambrian sandstone in DGR-2 are also shown. The stable hydrogen and oxygen isotope ratios (δD and δ^{18}O, respectively) are reported in the delta (δ) notation as the per mil (‰) deviation relative to the Vienna Standard Mean Ocean Water (VSMOW).

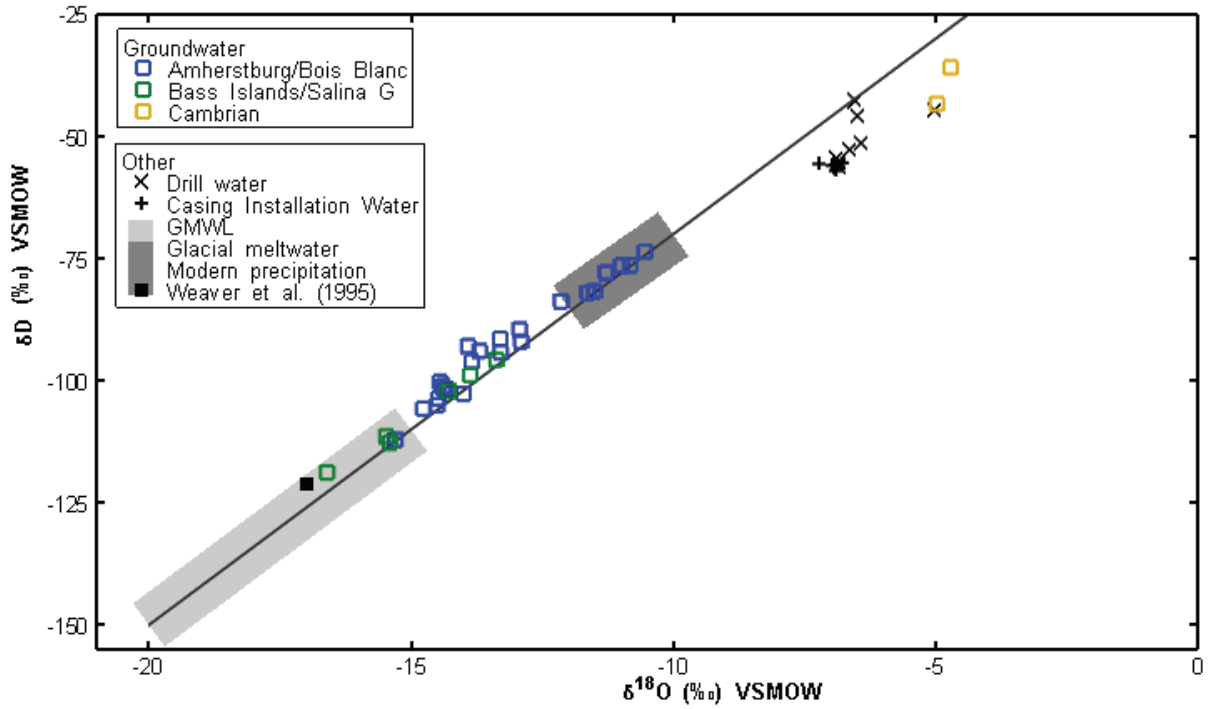

Note: Also shown is the range of modern precipitation (Fritz et al. 1987) and the range (Aravena et al. 1995) and best estimate (Weaver et al. 1995) of glacial meltwater for Southern Ontario.

Figure 4.45: Cross Plot of δD versus δ^{18}O for Drill Waters and Groundwater Samples from US-3, US-7, US-8, DGR-1 and DGR-2

Figure 4.45 shows that the Lake Huron water used for drilling and installing MP38 and MP55 casings has a characteristic evaporative enrichment signature and that the Cambrian groundwater is significantly enriched but plotting close to the GMWL. Both of these waters plot remotely from the Devonian and Upper Silurian dolostone groundwater, suggesting that the shallow bedrock groundwater is not influenced by drill water, casing installation water or Cambrian sandstone water.

Figure 4.45 shows that the deeper Upper Silurian dolostone groundwater is depleted relative to the Middle – Lower Devonian dolostone groundwater, suggestive of glacial meltwater presence in the deeper dolostone units (see Sections 4.5.2.3 and 4.6.6.1 for further discussion of this topic considering deeper opportunistic groundwater sample and porewater data, respectively).

4.5.1.3 Tritium

Groundwater from the US-series wells had < 35 tritium units (TU), but 14 out of 29 samples had tritium counts below the detection limit for direct counting analysis (6 TU) selected for initial analyses. Tritium in precipitation at the Bruce nuclear site is elevated and averaged 1800 TU during 2005-2007 (Bruce Power 2008). The $\delta^{18}O$ and δD ratios of the groundwater samples obtained from the Westbay samples above the Salina G Unit plot on or close to the GMWL, indicating the groundwater is of atmospheric origin (Figure 4.45). The low tritium counts in the groundwater samples suggest the groundwater does not contain recent atmospheric water that is affected by activities at the Bruce nuclear site. The Bruce nuclear site has been active since the late 1960's, which indicates the groundwater collected from US-3, US-7 and US-8 pre-dates the operation of the Bruce nuclear facility, or the groundwater recharged in an area not affected by the tritium emitted from the Bruce nuclear site.

Carbon-14 was also sampled from the shallow groundwater system. The results are presented and discussed in Section 4.7.1.

4.5.2 Intermediate and Deep Groundwater Chemistry - DGR Boreholes

Drilling of DGR-1, DGR-2, DGR-3 and DGR-4 provided opportunities to sample groundwater that flowed into the borehole at permeable intervals. These samples are referred to as opportunistic groundwater samples (OGW), although in DGR-3 and DGR-4 the sampled zones were targeted based on results of hydraulic testing of DGR-1 and DGR-2. This section characterizes the OGW samples from the four boreholes (TR-07-11, TR-08-18).

A total of seven OGW samples were obtained and analyzed in the course of drilling DGR-1 and DGR-2, as part of Phase 1. Permeable horizons were observed in the bedrock in the top 150 mBGS (Devonian and Silurian) and below 840 mBGS (Cambrian sandstone). Westbay installations in the US-series boreholes (TR-07-20) provide excellent coverage for the top 150 mBGS; therefore, the zones above 150 mBGS were not targeted for OGW sampling in Phase 2A.

Two additional permeable horizons were also identified by hydraulic testing in DGR-1 and DGR-2 that were not sampled in Phase 1. These horizons were 1) the top of Salina A1 Unit dolostone; and 2) the Guelph Formation dolostone. The permeable horizon in the Salina A1 Unit is referred to as the Salina Upper A1 Unit permeable zone. These two horizons as well as the Cambrian were sampled in both DGR-3 and DGR-4. There were a total of 13 OGW samples obtained in Phase 1 and Phase 2A. Opportunistic samples were collected and given identifiers as OGW-1 through OGW-13 (Table 4.6).

Once each permeable horizon was reached, drilling fluid was circulated in the hole and the drilling fluid was sampled when it returned to the surface. This sample is called the drill water return. The drill water return is a representative sample of the chemistry of the drilling fluid used to drill the sample horizon.

Table 4.6: Opportunistic Groundwater (OGW) Samples Used for Geochemical Interpretation

OGW #	OGW-3	OGW-6	OGW-7	OGW-8	OGW-9	OGW-10	OGW-11	OGW-12	OGW-13
Borehole & Sample No.	DGR1-111.22	DGR2-844.73	DGR2-852.70	DGR3-339.66	DGR3-389.99	DGR3-860.53	DGR4-327.08	DGR4-377.42	DGR4-848.50
Sampling Interval (mBGS)	107.81-114.63	841.96-847.50	843.70-860.70	337.80-341.51	386.61-393.36	851.89-869.17	324.83-329.33	373.66-381.18	840.01-856.98
Bedrock Formation	Bois Blanc	Cambrian	Cambrian	Salina Upper A1 Unit	Guelph	Cambrian	Salina Upper A1 Unit	Guelph	Cambrian

After the drill fluid was circulated, an inflatable packer was set above the top of the horizon to hydraulically isolate the permeable horizon. The drilling fluid and groundwater were then purged from the isolated permeable horizon by swabbing the drill rods. Swabbing deploys a rod-like device into the drill rods down to the top of the packer. The diameter of the rod is slightly less than the inside diameter of the drill rods. The rod is pulled to the surface as rapidly as possible, pulling drilling fluid and groundwater to the surface. OGW samples from the Cambrian formation (OGW-6, OGW-7, OGW-10 and OGW-13) were not purged. Artesian conditions in the Cambrian rocks purged the drill fluid from the borehole.

Field analyses of Na-Fluorescein (NaFl) tracer concentration and electrical conductivity (EC) of the purge water were used to estimate when the NaFl concentration was <3% of the drill water concentration and EC measurements were similar to the electrical conductivity of the previous swab samples. Once these criteria were met, the permeable horizon was sampled. Sampling was carried out by collecting fluid in the drill rods by one of three methods (TR-07-11 and TR-08-18). The first method used a submersible pump to bring the groundwater to surface was used when the water level in the drill rods was less than approximately 70 mBGS. The second method used Westbay sampling containers to retrieve water when the water level was too deep to pump the groundwater. The third method was to install a valve on the top of the drill rods to control the artesian groundwater flow from the Cambrian OGW samples. In all three cases, groundwater was discharge directly into flow cells (Figure 4.46).

In addition to NaFl concentrations, field measurements of pH, dissolved oxygen (DO), redox conditions (Eh) and EC were also made in flow cells as the OGW samples were obtained (Figure 4.46, Table 4.7).

Although NaFl and EC were used as the field indicators for drill fluid contamination, tritium is considered to be the final parameter for calculating the percent drill fluid contamination. Tritium is assumed not to be present in the formation waters; therefore, any tritium detected in the OGW samples is due to drill water contamination. The final percent drill water contamination was calculated by dividing the OGW sample tritium result (which is listed in Table 4.8) by the tritium in the first return water sample, and converting the result to a percentage.

Figure 4.46: Serially Connected Flow Cells with Electrodes Connected to Digital Voltmeters

Table 4.7: Field Geochemical Measurements for OGW Samples

Parameter	OGW-3	OGW-6	OGW-7	OGW-8	OGW-9	OGW-10	OGW-11	OGW-12	OGW-13
Formation/ Unit	Bois Blanc	Cam-brian	Cam-brian	Salina Upper A1	Guelph	Cam-brian	Salina Upper A1	Guelph	Cam-brian
% Drill Water Contamination	6%	<1%	<1%	3.1%	24%	0.2%	0.9%	0.3%	0%
pH	7.6	6.6	6.5	7.3	7.1	7.3	7.0	6.5	6.6
Eh (mV)	-48	165	166	-13	-165	-159	-98	-141.9	-123.4
DO (mg/L)	0.22	1.24	1.24	0.3	0.04	0.08	0.45	0.23	0
Ferrous Iron (mg/L)	1	>10	>10	>10	>10	>10	1	>10	>10
Sulphide (mg/L)	<0.5	<0.5	<0.5	5	<1	<1	4	<0.5	<0.5
Electrical Conductance (mS/cm)	1.76	200.4	130	52	236	197	51	228	226

Table 4.8: Major Ion and Environmental Isotope Chemistry Results for OGW Samples

Borehole	DRG-1	DGR-2		DGR-3			DGR-4		
Parameter	**OGW-3**	**OGW-6**	**OGW-7**	**OGW-8**	**OGW-9**	**OGW-10**	**OGW-11**	**OGW-12**	**OGW-13**
Formation/ Unit	Bois Blanc	Cam-brian	Cam-brian	Salina Upper A1	Guelph	Cam-brian	Salina Upper A1	Guelph	Cam-brian
General Parameters									
Calculated TDS (mg/L)	2156	238000	247800	26760	365604	224518	30455	375468	227001
Fluid Density (kg/m^3)	1008	1160	1170	1019	1258	1150	1017	1210	1150
Environmental Isotopes									
Tritium (TU)	8.1	4.3	2.5	9.4	133.1	1.6	2.3	5.2	<1
δD (‰)	-92.9	-43.3	-35.8	-104.3	-48.1	-31.7	-102.7	-50.0	-35.2
$\delta^{18}O$ (‰)	-13.91	-4.97	-4.71	-14.4	-2.3	-4.8	-14.5	-2.7	-5.2
Major Anions (mmol/kgw)									
Cl	0.58	4589	4790	388	7115	4453	462	7761	4584
Br	0.04	19.0	19.9	0.4	26.8	21.7	0.37	25.7	20.3
SO_4	15.7	5.6	4.1	37.5	0.0	3.9	39.9	2.6	4.5
Alkalinity as $CaCO_3$	2.2	0.35	0.36	3.6	1.8	0.90	4.8	0.71	0.82
Major Cations (mmol/kgw)									
Na	2.0	1817	1648	344	4482	1523	374	5168	1494
Ca	10.5	1080	1112	25.3	946	977	29.1	945	970
Mg	4.3	295	280	24.1	376	262	25.8	390	255
K	0.13	24.2	21.3	3.2	112	25.4	3.2	112	26.0
Sr	0.12	7.6	10.4	0.20	6.8	10.0	0.20	5.6	8.5
Charge Balance (%)	-3	-4	-10	-2	+1	-5	-6	+1	-7

The Phase 1 OGW samples were OGW-1 through OGW-7. High pH measurements for OGW-1 and OGW-2 (9.8 and 8.8 pH units respectively) indicated the sample water was affected by the casing cementing, and the geochemical results were not fit for interpretation. OGW-4 contained approximately 18% drill water and OGW-5 was almost 100% drill water, therefore, the OGW-4 and OGW-5 samples were not fit for interpretation. The tritium results confirmed the field-calculated drill water contamination results. Only OGW-3, OGW-6 and OGW-7 were deemed fit for interpretation, and the results for the other Phase 1 OGW samples are not shown.

The Phase 2A OGW samples were OGW-8 through OGW-13. The tritium calculations show OGW-9 had 24% drill water contamination, which is significantly higher than the 0.2% drill water

contamination shown using the NaFl concentrations. Despite the significant drill water contamination in OGW-9, corrections for drill water contamination applied to the OGW-9 sample data produced comparable results to the OGW-12 results (DGR-4 Guelph Formation sample), except for Na and Cl. The similarity of the OGW-9 and OGW-12 results increased the confidence in the OGW-9 results, however, the OGW-9 results should be interpreted with caution. All of the Phase 2A samples were deemed fit for interpretation.

4.5.2.1 Field Parameters, Major Ions and Trace Elements

Small amounts of DO in the OGW samples was likely due to swabbing and possibly due to oxygen diffusing through the tubing associated sampling. Field measurements of ferrous iron and sulphide are also listed in Table 4.7. Sulphide was detected in only the Salina Upper A1 Unit samples (OGW-8 and OGW-11). Dissolved iron in the filtered samples (Table 4.7) suggests ferrous iron was present, since ferric iron has a low solubility at near neutral pH ($K = 10^{-38.3}$, Appelo and Postma 1996, p. 253). The presence of reduced iron is considered to be a more appropriate indicator of redox conditions considering values obtained from Eh electrodes reflect mixed potentials (Stumm and Morgan 1981, pp. 490-493). Pyrite was detected, both visually and through lithogeochemical analyses (Section 3.7.2), at numerous depths throughout the Paleozoic formations. Pyrite provides mineralogical support for the ferrous iron observed in the OGW samples. The solubility constant for iron sulphide minerals is low (solubility product for FeS is $10^{-17.7}$, Appelo and Postma, 1996, pg. 287), which suggests water samples should have either iron or sulphide, not both. The presence of both ferrous iron and sulphide in the OGW-8 sample suggests particulate iron sulphide dissolved during both the iron and sulphide analyses.

Electrical conductivity (EC) is a function of the total dissolved solids in water. The EC results from OGW-3 (1.8 mS/cm) suggest the water was relatively fresh, whereas groundwater from the other permeable horizons was relatively saline. The EC in the Guelph Formation samples (OGW-9 and OGW-12) was the highest measured at the site, which is consistent with the calculated total dissolved solids concentration in the Guelph Formation water samples (Table 4.8).

Table 4.8 provides the results of laboratory analyses of the OGW samples. The Bois Blanc (OGW-3) sample water was characterized by Ca-SO_4 water, which has more sulphate than the samples near this depth obtained from US-8 (Figure 4.44). Section 4.5.1.1 identified the top of the bedrock to near 150 mBGS as a transition from a Ca:Na-HCO_3 type water to a Ca-SO_4 water. The difference between the US-8 results and OGW-3 results suggests the transition between the chemistries may have some small spatial variation. The Salina Upper A1 Unit (OGW-8 and OGW-11) sample water was a Na-Cl type water, the Guelph (OGW-9 and OGW-12) samples were a Na-Cl type water, and the Cambrian groundwater (OGW-6, OGW-7, OGW-10 and OGW-13) was Na:Ca-Cl water. Deep groundwater and porewater (see Section 4.6.5) ion concentrations were dominated by Na, Ca and Cl. K, Mg, sulphate and alkalinity (representative of carbonate species) concentrations were orders of magnitude less than Na, Ca and Cl. Additionally, porewater carbonate species were not directly determined. Piper diagrams, or other diagrams illustrating concentration ratios, were not produced as they would only illustrate the dominance of Na and Ca which is adequately described above.

The pH values for the OGW samples were measured in the flow cells to be 7.6, 6.6 and 6.5 for OGW-3, OGW-6 and OGW-7, respectively (Table 4.7). The measured pH may be higher than the actual pH since the OGW samples were effervescing at surface, likely due to the decrease in pressure as the fluid arrived at surface. Although the effervescing gas was not measured, it

was believed to be CO_2. Losing CO_2 to the atmosphere would raise the measured pH of the fluid. Despite the possible overestimation of pH, the range of pH values suggests that the carbonate content of the groundwater samples consists primarily of carbonic acid (H_2CO_3) and bicarbonate (HCO_3^-). Assuming all of the alkalinity in the samples was derived from carbonate species (i.e., alkalinity from silicate, boron, and organic carbon compounds was negligible), alkalinity in the groundwater samples was due to HCO_3^-.

The major ion concentrations for the two Salina Upper A1 Unit OGW samples (OGW-8 and OGW-11) are within 8% of each other, except for calcium and chloride, which are approximately 13 and 16% different, respectively (Table 4.8). The water isotopes showed small differences between OGW-8 and OGW-11.

The concentration differences between the Guelph Formation samples (OGW-9 and OGW-12) were less than 7% for the major ions, except for Na and Cl. The calculated groundwater sulphate concentration was zero for the OGW-9 sample, which is not likely true. The calculated sulphate concentration was likely affected by the drill water contamination (24%) and errors associated with analyzing the low sulphate concentration.

The difference between the $\delta^{18}O$ results in the OGW-9 and OGW-12 samples was near 0.5‰ and the δD values were offset by less than 2‰. The similarity between the major ions (except for sulphate) and the environmental isotopes between OGW-9 and OGW-12 suggests the correction factor to account for the high drill water contamination in OGW-9 was appropriate.

Small differences were calculated between the Cambrian samples OGW-10 and OGW-13 with the differences between the majority of solutes being below 4%. The $\delta^{18}O$ results differed by 0.4‰ and the δD by 3.4‰. The only OGW samples that were obtained from similar stratigraphic zones between the Phase 1 and Phase 2A boreholes were the Cambrian samples. Comparison of OGW-6 (Cambrian groundwater sample from DGR-2, TR-07-11) and OGW-13 (DGR-4, TR-08-18) shows between 0 and 18% difference between major ions. The chloride concentrations had a 0% difference, calcium was 10% greater in OGW-6 and sodium was 18% greater in OGW-6. Also, the difference in $\delta^{18}O$ was only 0.2‰ and the difference in δD was also small, 8.1‰.

The small differences between the isotope values from each borehole suggest the correction factors applied to the OGW samples were appropriate. Assuming the correction factors were appropriate, the environmental isotopes are similar between OGW samples at equivalent horizons in each borehole.

The data shown in Table 4.8 were input into PHREEQC (Parkhurst and Appelo 1999) to calculate mineral saturation indices (Table 4.9). All PHREEQC calculations were carried out using the USGS Pitzer activity coefficient database for PHREEQC. The sulphate concentration for OGW-9 was input as 1 mmol/kgw. The effect of analytical errors on the calculated SI values was examined by increasing the groundwater concentrations and decreasing the concentrations by 20% for each of the OGW samples and recalculating the saturation indices in PHREEQC. Changing all concentrations by 20% altered the charge balance for each of the samples, but the objective of this arbitrary concentration change was to examine the potential effect of 20% error in laboratory analyses on the interpretation of mineral saturation (Table 4.9).

The calculated SI values showed calcite and dolomite were saturated in all of the samples. Gypsum was saturated or near saturation (i.e., SI = 0 ±0.1) for all samples except for OGW-3 and OGW-9. The results from Table 4.9 show a 20% increase in the sulphate concentration of OGW-9, or 0.2 mm/kgw, raises the SI to -0.1. This basic comparison shows only a small error

in estimating the sulphate concentration in the Guelph Formation brine may lead to an erroneous conclusion regarding the sulphate chemistry, due to the small sulphate concentrations. The high TDS of the water in the Guelph Formation permeable horizon and the saturated gypsum result for OGW-11 (Table 4.9) suggests the water in the Guelph Formation is saturated with respect to gypsum. XRD results showed calcite and dolomite were in almost all rock samples (TR-08-01, TR-08-22, TR-08-23 and Table 3.6) Celestite was calculated to be at equilibrium or near equilibrium in all samples except OGW-9 (Table 4.9) in accordance with the mineralogical analyses showing celestite was occasionally observed throughout the Paleozoic bedrock sequence at the Bruce DGR site (Tables 3.13, 3.18). Halite was calculated to be supersaturated in the Guelph samples consistent with Table 3.13 and Figure 3.54 observations.

Table 4.9: Calculated Saturation Index Results for OGW Samples

OGW	pH	Calcite	Dolomite	Gypsum	Celestite	Halite
3	7.6	0.5 (0.6, 0.3)	0.9 (1.1, 0.6)	-0.2 (-0.1, -0.3)	0.0 (0.04, -0.16)	-7.7 (-7.5, -7.8)
6	6.6	0.4 (0.8, 0.1)	0.8 (1.6, 0.1)	0.4 (0.7, 0.1)	0.4 (0.8, 0.1)	-0.4 (0.1 -0.7)
7	6.5	0.4 (0.9, 0.1)	0.8 (1.7, 0.1)	0.3 (0.7, 0.03)	0.5 (0.9, 0.2)	-0.3 (0.1, -0.7)
8	7.3	0.4 (0.6,0.3)	1.2 (1.4, 0.9)	-0.1 (0.0, -0.2)	-0.1 (0.0, -0.2)	-2.8 (-2.6, -2.9)
9	7.1	1.9 (2.0,1.8)	4.0 (4.1,3.7)	-0.4 (-0.1,-0.7)	-0.3 (0.0,-0.7)	0.2 (0.5,-0.1)
10	7.3	1.6 (1.7, 1.5)	3.1 (3.4, 2.7)	0.0 (0.2, -0.2)	0.1 (0.3, -0.1)	-0.8 (-0.5, -1.0)
11	7.0	0.3 (0.5, 0.2)	0.9 (1.2, 0.6)	0.0 (0.1, -0.1)	-0.1 (0.0, -0.2)	-2.7 (-2.5, -2.8)
12	6.5	1.4 (1.5, 1.2)	3.0 (3.2, 2.6)	0.1 (0.4, -0.2)	0.1 (0.5, -0.2-)	0.4 (0.7, 0.1)
13	6.6	1.4 (1.6, 1.1)	2.6 (3.1, 2.0)	0.0 (0.3, -0.1)	0.1 (0.3, -0.1)	-0.8 (-0.5, -1.0)

The relatively large range of concentrations (±20%) that was applied to the sample results to examine the potential impact of analytical error on geochemical interpretation showed large potential analytical errors had a small impact on the interpretation of the OGW results. For example, calcite and dolomite were consistently calculated to be supersaturated. The high supersaturation for the carbonate minerals may be due to erroneously high pH values due to CO_2 degassing while sampling. The low sulphate concentrations should be considered when examining the SI results for any sulphate mineral. In the case of OGW-9, a 20% analytical error for sulphate is equivalent to 0.2 mm/kgw, and can impact the interpretation of gypsum saturation.

4.5.2.2 Evaporated Sea Water and OGW Chemistries

The potential for deep groundwater at the Bruce nuclear site to develop from sea water evaporation was investigated using the DGR-4 OGW results (OGW-11, OGW-12 and OGW-13). The DGR-4 samples were selected because of the negligible amount of drill water contamination in the samples (Table 4.7 and TR-08-18). Selecting samples with minimal drill water contamination minimizes the amount of uncertainty in the interpretation of the results of this analysis due to drill water contamination corrections.

The investigation was carried out using the geochemical modeling software PHREEQC. The objective of this modeling exercise was to use sea water evaporation, and dilution for OGW-11, as a diagnostic tool to examine the likelihood that deep groundwater at the Bruce nuclear site could be from sea water evaporation/dilution.

This modeling exercise is not meant to be a comprehensive examination of all of the potential reactions that occurred over the long time period. This exercise is meant to qualitatively determine if sea water evaporation/dilution alone can explain the present-day deep groundwater chemistry. The long time period from the deposition of the rock formations at the Bruce nuclear site to the present leaves an opportunity for many geochemical reactions to occur. Time constraints were not used in this model. This simple model is only intended to see if sea water evaporation (or dilution) and mineral precipitation can create the observed OGW chemistries. Also, this analysis does not account for ion transport or groundwater mixing, and temperature was assumed to be 25°C.

The sea water composition for the OGW samples in the Silurian formations (OGW-11 and OGW-12) was obtained from Lowenstein and Timofeeff (2008). The sea water composition for the Late Silurian was estimated from fluid inclusions extracted from Silurian sediments from the Michigan, Illinois, and Appalachian basins. Lowenstein et al. (2001) and Petrychenko et al. (2005) suggest the major ion ratios were generally similar in the Cambrian compared to the Ordovician and the Silurian. Therefore, the Silurian seawater chemistry was also used to examine the role of sea water evaporation on the evolution of the groundwater in the Cambrian.

The Pitzer database was used for the geochemical modeling due to the high ionic strengths of the water. The strategy for the modeling was to evaporate sea water in PHREEQC by removing water through the Reaction command until the calculated sea water chloride concentration was equal to the OGW chloride concentration. When the calculated gypsum saturation index reached the saturation index listed in Table 4.9, gypsum was fixed at the saturation index values listed in Table 4.9. Similarly, when the calculated halite saturation index reached the value listed in Table 4.9 for OGW-12, the halite saturation index was fixed at 1.0. Ion substitutions were not accounted for in this exercise, for example, strontium was not allowed to precipitate into gypsum.

The Salina Upper A1 Unit sample (OGW-11) had lower concentrations than sea water. Freshwater was added to the sea water until the chloride concentration of the calculated sea water was the same as OGW-11 (Table 4.10). The percent differences were calculated as the difference between the OGW concentration and the evaporated sea water concentration multiplied by 100 and divided by the OGW concentration. Positive percent difference values indicate the OGW concentration is greater than the calculated sea water concentration. For this analysis, concentration differences within 100% difference are considered to be similar given the time- scale for sea water evaporation and the number of geochemical and transport processes that may have affected the current OGW concentration.

Sea water was diluted by approximately 30% to lower the calculated sea water chloride concentration to the OGW-11 chloride concentration. The major ion results of the diluted sea water were similar to the OGW-11 results. This similarity suggests seawater dilution likely played a significant role in the evolution of the groundwater chemistry in the Salina Upper A1 Unit permeable zone. However, this does not preclude the role of other geochemical processes (e.g., dolomitization) on the geochemical evolution of the groundwater.

The calculated sea water was concentrated 12 times in order to match the chloride concentrations in the Guelph permeable horizon (OGW-12). Gypsum and halite were allowed to precipitate from the calculated seawater. The calculated K, Mg, and SO_4 results were greater than 100% different from the OGW-12 results. These large differences suggest other geochemical processes play a significant role in the evolution of the groundwater geochemistry at the site. However, the high concentrations in the groundwater suggest evaporation or

dissolution of soluble minerals played a significant role in the evolution of the groundwater chemistry.

The calculated sea water was concentrated 8.6 times in order to match the chloride concentration to the chloride concentration of the Cambrian groundwater (OGW-13). Only gypsum was allowed to precipitate. The large percent differences between the calculated seawater and the OGW-13 concentrations for all of the ions except for Ca suggest other processes besides seawater evaporation played a significant role in the evolution of the groundwater chemistry.

Table 4.10: Comparison of OGW Samples to Calculated Evaporated Sea Water Results (mmol/kgw)

Water Source		Na	K	Ca	Mg	Cl	SO_4
Sea Water		420	11	33	45	565	10
Salina Upper A1	OGW-11	344	3.0	25.4	23.6	442.2	35.9
	Calculated	328	8	25	35	442	7.8
	% Diff.	5	-186	-1	-49	0	78
Guelph	OGW-12	5107	111	933	334	7671	2.6
	Calculated	1502	429	982	1907	7648	7.4
	% Diff.	71	-286	-5	-470	0	-185
Cambrian	OGW-13	1494	26.0	970	254	4584	4.5
	Calculated	3407	89	204	365	4583	17.5
	% Diff.	-128	-242	79	-43	0	-288

4.5.2.3 Environmental Isotopes

The $\delta^{18}O$ and δD data for the opportunistic groundwater samples and the US well samples are shown on a cross plot of $\delta^{18}O$ vs δD (see Figure 4.47). Also shown for comparison purposes are the selected data for US and DGR well drill water obtained from Lake Huron that show a conventional evaporation signature.

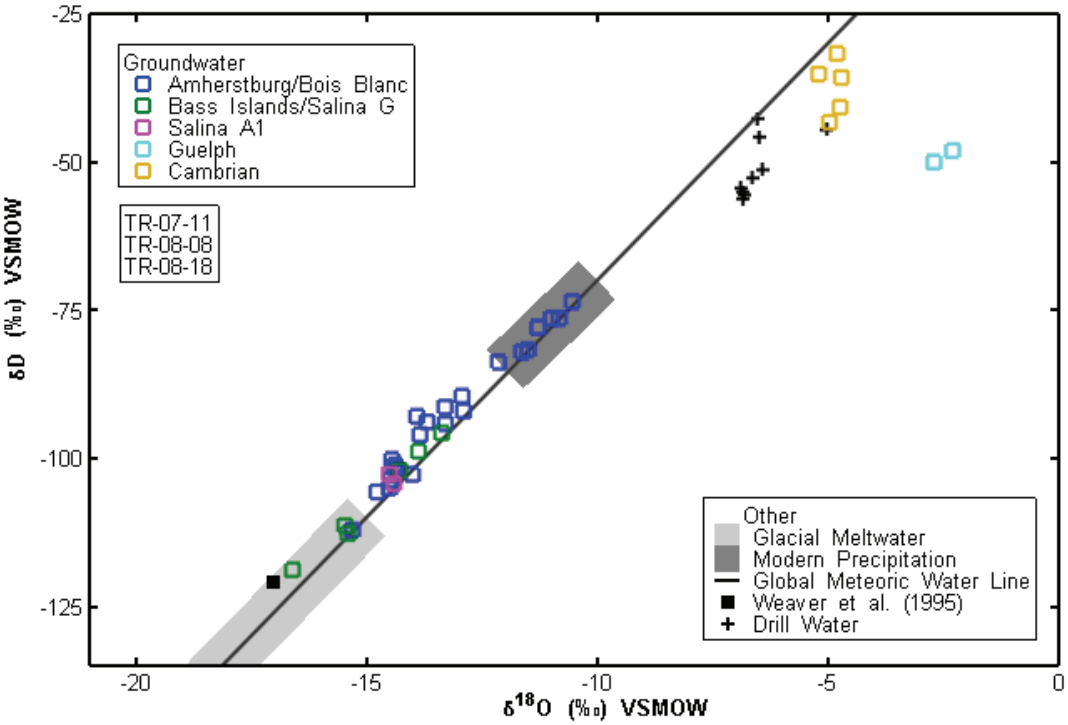

Figure 4.47: Cross Plot of δ^2H versus $\delta^{18}O$ for Groundwater from US-Series Wells and All OGW Samples from DGR Boreholes

A strictly modern groundwater would have a well-mixed mean-annual isotope composition rather than the observed range of values. The depleted values attributed here to glacial recharge are within the range suggested by Aravena et al. (1995) for southern Ontario, and are more depleted than the groundwater observed in the Alliston aquifer of Southern Ontario, to which Aravena et al. attribute a glacial meltwater component.

On their own, the OGW samples provide data for adequate interpretation of the flowing groundwater at each depth. However, more in depth interpretation of the groundwater chemistry at the site is augmented by examining the OGW and porewater chemistry together, which is performed in Section 4.6.

4.6 Porewater Characterization

4.6.1 Overview

Porewater characterization studies were undertaken by the University of Ottawa (TR-07-21, TR-08-19, TR-08-37, TR-08-38, TR-09-04), the University of Bern (TR-08-06, TR-08-40) and the University of New Brunswick (TR-07-17, TR-08-27). The presentation and discussion of porewater characterization given in this section, focuses primarily on University of Ottawa and University of New Brunswick data, as these data are the most complete sets of data. Porewater data generated by the University of Bern considered here include major and minor ions of Cl, Br, Na and Ca from boreholes DGR-2, DGR-3 and DGR-4.

Porewater chemistry was characterized using the crush and leach technique. Porewater was extracted from crushed DGR cores at the University of Ottawa by high-temperature vacuum distillation (150°C) for water isotopes. This was followed by deionized water leaching of the same crushed (2-4 mm grain size) rock samples to recover dissolvable salts (TR-07-21, DGR-1 and DGR-2; TR-08-19, DGR-3 and DGR-4; TR-09-04 , DGR-5 and DGR-6). For DGR-1 through DGR-4 cores, water leaching was performed by University of Ottawa in an open aerobic environment. For DGR-5 and DGR-6 cores, water leaching was completed by the University of Ottawa in an anaerobic chamber to minimize sulphide oxidation and generation of sulphate. The ion concentrations were calculated by dividing the mass of salts in the leachate solutions by the mass of water collected during the heating to produce values as mass of ions per kg H_2O.

The porewater data from the Universities of New Brunswick (TR-07-17, TR-08-27) and Bern (TR-08-06) were determined from crush and deionized water leach experiments with four solid:liquid weight ratios of 0.1. 0.25, 0.5 and 1.0. Subsequent porewater characterization completed by the University of Bern (TR-08-40) utilized only a 1:1 solid:liquid weight ratio and reduced leaching times from 48 hours to 10 minutes to minimize mineral dissolution. The ion concentrations were calculated by dividing the mass of salts leached by the mass of water collected from drying a subsample of the same rock core. The calculated ion concentrations are assumed to be representative of the porewater chemistries. However, the crush and leach technique does not directly measure the porewater ion concentrations and does not account for sample oxidation, mineral dissolution or the influence of clay on the porewater chemistry, which may affect the representativeness of the calculated porewater chemistries.

Some of the measured geochemical parameters, such as Cl and Br, and the stable isotopes of water ($\delta^{18}O$ and δD), are 'natural tracers' that may be used to constrain the hydrogeological and geochemical properties of the geological materials from which they are extracted (e.g., Desaulniers et al. 1981, Remenda et al. 1996, Hendry et al. 2000, Hendry et al. 2005, Boisson et al. 2001, Rübel et al. 2002, Gimmi et al. 2007). When plotted versus depth, the solutes, gases and isotopes provide information concerning paleo-hydrological and geochemical conditions within the rock column and allow inferences to be made concerning the validity of the assumed favourable site characteristics outlined in the Geoscientific Site Characterization Plan (INTERA 2006, INTERA 2008).

Estimations of major ion concentrations in the porewater using leaching techniques are susceptible to artefacts from the dissolution of naturally occurring soluble salts such as halite, anhydrite, gypsum and possibly carbonate minerals. Measured cation exchange capacities were between 2 and 40 meq/kg rock (TR-08-06), which is relatively low compared to the porewater concentrations (see Section 4.6.5). Cation exchange may affect relatively low porewater concentrations, <500 meq/kg.

The first task in estimating porewater chemistries was to correct the major ion analyses for these contributions from evaporite mineral dissolution during the crush and leach procedures. This is addressed in Section 4.6.2 by conditioning the raw porewater extraction data using PHREEQC to correct for mineral dissolution.

Porewater chloride is of particular concern because it is generally very mobile, although it can be precipitated as halite (NaCl) salt. The presence of halite within a formation or group of formations is a strong indicator that there has been no flow of fresh water through that rock sequence since the halite was precipitated. In their Regional Hydrogeochemical Synthesis, (Hobbs et al. (2011b) concluded that the Ordovician geochemistry indicated that the porewater brines had evolved from seawater by evaporation. Halite is commonly observed in the

Ordovician shales and several other formations in the DGR Paleozoic sequence by both SEM/EDS and XRD methods of identification (see Section 3.7.1.2); therefore the second task, described in Section 4.6.3, was to resolve why the extracted porewater was undersaturated with respect to halite when halite was present in rock cores (see Table 3.6).

The body of hydrogeochemical data given in this Section presents the results of major and minor ion analyses from the Universities of Ottawa, Bern and New Brunswick, and environmental isotope and gas analyses from the University of Ottawa. These data are described in the following sections:

- Section 4.6.5: the major-ion analytes from high-temperature vacuum distillation and crush leach testing;
- Section 4.6.6: the environmental isotopes of water ($\delta^{18}O$ and δD) and of strontium ($^{87}Sr/^{86}Sr$);
- Section 4.6.7: the major dissolved gases – CO_2 and CH_4;
- Section 4.6.8: the estimation of porewater pH and the redox potential; and
- Section 4.6.9: the distribution of helium gas isotopes.

Available data on porewater and groundwater radioisotopes (^{14}C, ^{36}Cl and ^{129}I) are discussed in Section 4.7.

4.6.2 Correction of Major Ion Concentrations for Potential Mineral Dissolution During Analyses

The porewater extraction results for the major ions were interpreted using PHREEQC to calculate mineral saturation indices for the principal evaporite minerals, i.e., gypsum, anhydrite, celestite and halite. Mineral saturation calculations showed that all of the porewater samples are saturated with respect to anhydrite and celestite ($SrSO_4$). Super saturation was likely a result of dissolution of sulphate minerals during the crush and leach extraction (TR-07-21 and TR-08-19). Also, the porewater was assumed to be saturated with respect to calcite due to the high carbonate content of the bedrock at the Bruce nuclear site.

To correct for mineral dissolution during porewater extraction, the porewater concentrations from each sample were adjusted to equilibrium with anhydrite and calcite using the Equilibrium Phases command within PHREEQC. The anhydrite and calcite equilibrium correction decreased the calcium and sulphate concentrations from the initial porewater results. Forcing calcite to equilibrium requires estimating alkalinity concentrations, which were calculated by satisfying the porewater charge balance and which are not considered to be representative of the true porewater alkalinities. The porewater pH was not directly measured, and was not input into PHREEQC. Porewater pH was estimated for DGR-2 samples and is described in Section 4.6.8.

Celestite was not forced to equilibrium due to the relatively low concentrations of strontium compared to other ions. Small analytical errors may account for the positive celestite saturation indices. Further discussion of porewater concentrations in subsequent sections refers to these anhydrite/calcite “corrected porewater concentrations”.

4.6.3 Apparent Porewater Halite Undersaturation in Halite-Containing Shales

Halite was also observed in small amounts in rock core samples in the Ordovician shales in DGR boreholes by SEM/EDS and XRD analytical techniques (Section 3.7.1.2, Table 3.6).

However, the calculated porewater halite saturation indices in the Ordovician shales were generally below saturation.

A porewater extraction experiment (TR-08-37) was designed to examine the apparent halite undersaturation in the Ordovician shale porewater. Rock core samples from adjacent carbonate (limestone) interbed and shale beds within the Georgian Bay Formation in DGR-4 were analyzed to examine the differences between water isotope results in the carbonate and shale beds in the Ordovician shales, which were noted when interpreting data from Phase 1 site characterization work. Porewater Na and Cl concentrations were also analyzed as part of this experiment, which is described in TR-08-37.

The adjacent rock core samples consisted of three samples from the shale beds from DGR4-550.32, DGR4-550.75 and DGR4-550.95, as well as one sample from a limestone interbed at DGR4-550.54. The results (blue and orange circles in Figure 4.48) show the porewater concentrations of sodium and chloride in the shale samples were less than the concentrations in the carbonate interbed. The small difference in depth between these samples (<1 m depth) suggests diffusion should have created similar concentrations over time.

The Na and Cl concentrations were interpreted using PHREEQC with the Pitzer database to determine if the porewaters were saturated with respect to halite. The porewater in the carbonate bed was saturated with respect to halite while the shale porewaters were below halite saturation. The PHREEQC calculations showed an increase in the Na and Cl concentrations in the shale samples by 15% (green and red data points in Figure 4.48) resulted in halite-saturated porewater in the shales and a more uniform chloride concentration. This 15% difference raises the question as to why the porewater Na and Cl concentration results from the Ordovician shales are 15% lower than halite saturation compared to adjacent carbonate bed/unit Na and Cl concentrations?

Visual inspection of the saturation indices from the anhydrite/calcite correction for all porewater samples from the Ordovician shales in DGR boreholes shows all porewater results are undersaturated with respect to halite, except for two Georgian Bay samples (DGR3-539.46 and DGR6-659.17) and the one carbonate bed sample from the Georgian Bay Formation that was discussed above (DGR4-550.54). However, halite was observed in core samples from the Ordovician shales in DGR boreholes by SEM/EDS and XRD analytical techniques (Section 3.7.1.2, Table 3.6). An example of halite saturation in the Blue Mountain formation is shown in Figure 4.49. Assuming the halite is in contact with the porewater, the porewater sodium and chloride concentrations are below what is expected for porewater in equilibrium with halite for the Ordovician shales.

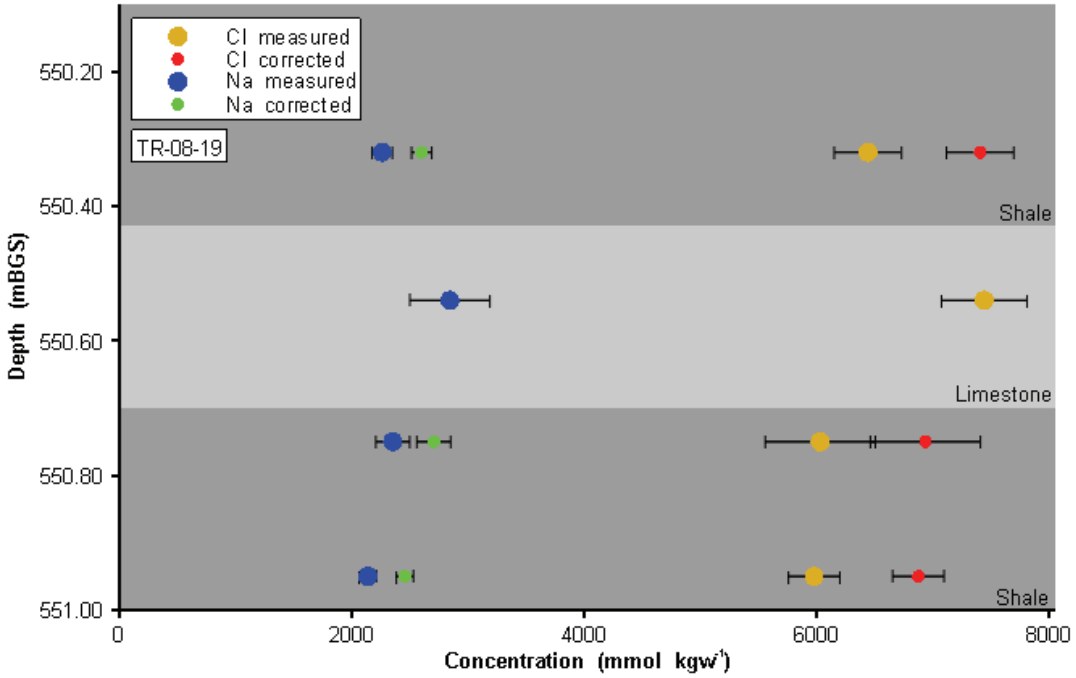

Figure 4.48: Chloride and Sodium Concentrations in Adjacent Shale and Limestone Beds in the Georgian Bay Formation in DGR-4

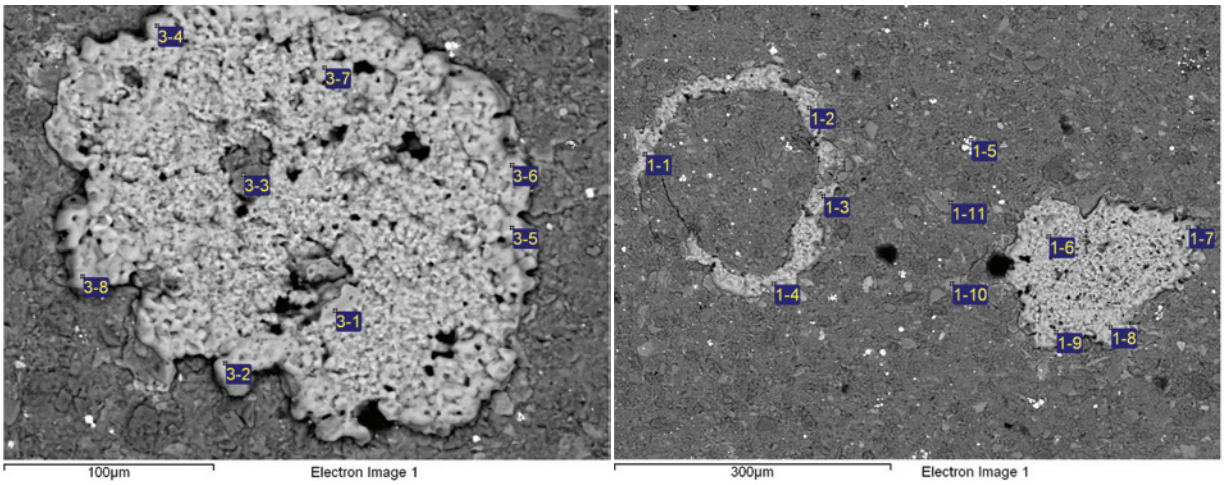

Note: The light grey areas are halite and black areas are pores. All spot analyses, except 1-6, 1-11, and 3-3, indicate halite.

Figure 4.49: SEM Photomicrograph of DGR3-628.54 Core – Blue Mountain Formation Showing Halite Presence as Rimming of Minerals and Interstitial to the Matrix

Porewater concentrations were increased in PHREEQC using the Reaction command by which water was “evaporated” from each porewater result from the shales until halite reached

saturation (log saturation index for halite = 0.0 ± 0.01). This process increased all of the porewater concentrations while keeping anhydrite and calcite at saturation indices of 0.0.

The difference between the "evaporated" porewater concentrations and the original concentrations is an indication of the amount of Na and Cl that would have to be added to the porewater (on a molal basis) in order to reach halite saturation (Figure 4.50). Also shown in Figure 4.50 is the percent increase in Na and Cl concentrations, which provides a relative comparison of the solute addition.

The results show Ordovician shale porewater in DGR-2 and DGR-3 required between an additional 8 to 38%, with an average of 17%, increase in Na and Cl to reach halite saturation. The DGR-4 samples required between 23 and 48% more Na and Cl (average of 33%) to reach halite saturation. The average increase in Na+Cl concentration from all of the boreholes was 20%, which is similar to the 15% concentration increase required to maintain a uniform porewater concentration between shales and a carbonate bed in the Georgian Bay Formation as shown above.

Lower porewater concentrations may be caused by underestimating the amount of solute in the rock core samples, over estimating the amount of water in the samples, or both. Each of the laboratories examined solute leaching in the course of completing the crush and leach process to determine porewater concentrations (TR-07-21, TR-08-06, TR-08-19, TR-08-40, TR-09-04). The amount of water used in the leach processes was significantly more than the amount of porewater in each rock core sample. Separate water/rock ratios were used to examine the potential for mineral dissolution and incomplete solute extraction. Additionally, solute leaching conducted by the University of Ottawa was carried out over 60 days, suggesting there was sufficient time to leach solute from the rock core samples.

The leach process likely dissolves some soluble and sparingly soluble minerals in the rock core samples, potentially leading to an overestimation of solute concentrations. For example, mineral saturation index calculations and the rock core petrography indicate high Ca, Sr, and SO_4 concentrations are due to dissolution of sulphate minerals. Even trace amounts of halite observed in the rock core samples (Table 3.6) should slightly overestimate the amount of Na and Cl in the porewater. Therefore, low porewater concentrations are not likely the result of underestimating the porewater solute mass in the rock core samples.

Lower porewater concentrations may also be due to extracting water from the rock that is not in contact with the porewater. Water in the pores is assumed to be free water or bound water. Free water is able to move between pores under a pressure or chemical gradient. Bound water includes water strongly adsorbed to negatively charged clay mineral surfaces and the hydration water associated with cations adsorbed to the clay surface. The surfaces of clay minerals commonly have a negative charge. Water is "bound" to the negative charge through hydrogen bonding. Water may also be bound to the edges of clay minerals where charge imbalances may exist. The volume of clay-bound water is proportional to the surface area of the clay. Clay-bound water is immovable by mechanical means although it can be removed by evaporation (Dacy and Martin 2006).

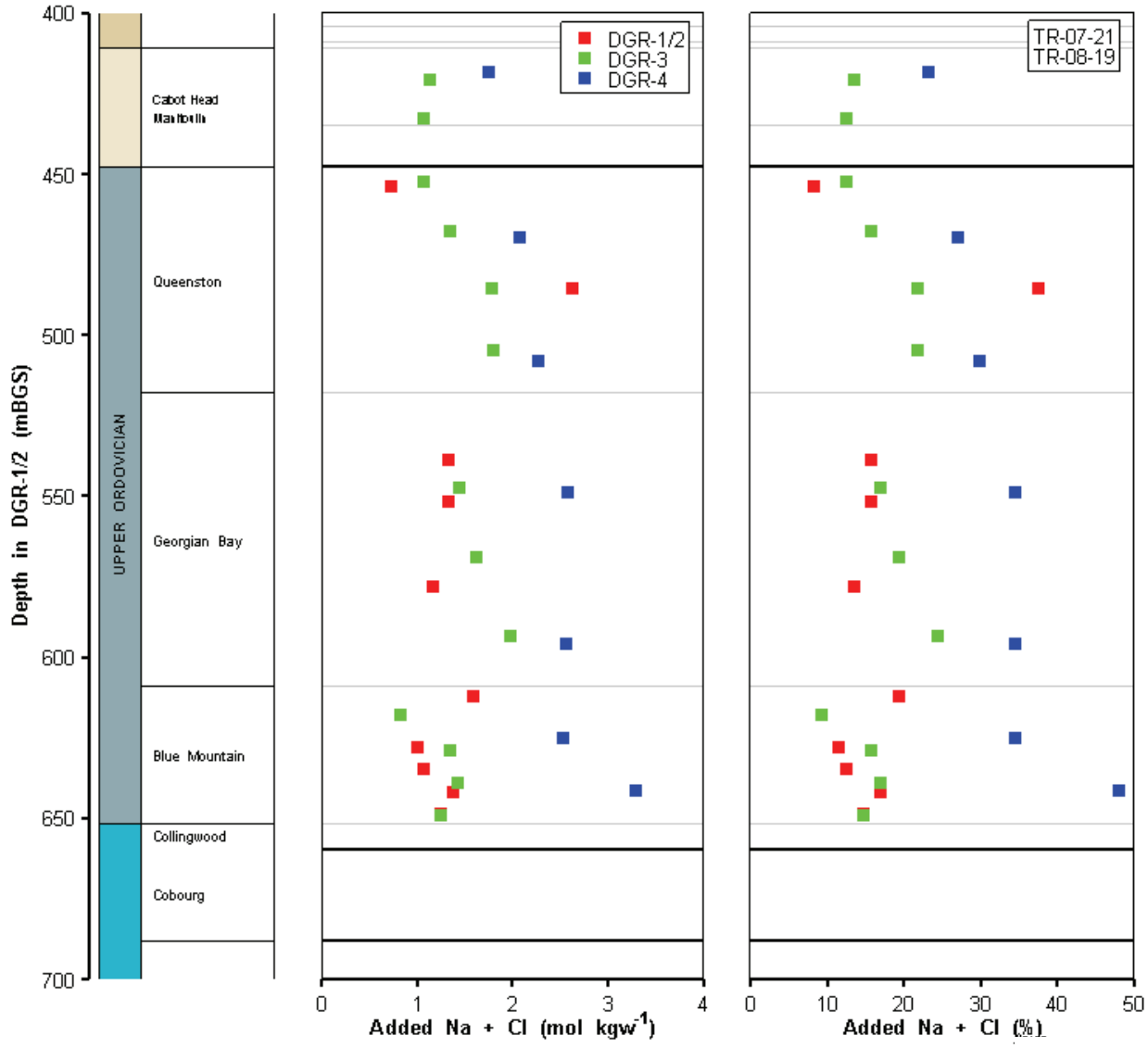

Figure 4.50: Na and Cl added to Porewater to Obtain Halite Saturation

The clays in the Ordovician shales are primarily illites and chlorites (TR-07-12, TR-08-20, TR-08-21, TR-09-06). Swelling clays with interlayers of water (e.g., smectites) were not identified in significant amounts. Therefore, the water associated with clays is not interlayer water, but is clay-bound water. The bound water does not associate with the free water in the pore. However, heating the rock core samples for determining water content in the rock core may release the bound water, leading to overestimation of the amount of free water in the pores. Dacy and Martin (2006) showed clay-bound water occupied approximately 20% of the liquid porosity in shaley sandstones with illite and chlorite clays. These results suggest underestimating porewater concentrations by 15-20% may be a result of releasing clay-bound water during the heating phase of the porewater analysis.

The amount of bound water required to underestimate the porewater concentrations by 15-20% was examined through the following calculation. The average dry bulk density for the Ordovician shales, is 2,590 kg/m^3 (Table 4.1). Figures 3.7 and 3.8 show illites and chlorites account for approximately 50% of the shale mass, which equates to 1300 kg of clay in 1 m^3 of shale.

The average water-loss porosity for the Ordovician shales was approximately 7% (Table 4.3), or 70 L of water in 1 m^3 of shale. If water adsorbed to the clays accounts for a 15% decrease in the porewater solute concentrations in the shales then there is approximately 10 L of water (70 L x 15%) adsorbed to 1300 kg of illite and chlorite in the Ordovician shales. If the water density is 1000 kg/m^3, then the adsorbed water has a mass of 10 kg, and 10 kg of adsorbed water is 0.8% of the clay mass by weight. By weight percentage, only a small amount of adsorbed water is required to dilute the porewater concentrations by 15% in 1 m^3 of rock because of the high clay content and low porosity of the shales.

The calculations presented above suggest the underestimated solute concentrations in the Ordovician shales may be due to the release of clay-bound water during the heating to estimate the water content of rock core samples. Clay-bound water does not have a significant effect on the porewater concentrations for the carbonate hard beds in the Ordovician shales or the Ordovician limestone units because the carbonate rocks have a significantly lower clay content (<20%) compared to the Ordovician shales (near 50%).

4.6.4 Anion Exclusion

Anion exclusion is a process where anion transport through pores is inhibited or prevented due to the negative charge of a mineral surface across small pore throats. Anions are unable to overcome the negative charge repulsion and cannot move through the small pore throats. The high clay content and relatively small porosities of the Ordovician shales potentially provide a suitable environment for solute transport to be affected by anion exclusion.

Through-diffusion analyses for determination of iodide-accessible pore space and effective diffusion coefficients showed iodide could only access approximately half of the pore spaces that were accessible to tritium in the Ordovician shales (TR-07-17, TR-08-27). This disparity of iodide accessibility compared to water accessibility was considered to be due to anion exclusion (Cavé et al. 2009).

The median pore-throat distributions measured in DGR-3 and DGR-4 Ordovician shale core samples by mercury porosimetry are shown in Figure 4.51. The small pore spaces may be an intrinsic property of the shale, and may also be due to mineral precipitation (halite, gypsum or other minerals) in the pores.

Pusch (2008) categorized discontinuities such as fractures, joints and smaller openings in crystalline rocks including both granites and clay shales into seven classes. The smallest class of openings is called crystalline pore spaces (Figure 4.52). Crystalline pore spaces can result at crystalline junctions or along crystalline edges. Crystal junctions might produce spherical pores while intercrystalline edges produce very small pores. The pore throat radii shown in Figure 4.51 are relatively small compared with the illustration in Figure 4.52. However, crystal junctions and mineral in-growth is a possible mechanism for creating small pore spaces in the Ordovician shales because evaporite minerals are common in the shales.

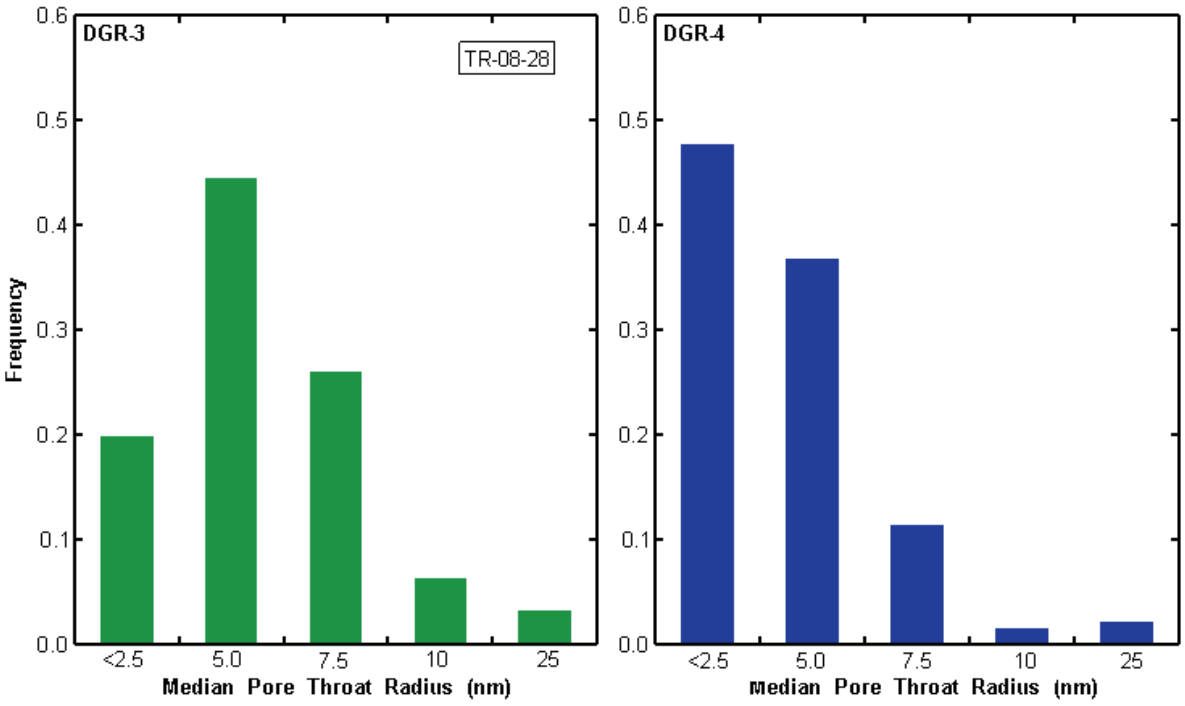

Figure 4.51: Median Pore Throat Radii from Mercury Injection Porosimetry Testing of DGR-3 and DGR-4 Shales

The presence of clay minerals in small pores can also cause anion exclusion. The negatively charged sites on the clay surface attract a layer of cations to the surface, which in turn attracts anions to the cation layer. Together, these two layers are referred to as the electric double layer (EDL). In the middle of the pore is the free porewater solution, which is the water that is outside of the influence of the EDL. The EDL may prevent anions from moving through pore throats, if the EDL occupies the pore throat.

The thickness of the EDL was determined in Section 4.4.1 as approximately 0.14 nm in brine with TDS ≈ 300 g NaCl/L. Because the equation used to calculate the EDL thickness was developed for freshwater and brackish systems, not the high ionic strength porewater in the Ordovician shales, the accuracy of this EDL thickness prediction is unknown. However, the results are used below to illustrate the potential for anion exclusion to occur.

If a pore is lined with clay, the cross section of the pore should have two EDLs, one on each pore wall. Therefore, the calculated EDL shown above was doubled (0.3 nm) to account for clay on both sides of a pore cross section. Since hydrated radii of many ions including I and Cl are near 0.3 nm (Nightingale 1959), pores less than approximately 0.6 nm are required for anion exclusion to occur. Even considering the uncertainty of the EDL calculation at high ionic strengths, these results suggest anion exclusion would only occur in very small pore throats.

Mercury porosimetry data presented in Section 4.3.5 has a method detection limit of 2.5 nm. Approximately 20% of the pores in DGR-3 were smaller than 2.5 nm and 48% of the pores in

DGR-4 were smaller than 2.5 nm (Figure 4.51). The relatively high proportion of pore throats <2.5 nm suggests there may be very small pore throats (<0.6 nm) capable of anion exclusion.

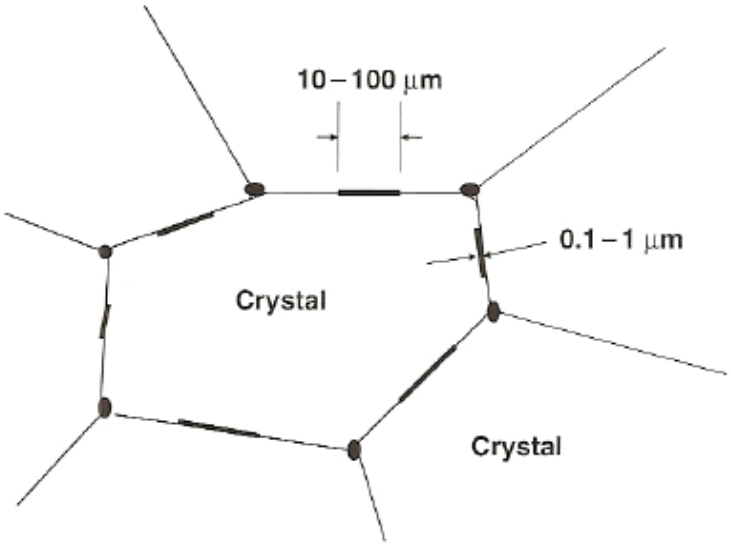

Figure 4.52: Schematic of Inter-crystalline Pore Spaces (after Pusch 2008)

The net effect of anion exclusion may be twofold. Firstly, the anions are made less mobile because they are restricted from moving through certain fine pore throats in which the EDLs prevent ready access. Secondly, when pore throats are extremely small, as in the case of the DGR Ordovician sequence, the aqueous concentration of ions in the outer layer of the EDL may be different from that in the centre of the pore beyond the influence of the EDL. This may create a case where the centre of spherical pores may have porewater at halite saturation, while along the edges of the sphere there is a chloride deficiency due to anion repulsion by the negatively charged crystalline surface. This second effect may also be a factor in the underestimation of shale porewater concentrations that was discussed in Section 4.6.3.

4.6.5 Major Ions

The discussion above suggests porewater concentrations from the crush and leach method underestimate porewater concentrations in the Ordovician shales. The magnitude of the underestimated porewater concentrations is likely different for each rock core sample. Therefore, it is difficult to accurately correct the underestimated porewater concentrations. The major ion results presented here are based on analyses performed by University of Ottawa and University of New Brunswick with some selected data (Cl, Br, Na, Ca and water activity) determined by the University of Bern. The presented major ion data do not account for the potential underestimation (approximately 15%, Figure 4.48) of ion concentrations in the Ordovician shales. The major ion results presented in this section account for mineral dissolution during porewater extraction, including anhydrite and calcite (see Section 4.6.2).

The ions considered are the following:

a) Na^+ and Cl^-: the source of these ions in brines is evaporated seawater and halite, which is a clear indicator of largely immobile brine porewater;
b) Ca^{2+} and Mg^{2+}: these ions are associated with the dolomitization of the Paleozoic rock sequence (Hobbs et al. 2011b);
c) K^+: low potassium concentrations are associated with Shield brines, and can be associated with transformation of smectite to illite;
d) B is a conservative tracer that also has a diagnostic signature in Shield brines; and
e) Br^- is a conservative tracer that is used to form Cl/Br ratios that are useful as tracers of seawater and brines.

Figures 4.53 and 4.54 present the depth profiles of Cl and Na and total dissolved solids (TDS) and water activity determined from porewater analyses of DGR cores and from analyses of groundwater samples collected from US-8 and DGR boreholes. The groundwater results from US-8 and DGR boreholes shown in the concentration-depth profiles were converted from measured concentration units (mg/L solution) to units of molality (mmol/kgw).

Water activity of core samples was determined by University of Bern (TR-08-06, TR-08-40) from direct measurements of the relative humidity immediately surrounding the samples using an activity meter. Activity measurements were made immediately after unpacking and removing the rim material from the core samples. Water activity is presented as an indicator parameter of TDS content. This simple measurement has the advantage that it does not have to consider the experimental complexities inherent in estimating porewater chemistries from conventional crush and leach testing. Water activity decreases with increasing TDS.

The shallow groundwater and porewater Cl concentrations are low from the Lucas Formation to the top of the Salina units (Figure 4.53), which is consistent with the permeable Devonian freshwater system. The porewater Cl concentrations generally increase from the Salina G Unit to the Salina B Evaporite Unit. Below the Salina B Evaporite Unit, the Cl concentration decreases to the top of the Salina A1 Unit. Below the top of the Salina A1 Unit, the Cl concentrations increase down to the Guelph Formation. Possible porewater dilution complicates the interpretation of chloride concentrations in the Ordovician shales and the Cabot Head shale. Below the Guelph Formation, concentrations generally decrease to the top of the Gull River Formation. The Cl concentrations increase from the bottom of the Gull River Formation to the Cambrian sandstone. The porewater and groundwater (OGW) Cl concentrations were similar for the Salina Upper A1 Unit, Guelph and Cambrian permeable horizons, which provides confidence in the porewater results.

The groundwater and porewater total dissolved solids (TDS) concentrations are also presented as g/L in Figure 4.54. Note the pattern of TDS is similar to the pattern of Cl due to the significant role chloride plays in the groundwater and porewater TDS. The similarity between the groundwater TDS and the porewater TDS suggests all of the major ions are accounted for in the porewater analyses.

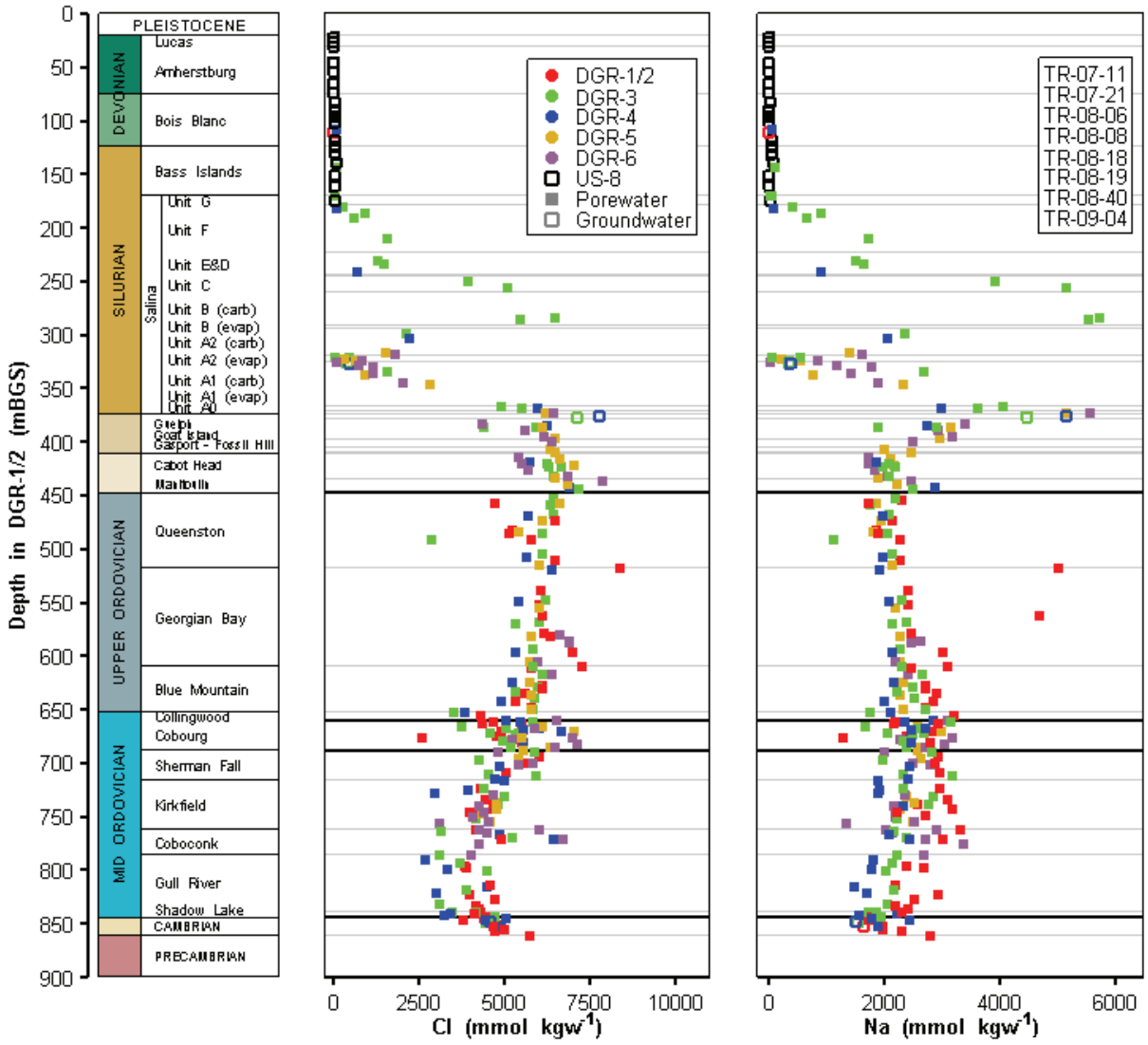

Figure 4.53: Profiles of Na and Cl Concentrations in Porewater and Groundwater from US-8 and DGR Boreholes

As expected the measured water activity of core samples shown on Figure 4.54, shows a mirrored depth profile to TDS. Activity decreases from near 1 within the Upper Silurian rocks to about 0.6 in the bottom of the Salina A2 Unit and then increases to about 0.9 near the Upper A1 Unit aquifer which has low TDS. Below the Upper A1 Unit aquifer activity deceases to about 0.6 for the high TDS groundwater in the Guelph Formation and then fluctuates between 0.6 and 0.7 through the Middle and Lower Silurian formations, the Ordovician shales and the bulk of the Ordovician limestones. In the very bottom of the Gull River Formation though the Shadow Lake Formation to the Cambrian sandstone and underlying Precambrian, the water activity shows dramatic increases from 0.65 to 0.8 reflecting the decreased salinity of the porewater in these rocks relative to overlying formations.

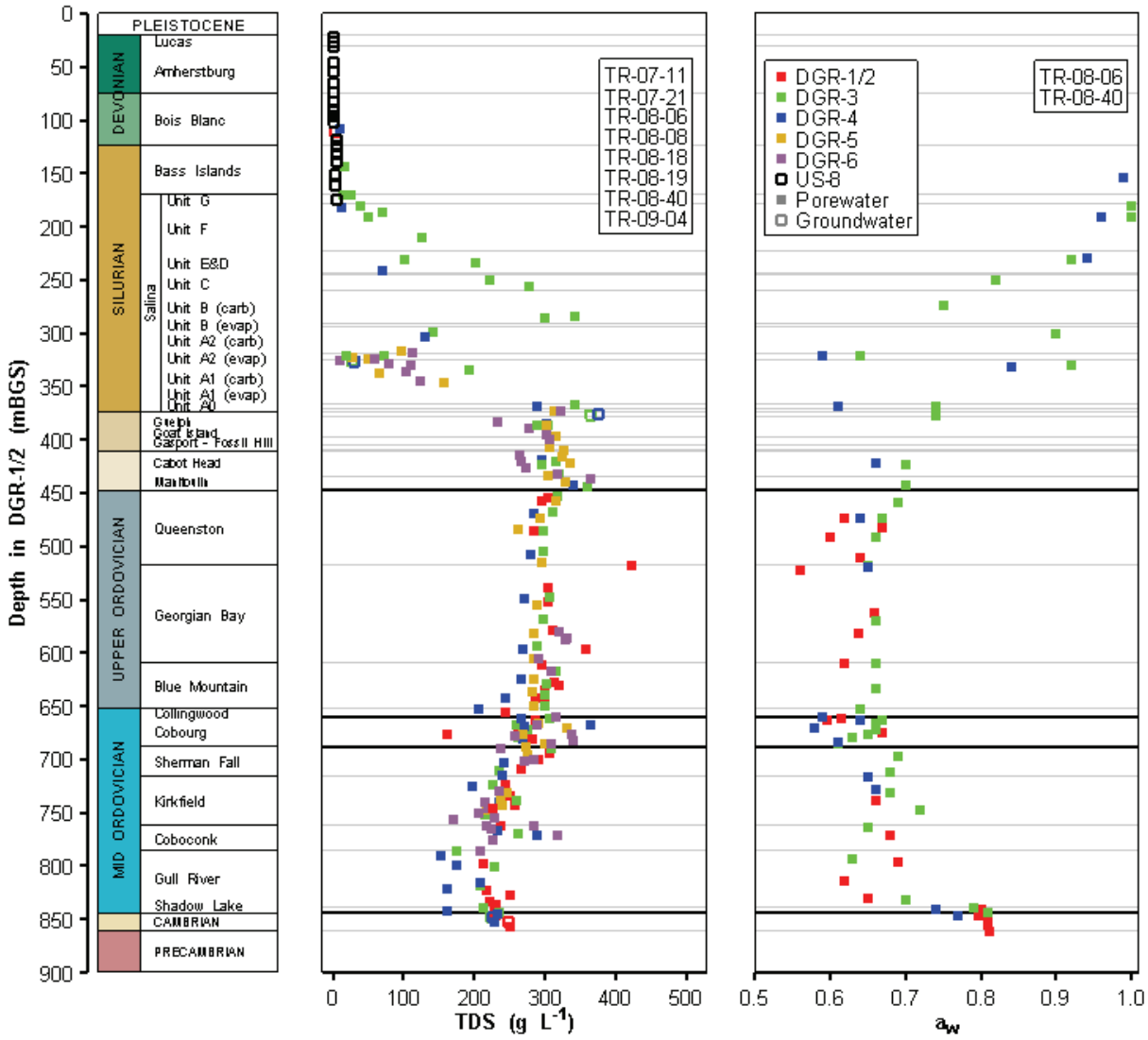

Figure 4.54: Profiles of TDS Concentrations and Water Activity in Porewater and Groundwater from US-8 and DGR Boreholes

For comparison, saturated NaCl solutions have a water activity of 0.75 (TR-08-40), which is a higher water activity than what was observed in samples from below the Guelph Formation to the Shadow Lake Formation. Although halite is observed in some rock samples in these formations, halite was not found throughout the section, even though the pore water in the Ordovician formations was primarily a Na-Cl type water (see Table 4.17 below). This indicates the measured water activity is lower than the mineralogy suggests, and the measured activity is lower than the water activity of the porewater concentrations determined by the University of Ottawa, the University of Bern and the University of New Brunswick. However, the qualitative comparison of porewater TDS and measured water activity suggests the trends in porewater salinity are true.

Not shown on Figures 4.53 and 4.54 are very high concentrations of Na, Cl and TDS for samples suspected to be affected by halite dissolution. For example, for sample DGR2-523.08 (e.g., Cl = 12,380 mmol/kgw) and sample DGR3-417.60 (Cl = 17,211 mmol/kgw), the very high concentrations, which exceed halite solubility, are attributed to halite dissolution during the solute leaching process for characterizing porewater solute concentrations. The DGR2-523.08 sample was obtained from the Georgian Bay Formation, which contains halite (Table 3.6) that was likely dissolved during the leaching procedure. The DGR3-417.60 sample is from the Fossil Hill Formation, which was not observed to contain halite. However, the concentrations were greater than halite solubility, which suggests a high uncertainty with the results. Porewater concentrations from sample DGR3-539.46 (Georgian Bay Formation) and ten samples from DGR-5 and DGR-6 (TR-09-04) collected mostly from Silurian dolostones, were not considered representative of porewater chemistry and were not plotted in order to preserve resolution of data trends with depth.

The patterns observed in the Cl concentration depth profile described above were also observed in the concentration depth profiles of Na and Br (Figures 4.53 and 4.55). Br concentrations from the University of Ottawa for DGR-1 and DGR-2 (TR-07-21) were not shown in Figure 4.55 due to analytical uncertainties in the Br data. The analytical uncertainties were addressed for Phase 2A and 2B, and the results are shown for DGR-3, DGR-4, DGR-5 and DGR-6. The DGR-2 porewater Br concentrations shown in Figure 4.55 are from the University of Bern and the University of New Brunswick. Br was not measured on dilute groundwater samples collected from the US-series boreholes.

The Na and Br profiles show the highest porewater concentrations near the bottom of the Silurian formations and for the Ordovician formations these ions shown minimum concentrations in the Coboconk or Gull River formations.

The Cl and K profiles (Figures 4.53 and 4.55) both show a slight decrease in concentration from the Guelph Formation to the Cobourg Formation, then a slight increase in concentration in the Cobourg Formation, which may be due to the analytical uncertainty in the Ordovician shales as discussed above. Below the Cobourg, Cl concentrations decrease down to the Gull River. Below the Gull River, CI concentrations increase into the Cambrian. K concentrations also decrease down to the Gull River, but unlike the Cl profile, the K concentrations continue to decrease into the Cambrian. Although it is not a major ion, B (Figure 4.55) has a similar depth profile to K.

Figures 4.56 and 4.57 present the groundwater and porewater chemistry profiles for Ca and Mg, and for Sr and SO_4, respectively.

The major ions, Ca, Mg, and SO_4, as well as minor ions including Sr and B, do not follow the same general concentration trends as Cl. Corrections for anhydrite saturation significantly affect the Ca and SO_4 results, making these results difficult to interpret. The Ca concentrations are also affected by the PHREEQC mineral saturation calculations that forced the porewater solution to equilibrium with calcite without a known pH. The confidence in the porewater results can be assessed by comparing the ion concentrations from the opportunistic groundwater samples to porewater samples in the same formation assuming the porewater and groundwater concentrations should be in equilibrium.

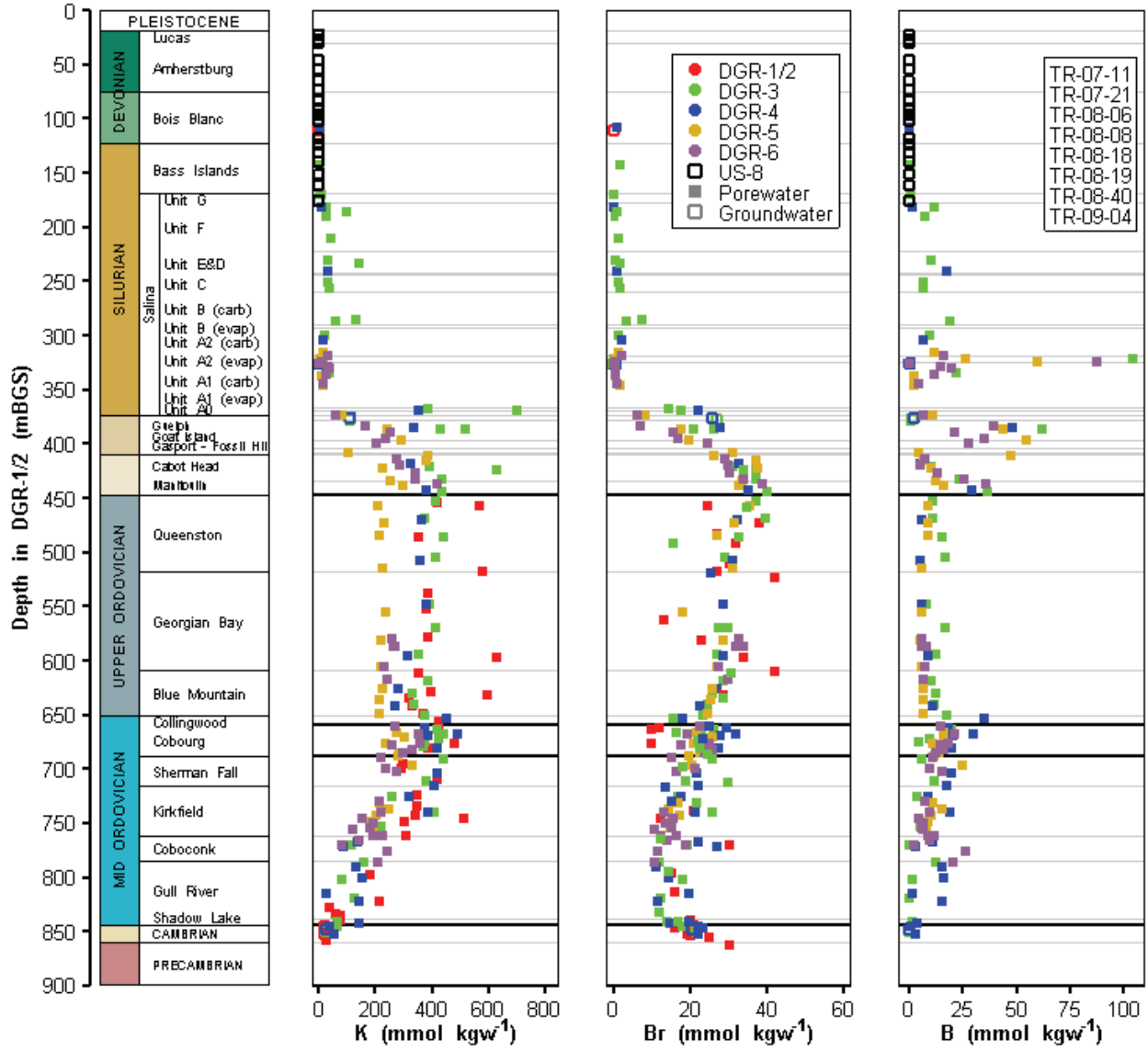

Figure 4.55: Profiles of Potassium, Bromide, and Boron Concentrations in Porewater and Groundwater from US-8 and DGR Boreholes

Ca porewater and groundwater concentrations are similar in the Salina Upper A1 Unit permeable horizon, are dissimilar in the Guelph Formation, and show more variability in the Cambrian. Corrections for calcite and anhydrite saturation significantly affect the Ca concentrations, making the Ca results difficult to interpret. Also, the Ca porewater concentrations within the Ordovician limestones in DGR-4 are significantly reduced relative to other DGR boreholes. Lower Ca concentrations may be due to 1) reactions that precipitate Ca (e.g., calcite or dolomite precipitation); 2) laboratory error; or 3) the concentrations are representative of actual heterogeneity between the porewater chemistries in the Ordovician limestones.

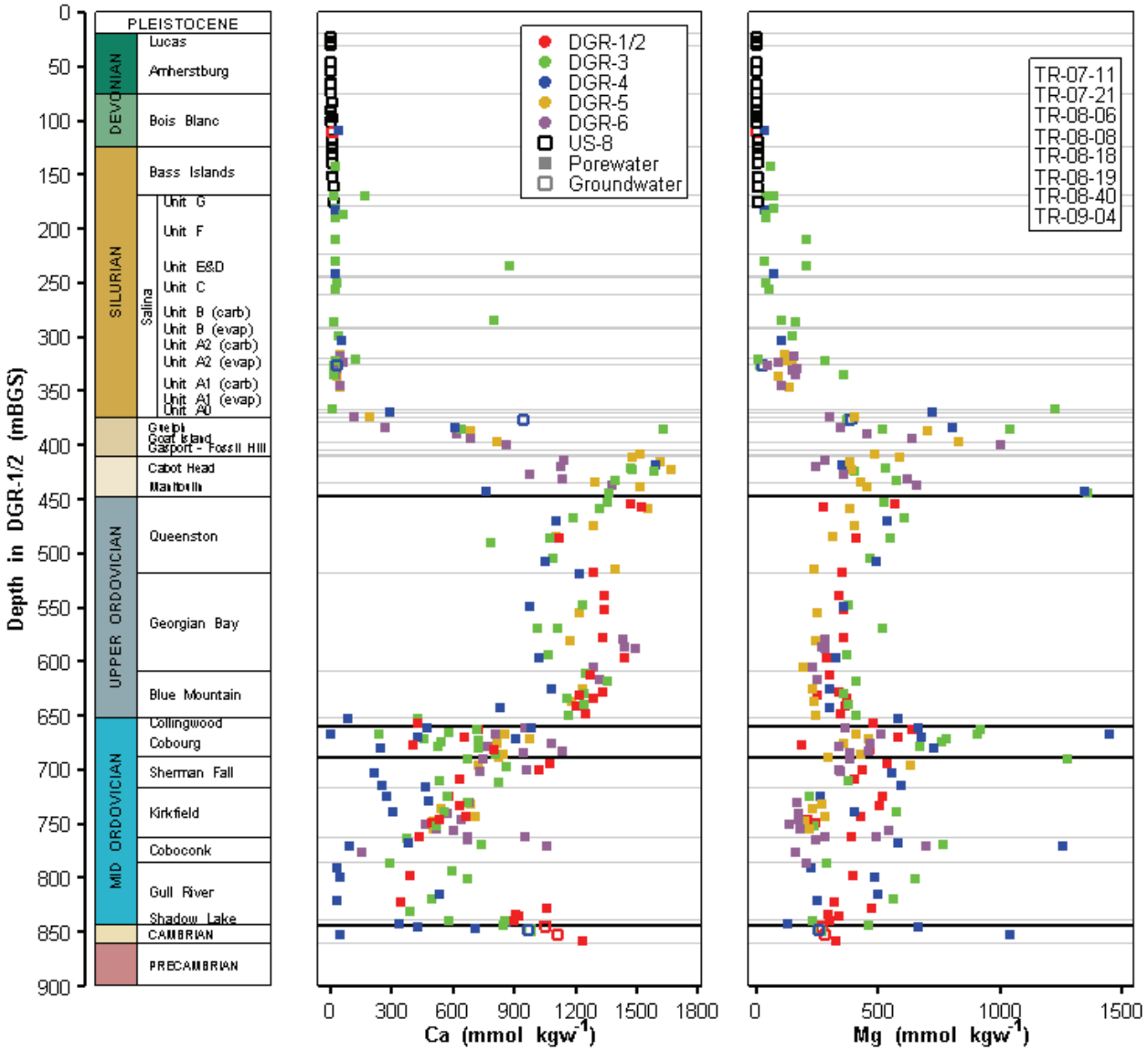

Figure 4.56: Profiles of Calcium and Magnesium Concentrations in Porewater and Groundwater from US-8 and DGR Boreholes

Mg porewater and groundwater concentrations are similar in the Salina Upper A1 Unit, the Guelph and the Cambrian permeable horizons. However, there is considerable scatter in the Mg concentrations profiles in DGR-3, DGR-4 and DGR-6 in the Ordovician limestones. The scatter may be due to the assumption that the porewater is in equilibrium with calcite and not a Mg bearing calcite or dolomite. Using only calcite as the equilibrium phase does not correct for Mg added to the leach water during the porewater characterizing process, which may overestimate porewater Mg concentrations.

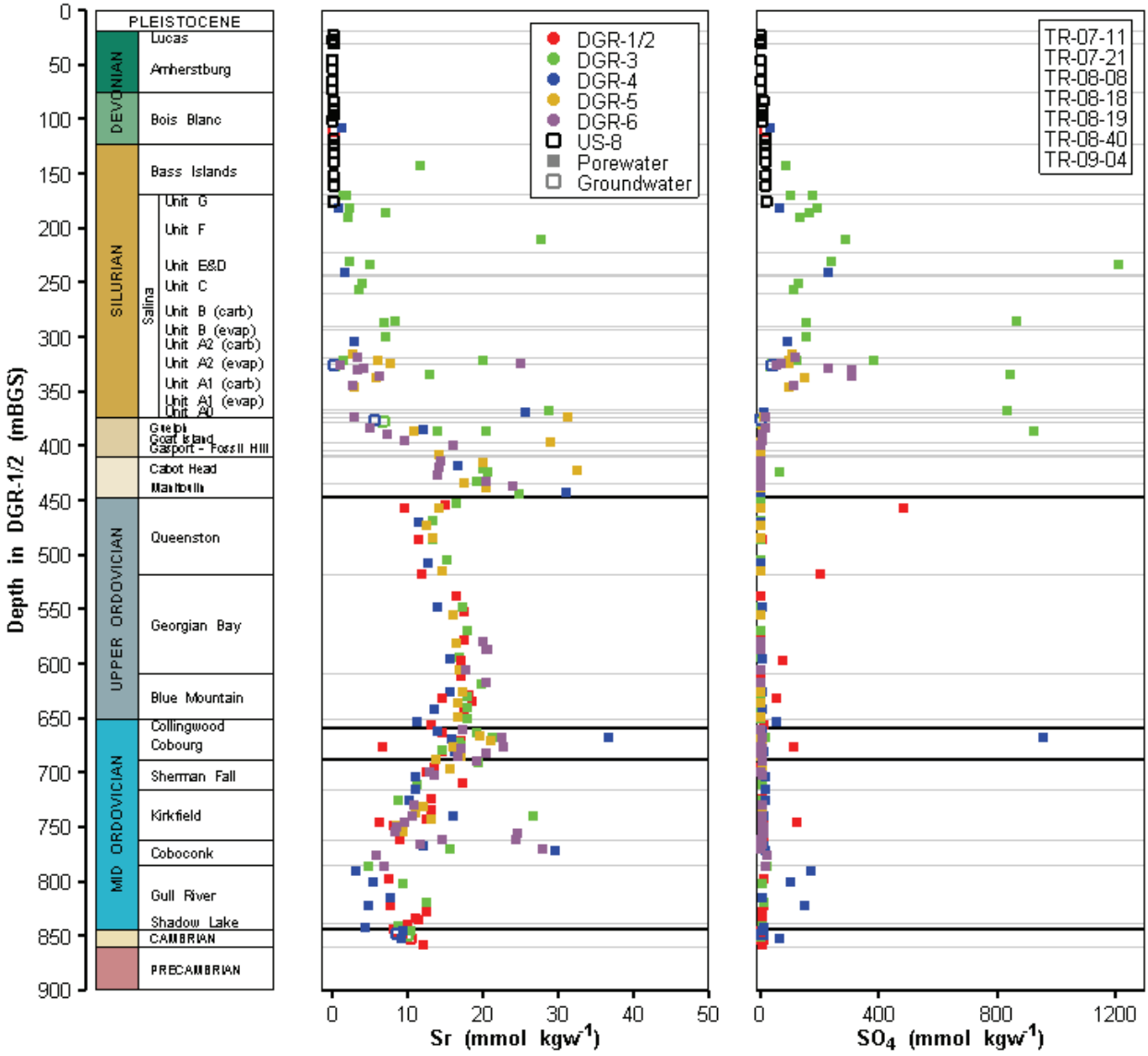

Figure 4.57: Profiles of Strontium and Sulphate Concentrations in Porewater and Groundwater from US-8 and DGR Boreholes

Sr porewater and groundwater concentrations are similar in the Salina Upper A1 Unit, the Guelph Formation and the Cambrian permeable horizons. The Sr concentrations from DGR boreholes in the Ordovician shales have a similar depth profile, but the Sr concentrations in the Ordovician limestones shows more scatter. Some scatter in the Sr concentrations may be due to dissolution of celestite, which was occasionally observed in the Silurian formations and the Ordovician shales (see Section 3.10.3, Table 3.13) during the mineralogical analyses.

Finally, porewater SO_4 concentrations were corrected assuming anhydrite equilibrium. Additionally, SO_4 may be affected by oxidative dissolution of pyrite and other iron sulphide minerals during laboratory procedures (which may also dissolve carbonate minerals) and

dissolution of SO_4 minerals (e.g., gypsum, anhydrite and celestite). Anhydrite and gypsum dissolution is a noted process in the Silurian rocks, affecting both SO_4 concentrations, and in the case of gypsum dissolution, water isotope results as well (see Section 4.6.6.1). In summary, the concentration profiles of Ca, Mg, SO_4 and Sr should only be used for limited interpretations.

The trends in groundwater and porewater major ion depth-profiles are also illustrated by considering the ion molal ratios shown in Figure 4.58.

Figure 4.58 shows the ion molal ratios of Cl/Na, Cl/Br and B/K in groundwater and porewater. An ion ratio of 1 for Cl/Na is expected if halite dissolution is the primary process controlling the Na and Cl concentrations. Stability in Cl/Br ratios is expected if halite dissolution is not an important process controlling Cl concentrations. Sea water Cl/Br ratio is 169 (Shouakar-Stash 2008), which would plot as 1.69 in Figure 4.58. Elevated B/K ratios can be indicative of dissolution of evaporite minerals and sedimentary basin brines.

Although there is some scatter of porewater Cl/Na in the Devonian, the Cl/Na ratios of groundwater in the Devonian and of porewater and groundwater in the Silurian increase from 1.0 in the Amherstburg Formation to about 1.5 in the Guelph Formation. Below the Guelph, the Cl/Na ratio increases to about 3.0 in the Cabot Head Formation and then decreases to about 1.25 at the top of Gull River Formation. The ratio increases from the top of the Gull River Formation to the Cambrian, where the Cl/Na ratio ranges from about 2 to 3. The Cl/Na data indicate most of the salinity in the Devonian and Silurian rocks is derived from halite dissolution, and the porewater and groundwater below the Guelph to the Cambrian did not evolve from the same Devonian/Silurian composition and/or the waters have been affected by processes that add Cl or remove Na over time.

The Cl/Br ratio is highest in the Salina units and is relatively constant in the Ordovician. There are small increases in the Cl/Br ratio in the Kirkfield, Gull River and Shadow Lake formations. These increased ratios may be due to halite dissolution increasing the Cl concentrations. Assuming Br is not contained within halite minerals, the relatively constant Cl/Br ratio in the Ordovician and Cambrian rocks suggests halite dissolution is not a significant factor affecting the Cl concentration in these rocks.

The B/K ratio (Figure 4.58) shows a relative enrichment in B associated with the Salina units, and a relative depletion of B in the Ordovician formations including the Cambrian sandstone. However, there is also a small trend of increasing B/K ratio from the Cambrian up to the Coboconk Formation.

4.6.6 Environmental Isotopes

4.6.6.1 Oxygen and Deuterium Isotopes

The combined $\delta^{18}O$ and δD plot for all DGR porewater and groundwater is shown in Figure 4.59. The ranges of $\delta^{18}O$ and δD for modern precipitation in southern Ontario are shown as $\delta^{18}O$: -12‰ to -10‰, and δD: -85‰ to -70‰. Figure 4.60 also presents the data for the many porewater samples, and the Guelph and Cambrian groundwater samples, that crowd the relatively enriched zone at the top right-hand corner of Figure 4.59 in expanded scale.

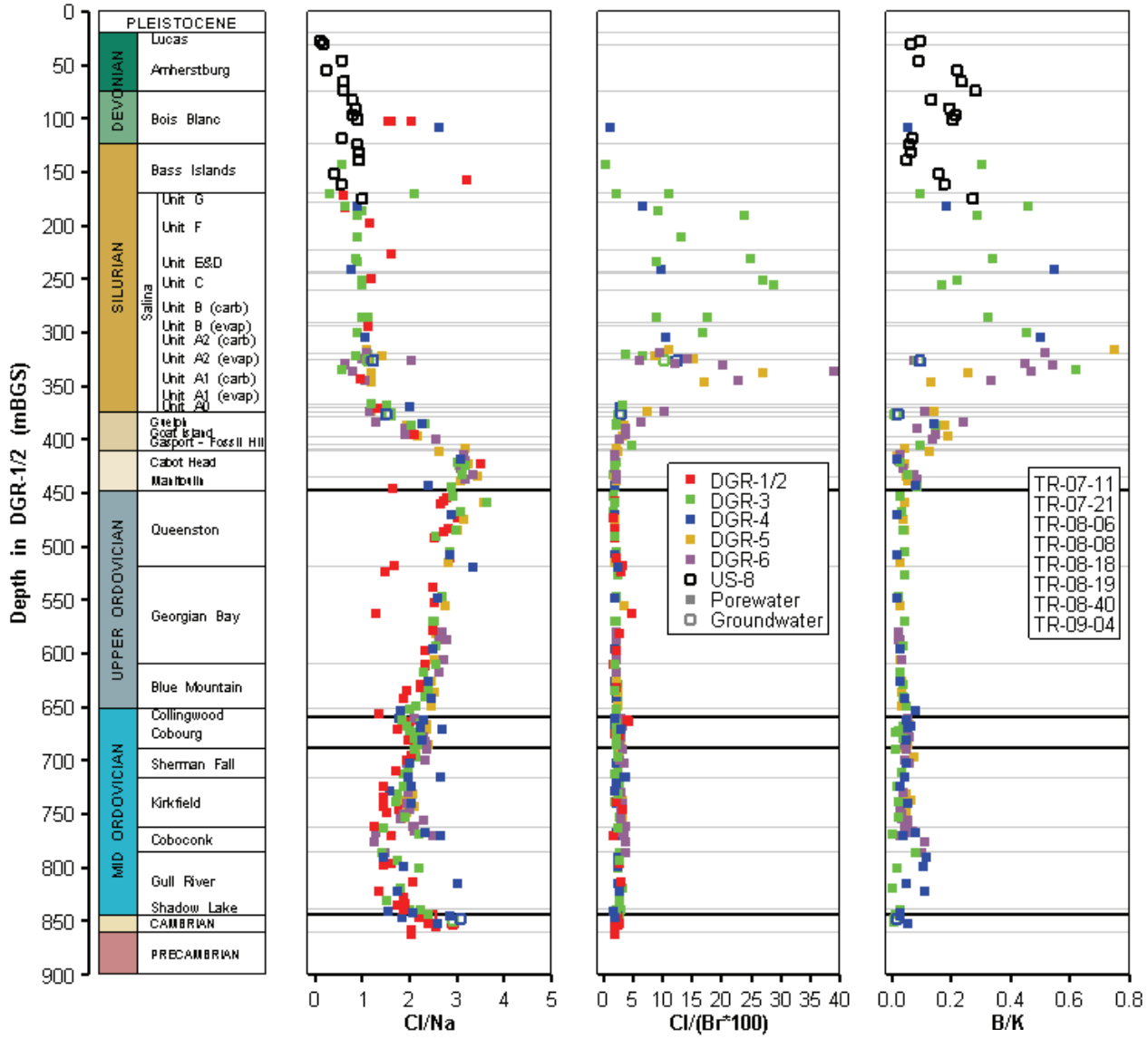

Figure 4.58: Profiles of Ion Molal Ratios of Porewater and Groundwater from US-8 and DGR Boreholes

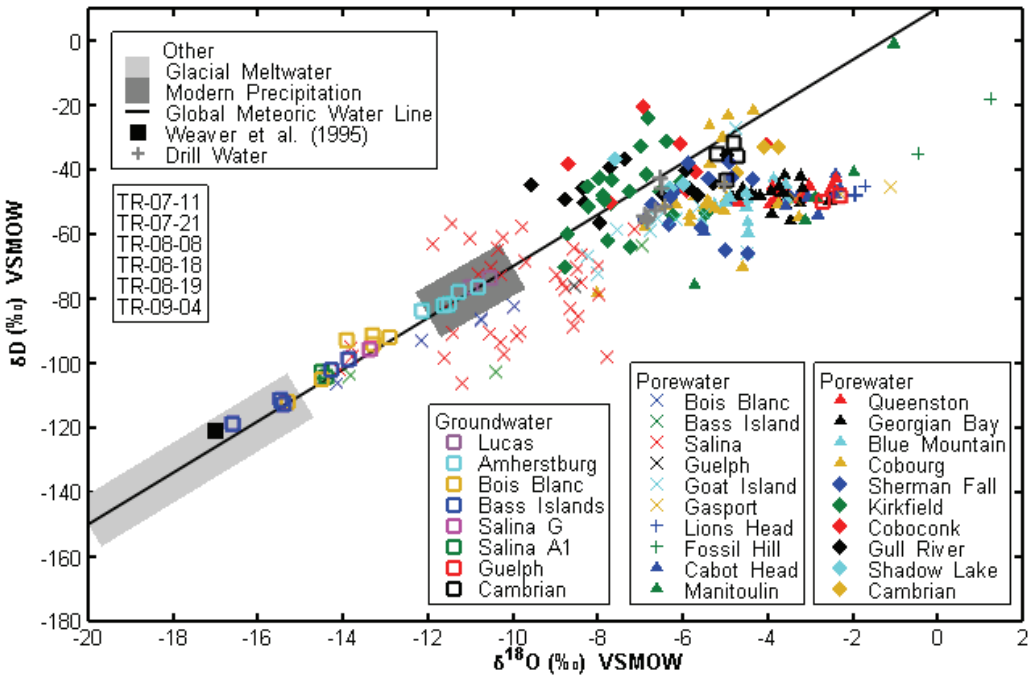

Figure 4.59: Cross Plot of δD versus $\delta^{18}O$ for all Groundwater and Porewater Samples from US Wells and DGR Boreholes

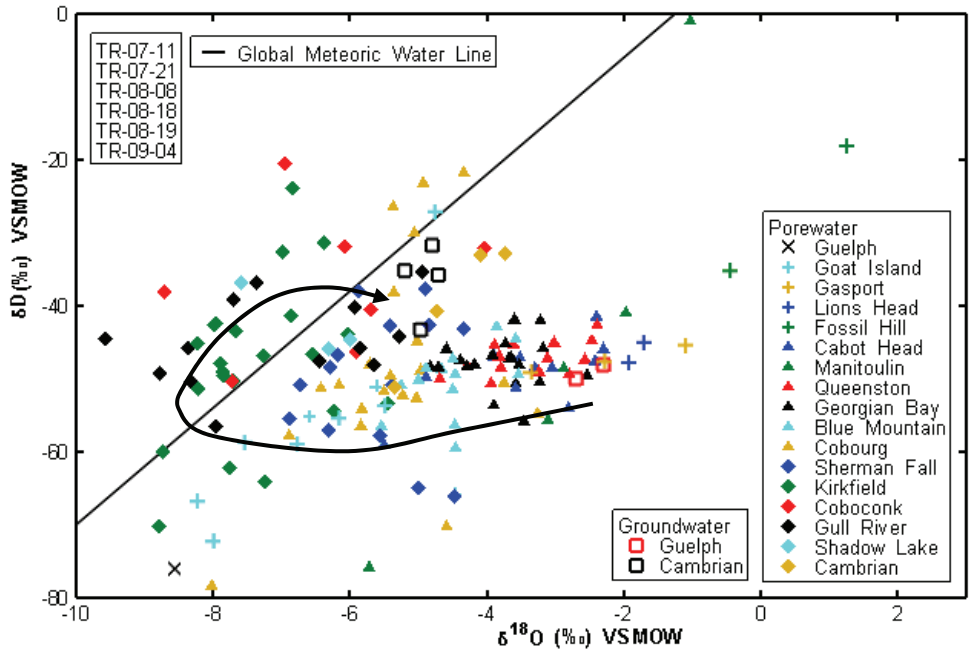

Note: Arrow shows evolutionary path with depth.

Figure 4.60: Expanded Scale for Porewater Samples and Guelph and Cambrian Groundwater from Figure 4.58

An assessment of the University of Ottawa porewater extraction method and isotope analyses (TR-08-37) suggests all of the porewater is removed during analysis. The porewater results and the OGW results were similar (Figure 4.61), except for the Guelph Formation, which decreases the uncertainty of the results. The Guelph Formation rock core samples were very porous and the porewater isotope results were similar to the drill fluid results, which suggests the rock core samples were contaminated with drill fluid (TR-09-04). The porewater isotope results from the Guelph Formation are not shown in the following figures. The analytical error associated with the results is small (±0.2‰ for $\delta^{18}O$ and ±2‰ for δD).

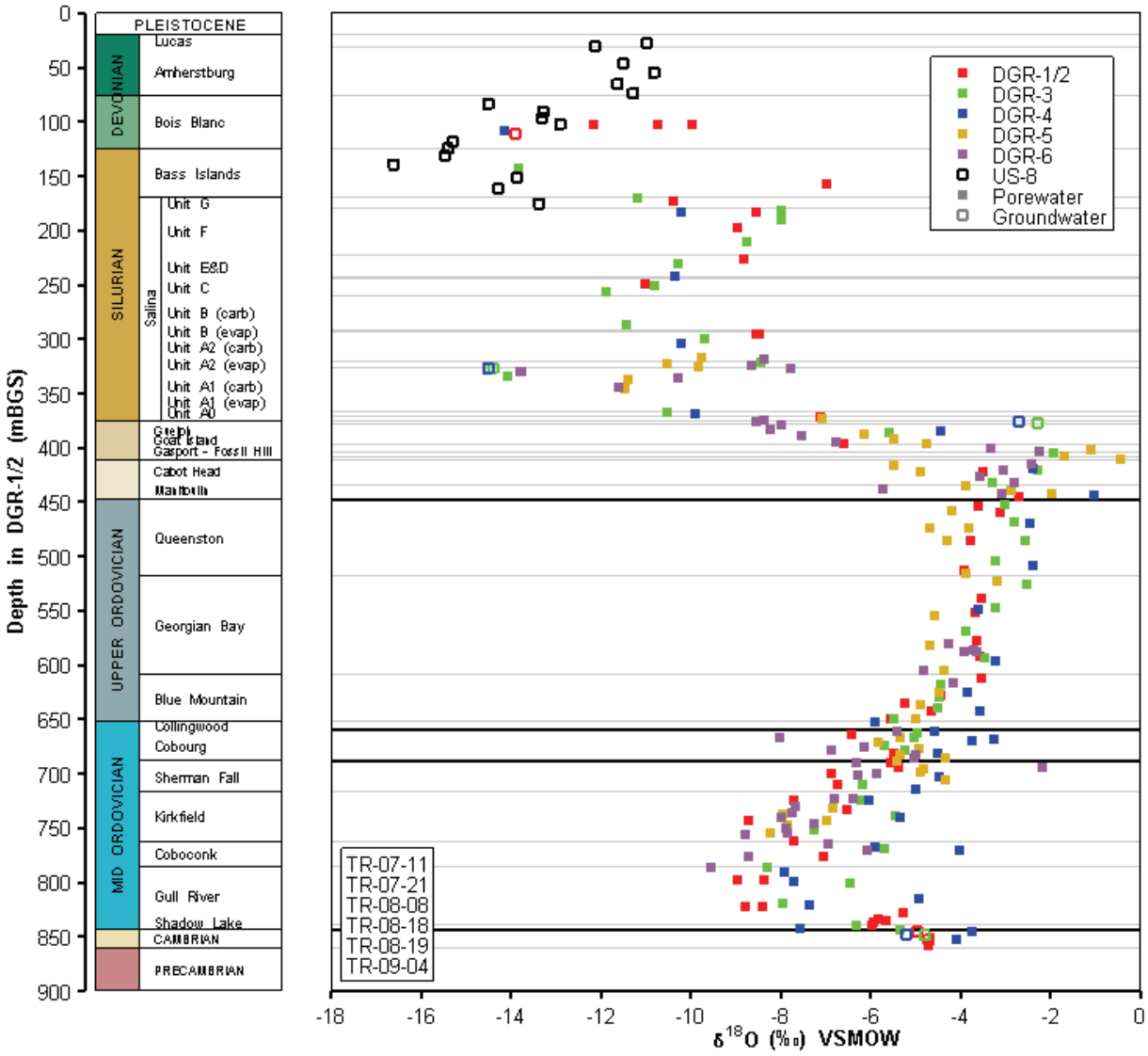

Figure 4.61: Profile of $\delta^{18}O$ of Porewater and Groundwater from US-8 and DGR Boreholes

The porewater $\delta^{18}O$ and δD results do not distinguish between water in the pore, water bound to clay or other mineralogical water (e.g. hydration water). Section 4.6.3 suggests approximately 15% of the water extracted by vacuum distillation may be clay-bound water, however, any difference in isotopic signature between the water in the pore and the clay-bound water.

As is typically the case, $\delta^{18}O$ and δD are shown as cross plots that permit evaluation of the data trends and results with respect to the Global Meteoric Water Line or GMWL i.e., $\delta D=8.13 \cdot \delta^{18}O + 10.8$) that defines the relationship between $\delta^{18}O$ and δD in worldwide fresh surface waters, including modern precipitation and glacial meltwater (shown on Figure 4.59). Typically sedimentary basin brines plot to the right of, and below, the GMWL, as is shown by most samples in Figure 4.59 and 4.60, although a few samples from the Trenton and Black River Groups (Kirkfield, Coboconk, Gull River limestones and the Shadow Lake siltstones) plot above the GMWL. Additionally, five samples from the Salina Formation that plot above the GMWL in Figure 4.59 are suspected to reflect isotope contributions from mineralogically bound water in gypsum and hence are not considered representative of porewater.

Review of Figure 4.60 shows a clustering and evolution of $\delta^{18}O$ and δD values from the Guelph and other Middle and Lower Silurian formations - including the Queenston Formation - with depth through the deeper Ordovician shales and limestones to the Cambrian. The evolutionary path with depth is primarily one of $\delta^{18}O$ depletion toward the GMWL, with a reversal above the GMWL followed by $\delta^{18}O$ and δD enrichment to the Cambrian groundwater and porewater values.

Figures 4.61 and 4.62 shows the $\delta^{18}O$ and δD groundwater data for US-8 multilevel well and OGW samples collected in the DGR boreholes together with similar data from core porewater plotted against the DGR-1/2 reference depth. Figure 4.61 shows there is some apparent $\delta^{18}O$ enrichment in porewater relative to groundwater for the Devonian and Upper Silurian dolostones, although the Salina Upper A1 Unit and Cambrian groundwater and porewater results are very similar.

The DGR porewater in the Devonian and Upper Silurian sequence show an $\delta^{18}O$ enrichment trend with depth, although some isotope values for gypsiferous samples from the upper Salina Formation likely have up to 3‰ $\delta^{18}O$ enrichment as an artefact of hydration waters released during extraction. Porewater and groundwater in the shallow Bois Blanc Formation have values that are close to the local groundwater (–12‰) with excursions to lower values that likely represent mixtures of modern meteoric water and glacial meltwater (–15 to –20‰; Aravena et al. 1995 and references therein). Deeper porewater in the Silurian formations trend towards the more enriched values observed in the Guelph Formation and Upper Ordovician shales ($\delta^{18}O$~–3.5‰) which are similar to Michigan Basin brines (Clayton et al. 1966). This trend suggests a gradual flushing of basin fluids in these Devonian and Upper Silurian formations with meteoric waters over time. This trend is observed in porewater salinity as well (see Figure 4.53). Within the Salina Upper A1 Unit aquifer, glacial meltwater has apparently penetrated to a depth of approximately 350 mBGS from the outcrops, as shown by the environmental isotope values from OGW-8: $\delta^{18}O$ =-14.4‰ and δD = -104‰.

Deuterium concentrations were similarly depleted in the shallow Devonian groundwater from the US-series multi-level wells (i.e., -75 to -120‰ for δD - see Figure 4.62), to those identified by Aravena et al. (1995) for the Alliston aquifer (δD: -101 to -95‰). The deuterium values increase throughout the upper Silurian formations to approximately -75‰ and, with the significant exception of the Salina Upper A1 Unit aquifer, continue this enriched trend reaching -50 to -40‰

in the formations in proximity to the Ordovician shales (i.e., the Cabot Head shale and the Manitoulin dolostone). The deuterium value of -104‰ in the Salina Upper A1 Unit aquifer is mid-way between the isotopic values for modern meteoric water and glacial meltwater (Figure 4.59) and is therefore a strong indicator of the deep penetration of Quaternary waters in that unit.

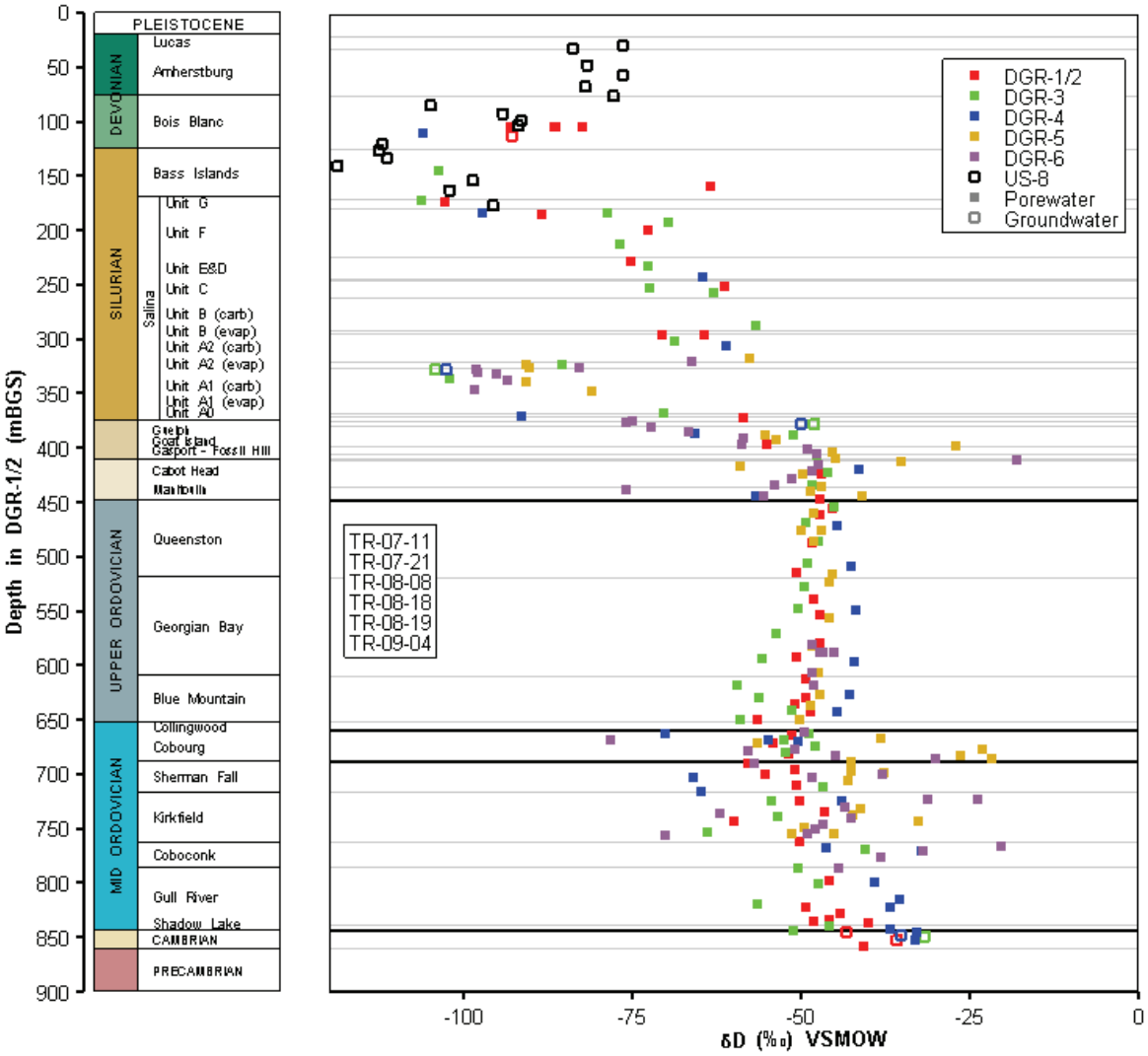

Figure 4.62: Profile of δD of Porewater and Groundwater from US-8 and DGR Boreholes

By contrast with the Devonian-Upper Silurian profile, the Middle and Lower Silurian through Ordovician porewater show a minor reverse trend with depth. $\delta^{18}O$ values show minor decreases from the Guelph Formation ($\delta^{18}O$ ~ -2.5‰ and δD ~ -48‰) downward through the Ordovician shales.

The δD profile is relatively similar from the Guelph through the Ordovician shales. Within the Ordovician limestones the δD profile is more scattered than the $\delta^{18}O$ profile. The Cambrian groundwater and porewater values are the most enriched at about -35‰.

As is shown in the depth profiles of Figures 4.61 ($\delta^{18}O$) and 4.62 (δD), several core samples in the Gull River and Coboconk formations have similar (enriched) isotopic compositions as the Cambrian samples. Figures 4.53 and 4.55 show that these samples also have enriched values for Cl and Br as well as $\delta^{18}O$.

Figure 4.63 presents the cross plot of $\delta^{18}O$ versus the deuterium excess, *d*, determined as the enrichment of D relative to ^{18}O where (Dansgaard 1964):

$$d = \delta D - (8 \times \delta^{18}O) \quad (4.8)$$

Figure 4.63 shows inverse correlation between $\delta^{18}O$ and *d* for the full Ordovician-Cambrian section. The depletion in $\delta^{18}O$ with depth from the Guelph Formation down through the stratigraphic column to the Gull River Formation is matched with an increase in deuterium excess. These trends then reverse through the Shadow Lake formation into the Cambrian to values with more enriched $\delta^{18}O$ and lower *d.*

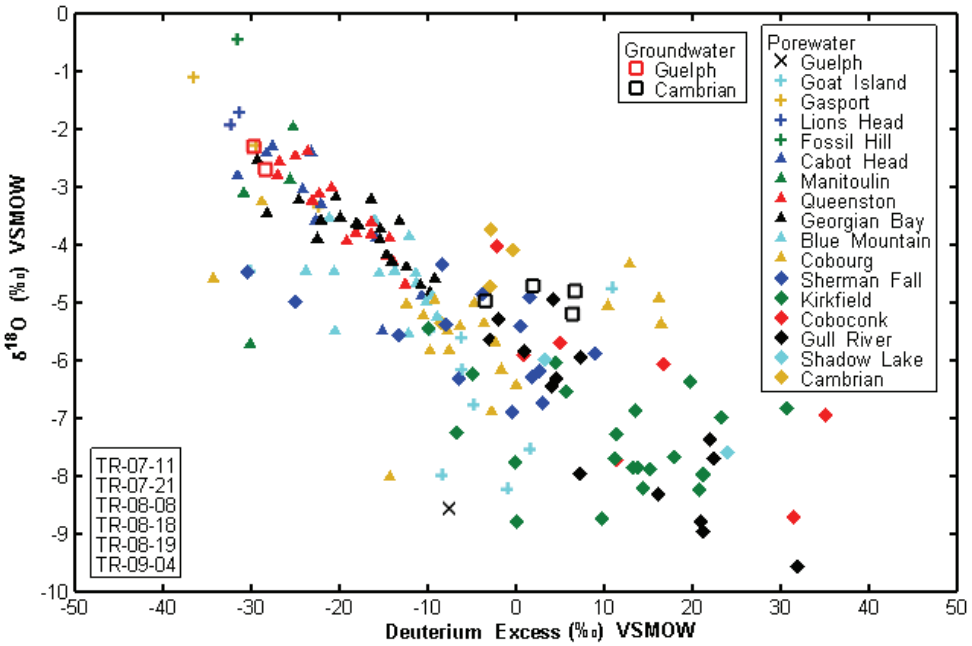

Figure 4.63: Deuterium Excess as a Function of $\delta^{18}O$ for DGR Porewater and Groundwater from the Guelph Formation to the Cambrian Sandstone

Figure 4.64 shows the variation of *d* with depth that indicates a common *d* value of +11‰ in the permeable Devonian and Upper A1 Unit aquifers, with systematic shift from a stable deuterium excess of about –30‰ in the Guelph and Lower Silurian formations down through the

Ordovician shales and limestones towards a very enriched value of about +20‰ in the Gull River limestone. This trend towards enriched deuterium excess then reverses in the Shadow Lake and Cambrian to lower values around 0‰.

The observed $\delta^{18}O$ depth trend also applies to Cl, Br, and TDS (see Section 4.6.5), as well as Sr (see below) where dilution trends are found in the sections with $\delta^{18}O$ depletion trends. Na^{+}, by contrast, shows the reverse trend and does not show the major ion dilution with the $\delta^{18}O$ depletion trend.

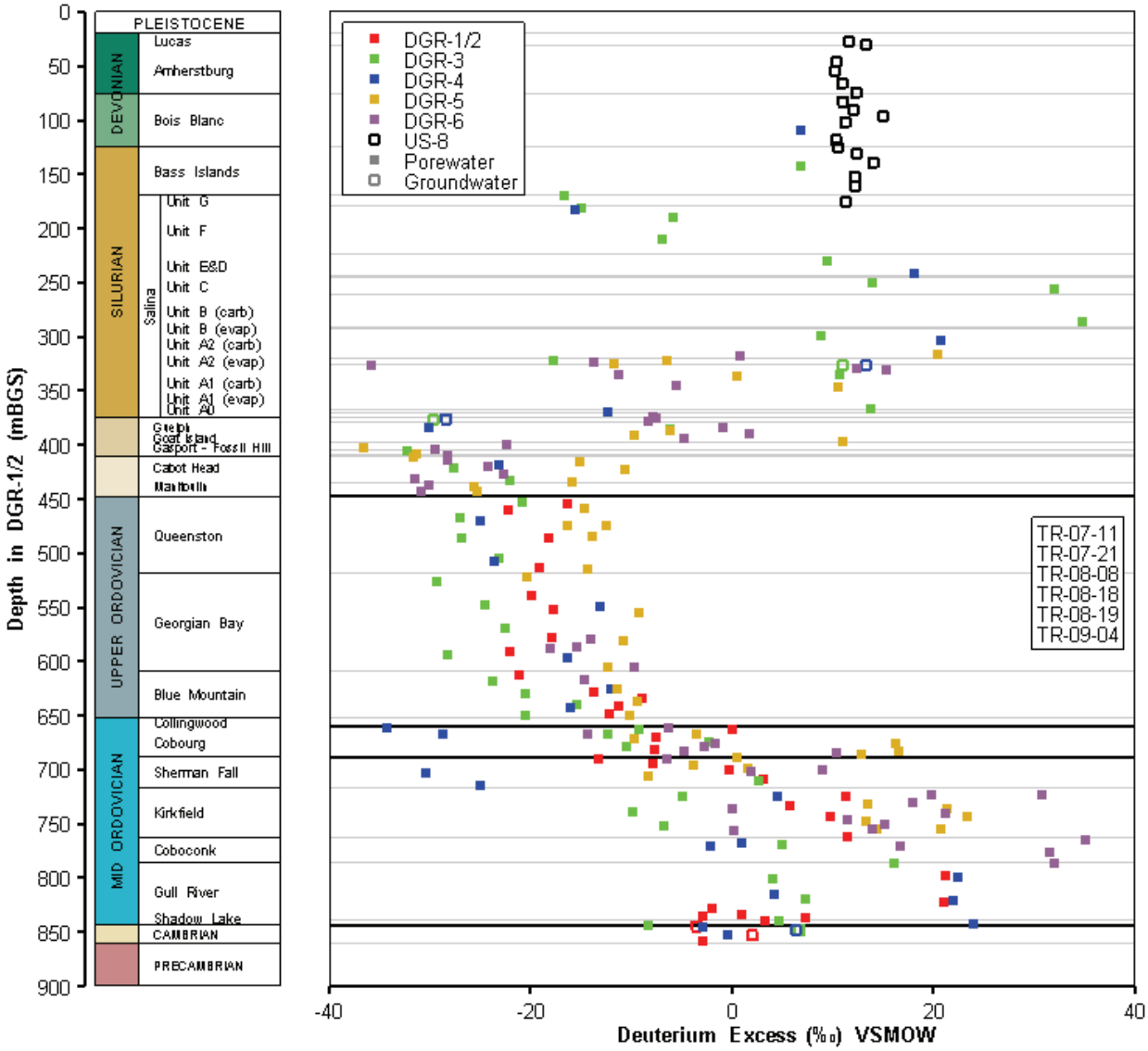

Figure 4.64: Profile of Deuterium Excess as a Function of Depth in US-8 and DGR Boreholes

4.6.6.2 Strontium Isotopes

The $^{87}Sr/^{86}Sr$ ratio in groundwater and porewater is a useful indicator of the source of Sr, which may be derived from seawater sources or through subsequent rock water interaction and mixing. ^{86}Sr is a stable isotope of Sr, while ^{87}Sr is produced by the decay of ^{87}Rb, which substitutes for K in crystalline rocks. The long half-life for ^{87}Rb ($T_{½}$ = 47.5 billion years) has produced a ^{87}Sr enrichment in potassium-bearing rocks of Precambrian age. The present $^{87}Sr/^{86}Sr$ ratio in seawater is a relatively constant value of 0.709, although this has varied over the Phanerozoic (Veizer 1989). The Ordovician to Devonian seawater Sr isotope curve varies between about 0.7077 and 0.7087. Increases in this value represent greater contributions of Sr from weathering of the continental crust, which displays enrichments in radiogenic ^{87}Sr from the decay of ^{87}Rb.

Sr isotopes were measured in groundwater, porewater and rock core samples. For the porewater samples, paired leaches were analyzed, including a rapid crush and deionized water leach (< 1 hr) to minimize mineral dissolution yet maximize uptake of porewater solutes, and an extensive leach in deionized water (using the leach water from the vacuum distillation experiments after 60 days contact with the rock fragments). This was undertaken to test the potential that Sr may be leached from the carbonate minerals in addition to the porewater solutes.

Results (TR-08-19) show less than 0.0002 difference in the measured $^{87}Sr/^{86}Sr$ ratios between paired leaches, suggesting no effect of matrix dissolution. Following leaching, the rock samples were rinsed extensively with deionized water and dried. These samples were then crushed to powder and leached with a mild acetic acid. This procedure leached Sr from the carbonate component of the rock. Sr was then removed from the leachate on ion exchange columns and re-eluted for preparation of filaments for analysis by thermal ionization mass spectrometry (TIMS) on a Triton instrument at Carleton University. Whole rock analyses were undertaken on two samples from the shales (including a shale hardbed) and two from the Middle Ordovician limestones to assess the potential contribution of ^{87}Sr from the aluminosilicate component. Whole rock samples were similarly rinsed and crushed, then dissolved in HCl. Remaining solids were dissolved in an HF/HNO_3 solution which was recombined with the HCl leachate before column extraction of Sr.

Results from the groundwater, porewater and rock Sr isotope analyses are shown in Figure 4.65. The $^{87}Sr/^{86}Sr$ ratios for acetic acid leachates of the host shales and limestones in Figure 4.65 fall close to the marine Sr curve (Veizer 1989). Also shown are rock measurements from Brand (2004) from eastern Ontario, two of which fall on the marine Sr isotope curve and one of which is more enriched, with a ratio close to the porewater profile. The whole rock analyses, which include Sr from the siliciclastic component, are more radiogenic than the Sr in the carbonate fraction. The two whole rock samples from the Georgian Bay include a shale with strongly radiogenic $^{87}Sr/^{86}Sr$ (0.7392) and carbonate hardbed with a less enriched value ($^{87}Sr/^{86}Sr$ = 0.7222). The whole rock measurements from the limestones, with minor aluminosilicate component (Figure 3.6), have minor enrichment above the seawater curve (0.7096 and 0.7087). The enrichment in the $^{87}Sr/^{86}Sr$ ratios in the shale sample and the shale hardbed sample suggests the enriched Sr signature is from the aluminosilicate component of these rocks, derived from weathering of the Shield during the Ordovician. Comparing the $^{87}Sr/^{86}Sr$ ratios for the whole rock results to the carbonate results shows the strongly radiogenic Sr from the aluminosilicates has not exchanged with or modified the $^{87}Sr/^{86}Sr$ ratio of the more labile (acetic acid leachable) carbonate fraction.

Figure 4.65 shows the DGR-2 and DGR-3 porewater analyses. Measurements show that most porewater is moderately to strongly enriched in ^{87}Sr with respect to the marine curve. Three distinct sections can be discussed, including (1) the upper profile in the Silurian dolostones where porewater $^{87}Sr/^{86}Sr$ ratios trend towards marine values, (2) the Upper Ordovician shale section characterized by $^{87}Sr/^{86}Sr$ ratios that are more radiogenic than the marine curve, and (3) the Middle Ordovician limestone section, which has variable but radiogenic $^{87}Sr/^{86}Sr$ values.

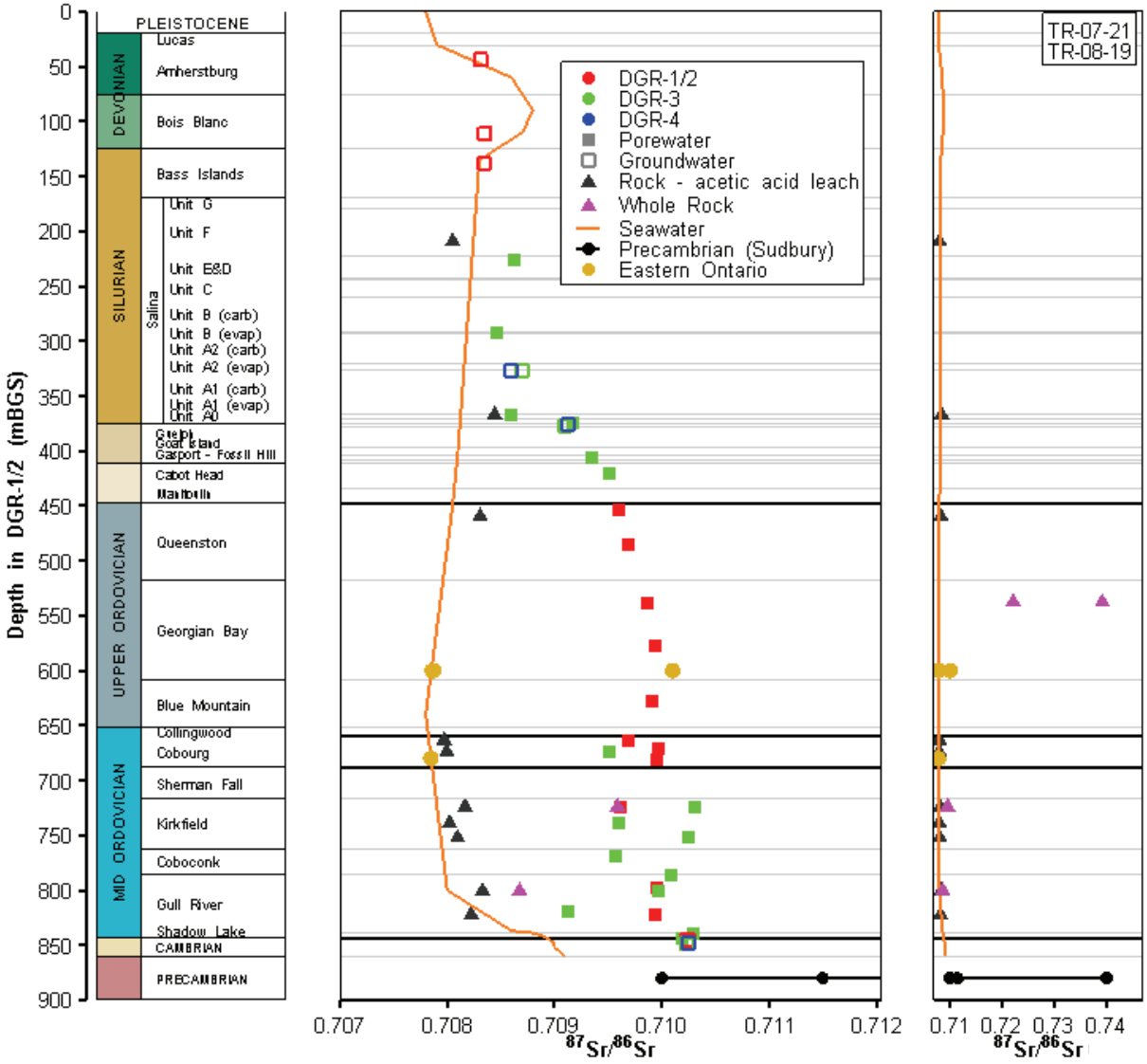

Figure 4.65: Profiles of Sr Isotopes in DGR Groundwater, Porewater and Rocks together with Seawater Strontium Isotope Curve from Veizer (1989), Precambrian Values from Sudbury (Frape et al. 1984)

Devonian and Silurian groundwater and porewater:

The Devonian groundwater Sr isotope ratio is the same as the seawater isotope signature (Veizer 1989), which is consistent with carbonate dissolution by shallow circulating groundwater. Below approximately 200 mBGS, the groundwater and porewater $^{87}Sr/^{86}Sr$ ratios increase through the Silurian section to the strongly radiogenic values in the Upper Ordovician shales. Both Silurian groundwater samples from the Salina Upper A1 Unit and the Guelph Formation plot close to or on this porewater trend, as is observed for the stable isotopes and solutes.

Ordovician shale porewater:

The porewater values measured in the Ordovician shales are significantly enriched in radiogenic ^{87}Sr in comparison with the marine curve, and are not in equilibrium with the minor labile carbonate component of this section. Here, any original marine signature in these porewaters has likely been modified by the uptake of radiogenic ^{87}Sr. Two potential sources of ^{87}Sr are (1) the leaching of the Precambrian-aged siliciclastic component weathered from the Shield, and (2) the in-growth of ^{87}Sr from the decay of ^{87}Rb associated with the high K content of these formations. The high K content is due to the high aluminosilicate content of the shales (Figure 3.6). The two whole-rock analyses for the Georgian Bay Formation (Figure 4.65 and in expanded scale plot) show that a significant source of ^{87}Sr exists in these shales.

Accumulation of radiogenic ^{87}Sr in the shales since the Paleozoic is enhanced by the high Rb concentrations from which it is ingrown, and the comparatively low Sr concentrations with which it is diluted (Figure 4.66). The overlain porewater $^{87}Sr/^{86}Sr$ profile shows this enrichment associated with the high Rb and low Sr shales. This illustrates that the radiogenic $^{87}Sr/^{86}Sr$ porewater ratios can be supported by enrichments in the parent Rb concentration. It is likely then, that in situ contributions of ^{87}Sr from possible leaching of ^{87}Sr from siliciclastics and decay of ^{87}Rb over Paleozoic time have contributed to the radiogenic $^{87}Sr/^{86}Sr$ ratios measured in the shale porewater.

Middle Ordovician limestone porewater:

The porewater from the Ordovician limestones, like the Ordovician shales, is enriched in radiogenic ^{87}Sr. However, the limestone porewater values are considerably more variable than those for the shales (Figure 4.65). The underlying Cambrian porewater samples fall very close to the two Cambrian groundwater samples, also with an enriched $^{87}Sr/^{86}Sr$ signature.

Both autochthonous and allochthonous ^{87}Sr sources can be considered in assessing the origin of the observed enrichment in these porewaters. In considering an autochthonous origin, the low Rb contents of the limestones would preclude a significant change in the $^{87}Sr/^{86}Sr$ ratio of the carbonate rocks via the process of ^{87}Rb decay alone. It is possible that preferential leaching of ingrown loosely-bound ^{87}Sr from the siliciclastic component of the argillaceous carbonates is the source of the ^{87}Sr enrichment in the Middle Ordovician limestone porewater (Figure 3.6) and that the porewater signatures represent a combination of both the siliciclastic $^{87}Sr/^{86}Sr$ and the carbonate (marine) $^{87}Sr/^{86}Sr$.

The Middle Ordovician limestone porewater is not in isotopic equilibrium with either the carbonate rock fraction or the siliciclastic rock fraction (nor are the Ordovician shale porewaters) which indicates that both sources could have contributed to the porewater $^{87}Sr/^{86}Sr$ ratios to varying degrees. An allochthonous source of radiogenic $^{87}Sr/^{86}Sr$ observed in the limestones may originate in the underlying crystalline Precambrian rocks. Highly radiogenic $^{87}Sr/^{86}Sr$ has been measured in Shield brines from Sudbury (Figure 4.65; Frape et al. 1984), with values as

high as 0.74. Movement of such Sr from the basement into these overlying strata can account for at least some of these enrichments. This is consistent with the elevated deuterium excess (Figure 4.64) and depleted $\delta^{18}O$ values (Figure 4.61) noted in the Middle Ordovician limestones, which both trend towards Shield brine values.

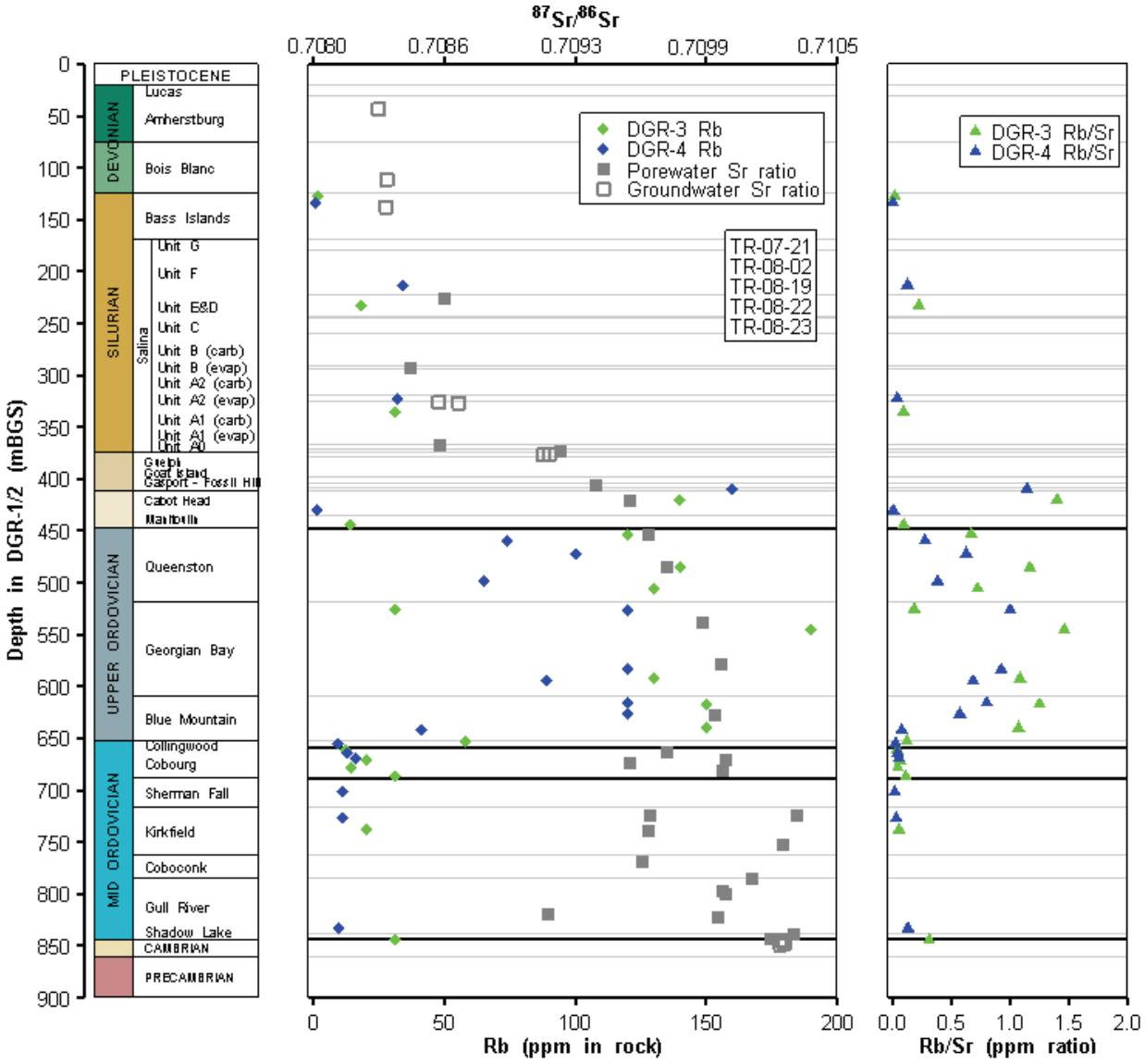

Figure 4.66: Profiles of Rb Concentration in DGR Rocks (lower x-axis) with $^{87}Sr/^{86}Sr$ in Porewater (Upper X-Axis) and the Rb/Sr ppm Ratio in DGR-3 and DGR-4 Rocks

4.6.7 CH_4 and CO_2 Gases

4.6.7.1 Methane

Methane concentrations in DGR-2, DGR-3 and DGR-4 cores core were measured in samples from Devonian carbonate formations down to the Cambrian (Figure 4.67). The amount of gas extracted from each rock core sample was normalized to water content to calculate a gas concentration. However, methane may be associated with organic carbon in the rocks, which is discussed further in Section 4.6.7.3. The normalization assumes all of the gas is dissolved in the porewater, which may not be the case. Therefore, these concentrations are considered to be apparent concentrations.

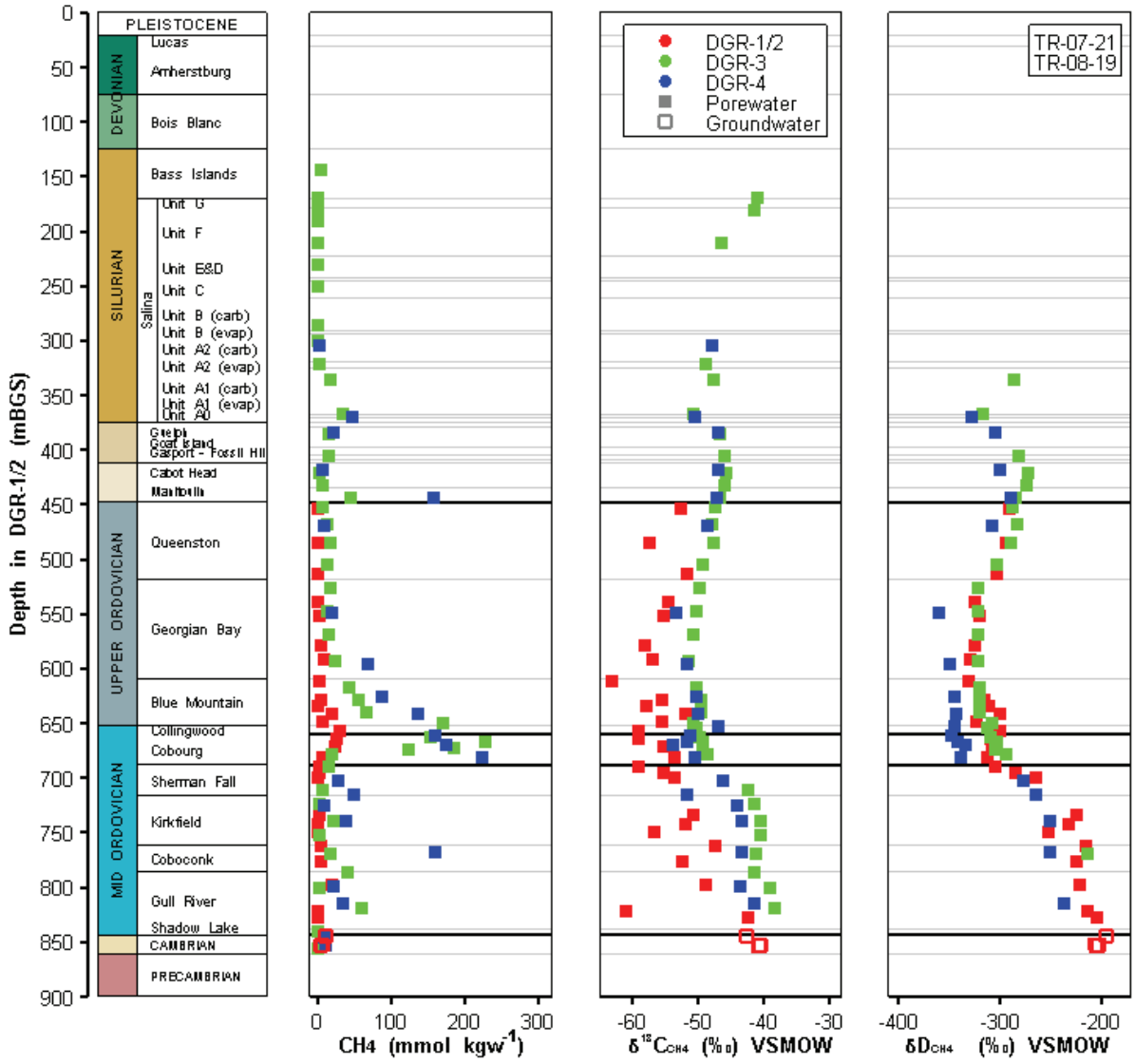

Figure 4.67: Profiles of CH_4 Apparent Porewater and Groundwater Concentrations and $\delta^{13}C$ and δD in CH_4 in DGR Boreholes

The DGR-2 results showed that the apparent methane concentrations increased from the Queenston Formation to the bottom of the Collingwood Member. The maximum methane concentration was measured in the Collingwood Member of the Cobourg Formation. Apparent methane concentrations in DGR-3 and DGR-4 increased from the Queenston Formation to a maximum in the Cobourg Formation, and one relatively high apparent methane concentration was observed in the Manitoulin Formation.

Relatively high apparent concentrations were also observed in the Coboconk and Gull River formations. Not shown on Figure 4.67, in order to maintain the ability to perceive trends, are two very high values of CH_4 (1210 and 460 mmol/kgw in the Collingwood and Cobourg, respectively). Although the magnitude of the methane concentrations was lower in DGR-2 (samples collected on-line by trapping on charcoal) than in DGR-3/DGR-4 (degassing from uncrushed core in IsoJars), the patterns were similar.

Isotope ratios are, perhaps, better indicators of methane production and movement at the DGR site because they do not rely on assumptions of gas saturation. $\delta^{13}C$ and δD isotope analyses of methane were carried out on the same samples from which the concentrations were obtained (Figure 4.67). The $\delta^{13}C$ and δD depth profiles from DGR-2 show depletion in the isotope signatures from the Cabot Head Formation to the top of the Blue Mountain Formation. Below the Cobourg Formation, the isotope signatures generally become more enriched with depth. The same general pattern is observed in DGR-3 and DGR-4.

A cross plot of $\delta^{13}C$ and δD in methane for all of the DGR cores (Figure 4.68) shows a trend from biogenic methane production at relatively shallower depths to methane production by thermocatalytic cracking of hydrocarbons at relatively greater depths. The boundaries for the biogenic and thermocatalytic fields in Figure 4.68 were taken from Whiticar (1999). Porewater methane from the Silurian formations down to the Sherman Fall Formation appears to have been generated biogenically. Although the Sherman Fall results could be a mix of thermocatalytic and biogenic methane. Below the Sherman Fall the methane results are dominantly thermocatalytic. The high methane concentrations in the Blue Mountain and Collingwood/Cobourg are considered to be derived from biogenic processes.

The isotope signatures (Figure 4.67) have a steep gradient near 700 mBGS between the biogenic and thermogenic isotope signatures. This steep gradient is observed below the high methane concentrations observed in the Collingwood Member and upper Cobourg Formation. The gradient is discussed further in the following section after methane saturation calculations are carried out in Section 4.6.7.3.

The ^{13}C and D isotopes can be used to examine methane transport; however, the data cannot be used to determine the age of the methane. Therefore, no insight can be gained from these data regarding the timing of the methane production.

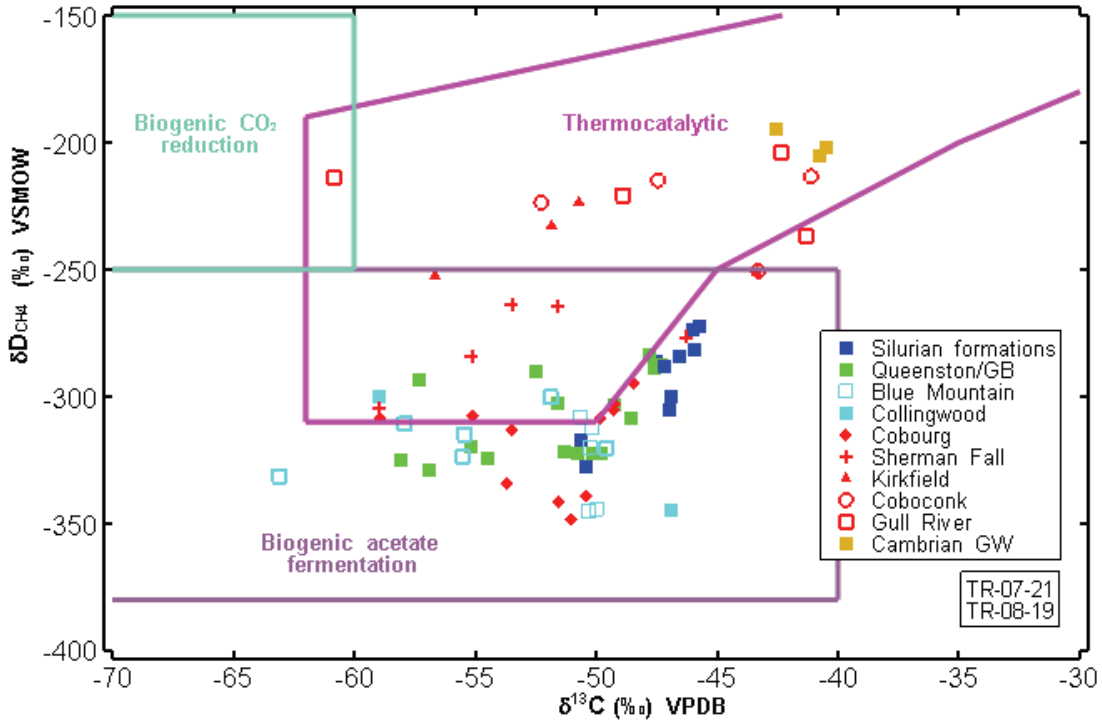

Figure 4.68: Cross Plot of δD vs $\delta^{13}C$ of Methane from DGR Porewater

4.6.7.2 Carbon Dioxide

Carbon dioxide concentrations and $\delta^{13}C$ values were measured on DGR core porewater and groundwater samples (TR-07-21 and TR-08-19). The carbon dioxide concentrations from DGR cores were also normalized to porewater mass. The error bars in Figure 4.69 are the standard deviation for each sample, calculated using the replicate analytical results. As with the methane, this assumes that all of the carbon dioxide is dissolved in the porewater; therefore, the carbon dioxide concentrations are apparent concentrations. Additionally the carbon dioxide results presented represent a maximum (or near maximum) concentration, since vacuum distillation likely converts almost all of the porewater carbonate species (H_2CO_3, HCO_3^- and CO_3^{2-}) to carbon dioxide. Although there is scatter in the carbon dioxide concentration and $\delta^{13}C$ isotope data, the results from DGR-2, DGR-3 and DGR-4 show the same general patterns (Figure 4.69).

The porewater $\delta^{13}C$ results show values close to the measured groundwater DIC $\delta^{13}C$ values at the same depth (Figure 4.69). The $\delta^{13}C$ in carbon dioxide is enriched in the lower part of the Georgian Bay Formation and in the Blue Mountain Formation, which suggests biological methanogenesis. Inorganic exchange or reaction with the carbonate rock is ruled out as such processes cannot produce such strong enrichments in this setting. It is noteworthy that this zone of $\delta^{13}C$ enrichment occurs above the zone of higher CO_2 and CH_4 concentrations. This suggests that the methane production may have occurred at this higher zone and accumulated in the deeper (high concentration) zone which is characterized by a high organic carbon content.

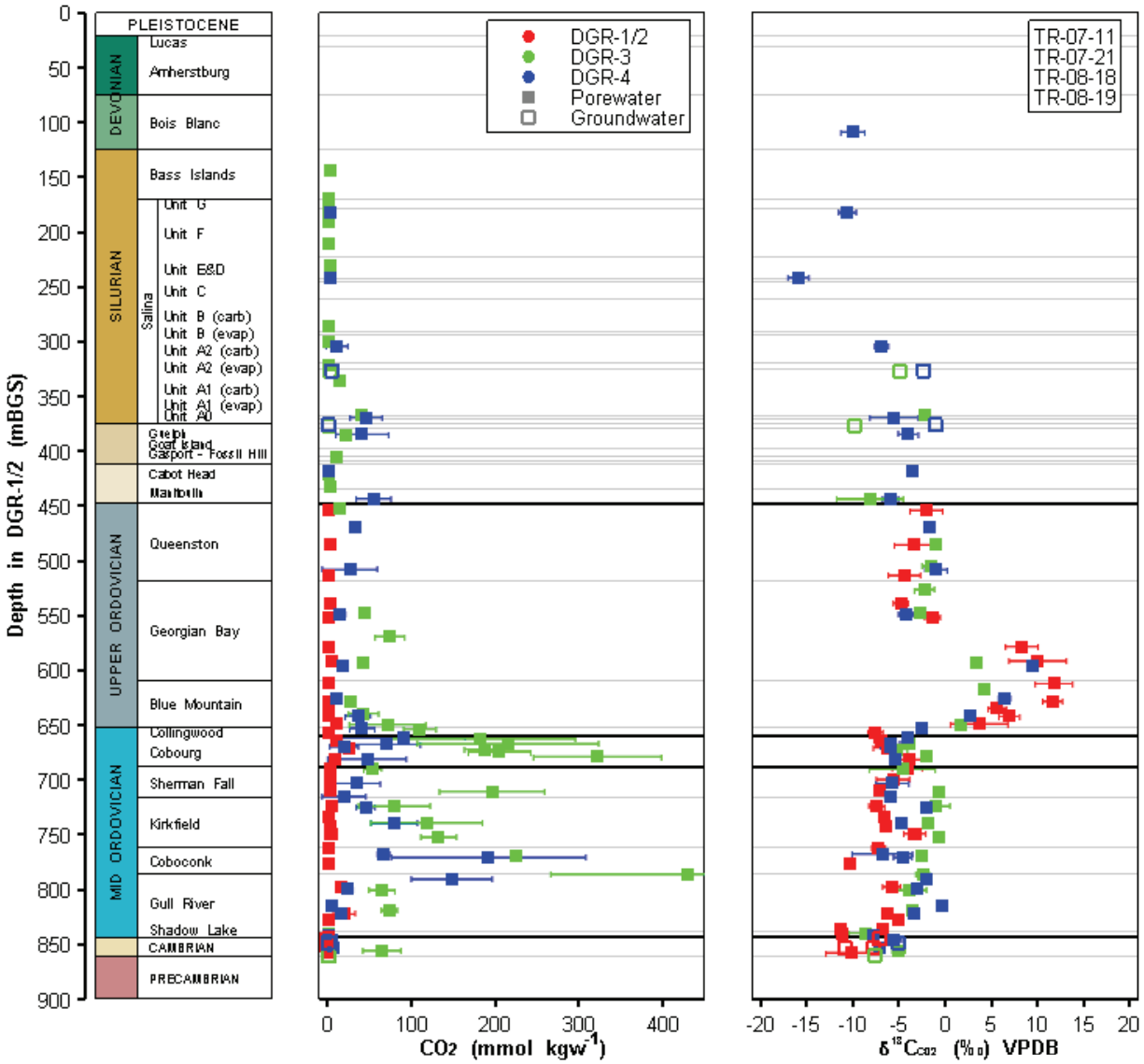

Figure 4.69: Profiles of CO_2 Apparent Porewater and Groundwater Concentrations and $\delta^{13}C$ in CO_2 in DGR Boreholes

4.6.7.3 Calculated Gas Saturations

The methane and carbon dioxide concentrations measured in the porewater were calculated by dividing the masses of methane and carbon dioxide released from a rock sample by the amount of water released from the same sample (TR-07-21, TR-08-19). Although this calculation assumes that all of the gas is dissolved in the porewater, this methodology allows a convenient comparison of the apparent porewater methane and carbon dioxide concentrations relative to the gas solubility. Apparent methane and carbon dioxide concentrations that exceed the solubility limits suggest a separate gas phase is present.

The thermodynamic-based model developed by Duan and Mao (2006) calculates the solubility

of methane and Duan and Sun (2003) calculates the solubility of carbon dioxide at a range of solute concentrations, water temperatures and water pressures. Due to the complexity of ion-ion interactions at high solute concentrations, the two models assume a binary solution, in this case NaCl.

Methane and carbon dioxide solubility curves were calculated using the Duan and Mao (2006) and Duan and Sun (2003) models at a constant temperature of 25°C and three pressures – 2, 6 and 11 MPa. These pressures were measured in the Ordovician shales, the Cobourg Formation and the Cambrian, through hydraulic testing and groundwater monitoring using the Westbay systems at the Bruce nuclear site (Section 4.12.2).

Both models require solute concentrations for binary salts (i.e., NaCl). Since the porewater at the Bruce nuclear site contains more than just Na and Cl, an equivalent NaCl concentration was calculated by two methods. The first method summed together all of the cations and anions and divided the result by two. This method assumes all of the ions in solution have the same ion-gas interaction as Na and Cl have with methane. The type of anion, for example chloride or sulphate, has a small effect on the solubility of methane in water; however, methane is more soluble with divalent cations than monovalent cations (Stoessell and Byrne 1982). This method assumes all cations are Na ions, which likely underestimates the solubility of methane because divalent calcium and magnesium are assumed to have the same interaction with methane as monovalent sodium.

The second method used to estimate the equivalent NaCl concentration summed together the porewater Na and Cl concentrations and divided by two. This method significantly underestimates the actual porewater solute concentrations, whereas the first method overestimated the equivalent NaCl concentration. A comparison of the results of the calculated gas saturations using the equivalent NaCl concentrations calculated by both methods was presented in TR-08-34. The comparison showed the method used to estimate the NaCl concentration had little effect on the assessment of gas saturation. Subsequent discussions refer to Figures 4.70 to 4.73, which present the first method for calculating the equivalent NaCl concentration.

The methane solubility curves for NaCl concentrations were calculated for concentrations from 0 to 6 molal NaCl for pressures of 2, 6, and 11 MPa (Figures 4.70 and 4.71). The Duan and Mao (2006) model was only applicable to a NaCl concentration of 6 molal for methane solubility. The dashed lines presented in Figures 4.70 and 4.71 are extrapolations of the calculated methane solubilities at each pressure. The solubility curves may not be applicable at these high molal concentrations due to ion-ion and ion-gas interactions.

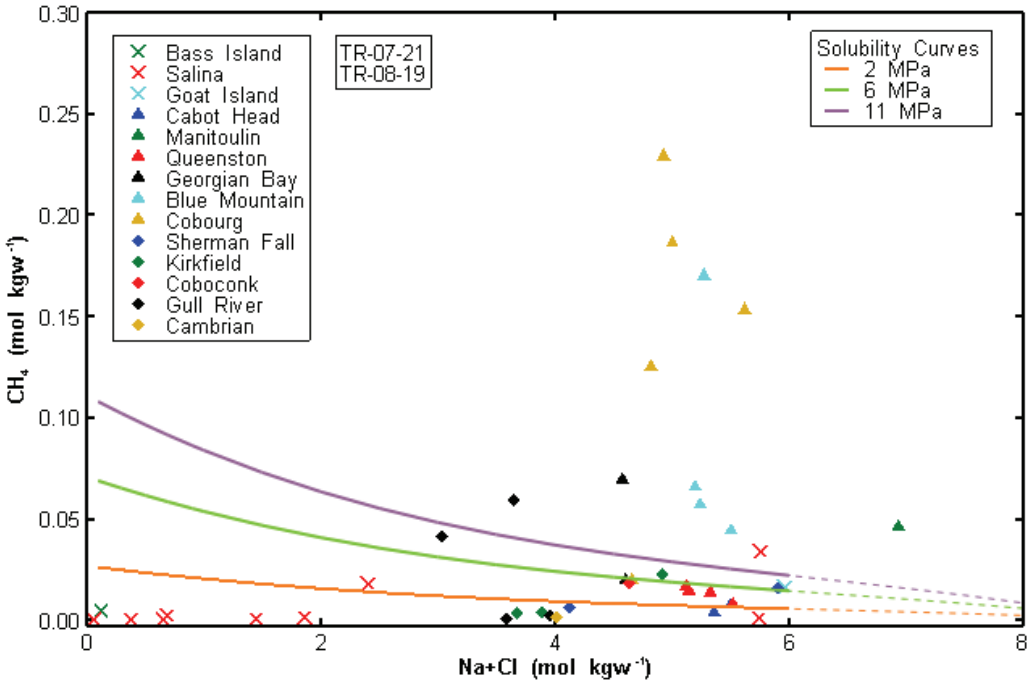

Figure 4.70: Cross Plot of Apparent CH_4 and Na+Cl Porewater Concentrations Compared to Calculated CH_4 Solubility in DGR-3

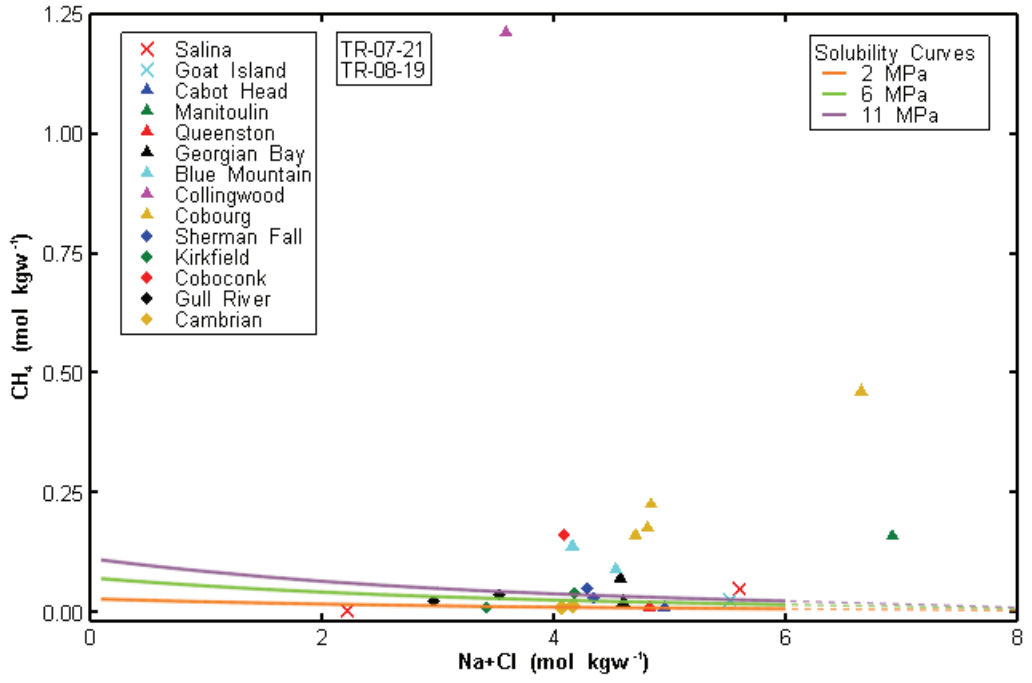

Figure 4.71: Cross Plot of Apparent CH_4 and Na+Cl Porewater Concentrations Compared to Calculated CH_4 Solubility in DGR-4

Considering the errors in analysis and solubility calculations, it is difficult to confidently identify samples with methane concentrations below the 11 MPa solubility curve as super-saturated for this initial analysis. Small errors in the thermodynamic model or laboratory analyses could move the samples located near the 6 MPa line below the 2 MPa line. Even with this consideration, there are several samples that plot above the methane solubility line. Methane concentrations above the 11 MPa solubility curve are primarily from the Collingwood/Cobourg and Blue Mountain formations, with one to two samples from each of the Salina A1 Unit, Manitoulin, Georgian Bay, Kirkfield and Gull River formations.

These results suggest a methane gas phase could be present in the Salina A1 Unit, the Manitoulin, the Georgian Bay, Blue Mountain, Collingwood, Cobourg, Coboconk, Sherman Fall and Kirkfield units/formations. This analysis does not account for methane adsorbed to organic carbon in the formations, however, which could result in an apparent methane concentration that is supersaturated with respect to the solubility limit of the porewater and the conclusion that a gas phase is present. However, methane is still likely present as a gas phase in the Collingwood Member and possibly the Cobourg and Blue Mountain formations.

The methane saturation concentrations and the steep methane isotope gradient shown in Figure 4.67 can be used to gain general insight into gas production and transport in the Ordovician rocks. If a separate methane gas phase does not exist, methane is not adsorbed to the organic carbon, and the pores are saturated with porewater, then the high methane concentration and methane isotope ratio gradients observed in Figure 4.67 can only be maintained by on-going or relatively recent methane production, since diffusive transport would decrease the peak methane concentrations.

The high methane concentration and methane isotope ratio gradients could also be maintained if the methane is adsorbed onto solid phase organic matter in the rock. If the methane is adsorbed, then a transport pathway may not be available and the concentration and isotope gradients shown in Figure 4.67 may not exist, and diffusion-driven transport may not be occurring.

Methane adsorption to organic carbon may be significant where high total organic carbon is present (Figure 3.15). High methane and total organic carbon content are co-located in the Manitoulin, Blue Mountain, Cobourg and Coboconk Formations. The high methane concentration in the Blue Mountain Formation (Figure 4.67) coincides with a high total organic carbon concentration in the rock (Figure 3.15). The high methane concentration could be due to methane released from solid organic carbon during laboratory analysis. Additionally, methane may be released from hydrocarbons in the pore space, where hydrocarbons are present. These two potential reservoirs of methane (solid organic carbon and hydrocarbons) can have a significant impact on the interpretation of the methane concentration and isotope data, which prevents conclusions regarding the storage of methane in the rocks (gas phase, dissolved in porewater or adsorbed) and the transport of methane.

Carbon dioxide solubility curves were calculated using the Duan and Sun (2003) model at a constant temperature of 25°C and three pressures – 2, 6 and 11 MPa (Figures 4.72 and 4.73). The equivalent NaCl concentrations used for this model were calculated using the first method described above, which summed together all of the anions and cations and divided the total by two.

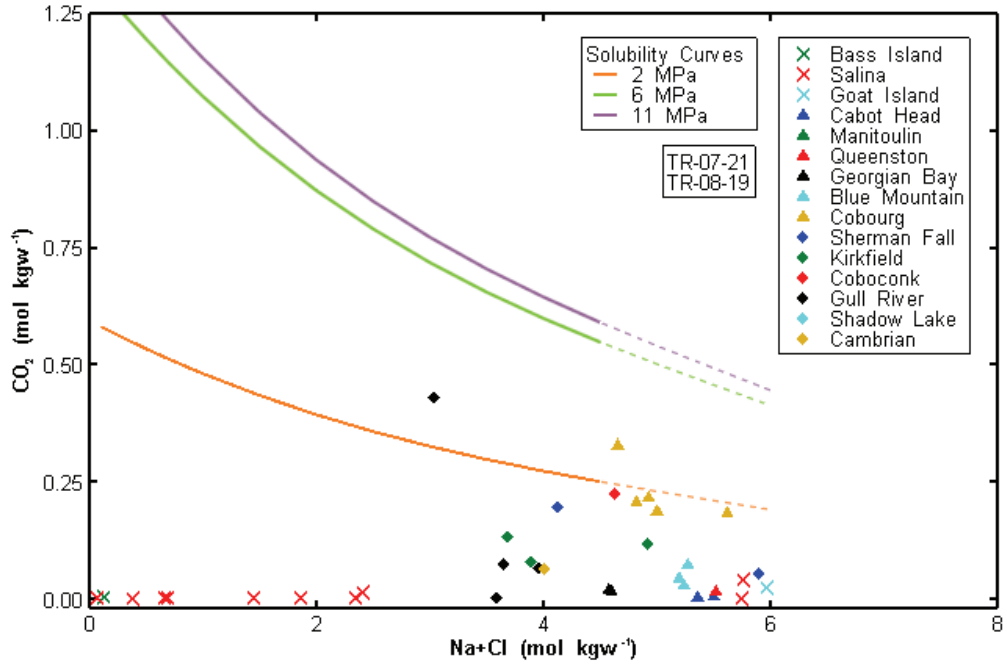

Figure 4.72: Cross Plot of Apparent CO_2 and Na+Cl Porewater Concentrations Compared to Calculated CO_2 Solubility in DGR-3

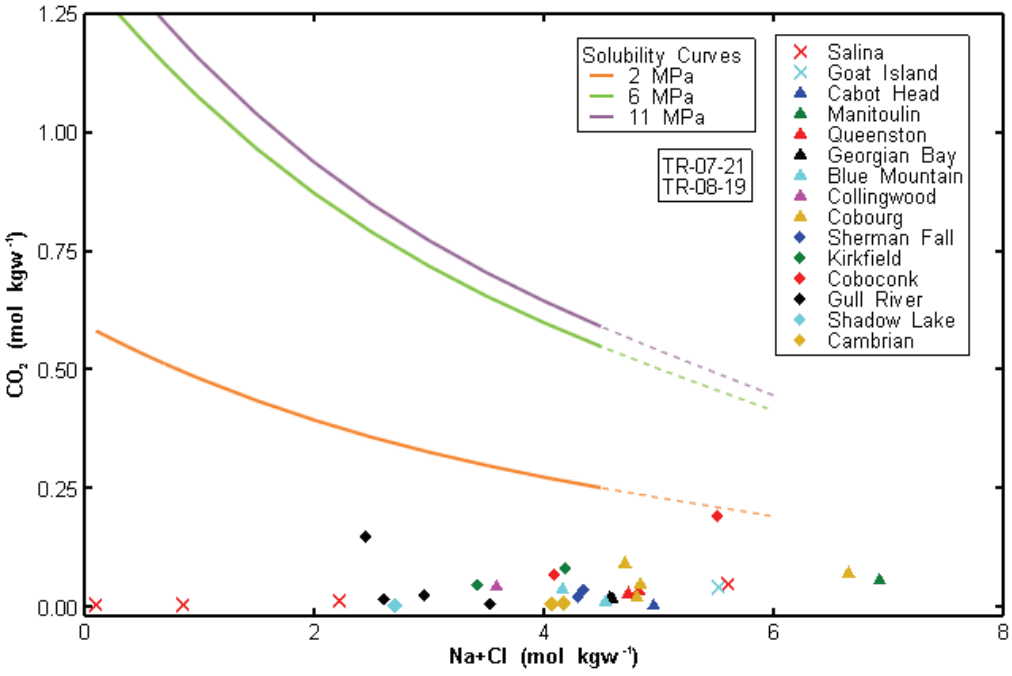

Figure 4.73: Cross Plot of Apparent CO_2 and Na+Cl Porewater Concentrations Compared to Calculated CO_2 Solubility in DGR-4

The Duan and Sun (2003) carbon dioxide model was only presented for NaCl concentrations from 0 to 4.5 molal. The dashed lines in Figure 4.72 and 4.73 represent the extrapolation of the thermodynamic model up to 6 molal NaCl. Molal NaCl concentrations were calculated as the summation of all of the anions and cations as described above.

Comparison of the carbon dioxide concentrations to the solubility limits show carbon dioxide has not exceeded the solubility limits. Therefore, a separate carbon dioxide gas phase is not likely present.

4.6.8 Estimated Porewater pH and Redox Conditions

Porewater was extracted at high temperature and under conditions that allow oxidation and could alter measurements of master variables of pH and redox potential. Therefore, pH and redox potential of these waters are determined by indirect estimation, using PHREEQC, for their use in hydrogeochemical modelling scenarios. PHREEQC calculations were used to estimate values of pH. The CO_2 obtained from the rock core samples was added to the PHREEQC calculations, forcing calcite to have a saturation index of 0.0.

The pH values were calculated for DGR-2 porewater using porewater major ion and porewater carbon dioxide concentration data from TR-07-21. The calculations were carried out in PHREEQC by inputting the major ion and carbon dioxide concentrations for each sample. Additionally, calcite was assumed to be in equilibrium (SI = 0.0) with the porewater, although it is not known if that is the case. The pH was calculated using the charge balance method in PHREEQC. The calculated pH values for the DGR-2 porewater are shown on Figure 4.74, and are in the pH range 5.0 – 6.2. By comparison, the artesian Cambrian brine of DGR-2 was measured on two occasions as having a pH = 6.5.

The calculated pH values are subject to errors associated with determining the CO_2 concentration. CO_2 may be liberated from hydrocarbons during vacuum distillation, which may erroneously raise the measured porewater CO_2 concentrations. Also, carbon dioxide measurements likely represent a maximum concentration (Section 4.6.7.2). Using maximum CO_2 concentrations would lower the calculated pH, which is what was observed (Figure 4.74). The pH calculations in PHREEQC were carried out by a charge balance method and are subject to errors in the major ion concentrations as well as with the assumption of calcite equilibria. Any errors associated with the estimation of water content will also be carried forward since water content is used to calculate the major ion and CO_2 concentrations. The porewater may not be in equilibrium with calcite, (i.e., the porewater saturation index may not be 0.0), it could be supersaturated with respect to calcite (saturation index >0) or undersaturated with respect to calcite (saturation index <0), or the porewater may be in equilibrium with another carbonate mineral such as a Mg-calcite, aragonite or dolomite.

To examine the potential error associated with pH calculations, the CO_2 concentration, major ion concentrations, and calcite saturation index were changed for the Cobourg Formation porewater. The CO_2 concentrations were increased and decreased by an order of magnitude, the major ion concentrations were adjusted by 20%, or the calcite saturation index was adjusted ± 0.3. The results of these adjustments are not shown here, but the results show the calculated pH values have a range of error of approximately 1 pH unit, particularly when errors in CO_2 concentration and carbonate equilibria are considered together. Therefore, the pH values shown in Figure 4.74 should be considered to have a range of +/- 1 pH unit. For the Ordovician shales, the average pH is 5.5 +/- 1, the Cobourg to Kirkfield formations have an average pH of 5.5 +/- 1, the Coboconk to Shadow Lake have an average pH of 5.5 +/- 1. Although pH values

were calculated for the Cambrian, the measured pH values during OGW sampling should be used (Table 4.7). The calculated pH values should be considered estimates of porewater pH. For this reason, pH calculations were only carried out for DGR-2. That notwithstanding, the high yields of CO_2 from the vacuum distillation, and the low porewater yields, particularly for the limestones, indicate that the solution pH must be less than neutral. Further, calculated pH values for the Cambrian and Shadow Lake samples are within approximately 0.6 pH units of the measured pH of the Cambrian groundwater, suggesting that the calculated pH values are reasonable estimates.

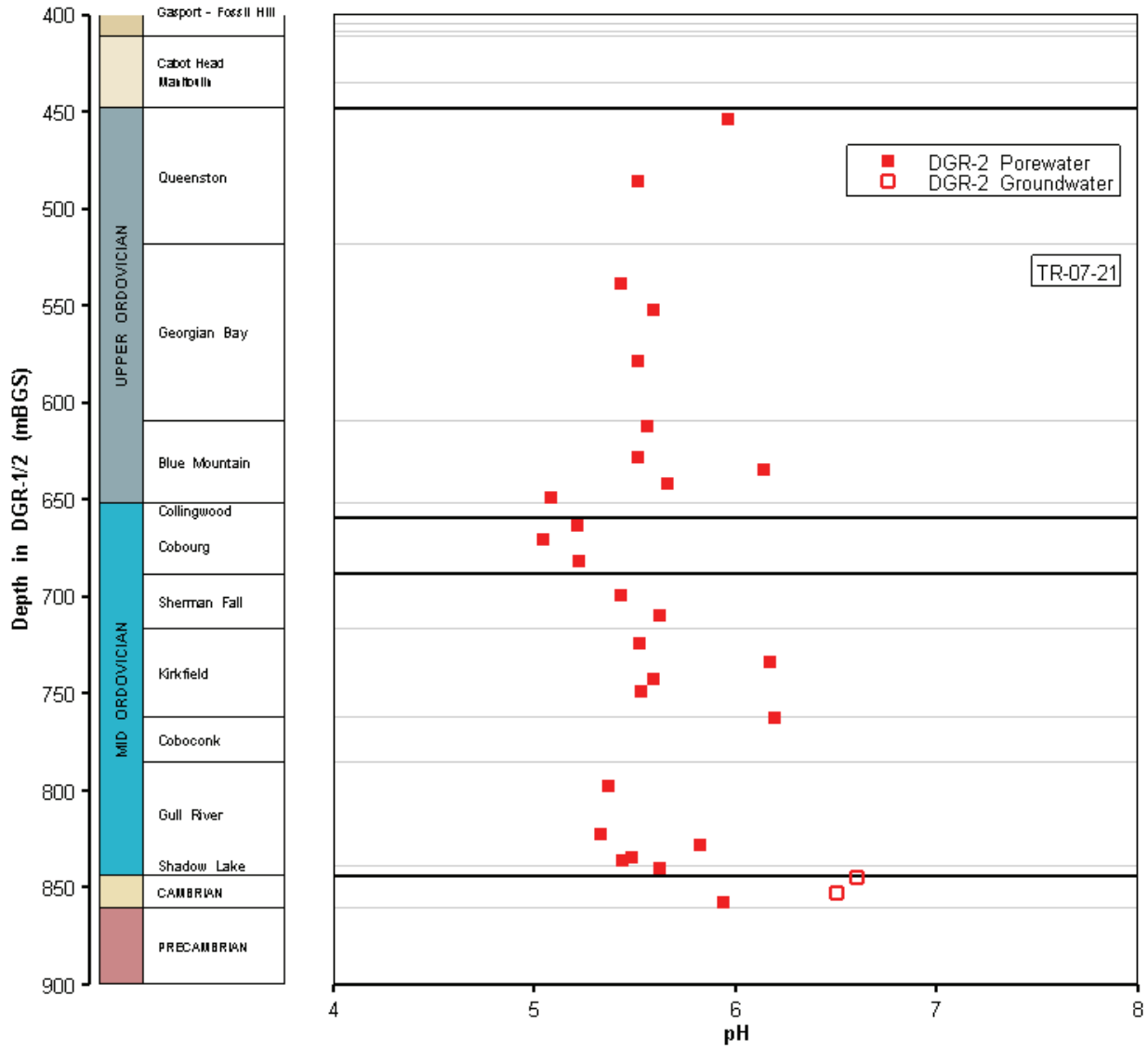

Figure 4.74: Profile of Measured Groundwater pH and Calculated Porewater pH from Measured CO_2 in DGR-2

It is also not possible to determine directly the redox state of porewater from an analysis of their composition due to the method of extraction. However, available mineralogical and hydrogeochemical evidence, points to the conclusion that the Paleozoic sequence of rocks beneath the Bruce nuclear site is an anoxic redox environment that is classifiable as either 'sulphidic', i.e., $H_2S \geq 1$ µM, or 'methanic' ($H_2S < 1$ µM) in the terminology of Berner (1981). Because pyrite is ubiquitous in the DGR Paleozoic sequence, it is reasonable to assume that the S(VI) - S(II-) redox potential is likely to provide a lower limit of Eh values that can be employed in geochemical modeling.

Langmuir (1997, p. 456) provides a equation to calculate Eh estimate based upon values of ∑S(aq) and ∑Fe(aq):

$$Fe^{2+} + 2SO_4^{2-} + 16H^+ + 14e^- \rightarrow FeS_2 + 8H_2O \quad (4.9)$$

for which:

$$Eh(V) = 0.355 + 0.00423\log\,[Fe^{2+}][SO_4^{2-}]^2[H^+]^{16}. \quad (4.10)$$

At a pH of 6.0, which is the estimated pH for equilibrium with calcite from PHREEQC simulations, and with ∑S(aq) = 0.03 mol/kg and ∑Fe(aq) = $1x10^{-4}$ mol/kg based on groundwater sampling of deep DGR boreholes, Eh = -0.08 V (or pE = -1.2). Equation 4.10 is sensitive to errors in concentration, particularly pH. Therefore, the basis of redox state of the porewater is mineralogical, e.g. the presence of pyrite or iron staining, rather than calculated pH and only broad ranges of redox state, such as methanogenic or sulphidic, are used.

4.6.9 Helium

He profiles have been shown to be reliable tracers with respect to the understanding of the mobility of dissolved gases in low-permeability formations (Hendry et al. 2005, Rübel et al. 2002) and, therefore, the potential for formations to retain contaminants. However, the total concentration of He in pore fluids is very difficult to measure accurately in the presence of a free gas phase, as may exist in parts of the DGR Paleozoic rock column (see Section 4.3.3). Normalizing He concentrations to pore fluid requires a precise measurement of both the liquid volume and any separate gas phase that exists. The low solubility of He in brines makes this an important measurement in establishing the pore-scale partial pressure of He that would drive diffusion.

The different sources of the isotopes ^3He and ^4He, however, provide insights to the generation and movement of He independent of its concentration. Therefore, this discussion is limited to the measured isotopic ratios of $^3He/^4He$ in DGR samples. This ratio is typically normalized to the ratio in air ($^3He/^4He$ = 1.4E–6) and so expressed as xRa = [$^3He/^4He$]sample/[$^3He/^4He$]air, as shown in Figure 4.75. Atmospheric He has a ratio of 1. Decreases in this ratio reflect incorporation of He produced in the subsurface, also called geogenic He, is produced from radiogenic sources, which can have variable ratios of these isotopes. Underlying the Bruce nuclear site, the shale formations with high U and Th will be enriched in ^4He from alpha decay. Shield rocks, with high U and Th, will also produce abundant ^4He but will also produce ^3He from Li fission. These distinctly different geological terrains then provide contrasting source terms for He at this site.

The DGR-2 profile is reproduced by the DGR-3 and DGR-4 profile. The remarkably good overlay of the two profiles (Figure 4.75) adds confidence to the interpretation that the lower Cobourg/upper Sherman Fall is characterized by exceedingly low gas permeability. This is consistent with the low-diffusivity zone observed in the methane isotope profile (see Section 4.6.7.1) and the very low field measurements of hydraulic conductivity at this depth in DGR boreholes (see Figure 4.88).

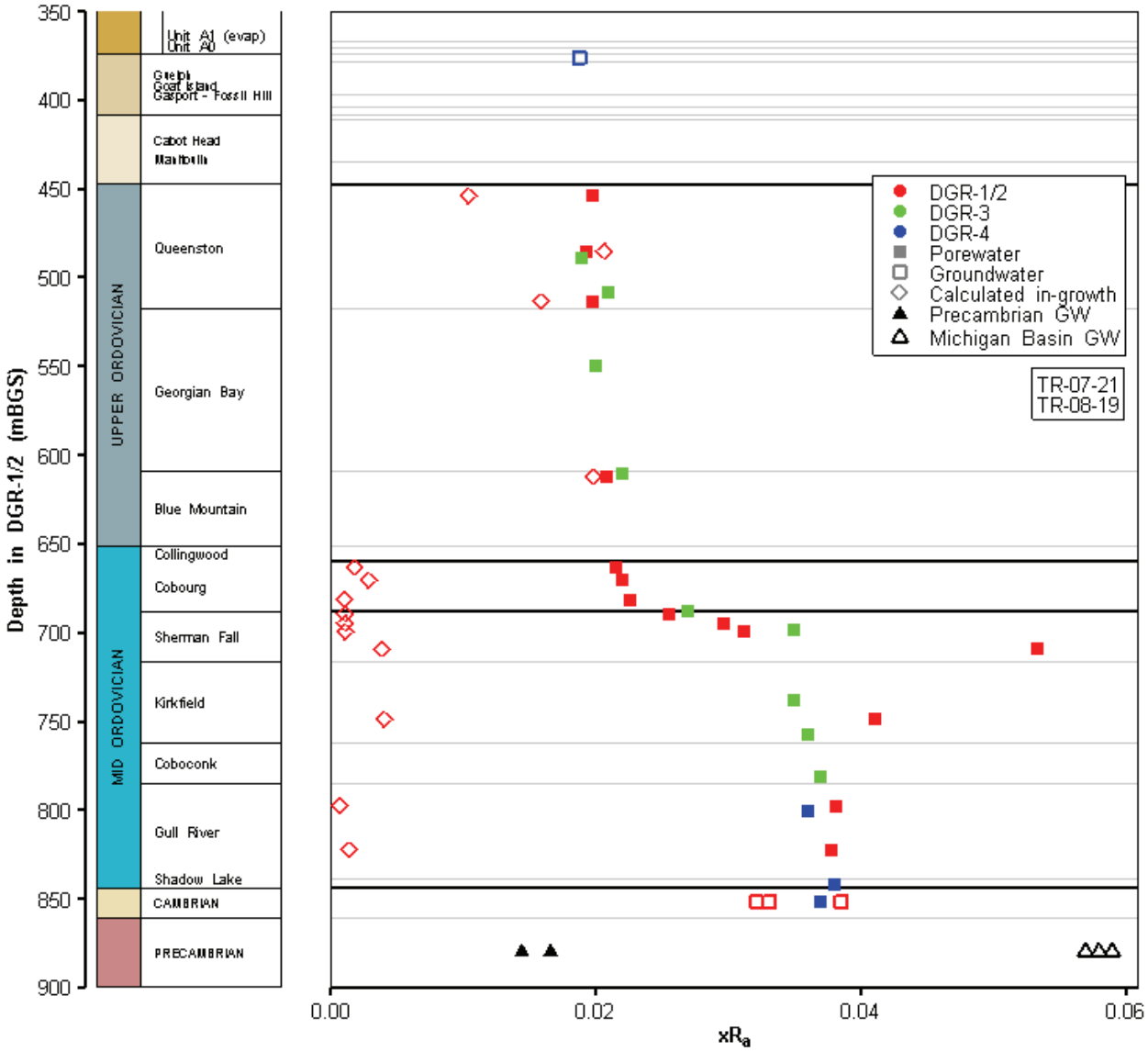

Note: Values for the Precambrian (Kotzer et al. 1998) and the Michigan Basin (Ma et al. 2009) shown for reference.

Figure 4.75: Profile of Ratio $^{3}He/^{4}He$ in DGR Porewater and Groundwater Normalized to He in Air (xRa) Together with Calculated He Isotope Ratios

The $^{3}He/^{4}He$ ratio profile brings a supporting perspective that is independent of the normalization uncertainties that affect the He concentration data. Consistent with the CH_4

isotope ratios, the $^{3}He/^{4}He$ ratio suggests a two-component source for He in this section. The Ordovician shales have a relatively uniform ratio close to xRa ~ 0.02, which transitions over less than about 50 m to a higher $^{3}He/^{4}He$ ratio (xRa ~ 0.04) in the deeper limestones. This value for the Ordovician limestone porewater is within the range reported for Cambrian gas field He in southwestern Ontario by Sherwood Lollar et al. (1994; mean xRa = 0.035). Further, this transition is also found at the base of the Cobourg, providing further evidence for a diffusional barrier at this horizon. The $^{3}He/^{4}He$ gradient at the base of the Cobourg is similar to that observed in the methane isotopic data (see Figure 4.67), as well as that suggested by the gas entry pressure data (Section 4.3.6).

The production of ^{3}He and ^{4}He can be used to examine solute residence time. Geogenic He is produced by ingrowth of radiogenic ^{4}He from the decay of U and Th, while the ingrowth of ^{3}He arises from neutron-induced fission of ^{6}Li.

$$^{6}Li + n \rightarrow \alpha + {}^{3}H \rightarrow {}^{4}He + {}^{3}He + \beta^{-} \quad (4.11)$$

The concentrations and ratios of these two He isotopes can be used to constrain age in very old groundwater and porewater systems. Note that unlike ^{36}Cl and ^{129}I which are radioactive isotopes produced radiogenically, He is not radioactive and so no secular equilibrium between radiogenic production and decay is established.

Concentrations of Li, U and Th in the DGR rocks are shown in Figure 4.76. Although the pore fluid He concentrations may not be determined due to the requirement of precise measurements of both the liquid volume and any separate gas phase that exists (see above), the He concentration can be determined for a whole rock sample (cc He STP/g of rock). Accordingly, the concentrations do not necessarily reflect the porewater concentration profile that would drive diffusion through connected porosity. However, the measured profiles present total He accumulation in these rocks that can be used to constrain age, depending on how easily He can leave the system. The loss of He from rock between the time the cores were sampled and analysed were accounted for in DGR core samples (TR-08-38). The He loss was not significant for most samples and the data presented here include the estimated He loss.

Figure 4.77 presents the He concentration normalized to rock mass. Due to the high concentrations for the Guelph Formation and Cambrian rocks the data are not plotted to scale in order to maintain a suitable plotting resolution. The concentrations for these two samples are plotted below the data points.

The accumulations presented in Figure 4.77 are minimum amounts for the radiogenic production of He since He may have been removed from the sedimentary formations. The He concentration profiles for DGR-2 and DGR-3 are similar and closely resemble the U concentration profile, showing higher concentrations in the Upper Ordovician shales and lower concentrations in the Middle Ordovician limestones. This close affiliation of He concentration with the primary production term (^{238}U is the principal source of alpha decay and ^{4}He production, whereas ^{232}Th accounts for about one quarter of radiogenic He) suggests that the system has remained relatively closed. If so, then the accumulated He can be used to constrain age. He will continue to accumulate unless loss by diffusion or advection under open system conditions occurs.

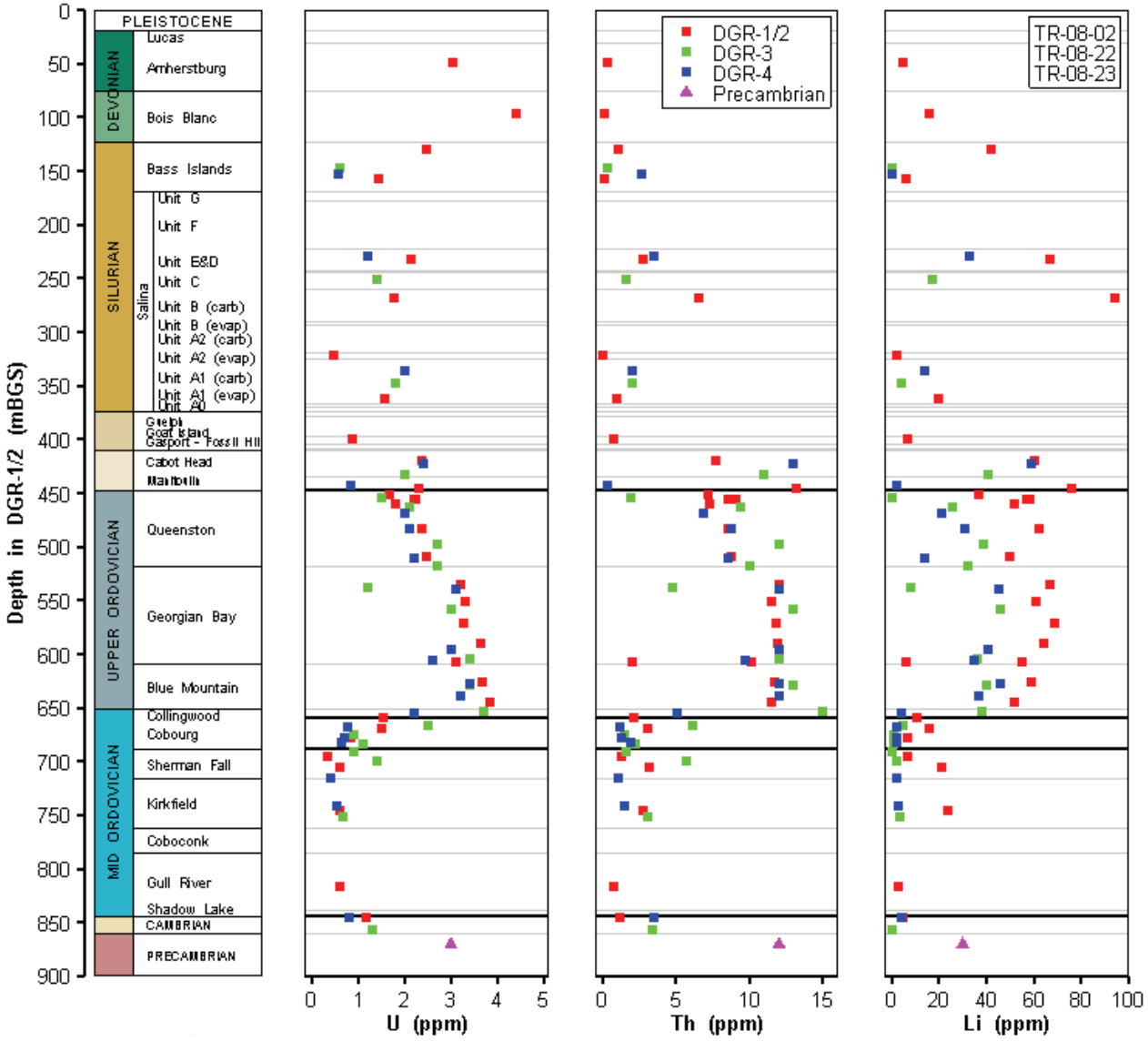

Note: Concentrations in the Precambrian are approximations (Ma et al. 2009 and references therein, Faure 1998).

Figure 4.76: Uranium, Thorium and Lithium Concentrations in Cores from DGR-2, DGR-3 and DGR-4

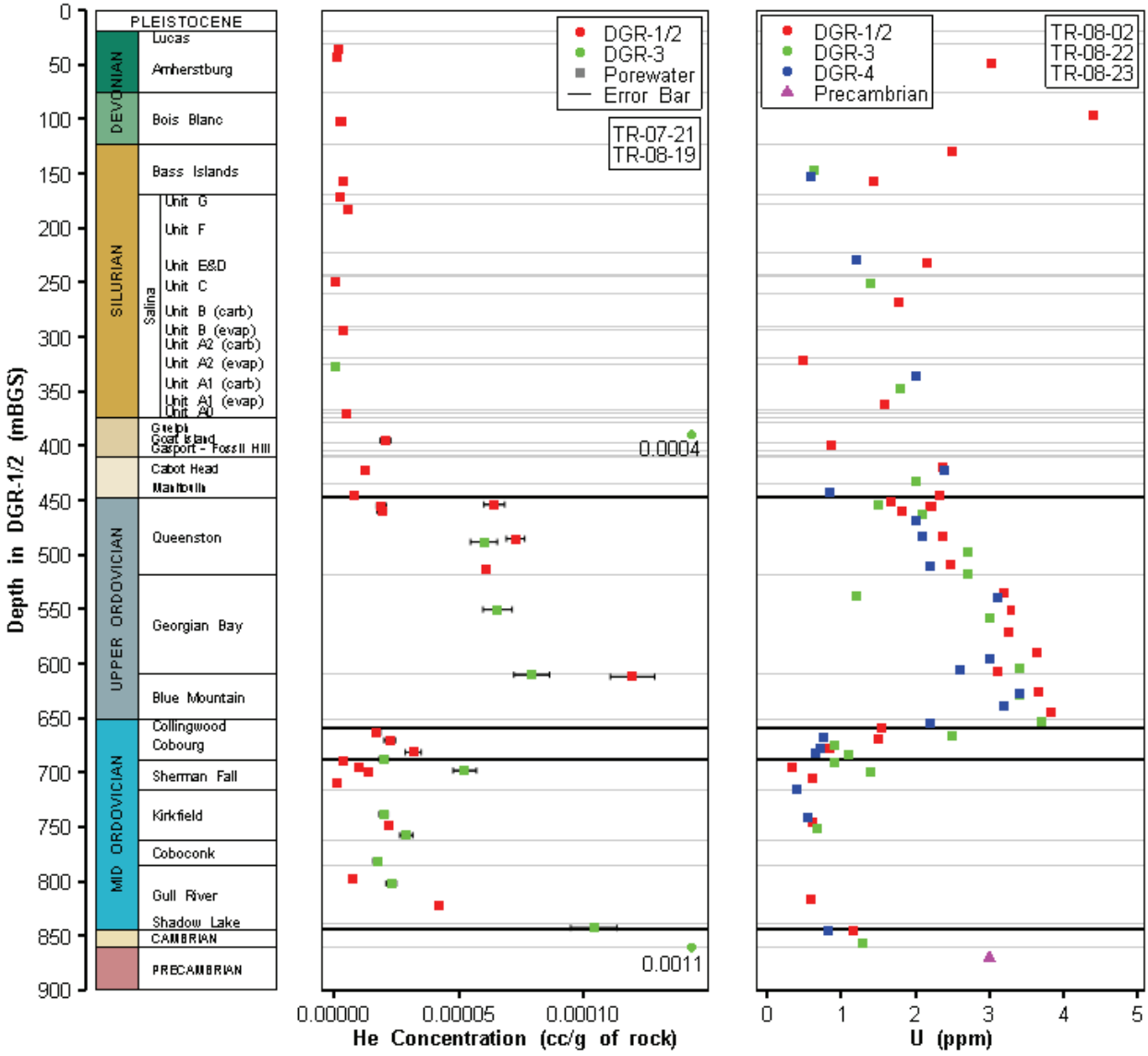

Note: He concentrations for the Guelph Formation and Cambrian are indicated below data points. Uranium value for Precambrian rocks is based on estimates from Faure (1998) and Ma et al. (2009). Samples (normalized to rock concentration with density and porosity).

Figure 4.77: Left: Helium Concentrations from DGR-2 and DGR-3 and for Groundwater Samples. Right: Uranium Concentrations in DGR-2, DGR-3 and DGR-4 Rocks.

The He concentration in the groundwater samples from the Guelph Formation and Cambrian rocks are higher than the adjacent porewater results. High groundwater He concentrations may be due to He production from deeper in the Michigan Basin and eventual movement towards the basin margins (i.e. the Bruce nuclear site). The primary method that could produce high He concentrations is a bubble forms in a sampling apparatus that allows He to partition into the bubble. This could artificially increase the sample volume since water passing by the bubble will

lose He to the bubble, increasing the amount of He captured during the sampling process. This is not likely an issue for the sample collected from the Cambrian rocks. Artesian groundwater flow allowed the sample to be taken with minimal sample disturbance, such as gas ebullition and turbulent water flow. Additionally, the He profile from the Cambrian to the top of the Gull River improves the confidence in the groundwater result. The groundwater sample from the Guelph Formation as sampled using the Westbay sample containers. During this procedure only 1L of liquid is collected at a time. Concentrating He in a bubble is not likely an issue since a known volume of groundwater was sampled. However, the adjacent porewater samples do not show a concentration gradient like what is observed with the Cambrian sample, which suggests sampling and analytical uncertainty may be a factor with the Guelph Formation sample.

The degree of closure of the systems to He loss can be examined by comparing the measured $^{3}He/^{4}He$ ratio with the ratios calculated from the different modes of formation of these two isotopes (^{3}He by ^{6}Li fission and ^{4}He by alpha decay in the ^{238}U and ^{232}Th series). This is shown in Figure 4.75 where the measured ratios (xRa = ^{3}He /^{4}He normalized to the ratio in air) are shown for samples from DGR-2 and DGR-3 together with the calculated ratios based on the respective production rates of ^{3}He and ^{4}He (^{3}He by ^{6}Li fission and ^{4}He by alpha decay in the ^{238}U and ^{232}Th series). Calculations for the ^{3}He and ^{4}He production rates, summarized by Ballentine and Burnard (2002), are based on the production of thermal neutrons generated by alpha-n reactions together with modulation by interaction with Mg, Na, Al, Si and C in the rock matrix (TR-08-38).

The ratio of the production rate of ^{3}He and ^{4}He gives the $^{3}He/^{4}He$ isotope ratio for in-situ production. Important to note is the similarity between measured and calculated $^{3}He/^{4}He$ ratios in the Upper Ordovician shales (Figure 4.75), which indicates in-situ U, Th and Li to be the source term for He in the shales. One can conclude that the He is autochthonous (internally or locally-derived), which allows the He concentrations to be used to estimate minimum ages for pore fluids (Figure 4.78).

Considering that the calculated xRa is close to measured values and that the He and U profiles are similar, the He in the Upper Ordovician shales can be considered autochthonous, with an age of accumulation of at least 100 million to 200 million years. This range is within the range of published values for heating in the Michigan Basin. Ma et al. (2009) place the timing of the last major thermal event at 130 Ma before present. Heaman et al. (2000) traced kimberlite hot spots near Timiskaming, Quebec (450 km north-east of the Bruce nuclear site), between 134 Ma and 155 Ma and Wang et al. (1994) indicate the peak temperature (primarily due to burial) in the basin occurred between 200 and 250 Ma.

He isotopes measured in the Middle Ordovician limestones below the Cobourg are more enriched in ^{3}He than would be expected for in-situ production. The He concentrations are close to the measured concentrations in the Cambrian groundwater and intermediary between literature values for groundwater from the Precambrian (Kotzer et al. 1998) and Michigan Basin groundwater (Ma et al. 2009). Note, the range of results in the Michigan Basin is between 0.057 and 0.133, only results less than 0.06 are shown in Figure 4.75. It can be concluded that He in this section is allochthonous, by migration from a mixture of basin-derived and Shield-derived He via the Cambrian sandstone. This is consistent with the measured He concentrations (Figure 4.77, left chart) which show a steep gradient into the Cambrian sandstone.

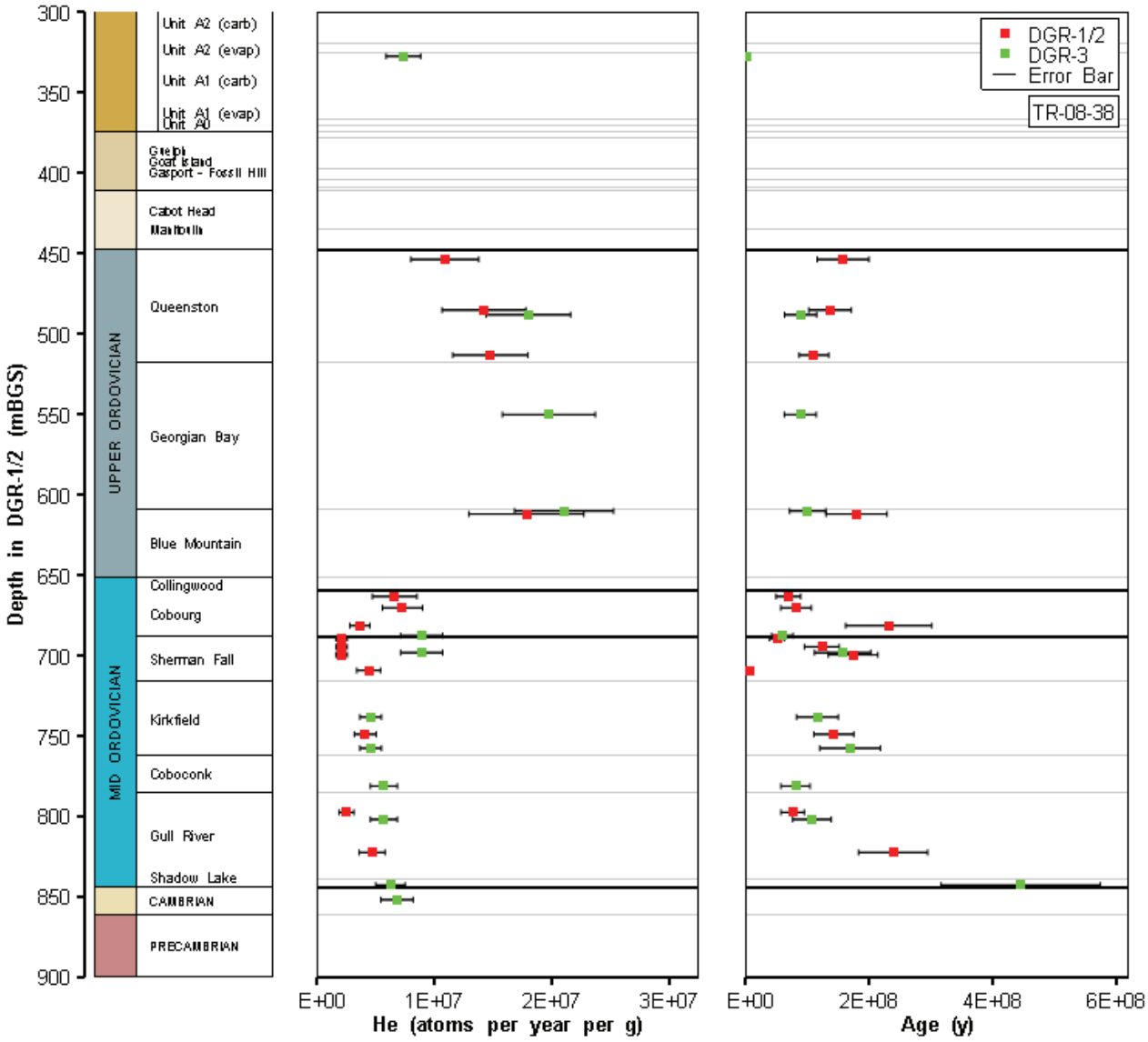

Note: Left: Helium production based on U and Th concentrations. Right: helium ages calculated for DGR porewater based on measured He per g rock and in-situ He production based on U and Th concentrations assuming a closed system, i.e., no advection or diffusion. Error bars include He measurement uncertainties (most near 9%) and uncertainties in interpolation of U and Th measurements (assessed at 20%).

Figure 4.78: Calculated Helium Production and Ages from DGR Cores

Within the Cobourg Formation limestone, measured $^{3}He/^{4}He$ ratios are consistent with the overlying shales, yet enriched in ^{3}He over the calculated in-situ values. Here it is apparent that movement of He from the shales into the limestones has occurred, with little to no exchange with He from the underlying Sherman Fall or deeper limestone formations. This is consistent with the CH_4 profiles (TR-08-19) that show a strong impediment to migration of this gas below

the Cobourg Formation. Also, hydraulic conductivity tests showed horizontal hydraulic conductivities in this section are as low as 10^{-15} m/s (TR-08-32) and are likely to be even lower in the vertical direction. These low hydraulic conductivities inhibit gas and solute migration.

The calculated ages for the Middle Ordovician limestones are invalid as they assume a closed system with in-situ production and accumulation of He. From the He production profile (left chart - Figure 4.78) and He age profile (Figure 4.78- right chart), the accumulated He measured in the limestones provides ages as old or older than those for He in the Upper Ordovician shales, and ages below 800 mBGS that approach the age of the sedimentary units themselves. As the $^{3}He/^{4}He$ ratios (Figure 4.75) demonstrate, He in this section is allochthonous showing an almost uniform profile from the Cambrian up to the Sherman Fall Formation. Therefore it is concluded that the Middle Ordovician limestones are open to exchange with the underlying Cambrian sandstone over very long geological time frames. Porewater in the Cobourg Formation limestone, however, must be considered to be as old as the overlying shales, given that their He isotope signature is derived from He produced in the shales and has migrated downward, presumably by diffusion. While, in-situ production has been minimal as shown by the low He concentrations (Figure 4.77 - left chart), He from the shales has dominated the Cobourg Formation porewater over the past 100 to 200 million years.

4.7 Radioisotopes in Groundwater and Porewater

The Geoscientific Site Characterization Plan was prepared making the assumption that the deep groundwater system in the shales and limestones is saline, stable and ancient (INTERA 2008). The measured low permeability of the argillaceous sedimentary rocks reported elsewhere in this DGSM (Section 4.9.2) suggests diffusion is the controlling process in solute transport throughout most of the Paleozoic bedrock sequence from Salina Formation down to the Black River limestones. Notable exceptions to this general observation are the permeable aquifers of the Salina Upper A1 Unit and the Guelph Formation. This general assumption has not been considered applicable to the shallow groundwater flow system in the Devonian and Upper Silurian formations for which there is strong evidence that they have been penetrated by recharge that occurred during the Quaternary period, similar to that reported in Michigan by McIntosh and Walter (2005 and 2006).

Consequently, an independent means of estimating the residence times of the porewater or groundwater in the depth profile modeled would help justify the assumptions of diffusion-controlled radionuclide migration in the Ordovician shales and limestones and modern recharge in the shallow dolostones. Given the range in potential residence times of the groundwater and porewater in the Paleozoic rock sequence at the DGR, radioisotope dating provides an appropriate tool to estimate the residence times of the groundwater and porewater and to improve our understanding of solute transport at the Bruce nuclear site. The radioisotopes considered for use are ^{14}C ($t_{½}$=5730 yr), ^{36}Cl ($t_{½}$=301,000 yr) and ^{129}I ($t_{½}=1.6x10^{7}$ yr) because their long half lives permit estimation of solute residence times in the groundwater and porewater of the DGR rocks. TR-08-38 provides a detailed description and discussion of the characterization of radioisotopes in DGR groundwater and porewater.

4.7.1 ^{14}C in Shallow Groundwater

The ages of shallow Devonian and Upper Silurian groundwater present in fractures and solution cavities above the Salina F Unit shale have been investigated by ^{14}C dating. The $\delta^{13}C$ mixing model of Pearson (1965) and Pearson and Hanshaw (1970) was applied to correct the apparent

radiocarbon ages as described by Clark and Fritz (1997, pp. 210-211). Table 4.11 presents the results from groundwater samples collected from the US series of Westbay multi-level wells.

Table 4.11: Apparent Radiocarbon Ages in Years before Present and the Percent Modern Carbon (pmC) of Selected Shallow Groundwater Samples as well as Radiocarbon Ages Corrected Using the $\delta^{13}C$ Mixing Model

Borehole and Depth (mBGS)	Tritium (TU)	Apparent ^{14}C Age (Years BP)	% Modern Carbon (pmC)	Corrected ^{14}C Age (Years BP)
US3-32.30	1.9	12550 ± 70	20.96 ± 0.18	4741
US3-68.50	1.8	12100 ± 70	22.16 ± 0.19	4468
US7-68.90	<0.8	14450 ± 80	16.54 ± 0.16	7290
US8-40.60	3.7	5810 ± 50	48.50 ± 0.30	4447
US8-120.80	33.8	8030 ± 60	36.79 ± 0.27	4666
US8-158.00	12.5	13270 ± 70	19.16 ± 0.17	7709
US8-179.40	<6	12070 ± 70	22.25 ± 0.19	4732
DGR4-327.08	3.0	13560 ± 80	18.49 ± 0.18	5442

Corrected ages suggest mid-Holocene recharge at most depths. There is no general trend towards older ^{14}C ages with depth. The samples from 68.9 m and 158.0 m depth have comparatively greater corrected ages. The deeper (158.0 mBGS) sample was recovered from the Upper Silurian dolostones and has a depleted $\delta^{18}O$ value (–16.6‰) and the oldest ^{14}C age (7700 yrs BP) that indicate a component of glacial meltwater recharge. The sample from the Salina Upper A1 Unit permeable horizon (DGR4-327.08) had a mid Holocene 14C age, which is considered to be a minimum age.

The ^{14}C data show relatively young carbon corrected ages (<8,000 years since groundwater recharge) in the groundwater in Devonian formations as well as the Salina Upper A1 Unit permeable horizon, which is similar to the water isotope results that showed water isotope signatures representative of glacial melt water (Section 4.6.6.1). Also, groundwater results from samples taken from the Devonian formations and the Salina Upper A1 Unit were relatively dilute, which may be due to dilution by glacial melt water.

The ages presented suggest the groundwater is relatively old Holocene groundwater and tritium should not be present (Table 4.11). The tritium in the groundwater indicates the groundwater samples are mixed, which is not accounted for in the calculation of radiocarbon ages. Therefore, some error is expected with these calculated ages, although the overall finding of relatively old Holocene groundwater is considered to be appropriate.

4.7.2 ^{36}Cl in Porewater and Groundwater

Radioisotopes provide a means of tracing the potential migration of solute in porewater. In particular, ^{36}Cl ($t_{½}$=301,000 yr) and ^{129}I ($t_{½}$=1.6x10^{7} yr) have relatively long half lives and subsurface production that may permit estimation of residence times of solutes in the groundwater and porewater of the rocks at the Bruce nuclear site. Both Cl and I are halides that

share similar geochemical characteristics including the solubility and relatively conservative transport characteristics.

Measured concentrations can be attributed to in-growth towards secular equilibrium in the host formation, or to transport of ^{129}I and ^{36}Cl from higher or lower geogenic production zones in the subsurface (Bentley et al. 1986). The in-growth of ^{36}Cl and ^{129}I are also strongly dependent on the concentration of U in the rocks, although their modes of production differ. Bottomley et al. (2002) employed ^{129}I to identify a residence time of greater than 80 million years for the Shield groundwater collected in the Con Mine, Yellowknife, NWT. The coupled use of these two radioisotopes has resulted in several successful hydrogeological studies according to Fabryka-Martin (1999).

He evidence (Section 4.6.9) demonstrated that the shale porewater is much older than the approximately 1 million years required to reach secular equilibrium for ^{36}Cl in these rocks, and so these low measured ^{36}Cl contents can be reasonably assumed to have reached secular equilibrium. When ^{36}Cl concentrations have reached secular equilibrium, the measured ^{36}Cl concentration can be used to determine the U and Th concentrations as a basis for more precise calculation of secular equilibrium ^{129}I concentrations (TR-08-38).

Groundwater samples were collected from the Salina Upper A1 Unit permeable horizon, the permeable horizon in the Guelph Formation and from the Cambrian rocks. Additionally, Cl and I from nine rock core samples from the Ordovician shales and limestones were extracted by the vacuum distillation crush and leach procedure and were analyzed for solute concentrations and radioisotope concentrations.

The in-situ ^{36}Cl concentrations for secular equilibrium were calculated based on the method outlined by Andrews et al. (1986). In Figure 4.79, measured $^{36}Cl/Cl$ ratios are plotted with depth (left hand chart) for both porewater samples and groundwater samples. One measurement (DGR4-725.92) had a low ^{36}Cl mass and is considered to have been contaminated during analysis by a high ^{36}Cl background signal during the analytical procedure and so is considered anomalous. Calculations for the U and Th concentrations at this depth were taken from the next lower sample.

The centre and right panels of Figure 4.79 present measured U and Th concentrations (for DGR-2, DGR-3 and DGR-4 corrected to DGR1/2 reference depths) together with the back-calculated U and Th concentrations to provide values for secular equilibrium that are the same as the measured porewater ^{36}Cl contents. The back calculated U and Th ratios were determined assuming the ratio of U to Th was constant for all samples, which allows both U and Th could be estimated using the measured porewater ^{36}Cl contents. For the one anomalous ^{36}Cl analysis, the U content calculated for secular equilibrium is the adjacent (lower) sample. For the shale samples, the calculated U concentrations fall near or below the range of measured U concentrations. In the Ordovician limestones, they fall near or above the range of measured U concentrations.

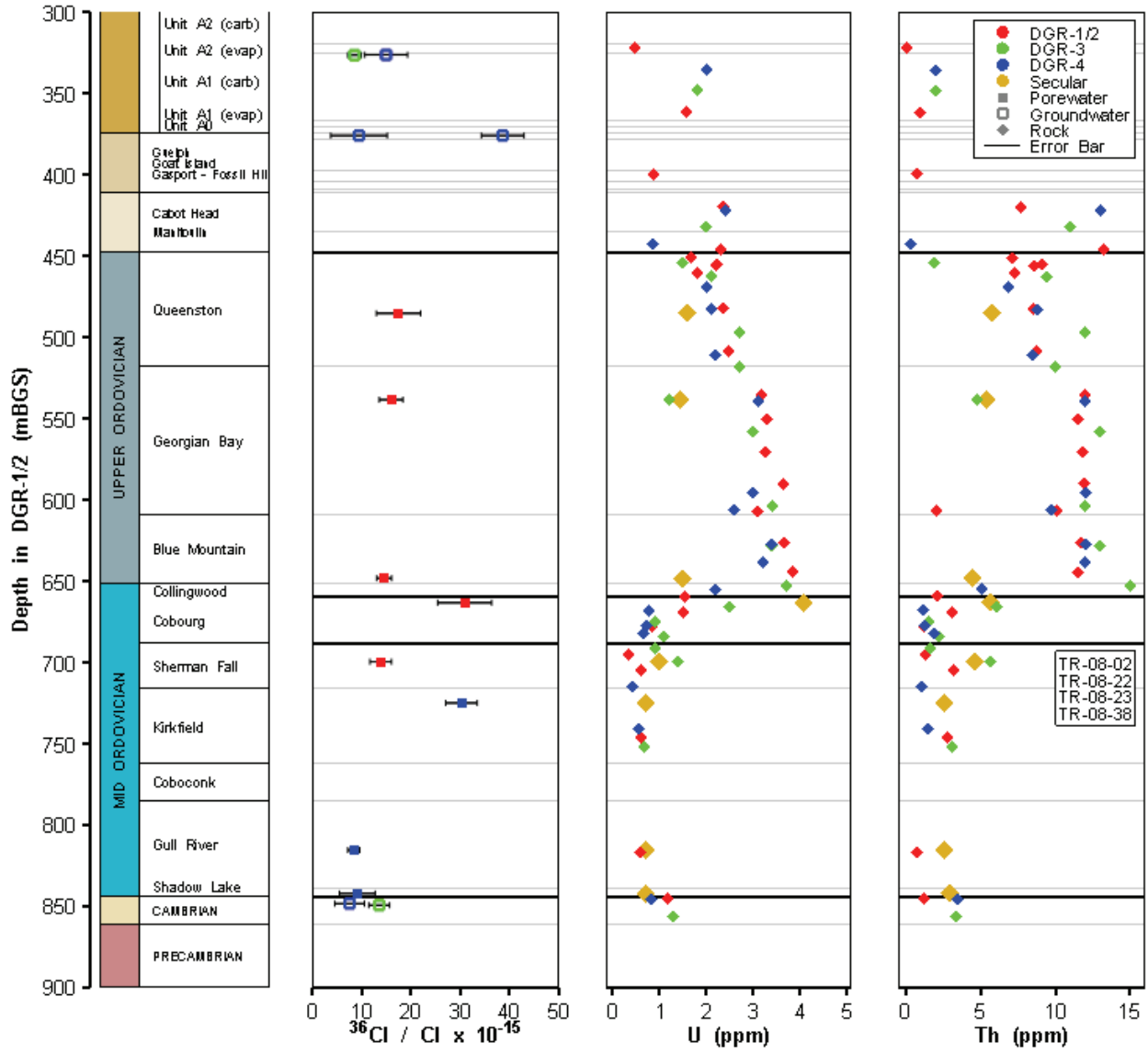

Notes: Left: Measured groundwater and porewater $^{36}Cl/Cl$ concentrations from DGR-2, DGR-3 and DGR-4, error bars are +/- 1 sigma for the analytical run. Centre: Measured U concentrations and calculated U concentrations in rock based on ^{36}Cl secular equilibrium. Right: Measured Th concentrations and calculated Th concentrations in rock based on ^{36}Cl secular equilibrium.

Figure 4.79: ^{36}Cl Concentrations in Porewater and Groundwater with U and Th Concentrations in Rock

Secular equilibrium values were calculated for the groundwater samples using the same modeled U and Th concentrations as for similar units (Salina Upper A1 Unit and Guelph Formation as limestone and Cambrian as shale). ^{36}Cl contents in the Salina Upper A1 Unit were close to secular equilibrium values, suggesting that Cl in this formation has had a significant local residence time. The higher of the two $^{36}Cl/Cl$ ratios measured in the Guelph Formation

groundwater is likely due to drill fluid contamination, which was estimated to be 24% drill fluid based on tritium results (TR-08-18). The lower ^{36}Cl value for groundwater in the Guelph Formation is close to that measured in the Upper A1 Unit, suggesting a common source of Cl in this section. The higher values for secular equilibrium may reflect a poor understanding of the actual U and Th content for the Guelph Formation. The range of values for the Cambrian groundwater gives no clear indication that the Cl in this groundwater has achieved secular equilibrium or whether it has contributions from any underlying Precambrian groundwater.

4.7.3 ^{129}I in Porewater and Groundwater

The production of ^{129}I measured in groundwater can be a mixture of both cosmogenic production through interaction of cosmic rays with ^{129}Xe in the atmosphere, or through the spontaneous fission of ^{238}U in the subsurface. The increase in human nuclear activities since the 1950s represents a third source of anthropogenic ^{129}I in the environment. Cosmogenic ^{129}I in groundwater is difficult to assess due to the overprint from nuclear era ^{129}I, but has been estimated to be in the range of 1000 to 20,000 atoms per kg water (Rao and Fehn 1999). Pre-nuclear era seawater has a $^{129}I/I$ ratio of about 1.5×10^{-12} or about 11.4 million atoms per kg water. Geogenic production can be similar to or higher than this (Rao and Fehn 1999, Renaud et al. 2005). In the case of halides in DGR porewater and groundwater, no residual ^{129}I from atmospheric or marine sources is anticipated, and so measured ^{129}I can be attributed to geogenic production.

The movement of ^{129}I in pore fluids and groundwater is closely linked with halide movement in general and specifically with stable I (^{127}I). The $^{129}I/I$ ratio is a useful tool for interpreting ^{129}I as a tracer. In the DGR porewater, total I (^{127}I + ^{129}I) was measured by ICP-MS.

Measurements of ^{129}I concentrations are presented in Figure 4.80 for both porewater and groundwater from DGR-2 and DGR-4. Values are expressed both as atoms ^{129}I per litre of water (molal concentration) and as the atomic ratio of ^{129}I to total I (essentially stable ^{127}I). For groundwater these were measured directly on submitted samples. For groundwater from the Upper A1 Unit (~330 m depth) total I measurements were below detection of 0.3 ppm, which was used to calculate a minimum $^{129}I/I$ ratio for comparison with the calculated secular equilibrium values. The reported values for total I in the Cambrian (0.6 and 2.8 ppm; TR-08-18) are low, and were likely affected by the high salinity of the samples which reduces the counts measured. For the porewater, measurements were made by ICP-MS on leach solutions and the measured mass of ^{129}I was normalized to the porewater content from that sample.

In addition to measured values are ^{129}I concentrations calculated for in-growth to secular equilibrium (concentration of ^{129}I to the point where production is matched by radioactive decay in a closed system). Values for $^{129}I_{se}$ (calculated ^{129}I at secular equilibrium) were determined using the U concentrations of the rock calculated from ^{36}Cl measurements, as discussed in Section 4.7.2, and the approach of Fabryka-Martin et al. (1999). Concentrations of U, Th and Li in the DGR rocks are shown in Figure 4.76.

Ratio calculations ($^{129}I/I$) for the Salina Upper A1 Unit groundwater was not possible as the measured concentration of stable I was below the analytical detection limit. Both samples from the Upper A1 Unit had ^{129}I concentrations below the values calculated for secular equilibrium. This is consistent with the dilution of groundwater in this aquifer by the incursion of glacial melt water, and is consistent with radiocarbon dating which shows these groundwaters to be late Pleistocene to Holocene in age.

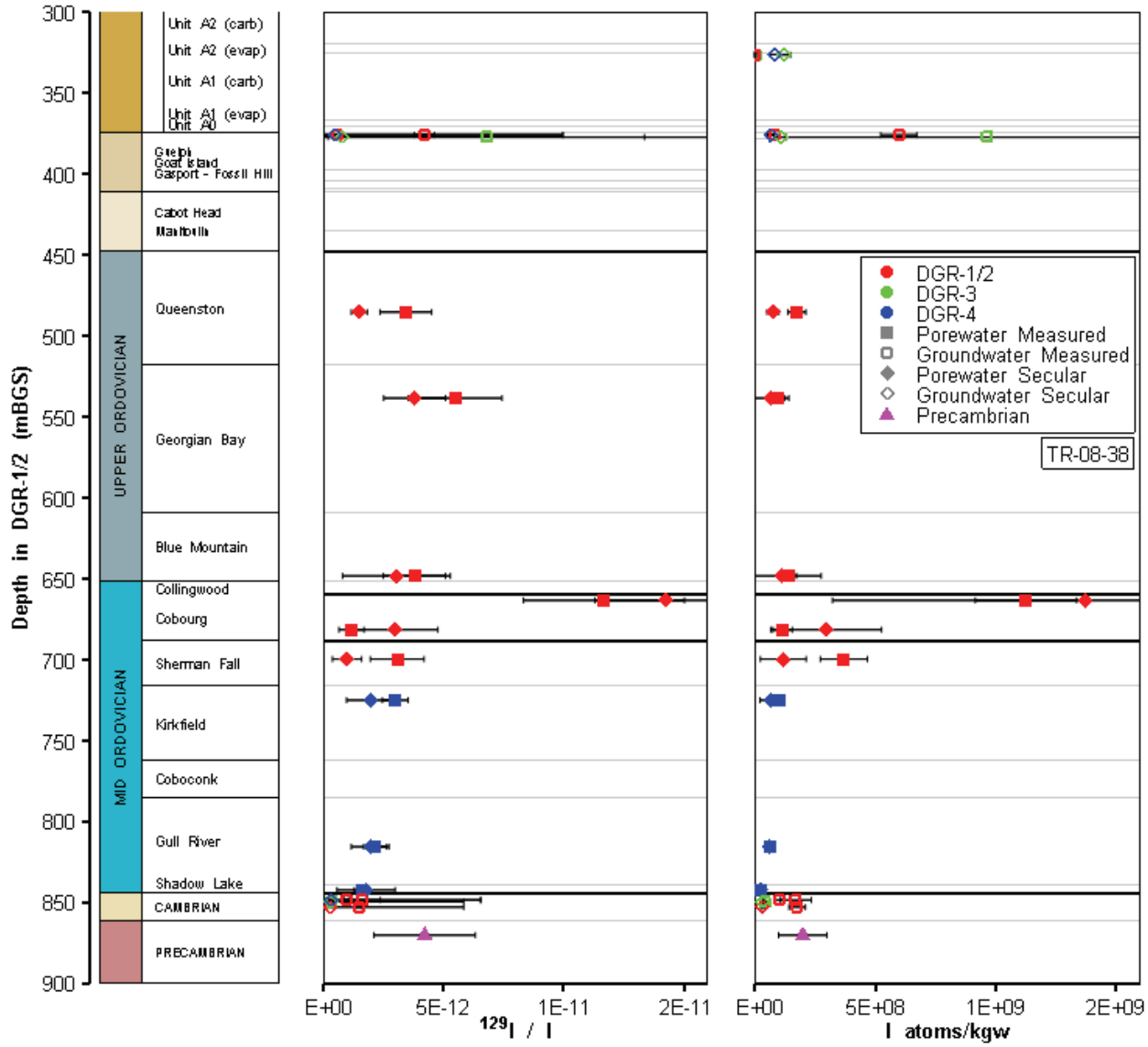

Notes: Left: ^{129}I normalized to total iodine concentration. Right: ^{129}I as atoms per kg porewater or groundwater. Uncertainty in the stable I concentrations for the Salina Upper A1 Unit groundwater precludes determination of their ^{129}I/I ratio. The concentrations in the Precambrian groundwater were measured at Sudbury mines (Bottomley et al. 2002). Error bars on secular equilibrium values are based on uncertainties in Uranium concentrations through section and are all positive values.

Figure 4.80: ^{129}I Measured in DGR-2 and DGR-4 Porewater and Groundwater Together with Secular Equilibrium ^{129}I Calculated from U Concentration and Assuming Secular Equilibrium (Production = Decay)

Guelph Formation groundwater analyses were complicated by the high salinity in these samples, and therefore the measured ^{129}I concentrations and ratios are accompanied by large errors. The sample with the highest value (964×10^6 atoms L^{-1}) is contaminated with 24% drilling

fluid (133 TU, TR-08-18) and so can be discounted. The remaining two Guelph Formation groundwater samples had contrasting ^{129}I concentrations (82.9×10^6 atoms L^{-1} at Purdue; and 598×10^6 atoms L^{-1} at IsoTrace) which are similar to, or greater than the secular equilibrium concentration. There are no adjacent formations with sufficiently high U to account for the higher ^{129}I measurement.

The groundwater in the Cambrian rocks has 100 to 200 million atoms ^{129}I kgw^{-1}. Both are close to, or above, the calculated ^{129}I concentrations for secular equilibrium with the formational U content. These compare with an estimated value for Precambrian groundwater of close to 200 million atoms ^{129}I kgw^{-1} based on measurements from the Victor mine in Sudbury (Bottomley et al. 2002). This enrichment in ^{129}I in the Cambrian groundwater toward values in the Precambrian is also seen in the ^{129}I/I values, which exceed the values calculated for secular equilibrium. This suggests that the groundwater in the Precambrian Shield is a potential source of ^{129}I in the Cambrian.

The measured porewater ^{129}I concentrations and ^{129}I/I ratios in the Upper Ordovician shales (Figure 4.80) are close to their respective calculated secular equilibrium values. The four Trenton Group samples, including two Cobourg limestone samples also have measured values for both the ^{129}I/I ratio and concentration of ^{129}I per kg porewater that are close to their calculated secular equilibrium values.

The concentration of ^{129}I for the upper Cobourg at 663.34 mBGS is the most enriched sample in the profile, and coincides with a high value for ^{36}Cl in this sample. Diffusion from the overlying shales is unlikely as the ^{129}I/I ratio should be similar to that found in the shales. An allochthonous (external) source for this excess ^{129}I is unlikely, as no other enriched sources are identified in the section. Locally higher U and Th concentrations in rock may be responsible for the production of ^{129}I and ^{36}Cl in this zone. Organic carbon can adsorb I, and high I concentrations can be associated with high organic carbon content. However, ^{129}I has reached secular equilibrium, indicating ^{129}I would decay unless a source was present.

The two deeper porewater ^{129}I values for the Gull River and upper Shadow Lake formations show ^{129}I/I ratios and concentrations that are lower than most of those in the Trenton Group limestones. However, with lower U concentrations at these depths, the measured values are the same as calculated secular equilibrium values. The ^{129}I contents of these two deep porewater samples are unlike those measured in the Cambrian groundwater, having lower ^{129}I concentrations (atoms/kgw) and higher ^{129}I/I ratios. This is consistent with Cl, Na, Br, δ^{18}O and δD results that showed the lower-salinity porewater in the lower Black River Group rocks does not have a significant component of current Cambrian groundwater.

^{129}I measurements in the Ordovician shales are close to values for secular equilibrium, which requires a period of 80 million years. This is a similar time frame for the calculated helium ages described above (Figure 4.78). Assuming iodine is conservative, the ^{129}I results indicate there has not been an input of atmospheric iodine to these formations for at least 80 million years. It is not known whether or not the iodide dissolved in the porewater has been in contact with the same porewater over that time frame, therefore, the ^{129}I results cannot be explicitly used as an indicator for water residence time. However, the ^{129}I results, He results, and the estimated time required to produce the ^{18}O profile (NWMO 2011) suggests that the porewater solute has been equilibrating in the Ordovician shales and the Cobourg Formation for between 80 million and 200 million years. This long equilibration time indicates water and solute movement are very slow within the Ordovician shales and solute exchange with overlying and underlying permeable units is also very slow.

^{129}I measurements in the Ordovician limestones are close to secular equilibrium, which suggests there has not been an input of atmospheric iodine to these formations for at least 80 million years. He in the Middle Ordovician limestones below the Cobourg Formation appears to be open to exchange with the underlying Cambrian sandstone over very long geological time frames (Section 4.6.9). Therefore, the calculated ages for the Middle Ordovician limestones (except for the Cobourg Formation) are invalid as they assume a closed system with in-situ production and accumulation of He.

4.8 Fluid Density

Groundwater (GW) and porewater (PW) chemistry data and field and laboratory fluid density measurements were used to generate a profile of formation fluid density for the Paleozoic bedrock column at the Bruce nuclear site (TR-08-31). Figure 4.81 shows the fluid density versus depth and formation data, the recommended or reference density profile selected for the DGR bedrock sequence, and arithmetic formation averages. A reference density profile is required to calculate environmental water heads from fresh water heads in variable density fluid systems as exist at the Bruce nuclear site. Figure 4.81 includes 1) laboratory measurements of fluid density on groundwater samples collected during drilling of DGR boreholes (TR-07-11, TR-08-18), 2) laboratory measurements of fluid density on groundwater samples collected from Westbay MP38 casing completion in US-8 (TR-08-08), 3) calculations of fluid density from major ion analyses of porewater reported by University of Ottawa (TR-07-21, TR-08-19, TR-09-04), and 4) calculations of fluid density by the University of New Brunswick based porewater concentrations determined from crush and leach analyses (TR-07-17, TR-08-27). For groundwater samples collected from the Salina Upper A1 Unit aquifer in DGR-4, the fluid density was calculated from the measured TDS values, as the laboratory density value was judged to be unreliable. University of Ottawa and University of New Brunswick fluid density data are discriminated in Figure 4.81 based on charge balance (CB) error.

Fluid densities were reported in various units, all of which were scaled to units of kg/m^3 for comparison purposes. Porewater chemistries reported in units of g/kg of water were converted to kg/m^3 of solution by scaling the porewater TDS in units of g/kg of water to the known average groundwater density of the Guelph Formation (1234 kg/m^3) and the calculated average groundwater TDS of the Guelph Formation (451.8 g/kg of water). The similarity of fluid densities reported for porewater by different laboratories, and from direct measurements on groundwater samples from non-Guelph aquifers to those calculated from porewater analyses, provides confidence in the reference density profile.

Figure 4.81 shows a density profile that transitions from fresh water (ρ=990-1000 kg/m^3) in the upper dolostone units (Lucas, Amherstburg, Bois Blanc and Bass Islands formations) though brackish water (ρ=1004 kg/m^3) in the Salina G Unit to the brine (ρ=1072 kg/m^3) in the Salina Formation B Unit. From the Salina B Unit down to the Salina Upper A1 Unit aquifer, the water density significantly decreases to the saline water that characterises the Salina Upper A1 Unit aquifer (ρ=1013 kg/m^3). There is then a significant increase in water density from the Salina Upper A1 Unit aquifer to the brine found within the Guelph Formation (ρ=1234 kg/m^3) which is the highest TDS and highest density fluid measured at the Bruce nuclear site.

From the Guelph downward, the porewater density decreases to 1164 kg/m^3 in the Goat Island Formation to 1210 kg/m^3 in the Manitoulin Formation. Through the Ordovician shales, the fluid density decreases slightly from 1177 kg/m^3 in the Queenston Formation to 1173 kg/m^3 in the Blue Mountain Formation before decreasing to 1128 kg/m^3 in the Collingwood Member. Porewater density decreases from 1168 kg/m^3 in the Lower Member of the Cobourg Formation

to 1115 kg/m^3 in the Gull River Formation. Fluid density then increases through the bottom of the Gull River and Shadow Lake formations to an average groundwater density of 1145 kg/m^3 within the Cambrian sandstone. The average porewater density within the Coboconk Formation at 1148 kg/m^3 is similar to that of the Cambrian sandstone.

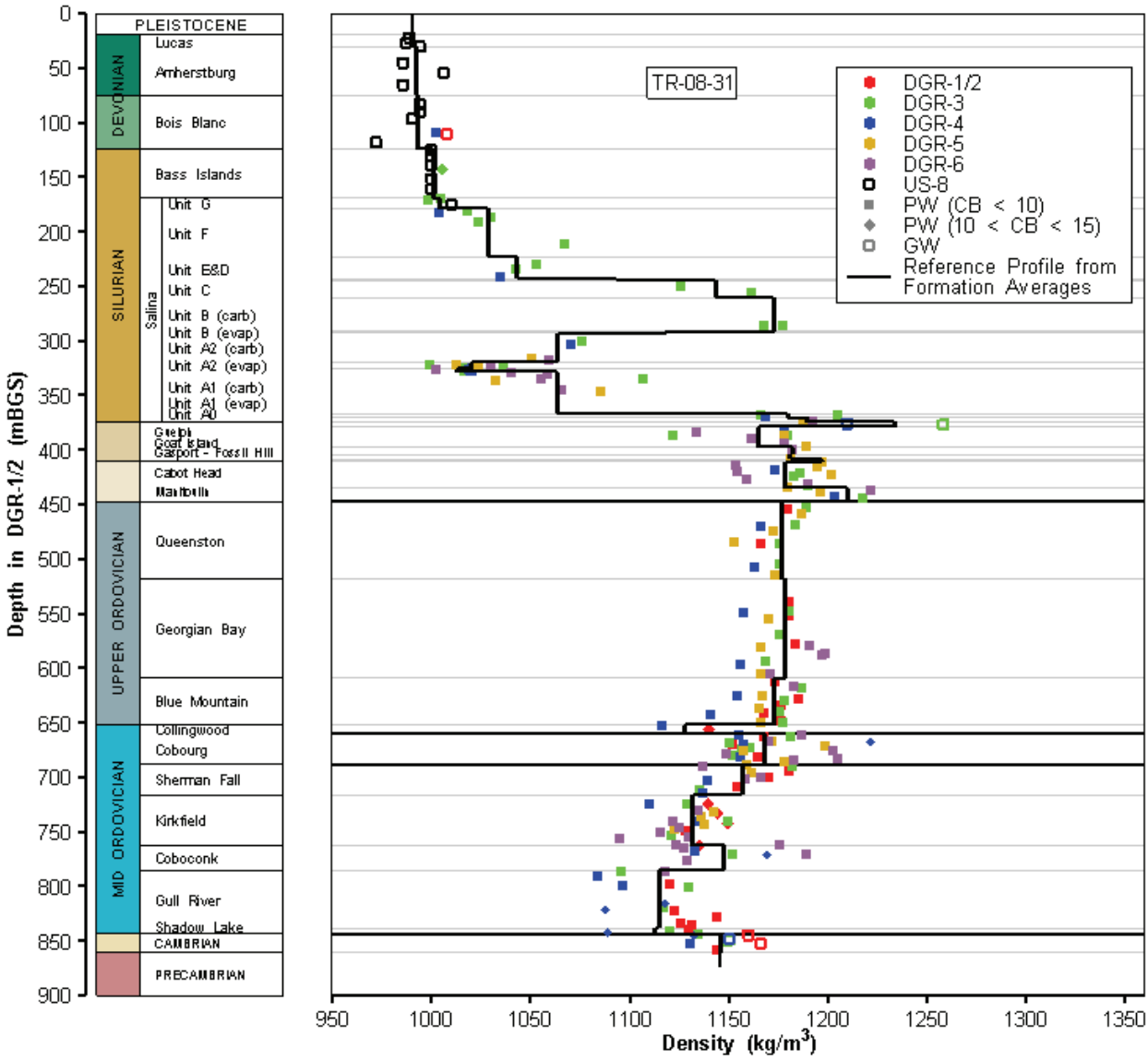

Figure 4.81: Reference Fluid Density Profile and Formation Averages Based on US-8 and DGR Borehole Groundwater and Porewater Data

4.9 Formation Hydraulic Conductivity

4.9.1 Shallow Bedrock – US Wells

Data on formation horizontal hydraulic conductivity for the shallow bedrock (Lucas, Amherstburg, Bois Blanc and Bass Islands formations) are available from summaries of geotechnical bedrock investigations; Bruce A and B cooling water intake tunnelling experience (GOLDER 2003); straddle-packer testing of US-1 to US-7 (106 tests - Lukajic 1988); slug testing of Westbay test intervals in US-5 and US-6 (14 tests – GOLDER 2003); and from drilling fluid loss observations made during drilling of US-8 (TR-07-19) and DGR boreholes (TR-07-06, TR-08-13). Packer test flow rates and injection pressures and drilling fluid loss rates and heads were converted to equivalent hydraulic conductivities assuming conditions of confined steady radial flow.

Table 4.12 summarizes representative estimates of horizontal hydraulic conductivities for the Lucas, Amherstburg, Bois Blanc and Bass Islands formations, the basis/rationale for the estimate and the data source for their inclusion in this report. Of note are the very permeable sections ($1x10^{-4}$ m/s) of the upper 20 m of Bass Islands Formation that created significant drilling fluid losses during drilling of all DGR boreholes and US-8.

Table 4.12: Summary of Horizontal Hydraulic Conductivities for Lucas, Amherstburg, Bois Blanc and Bass Islands Formations

Formation	Hydraulic Conductivity (m/s)	Basis/Rationale	Source
Lucas and Amherstburg (<30 m)	$6x10^{-9}$ to $3x10^{-5}$ $2x10^{-6}$	Range, geometric mean from packer tests in US boreholes	Analysis of Lukajic (1988) Data
Lucas and Amherstburg (<30 m)	$4x10^{-9}$ to $2x10^{-4}$ $5x10^{-7}$	Range, geometric mean from Bruce A site investigations	GOLDER 2003
Amherstburg (>30 m)	$8x10^{-10}$ to $8x10^{-5}$ $8x10^{-8}$	Range, geometric mean from packer tests in US boreholes	Analysis of Lukajic (1988) Data
Amherstburg (>30 m)	$1x10^{-8}$ to $2x10^{-5}$ $2x10^{-7}$	Range, geometric mean from Bruce A site investigations	GOLDER 2003
Bois Blanc (to 100 m)	$6x10^{-10}$ to $1x10^{-5}$ $1x10^{-7}$	Range, geometric mean from packer tests in US boreholes	Analysis of Lukajic (1988) Data
Combined Amherstburg and Bois Blanc	$1x10^{-6}$ to $1x10^{-4}$ $1x10^{-5}$	Range, geometric mean from tunnel dewatering experience and slug testing of US-5 & US-6 casings	GOLDER 2003
Bass Islands (upper 20 m)	$1x10^{-5}$ to $3x10^{-4}$ $1x10^{-4}$	Range, geometric mean from analysis of drilling fluid losses in US-8 and DGR boreholes	TR-07-06, TR-07-19, TR-08-13
Bass Islands	$1x10^{-5}$	Estimated average representative value	GOLDER 2003

4.9.2 Deep Bedrock – DGR Boreholes

4.9.2.1 Field Testing

Field measurements of deep bedrock formation horizontal hydraulic conductivity were made in all DGR boreholes using a custom-built straddle-packer hydraulic testing tool (TR-08-32) as well as during opportunistic groundwater sampling using a bottom-hole, production-injection packer (PIP) during drilling. Hydraulic test responses were collected from 3 intervals (12-m test zone) in DGR-1, 15 intervals (30.5-m test zone) in DGR-2, 23 intervals (30.7-m test zone) in DGR-3, 24 intervals (30.7-m test zone) in DGR-4, 11 intervals (30.3-m test zone) in DGR-5 and 12 intervals (10.2-m test zone in DGR-6. The hydraulic tests performed in DGR boreholes included pulse, slug, and drill-stem tests (DST) using a workover rig and drill tubing to position the test tool in the borehole (see Figure 4.82).

Figure 4.82: Straddle-packer Hydraulic Testing at DGR-4 Using Workover Rig and Drill Tubing

During each straddle-packer hydraulic test, pressures within, below and above the test interval (within drill tubing and borehole annulus), and pressures controlling 1) packer inflation, 2) the downhole open-close shut-in valve and 3) the downhole pulse piston, as well as atmospheric pressure were continuously monitored in real time. Figure 4.83 provides an example of the pressure data obtained during each straddle-packer hydraulic test performed in DGR boreholes.

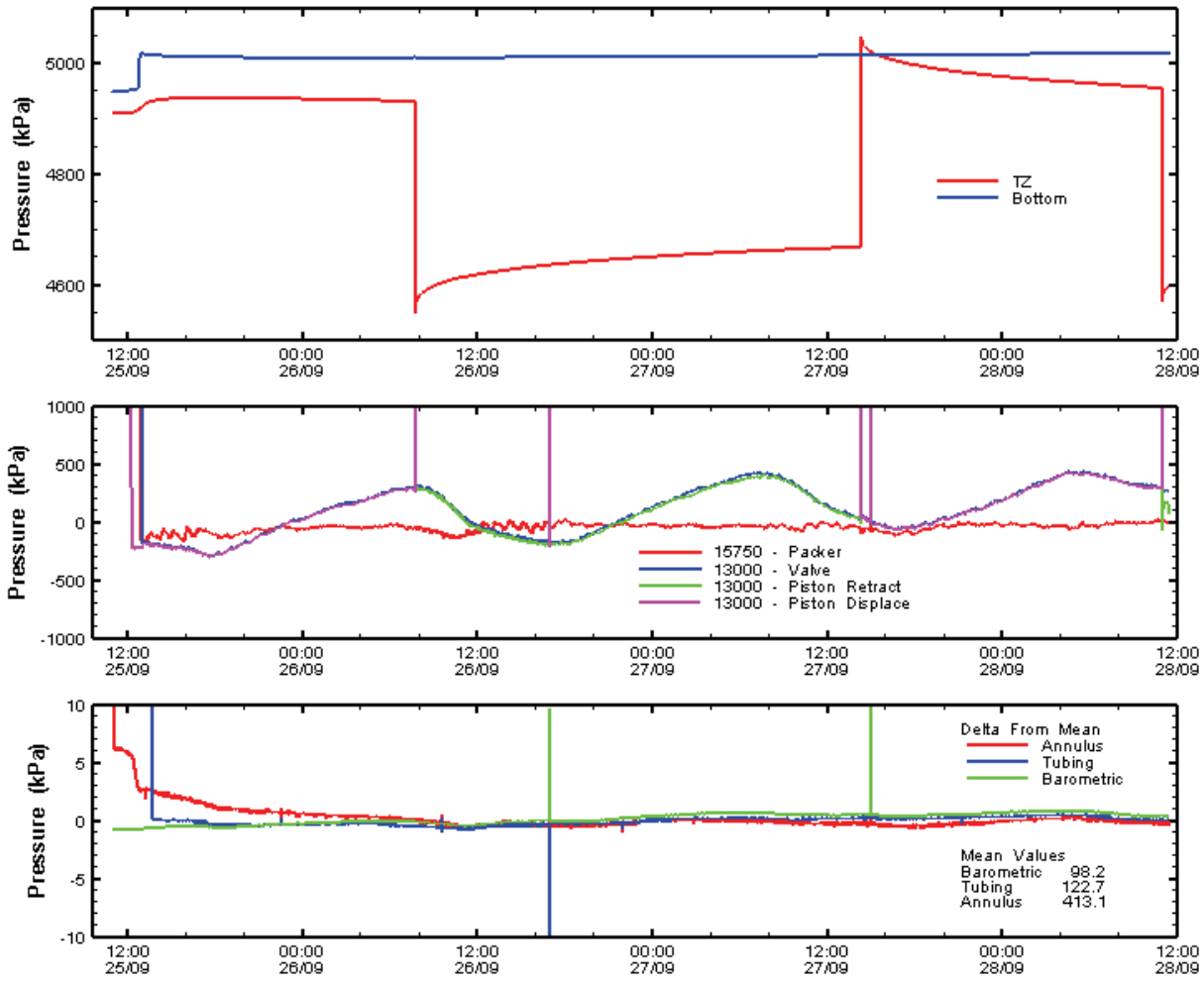

Figure 4.83: Pressure Data Recorded During Pulse Hydraulic Testing of Interval 471.41-502.15 mBGS in DGR-3 in Queenston Formation

The DGR borehole hydraulic test data were analysed to determine best-fit, minimum, maximum and mean estimates of formation hydraulic conductivity and formation pressure, and other formation parameters including borehole skin thickness and hydraulic conductivity, and formation specific storage. Test analyses included consideration of test interval pressure history based on drilling and drilling fluid density information and in-hole pressures recorded prior to packer isolation of the test interval.

The computer code used for analysis of the hydraulic tests was Sandia National Laboratories' numerical hydraulic-test simulator, nSIGHTS (**n**-dimensional **S**tatistical **I**nverse **G**raphical **H**ydraulic **T**est **S**imulator), a numerical well-test analysis code. Description of the straddle-packer hydraulic testing program including: testing and analysis methodologies, quantification of uncertainty using perturbation analyses, and detailed analysis of DGR-1, DGR-2, DGR-3, DGR-4, DGR-5 and DGR-6 tests are given in TR-08-32.

Figures 4.84 to 4.87 show examples of simulated tests and field test data used to determine horizontal formation hydraulic conductivity and static formation pressure. Figure 4.84 shows the comparison of best-fit simulated and measured test pressure for the pulse test of the 471.41-502.15 mBGS interval of the middle of the Queenston Formation in DGR-3. Figure 4.85 is the XY-scatter plot for the same test showing the goodness of fit for different estimates of formation hydraulic conductivity and static formation pressure derived from the perturbation analysis of the test data.

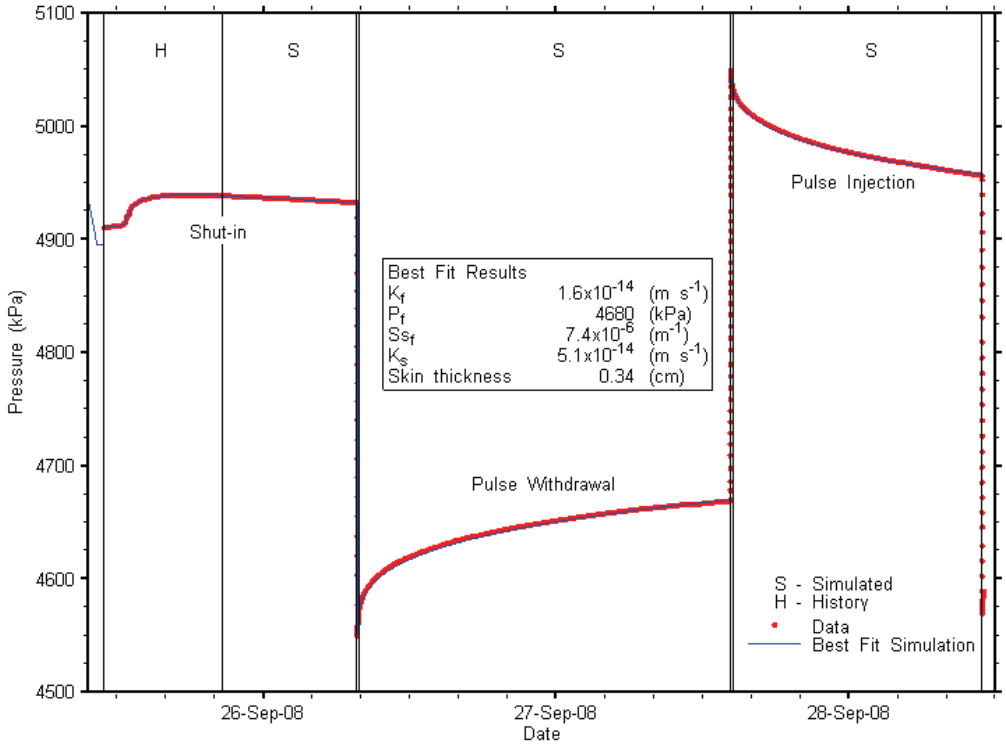

Note: Test Interval 471.41-502.15 mBGS in DGR-3 in the Queenston Formation.

Figure 4.84: Annotated Pulse Testing Sequence Showing Test Data, Best-fit Simulation and Parameter Estimates

Figure 4.84 shows the test sequence including the pre-shut-in period (with quantified pre-test pressure history – H), and the post-shut-in simulated (S) test phase comprising a pulse withdrawal and pulse injection that were completed over a three-day period. Analysis of this straddle-packer hydraulic test indicates an average horizontal formation hydraulic conductivity (K_f) of 1.6×10^{-14} m/s, negative skin of thickness 0.34 cm and hydraulic conductivity (K_s) of

5.1x10^{-14} m/s, and static formation pressure (P_f) of 4680 kPa. An estimate of test interval formation specific storage (Ss_f) of 7.4x10^{-6} m^{-1} is also generated from the test; however, the analysis is not particularly sensitive to this parameter.

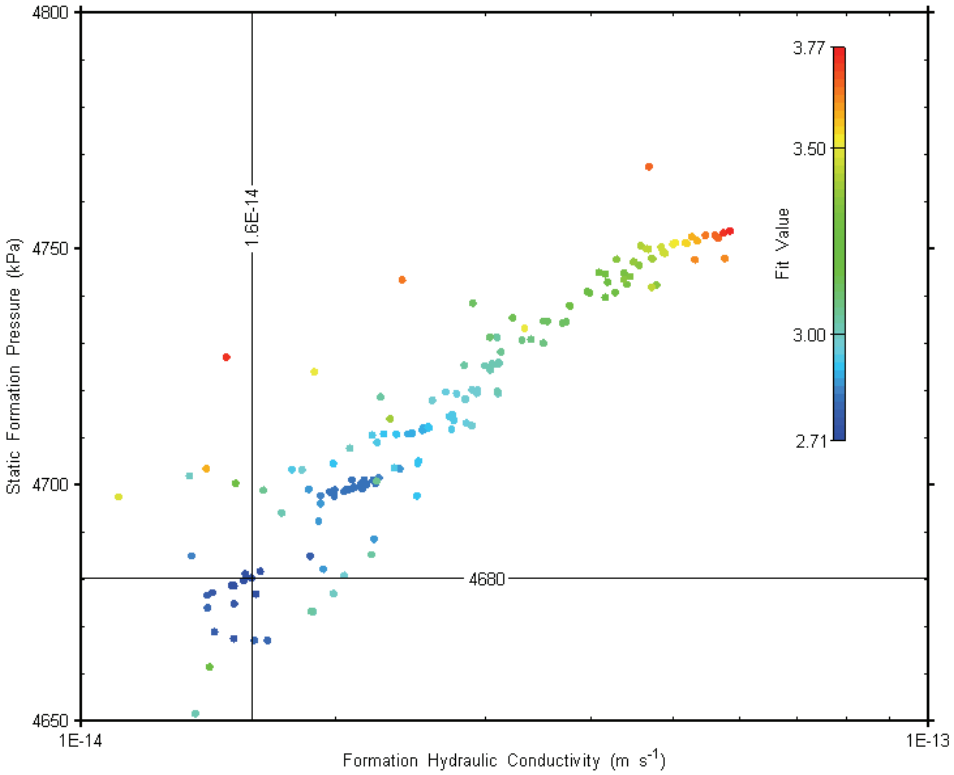

Note: Test Interval 471.41-502.15 mBGS in DGR-3 in Queenston Formation.

Figure 4.85: XY-scatter Plot Showing Estimates of Formation Hydraulic Conductivity and Raw Static Formation Pressure Derived from Perturbation Analysis

Figure 4.86 shows the comparisons of the best-fit simulated and measured test pressures for the pulse test of the 658.46-689.20 mBGS interval covering all of the Cobourg Formation limestone (the repository horizon) and the lower 3.0 m of the overlying Collingwood Member shale in DGR-4. Figure 4.87 is the XY-scatter plot for the same test showing the goodness of fit for different estimates of formation hydraulic conductivity and static formation pressure derived from the perturbation analysis of the test data.

Similar to Figure 4.84, Figure 4.86 shows the test sequence including the pre-shut-in period (with quantified pre-test pressure history – H), and the post-shut-in simulated (S) test phase comprising a pulse withdrawal and pulse injection that were completed over a three-day period. Analysis of this straddle-packer hydraulic test indicates an average horizontal formation hydraulic conductivity (K_f) of 2.4x10^{-14} m/s, a positive skin with thickness of 10.2 cm and hydraulic conductivity (K_s) of 6.6x10^{-15} m/s, and static formation pressure (P_f) of 5606 kPa. The formation specific storage value for this test analysis was set at 1.0x10^{-6} m^{-1}, a value estimated from preliminary perturbation analysis.

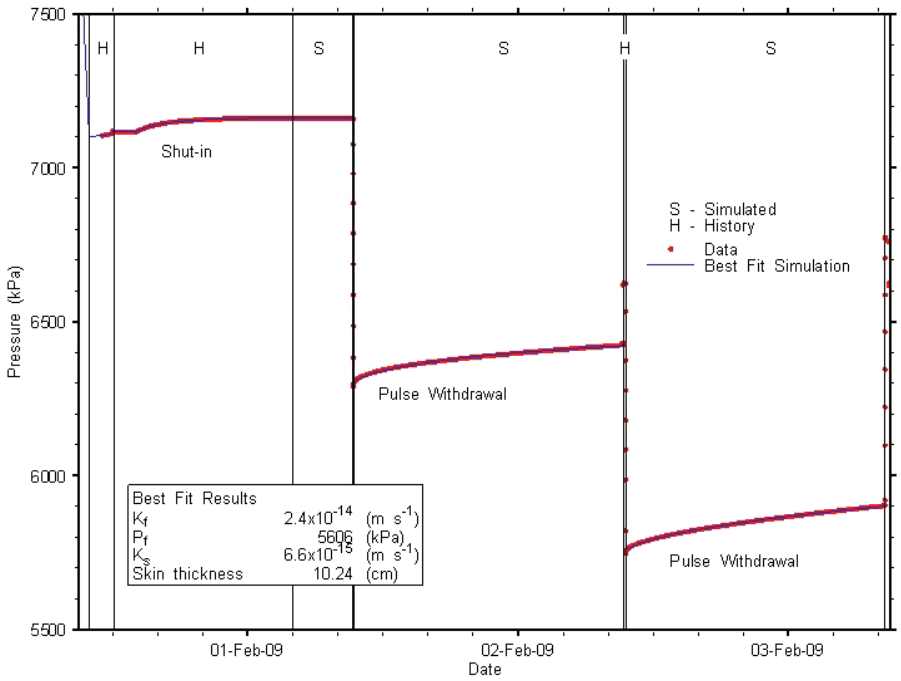

Note: Test Interval 658.46-689.20 mBGS in DGR-4 in the Cobourg Formation.

Figure 4.86: Annotated Pulse Testing Sequence Showing Test Data, Best-Fit Simulation and Parameter Estimates

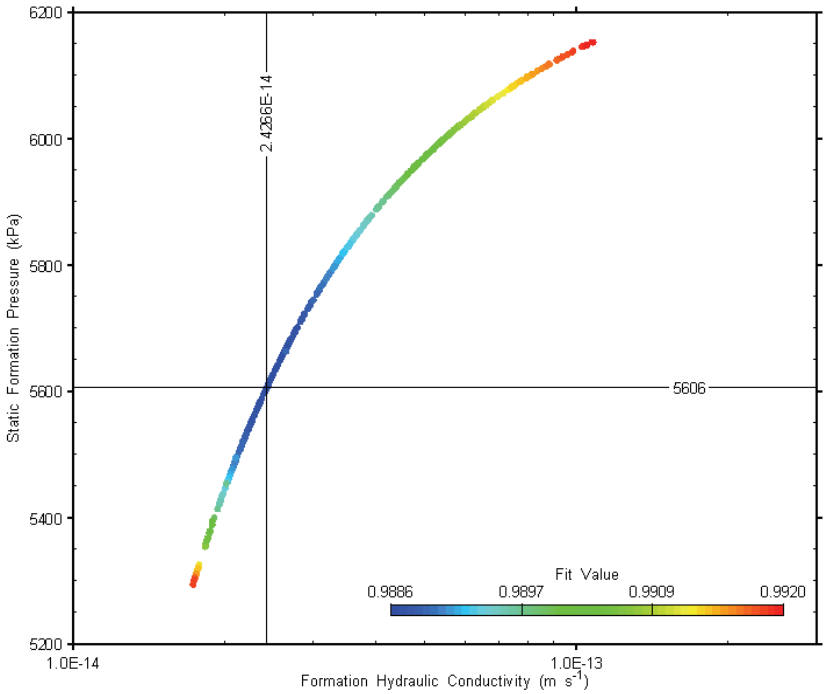

Note: Test Interval 658.46-689.20 mBGS in DGR-4 in the Cobourg Formation.

Figure 4.87: XY-scatter Plot Showing Estimates of Formation Hydraulic Conductivity and Raw Static Formation Pressure Derived from Perturbation Analysis

The results of the straddle-packer hydraulic testing of DGR boreholes are summarized versus depth and formation in Figures 4.88 and 4.89. Figure 4.88 shows calculated formation hydraulic conductivities and Figure 4.89 shows calculated test interval compressibilities. No straddle-packer hydraulic test results are available for the Shadow Lake Formation and Cambrian sandstone because of the installation of temporary PIPs to control formation fluid flow from the Cambrian sandstone.

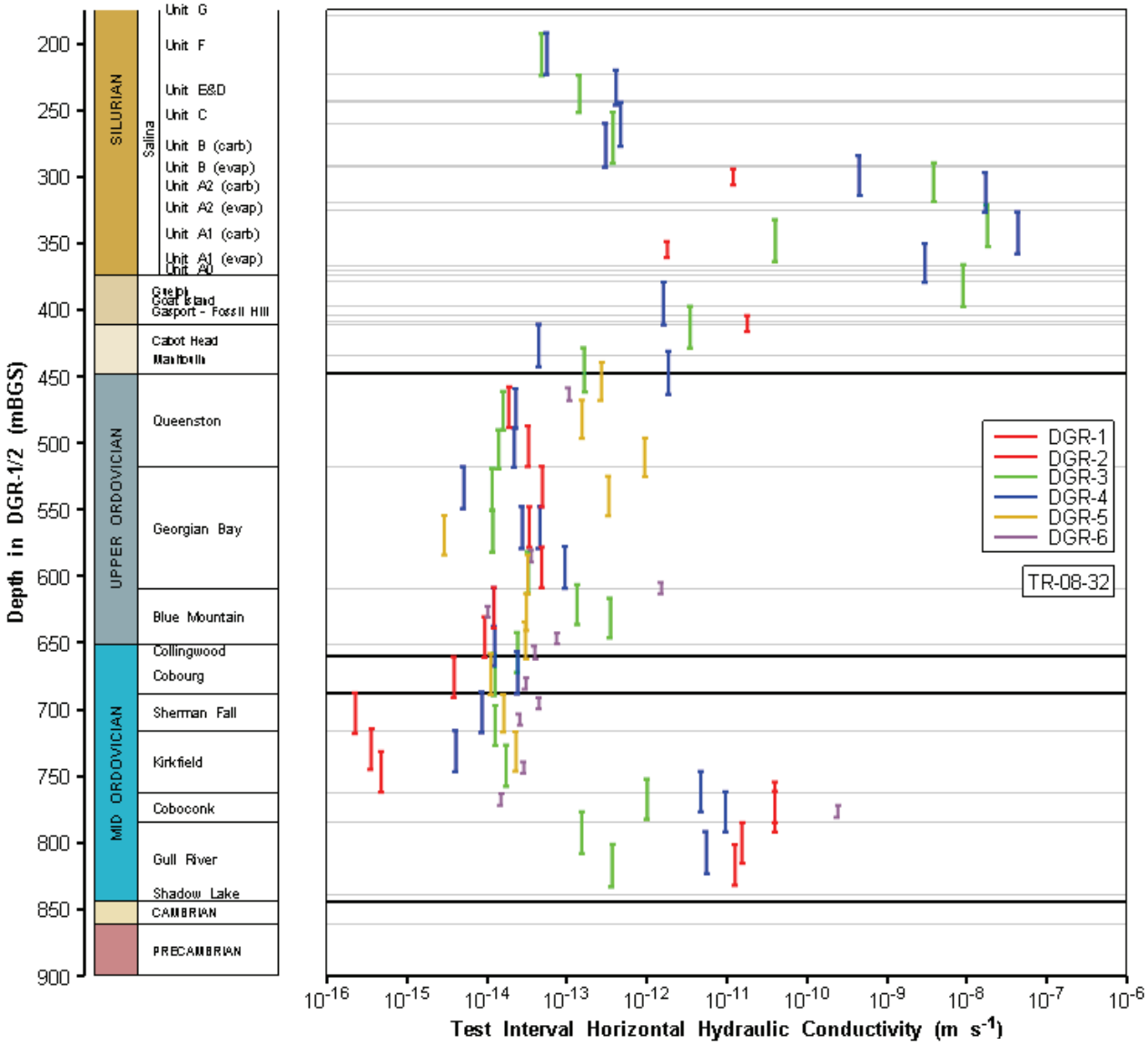

Figure 4.88: Profile of Test Interval Hydraulic Conductivity Estimates Determined from Field Straddle-Packer Testing in DGR Boreholes

Figure 4.88 shows that the calculated test interval hydraulic conductivities in DGR boreholes below the Salina G Unit range from approximately 10^{-16} to 10^{-8} m/s. The lowest measured test interval hydraulic conductivities of less than 10^{-15} m/s were determined from testing of the Sherman Fall and Kirkfield formations in DGR-2. The highest test interval hydraulic conductivities of greater than 10^{-8} m/s were determined for tests that included the porous and permeable sections of the Salina Upper A1 Unit and the Guelph Formation. The bedrock below the Guelph Formation to the Queenston shale has test interval hydraulic conductivity between $1x10^{-14}$ and $2x10^{-11}$ m/s.

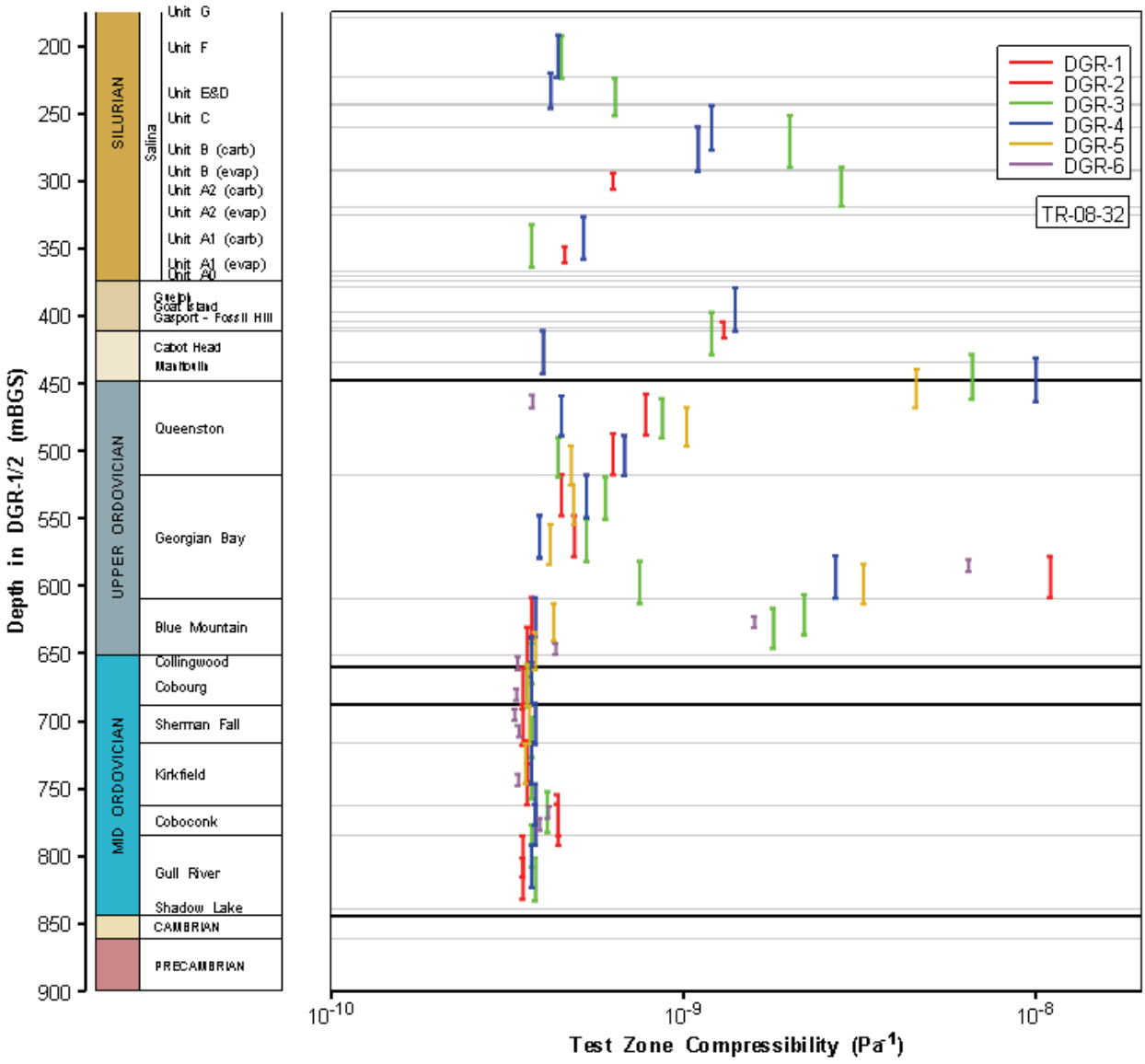

Figure 4.89: Profile of Test Interval Compressibilities Determined from Field Straddle-packer Testing in DGR Boreholes

The bulk of the Ordovician shales and all the Ordovician limestones from the Cobourg to the Kirkfield formation (i.e., the Trenton Group) have very low test interval hydraulic conductivity of less than 10^{-15} to $5x10^{-14}$ m/s. Slightly higher test interval hydraulic conductivities ($1x10^{-13}$ to $2x10^{-12}$ m/s), attributed to identified single fractures or zones of closely spaced fractures, were measured within one test interval in DGR-3 (Blue Mountain), one test interval in DGR-4 (lower Georgian Bay), three test intervals in DGR-5 (Queenston and Georgian Bay) and one test interval in DGR-6 (lower Georgian Bay). The deeper Ordovician limestones of the Black River Group (Coboconk and Gull River formations) have higher test interval hydraulic conductivity of between $1x10^{-13}$ and $2x10^{-10}$ m/s, which also may reflect the influence of thin, suspected increased permeability zones (e.g., dolomitized zones and volcanic ash layer).

Figure 4.89 shows the calculated test interval compressibilities from known fluid volume displacements of the pulse piston, calculated test interval volumes and the measured test interval pressure pulse magnitudes. Test interval compressibility is reported because it can be a diagnostic measure of packer compliance, formation compressibility, presence of gas within the test interval and adjacent formation or fractures, and/or dilation/closure of fractures or other permeable planar features that extend from the borehole into the formation.

Figure 4.89 shows that the test interval compressibilities are remarkably uniform and low within the Ordovician limestones and variable and larger within the overlying Ordovician shales and Silurian formations. The test interval compressibilities within the Ordovician limestones are all about 3-4 $x10^{-10}$ Pa^{-1}, which is essentially the compressibility of brine (TR-08-10). These very low test interval compressibilities demonstrate the extreme rigidity of the test equipment and that packer compliance is negligible in the pulse hydraulic tests. Consequently, the increased test interval compressibilities observed for Ordovician shales and Silurian formations (up to $1x10^{-8}$ Pa^{-1}) may be attributed to softer formations (e.g., Blue Mountain shales, Silurian evaporites), the presence of gas, or permeable fractures/features that exhibit near-borehole pressure-dependent dilation or closure during pressure pulse application.

4.9.2.2 Targeted Hydraulic Testing in DGR-6

In contrast to the continuous profile testing completed in DGR-2, DGR-3 and DGR-4, straddle-packer hydraulic testing in DGR-6 was completed with shorter test intervals and focused on evaluation of the hydraulic properties of specific targeted zones within the Ordovician shales and limestones. Typically, half of the test intervals were selected to evaluate massive intact sections of the Ordovician rocks and half of the test intervals were selected to evaluate sections with potential for enhanced permeability due to fractures and other features (e.g., dolomitized zones and ash layers). The selection of DGR-6 test intervals was made based on review of core logs and borehole geophysical logs, particular ATV images of the borehole walls and fluid temperature logs. Hydraulic properties of interest in the DGR-6 testing program included hydraulic conductivity, formation pressure and test zone compressibility.

A specific objective of the DGR-6 testing program was to determine if the occurrence of underpressured, normally pressured and overpressured zones within the Ordovician shales and limestones correlated with the presence or absence of fractures. This testing was completed within the Georgian Bay, Blue Mountain and Sherman Fall formations.

Table 4.13 summarizes the intervals tested in DGR-6, the rationale for the testing and the results of the testing. Table 4.13 lists the mean or best estimate of formation hydraulic conductivity (K), formation pressure (P_f) and an indication of whether the zone is normally pressured (=), overpressured (+) or underpressured (-), and test zone compressibility (Ctz).

Review of Table 4.13 shows that there is no apparent correlation of formation hydraulic conductivity and formation pressure conditions with the presence of fractures within the Ordovician shales and limestones in DGR-6. This observation suggests that fractures within the Ordovician shale and limestone formations tested are effectively sealed. Table 4.13 also shows that the cause of the elevated hydraulic conductivity within the Coboconk Formation in DGR-6 is the occurrence of fractures and dolomitized zones, not the volcanic ash layer. The occurrence of underpressures in DGR-6 appears to be limited to the Ordovician shales. Further discussion of formation pressure conditions in DGR boreholes is presented in Section 4.12.2.

4.9.2.3 Estimates of Average Formation Values

Figure 4.90 summarizes the estimates of formation horizontal hydraulic conductivity based on review of: 1) the consolidated results of all DGR borehole hydraulic testing, 2) hydraulic testing of US-series boreholes (Table 4.13), 3) core inspection, 4) observations of fluid loss during drilling of DGR boreholes and US-8 as discussed in Section 4.9.1, and 5) observations on fluid volume production and drawdown during opportunistic groundwater sampling of DGR boreholes and other data as discussed in TR-08-10.

Table 4.13: Summary of Straddle-packer Hydraulic Testing Results in DGR-6

Test No.	Formation	DGR-1/2 Reference Depth (mBGS)	Testing Rationale	K (m/s)	P_f (kPa)	Ctz (Pa)
1	Queenston	453.30 – 462.80	Massive shale	$1.1x10^{-13}$	4992 =	$3.7x10^{-10}$
2	Georgian Bay	572.46 – 581.09	Shale with fractures and limestone interbeds	$3.6x10^{-14}$	5661 -	$6.4x10^{-9}$
3	Georgian Bay	596.02 – 604.60	Interbedded shale and limestone	$1.5x10^{-12}$	5004 -	$2.5x10^{-8}$
4	Blue Mountain	614.49 – 623.14	Shale with fractures	$1.0x10^{-14}$	3340 -	$1.6x10^{-9}$
5	Blue Mountain	635.61 – 644.22	Massive shale	$7.4x10^{-14}$	6231 -	$3.6x10^{-10}$
6	Collingwood	645.71 – 654.31	Massive shale	$4.0x10^{-14}$	7302 +	$3.4x10^{-10}$
7	Cobourg	668.34 – 676.89	Massive limestone – repository horizon	$3.1x10^{-14}$	8296 +	$3.4x10^{-10}$
8	Sherman Fall	683.39 – 691.94	Massive limestone	$4.5x10^{-14}$	7484 =	$3.3x10^{-10}$
9	Sherman Fall	695.94 – 704.51	Limestone with fractures	$2.6x10^{-14}$	8258 +	$3.4x10^{-10}$
10	Kirkfield	732.76 – 741.35	Massive limestone	$2.9x10^{-14}$	9574 +	$3.4x10^{-10}$
11	Coboconk	756.93 – 765.55	Volcanic ash layer	$1.5x10^{-14}$	12023 +	$3.9x10^{-10}$
12	Coboconk	765.55 – 774.24	Limestone with fractures and dolomitized zone	$2.4x10^{-10}$	8943 +	$3.9x10^{-10}$

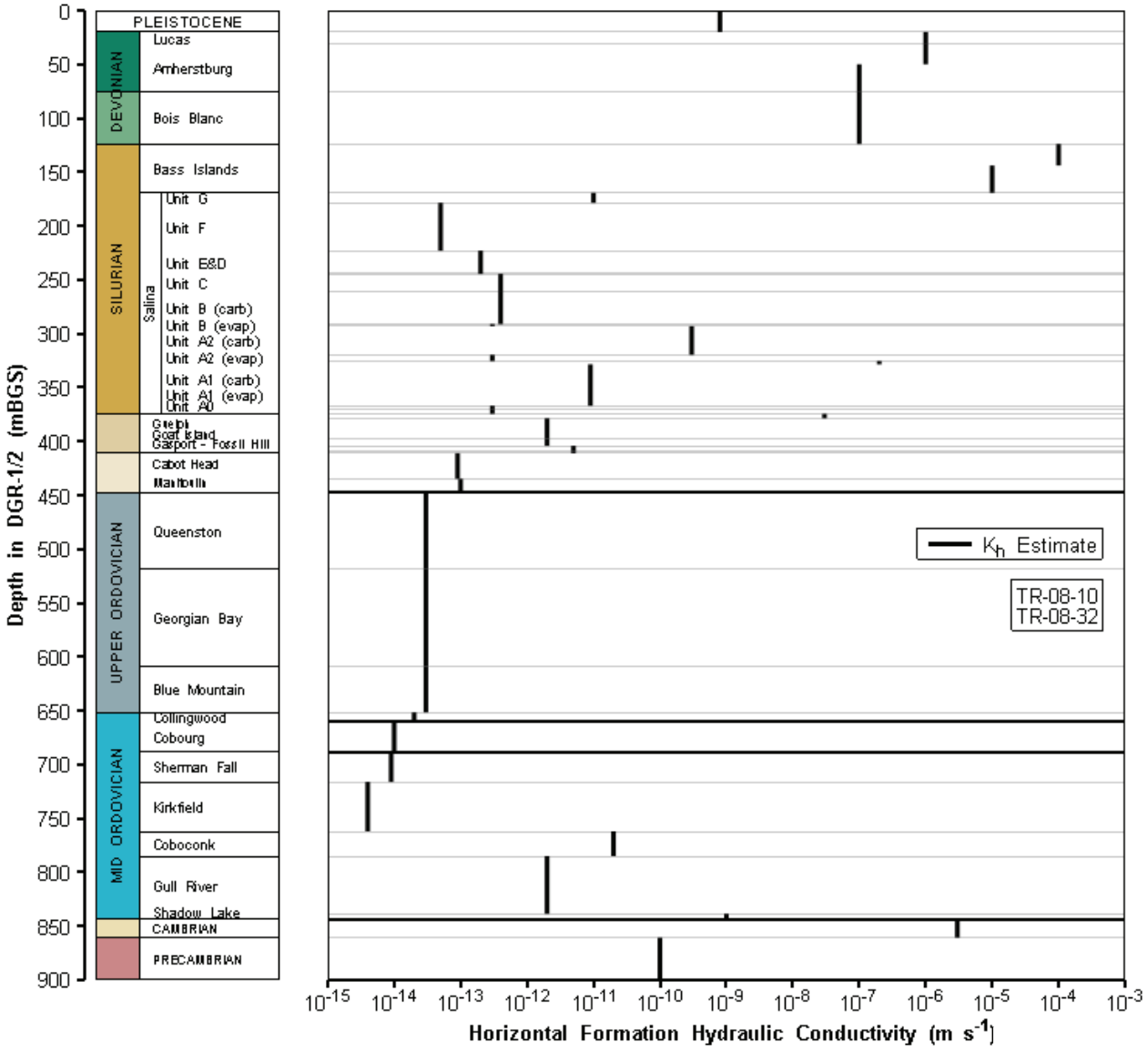

Figure 4.90: Estimates of Formation Horizontal Hydraulic Conductivity for Overburden and Bedrock Formations at the DGR Site

Table 4.14 provides the tabular summary of the representative estimates of formation horizontal hydraulic conductivity shown in Figure 4.90.

A review of Figure 4.90 and Table 4.14 shows that the Devonian and Upper Silurian dolostone formations (Lucas to Bass Islands) have moderate to high horizontal hydraulic conductivity, typically larger than 10^{-7} m/s, with an important high-permeability (drill fluid loss) zone in the upper 20 m of the Bass Islands Formation.

Table 4.14: Summary of Representative Horizontal Hydraulic Conductivities of DGR Formations

Formation	Depth of Top in DGR-1/2 (mBGS)	K_h (m/s)
Clay till overburden	0	$8x10^{-10}$
Lucas	20.0	$1x10^{-6}$
Amherstburg (top 20 m)	30.4	$1x10^{-6}$
Amherstburg (lower 25 m)	50.0	$1x10^{-7}$
Bois Blanc	75.0	$1x10^{-7}$
Bass Islands (upper 20m)	124.0	$1x10^{-4}$
Bass Islands (lower 25 m)	144.0	$1x10^{-5}$
Salina G Unit	169.3	$1x10^{-11}$
Salina F Unit	178.6	$5x10^{-14}$
Salina E Unit	223.0	$2x10^{-13}$
Salina D Unit	243.0	$2x10^{-13}$
Salina C Unit	244.6	$4x10^{-13}$
Salina B Unit - Carbonate	260.3	$4x10^{-13}$
Salina B Unit - Evaporite	291.2	$3x10^{-13}$
Salina A2 Unit - Carbonate	293.1	$3x10^{-10}$
Salina A2 Unit - Evaporite	319.7	$3x10^{-13}$
Salina A1 Unit – Upper Carbonate	325.5	$2x10^{-7}$
Salina A1 Unit - Lower Carbonate	328.5	$9x10^{-12}$
Salina A1 Unit - Evaporite	367.0	$3x10^{-13}$
Salina A0 Unit	370.5	$3x10^{-13}$
Guelph	374.5	$3x10^{-8}$
Goat Island	378.6	$2x10^{-12}$
Gasport	397.4	$2x10^{-12}$
Lions Head	404.2	$5x10^{-12}$
Fossil Hill	408.7	$5x10^{-12}$
Cabot Head	411.0	$9x10^{-14}$
Manitoulin	434.8	$1x10^{-13}$
Queenston	447.7	$3x10^{-14}$
Georgian Bay	518.0	$3x10^{-14}$
Blue Mountain	608.9	$3x10^{-14}$
Cobourg – Collingwood Member	651.6	$2x10^{-14}$
Cobourg - Lower	659.5	$1x10^{-14}$

Formation	Depth of Top in DGR-1/2 (mBGS)	K_h (m/s)
Sherman Fall	688.1	$9x10^{-15}$
Kirkfield	716.1	$4x10^{-15}$
Coboconk	762.0	$2x10^{-11}$
Gull River	785.0	$2x10^{-12}$
Shadow Lake	838.6	$1x10^{-09}$
Cambrian	843.8	$3x10^{-06}$
Upper Precambrian	860.7	$1x10^{-10}$

The majority of the Upper Silurian formations have very low horizontal formation hydraulic conductivities of $5x10^{-14}$ to $5x10^{-13}$ m/s, with the exception of the G Unit dolostone and the A2 Unit dolostone with formation K_h of $1x10^{-11}$ and $3x10^{-10}$ m/s, respectively, and a vuggy zone in the upper part of the A1 Unit dolostone, which has hydraulic conductivity of about $2x10^{-7}$ m/s. The hydraulic conductivity for the upper part of the A1 Unit dolostone was determined by assuming that all of the flow in the longer straddle-packer test interval occurred within the average 3.5 m length of vuggy and porous core. Figure 3.22 shows the core photograph of this permeable vuggy zone of the Salina Upper A1 Unit in DGR-4.

The Middle and Lower Silurian formations have very low formation hydraulic conductivity of about $1x10^{-13}$ m/s (Cabot Head and Manitoulin formations) to $2x10^{-12}$ to $5x10^{-12}$ m/s (Goat Island, Gasport Lions Head and Fossil Hill formations). The most permeable interval in the Middle to Lower Silurian formations in DGR boreholes is the vuggy Guelph Formation dolostone with K_h of $3x10^{-8}$ m/s, again based on an average effective zone length of about 5.1 m determined from core logging applied to the longer interval straddle-packer test result (i.e., assuming all of the test flow occurs within this 5.1-m vuggy zone). Figure 3.25 shows the appearance of the Guelph Formation in DGR-1. Figure 4.91 shows this same permeable vuggy section of the Guelph Formation dolostone found in DGR-4.

The average formation horizontal hydraulic conductivities of the Ordovician shales, based mostly on 30-m test interval lengths, are relatively uniform ranging from $2x10^{-14}$ to $3x10^{-14}$ m/s with the lower value estimated for the Collingwood Member. The Trenton Group limestones consisting of the Cobourg, Sherman Fall and Kirkfield formations, have estimated formation K_h values of $1x10^{-14}$, $9x10^{-15}$ and $4x10^{-15}$ m/s, respectively. The Black River Group limestones consisting of the Coboconk and Gull River formations have higher estimated formation K_h of $2x10^{-11}$ and $2x10^{-12}$ m/s, respectively. All of the current estimates of formation K_h are based on the final results of the analysis of straddle-packer tests in DGR-1 through DGR-6 boreholes (TR-08-32).

Formation K_h estimates for the Shadow Lake Formation and the upper several tens of metres of the Precambrian basement rocks are based on review of borehole test results completed and compiled by Raven et al. (1992a, 1992b). The Shadow Lake Formation has an estimated formation K_h of $1x10^{-9}$ m/s and the upper Precambrian basement has an estimated formation K_h of $1x10^{-10}$ m/s. The permeable Cambrian sandstone has an average K_h of $3x10^{-6}$ m/s based on completion of flow tests in the Cambrian during opportunistic groundwater sampling in DGR-2, DGR-3 and DGR-4, and general observations of volumes and heads of produced formation fluids during drilling.

Figure 4.91: Permeable Vuggy Core in Guelph Formation Dolostone, 375 mBGS, DGR-4

4.9.3 Comparison of Field and Laboratory K Data

Figure 4.92 shows comparison of the field and laboratory hydraulic test data expressed as hydraulic conductivity (K). For ease of presentation, field K data in Figure 4.92 are shown as the representative best estimates of formation horizontal hydraulic conductivity (K_h) which are derived primarily from review of borehole hydraulic testing data. Figure 4.92 also shows the laboratory-derived estimates of horizontal and vertical permeability determined from gas pulse permeability testing of "as received" cores and from brine pulse permeability testing, which are the test results least affected by sample preparation (see Section 4.3.4). Lab results were converted from permeability to hydraulic conductivity assuming an average brine density of 1150 kg/m^3 and a dynamic viscosity of 0.002 Pa·s. The clustering of K values at $5x10^{-14}$ m/s represents the lower testing limit of the Core Labs gas and brine pulse testing equipment. Actual lab K data for these tests will be less than the plotted values.

Figure 4.92 clearly shows the overestimation of in situ K by laboratory gas and brine pulse testing for most of the samples tested within the Ordovician shales and, to a lesser degree, within the Ordovician Trenton limestones, as discussed in Section 4.3.4. The overestimation of K for the Ordovician shales ranges from 1 to 4 orders of magnitude, whereas the overestimation for the Ordovician Trenton limestones typically ranges from 1 to 3 orders of magnitude. The Ordovician Black River limestones show comparable field and lab estimates of K, with increasing lab K with depth into the Gull River Formation. The estimated field result (Raven et al. 1992a – borehole OHD-1) and the lab data for the Shadow Lake Formation are comparable at about $1x10^{-9}$ m/s.

Figure 4.92 also shows similar overestimation of K for the Salina F Unit shale and Cabot Head shale with lab data ranging up to 3 orders of magnitude larger than in situ field estimates. The remaining Silurian dolostone, shale and evaporite rocks show significant scatter in lab test data

but generally show the field best estimates represent the central tendency of the lab data. The notable exception to this general observation is the Salina A2 Unit Carbonate which shows higher field estimate than lab data. This is most likely due to the occurrence of several permeable fractures (evident from review of hydraulic testing (TR-08-32), core logging (TR-07-06) and borehole geophysical logging (TR-07-08)) identified in the upper half of the carbonate unit that was subject to packer testing.

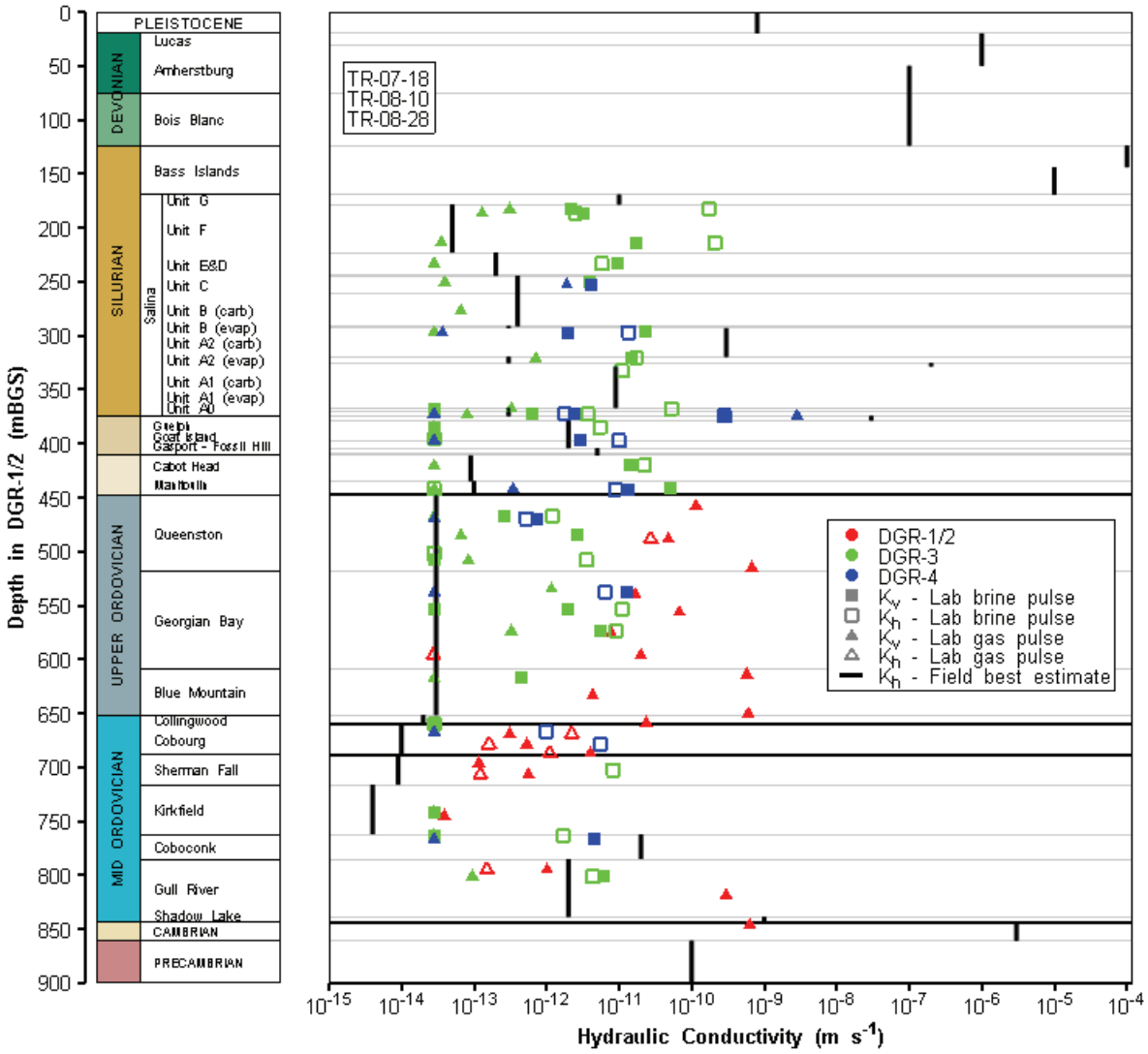

Figure 4.92: Comparison of Best Estimates of Formation K_h Based on Field Testing and Laboratory K_h and K_v Determined from "As Received" Gas Pulse Testing and Brine-saturated Pulse Testing of DGR Cores

Comparison of the field and laboratory K data for the Cambrian sandstone shows that the field estimate is more than a thousand times higher than the lab test. This difference is mostly a reflection of facies changes in the Cambrian (the upper Cambrian sample that was subject to

lab testing is primarily fine-grained dolostone) and the occurrence of open permeable fractures in the deeper Cambrian sandstone.

Figure 4.92 clearly shows that the best and most reliable estimates of hydraulic conductivity for the majority of low-permeability DGR bedrock formations are derived from in situ hydraulic testing.

4.10 Rock Matrix Compressibility

Uniaxial compression testing (TR-07-03, TR-08-24, TR-08-39, TR-09-07) and porosity characterization (Section 4.3.2) of intact cores collected from DGR boreholes allow estimation of formation matrix compressibility and specific storage properties (TR-08-10) (see Figure 4.93). Such matrix properties do not consider the effects of any fractures or the presence of gas, and hence might be expected to underestimate overall formation properties if fractures or gas were present. Quantification of such poroelastic properties are important for understanding and predicting both short-term and long-term transient hydraulic responses of the Paleozoic bedrock sequence at the Bruce nuclear site to hydraulic and geomechanical perturbations such as DGR excavation and glacial and erosional unloading. Independent quantification of specific storage also allows for more accurate interpretation of straddle-packer hydraulic tests and determination of formation hydraulic conductivity.

Stress-strain data collected during uniaxial compression testing were analysed to determine Young's moduli and Poisson's ratio (see Chapter 5), undrained and drained bulk moduli, and undrained and drained rock compressibility considering uniaxial and triaxial loading conditions. Because of uncertainty over drained versus undrained laboratory testing conditions and uniaxial versus triaxial field conditions, low and high estimates of rock formation compressibility are determined (see Figure 4.93). Specific storage values were then calculated from formation-averaged total porosity and pore fluid density values and low and high estimates of individual core rock compressibility data. The methods and results of these compressibility and specific storage calculations are provided in TR-08-10.

Figure 4.93 shows the calculated low and high values of rock matrix compressibility by depth and formation from testing of DGR core as well as the low and high geometric mean formation averages. Figure 4.93 shows that the competent Devonian and Silurian dolostones and the Ordovician limestones generally have formation compressibility of about 10^{-11} to 10^{-10} Pa. The Salina B Unit Carbonate, Cabot Head shale and the Ordovician shales are more compressible with compressibilities of about 10^{-10} to 10^{-9} Pa. There is noticeable increase in rock compressibility with increasing depth within the Ordovician shales, with maximum values evident within the Blue Mountain Formation. The calculated compressibility values for the Ordovician shales are typically an order of magnitude greater than those properties of the Ordovician limestones. The most compressible formations in DGR boreholes are the Salina B Unit Carbonate, and the Cabot Head and Blue Mountain shales.

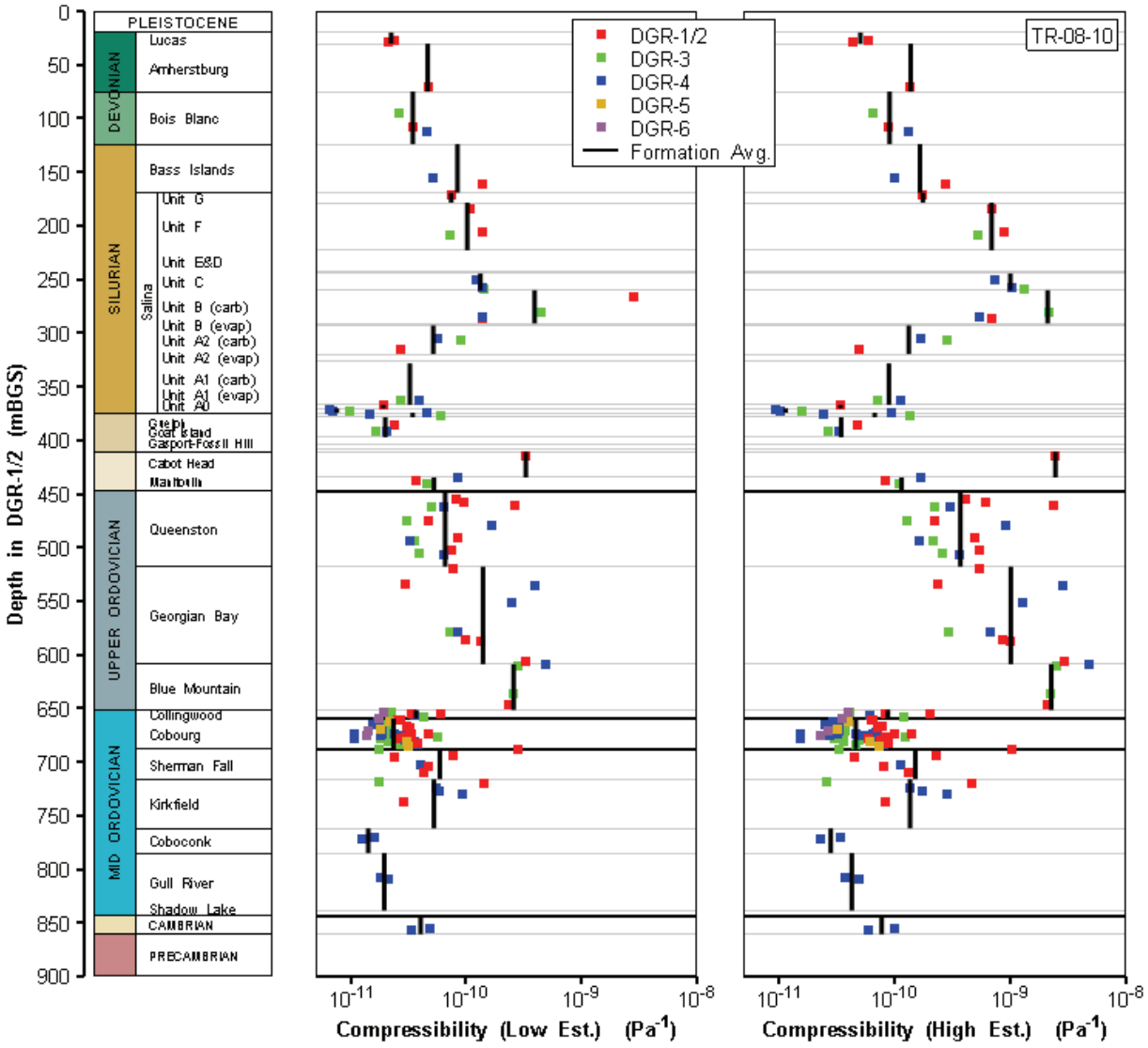

Figure 4.93: Profiles of Low and High Estimates Rock Matrix Compressibility in DGR Boreholes Showing Point Data and Formation Averages

4.11 Rock Matrix and Formation Specific Storage

Figure 4.94 shows the comparison of low and high estimates of rock matrix specific storage determined from laboratory geomechanical testing and formation values determined from analysis of field hydraulic testing in DGR boreholes (TR-08-32). The geometric mean best estimates from lab testing are shown in Figure 4.94 as boxes based on low and high best estimates of rock compressibility. The formation specific storage values for all DGR borehole hydraulic tests are also shown for each test interval.

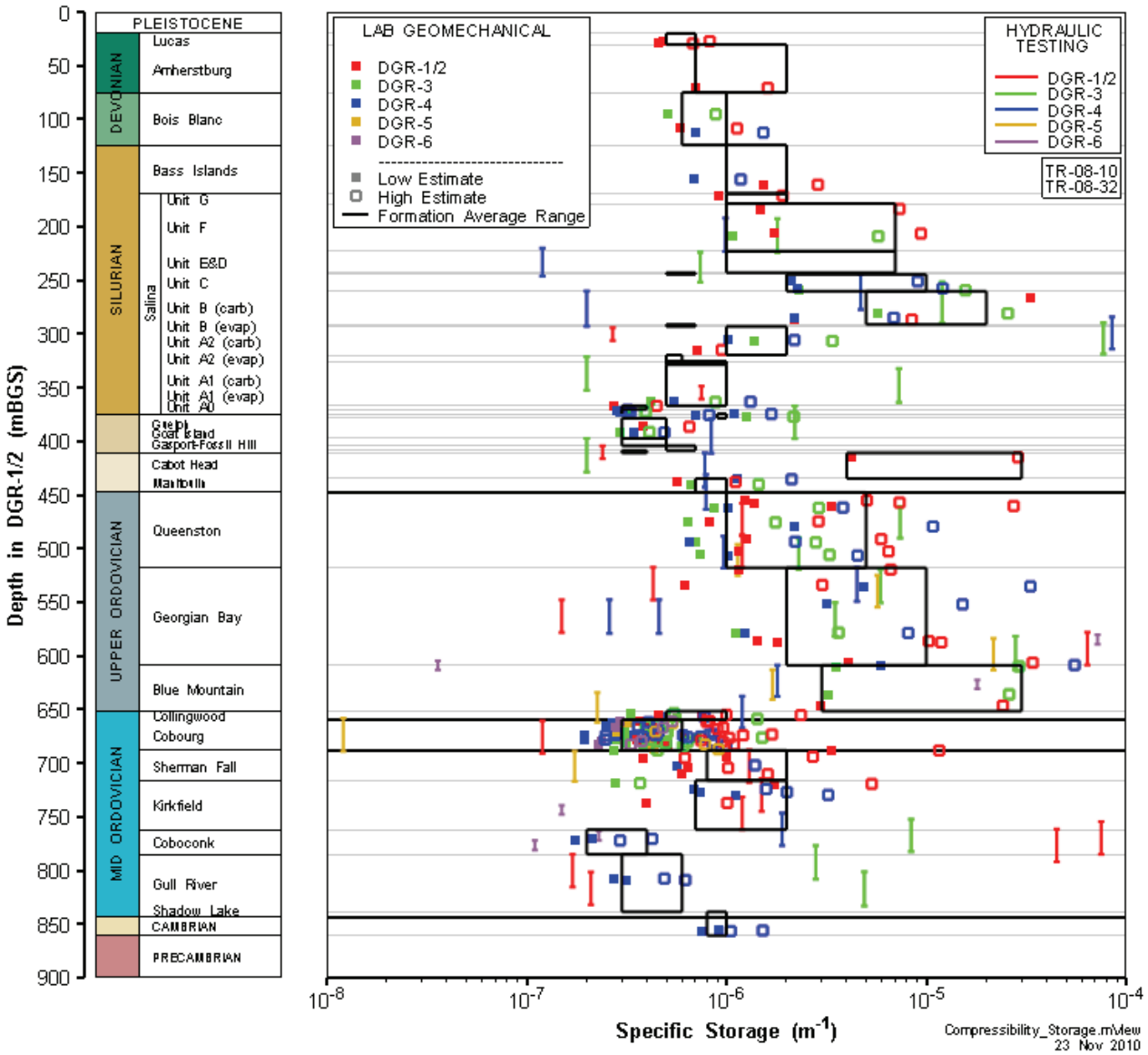

Figure 4.94: Profiles of Low and High Estimates of Specific Storage in DGR Boreholes Showing Point Data and Formation Averages from Laboratory Testing and Field Values Determined from Straddle-packer Testing

Two observations are noteworthy for Figure 4.94. Firstly, the calculated specific storage values from lab geomechanical testing track very closely with the ranges of rock compressibility indicating that formation porosity and fluid density are not significant contributors to specific storage. Specific storage is determined primarily from rock compressibility data. Secondly, formation specific storage values determined from field hydraulic testing show a much wider range than values determined from lab geomechanical testing. The reported range of specific storage from analysis of straddle-packer testing is about $1x10^{-8}$ to $1x10^{-4}$ m, with most values falling the range of $1x10^{-7}$ to $1x10^{-5}$ m. There is noticeable increase in matrix specific storage with increasing depth within the Ordovician shales and the presence of lower values within the

more competent Silurian dolostones and Ordovician limestones. The Silurian B Unit Carbonate, Cabot Head shale and Blue Mountain shale have the highest specific storage values approximating $1x10^{-5}$ m.

The values of formation specific storage from field hydraulic testing that are more than an order of magnitude greater than laboratory values are most likely reflective of fracture and/or gas presence effects. For example, field tests of the Salina A2 Unit Carbonate in DGR-3 and DGR-4, the Georgian Bay Formation in DGR-2 and DGR-6, and the Coboconk Formation in DGR-2 are of intervals that contain clearly defined fractures (see Figures 3.51 and 3.61) or thin permeable dolomitized zones, that may show dilational effects during testing and may contain compressible gas.

4.12 Formation Pressures and Hydraulic Heads

4.12.1 Shallow Bedrock – US Wells

Shallow bedrock boreholes US-3, US-7 and US-8, instrumented with Westbay MP38 multi-level monitoring casings (TR-07-20), provide profiles of formation pressures from 31 packer-isolated intervals in the shallow bedrock at the Bruce nuclear site to depths of 200 m (TR-08-08, TR-08-30). Formation pressures in US-3, US-7 and US-8 are analyzed and presented as freshwater hydraulic heads (Figure 4.95) as the groundwater densities in these wells, based on groundwater sampling, are all about 990-1000 kg/m^3 or less (see Section 4.8).

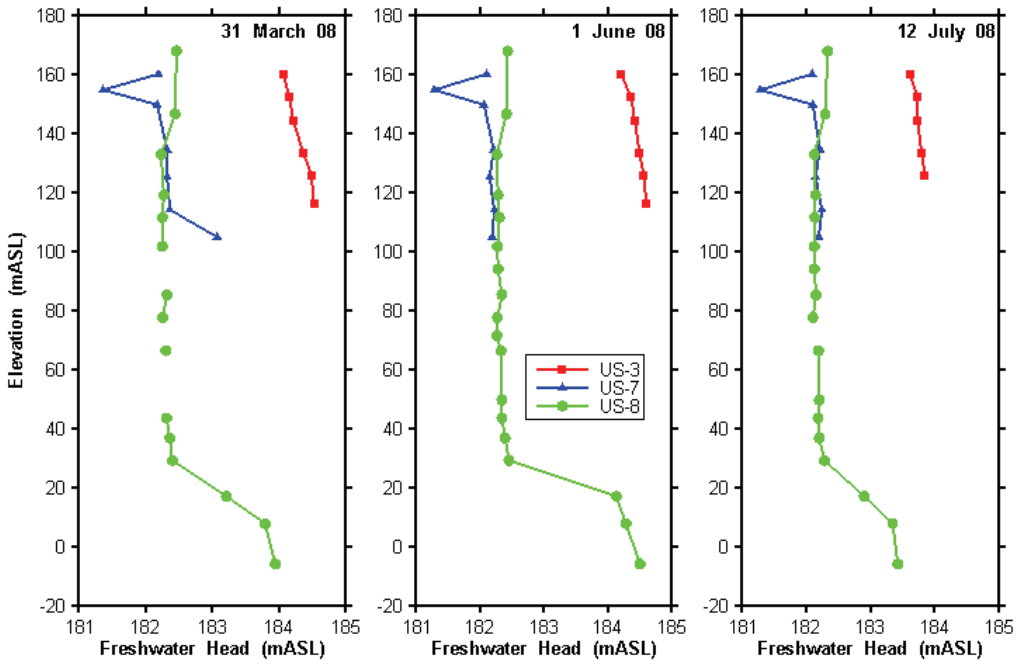

Figure 4.95: Hydraulic Head Profiles – US-3, US-7 & US-8 from March to July, 2008

Pressure profiles were completed in US-3, US-7 and US-8 in March, late May-early June and July, 2008 (Figure 4.95) following casing installation in US-3 and US-7 on December 10 and 11, 2007 and in US-8 on March 6, 2008. Subsequent to summer 2008, pressure profiles were completed on a quarterly basis.

Figure 4.95 shows stable hydraulic head profiles indicating slight upward hydraulic gradients (0.001 to 0.01 m/m) and lateral flow to the northwest toward Lake Huron. Quarterly pressure profiles completed after this spring/summer 2008 monitoring (TR-08-30), have shown similar hydraulic gradients and groundwater flow directions.

4.12.2 Deep Bedrock – DGR Boreholes

Boreholes DGR-1, DGR-2, DGR-3 and DGR-4 were completed with Westbay stainless steel and PVC MP55 multi-level monitoring casings, primarily to provide access for formation pressure measurement, but also to allow for future groundwater sampling. MP55 casings were not installed in DGR-5 and DGR-6. DGR-5 and DGR-6 were sealed with PIPs (TR-09-10).

MP55 casings were installed in DGR-1 and DGR-2 on September 25 and December 13, 2007. MP55 casings were installed in DGR-3 and DGR-4 on September 28 and April 30, 2009. For reasons outlined below, the MP55 casing installed in DGR-2 on December 13, 2007 was successfully removed on June 5, 2009. An improved and upgraded MP55 casing system was installed in DGR-2 on December 2, 2009. Table 4.15 summarizes the design elements of the MP55 casing systems installed in DGR boreholes. Pressure measurement ports in MP55 casings are typically located 3 m below the top of each monitoring interval (TR-07-10, TR-08-17).

Table 4.15: Major Design Elements of MP55 Casing Systems Installed in DGR Boreholes

MP55 Casing Element	DGR-1	DGR-2 (old)	DGR-2 (new)	DGR-3	DGR-4
Monitored Depth Range (mBGS)	190.7 to 462.9	460.4 to 848.0	460.7 to 846.7	218.3 to 869.2	194.3 to 852.5
Number of Packers	23	28	27	43	43
Number of Formation Pressure Monitoring Intervals	22	25	24	42	42
Average Monitoring Interval Length (m)	11.3	14.4	14.7	14.0	14.3
Range of Monitoring Interval Lengths (m)	3.4 to 24.0	3.0 to 23.0	5.2 to 24.2	4.7 to 28.7	3.2 to 24.2
Number of Pressure Profiles Completed to June 2010	13	6 + Continuous MOSDAX	2	3	4

Profiles of formation pressure were typically measured in DGR boreholes immediately following casing installation (i.e., packer inflation), on an approximate monthly basis for the next three months, and then on a quarterly basis. Table 4.15 lists the total number of continuous pressure profiles completed in each DGR borehole up to June 30, 2010 including initial post-inflation profiles. On March 4, 2008 a MOSDAX string of 10 pressure transducers was installed in DGR-

2 to provide continuous records of formation pressure in 10 key test intervals. This MOSDAX system operated for approximately 13 months, until this pressure-measurement system was removed from DGR-2 on April 2, 2009.

In the very low permeability formations that characterize large sections of all DGR boreholes, formation pressures are slow to equilibrate. Consequently, measured formation pressures in DGR boreholes are reported here for selected monitoring dates that provide a reasonable representation of the temporal evolution of formation pressures. For each DGR borehole, the measured formation pressures are plotted relative to freshwater hydrostatic and density-compensated hydrostatic pressure lines and for each pressure survey, the elapsed time after casing installation is identified in parentheses. The measured in situ pressures are also plotted with the best-fit estimates of test interval formation pressure from analyses of the straddle-packer hydraulic tests as described in TR-08-32. All formation pressures are plotted using the test interval lengths.

In addition to pressure plots, the pressure data are converted to environmental head considering the reference formation fluid density profile provided in Figure 4.81. Calculated environmental heads are plotted with the vertical ground surface elevation line as a reference point for the calculated heads. Environmental heads from MP55 casings are plotted as the value at the pressure measurement port; heads from hydraulic testing are plotted as the test interval length. Fresh water and environmental heads were calculated from formation pressures following the methods of Lusczynski (1961) and Jorgensen et al. (1982) as described in TR-08-31. Environmental heads are suitable for assessing vertical groundwater flow potentials in variable-density groundwater flow systems. Detailed description of the calculations for determination of freshwater hydrostatic and density-compensated hydrostatic pressure lines, and of environmental heads is also provided in TR-08-31.

4.12.2.1 DGR-1 and DGR-2 (Old)

Figure 4.96 shows the temporal evolution of pressures and heads in DGR-1 over a 1.5- to 29-month period after casing installation on September 25, 2007. Figure 4.96 shows that stable formation pressures and heads occur in almost all of the Salina Formation after an equilibration period of about 5 months. The environmental head profile is accurate with the minimum environmental head of about 170 mASL occurring in the middle of the formation at the bottom of the Salina B Unit.

Formation pressures and heads for the permeable Salina Upper A1 Unit and Guelph Formation aquifers are stable in all pressure profiles. Elevated pressures and environmental heads are observed within lower Salina A1 evaporite and A0 Units and the underlying Goat Island to upper Cabot Head formations. These Westbay pressures measured in the Lions Head, Fossil Hill and upper Cabot Head formations are very similar to the estimated formation pressures from borehole hydraulic testing. The increasing and high pressures measured in these formations may be related to gas occurrence, as hydrocarbons in the form of crude oil were observed in the bottom of the Salina A1 Unit. Gas occurrence and up-dip migration have been credible explanations for overpressures measured in tight Paleozoic rocks in southern Ontario (Raven et al. 1992a).

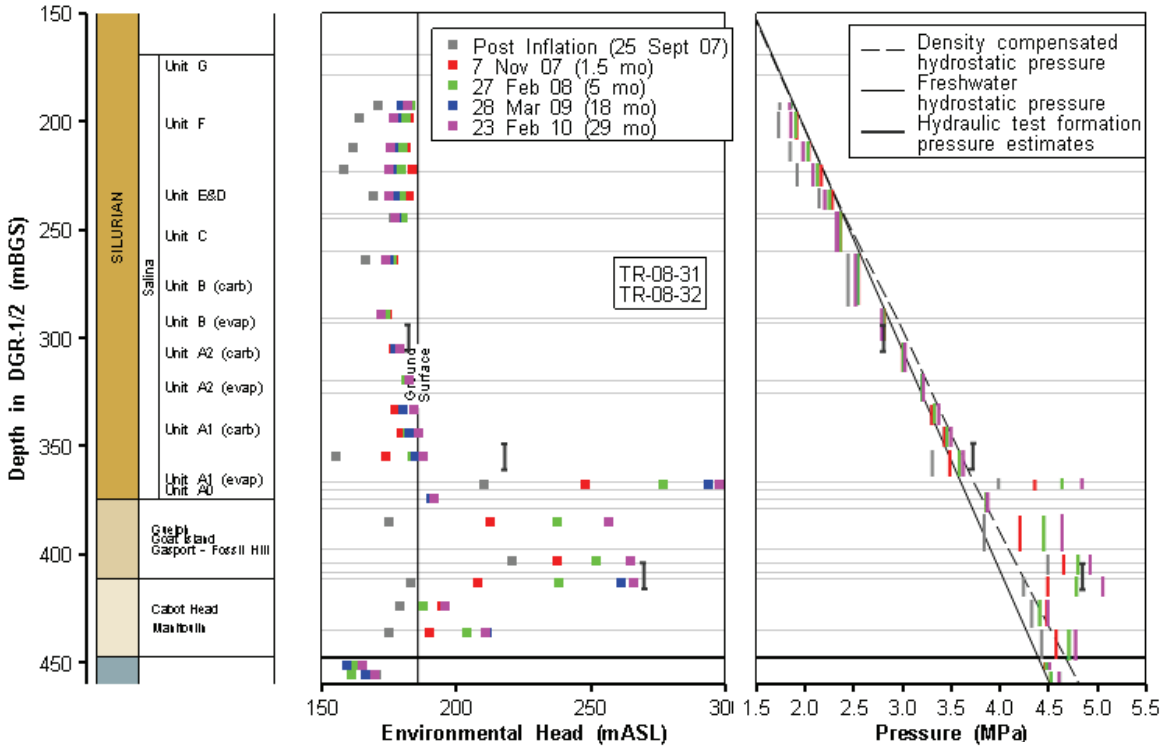

Figure 4.96: DGR-1 Formation Pressure and Environmental Head Profiles, September 2007 (Post Inflation), February 2008, March 2009 and February 2010

The very bottom of DGR-1 shows environmental heads that are underpressured relative to the vertical ground surface line and all other environmental heads in DGR-1. These underpressures and low environmental heads are entirely consistent with deeper data recorded in DGR-2 (Figure 4.97).

Figure 4.97 shows the temporal evolution of pressures and heads in DGR-2 over about a 1- to 4-month period after casing installation in DGR-2 on December 11, 2007, plotted together with data from DGR-1. Figure 4.97 shows the development of significant underpressures within the Ordovician shales and Trenton Group limestones with environmental heads approaching -70 mASL or 255 mBGS.

Pressure data collected from DGR-2 also show the occurrence of a slightly overpressured zone within the lower part of the Georgian Bay that has elevated test interval compressibility from hydraulic testing and is suspected to be associated with an inclined fracture at 585.7 mBGS possibly containing gas (see Figure 3.61). This slightly overpressured zone also shows interval hydraulic conductivity $5x10^{14}$ m/s, comparable to the surrounding rock mass. Figure 4.97 also shows that large overpressure extends downward from the Coboconk Formation to the Cambrian sandstone. The deepest formation pressures in DGR-2 are equivalent to an environmental head of about 350 mASL or 165 m above ground surface (AGS). Both the underpressures and overpressures were also estimated from interpretation of Phase 2 borehole hydraulic tests.

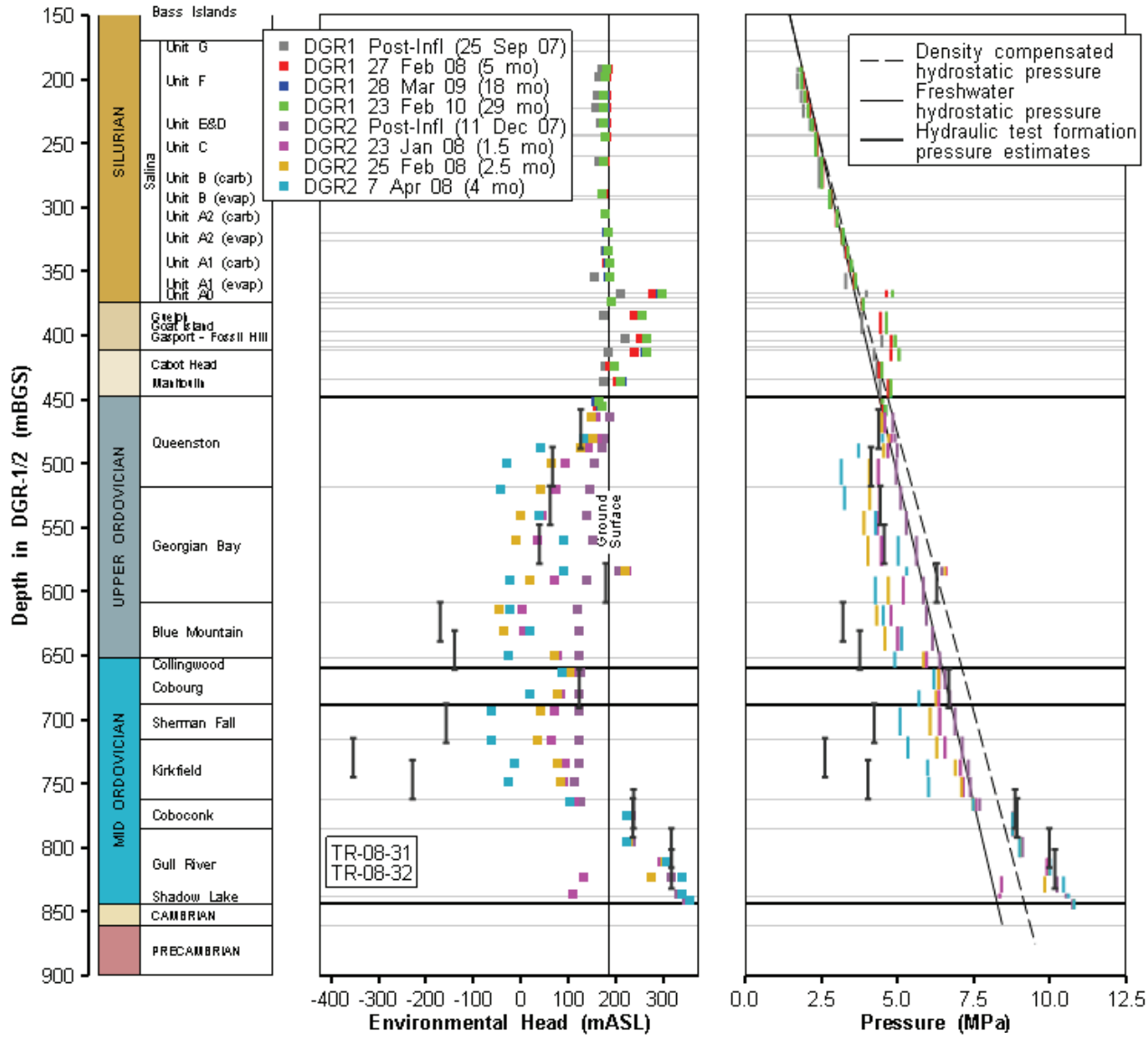

Figure 4.97: Combined DGR-1 and DGR-2 (Old) Formation Pressure and Environmental Head Profiles: Old DGR-2 (December 2008 - Post Inflation, January 2008 and April 2008), DGR-1 (September 2007- Post Inflation, February 2008, March 2009 and February 2010)

The January 23, 2008 pressure measurements from two of the deeper intervals in DGR-2 show pressures and calculated environmental heads that appear to be too low and are attributed to leakage of Shadow Lake and Gull River pressure into the MP55 casing (i.e., around MOSDAX probe) due to a poor probe seal on the pressure measurement port. This phenomenon is also observed with the continuous pressure monitoring data for the Cambrian port as discussed below.

In the period of March 2008 to April 2009, ten pressure transducers were installed in DGR-2 to continuously monitor formation pressures. Figure 4.98 shows the continuous pressure plots generated from this MOSDAX installation.

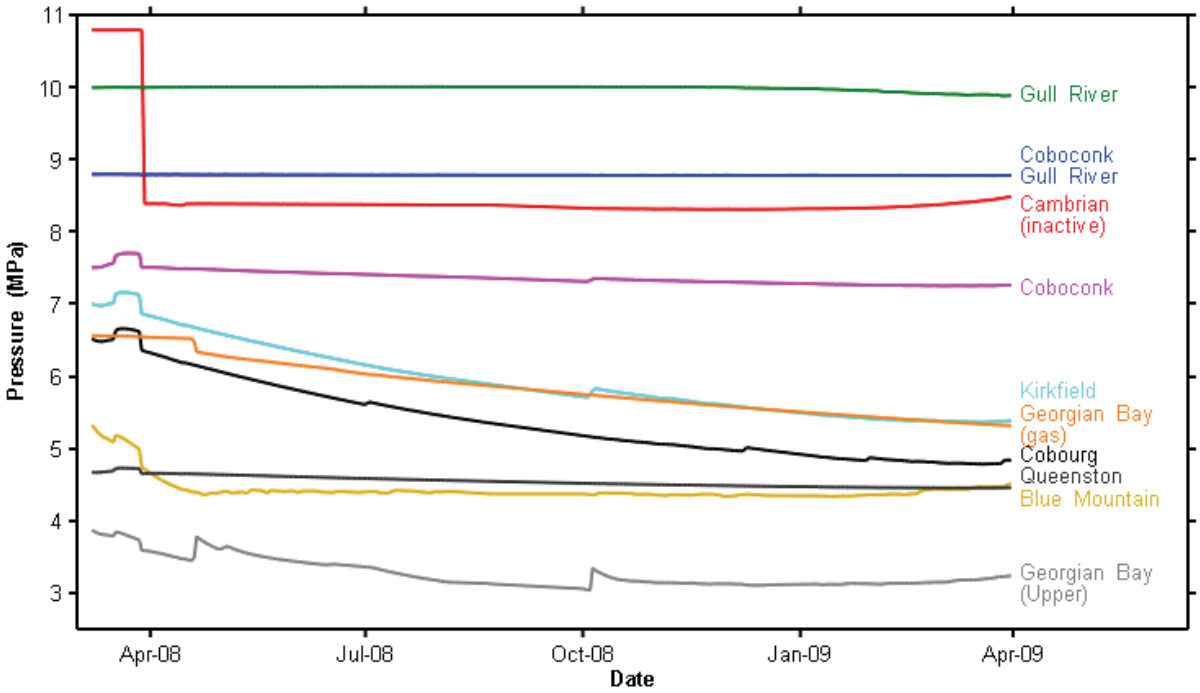

Figure 4.98: Continuous Formation Pressure Measurements, March 2008 to April 2009 in DGR-2

Figure 4.98 shows that even after 18 months, pressures within DGR-2 continue to show changes with decreasing pressures in the Georgian Bay, Cobourg and Kirkfield formations and apparent stabilization of pressures within the Queenston, Blue Mountain and Coboconk/Gull River formations. The step pressure increase and decrease shown in mid to late March is leakage of Cambrian pressure into the sealed casing and correction of this leakage by disconnecting the pressure transducer from the Cambrian measurement port. Figure 4.98 also shows periodic “bumps” or pressure increases for the upper Georgian Bay, Blue Mountain, Cobourg and Kirkfield formations that are thought to be due to leakage around packer seals and/or leakage from the inside of the MP55 casing to these underpressured formations.

Figures 4.97 and 4.98 show that the only truly stable environmental heads in DGR-2 during the monitoring period are in the deeper Coboconk and Gull River formations, as well as the underlying Shadow Lake Formation where pressures are probably controlled by the stable high pressure measured in the Cambrian sandstone. While environmental heads in the Ordovician shales appear close to stabilizing, the heads in the Cobourg and Kirkfield formations show near uniform pressure decreases throughout the 18-month monitoring period.

4.12.2.2 DGR-2 Casing Removal and Re-installation

Removal of the 848-m length of MP55 casing in DGR-2 was undertaken in early June 2009 for the reasons listed below.

- To eliminate the suspected MP55 casing leaks by upgrading the design of the system - increasing the amount of stainless steel components and the use of high pressure Geopro™ packers in zones expected to experience very high differential pressures.
- To allow for additional borehole acoustic televiewer logging of the borehole walls to further assess possible borehole breakouts for assessment of in situ stresses (see Section 5.4).
- To allow for retesting of DGR-2 to address concerns over possible test equipment leaks identified by comparison of test results between borehole DGR-2 and boreholes DGR-3 and DGR-4.
- To demonstrate retrieveability of MP55 casings in DGR boreholes, which was a requirement of the Phase 1 GSCP (Section 5.2.7.4, INTERA 2006).

4.12.2.3 DGR-2 (New)

The new MP55 casing system was installed in DGR-2 on December 2, 2009. In addition to the post-inflation pressure profile completed on December 3, 2009, one other pressure profile was completed in the New DGR-2 casing system on February 10, 2010, approximately 2.5 months following casing installation. Figure 4.99 shows the results of the pressure profiling completed in DGR-2 in combination with available DGR-1 pressure and head data.

Figure 4.99 shows similar formation pressure and environmental head profile evolution for the New DGR-2 casing installation to the Old DGR-2 casing installation with several notable exceptions. There is a similar distribution of overpressures and underpressures throughout the stratigraphic sequence in the new casing completion compared to Old DGR-2 casing completion. The Black River limestones are similarly overpressured, and the Trenton limestones and Ordovician shales are underpressured. The isolated zone of slight overpressure in the lower part of the Georgian Bay Formation is also reproduced in the New DGR-2 pressure profiles.

Noteworthy differences between the Old and New DGR-2 pressure profiles are the lower pressures recorded in the bottom of the Trenton limestones and the higher pressure gradients measured across the Black River – Trenton contact in the New DGR-2 data. These more pronounced pressure conditions in the New DGR-2 data reflect the use of stainless steel and high integrity packers in this part of the New DGR-2 MP55 casing installation.

What is noteworthy in both the Old and New DGR-2 casing installations is the rapid equilibration of formation pressures within the Black River limestones compared to the Trenton limestones and Ordovician shales. This more rapid equilibration indicates the Black River limestones are more permeable than the Trenton limestones and the bulk of the Ordovician shales.

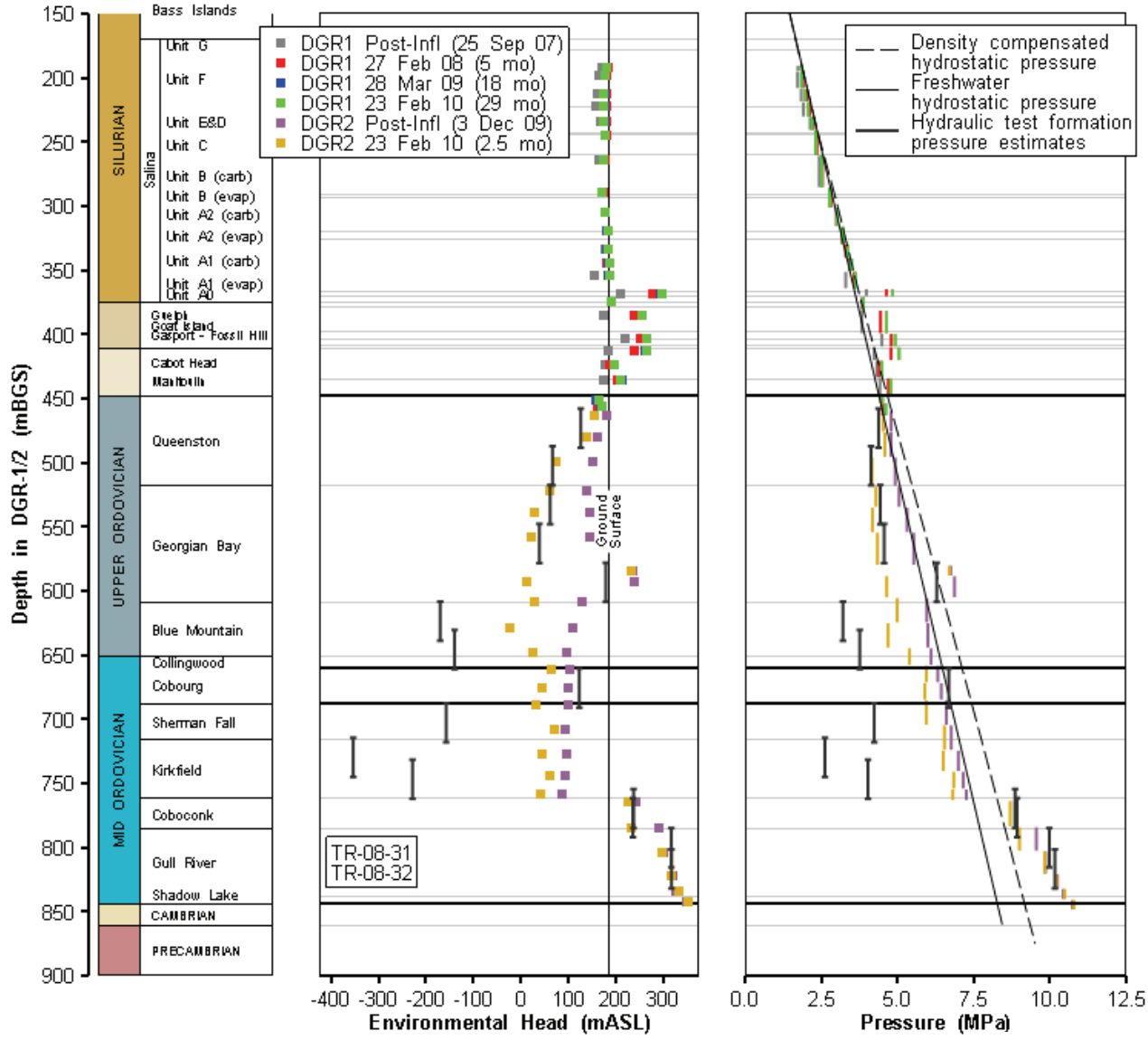

Figure 4.99: Combined DGR-1 and DGR-2 (New) Formation Pressure and Environmental Head Profiles: New DGR-2 (December 2009 - Post Inflation, February 2008), DGR-1 (September 2007- Post Inflation, February 2008, March 2009 and February 2010)

4.12.2.4 DGR-3

Figure 4.100 shows two profiles of formation pressures and environmental heads in DGR-3, 1.5 and 5 months after casing installation in late September, 2009. Although only two pressure profiles are available for this borehole after completion of the post-inflation profile, the pressure and head data illustrated in Figure 4.100 are remarkably similar to data from DGR-1 and DGR-2.

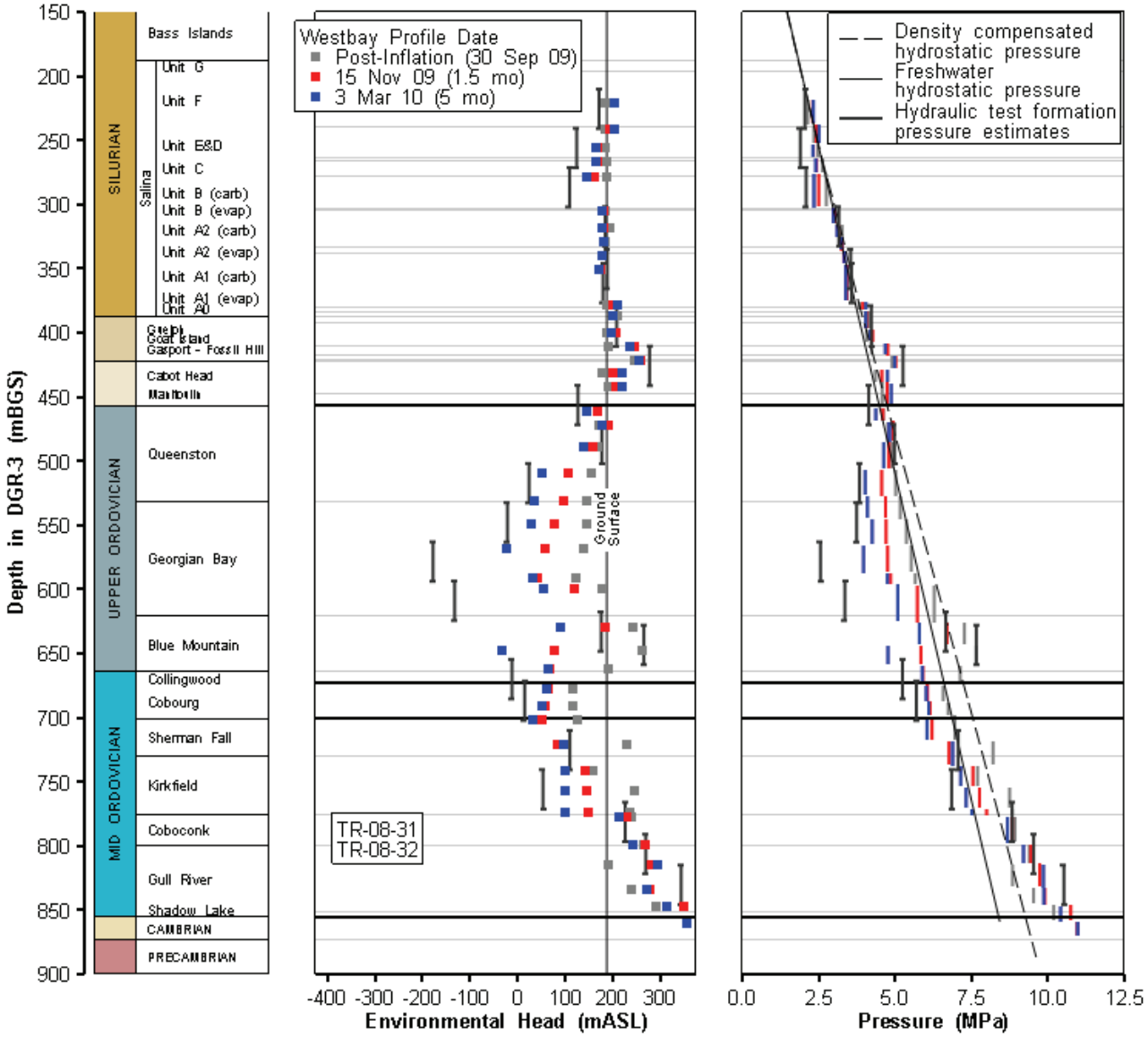

Figure 4.100: DGR-3 Formation Pressure and Environmental Head Profiles, September 2009 (Post Inflation), November 2009 and March 2010

The pressure and head data for DGR-3 show minor underpressure in the Salina Formation that increases to overpressure in the Gasport to Fossil Hill formations and then rapidly transitions to significant underpressure within the Ordovician shales and the Trenton Group limestones. Similar to DGR-2, all of the deeper Black River Group formations are overpressured. Figure 4.100 shows that the overpressured and underpressured intervals measured in the MP55 casing were all reasonably well determined from borehole hydraulic testing. Comparison of the formation pressures determined from hydraulic testing to MP55 casing measurements indicates that final or stable underpressures and environmental heads in the Ordovician shales and limestones are likely to be much lower than those measured during March, 2010. Stable

formation pressures are evident for the permeable sections of DGR-3, including the Salina Upper A1 Unit, the Guelph and the Cambrian sandstone.

What is also remarkable is that the development of the overpressures and underpressures are very similar in DGR-3 and DGR-2. For example, the environmental head profiles determined from the DGR-3 pressure measurements completed approximately 1.5 and 5 months after casing installation are very similar in both shape and magnitude to the environmental head profile determined from DGR-2 for the same time period after casing installation.

Note: Pitting or minor core breakage at the low point on the elliptical fracture trace.

Figure 4.101: Closely Spaced, Inclined, Calcite-infilled Fractures at 638.5 mBGS in Blue Mountain Formation, DGR-3

As in DGR-2, there is one normally pressured interval in the Ordovician shales; in DGR-3 it occurs within the Blue Mountain Formation that has environmental head at least 200 m greater than heads in the surrounding shales (based on the November 2009 profile), and test interval hydraulic conductivity that is about 1.5 orders of magnitude greater than the surrounding rock mass. This higher pressure and permeability interval may be attributed to a single inclined fracture at 632.4 mBGS or a set of inclined, cm-spaced, calcite-infilled fractures found at 638 to 639 mBGS in DGR-3. Figure 4.101 shows a close-up of the appearance of the set of inclined closely spaced fractures. Borehole acoustic televiewer logs indicate that at least one of these inclined fractures has an identifiable trace on the borehole wall and hence may have increased permeability relative to the intact rock mass. In both core and borehole wall images, these inclined fractures show pitting or minor breakage at the high and low points of the elliptical fracture traces. This normally pressured interval also shows elevated test interval compressibility from straddle-packer hydraulic testing.

4.12.2.5 DGR-4

Figure 4.102 shows the temporal evolution of pressures and heads in DGR-4 over the 1- to 10-month period following casing installation on April 28, 2009. The temporal development and spatial distribution of overpressures and underpressures in DGR-4 is essentially identical to that observed in boreholes DGR-1, DGR-2 and DGR-3.

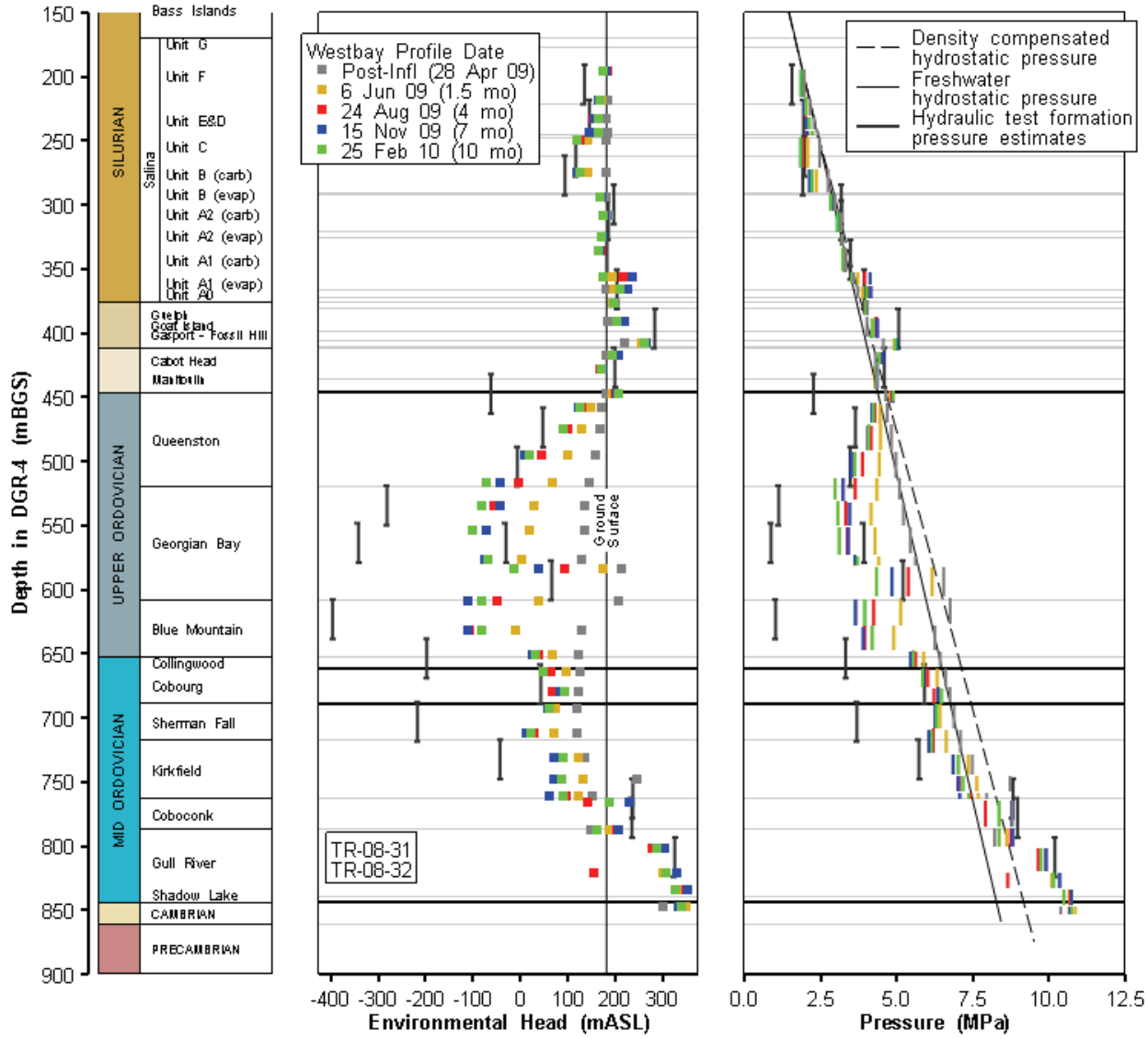

Figure 4.102: DGR-4 Formation Pressure and Environmental Head Profiles, April 2009 (Post Inflation), June 2009, August 2009, November 2009 and February 2010

As in other DGR boreholes, the pressure and head data for DGR-4 show underpressure in the Salina Formation that increases to overpressure in the Gasport to Fossil Hill formations and

then rapidly transitions to significant under-pressure within the Ordovician shales and the Trenton Group limestones. Similar to DGR-1, formation pressures within the permeable Salina Upper A1 Unit and Guelph aquifers are stable in all pressure surveys. Similar to DGR-2 and DGR-3, all of the deeper Black River Group formations are overpressured. The pressure in the Cambrian sandstone in DGR-4 is equivalent to an environmental head of 165 mAGS.

The underpressures in DGR-4 are greater in magnitude than in DGR-1, DGR-2 or DGR-3, being equivalent to environmental heads of 117 mASL in the middle of the Salina Formation and -115 mASL (300 mBGS) in the Blue Mountain Formation. This observation is not unexpected as the MP55 casing in DGR-4 is a more robust design than casing in DGR-1 and DGR-2 (Old) and has been in the ground longer than DGR-2 (New) and DGR-3. Figure 4.102 shows that the overpressured and underpressured intervals measured in the MP55 casing in DGR-4 were all reasonably well determined from borehole hydraulic testing. Again, comparison of the formation pressures determined from hydraulic testing to MP55 casing measurements indicates that final or stable underpressures and environmental heads in the Ordovician shales and limestones are likely to be much lower than those measured in February 2010.

As in DGR-2 and DGR-3, there is one normally pressured interval within the Ordovician shales; in DGR-4, it occurs within the lower Georgian Bay Formation and has environmental head at least 200 m greater than heads in the surrounding shales. Reductions in pressure and head in this overpressured zone throughout the period of monitoring suggest leakage from the interval around packer seals or through the pressure measurement port. In DGR-4, this normally pressured zone appears to have slightly elevated hydraulic conductivity relative to the surrounding rock mass. It appears to be associated with a sub-horizontal calcite-infilled fracture at 594.8 mBGS. Similar to other normally pressured zones in the Ordovician shales in DGR boreholes, it shows elevated test interval compressibility from straddle-packer hydraulic testing.

4.12.2.6 DGR-5

Because MP55 casing systems were not installed in DGR-5, the only data on formation pressures and environmental heads for DGR-5 are from borehole hydraulic testing. Hydraulic testing in DGR-5 was limited to continuous profiling of the Ordovician shales and the Trenton Group limestones. Figure 4.103 shows the measured formation pressures determined from hydraulic testing (TR-08-32) and the calculated environmental heads based on the fluid density profile as shown in Figure 4.81 and described in TR-08-31.

The estimated underpressures in DGR-5 are similar to those described for DGR-2, DGR-3 and DGR-4. In DGR-5 there is one overpressured interval in the bottom of the Georgian Bay Formation, one or two normally pressured intervals within the upper part of the Queenston Formation, and seven to eight underpressured intervals within the Ordovician shales and limestones. The maximum underpressure approaches -400 mASL within the middle of the Georgian Bay Formation. The overpressured interval within the lower Georgian Bay Formation and has elevated test zone compressibility (Figure 4.89), but not elevated hydraulic conductivity.

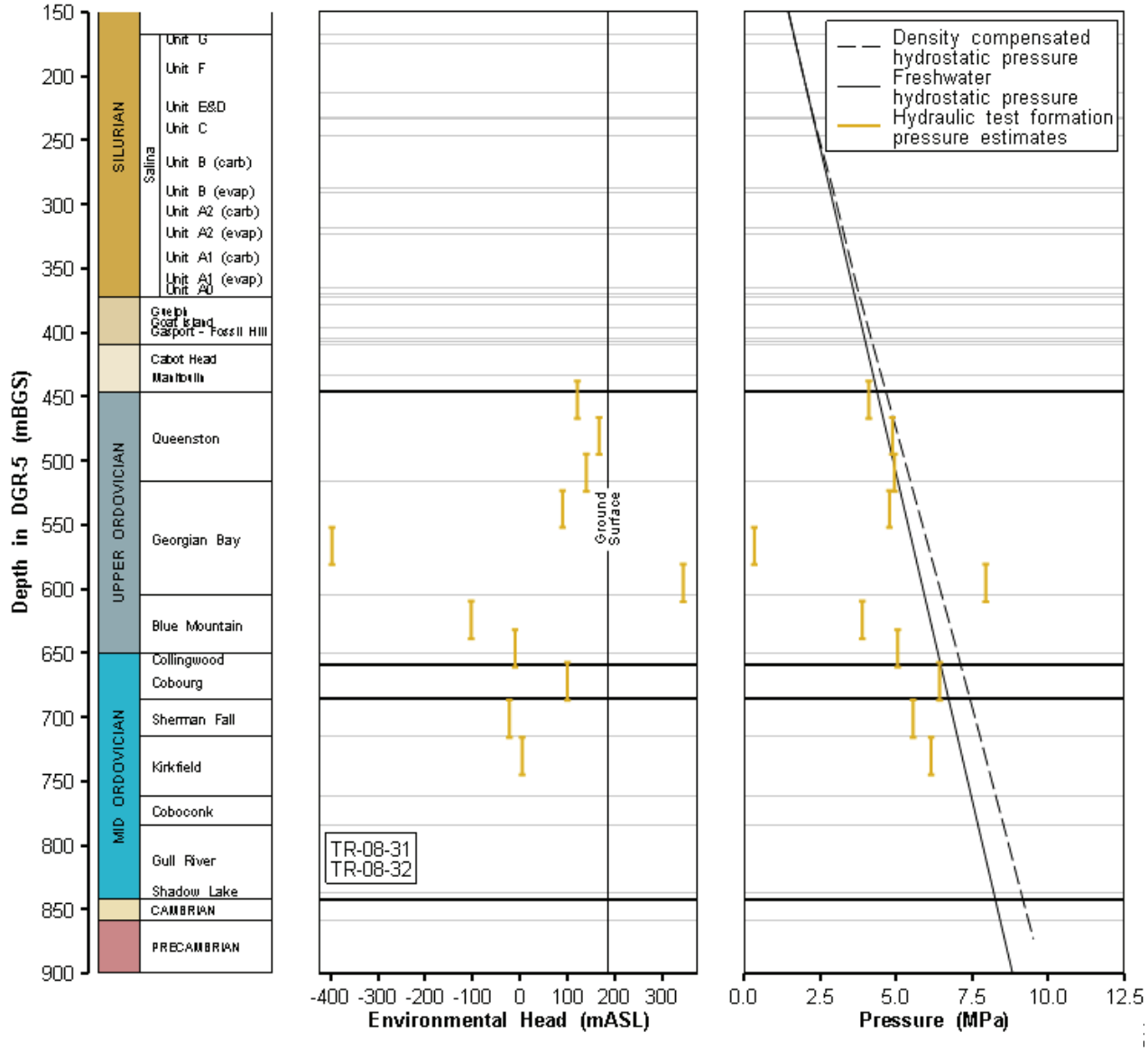

Figure 4.103: DGR-5 Formation Pressure and Environmental Head Profiles Determined from Borehole Hydraulic Testing

4.12.2.7 DGR-6

Similar to DGR-5, because MP55 casing systems were not installed in DGR-6, the only data on formation pressures and environmental heads for DGR-6 are from borehole hydraulic testing. Hydraulic testing in DGR-6 was limited to shorter interval (~10 m length) testing of targeted zones of intact and fractured rock within the Ordovician shales and the Trenton Group limestones (see Section 4.9.2.2). Figure 4.104 shows the measured formation pressures and the calculated environmental heads based on the fluid density profile as described in TR-08-31.

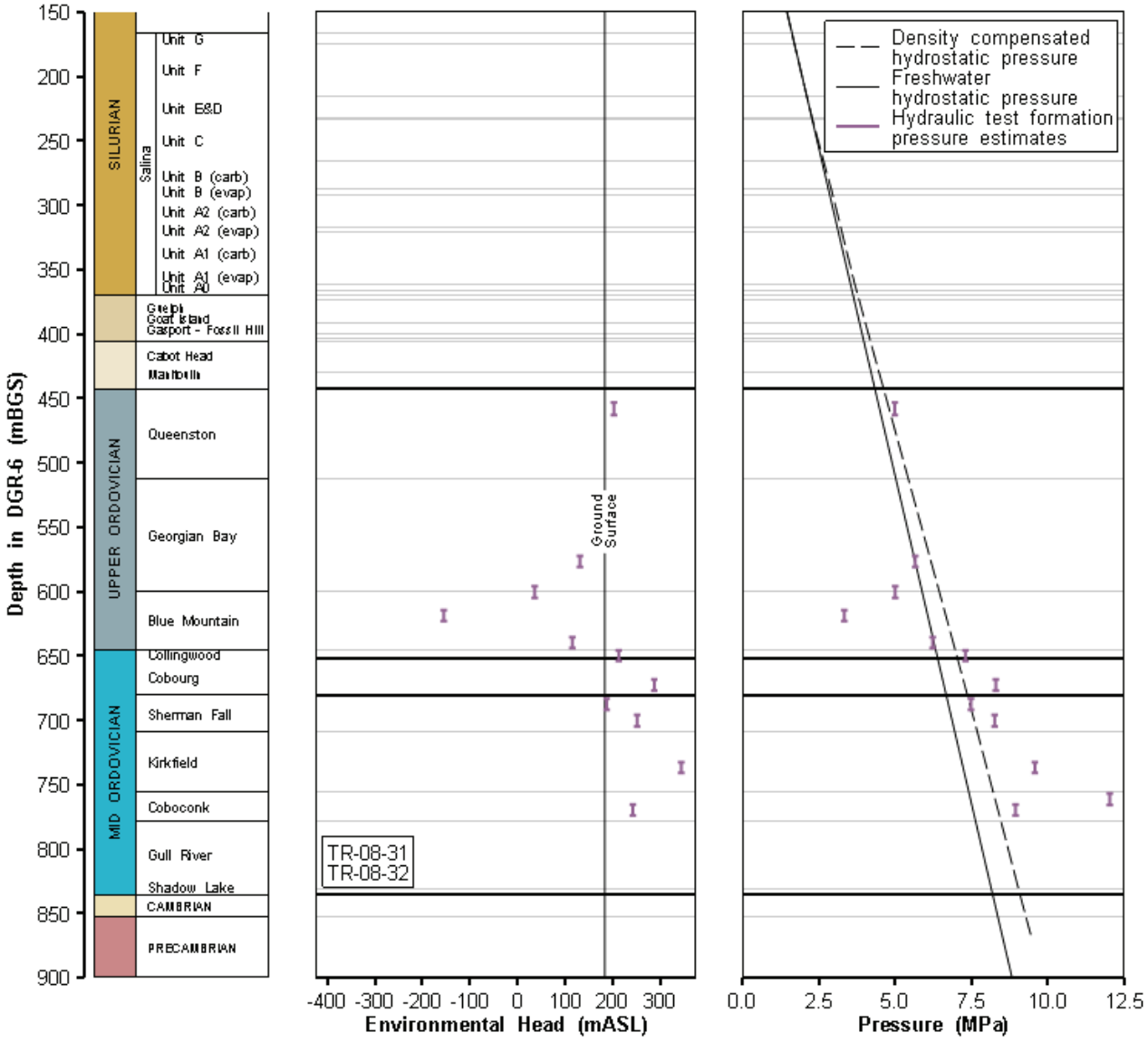

Figure 4.104: DGR-6 Formation Pressure and Environmental Head Profiles Determined from Borehole Hydraulic Testing

The estimated underpressures in DGR-6 are dissimilar to those described for DGR-2, DGR-3, DGR-4 and DGR-5. In DGR-6 there are six overpressured intervals within the Trenton Group limestones, two normally-pressured intervals within the Ordovician shales and limestones, and four underpressured zones within the Ordovician shales. The estimated maximum underpressure approaches only -150 mASL within the middle of the Blue Mountain Formation. The largest overpressured interval within the upper part of the Coboconk Formation is from testing of the volcanic ash layer, although this interval shows neither elevated test zone compressibility or hydraulic conductivity.

4.12.2.8 Summary of Underpressures and Overpressures

The available pressure measurements from borehole hydraulic testing and monitoring of MP55 casings shows the following general environmental head conditions in DGR boreholes related to overpressures and underpressures.

- Underpressures in the Salina Formation, with maximum underpressures occurring within the C and B Units equal to environmental heads of 70 mBGS.
- Overpressures in the Salina A1 and A0 Units, and Gasport to Fossil Hill formations, with maximum overpressures equal to environmental heads of 75 mAGS.
- Underpressures in the Ordovician shales and Trenton Group limestones, with maximum underpressures occurring within the Blue Mountain Formation equal to environmental heads of about 300 mBGS.
- Overpressures in the Black River Group limestones and siltstones and the Cambrian sandstone, with maximum overpressures equal to environmental heads of 165 mAGS.

It is important to understand that for the majority of the underpressures, the currently available data provide indications of what the actual equilibrium formation pressures may be, assuming such equilibria exist. The formation pressures from straddle-packer testing are values determined from analysis of the pressure transient data similar to values of formation hydraulic conductivity. As illustrated in Figure 4.105, the actual time it would take to reach equilibrium formation pressures with the straddle-packer testing equipment is on the order of 1-2 years for a formation hydraulic conductivity of 9×10^{-15} m/s.

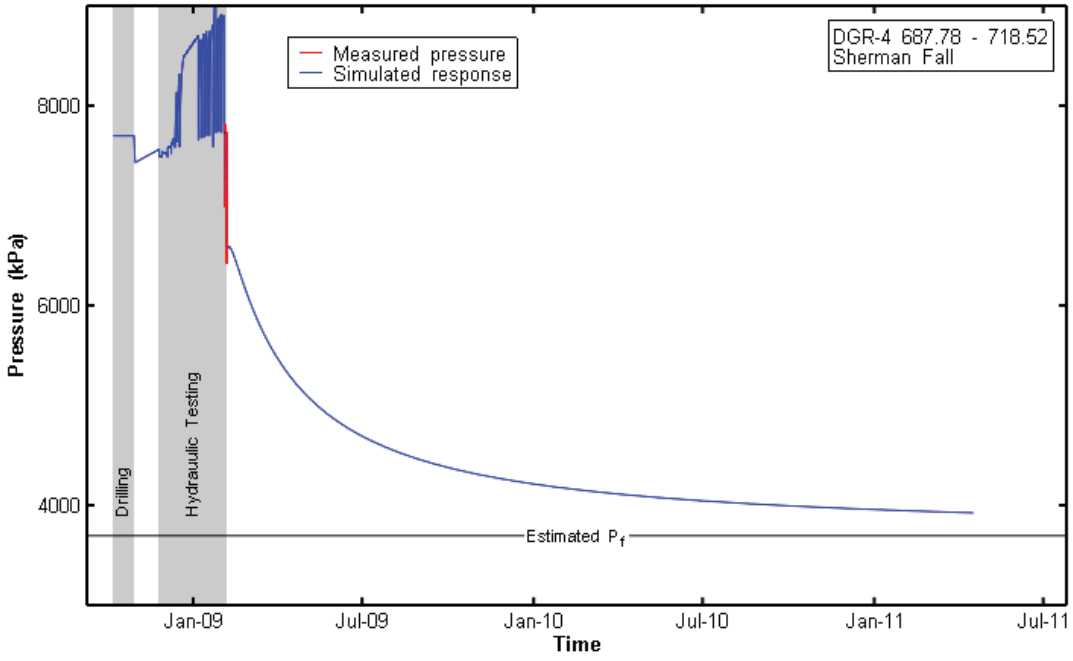

Figure 4.105: Calculated Time to Reach Equilibrium Formation Pressure with Straddle-Packer Testing Equipment, Sherman Fall Formation in DGR-4

Because the test interval compressibility of MP55 casing is likely an order or magnitude greater than the very stiff straddle-packer test equipment, the time to reach equilibrium formation pressures with the MP55 installations is on the order of 5-10 years. Since pressure monitoring in the MP55 casing systems has only been undertaken for a maximum of 1.5 years, the bulk of the data from these installations are overestimates of actual formation pressures. Given these constraints, the best current estimates of formation underpressures are likely those determined from analysis of straddle-packer hydraulic tests.

The causes of the observed underpressures and overpressures and heads in DGR boreholes are not evident at this time. Certainly, both the underpressures and larger overpressures are not in hydrodynamic equilibrium with local topography and surface water elevations.

While the moderate overpressures observed within the Salina A1 and A0 Units, Goat Island, Gasport, Lions Head and Fossil Hill formations and the middle of the Georgian Bay Formation (DGR-2 and DGR-3) and the Blue Mountain Formation (DGR-4) may be gas related, the Cambrian overpressure is much larger and is associated with a locally permeable formation (i.e., $K_h \sim 10^{-6}$ m/s). Possible explanations for the Cambrian overpressures include: hydraulic connection to a remote elevated regional recharge area (e.g., Niagara Escarpment, Canadian Shield); remnant overpressure from deep basin glacial meltwater recharge (Bense and Person 2008) and post-glacial basin isostatic rebound; and/or up-basin regional fluid (brine or gas) migration and pressurization, as has been reported by Bahr et al. (1994) for deep Middle Ordovician formations on the east side of Lake Huron near Saginaw Bay, and by Raven et al. (1992a) for southern Ontario. The fact that the groundwater flow directions in the overpressured Cambrian today at the Bruce DGR site are outward from the centre of the Michigan Basin (see Section 4.12.3) suggests that the Cambrian overpressures are likely sourced from the centre of the Michigan Basin.

There is much more literature on the occurrence and genesis of underpressures, particularly in very low permeability argillaceous formations as exist at the Bruce nuclear site. Similar underpressures have been reported for the Pierre shale in South Dakota (Neuzil 1993), the western Canada sedimentary basin (Corbet and Bethke 1992) and the marl-shale aquitard at Wellenberg, Switzerland (Vinard 1988). Neuzil (1995) provides a good summary of the various mechanisms for generation of abnormal pressures in hydrogeologic systems.

Based on available literature and considering the Bruce nuclear site geology/hydrogeology and geological history, possible explanations for the observed underpressures include: 1) poroelastic response to glacial unloading and flexure; 2) poroelastic response to Cenozoic erosional unburdening; 3) capillary pressure effects due to the presence of a separate gas phase; and/or 4) chemical osmosis. Poroelastic response is an attractive explanation because the lowest pressures appear to occur within the most compressible formations (i.e., Georgian Bay and Blue Mountain shales, but also the Salina B and C Units). Presence of a gas phase within the Ordovician shales and limestone as suggested in Sections 4.3.3 and 4.6.7.3 is also a credible explanation based on recent brine-gas modeling (NWMO 2011) that shows similar underpressures within these formations. Osmosis cannot be eliminated from the list of potential explanations as water within the packer-isolated test intervals of DGR boreholes has lower salinity than most adjacent formation porewater. These chemical gradients may potentially create osmotically induced flow of water from the test interval to the formation resulting in under-pressuring of the test interval (Neuzil 2000).

Regardless of which explanation is favoured, the occurrence of such underpressures implies that the formations in which they are measured must be of extremely low permeability in order

for them to persist. Based on underpressure occurrences reported for the Pierre shale, which is quite analogous to the Bruce Ordovician shale and limestone sequence (i.e., 300-m-thick shale sequence with similar underpressure head magnitude [130 m] and pattern [maximum underpressure at centre of sequence]), the Ordovician shale and limestone sequence at the Bruce nuclear site would be expected to have formation–scale permeabilities of less than 10^{-20} m^2 (hydraulic conductivity less than 10^{-13} m/s). These hydraulic conductivity estimates are very similar to those estimated from interpretation of field hydraulic test data discussed in Sections 4.9.2 and 4.9.3.

4.12.3 Groundwater Flow Directions in Permeable Units

As evident in Figure 4.90 and Table 4.14, there are four sections of the Paleozoic stratigraphic sequence at the Bruce nuclear site with sufficient permeability (e.g., > 10^{-10} m/s) to support active groundwater movement or flow. These permeable units and their reference depths include:

- The permeable Devonian and Upper Silurian dolostone aquifer of the Lucas, Amherstburg, Bois Blanc and Bass Islands formations at depths of 20 to 169.3 mBGS in DGR-1;
- The vuggy Salina Upper A1 Unit at depths of 325.5 to 328.5 mBGS in DGR-1;
- The vuggy Guelph Formation at depths of 374.5 to 378.6 mBGS in DGR-1; and
- The overpressured Cambrian sandstone at depths of 843.8 to 860.7 mBGS in DGR-2.

Groundwater flow directions in these four permeable units are estimated based on measurements of formation pressures and hydraulic heads in boreholes instrumented with MP38 and MP55 multi-level monitoring casings.

Groundwater flow in the permeable Devonian and Upper Silurian dolostones is discussed in Section 4.12.1. Formation pressure measurements in boreholes US-3, US-7 and US-8 show stable hydraulic head profiles indicating slight upward hydraulic gradients (0.001 to 0.01 m/m) and lateral flow to the northwest toward Lake Huron.

For the deeper permeable units intersected by DGR boreholes, horizontal groundwater flow directions are calculated from measured formation pressures obtained from MP55 casings considering the density of the aquifer fluids and the dip of the formations. Table 4.16 summarizes the results of this assessment, the details of which are given in TR-08-31.

Groundwater flow directions and hydraulic gradients were calculated from measured in situ pressures in MP55 casings using the procedure described below.

- Correct measured absolute MP pressures for the interval that contains the permeable unit for atmospheric pressures measured at the time of the field survey.
- Express atmospheric-corrected MP pressures as the formation pressure at the mid-depth point of the permeable unit considering the density of the formation fluid and the elevation difference between the MP pressure measurement port and the mid-depth point.
- Express the mid-point formation pressures as an equivalent pressure for a horizontal permeable unit considering the orientation of the unit as listed in Table 3.2, determined from TR-09-11. These equivalent horizontal unit pressures are listed in Table 4.16.
- Solve the three-point pressure problem to determine the strike and dip of the equivalent horizontal formation pressure surface considering true location of pressure measurement ports considering borehole tilts.

- Express the calculated formation pressure surface as equipotential lines, groundwater flow directions and hydraulic gradients.

Table 4.16: Formation Pressures and Groundwater Flow Directions in DGR Deep Permeable Bedrock Units

Salina Upper A1 Unit			
Parameter (Units)			
Date of Pressure Measurements	October 30, 2009	January 27, 2010	April 26 & 27, 2010
Adjusted Pressures for Mid-depth of Horizontal Permeable Unit (kPa)	DGR-1: 3408.98 DGR-3: 3348.85 DGR-4: 3297.48	DGR-1: 3402.92 DGR-3: 3332.44 DGR-4: 3294.65	DGR-1: 3400.92 DGR-3: 3348.43 DGR-4: 3300.44
Equipotential Line (Azimuth)	231	221	232
Hydraulic Gradient (m/m)	0.0086	0.0084	0.0077
Groundwater Flow Direction (Azimuth)	321	311	322
Guelph Formation			
Parameter (Units)			
Date of Pressure Measurements	October 30, 2009	January 27, 2010	April 26 & 27, 2010
Adjusted Pressures for Mid-depth of Horizontal Permeable Unit (kPa)	DGR-1: 4066.82 DGR-3: 4103.91 DGR-4: 4060.99	DGR-1: 4036.28 DGR-3: 4079.44 DGR-4: 4058.17	DGR-1: 4036.69 DGR-3: 4071.78 DGR-4: 4056.72
Equipotential Line (Azimuth)	313	344	348
Hydraulic Gradient (m/m)	0.0039	0.0032	0.0026
Groundwater Flow Direction (Azimuth)	43	74	78
Cambrian Sandstone			
Parameter (Units)			
Date of Pressure Measurements	December 8 & 9, 2009	January 27, 2010	April 26 & 27, 2010
Adjusted Pressures for Mid-depth of Horizontal Permeable Unit (kPa)	DGR-2: 10990.64 DGR-3: 11015.98 DGR-4: 11010.58	unreliable data	DGR-2: 10984.09 DGR-3: 11022.60 DGR-4: 11012.38
Equipotential Line (Azimuth)	2	unreliable data	359
Hydraulic Gradient (m/m)	0.0020	unreliable data	0.0031
Groundwater Flow Direction (Azimuth)	92	unreliable data	89

The results of these calculations, listed in Table 4.16, show the groundwater flow directions in the Salina Upper A1 Unit aquifer are the same as those in the shallow dolostones, being to the northwest toward Lake Huron. In contrast, the calculated groundwater flow directions for the

Guelph Formation and the Cambrian sandstone are outward from the middle of the Michigan Basin toward the northeast (Guelph Formation) and to the east (Cambrian sandstone).

4.13 Hydrostratigraphic Units

Because of natural variability, hydrogeological and geochemical properties can be expected to vary within and across every stratigraphic formation and unit beneath the Bruce nuclear site as defined in Chapter 3 of this report. For the purpose of preparation of the descriptive hydrogeological site model, the overburden and bedrock formations at the Bruce nuclear site have been categorized and grouped into hydrostratigraphic (HS) units (see Figure 4.106).

Hydrostratigraphic units are formations, parts of formations, or groups of formations that have similar hydrogeologic characteristics that allow for grouping into aquifers, aquitards and aquicludes. Hydrostratigraphic units are operational definitions that facilitate hydrogeologic assessment. Nine hydrostratigraphic units have been defined, as noted below and shown in Figure 4.106, based on data and reference stratigraphy depths at DGR-1 and DGR-2.

- HS Unit 1: Overburden Aquitard; 0 to 20 mBGS.
- HS Unit 2: Devonian and Upper Silurian Dolostone Aquifer, 20 to 169.3 mBGS.
- HS Unit 3: Silurian Shale, Dolostone and Anhydrite Aquitards, 169.3 to 447.7 mBGS, excluding Unit 4.
- HS Unit 4: Silurian Dolostone Aquifers, 325.5 to 328.5 mBGS (4A) and 374.5 to 378.6 mBGS (4B).
- HS Unit 5: Ordovician Shale Aquiclude, 447.7 to 659.5 mBGS.
- HS Unit 6: Ordovician Limestone Aquiclude, 659.5 to 762.0 mBGS,
- HS Unit 7: Ordovician Limestone Aquitard, 762.0 to 836.6 mBGS.
- HS Unit 8: Cambrian Sandstone Aquifer, 838.6 to 860.7 mBGS.
- HS Unit 9: Precambrian Aquitard, >860.7 mBGS.

Aquifers are defined as formations or units that are sufficiently porous and permeable to store, transmit and yield significant quantities of groundwater. For the Bruce DGSM, aquifers are practically defined as formations or units that yield sufficient water to allow for groundwater sampling.

Use of the word aquifer in this report in no way implies that the formation or unit contains potable water. The formations here referred to as aquifers are classified as such based on their physical properties (permeability, hydraulic conductivity, etc.), but these classifications do not take water quality into consideration. All units below HS Unit 2 contain only non-potable water (brines) and the designation as “aquifer” is based solely on the physical characteristics of the host rock. Aquitards are formations or units that retard but do not prevent flow of water to or from adjacent aquifers. Aquitards do not readily yield water, but over long periods of time may exhibit evidence of advection. Aquicludes are formations or units with very low permeability such that they are almost impermeable and do not exhibit evidence of advection even over very long periods of time.

4.13.1 HS Unit 1: Overburden Aquitard

HS Unit 1 comprises the overburden deposits at the Bruce nuclear site. Overburden at the Bruce nuclear site (Section 3.8.1) is of variable thickness ranging from a thin veneer near Lake Huron to upwards of 20 m in the southeastern part of the site near US-6 and DGR-1 (Figure 1.2). In the vicinity of the proposed DGR at DGR-1, the overburden consists of 2-3 m

layers of granular fill and basal gravel overlying and underlying 15 m of sandy silt till, which classifies the overburden as an aquitard.

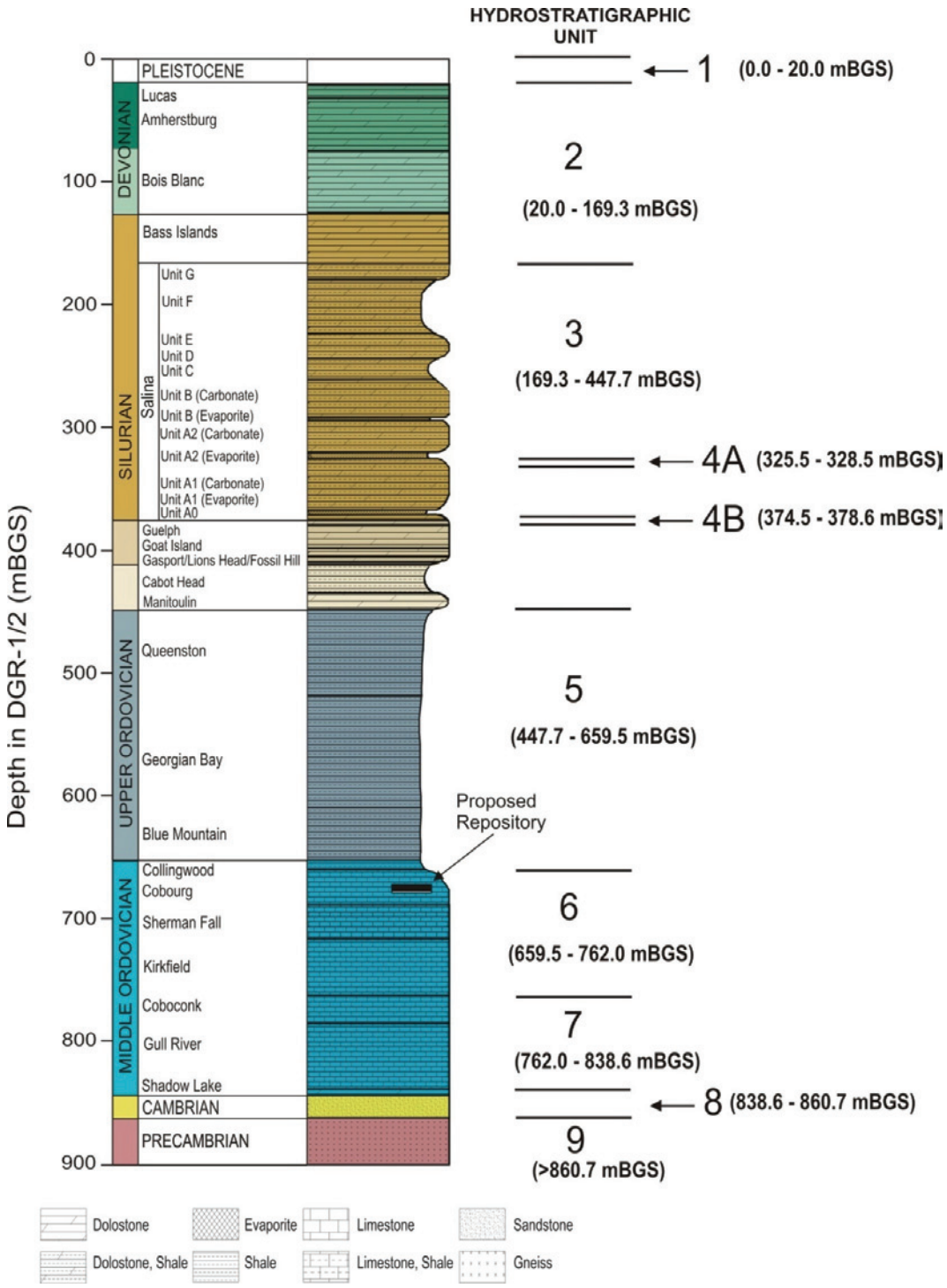

Figure 4.106: Reference Stratigraphic Column Showing Hydrostratigraphic Units at the Bruce Nuclear Site

Although hydraulic testing of overburden deposits was not undertaken as part of the GSCP, there is an extensive database of hydraulic tests of the overburden at the Bruce nuclear site completed as part of radioactive and non-radioactive waste management investigations (Jensen and Heystee 1987, Jensen and Sykes 1995, GOLDER 2003). Based on these sources, the bulk horizontal hydraulic conductivity for unweathered sandy silt till at the Bruce nuclear site ranges from $1x10^{-10}$ to $6x10^{-9}$ m/s with an average or estimated value of $8x10^{-10}$ m/s. Horizontal:vertical K anisotropy has been evaluated at 2:1 with water-loss porosity of 20% (Jensen and Sykes 1995).

Specific storage values for HS Unit 1, based on literature review of similar soils and review of on-site hydraulic testing, are estimated to be about $1x10^{-3}$ m^{-1}.

Vertical hydraulic gradients are typically about 0.1 m/m in both upward and downward directions depending upon proximity to the regional groundwater discharge area of Lake Huron.

Effective diffusion coefficients (D_e, chloride) in HS Unit 1 have been reported as $6x10^{-10}$ m^2/s (GOLDER 2003) with diffusion porosity equal to water-loss porosity. Diffusion properties in the overburden are assumed to be isotropic.

Groundwater chemistry is typically fresh Ca:Na-HCO_3 with TDS less than 500 mg/L (INTERA 2007) and under oxidizing redox conditions. Master variables of pH and Eh approximate 7-8 and +200 to +400 mV, respectively.

4.13.2 HS Unit 2: Devonian and Upper Silurian Dolostone Aquifer

HS Unit 2 comprises the permeable upper dolostone aquifer at the Bruce nuclear site from top of bedrock to reference depth of 169.3 m BGS at DGR-1. HS Unit 2 includes the Lucas Formation, where present, and the underlying Amherstburg, Bois Blanc and Bass Islands formations. In DGR boreholes, the Unit is 149 to 179 m thick. HS Unit 2 includes the regional groundwater supply aquifer that typically extends to depths of 50 to 100 m and the deeper less permeable bedrock to the top of the Salina Formation.

Extensive packer testing and observations of drilling fluid loss show that the average horizontal hydraulic conductivities in the upper 100 m range from $8x10^{-8}$ to $2x10^{-6}$ m/s, generally decreasing with depth. However, the upper part of the Bass Islands Formation in all DGR boreholes at DGR-1 reference depths of 140 to 145 mBGS contains very permeable sections with hydraulic conductivity approximating $1x10^{-4}$ m/s. Below 145 mBGS at DGR-1, the hydraulic conductivity of HS Unit 2 deceases to average values of about $1x10^{-6}$ m/s. The horizontal:vertical K anisotropy is assumed to be 10:1. Based on lab testing of the Bois Blanc and Bass Islands formations in DGR boreholes, an average total porosity of 7.0% is assumed for HS Unit 2.

Specific storage values for HS Unit 2, based on literature review of similar rock, review of on-site hydraulic testing, and calculations from lab measurements of rock compressibility and total porosity, (see Section 4.11) are estimated to be in the range of $5x10^{-7}$ to $2x10^{-6}$ m^{-1}, generally increasing with depth.

Vertical and horizontal hydraulic gradients in HS Unit 2 are low (i.e., 0.001 to 0.01 m/m) reflecting the high hydraulic conductivities with flow gradients directed upward and laterally to the northwest toward Lake Huron.

Diffusion testing was not undertaken in HS Unit 2 in Phase 1 or Phase 2. Based on core observations, measured porosities, results from testing on similar DGR core, and scientific literature, the vertical effective diffusion coefficient for iodide in HS Unit 2 is estimated at $8x10^{-12}$ m^2/s. The horizontal:vertical D_e anisotropy is assumed to be 1:1 based on DGR core observations and the elevated formation hydraulic conductivities. Average diffusion porosity is assumed equal to average total porosity of 7.0%.

Groundwater and porewater chemistries in HS Unit 2 are transitional from fresh Ca:Mg-HCO_3 water (TDS ~500 mg/L) near the top of the bedrock to brackish Ca-SO_4 water (TDS ~5,000 mg/L) at the bottom of the Unit. Master variables of pH and Eh (field measured) approximate 7-8 and +400 to -100 mV respectively, with Eh decreasing with depth.

The deeper parts of HS Unit 2 including the Bass Islands Formation show a depleted ^{18}O and D signature, and ^{14}C ages indicative of a glacial meltwater component. Mixing and exchange of higher TDS Ca-SO_4 water from underlying HS Unit 3 is also evident in HS Unit 2.

4.13.3 HS Unit 3: Silurian Shale, Dolostone and Anhydrite Aquitards

HS Unit 3 comprises the low-permeability Silurian shale, dolostone and anhydrite rocks at the Bruce nuclear site from DGR-1 reference depths of 169.3 to 447.7 mBGS. HS Unit 3 includes three aquitards: upper, middle and lower separated by two Silurian dolostone aquifers (HS Units 4A and 4B) which are found at DGR-1 reference depths of 325.5 and 374.5 mBGS. The upper aquitard comprises the Salina Units G, F, E, D, C, B and most of A2 found at reference depths of 169.3 to 325.5 mBGS. The middle aquitard includes the Salina A1 and A0 Units found at reference depths of 328.5 to 374.5 mBGS. The lower aquitard consists of the Goat Island, Gasport, Lions Head, Fossil Hill, Cabot Head and Manitoulin formations found at reference depths of 378.6 to 447.7 mBGS. HS Unit 3 has a combined thickness of 260.7 to 271.3 m in DGR boreholes.

Borehole straddle-packer testing shows that the average horizontal hydraulic conductivities for formations and units that comprise HS Unit 3 range from $5x10^{-14}$ to $3x10^{-10}$ m/s, with most values at or less than $1x10^{-12}$ m/s. Based on lab permeability testing (Figures 4.19 and 4.92), the horizontal:vertical K anisotropy is estimated to be 10:1. Based on lab testing (Section 4.3.2, Figure 4.3, Table 4.3), average total porosity for HS Unit 3 formations and units range from 0.5 to 19.4% with a calculated bulk HS Unit 3 average value of 8.9%. The upper aquitard and the Cabot Head shale of the lower aquitard have higher average porosity (~15%) than the middle aquitard and the remaining formations comprising the lower aquitard (average 3%).

Specific storage values for HS Unit 3, based on calculations from lab measurements of rock compressibility and total porosity are estimated to be in the range of $3x10^{-7}$ to $7x10^{-6}$ m^{-1}, generally decreasing with depth into the more competent Silurian dolostones. Elevated specific storages are noted for the Salina B and C Units and the Cabot Head shale with upper estimate values of $2x10^{-5}$, $1x10^{-5}$ and $3x10^{-5}$ m^{-1}, respectively.

The upper and middle aquitards of HS Unit 3 are moderately underpressured with the maximum underpressure (~ 70 mBGS) occurring in the middle of the sequence in the Salina C and B Units. Based on environmental heads, vertical hydraulic gradients in the upper and middle aquitards of HS Unit 3 are moderately (0.1 to 0.5 m/m) upward and downwards to the maximum underpressure zone, reflecting the low vertical hydraulic conductivities of the aquitard. However, vertical hydraulic gradients in the lower aquitard are much higher (1.0 to 3.0 m/m) being both upwards and downwards from the high-pressure zone straddling the Salina A1 and

A0 Units and the Goat Island, Lions Head and Fossil Hill formations. These high vertical gradients suggest that the bedrock of the bottom part of the middle aquitard and lower aquitard must be of very low permeability in order to maintain such high hydraulic gradients.

Laboratory diffusion testing undertaken on shale, dolostone and anhydrite core samples collected from HS Unit 3 shows a wide range of vertical effective diffusion coefficients for iodide of about $3x10^{-14}$ m^2/s for anhydrite to $1\text{-}2x10^{-11}$ m^2/s in the higher porosity shales. The available diffusion data indicate that the vertical effective diffusion coefficient for iodide in the upper aquitard and the Cabot Head shale of the lower aquitard is about $5x10^{-12}$ m^2/s with horizontal:vertical D_e anisotropy of 2:1. The average iodide diffusion porosity in these rocks is 6% or about 67% of the total porosity. The vertical effective diffusion coefficient for iodide in the middle and lower aquitard (excluding the Cabot Head shale) is about $1x10^{-13}$ m^2/s with horizontal:vertical D_e anisotropy of 2:1. The average iodide diffusion porosity in the middle and lower aquitard, excluding the Cabot Head shale, is 1.5% or about 50% of the total porosity.

Groundwater and porewater chemistries in HS Unit 3 are transitional from brackish Ca-SO_4 water (TDS ~10,000 mg/L) near the top of the Unit to Na-Cl brine (TDS ~325,000 mg/L) at the bottom of the Unit. The dramatic increase in TDS with depth in this unit is reflected in the major ion profiles (Figures 4.53 to 4.56) and the fluid density profile (Figure 4.81). Master variables of pH and Eh approximate 7.0 and -100 to -150 mV, respectively, reflecting iron and/or sulphur-reducing conditions.

Superimposed on this major ion chemistry profile are significant decreases and increases in the salinity and chemistry of groundwater measured in the Upper A1 Unit aquifer and the Guelph aquifer, respectively. The moderate salinity profile in the upper aquitard suggests that exchange or mixing of porewater from this part of the aquitard has occurred and that the upper aquitard is likely more permeable than the middle and lower aquitards. The salinity contrast in the middle aquitard from TDS of about 30,000 mg/L at 328.5 mBGS to 370,000 mg/L at 374.5 mBGS is remarkable and suggests that the middle aquitard comprising the Salina A1 and A0 Units is of very low permeability, such that solute transport is likely by diffusion. Based on the changes in concentrations of major ions and TDS across the lower aquitard, it is also likely of very low permeability.

4.13.4 HS Unit 4: Silurian Dolostone Aquifers

HS Unit 4 comprises two thin porous and permeable aquifers evident in core logging, borehole geophysical logging, hydraulic testing and groundwater sampling completed in DGR boreholes. The upper aquifer (4A) is found at reference depths 325.5 to 328.5 mBGS in DGR-1 and is the upper 3.0 to 3.7 m of the Salina A1 Unit dolostone in DGR boreholes. The lower aquifer (4B) is found at reference depths 374.5 to 378.6 mBGS in DGR-1 and is the entire thickness of the Guelph Formation dolostone. The lower aquifer ranges in thickness from 3.8 to 5.4 m thickness in DGR boreholes. Core photographs of these porous and permeable aquifers are given in Figures 3.22, 3.25 and 4.91.

Borehole straddle-packer testing and observations during targeted groundwater sampling show that the average horizontal hydraulic conductivities in these Silurian dolostone aquifers 4A and 4B approximate $2x10^{-7}$ and $3x10^{-8}$ m/s, respectively in DGR-3 and DGR-4 (Table 4.14). Based on core observations, the horizontal:vertical K anisotropy is assumed to be 1:1. Again, based on core observations and limited lab testing (TR-08-10), an average total porosity of 6.3% is assumed for HS Unit 4A and 13.1% for HS Unit 4B.

Specific storage values for HS Units 4A and 4B, based on calculations from lab measurements of rock compressibility and total porosity, are estimated to be about at $5x10^{-7}$ to $1x10^{-6}$ m^{-1}. Average specific storage value of $8x10^{-7}$ m^{-1} and $1x10^{-6}$ m^{-1} are assumed to be applicable to HS Unit 4A and HS Unit 4B, respectively.

Vertical hydraulic gradients in both dolostone aquifers of HS Unit 4 are negligible based on the observed high permeability and limited thickness. Horizontal hydraulic gradients for HS Unit 4A are calculated from MP55 casing pressure measurements at 0.0077 to 0.0086 m/m with groundwater flow directed to the northwest toward Lake Huron (Table 4.16). Horizontal hydraulic gradients for HS Unit 4B, also calculated from MP55 casing pressure measurements, are 0.0026 to 0.0039 m/m with groundwater flow directed to the east-northeast.

Diffusion testing was not undertaken in HS Unit 4 in Phase 1, 2A or 2B. Based on core observations, measured porosities, results from testing on similar DGR core, and scientific literature, the vertical effective diffusion coefficient for iodide is estimated at $5x10^{-12}$ m^2/s for MS Unit 4A and $3x10^{-12}$ m^2/s for MS Unit 4B (TR-08-10). The horizontal:vertical D_e anisotropy is assumed to be 1:1 based on core observations. Diffusion porosity in these porous permeable aquifers is assumed equal to total porosity at 7.7% and 7.5% for Units 4A and 4B, respectively.

Groundwater and porewater chemistries in HS Unit 4 are remarkably different in each aquifer based on results of targeted groundwater sampling in DGR-3 and DGR-4. The aquifer of the Salina Upper A1 Unit contains saline Na-Cl water with TDS of 30,000 mg/L. The lower aquifer of the Guelph Formation contains Na-Cl brine with TDS of 370,000 mg/L. Master variable of pH for the upper and lower aquifers approximate 7.0 to 7.3 and 6.5 to 7.1 (field measured), respectively. Eh in the upper and lower aquifers is about -100 mV and -150 mV, respectively, reflecting iron and/or sulphur-reducing conditions.

4.13.5 HS Unit 5: Ordovician Shale Aquiclude

HS Unit 5 comprises the very low permeability massive Ordovician shale sequence at the Bruce nuclear site from reference depths of 447.7 to 659.5 mBGS at DGR-1 and DGR-2. HS Unit 5 includes the Queenston, Georgian Bay and Blue Mountain Formation shales and Collingwood Member shale of the Cobourg Formation. The Unit is 209.5 to 216 m thick in DGR boreholes.

Borehole straddle-packer testing shows that the average horizontal hydraulic conductivities for formations and members that comprise HS Unit 5 range from $2x10^{-14}$ to $3x10^{-14}$ m/s, with several individual straddle-packer test results reported at values greater than and less than these average formation values. Based on laboratory petrophysical testing, the horizontal:vertical K anisotropy is assigned a value of 10:1. Based on extensive testing by different laboratories using different testing methods (Section 4.3.2, Figure 4.3, Table 4.3), an average total porosity of 7.4% is assumed for the massive shales of HS Unit 5. The siltstone and argillaceous limestone hard beds that occur within the shales have lower average total porosity of about 2.5%.

Specific storage values for HS Unit 5, based on calculations from lab measurements of rock compressibility and total porosity are estimated to be in the range of $5x10^{-7}$ to $3x10^{-5}$ m^{-1}, generally increasing with depth into the softer Blue Mountain shales.

The Ordovician shales are significantly underpressured. As discussed in Section 4.12.2, after shut-in periods of up to 18 months, formation pressures in HS Unit 5 are not yet stable, with maximum underpressures of about 300 mBGS expressed as environmental water head occurring within the Blue Mountain Formation. Based on environmental heads, vertical

hydraulic gradients in HS Unit 5 are generally strongly downward (~1.2 to 1.5 m/m) to the Blue Mountain Formation. Although the genesis of these underpressures is ambiguous, their occurrence and persistence are clearly indicative of very low formation permeability.

It is a characteristic of HS Unit 5 that a normally pressured zone of higher test interval compressibility and often hydraulic conductivity occurs within the otherwise underpressured and very low hydraulic conductivity aquiclude. These features appear to be associated with discrete inclined and subhorizontal fractures as described in Section 4.12.2.

Laboratory diffusion testing undertaken on DGR shale core samples collected from HS Unit 5 shows vertical effective diffusion coefficients for iodide of about $4x10^{-13}$ to $3x10^{-12}$ m^2/s generally decreasing with depth and showing a horizontal:vertical D_e anisotropy of about 2:1. A bimodal distribution of iodide effective diffusion coefficient and porosity is recognized from diffusion testing based on the presence of two distinct lithologies (shale and limestone/siltstone hardbeds) within HS Unit 5. The vertical effective diffusion coefficients for the HS Unit 5 hardbeds range from $3x10^{-14}$ to $4x10^{-13}$ m^2/s. The estimated iodide diffusion porosity values are 4.5% for the massive shales and 2% for the siltstone/limestone hardbeds within those shales.

Porewater chemistries in HS Unit 5 are relatively uniform consisting of Na-Cl brine (average TDS ~300,000 mg/L, Figures 4.53 and 4.54) showing minor (up to 10%) decreases in TDS with depth through the Unit. This uniform chemistry profile is evident in the major ion profiles (Figures 4.53 to 4.56), the ^{18}O and D profiles (Figures 4.61 and 4.62) and the fluid density profile (Figure 4.81). Master variables of pH and Eh approximate 5.5 ± 1 (computed from measured pCO_2) and -150 mV respectively, reflecting iron and/or sulphur-reducing conditions.

The persistent formation underpressures and the uniform porewater chemistry profiles indicate that no significant fluid flow has occurred within HS Unit 5, supporting its designation as an aquiclude.

4.13.6 HS Unit 6: Ordovician Limestone Aquiclude

HS Unit 6 comprises the very low permeability argillaceous limestone of the Lower Member of the Cobourg Formation – the DGR repository horizon – and the underlying limestones of the Sherman Fall and Kirkfield formations. Geologically, this HS Unit 6 is composed of the Trenton Group limestones. HS Unit 6 is found at reference depths of 659.5 to 762.0 mBGS at DGR-2. The Unit is 101.5 to 104.1 m thick in DGR boreholes.

Borehole straddle-packer testing and some laboratory petrophysical testing show that the average horizontal hydraulic conductivity for the formations that comprise HS Unit 6 range from $4x10^{-15}$ to $1x10^{-14}$ m/s, with bulk Unit average of about $1x10^{-14}$ m/s. Based on laboratory petrophysical testing, the horizontal:vertical K anisotropy is assigned a value of 10:1. Based on extensive testing by different laboratories using different testing methods (Section 4.3.2, Figure 4.3), an average total porosity of 2.4% is assumed for the argillaceous limestones of HS Unit 6 based on a range of average formation total porosity of 1.9 to 2.9%.

Specific storage values for HS Unit 6, based on calculations from lab measurements of rock compressibility and total porosity, are estimated to be in the range of $3x10^{-7}$ to $2x10^{-6}$ m.

The Cobourg, Sherman Fall and Kirkfield formations are under pressured and very slow to achieve stable conditions. As discussed in Section 4.12.2, stable formation pressures in HS Unit 6 have not yet been measured following shut-in periods of 18 months after initial installation of MP55 casing systems in DGR-2. The current best estimates of underpressures in HS Unit 6

expressed as environmental heads approximate 250 mBGS. Based on environmental heads, vertical hydraulic gradients in HS Unit 6 are moderately to strongly upward (~0.5 to 1.0 m/m) to the Blue Mountain Formation. Although the genesis of these underpressures is ambiguous, their occurrence is clearly indicative of very low formation permeability.

Laboratory diffusion testing undertaken on DGR core samples collected from HS Unit 6 shows vertical effective diffusion coefficients for iodide of about $1x10^{-13}$ to $9x10^{-13}$ m^2/s with an average value of about $3x10^{-13}$ m^2/s. Similar to other low-permeability HS units, a horizontal:vertical D_e anisotropy of about 2:1 is determined for HS Unit 6 from available diffusion testing. Average iodide diffusion porosity was measured at about 1.3%.

Porewater chemistries in HS Unit 6 show minor decreases in concentration from the top to the bottom of HS Unit 6. Porewater in HS Unit 6 consists of Na-Cl brine decreasing in TDS from about 285,000 mg/L at the top of unit to about 230,000 mg/L at the bottom of the unit (Figure 4.54). This chemistry profile is evident in the major ion profiles (Figures 4.53 to 4.56), the ^{18}O and D profiles (Figures 4.61 and 4.62), and the fluid density profile (Figure 4.81). Master variables of pH and Eh approximate 5.5 ± 1 (computed from measured pCO_2) and -150 mV respectively, reflecting iron and/or sulphur-reducing conditions.

The formation underpressures and the porewater chemistry profiles indicate that no significant fluid flow has occurred within HS Unit 6, supporting its designation as an aquiclude.

4.13.7 HS Unit 7: Ordovician Limestone Aquitard

HS Unit 7 comprises the low-permeability Ordovician limestone sequence at the Bruce nuclear site from reference depths of 762.0 to 838.6 mBGS at DGR-2. HS Unit 7 includes the Coboconk and Gull River formations (i.e., the Black River Group of limestones). In DGR boreholes, the Unit is 75.4 to 76.6 m thick.

Borehole straddle-packer testing and laboratory petrophysical testing show that the average horizontal hydraulic conductivity for HS Unit 7 ranges from $2x10^{-12}$ to $2x10^{-11}$ m/s, with some higher lab values reported in the bottom of the Gull River Formation. The estimated average horizontal hydraulic conductivity for the HS Unit is $6x10^{-12}$ m/s. Based on laboratory petrophysical testing, the horizontal:vertical K anisotropy is assumed to be 10:1 throughout HS Unit 7. However, this anisotropy estimate may be low within the Coboconk Formation if formation permeability is preferentially associated with some thin zones (e.g., tan dolostone marker beds) that are suspected to have increased hydraulic conductivity based on interpretation of borehole geophysical logs and straddle-packer testing results. Under these circumstances, the horizontal:vertical K anisotropy may be upwards of 1000:1. Based on extensive testing by different laboratories using different testing methods (Section 4.3.2, Figure 4.3), an average total porosity of 1.5% is assumed for the limestones of HS Unit 7.

Specific storage values for HS Unit 7, based on calculations from lab measurements of rock compressibility and total porosity, are estimated to be in the range of $2x10^{-7}$ to $6x10^{-6}$ m, with an overall average value of about $5x10^{-7}$ m.

Formation pressures and calculated fresh water and environmental heads in HS Unit 7 are normally pressured to overpressured and achieve stable conditions quickly within several days to a few months of casing installation (see Figures 4.97 to 4.100 and 4.102), reflecting the higher formation permeabilities relative to the overlying lower permeability units. Based on environmental heads, vertical hydraulic gradients in HS Unit 7 are strongly upward (~ 1.6 to 2.2 m/m) toward the Kirkfield Formation. These upward gradients, as per Darcy's Law, indicate

potential for upward advection of groundwater through HS Unit 7. The amount of advection will be controlled by the vertical hydraulic conductivity of the rock mass, which is unknown but certainly low.

Laboratory diffusion testing undertaken on DGR core samples collected from HS Unit 7 shows vertical effective diffusion coefficients for iodide of about $5x10^{-14}$ to $9x10^{-13}$ m^2/s with an average value of about $3x10^{-13}$ m^2/s. Similar to other low-permeability HS units, a horizontal:vertical D_e anisotropy of about 2:1 is determined for HS Unit 7 from available diffusion testing. Average iodide diffusion porosity in HS Unit 7 was measured at about 1.2%.

Porewater chemistries in HS Unit 7 are Na-Cl brine but are transitional with depth from the chemistry of the overlying Kirkfield Formation to that of the underlying Cambrian sandstone. TDS decreases from ~230,000 mg/L at the top of Coboconk Formation to ~200,000 mg/L in the top to middle of the Gull River Formation and then increases to ~230,000 mg/L at the bottom of the Gull River Formation (Figure 4.54). There are numerous excursions in porewater chemistry from this general trend, with both higher and lower concentrations evident in HS Unit 7. The changes in porewater TDS chemistry with depth are evident in the major ion profiles (Figures 4.53, 4.54 and 4.55 – especially for potassium), the ^{18}O and D profiles (Figures 4.60 and 4.61) and the fluid density profile (Figure 4.81). Master variables of pH and Eh approximate 5.5 ± 1 (computed from measured pCO_2) and -150 mV respectively, reflecting iron and/or sulphur-reducing conditions.

4.13.8 HS Unit 8: Cambrian Sandstone Aquifer

HS Unit 8 comprises the permeable Cambrian sandstone and the overlying permeable Shadow Lake siltstone found at reference depths of 838.6 to 860.7 mBGS at DGR-2. In DGR boreholes, the Unit is estimated to be 22.1 m thick. The hydraulic properties of HS Unit 8 are dominated by the high hydraulic conductivity and hydraulic heads of the middle to lower parts of the Cambrian rocks.

Borehole packer testing, opportunistic groundwater sampling and laboratory petrophysical testing show that the average horizontal hydraulic conductivity for HS Unit 8 ranges from $1x10^{-9}$ m/s for the Shadow Lake Formation (Raven et al. 1992a) and upper parts of the Cambrian sandstone to $3x10^{-6}$ m/s for the bulk of the Cambrian rocks. Given the permeable nature of HS Unit 8, the hydraulic conductivity of HS Unit 8 is assumed to be isotropic. Based on extensive testing by different laboratories using different testing methods (Section 4.3.2, Figure 4.2), an average total porosity of 10.1% is assumed for the Cambrian sandstones of HS Unit 8. Lower values of about 2 to 10% have been measured in the less permeable upper part of the Cambrian sequence that shows fine-grained dolostone facies and in the Shadow Lake Formation. The overall average total porosity for HS Unit 8 is 9.5%.

Specific storage values for HS Unit 8, based on calculations from lab measurements of rock compressibility and total porosity, are estimated to be in the range of $8x10^{-7}$ to $1x10^{-6}$ m^{-1}, with an overall average value of about $9x10^{-7}$ m^{-1}.

Formation pressures and calculated fresh water and environmental heads in HS Unit 8 are significantly overpressured with formation pressures of about 11,000 kPa and environmental heads of 350 mASL (165 m above ground surface). These pressures and heads have been consistently measured during opportunistic groundwater sampling and flow tests of the Cambrian sandstone and with Westbay MP55 casing installations in all DGR holes. Vertical hydraulic gradients in HS Unit 8 are assumed to be negligible based on the observed high

hydraulic conductivities. Horizontal hydraulic gradients for HS Unit 8 are calculated from MP55 casing pressure measurements at 0.0020 to 0.0031 m/m with groundwater flow directed to the east away from the centre of the Michigan Basin (Table 4.16).

Diffusion testing was not undertaken in HS Unit 8 in Phase 1, 2A or 2B. Based on core observations, known porosity, results from testing on comparable DGR core, and scientific literature, the vertical effective diffusion coefficient for iodide in HS Unit 8 is estimated at $1x10^{-11}$ m^2/s. The horizontal:vertical D_e anisotropy is assumed to be 1:1 based on core observations. Diffusion porosity is assumed equal to total porosity at 9.5%.

Groundwater and porewater chemistries in HS Unit 8 are Na:Ca-Cl brine (TDS ~205,000 to 235,000 mg/L) but of lower salinity than the porewater of the upper parts of HS Unit 7 and of HS Units 6 and 5. Master variables of pH and Eh approximate 6.5 to 7.3 (field measured, average 6.7) and -150 mV reflecting iron and/or sulphur-reducing conditions.

The collection of reliable and representative samples of groundwater from the overpressured Cambrian rocks allows assessment of the reliability and representativeness of the porewater chemistry data determined for the Cambrian strata and the Shadow Lake Formation. Where this comparison is possible, it shows that the major ion (Figures 4.53 to 4.56), environmental isotope (Figures 4.61 and 4.62) and gas (Figures 4.67, 4.69 and 4.75) chemistries are quite similar, providing confidence in the porewater chemistry results.

4.13.9 HS Unit 9: Precambrian Aquitard

HS Unit 9 comprises the moderate to low-permeability basement rock of the Precambrian granite gneiss underlying the Cambrian sandstone. At DGR-2, the Unit is found at reference depths of 860.7 mBGS. Based on the appearance of the 1.55 m of core obtained from DGR-2, HS Unit 9 is comprised of competent moderately fractured felsic granite gneiss.

No field or laboratory testing of the hydraulic properties of the Precambrian basement has been performed as part of Phase 1 or 2A site characterization work. However, there is a large amount of information on both the hydraulic and diffusive properties of similar rock types at similar depths in the Canadian Shield based on Canadian and international studies completed in support of deep geological disposal of nuclear fuel wastes. Based on review of these studies (Raven et al. 1992b), representative estimates of hydraulic conductivity and total porosity of the majority of HS Unit 9 are $1x10^{-12}$ m/s and 0.5%, respectively and the rocks are assumed to be isotropic. The upper several metres to tens of metres of the Precambrian basement is often weathered, fractured and more permeable than the deeper basement rocks. Based on testing reported by Raven et al. (1992a) for borehole OHD-1 at a depth of about 400 mBGS at the Lakeview Generating Station, the upper weathered and fractured part of the Precambrian may have hydraulic conductivity of about 10^{-10} to 10^{-9} m/s, with a higher total porosity equivalent to the 3.8% measured by testing of DGR-2 core (Figure 4.3) to reflect weathering and fracturing. Based on these estimated hydraulic properties, the Precambrian, relative to the overlying Cambrian sandstone aquifer, is an aquitard, although the upper part of the Unit is more permeable.

There is no information available on formation pressures or hydraulic heads within HS Unit 9 at the Bruce nuclear site. Based on review of scientific literature (Raven et al. 1992b), a hydraulic gradient of $1x10^{-3}$ m/m is likely appropriate for HS Unit 9. The actual magnitude and direction of this assumed gradient is unknown at the Bruce nuclear site.

Diffusion testing was not undertaken in HS Unit 9 in Phase 1 or 2. Based on core observations, total porosity and review of international scientific literature (Raven et al. 1992b), the effective diffusion coefficient for iodide is estimated at $3x10^{-13}$ m^2/s. The horizontal:vertical D_e anisotropy is assumed to be 1:1. Diffusion porosity is assumed equal to total porosity at 0.5%.

Groundwater and porewater chemistries in HS Unit 9 are not known at the Bruce nuclear site, but have been extensively characterized elsewhere in Ontario (Frape and Fritz 1987, Gascoyne et al. 1987), including the Sudbury mining region. Canadian Shield groundwater from comparable depths (>860 m BGS) are typically Ca:Na-Cl brine with TDS greater than 50,000 mg/L towards an estimated Shield source brine of more than 350,000 mg/L (Gascoyne et al. 1987, Pearson 1987). Based on literature review, master variables of pH and Eh approximate 6.0 and -150 mV respectively, reflecting iron and/or sulphur-reducing conditions.

4.13.10 Summary of HS Unit Properties

Table 4.17 provides a summary of the representative estimates of hydrogeologic properties of the hydrostratigraphic units identified for the Bruce nuclear site as discussed in Sections 4.13.1 to 4.13.9. Table 4.17 lists recommended estimates of formation-scale properties based on review of available Phase 1, 2A and 2B site characterization data, experience from investigation of similar formations elsewhere and professional judgment. Table 4.17 lists single recommended estimates or ranges of recommended estimates for formations where changes with depth are apparent. Table 4.17 lists parameter values for specific storage (S_s), horizontal hydraulic conductivity (K_h), hydraulic conductivity anisotropy ratio (K_h:K_v), total porosity (ϕ_t), vertical effective diffusion coefficient (D_{e-v}), diffusion coefficient anisotropy ratio (D_{e-h}:D_{e-v}), iodide accessible diffusion porosity (ϕ_l) and groundwater/ porewater chemistry.

4.14 Hydrogeological Systems

Physical hydrogeological data (i.e., K and formation pressure/environmental head) and chemical hydrogeological data (i.e., porewater and groundwater major ion concentrations and environmental isotopes) presented and discussed in Sections 4.3 to 4.13 of this report indicate the presence of three hydrogeological systems or regimes at the Bruce nuclear site:

- Shallow System;
- Intermediate System; and
- Deep System.

4.14.1 Shallow System

The shallow freshwater to brackish hydrogeological system includes HS Units 1 and 2 and extends to reference depths of about 169.3 mBGS at DGR-1. Groundwater flow within the normally pressured permeable bedrock system is upward and laterally toward Lake Huron. Groundwater and porewater chemistries are transitional from fresh Ca:Mg-HCO_3 water (TDS ~500 mg/L) near the top of the bedrock to brackish Ca-SO_4 water (TDS ~5,000 mg/L) at the bottom of the system. Solute migration within this permeable shallow groundwater system is principally by advection.

Table 4.17: Summary of Representative Estimates of Hydrogeologic Properties of Bruce Nuclear Site Hydrostratigraphic Units

HS Unit	Depth (mBGS)	Hydraulic Properties				Iodide Diffusive Properties			Groundwater/Porewater Properties			
		S_s (m^{-1})	K_h (m/s)	K_h:K_v (-)	Φ_t (%)	D_{e-v} (m^2/s)	D_{e-h}: D_{e-v} (-)	Φ_l (%)	TDS (mg/L)	Type	pH	Eh (mV)
1: Overburden Aquitard	0-20	$1x10^{-3}$	$8x10^{-10}$	2:1	20	$6x10^{-10}$	1:1	20	<500	Ca,Na-HCO_3	7-8	+200 to +400
2: Dolostone Aquifer	20-169.3	$5x10^{-7}$ to $2x10^{-6}$	$1x10^{-7}$ to $1x10^{-4}$	10:1	7.0	$8x10^{-12}$	1:1	7.0	500 to 5000	Ca,Mg-HCO_3 to Ca-SO_4	7-8	+400 to -100
3: Silurian Aquitards	169.3-447.7	$3x10^{-7}$ to $3x10^{-5}$	$5x10^{-14}$ to $3x10^{-10}$	10:1	0.5 to 19	$1x10^{-12}$	2:1	0.5 to 8.7	10,000 to 350,000	Ca-SO_4 to Na-Cl	7.0	-100 to -150
4A: Silurian Aquifer	325.5-328.5: 374.5-378.6	$8x10^{-7}$	$2x10^{-7}$	1:1	6.3	$7x10^{-12}$	1:1	6.3	30,000	Na-Cl	7.1	-100
4B: Silurian Aquifer		$1x10^{-6}$	$3x10^{-8}$	1:1	13.1	$3x10^{-11}$	1:1	13.1	370,000	Na-Cl	6.8	-150
5: Ordovician Shale Aquiclude	447.7-659.5	$5x10^{-7}$ to $3x10^{-5}$	$2x10^{-14}$ to $3x10^{-14}$	10:1	2.5 & 7.4	$1x10^{-13}$ & $1x10^{-12}$	2:1	2.0 & 4.5	300,000	Na-Cl	5.5 ± 1	-150
6: Ordovician Lmst Aquiclude	659.5-762.0	$3x10^{-7}$ to $2x10^{-6}$	$4x10^{-15}$ to $1x10^{-14}$	10:1	2.4	$3x10^{-13}$	2:1	1.3	285,000 to 230,000	Na-Cl	5.5 ± 1	-150
7: Ordovician Lmst Aquitard	762.0-838.6	$5x10^{-7}$	$6x10^{-12}$	10-1000:1[2]	1.5	$3x10^{-13}$	2:1	1.2	230,000 to 200,000	Na-Cl	5.5 ± 1	-150
8: Cambrian Aquifer	838.6-860.7	$9x10^{-7}$	$1x10^{-9}$ to $3x10^{-6}$	1:1	9.5	$1x10^{-11}$	1:1	9.5	205,000 to 235,000	Na,Ca-Cl	6.7	-150
9: Precambrian Aquitard[1]	>860.7	$1x10^{-6}$	$1x10^{-10}$ & $1x10^{-12}$	1:1	3.8 & 0.5	$3x10^{-13}$	1:1	3.8 & 0.5	50,000 to 350,000	Ca,Na-Cl	6.0	-150

Notes: Unless otherwise flagged, all data are derived or interpreted from investigations of the Bruce nuclear site as described in relevant technical reports and discussed in Section 4.13 and earlier sections of this report.

1. All hydraulic and iodide diffusive property values for HS Unit 9 are from Raven et al. (1992b). All groundwater porewater property data for HS Unit 9 are from Gascoyne et al. (1987) and Pearson (1987).

2. Anisotropy will be high if permeability is preferentially associated with thin dolomitized zones in the Coboconk and Gull River formations.

This shallow groundwater flow system contains stable-isotope evidence of circulation of glacial meltwater mixing with older brackish waters. Although redox potentials of up to 400 mV have been measured (with Pt electrodes) on collected groundwater samples, this flow system is predominately anoxic as is demonstrated by the presence of trace pyrite in core samples. The deepest penetration of water with significant amounts of dissolved oxygen (i.e., DO > 0.3 mg/L) is 170 m BGS in US-8 in which DO=7 mg/L (TDS=2670 mg/L). Radiocarbon analyses of dissolved inorganic carbon in groundwater from 158 and 179 mBGS in US-8 indicate ($\delta^{13}C$ corrected) ^{14}C ages of 4,000 to 8,000 years B.P. Both of these samples had non-detectable DO.

4.14.2 Intermediate System

The intermediate hydrogeological system includes HS Unit 3 and both Silurian aquifer zones that comprise HS Unit 4, and occurs at reference depths of 169.3 to 447.7 mBGS at DGR-1. The intermediate system includes dolostones, shales and evaporites of the Salina Formation and the Middle and Lower Silurian dolostones and shales. This is a predominantly a low-permeability system (K_h=5x10^{-14} to 3x10^{-10} m/s) with groundwater flow likely restricted to the two permeable aquifer zones present at reference depths of 325.5 – 328.5 mBGS in the top of the Salina A1 Unit and at 374.5 – 378.6 mBGS in the Guelph Formation.

There are moderate underpressures evident within Salina B and C Units and moderate overpressures in the Gasport to Fossil Hill formations, attesting to the low permeabilities of the intermediate system. Based on formation pressure measurements, flow in the two permeable units is not coupled as the flow direction in the Salina Upper A1 Unit is towards Lake Huron, whereas in the Guelph Formation the flow direction is eastwards or inland.

Opportunistic groundwater samples from the two permeable zones contained ferrous iron and dissolved sulphide and were approximately neutral in pH. The Salina Upper A1 Unit aquifer shows evidence of deep meltwater recharge, i.e., OGW-8: $\delta^{18}O$=-14.4 ‰ and δD= -104‰. Groundwater and porewater chemistries in this intermediate system are transitional from saline Ca-SO_4 water (TDS ~10,000 mg/L) near the top of HS Unit 3 to Na-Cl brine (TDS ~370,000 mg/L) in the lower part of the system, i.e., the Guelph Formation. Below the Guelph Formation the porewater TDS ranges from 290,000 to 350,000 mg/L of Na-Cl brine.

The salinity and tracer profiles (e.g., $\delta^{18}O$ and δD, Cl, Sr) in the upper part of the system (Salina G to A1 Units) suggest that diffusive exchange of porewater from this part of the aquitard with the meltwater in the overlying Bass Islands Formation and underlying Salina Upper A1 Unit aquifers has occurred. There is also a pronounced $\delta^{18}O$, δD, major ion, TDS and fluid density increase downward from the Salina Upper A1 Unit to the Guelph that is likely diffusional in origin due to upward diffusion from the Guelph. The TDS in this middle part of the system increases by over an order of magnitude in a vertical distance of only 46 m from 30,000 mg/L at reference depth of 328.5 mBGS to 370,000 mg/L at reference depth of 374.5 mBGS. Below the Guelph Formation, the $\delta^{18}O$, δD, major ion, TDS and fluid density profiles are similar to those measured in the upper part of Queenston shale suggesting that diffusion-controlled solute transport also occurs in the lower part of the intermediate system.

4.14.3 Deep System

The deep hydrogeological system includes a deep aquiclude and an underlying deep aquitard and aquifer. The deep system includes HS Units 5, 6, 7 and 8 and occurs at reference depths of 447.7 to 860.7 mBGS at DGR-1 and DGR-2. This deep system consists of the Upper

Ordovician shales, the Trenton and Black River Group limestones and the Cambrian sandstone. The upper part of the system comprising an aquiclude and the lower part of the system comprising an aquitard and non-potable aquifer, are described separately.

Porewater chemistries of the deep aquiclude system are Na-Cl brine with 4500 to 6000 mmol Cl^- /kgw and TDS of 220,000 to 300,000 mg/L that decrease in concentration with depth. The rocks are of exceptionally low hydraulic conductivity (K_h=8x10^{-15} to 5x10^{-14} m/s), are and significantly underpressured in the deeper Ordovician shales and Trenton Group limestones that likely contain a free gas phase of approximately 10% of the pore volume. These hydrogeological properties indicate an aquiclude with no advection of brine, and a system in which gas flow would also be diffusion controlled.

Within each DGR borehole monitoring the deep aquiclude using MP55 casing systems there is one normally pressured horizon that appears to be associated with specific subvertical (DGR-2 and DGR-3) and subhorizontal fractures (DGR-4). The remaining parts of the deep aquiclude system are significantly underpressured. The normally pressured zones also often show formation hydraulic conductivity that is often 1 to 1.5 orders of magnitude greater than the surrounding rock mass based on the straddle-packer test intervals and with increased test interval compressibility measured during packer testing. Assuming the increased test interval values of hydraulic conductivity are associated with thin zones, the bulk hydraulic conductivity of these thin zones is more than 1 to 1.5 orders of magnitude greater than that of the surrounding rock mass. However, targeted hydraulic testing using shorter test intervals in DGR-6 suggests this may not be the case, as there was no clear enhancement of formation hydraulic conductivity associated with suspected permeable fractures.

Environmental isotope profiles from DGR boreholes indicate no significant migration of solutes in this deep aquiclude system other than by diffusion upwards to the intermediate system and possibly downwards to the underlying more permeable limestones of the Black River Group. The limited number of fractures detected appear to have healed and are infilled with halite and calcite. The presence of soluble halite throughout the 230 m of rocks above and occasionally in the 75 m of rocks below the proposed repository formation is a clear indicator of the absence of active fluid circulation in this system. This diffusion-dominated system has likely existed over a time scale of hundreds of millions of years (NWMO 2011).

Several lines of evidence point to the presence of capillary barriers to solute migration immediately above the proposed repository formation in the deep aquiclude system. Firstly, the estimated pore throat radii for the Cobourg and Lower Blue Mountain formations are <4 nm and the gas entry pressures are in excess of 20 MPa, which is approximately the lithostatic confining pressure at that depth. Also, the helium gas isotope ratios and the methane isotope ratios show strong gradients at the shale-limestone contact represented by the Collingwood Member. These data indicate that upward migration of gaseous radionuclides would be inhibited by capillary effects while downward migration would be prevented by a combination of the extremely low hydraulic conductivity and a strong upward hydraulic gradient.

The deep aquitard and aquifer system is an overpressured hydrogeological system, most likely sourced from the permeable Cambrian sandstone. This deep overpressured system includes the Middle Ordovician Coboconk, Gull River and Shadow Lake formations and the Cambrian sandstone, which all exhibit increased permeability relative to the overlying deep aquiclude system. The formation horizontal hydraulic conductivities in this system decrease upwards from the Cambrian sandstone (K_h=3x10^{-6} m/s) through the Shadow Lake Formation (K_h=1x10^{-9} m/s) to the Gull River and Coboconk (K_h=2x10^{-12} and 2x10^{-11} m/s), with locally higher estimates of up

to $2x10^{-10}$ m/s reported from some straddle-packer testing. Groundwater and porewater chemistries in this regime are Na:Ca-Cl to Na-Cl brine with TDS of about 200,000 to 255,000 mg/L.

Groundwater flow within the permeable Cambrian sandstone is lateral with flow gradients directed to the east away from the centre of the Michigan Basin. Based on Darcy's Law and the observed upward hydraulic gradients, that approximate 2 m/m, there is potential for upward vertical groundwater movement from the Cambrian sandstone toward the Coboconk Formation. As the magnitude of any upward vertical groundwater flow is controlled by the vertical hydraulic conductivity of the aquitard which is unknown, the magnitude of such flow is also unknown. If the horizontal:vertical K anisotropy for the aquitard approaches 1000:1, which has been suggested for the Ordovician aquitard (Sykes et al. 2011), the resultant vertical groundwater flow would be insignificantly small and comparable to that estimated for the overlying Ordovician aquiclude.

The major ion and environmental isotope profiles from DGR boreholes show that the current groundwater and porewater chemistry in the Cambrian sandstone is significantly different than the porewater chemistry profile evident within the overlying formations from the Guelph Formation to the Black River Group of formations, that NWMO (2011) attribute to a very old (300 million years) diffusion profile. The reversals of Cl, Br, TDS, $\delta^{18}O$, deuterium excess and Sr depth trends evident within the Gull River and Shadow Lake formations suggest that a hydrological perturbation occurred within the Cambrian within the geological past, the timing of which is uncertain. The occurrence of sporadic, but coherent, Cambrian-like Cl, Br and $\delta^{18}O$ porewater signatures within the Black River limestones may reflect localized upward transport along increased porosity and permeability pathways within the Black River Group limestones. An alternate explanation for the observed geochemical reversals and Cambrian-like geochemical excursions in the Black River limestones is that these geochemical patterns are ancient signatures that may have existed since the early Mesozoic due to the effects of separate gas and liquid hydrocarbon phases in retarding diffusion.

4.15 Representative Estimates of Descriptive Hydrogeological Model Properties

Tables 4.18 and 4.19 summarize the representative estimates of the main hydrogeological properties of the 39 layers that comprise the descriptive hydrogeological model for the Bruce DGR site. Data given in Tables 4.18 and 4.19 are consistent with and provide a more detailed description of the hydrogeological information given in Table 4.17 on the nine hydrostratigraphic units that represent the Bruce DGR site.

The descriptive hydrogeological model includes three additional layers that were not included in the geological model. The hydrogeological model includes separate model layers to account for increased permeability associated with the upper parts of the Amherstburg Formation, Bass Islands Formation and Salina Upper A1 Unit Aquifer (HS Unit 4A). The descriptive geological model does not differentiate the upper and lower parts of these formations and units.

Estimates presented in Tables 4.18 and 4.19 are based on assessment of data obtained from all DGR boreholes, that is DGR-1 through DGR-6. Earlier interim assessments of hydrogeological data were based on assessment of data from boreholes DGR-1 through DGR-4. These earlier interim estimates of layer hydrogeological properties were used in Post Closure Safety Assessment modeling and regional groundwater modeling completed as part of Geosynthesis work. In general the changes in hydrogeological properties used in the modeling and given this DGSM report are not large and are thought not to be significant. Appendix A

presents a tabular listing parameter values used in modeling and as outlined in Tables 4.18 and 4.19. Appendix A shows values for formation hydraulic conductivity, liquid, diffusion and total porosity, specific storage, effective diffusion coefficients, fluid TDS and gas saturations.

Table 4.18: Representative Estimates of Rock Density, Porosity and Gas Saturation Properties of Hydrogeological Model Layers

Model Layer	Wet Bulk Density (g/cm^3)	Dry Bulk Density (g/cm^3)	Grain Density (g/cm^3)	Liquid Porosity (%)	Diffusion Porosity (%)	Total Porosity (%)	Gas Saturation (% PV)
Clay till overburden	-	-	-	20	20	20	-
Lucas	2.70	2.62	2.84	7.8	7.8	7.8	-
Amherstburg (upper 20m)	2.70	2.62	2.84	7.8	7.8	7.8	-
Amherstburg (lower 20m)	2.70	2.62	2.84	7.8	7.8	7.8	-
Bois Blanc	2.70	2.62	2.84	7.8	7.8	7.8	-
Bass Islands (upper 20 m)	2.76	2.71	2.84	5.5	5.5	5.5	-
Bass Islands (lower 25 m)	2.76	2.71	2.84	5.5	5.5	5.5	-
Salina G Unit	2.48	2.32	2.78	16.7	0.9	16.7	-
Salina F Unit	2.54	2.38	2.80	10.7	4.8	10.7	15.8
Salina E Unit	2.60	2.49	2.82	11.9	5.5	11.9	17.8
Salina D Unit	2.80	2.73	2.93	6.7	0.7	8.9	-
Salina C Unit	2.46	2.25	2.74	18.5	8.5	19.4	18.0
Salina B Unit - Carbonate	2.56	2.31	2.81	15.8	8.7	15.8	0
Salina B Unit - Evaporite	2.80	2.73	2.93	6.7	0.7	8.9	-
Salina A2 Unit - Carbonate	2.68	2.42	2.86	12.4	3.9	12.4	0.7
Salina A2 Unit - Evaporite	2.71	2.87	2.85	6.7	0.7	8.9	15.7
A1 Unit – Upper Carb	2.81	2.74	2.93	6.3	6.3	6.3	-
A1 Unit – Lower Carb	2.63	2.60	2.73	4.0	1.1	4.0	-
Salina A1 Unit - Evaporite	2.89	2.87	2.93	1.1	0.1	1.2	0
Salina A0 Unit	2.64	2.71	2.79	2.7	1.8	5.4	16.9

Model Layer	Wet Bulk Density (g/cm^3)	Dry Bulk Density (g/cm^3)	Grain Density (g/cm^3)	Liquid Porosity (%)	Diffusion Porosity (%)	Total Porosity (%)	Gas Saturation (% PV)
Guelph	2.65	2.58	2.81	13.1	13.1	13.1	-
Goat Island	2.68	2.65	2.73	2.8	1.2	2.8	0.1
Gasport	2.70	2.68	2.73	1.9	1.2	1.9	-
Lions Head	2.59	2.50	2.73	8.3	8.3	8.3	-
Fossil Hill	2.72	2.72	2.73	0.5	0.5	0.5	-
Cabot Head	2.60	2.52	2.79	10.4	6.8	10.4	-
Manitoulin	2.67	2.65	2.72	2.4	1.2	3.1	0
Queenston	2.65	2.57	2.77	7.5	3.7	7.5	6.7
Georgian Bay	2.64	2.61	2.76	7.1	3.4	7.1	6.6
Blue Mountain	2.64	2.55	2.77	7.1	4.3	7.1	14.5
Cobourg – Collingwood Member	2.64	2.57	2.70	1.1	1.7	2.3	18.3
Cobourg - Lower	2.68	2.66	2.71	1.4	1.3	1.9	11.9
Sherman Fall	2.70	2.66	2.72	1.7	0.45	2.9	15.2
Kirkfield	2.68	2.63	2.71	2.3	2.1	2.3	19.9
Coboconk	2.66	2.67	2.69	0.9	1.1	0.9	4.0
Gull River	2.71	2.67	2.73	2.2	1.4	2.2	20.0
Shadow Lake	2.65	2.58	2.76	8.9	8.9	8.9	-
Cambrian	2.58	2.51	2.70	6.7	6.7	10.1	3.3
Upper Precambrian	2.54	2.49	2.59	3.7	3.7	3.8	-

Table 4.18 summarizes the estimates of wet bulk density, dry bulk density, grain density, liquid porosity, diffusion porosity, total porosity and gas saturation for the 39 layers that comprise the descriptive hydrogeological site model. Table 4.19 summarizes estimates of the main transport properties, including formation horizontal hydraulic conductivity, hydraulic conductivity anisotropy, specific storage, vertical effective diffusion coefficients for iodide, effective diffusion coefficient anisotropy and groundwater/porewater total dissolved solids (TDS) of the 39 model layers.

Tables 4.18 and 4.19 do not list all hydrogeological properties determined for the descriptive hydrogeological model, only those main properties for which data is available for most of the model layers and for which representative estimates are appropriate and reasonably calculated. For example, information on gas entry pressures, surface areas and gas-brine flow properties are available primarily for the Cobourg Formation and the Ordovician shales and are not summarized here. Similarly, estimates of porewater and groundwater geochemistry, and

formation pressures and environmental heads are not given here because many of the model layers show important spatial and/or temporal changes within layers that are poorly represented by single estimated values.

Table 4.19: Representative Estimates of Hydraulic, Diffusive and Pore Fluid TDS Properties of Hydrogeological Model Layers

Model Layer	K_h (m/s)	K_h:K_v (-)	S_s (m^{-1})	Iodide D_{e-v} (m^2/s)	D_{e-h}:D_{e-v} (-)	Fluid TDS (g/L)
Clay till overburden	$8x10^{-10}$	2:1	$1x10^{-3}$	$6.0x10^{-10}$	1:1	0.5
Lucas	$1x10^{-6}$	10:1	$5x10^{-7}$ - $7x10^{-7}$	$1.0x10^{-11}$	1:1	0.5
Amherstburg (upper 20m)	$1x10^{-6}$	10:1	$7x10^{-7}$ - $2x10^{-6}$	$1.0x10^{-11}$	1:1	0.5
Amherstburg (lower 20m)	$1x10^{-7}$	10:1	$7x10^{-7}$ - $2x10^{-6}$	$1.0x10^{-11}$	1:1	0.5
Bois Blanc	$1x10^{-7}$	10:1	$6x10^{-7}$ - $1x10^{-6}$	$1.0x10^{-11}$	1:1	3.2
Bass Islands (upper 20m)	$1x10^{-4}$	10:1	$1x10^{-6}$ - $2x10^{-6}$	$5.0x10^{-12}$	1:1	6.0
Bass Islands (lower 25m)	$1x10^{-5}$	10:1	$1x10^{-6}$ - $2x10^{-6}$	$5.0x10^{-12}$	1:1	6.0
Salina G Unit	$1x10^{-11}$	10:1	$1x10^{-6}$ - $2x10^{-6}$	$4.3x10^{-13}$	2:1	14.8
Salina F Unit	$5x10^{-14}$	10:1	$1x10^{-6}$ - $7x10^{-6}$	$4.1x10^{-12}$	2:1	59.6
Salina E Unit	$2x10^{-13}$	10:1	$1x10^{-6}$ - $7x10^{-6}$	$4.7x10^{-12}$	2:1	124
Salina D Unit	$2x10^{-13}$	10:1	$5x10^{-7}$ - $7x10^{-7}$	$4.7x10^{-12}$	2:1	200
Salina C Unit	$4x10^{-13}$	10:1	$2x10^{-6}$ - $1x10^{-5}$	$1.1x10^{-11}$	2:1	249
Salina B Unit - Carbonate	$4x10^{-13}$	10:1	$5x10^{-6}$ - $2x10^{-5}$	$1.2x10^{-11}$	2:1	321
Salina B Unit - Evaporite	$3x10^{-13}$	10:1	$5x10^{-7}$ - $7x10^{-7}$	$7.7x10^{-14}$	2:1	321
Salina A2 Unit - Carbonate	$3x10^{-10}$	10:1	$1x10^{-6}$ - $2x10^{-6}$	$1.2x10^{-12}$	2:1	120
Salina A2 Unit - Evaporite	$3x10^{-13}$	10:1	$5x10^{-7}$ - $6x10^{-7}$	$7.7x10^{-14}$	2:1	45.6
A1 Unit – Upper Carb	$2x10^{-7}$	1:1	$5x10^{-7}$ - $1x10^{-6}$	$6.8x10^{-12}$	1:1	22.4
A1 Unit –	$9x10^{-12}$	10:1	$5x10^{-7}$ -	$1.8x10^{-13}$	2:1	118

Model Layer	K_h (m/s)	K_h:K_v (-)	S_s (m^{-1})	Iodide D_{e-v} (m^2/s)	D_{e-h}:D_{e-v} (-)	Fluid TDS (g/L)
Lower Carb			$1x10^{-6}$			
Salina A1 Unit - Evaporite	$3x10^{-13}$	10:1	$3x10^{-7}$ - $4x10^{-7}$	$3.0x10^{-14}$	2:1	325
Salina A0 Unit	$3x10^{-13}$	10:1	$3x10^{-7}$ - $3x10^{-7}$	$3.0x10^{-14}$	2:1	318
Guelph	$3x10^{-8}$	1:1	$9x10^{-7}$ - $1x10^{-6}$	$2.9x10^{-11}$	1:1	370
Goat Island	$2x10^{-12}$	10:1	$3x10^{-7}$ - $5x10^{-7}$	$1.5x10^{-13}$	2:1	290
Gasport	$2x10^{-12}$	10:1	$3x10^{-7}$ - $5x10^{-7}$	$1.5x10^{-13}$	2:1	307
Lions Head	$5x10^{-12}$	10:1	$5x10^{-7}$ - $7x10^{-7}$	$1.2x10^{-11}$	2:1	306
Fossil Hill	$5x10^{-12}$	10:1	$3x10^{-7}$ - $4x10^{-7}$	$4.3x10^{-14}$	2:1	327
Cabot Head	$9x10^{-14}$	10:1	$4x10^{-6}$ - $3x10^{-5}$	$3.1x10^{-12}$	2:1	301
Manitoulin	$1x10^{-13}$	10:1	$7x10^{-7}$ - $1x10^{-6}$	$1.5x10^{-13}$	2:1	349
Queenston	$3x10^{-14}$	10:1	$1x10^{-6}$ - $5x10^{-6}$	$1.0x10^{-12}$	2:1	304
Georgian Bay	$3x10^{-14}$	10:1	$2x10^{-6}$ - $1x10^{-5}$	$4.3x10^{-13}$	7:1	302
Blue Mountain	$3x10^{-14}$	10:1	$3x10^{-6}$ - $3x10^{-5}$	$8.2x10^{-13}$	2:1	294
Cobourg – Collingwood Member	$2x10^{-14}$	10:1	$5x10^{-7}$ - $1x10^{-6}$	$4.9x10^{-13}$	2:1	225
Cobourg - Lower	$1x10^{-14}$	10:1	$3x10^{-7}$ - $6x10^{-7}$	$3.7x10^{-13}$	2:1	286
Sherman Fall	$9x10^{-15}$	10:1	$8x10^{-7}$ - $2x10^{-6}$	$2.2x10^{-13}$	2:1	269
Kirkfield	$4x10^{-15}$	10:1	$7x10^{-7}$ - $2x10^{-6}$	$4.2x10^{-13}$	2:1	230
Coboconk	$2x10^{-11}$	10-1000:1	$2x10^{-7}$ - $4x10^{-7}$	$2.7x10^{-13}$	2:1	255
Gull River	$2x10^{-12}$	10-1000:1	$3x10^{-7}$ - $6x10^{-7}$	$2.6x10^{-13}$	2:1	204
Shadow Lake	$1x10^{-9}$	10:1	$8x10^{-7}$ - $1x10^{-6}$	$1.3x10^{-12}$	2:1	201

Model Layer	K_h (m/s)	K_h:K_v (-)	S_s (m^{-1})	Iodide D_{e-v} (m^2/s)	D_{e-h}:D_{e-v} (-)	Fluid TDS (g/L)
Cambrian	$3x10^{-6}$	1:1	$8x10^{-7}$ - $1x10^{-6}$	$1.7x10^{-11}$	1:1	235
Upper Precambrian	$1x10^{-10}$	1:1	$1x10^{-6}$	$3.0x10^{-13}$	1:1	-

Table 4.18 lists the estimates of rock densities based on laboratory testing by Core Labs, University of New Brunswick and the University of Bern (TR-07-17, TR-08-06, TR-08-27, TR-08-28 and TR-08-40). Estimates of rock densities were determined from arithmetic averages for layers presented in Figure 4.1. Where rock density data were not available for shallow layers and some thin layers (e.g., Lucas to Bass Islands, Salina D Unit anhydritic dolostone, B Unit evaporite, A0 Unit dolostone, Gasport, Lions Head and Fossil Hill dolostones), densities were estimated from lithologically similar units or formations. If wet or dry density values were unavailable they were calculated from grain density and porosity data as described in TR-08-10.

Estimates of liquid and total porosity for each of the hydrogeological model layers are based on a coherent analysis and interpretation of testing completed by Core Labs, University of Ottawa, University of New Brunswick and University of Bern as summarized in TR-08-10 and TR-08-34. The estimated values of liquid and total porosities for each model layer are generally the arithmetic averages shown on Figures 4.2 and 4.3 that are based on testing of unconfined cores. For the Salina G Unit to A2 Unit where gypsum is an important secondary mineral, liquid porosities are frequently larger than total porosities due to release of mineralogically-bound water during heating. For these units the representative liquid porosity values are set equal to the total porosity values. For most of the Ordovician shales and limestones, as well as the Guelph dolostone and the Cabot Head shale, the number of total porosity results are limited compared to the liquid porosity, and the liquid porosity averages are considered representative of total porosity averages. Estimates of diffusion porosity are the arithmetic average values of iodide tracer-accessible porosity from University of New Brunswick testing completed normal to bedding planes (TR-07-17, TR-08-27) as listed in Figure 4.38. As with rock density, where porosity data were not available for shallow layers and some thin layers, porosities were estimated from lithologically similar units or formations.

Estimates of gas saturations, expressed as a percentage of the pore space volume (PV), are determined from analysis and interpretation of testing completed by Core Laboratories (TR-07-18, TR-08-28) as described in TR-08-34. Dashes in Figure 4.19 indicate that no data are available for model layers. The estimates are the arithmetic averages shown on Figure 4.8. Given the observed variability of these data, extrapolation of data to other layers that were not tested was not done. As the calculations of gas saturations were completed on a subset of samples tested for total and liquid porosity, there are some inconsistencies evident in the comparison of total and liquid porosities and gas saturations. That is for some model layers total porosity volume does not equal liquid porosity volume plus gas saturation volume.

Similar to the descriptive geological model, Table 4.18 provides representative estimates of properties mostly on a unit, member and formation basis, regardless of any major lithofacies changes within such units, members and formations. Thus, for the Queenston and Georgian Bay formations where two sets of lithofacies are evident (massive shale and limestone/siltstone hardbeds), the reported estimates of rock densities, porosities and gas saturations are averages

of cores that sample these different lithofacies. Similarly, for the Cambrian rocks that are comprised of an upper argillaceous dolostone facies and a lower quartzitic sandstone facies, the reported estimate values represent an average of these two different lithofacies.

The estimates of formation hydraulic conductivity (K) for each of the 39 hydrogeological model layers given in Table 4.19 are geometric mean values determined primarily from field testing of DGR and US boreholes (TR-08-10). The values listed in Table 4.19 are those listed in Table 4.14 and shown in Figure 4.90. Field data from straddle packer testing of all DGR boreholes are considered in these determinations for layers below the Salina G Unit. No weight was given to laboratory gas pulse permeability testing due to the recognized effects of core damage on the reported results. Estimates of hydraulic conductivity anisotropy are based primarily on laboratory core testing, with the proviso that thin permeable layers (i.e., Salina Upper A1 Unit, Guelph and Cambrian aquifers), based on core observations, are isotropic with respect to hydraulic conductivity.

The estimates of effective diffusion coefficient listed in Table 4.19 are, with the exception of the Georgian Bay Formation, the geometric mean estimates for iodide testing normal to bedding planes based on University of New Brunswick X-ray radiography and conventional through-diffusion testing (TR-07-17, TR-08-27). For the Georgian Bay, the formation scale D_e estimates are those of Cavé et al. (2010) developed from harmonic and arithmetic means considering the cumulative thickness of shale and carbonate hard beds. Otherwise, the estimates given in Table 4.19 are the average values shown in Figure 4.38 and calculated values for other layers not subject to testing based on measured porosity using Equation 4.7 assuming m=2 as described in Section 4.4.3 and tabulated in TR-08-10. Anisotropy in effective iodide diffusion coefficients given in Table 4.19 are based on testing completed by the University of New Brunswick on intact low-permeability DGR cores and the assumption that rocks with hydraulic conductivity equal to or greater than 10^{-8} m/s are isotropic with respect to diffusion.

Average salinity of each model layer is listed in Table 4.19 as TDS in units of g/L solution based on porewater and groundwater analyses of US and DGR boreholes from TR-07-11, TR-07-21, TR-08-08, TR-08-18, TR-08-19, TR-08-27 and TR-09-04. The conversion of these data, which are given in mixed concentration units to common units of g/L solution, is described in TR-08-34.

4.16 Confidence Assessment of Hydrogeological Data and Model

Confidence in the descriptive hydrogeological site model presented in Chapter 4 is assessed based on an evaluation of the quality and uncertainty in the key data that comprise the model, consistency of the data sets that comprise the model and consistency of the hydrogeological model with other geoscientific models presented in Chapter 3 (descriptive geological site model) and Chapter 5 (descriptive geomechanical site model).

The following key hydrogeological data sets are subject to confidence assessment:

- Rock densities;
- Liquid and total porosities;
- Gas saturations;
- Gas-brine flow properties;
- Diffusion properties;
- Porewater characterization;

- Formation hydraulic properties;
- Formation pressures and heads; and
- Groundwater flows in bedrock aquifers.

4.16.1 Rock Densities

Confidence in the reported wet bulk, dry bulk and grain densities of the 39 layers that comprise the descriptive hydrogeological model is judged to be high. The estimates are based on extensive testing of strata from the Salina F Unit shale to the Precambrian basement using different testing techniques on different sized core subsamples by different testing laboratories. The resultant scatter and range in the reported densities as evident in Figure 4.1 and Table 4.1 are minor and generally in accordance with expectations given the known formation mineralogies and porosities.

The highest standard deviations on wet bulk, dry bulk and grain densities for major groups of formations, as given in Table 4.1, are for the Silurian formations and the Cambrian strata – rocks that show a wide range of mineralogy and porosity. The standard deviations for the reported densities of the Ordovician shales and limestones are all small, at less than 0.05, reflecting the uniform mineralogy and porosity of these strata. The agreement between observed scatter in densities and known variability in formation mineralogy and porosity provides confidence in these data sets.

The relative differences between wet bulk/dry bulk and grain densities are also in agreement with expectations given the magnitudes of porosity reported for the different model layers. The differences are greatest for those layers with the largest porosity. For example, within the higher porosity Silurian and Ordovician shales, the difference between wet bulk density and grain density approximates 0.11 to 0.30 kg/m^3. The differences between these densities for the low-porosity Ordovician limestones averages 0.02 kg/m^3 or about 10 times less, which corresponds to the ratio of porosities for these different formations. A similar correspondence exists between dry bulk density and grain density and formation porosity. This agreement between observed difference in wet bulk/dry bulk and grain densities and expectations based on reported porosities, increases confidence in the density data.

4.16.2 Liquid and Total Porosities

Confidence in the reported liquid and total porosities of the 39 layers that comprise the descriptive hydrogeological model is judged to be moderate. The initial assessment of confidence in the liquid and total porosity data was less than moderate due to observation that liquid porosity values were often greater than total porosity values, an occurrence that is physically impossible. This occurrence was thought, in part, to be due to application of different testing and data reduction and interpretation methods by different testing laboratories in the determination of liquid porosities (see Section 4.3.2.3).

In an effort to address the different data reduction and interpretation methods for liquid porosity determination, all basic water-loss measurements made by different testing laboratories upon sample heating were converted to liquid porosities based on a standardized approach (TR-08-34) considering the average density and TDS of porewater determined from porewater characterization studies. Detailed assessment of the standardized liquid porosity values, in conjunction with consideration of the effects of release of mineralogically bound water (see Section 4.6.3), possible presence of a gas phase, variable testing procedures, lower testing limit errors, sample size, heterogeneity and anisotropy, indicates that confidence in liquid

and total porosity is at least moderate for the DGR bedrock formations. Confidence is highest for the porosities determined for limestone, dolostone and sandstone layers with porosity greater than 2% (e.g., Devonian dolostones, Salina A2, A1 and A0 Unit dolostones, Guelph to Fossil Hill dolostones, Manitoulin dolostone, Kirkfield limestone, Shadow Lake siltstone and Cambrian sandstone).

Confidence in the determination of liquid and total porosity is most easily evaluated with data sets that minimize the number of confounding effects on the measurements. The porosity data set with the least number of potential confounding effects is the Core Labs data for liquid and total porosity based on unconfined testing of identical core plugs (i.e., Figure 4.6). These data show very good correlation between liquid and total porosity, where the higher total liquid porosities apparent in the Silurian and Ordovician rocks are attributed to the presence of a separate gas phase. The next best comparable data set is that of the University of Bern, where different sub-samples of different sizes collected from the same core were tested. These results, which are illustrated in combination with Core Labs results in Figure 4.4, show a much greater difference in liquid and total porosity values for cores of all DGR rocks. The observed larger liquid porosities compared to total porosities in this data set are most likely due to release of mineralogically bound water for the samples of Silurian formations (i.e., gypsum and clays) and Ordovician shales (clays), and lower testing limit errors for the low porosity (<2%) Ordovician limestones.

4.16.3 Gas Saturations

Confidence in the reported gas saturations of the 39 layers that comprise the descriptive hydrogeological model, for which such data are available, is judged to be low. Confidence in gas saturations (S_G) is considered low, principally because of the concern that the generally small values reported (formation group means of 7-14%, formation means of 0-20%) may be artefacts due to sample drying and irrecoverable core relaxation effects during sample collection, handling and preparation for testing, and the difficulty of accurately measuring such properties in low porosity (<2%) formations. In Dean Stark testing of fluid saturations, gas saturations are determined as the difference between calculated total porosity and calculated brine and oil saturations. Thus, the estimate of S_G incorporates all of the errors accumulated in estimating total porosity and both S_W and S_G.

As discussed in Section 4.3.3, irrecoverable core damage cannot fully explain the resultant gas saturations, but sample drying and measurement error remain potential explanations for the reported gas saturations. Uncertainty in gas saturations due to measurement error associated with Dean Stark testing is significant (+/- 50 to 100%) for formations with porosity of <2%. Consequently, all of the reported gas saturations for the Ordovician limestones which have porosity of less than 2%, may be the result of measurement error. For the higher porosity Ordovician shales, measurement error is not a reasonable explanation for the reported gas saturations.

In contrast to the sample drying and measurement error, the following data and observations listed below support the occurrence of a discontinuously distributed gas phase in the DGR formations.

- Testing of brine and gas saturations using Nuclear Magnetic Resonance and He gas expansion on Ordovician shale and limestone cores from DGR-4, DGR-5 and DGR-6 that confirm the Dean Stark results on the same core samples (Figure 4.9).
- Observation of presence of discontinuous oil, bitumen and petroliferous odours in DGR

formations (Section 3.7.4) and the expectation that gas would also be associated with such hydrocarbon presence.
- Carbon isotope signatures of methane (Figure 4.68) that indicate biogenic generation of methane gas within the Ordovician shales and underlying limestones.
- Comparison of measured methane concentrations in Ordovician shale and limestone cores from DGR-3 and DGR-4 (Figures 4.70 and 4.71, Section 4.6.7.3) against calculated methane solubility that show supersaturation and therefore likely presence of separate methane gas phase.
- Occurrence of high test interval compressibility from straddle-packer hydraulic testing (i.e., 16 of 89 test intervals show compressibility greater than $1x10^{-9}$ Pa – see Figure 4.89), that may be due to the presence of gas within fractures which show increased permeability relative to the intact rock matrix.
- Results of TOUGH2 brine-gas modeling of the DGR formations (NWMO 2011, Section 5.5.4) that shows that transient brine-gas flow modeling can reproduce the general features of the underpressures and occasional normally pressured zones observed in the DGR Ordovician shales and limestones.

On balance, the available data indicate that gas is likely present as a separate phase within the pore space of some of the Silurian and Ordovician formations, although confidence in this assessment remains low.

4.16.4 Gas-Brine Flow Properties

Confidence in the reported gas-brine flow properties of the layers that comprise the descriptive hydrogeological model, for which such data are available, is judged to be low to moderate, depending upon the property considered. Confidence in pore size distributions, median pore throat sizes and gas entry pressures determined from high-pressure mercury injection testing are considered moderate, whereas confidence in van Genuchten fitting parameters for capillary pressure – liquid saturation curves and relative permeability – liquid saturation curves are considered low.

High-pressure mercury injection testing is a well-established testing technique for determination of pore size distributions of rock cores and with extrapolation, the gas entry pressures for brine-filled pores. The results of the mercury injection testing shown as mercury saturation – injection pressure profiles (Figure 4.21), gas entry pressures (Figure 4.22) and median pore throat radii (Figures 4.23 and 4.24) are comparable between tests completed on cores collected from within the same formation and with core from different DGR boreholes and generally consistent with expectations based on core observations and other testing (e.g., lab porosity testing, field hydraulic conductivity testing). For example, mercury saturation – injection pressure profiles and gas entry pressures for the Salina A2 and A0 Units, the lower Gull River and Cambrian cores are distinctly different than those for the bulk of the Ordovician shales and limestones, and show results in accordance with the increased porosity and permeability of these horizons evident from other testing and core observations.

Brine-gas flow properties of capillary pressure-brine saturation and relative permeability-brine saturation were determined from fitting mercury injection porosimetry data, fluid saturation data and gas pulse permeability data for “as received” and “clean and dry” core samples to standard van Genuchten fitting parameters. Confidence in these data is judged to be low based on the low confidence assigned to the gas and brine saturations, the unreliable overestimates of lab permeability data, and the fact that the relative permeability-saturation curves are fit to only one relative permeability-saturation data point (the “as received” test results).

4.16.5 Diffusion Properties

Confidence in the reported diffusion properties (effective diffusion coefficients, coefficient anisotropy and tracer-accessible porosity) of the 39 layers that comprise the descriptive hydrogeological model is judged to be high. The estimates of effective diffusion coefficients for iodide normal and parallel to bedding planes and iodide tracer-accessible porosity are based on University of New Brunswick (UNB) laboratory testing by X-ray radiography using iodide tracer and by conventional through-diffusion testing techniques using both iodide and tritium as tracers. A total of 113 diffusion experiments were completed to support the estimated values listed in Table 4.19. A cursory review of diffusion data plotted by DGR boreholes (Figure 4.38) shows that there are no discernable differences in D_e values between individual DGR boreholes, and hence the geometric mean D_e formation values are representative.

Although a new diffusion testing technique (X-ray radiography) was used for iodide diffusion testing of rocks other than the low-porosity Ordovician limestones, the results of this new technique were benchmarked against conventional through-diffusion testing also using iodide as a tracer. University of New Brunswick results for the Queenston shale and Cobourg limestone were also benchmarked against radioiodine (^{125}I) diffusion completed by Paul Scherrer Institute, Switzerland in an inter-laboratory comparison study using DGR core. All diffusion testing was completed by University of New Brunswick using synthetic porewater designed to match porewater chemistries determined from porewater characterization studies (Section 4.6.5) and therefore minimizing mineral dissolution and precipitation during the testing and increasing confidence in the testing results.

The testing program completed by UNB also reported on comparison of water-loss (liquid) porosities measured on the same cores subject to diffusion testing and determination of iodide tracer-accessible porosity. This comparison, which showed that iodide-accessible porosity was typically 50% of liquid porosity in the Silurian and Ordovician shales, is in accordance with anion exclusion theory (Section 4.6.4) and provides confidence in the estimates of iodide-accessible porosity determined from UNB testing.

The results of the UNB diffusion testing using both tritium and iodide tracers were also compared to diffusion coefficient and porosity data generated for argillaceous rocks as part of the OECD Claytrac Project. Effective diffusion coefficients and tracer-accessible porosities for both tritium and iodide compare very favourably with international data considering the lower porosity of the DGR rocks, and with the porosity-diffusion coefficient relationship derived from Archie's Law (see Section 4.4.3). These favourable comparisons show that the UNB diffusion property data are reliable, representative, and of high quality.

4.16.6 Porewater Characterization

Confidence in the reported porewater chemistry profiles of the DGR rocks that comprise the descriptive hydrogeological model is judged to be low to high depending upon the porewater parameter considered (i.e., major/minor ions, environmental isotopes, strontium isotopes, and gases). Concentrations of major/minor ions in porewater were reported by University of Ottawa, University of New Brunswick and University of Bern using different laboratory methods that allow for inter-laboratory comparisons. SGS Laboratories completed major ion analyses of groundwater samples. Environmental isotopes, strontium isotopes and gases in porewater were only determined by the University of Ottawa. However, measurement of all porewater parameters were also completed on groundwater samples from permeable aquifers (e.g., Salina

Upper A1 Unit, Guelph and Cambrian) allowing for direct comparison of porewater and groundwater concentrations.

Confidence in major and minor ion profiles (Na, Ca, K, Mg, Sr, B, Cl, Br, SO_4, TDS) presented as part of the descriptive hydrogeological model (Section 4.6.5) range from low to moderate. Confidence in Na, B, Cl, Br and TDS porewater profiles is considered to be moderate, based on similarity of the concentration depth profiles for these analytes, inter-laboratory comparisons (Figure 4.107) and expectation that for Na, Cl and TDS, the reported results may only be influenced by halite presence and release of mineralogically bound water during heating. Dissolution of halite during crush and leach experiments will result in overestimation of these parameters, whereas release of mineralogically bound water will result in underestimation of the parameters in porewater due to overestimation of the volume of water within the pore that contains the parameters.

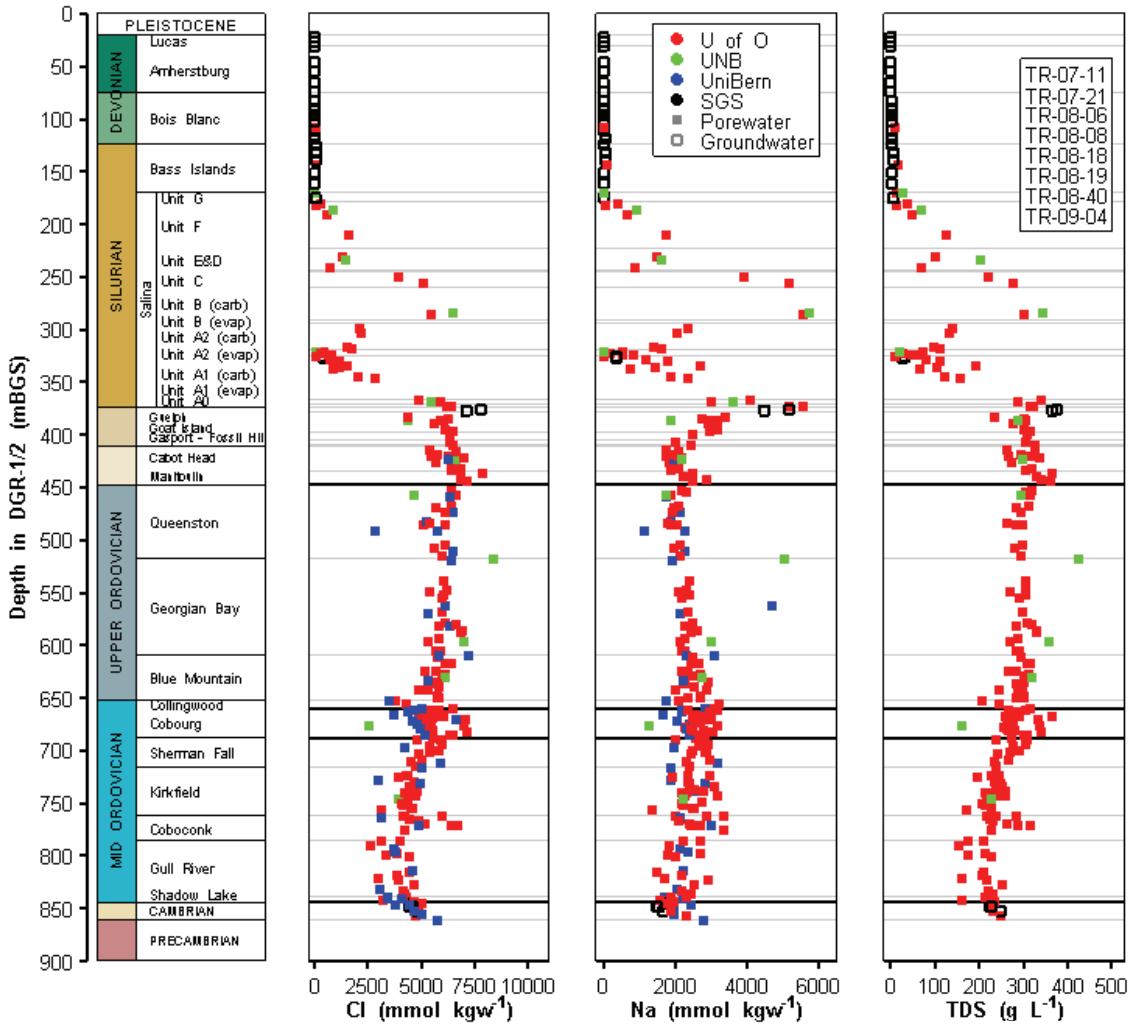

Figure 4.107: Profiles of Porewater and Groundwater Cl, Na and TDS Profiles in DGR Boreholes Distinguished by Analytical Laboratory

Confidence in Ca, Mg, K, Sr, and SO_4 profiles are judged to be low due to potential effects of dissolution of anhydrite, gypsum and celestite, interaction with clays, and oxidation of pyrite during leaching experiments and the effects of solubility controls exerted by these minerals, as well as calcite and dolomite, on reported concentrations. The reported concentrations of these ions only account for mineral dissolution for anhydrite and calcite. As evident in Figures 4.55 4.56 and 4.57, the depth profiles of Ca, Mg, Sr and SO_4 do not follow the same general concentration trends of Cl and Br. Consequently, the Ca, Mg, Sr and SO_4 concentrations in porewater should be interpreted with caution.

Confidence in profiles of the environmental isotopes of $\delta^{18}O$, deuterium (δD) and deuterium excess (*d*) presented as part of the descriptive hydrogeological model (Section 4.6.6.1) is judged to be high. The depth profiles of these parameters are smooth with some variability between DGR boreholes that is interpreted to reflect site conditions and not analytical uncertainty. These porewater parameters are not significantly influenced by rock interactions during vacuum distillation, and a laboratory test program completed by the University of Ottawa (TR-08-37) demonstrated that a standard extraction temperature of 150°C and extraction time of 6 hours produced reliable estimates of porewater isotope and major ions (Na, Cl) concentrations. Additional explanations for the high confidence in environmental isotopes data determined by vacuum distillation by the University of Ottawa, including international experience (Altinier et al. 2007), provided in TR-07-21.

Confidence in porewater major ion (e.g., Cl, Br) and environmental isotope (e.g., $\delta^{18}O$, δD and *d*) values can also be assessed based on the similarity of depth trends in these parameters. If the depth trends in these largely conservative tracers show coherence, there is confidence in the porewater values for these parameters. Figure 4.108 shows a composite plot of Cl, Br, $\delta^{18}O$ and deuterium excess concentrations for University of Ottawa porewater data and US-series and DGR borehole groundwater data. To facilitate comparison of trends on one plot, translation and scaling of data are necessary. The Cl data are plotted in mmol/kgw, Br data are plotted as Brx100 in mmol/kgw, ^{18}O data are plotted as $\delta^{18}Ox2+40$ in ‰ (VSMOW), and deuterium excess data are plotted as 1-*d*/2 in ‰ (VSMOW). Figure 4.108 shows similarity of depth trends in Cl, Br, $\delta^{18}O$ and *d* data, which provides confidence in these porewater data.

Confidence in profiles of the strontium isotopes ($^{87}Sr/^{86}Sr$) in porewater, groundwater and rock presented as part of the descriptive hydrogeological model (Section 4.6.6.2) is judged to be high. The high confidence is based on the reproducibility between measured porewater strontium isotopes in different DGR boreholes. Also raising the confidence is the acid leach and whole rock analyses results which show there is little to no influence of either the carbonate matrix or the aluminosilicate component of the rocks on the porewater strontium ratios. The minor aluminosilicate component of the rocks is further evidence that Sr from this fraction is likely small. Confidence in the whole-rock strontium isotope results is also evident from the similarity between reported values and both marine strontium and rock measurements from eastern Ontario.

Confidence in reported profiles of apparent methane concentrations and isotopes ($\delta^{13}C_{CH4}$, δD_{CH4}) is moderate based on confidence in the analytical methods, reproducibility of analytical results between boreholes, and similar smooth depth profiles for these parameters in DGR boreholes. Confidence in reported profiles of carbon dioxide concentrations and isotopes ($\delta^{13}C_{CO2}$) is judged to be low, based on the scatter in observed profiles and the uncertain role of the carbonate rock matrix in controlling CO_2 concentrations and isotopes, especially within the Ordovician limestones. Also, the pH of the porewater is not explicitly known.

Confidence in reported helium isotope ratios is judged to be moderate based on the similarity between the helium isotope profile and the methane isotope profile. There is low confidence in the porewater helium concentration data due to recognized difficulty in retaining this highly volatile gas in core samples (TR-07-21, TR-08-38) and the associated difficulties in partitioning helium to brine and any separate gas phase that may be present in the pore space due to low solubility of helium in brine. To overcome these difficulties in reporting helium concentrations, the measured isotopic ratio of $^{3}He/^{4}He$ in DGR samples is reported relative to that in air. This reporting approach increases the confidence in the helium isotope data to moderate.

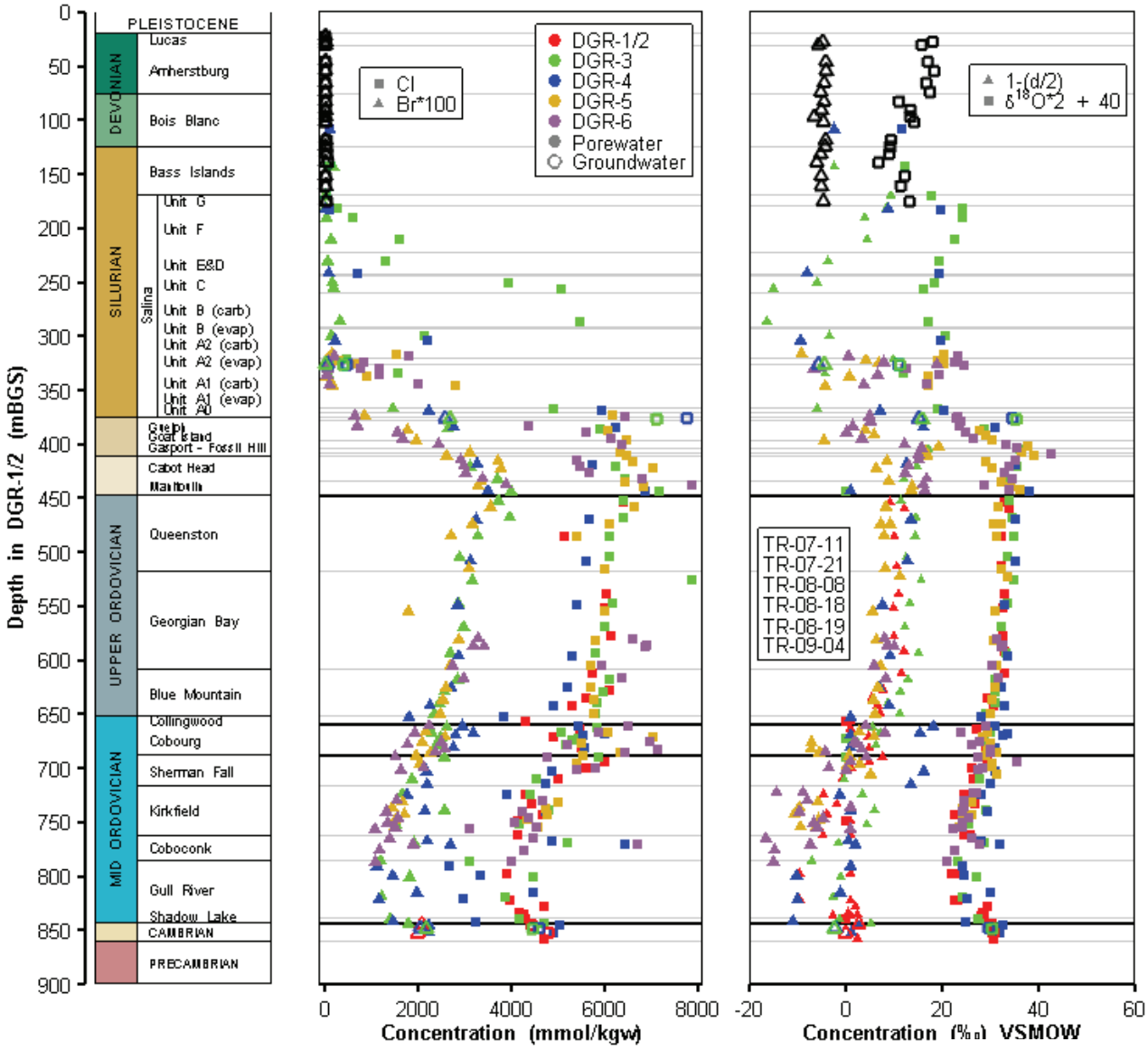

Figure 4.108: Consolidated Depth Profiles of Cl, Br, $\delta^{18}O$ and Deuterium Excess in DGR Porewater and Groundwater

There is moderate confidence in the helium concentrations normalized to rock mass (cc/g rock) due to the similarity between the helium concentrations (cc/g rock mass) and the uranium

concentrations in the rock (Figure 4.77). The difficulty normalizing the results to porewater content (described above) is eliminated by considering the whole rock sample. The age of He in porewater is calculated based on lithogeochemistry results and production rates of He isotopes from thermal neutron generation (Ballentine and Burnard 2002). Uncertainty in these calculations arises from porewater residence times and how easily He can leave the system. There is low confidence in the He age estimates, but moderate confidence that the age estimates are accurate to within one order of magnitude.

There is a high degree of confidence in the ^{14}C results since the corrected ages were calculated using a common mixing model (Pearson and Hanshaw 1970, Clark and Fritz 1997) and the results were consistent with tritium concentrations and stable water isotope results. The confidence in the analytical results for ^{36}Cl and ^{129}I is moderate due to the similarity of the isotope and isotope/concentration ratios in the Ordovician shales. Also, the reproducibility of the three Cambrian groundwater samples for ^{129}I was acceptable. There is low confidence in the calculated secular equilibrium values for ^{36}Cl and ^{129}I results due to the unknown residence time of these radioisotopes in porewater and the complicated history of solute movement in the Michigan Basin. Therefore, there is low confidence in the interpretation of ages from these radioisotopes.

4.16.7 Formation Hydraulic Properties

Confidence in the reported hydraulic properties (hydraulic conductivity, conductivity anisotropy and specific storage) of the 39 layers that comprise the descriptive hydrogeological model is judged to be moderate to high depending upon the property considered.

The representative estimates of formation hydraulic conductivity (K) are based on historical packer testing of the shallow Devonian dolostones, observation during DGR drilling, and continuous-profile field hydraulic testing using a custom-fabricated straddle-packer testing tool (TR-08-32). The resultant K estimates range from 10^{-15} to10^{-4} m/s and are consistent with expectations based on formation lithology, field testing in similar formations remote from the Bruce nuclear site (Raven et al. 1992a, Neuzil 1993, Neuzil 1994, GOLDER 2003), and controlled lab testing of cores from the same formations elsewhere in Ontario (Vilks and Miller 2007). Typically, confidence in very low hydraulic conductivity estimates ($<10^{-12}$ m/s) is difficult to achieve and demonstrate. Such confidence was achieved in the DGR borehole hydraulic testing program by use of very stiff, high-pressure hydrofracturing packers, completion of leak testing in steel casing installed in each DGR borehole, and detailed analyses of the pulse test results using a numerical well test simulator (nSIGHTS) developed by Sandia National Laboratories.

Quantification of the lower testing limit of straddle-packer testing equipment provides confidence in the reported K values above the testing limit. Leak testing was attempted in the steel casing of DGR boreholes to establish the lower testing limit of the test tool, but casing joints within the test intervals were found to have apparent hydraulic conductivities of approximately $5x10^{-15}$ to $2x10^{-14}$ m/s. An alternate method of defining the lower testing limit is the lowest reported K value from field testing. Based on analysis of testing of the Sherman Fall formation in DGR-2, the lower testing limit of the test tool is about $2x10^{-16}$ m/s. Given this lower testing limit, it is reasonable to conclude that K values of greater than and equal to 10^{-15} m/s can be reported with high confidence.

Confidence in the K anisotropy assigned to the 39 layers that comprise the descriptive hydrogeological model is judged to be moderate to high. For the thin permeable aquifer units

and the Precambrian basement, confidence in the assumption of isotropic K is high. For the majority of low to intermediate K model layers, the assumption of 10:1 horizontal:vertical K is based principally on lab petrophysical testing and core observations of the occurrence of cm-scale low-K bedding layers in these DGR rocks. Confidence in this assumption is moderate. For parts of the Black River formations where thin higher permeability zones are suspected (e.g., thin dolomitized layers), the assumed anisotropy value of 10:1 is likely underestimated because the horizontal hydraulic conductivity for most of the rock is overestimated.

Confidence in the specific storage reported for the 39 model layers that comprise the descriptive hydrogeological model is judged to be moderate. Specific storage values are difficult to reliably measure during single-hole hydraulic testing as the test results are not particularly sensitive to changes in this parameter. Given this difficulty, representative estimates of formation specific storage values were calculated as geometric means of component values including drained compressibility from geomechanical testing and formation averages of porosity and pore fluid density. Moderate confidence in the reported specific storages are supported by the observation that the values calculated from component values were generally similar to those values determined from analyses of field hydraulic tests.

4.16.8 Formation Pressures and Heads

Confidence in the reported profiles of formation pressure and environmental head that comprise the descriptive hydrogeological model is judged to be low and high for zones of underpressure and high for zones of normal to overpressure.

Low confidence is assessed for the values of formation underpressure and associated environmental head because such pressures are associated with formations of very low hydraulic conductivity, and equilibrium values of such underpressure have not been measured with MP55 casing systems, but rather inferred from estimates determined from nSIGHTS analyses of straddle-packer hydraulic tests. Based on the analysis and discussion presented in Section 4.12.2.8, the time to reach formation pressure equilibration in the MP55 casings is on the order of 5-10 years. As this time frame is longer than the current monitoring period, measurements of stable formation pressures with MP55 casing have not been reported to date. Although there is low confidence in the magnitude of the formation underpressures, there is high confidence in the occurrence of such underpressures, particularly in the tight Ordovician shales and the Trenton Group limestones.

In contrast, high confidence is associated with the stable normal and overpressured formation pressures found in the DGR boreholes. Where comparisons are possible, there is coincidence of stable formation normal pressure and overpressures from monitoring of MP55 casings and from interpretation of straddle-packer hydraulic tests. This coincidence is evident for the overpressured Cambrian and Black River Group formations as well as the single isolated zones of normal pressure found within the Ordovician shales. As evident from repeated formation pressure profiles of the MP55 casings installed in DGR boreholes and the dedicated DGR-2 MOSDAX transducer installation in DGR-2, stable formation pressures are attained in these more permeable intervals within several days to weeks following casing installation. Based on the elevated hydraulic conductivity of the Silurian aquifers of the Salina Upper A1 Unit and Guelph and repeated stable formation pressures measured in these aquifers using MP55 casing, there is also high confidence in the formation pressures and environmental heads of these horizons in DGR boreholes.

4.16.9 Groundwater Flow Directions and Gradients in Bedrock Aquifers

Confidence in the reported groundwater flow directions and gradients in bedrock aquifers that comprise the descriptive hydrogeological model is judged to be low to high depending upon the aquifer considered. Confidence is based on accuracy of formation pressure measurements and accuracy in known depths and horizontal positions of the pressure measurement ports.

There is high confidence in the groundwater flow directions and gradients within the permeable Devonian dolostone bedrock that is monitored via the MP38 multi-level monitoring casings installed in boreholes US-3, US-7 and US-8. Pressures within these permeable units are stable and reproducible based on quarterly pressure profiling using a pressure transducer sensitive to 0.07 kPa and accurate to about 1 kPa. Positions of the measurement ports are known to within an accuracy of 1 to 3 cm and related uncertainty in these positions does not affect the calculated groundwater flow directions and gradients.

Groundwater flow directions and gradients within the Salina Upper A1 Unit and Guelph are reported (Table 4.16) with moderate confidence based on similar transducer sensitivity of 0.07 kPa and accuracy of about 3 kPa and the observation that the maximum difference in adjusted pressures between the DGR boreholes at 100-111 kPa (Upper A1 Unit) and 35-43 kPa (Guelph) is much greater than the accuracy or sensitivity of pressure measurement and the possible errors in adjusted formation pressures associated with variability and uncertainty in formation fluid densities. Because the true borehole depths and horizontal positions are used in the calculation of groundwater flow directions in these aquifer units, the only uncertainty in measurement port position is that associated with stretch of MP55 casing. This uncertainty is estimated at a maximum of 10 cm given the depth of ports, which translates to a pressure uncertainty of 1.0 kPa.

The calculations of adjusted formation pressures used to quantify gradients and flow directions also assume a uniform but different formation fluid density in each of the permeable bedrock units based on groundwater sampling. The adjustments in formation pressures are necessary to quantify formation pressures at the mid-depth point in an equivalent flat-lying formation. The error in adjusted formation pressures can be estimated as the product of the maximum net depth adjustment between DGR boreholes and the differences in reported formation densities from groundwater sampling (Table 4.8). For the Salina Upper A1 Unit and the Guelph the calculated errors are 0.2 and 4.7 kPa, respectively. As these errors represent about 0.2% and 12% of the maximum differences in adjusted pressures between DGR boreholes, uncertainty in formation fluid densities is unlikely to alter the calculated groundwater flow gradients and directions in the Salina Upper A1 Unit and Guelph aquifers.

While these computations suggest high confidence in the accuracy of the calculated flow directions and gradients in these aquifers, moderate confidence is assigned based on the fact that formations pressures were recorded in the MP55 casings when borehole DGR-5 was open. Such an open borehole in proximity to borehole DGR-1 would allow drainage from the Guelph aquifer to the Upper A1 Unit aquifer and potentially affect the measured pressures in these formations in DGR-1. Future pressure measurements to be obtained following sealing of boreholes DGR-5 and DGR-6 will allow for more accurate assessment of groundwater flow directions and gradients within these thin Silurian aquifers. Both borehole DGR-5 and DGR-6 were sealed in July 2010.

Groundwater flow directions and gradients within the Cambrian sandstone aquifer are reported (Table 4.16) with low confidence. Although the transducer sensitivity and accuracy are similar

for pressure measurements in the Cambrian to those made in the Salina Upper A1 Unit and Guelph aquifers, the maximum difference in adjusted pressures (25-38 kPa) is less and the uncertainty in depth location of the measurement ports is greater at about 30 cm or 3 kPa. The calculated error in adjusted formation pressures for the Cambrian sandstone considering the maximum net depth adjustments and the differences in reported fluid density from groundwater sampling is 3.1 kPa, or 8.4 to 12% of the maximum differences in adjusted formation pressures.

Additional potential uncertainties in quantification of groundwater flow directions and gradients within the Cambrian sandstone are due to uncertainty in the depth of the mid-point of the Cambrian within boreholes DGR-3 and DGR-4, as these boreholes did not fully intersect the complete thickness of the Cambrian sandstone. In the gradient calculations, the complete thickness of the Cambrian found in DGR-2 was assumed to present in DGR-3 and DGR-4. This uncertainty in thickness of the Cambrian will only be important if the a more permeable part of the Cambrian exists below the bottom of DGR-3 and DGR-4 and is separated from the bottom of these boreholes by a reduced permeability horizon that creates upward hydraulic gradients. As DGR-3 and DGR-4 were intentionally drilled to fully access the permeable and high head parts of the Cambrian, this uncertainty in thickness of the Cambrian is not thought to be significant.

An assessment of low confidence in groundwater flow directions in the Cambrian sandstone is further supported is by the limited set of data from two pressure profiles that yielded reliable data for gradient calculations. Confirmation of these initial data from ongoing pressure monitoring in DGR boreholes is considered necessary to support the continued assessment of confidence in groundwater flow directions in the Cambrian sandstone.

5. DESCRIPTIVE GEOMECHANICAL SITE MODEL

5.1 Model Elements and Scope

The geomechanical site model describes and summarizes our current understanding of the principal geomechanical properties of the rock materials and rock mass beneath the Bruce DGR site. The geomechanical site model focuses on presentation of quantitative estimates of physical properties that will control the geomechanical behaviour of the rock mass beneath the Bruce nuclear site during and after construction of the sub-surface infrastructure required for development of the DGR. Estimated values are based on combining the specific quantitative values of various parameters derived from field and laboratory testing with expert judgement, where appropriate. Thus, while taking full account of all relevant test data, representative estimate values may or may not be synonymous with simple average or median values of test results, and are intended to provide guidance as to values of geomechanical parameters that may be reasonably relied upon for purposes of preliminary design.

The descriptive geomechanical site model has been divided into five broad units for the purposes of presentation of summary data and representative parameter values, as discussed below.

5.1.1 Mechano-Stratigraphic Units

Because of natural variability, geomechanical properties can be expected to vary within and across every stratigraphic rock unit beneath the Bruce nuclear site. However, it would be neither useful nor necessary for the purposes of site description to present geomechanical data separately for every stratigraphic unit, and detailed data are available from within the data sources listed in Section 5.2, if required. The intent of this part of the report is to summarize the geomechanical data in a manner that is meaningful within the context of overall development and performance of the sub-surface infrastructure. For this purpose, five mechano-stratigraphic (MS) units have been defined, as noted below and shown in Figure 5.1, based on data from DGR boreholes. Depths of these MS units are described below and throughout this section based on reference stratigraphy as defined in boreholes DGR-1 and DGR-2 (Figure 5.1).

- MS Unit 1:. Comprising principally dolostones, this MS Unit includes all Devonian formations encountered at the Bruce nuclear site, as well as the Upper Silurian Bass Islands Formation and the Salina G Unit dolostone. In DGR-1, MS Unit 1 lies from 20 to 178.6 mBGS.
- MS Unit 2: Comprising a sequence of interbedded shales, dolostones and anhydrites, this MS Unit includes the strata from the top of the Silurian F Unit to the base of the Silurian Fossil Hill Formation. In DGR-1, MS Unit 2 lies from 178.6 to 411 mBGS.
- MS Unit 3: Comprising principally the sequence of shales that overlie the repository horizon, this MS Unit includes the strata from the top of the Lower Silurian Cabot Head Formation, through all of the Upper Ordovician strata, to the base of the Middle Ordovician Collingwood Member. In DGR-1 and DGR-2, MS Unit 3 lies from 411 to 659.5mBGS.
- MS Unit 4: This MS Unit includes the repository horizon and comprises the Middle Ordovician Cobourg Formation argillaceous limestone. In DGR-2, MS Unit 4 lies from 659.5 to 688.1 mBGS.
- MS Unit 5: This MS Unit comprises all units below the Cobourg Formation, including Middle Ordovician Sherman Fall Formation and deeper Cambrian and Precambrian units. In DGR-2, MS Unit 5 lies below 688.1 mBGS.

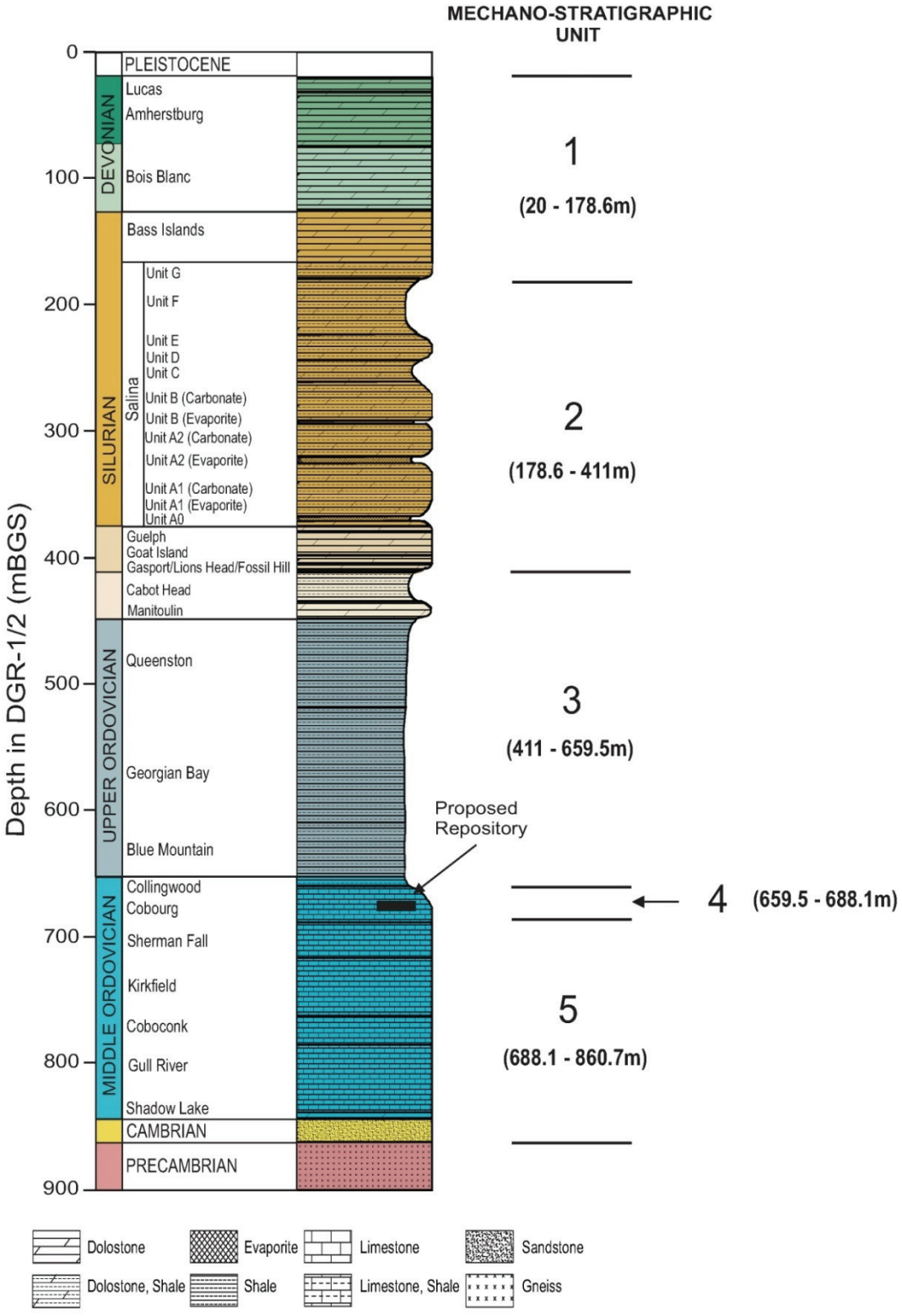

Figure 5.1: Reference Stratigraphic Column Showing Mechano-stratigraphic Units at the Bruce Nuclear Site

The rock formations lying above the target host horizon for the repository have been grouped into the upper three MS units. These units will house the vertical access penetrations (shafts) and associated seals to the repository horizon. The fourth unit will house the repository itself, and the fifth unit comprises the rocks lying below the repository. Portions of the shaft sumps will extend into the fifth unit. Each unit has been defined so that the overall geomechanical properties of the rocks in the unit can be presented and discussed in a context that is meaningful to the geomechanical issues associated with repository design and performance.

For each MS Unit, descriptive geomechanical site data are presented under two broad headings – rock material characteristics and rock mass characteristics, respectively. At the current stage, available site data deal primarily with characteristics of the rock material itself, derived from field and laboratory tests on core from DGR-1, DGR-2, DGR-3, DGR-4, DGR-5 and DGR-6. Data concerning rock mass characteristics at the site are relatively limited at the current stage of investigation.

5.1.1.1 MS Unit 1: Devonian and Upper Silurian Dolostones

The MS Unit 1 has a total thickness of approximately 154 to 188 m in DGR boreholes. At DGR-1, MS Unit 1 comprises the fossiliferous limestone/dolostone of the Devonian Lucas and Amhertsburg formations from ~ 20 to 75 mBGS, the cherty dolostone of the Devonian Bois Blanc Formation from ~75 to 124 mBGS, the argillaceous dolostone of the Upper Silurian Bass Islands Formation from ~124 to 169 mBGS, and the Salina G Unit argillaceous dolostone from 169 to 179 mBGS (Sections 3.8.2, 3.8.3). This MS unit will house the uppermost bedrock portion of the shaft excavations (approximately 154-179 m thickness). From a geomechanical viewpoint, the lithology (dolostone) is relatively consistent within this unit. MS Unit 2: Upper and Middle Silurian Shales, Dolostones and Anhydrite

The MS Unit 2 has a total thickness of approximately 226 to 235 m in DGR boreholes. It consists primarily of the alternating dolostones, shales and anhydrites of most of the 189.9- to 198.1-m-thick Upper Silurian Salina Formation, underlain by 33.7 to 35.0 m of dolostones and limestones in the Middle Silurian Guelph/Goat Island/Gasport/Lions Head/Fossil Hill formations (Sections 3.8.3, 3.8.4). The upper half of this MS Unit is largely brecciated due to formation collapse following paleo-dissolution of salt beds. Geomechanically, properties within this unit can be expected to be highly variable due to frequent lithological changes, giving rise to local variation in the performance of the rock units around the shaft excavations (Section 5.6).

5.1.1.2 MS Unit 3: Lower Silurian and Upper Ordovician Shales and Dolostones

The MS Unit 3 has a total thickness of approximately 246 to 251 m in DGR boreholes. With the exception of the included Lower Silurian Manitoulin Formation, the MS Unit 3 was defined primarily for the purpose of including the shale caprock formations overlying the repository horizon (Section 5.7). In descending order in DGR boreholes, MS Unit 3 includes:

- 23.4 to 24.7 m of Cabot Head Formation shale (Lower Silurian);
- 9.5 to 13.2 m of Manitoulin Formation dolostone (Lower Silurian);
- 69.3 to 74.4 m of Queenston Formation shale (Upper Ordovician);
- 88.2 to 90.9 m of Georgian Bay Formation shale (Upper Ordovician);
- 42.7 to 45.1 m of Blue Mountain Formation shale (Upper Ordovician); and
- 6.5 to 8.7 m of Collingwood Member, Cobourg Formation shale (Middle Ordovician).

5.1.1.3 MS Unit 4: Middle Ordovician Cobourg Formation

The MS Unit 4 in DGR boreholes comprises the 27.1- to 28.6-m-thick argillaceous limestone of the lower part of the Cobourg Formation, i.e., the host horizon of the repository. In terms of the DGR itself, the geomechanical properties within this MS Unit will be critical to design and performance assessment issues of the repository rooms (Section 5.8).

5.1.1.4 MS Unit 5: Middle Ordovician Sherman Fall and Deeper Formations

All rock formations encountered in DGR boreholes lying beneath the repository horizon are included in the MS Unit 5. While the geomechanical properties of the different lithological units within MS Unit 5 may vary widely, in practical terms this variation will have little or no impact on the design and performance issues of the DGR (Section 5.9).

5.2 Data Sources

Primary data sources for the descriptive geomechanical site model include:

- The descriptive geological site model given in Chapter 3 of this report;
- Observations during drilling, logging and sampling of DGR-1 and DGR-2 (TR-07-06), DGR-3 and DGR-4 (TR-08-13) and DGR-5 and DGR-6 (TR-09-01, TR-09-09);
- Field geomechanical testing of DGR-1 and DGR-2 core (TR-07-07) and of DGR-3 and DGR-4 core (TR-08-14);
- Laboratory geomechanical strength testing of DGR-1 and DGR-2 core (TR-07-03, TR-09-07), of DGR-3 and DGR-4 core (TR-08-24, TR-08-39, TR-09-07) and of DGR-5 and DGR-6 core (TR-09-07);
- Laboratory abrasiveness testing of DGR-2 core (TR-07-04) and of DGR-3 and DGR-4 core (TR-08-25);
- Borehole geophysical logging of DGR-1 and DGR-2 (TR-07-08), of DGR-3 and DGR-4 (TR-08-15) and of DGR-5 and DGR-6 (TR-09-03);
- Laboratory swell testing of DGR-2 core (TR-07-16) and of DGR-3 and DGR-4 core (TR-08-26);
- Laboratory long-term strength degradation testing of DGR-2 core (TR-08-11) and of DGR-3 and DGR-4 core (TR-08-36);
- Assessment of in situ stresses from analyses of borehole wall behaviour in DGR boreholes (TR-08-35):
- Field in situ stress measurements in MS Unit 1 in US6 (McKay 1989);
- Seismic monitoring at and in the vicinity of the Bruce nuclear site completed by the Canadian Hazards Information Service (Hayek et al. 2010); and
- Regional geomechanics of southern Ontario geosynthesis study (NWMO 2011, NWMO and AECOM 2011).

5.3 Local Seismicity

Seismic monitoring at and in the vicinity of the Bruce nuclear site is undertaken to obtain understanding of the contemporary seismic activity within a few hundred kilometres of the Bruce nuclear site, which in turn will be used to conduct a seismic hazard evaluation for the DGR. As described in the GSCP, such an evaluation also provides information on the contemporary seismicity and microseismicity that can be used in identification of seismogenic features in the region surrounding the Bruce nuclear site.

Seismic monitoring has historically been completed for the Bruce nuclear site for magnitude 2.0 (M2.0) and above. The Canadian National Seismic Network (CNSN) provided an earthquake detection threshold of magnitude 3.0. With the expended POLARIS (Portable Observatories for Lithospheric Analysis and Research Investigating Seismicity) network in 2002, the detection threshold in the region has reduced to M2.0. To further lower the earthquake detection threshold to M1.0, University of Western Ontario, under contract to OPG, installed three bedrock borehole microseismic monitoring stations approximately 40 km from the Bruce nuclear site during the summer of 2007. The seismic monitoring network for the Bruce nuclear site includes the following stations, the locations of which are shown in Figure 5.2:

- Station BRCO (existing Bruce nuclear station) near Tiverton;
- Station BWLO at Walkerton;
- Station BASO at Ashfield; and
- Station BMRO at Maryville Lakes.

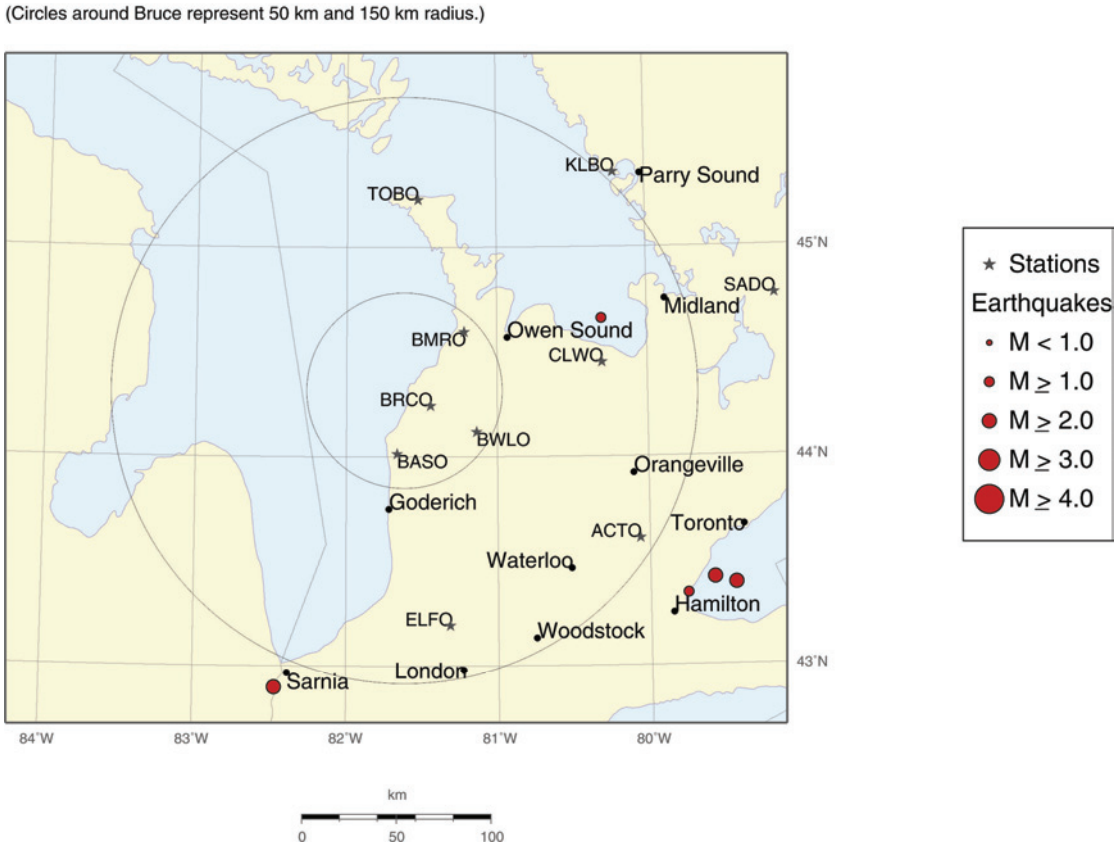

Note: M=mN (Nuttli scale).

Figure 5.2: Earthquakes in the Vicinity of the Bruce Nuclear Site, 2009 (after Hayek et al. 2010)

Hayek et al (2010) also reviews historical seismicity for the Bruce area (see Figure 5.3). Hayek et al notes that only four earthquakes have historically been detected within 50 km of the Bruce nuclear site. Including the M1.2 event recorded in 2008, the four events occurred in Lake Huron

about 20 km northwest of Southampton with M1.2 to M2.1. These current and historical monitoring data show that the Bruce nuclear site is located in a seismically quiet area.

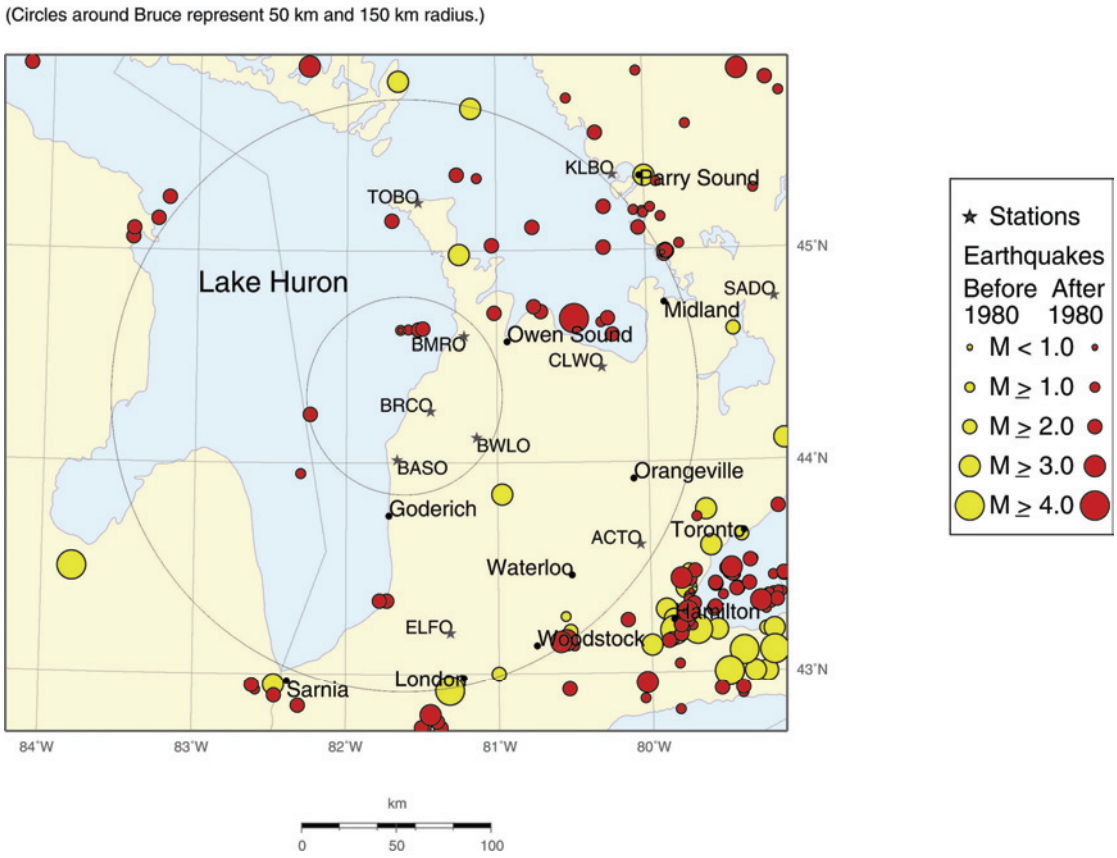

Note: M=mN (Nuttli scale).

Figure 5.3: Historical Earthquakes in the Vicinity of the Bruce Nuclear Site (after Hayek et al. 2010)

5.4 In Situ Stresses

The in situ state of stress below the DGR site, and particularly at the repository elevation, is a key geomechanical parameter affecting the design of the repository facilities. The vertical stress magnitude and orientation will closely match the gravitational stress caused by the weight of rock above any elevation of interest, and this magnitude can be accurately estimated. The challenge lies in trying to evaluate the magnitudes and orientations of the horizontal stress components at depth.

Unfortunately, there are great challenges in trying to obtain, with confidence, direct measurements of in situ stresses at the depths of interest from a surface-based exploratory borehole. This is particularly true in horizontally bedded formations where the vertical stress is less than the horizontal stresses, as hydrofracture techniques cannot be used with confidence in

this situation. While traditional strain-relief methods (e.g., overcoring) are suitable for relatively shallow measurements, such testing from within an exploration borehole at the ~680 m depth of the DGR has not been successfully completed elsewhere in sedimentary rocks and, if attempted, would in all likelihood not provide reliable results. Consequently, no direct measurements of the in situ stresses at the depth of the proposed repository at the Bruce nuclear site have been undertaken during the Phase 1 and 2 site characterization investigations.

Although no direct stress measurements are available at repository depth beneath the Bruce nuclear site, indirect evidence is available from three primary sources:

- Compilation of regional stress measurement data undertaken as part of the Phase 1 Regional Geomechanics Report (NWMO and AECOM 2011);
- Modelling of the Bruce nuclear site as a layered series of rock units subjected to imposed horizontal compression of a magnitude that matches stresses that have been measured at a depth of 680 mBGS in the Norton Mine in Ohio; and
- Behaviour of the DGR-1, DGR-2, DGR-3 and DGR-4 borehole walls and recovered core (TR-08-35).

The Phase 1 Regional Geomechanics Report (NWMO and AECOM 2011) provides detailed presentation and discussion of regional stress data, derived from numerous sources. Virtually all of the data at depths beyond 100 mBGS have been derived from hydrofracture testing, and there is uncertainty regarding the validity of these data in horizontally bedded rock formations with relatively high horizontal stresses – a condition that is well known to exist widely throughout the sedimentary rocks of Southern Ontario. However, there are some stress measurements that have been made from the deep Norton Mine in Ohio using short overcoring holes from within the mine, and these measurements are particularly valuable in helping to evaluate the probable stress conditions at similar depth beneath the Bruce nuclear site.

Figure 5.4 summarizes the results of this regional database evaluation (using a 7-point moving median technique), showing the potential variation with depth of the maximum horizontal stresses respectively, expressed as a ratio of the vertical (gravity) stress. Confidence in these regional data is low, as noted above. This view is further supported by the observation that the plot of regional data in Figure 5.4 does not appear to indicate that the in situ stresses vary as a function of the stiffness (modulus) of the various rock units, as would be expected. In fact, there seems to be an inverse relationship, suggesting that stresses increase in the softer shale units compared to the stiffer dolostone units. This is unlikely.

A second line of reasoning is based on numerical modeling of the Bruce nuclear site as a series of rock layers of different elastic modulus values (as determined from laboratory testing of rock cores) that have been subjected to an imposed horizontal compression sufficient to cause the same in situ stresses that were actually measured at the Norton Mine. Stresses in the various rock strata will then vary as a function of their stiffness (modulus). The results of this modelling, conducted by Itasca Consulting Group (2010), are also shown in Figure 5.4.

The third, and most important, line of reasoning concerning the horizontal stresses at depth at the Bruce nuclear site comes from careful examination of the borehole wall behaviour during and after drilling of DGR exploratory boreholes. These boreholes are, in fact, small diameter trial excavations, around which concentration of the in situ stresses will occur. If the in situ stresses are sufficiently high relative to the strength of the rock in the borehole wall, then

borehole breakouts will occur, and these will be visible from optical and acoustic downhole logging of the holes.

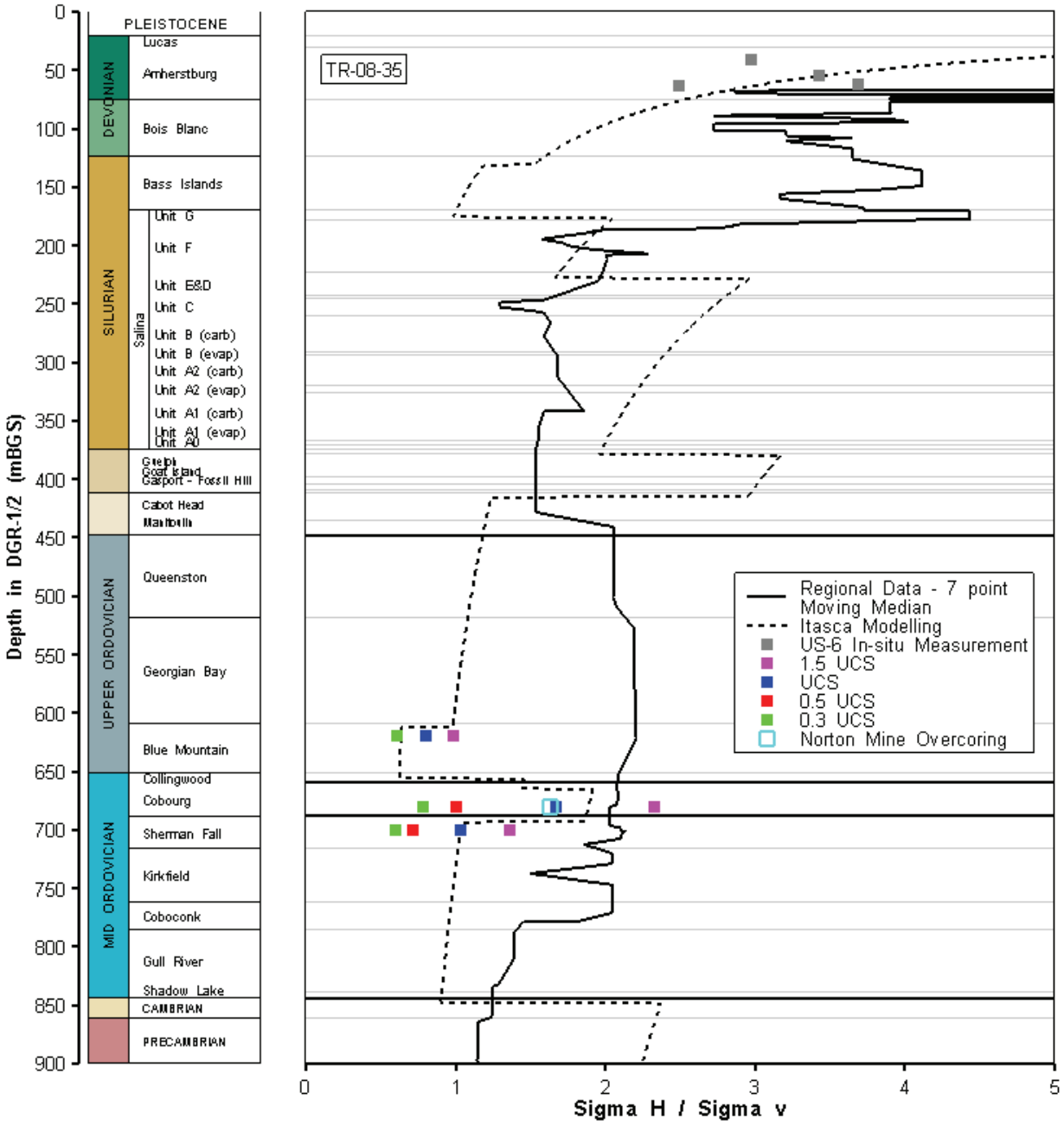

Note: UCS is mean peak uniaxial compressive strength and the listed values are the assumed borehole wall strengths for borehole breakout analyses. Data from the Norton Mine are shown at the depth of that mine, not at its stratigraphic location.

Figure 5.4: Potential Magnitudes of Maximum In Situ Horizontal Stresses (σ_H) Compared to Vertical Stress (σ_V)

This phenomenon is well known, and can be used to provide some bounds on the possible magnitude of the in situ stresses, depending on whether or not such breakouts have occurred. In a significant sense, observation and analysis of this mechanism provides very direct evidence of the actual stress-to-strength situation in the rock formations at depth. Importantly, no evidence of stress-induced borehole breakouts was found at any location in any of the six DGR boreholes (TR-07-08, TR-08-15, TR-09-03). Of particular note is the fact that down-hole televiewer logs were re-run after the exploratory holes had been open for about 24 months in DGR-2 and for 6 months in DGR-3, and no break-out damage was evident. As noted below, it is considered probable that if the induced stresses in the borehole walls had exceeded the "crack initiation" threshold for the rock materials, then visible breakout damage would be expected after these time periods.

Results from analysis of the downhole images from DGR-1 to DGR-4 for the purpose of characterizing or limiting the in situ state of stress at the DGR location are reported in TR-08-35. In undertaking these analyses, one critical parameter is the effective magnitude of the rock material strength at the borehole wall and, in particular, the strength value at which borehole breakout will occur if it is exceeded by the stresses induced around the borehole.

As there is uncertainty regarding the "correct" value to use for the borehole wall strength, analyses were conducted for a number of possible values.

- Mean value of peak uniaxial compressive strength (UCS - laboratory measured on cores) available at the time of completion of the analyses.
- 150% of UCS, assuming that borehole wall breakout strength is actually 50% higher than UCS.
- 75%, 50%, and 30% of UCS, assuming that borehole wall breakout strength is actually lower than UCS.

The results of these analyses are shown below in Table 5.1 for depths corresponding to the repository horizon (within the Cobourg Formation at 680 mBGS), just above the repository horizon (in the Blue Mountain Formation at 620 mBGS), and just below the repository horizon (in the Sherman Fall Formation at 700 mBGS). Based on the absence of borehole breakouts, and on a number of assumptions regarding the ratio of principal stresses in the earth's crust under various faulting regimes (TR-08-35), these analyses are capable only of evaluating:

a) The maximum possible magnitude of the larger of the two horizontal in situ stresses (σ_H), beyond which borehole breakout would occur; and
b) The corresponding range of minimum-to-maximum possible magnitudes of the smaller of the two horizontal stresses (σ_h).

Table 5.1 shows that the assumptions of UCS used in the analyses are slightly different than those considered representative based on formation estimates (see Section 5.10, Table 5.22). The UCS values listed in Table 5.1 and used in the stress analyses were based on depth-specific statistical analysis of the available UCS data from DGR-1 to DGR-4 (TR-08-35), whereas representative formation estimates are based on simple formation averages.

The results indicate that the ratio of the maximum horizontal stress to vertical stress (σ_H/σ_v) at the repository horizon depth (680 mBGS) could potentially lie between 0.78 to 2.33, depending on the actual breakout strength of the rock at the borehole wall. However, both ends of the quoted range of results (i.e., for assumed borehole wall strengths of 150% of UCS and 30% of UCS) are considered to be unlikely, as they represent cases in which the assumed borehole

wall strength is very significantly different from the laboratory-measured values. Removing these outer bounds, a range of $1.67<\sigma_H/\sigma_v<1.00$ is considered more realistic at the repository horizon, based on a range of borehole wall strengths from UCS to 50% UCS.

It is important to note that the lower bound of this range (i.e., assuming 50% UCS) is roughly equal to (slightly higher than) the "crack initiation stress" measured in the laboratory, which has a consistent value of 40% UCS in the rock at the repository horizon (see Section 5.8.1.1). In our opinion, it is probable that borehole breakout would occur if the induced stresses at the borehole walls exceeded the crack initiation stress level, particularly after the holes had stood open for several too many months. No such damage was observed (TR-07-08, TR-08-15).

Table 5.1: Constraints on the Horizontal Stress Magnitude at Depths of 620, 680 and 700 mBGS, Assuming Various Scenarios for the Borehole Wall Strength

Formation and Depth	Assumed Borehole Wall Strength	~Vertical Stress, σ_v, MPa	Bounding Horizontal Stress Values		Maximum Ratio σ_H/σ_v
			Maximum Value of σ_H	Range: Minimum-to-Maximum Value of σ_h	
Blue Mountain 620 mBGS	1.5 UCS	16.4	16	8-16	0.98
	UCS (20 MPa)	16.4	13	8-13	0.80
	0.75 UCS	16.4	11	8-11	0.68
	0.5 UCS	16.4	10	8-10	0.61
	0.3 UCS	16.4	10	8-10	0.61
Cobourg 680 mBGS	1.5 UCS	18.0	42	9-42	2.33
	UCS (107 MPa)	18.0	30	9-30	1.67
	0.75 UCS	18.0	24	9-24	1.33
	0.5 UCS	18.0	18	9-18	1.00
	0.3 UCS	18.0	14	9-14	0.78
Sherman Fall 700 mBGS	1.5 UCS	18.5	25	9-25	1.36
	UCS (70 MPa)	18.5	19	9-19	1.03
	0.75 UCS	18.5	16	9-16	0.86
	0.5 UCS	18.5	13	9-13	0.71
	0.3 UCS	18.5	11	9-11	0.60

Note: Vertical Stress at repository depth (680 mBGS) is about 18 MPa.

Maximum possible stresses immediately above and below the repository horizon (at 620 and 700 mBGS, respectively) are indicated to be much lower, due to lack of borehole damage in the weaker rocks of the Blue Mountain and Sherman Fall formations.

The results of these lines of reasoning regarding in situ stress levels are summarized in Figure 5.4 for the maximum horizontal stress magnitude and for the range of assumptions noted above regarding borehole wall strength.

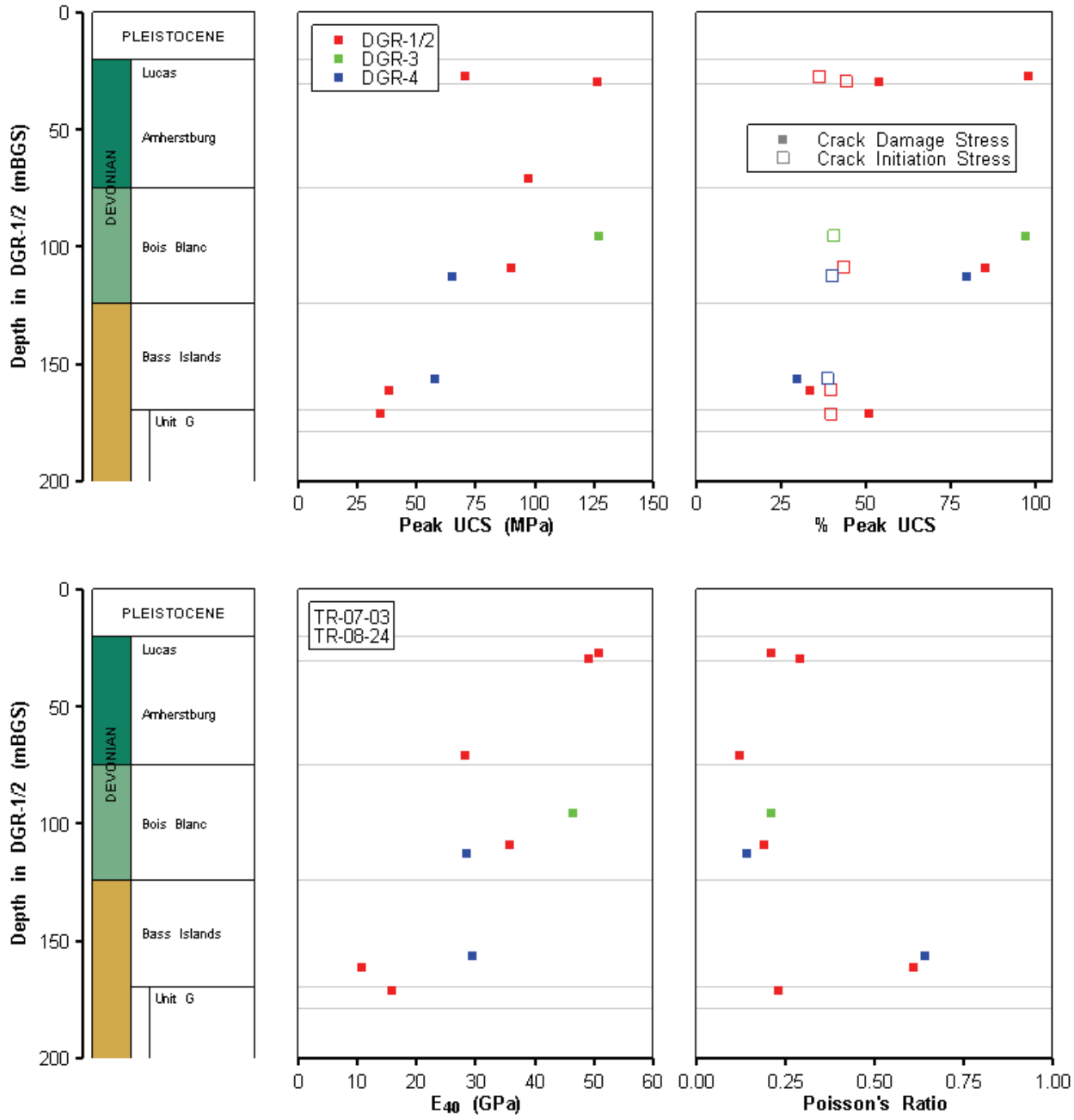

Figure 5.5: MS Unit 1: Uniaxial Compression Test Data

Based on review of the available data and the lines of argument summarized above, the following in situ stress levels are indicated as current recommended conservative values at the elevation of the DGR (~680 mBGS).

- Vertical stress (σ_v) ~ gravity load of super-incumbent materials, ~18 MPa.
- Maximum horizontal stress (σ_H): $1.5<\sigma_H/\sigma_v<2.0$.

- Minimum horizontal stress (σ_h): $1.0<\sigma_h/\sigma_v<1.2$.

Detailed measurements of the borehole dimensions indicated a consistent trend for the boreholes to deform by elongating in a SE direction (TR-08-35), indicating a high probability that the major horizontal in situ stress was acting perpendicular to this, in a NE-SW direction.

5.5 MS Unit 1: Devonian and Upper Silurian Dolostones

The geomechanical data available from within MS Unit 1 (20 to 178.6 mBGS in DGR-1) are relatively limited, as the geomechanics focus of the Phase 1, 2A and 2B site investigation has been, primarily, on the rock units hosting or immediately overlying the DGR.

5.5.1 Rock Material Geomechanical Characteristics

5.5.1.1 Uniaxial Compression

Nine laboratory test specimens were prepared from DGR core recovered in the MS Unit 1 interval, then tested in uniaxial compression. Key results are summarized in Figure 5.5 for each specimen in terms of their peak uniaxial compressive strength (UCS), the percentage of UCS at which crack initiation and crack damage occurred, and the Modulus of Elasticity and the Poisson's Ratio values (measured at 40% of UCS). For two of the UCS tests completed in the lower part of the Bass Islands Formation (i.e., DGR1-160.93 and DGR4-157.25), the Poisson's Ratio is greater than 0.5 and the crack damage stress is less than the crack initiation stress, due to gross specimen dilation during early loading. For these tests, the Poisson's Ratios and crack damage stresses are unreliable and the tests should be interpreted with caution.

Figure 5.6 summarizes the Point Load Test (PLT) data from field tests on core recovered in the MS Unit 1, in terms of axially oriented tests (left), and in terms of the ratio of diametral-to-axial PLT values (right). The isotropic line defined as equal diametral and axial strength is shown on the right panel of Figure 5.6.

Laboratory test data in the MS Unit 1 are relatively sparse. The more frequent point load testing was conducted in an attempt to provide more extensive index information concerning the variability of rock strength throughout MS Unit 1. It was recognized, and is emphasized here, that individual test results from point load testing are intended to provide a qualitative indication of strength variability only, and should not be used for direct estimation of compressive strength.

Overall, the data indicate there is an apparent distinction between the relatively stronger upper formations (Lucas, Amherstburg and Bois Blanc), and the lower Bass Islands Formation and Salina G Unit. This distinction is visible both in the laboratory-based peak UCS values, which average ~95 MPa in the upper units (range 70-126 MPa) and fall to ~36 MPa in the lower Bass Islands and Salina G Unit (range 34-38 MPa), as well as in the overall PLT test results which indicate an $I_{s(50)}$ value of ~5 MPa in the upper units, falling to ~1 MPa in the Bass Islands and Salina G Unit.

Although the peak UCS varies as noted above, the relative stress level at which internal cracking is initiated is remarkably consistent (defined as the point at which internal cracking causes the volumetric strain curve to deviate from linear contraction), remaining virtually constant at ~40% of the peak UCS (range 36%-44%). However, the stress level at which significant crack damage has accumulated in each sample is highly variable as a percentage of the peak UCS, ranging from ~35% to ~98% (defined as the point at which the incremental volumetric expansion caused by crack opening becomes greater than the incremental

volumetric contraction of the rock material). These results indicate that whereas crack initiation as a proportion of peak UCS is a robust and useful parameter, crack damage cannot be reliably predicted.

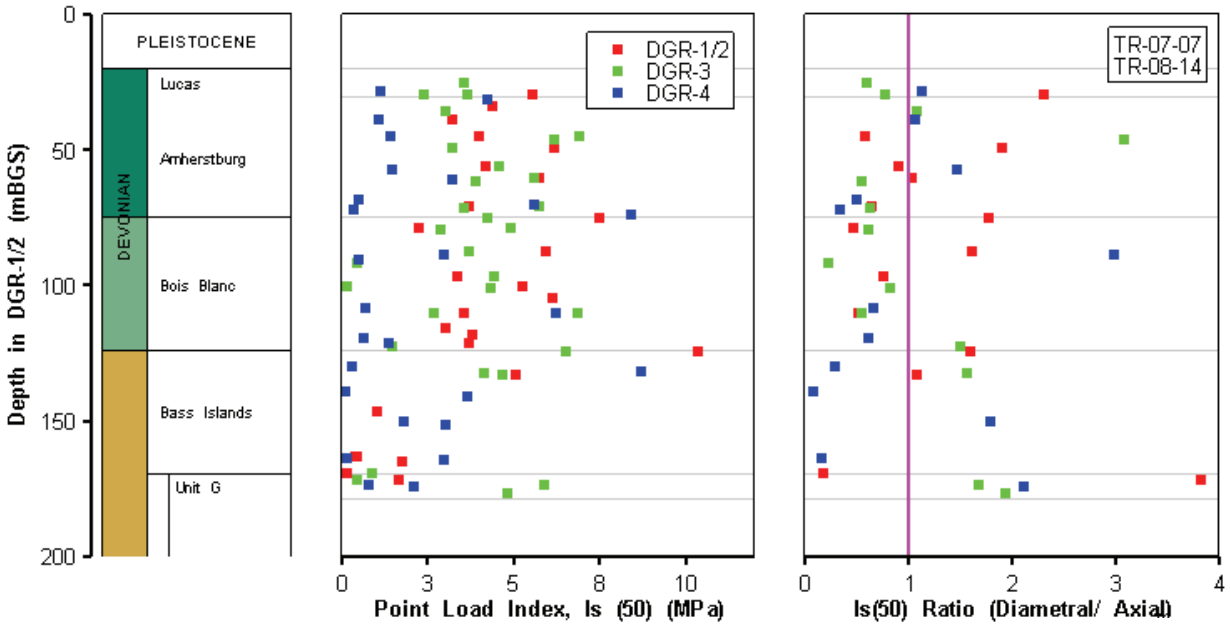

Figure 5.6: MS Unit 1: Point Load Test Data

As expected, Modulus of Elasticity values (measured at 40% of UCS) are generally higher in the higher strength materials, and lower in the weaker materials, averaging ~40 GPa in the upper Amherstburg/Bois Blanc units (range 28-51 GPa), and 13 GPa in the lower Bass Islands and Salina G Unit (range 11-16 GPa).

Poisson's Ratio (computed at stress levels of 40%UCS) does not generally show significant variability in MS Unit 1 except in two samples near the base of the Bass Islands Formation discussed above. Other than these unreliable tests, the Poisson's Ratio is fairly constant in all units at ~0.20, which is somewhat lower than might be expected, although not significantly so. Testing results for the two samples at the base of the Bass Islands are distinctly anomalous, as both cases show very early onset of significant crack damage (at about 30% of peak strength), leading to rapid volume expansion and consequent Poisson Ratio values greater than 0.5 when measured at 40% UCS.

Based on the ratio of diametral-to-axial PLT results, rock materials in MS Unit 1 do not appear to be strongly anisotropic. However, this conclusion should be treated with caution, due to the uncertainties that are inherent in PLT data.

There are no data available for the rocks in MS Unit 1 regarding possible relationships between short-term strength and the stress threshold at which long-term strength degradation (LSD) may commence.

Based on the available data, Table 5.2 summarizes estimated values of geomechanical parameters associated with behaviour under uniaxial compression for the rock materials in MS Unit 1.

Table 5.2: MS Unit 1: Estimated Geomechanical Parameters in Uniaxial Compression

Parameter	Mean	Range	Estimate
Peak UCS	20-124 mBGS: 96 MPa 124-178 mBGS: 43 MPa	20-124 mBGS: 65-127 MPa 124-178 mBGS: 34-58 MPa	20-124 mBGS: 90 MPa 124-178 mBGS: 35 MPa
Crack Initiation	40% (UCS)	36-44% (UCS)	40% (UCS)
Crack Damage	Data inconsistent	33-98% (UCS)	No consistent estimate.
Modulus of Elasticity (E_{40})	20-124 mBGS: 40 GPa 124-178 mBGS: 18.6 GPa	20-124 mBGS: 28-51 GPa 124-178 mBGS: 11-29 GPa	20-124 mBGS: 35 GPa 124-178 mBGS: 12 GPa
Poisson's Ratio	0.19	0.1–0.29 (excluding outliers)	0.20
PLT Strength Anisotropy (Diametral/Axial)	Low (~1)	Large scatter	~0.8
Long-Term Strength Degradation (initiating stress level as %UCS)	No data	No data	No data

5.5.1.2 Tension

No data regarding behaviour of MS Unit 1 rock materials under tension were generated during Phase 1, 2A and 2B site investigations.

5.5.1.3 Shear

No data regarding behaviour of MS Unit 1 rock materials under shear were generated during Phase 1, 2A and 2B site investigations.

5.5.1.4 Slake Durability

In general, standard slake durability tests were run in the field only on specimens from core samples that, based on visual inspection, contained significant argillaceous (clayey) material. In the MS Unit 1 interval, however, slake durability tests were conducted not only on two samples of argillaceous dolostone from the Salina G Unit, but also on two samples of dolostone that did not appear to be argillaceous.

The results, summarized in Figure 5.7, indicated that as expected the non-argillaceous materials showed no significant degradation when subjected to slaking (wetting-drying) cycles (Slake Durability Index 95-100%), whereas argillaceous dolostones can be expected to show some degradation, with the degree dependent on both the quantity and the nature of the clay content (Slake Durability Index 30-80%). No overall estimated values are presented as these would be meaningless - susceptibility to slaking degradation is completely specific to the clay content (amount and type) which is variable within each rock unit (see Figures 3.6 and 3.7 in Section 3.7.1).

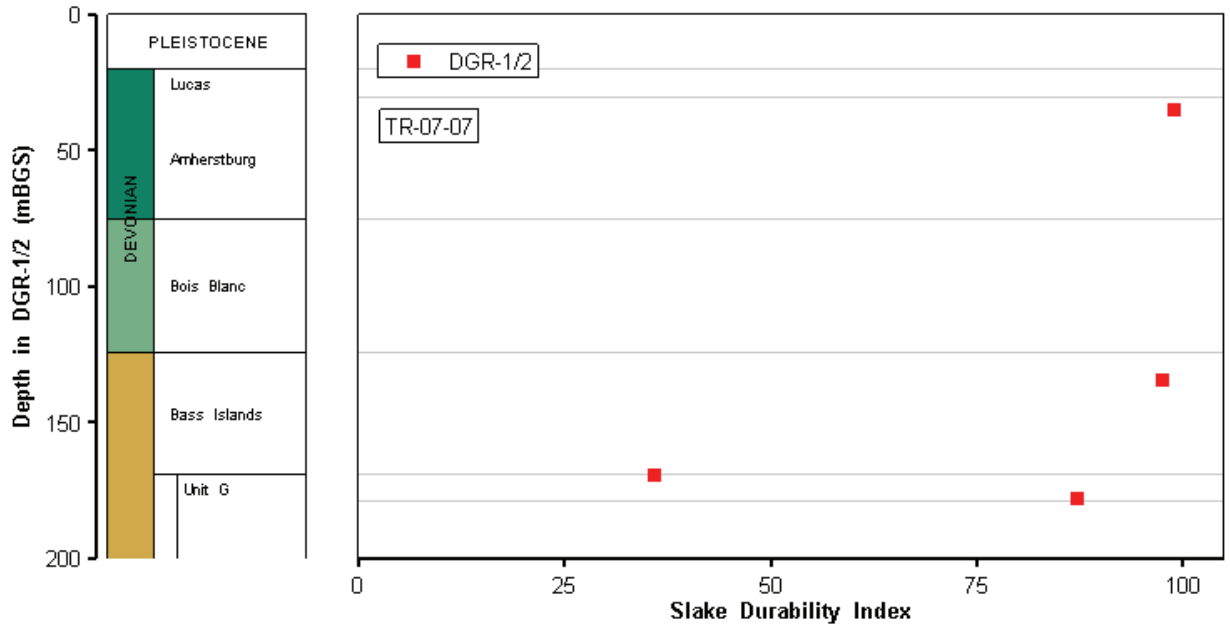

Figure 5.7: MS Unit 1: Slake Durability Index Data

5.5.1.5 Free Swell

No data regarding the swelling behaviour of MS Unit 1 rock materials were generated during Phase 1, 2A and 2B site investigations.

5.5.1.6 Abrasiveness

No data regarding the abrasive behaviour of MS Unit 1 rock materials were generated during Phase 1, 2A and 2B site investigations.

5.5.1.7 Dynamic Properties

Compression wave (P-wave) and shear wave (S-wave) velocities were measured on core samples both in the field (TR-07-07, TR-08-14) and in the laboratory (TR-07-03, TR-08-24), from which dynamic elastic constants were calculated. Variations between field and laboratory results occur, and this is not unusual. However, as noted in Section 5.5.1.1, there appears to be a distinct change in character between the upper Amherstburg/Bois Blanc formations and the lower Bass Islands – Salina G Unit, with the latter showing significantly reduced P- and S-wave velocities.

Dynamic elastic constants are calculated from P-wave and S-wave velocities using the following relationships (ASTM 2005):

Dynamic Modulus of Elasticity:

$$E_d = \frac{\rho V_s^2 \left(3V_p^2 - 4V_s^2\right)}{V_p^2 - V_s^2} \tag{5.1}$$

where: E_d = dynamic Young's modulus;

V_s = S-wave velocity;

V_p = P-wave velocity;

ρ = bulk density of specimen.

Dynamic Shear Modulus:

$$G_d = \rho V_s^2 \tag{5.2}$$

where: G_d = dynamic shear modulus;

V_s = shear wave velocity;

ρ = bulk density of specimen.

Dynamic Poisson's Ratio (based on velocity data):

$$\nu_d = \frac{V_p^2 - 2V_s^2}{2\left(V_p^2 - V_s^2\right)} \tag{5.3}$$

where: ν_d = Poisson's Ratio;

V_s = S-wave velocity;

V_p = P-wave velocity.

Based on review of the data, estimated values of wave velocities and dynamic elastic constants for the intact rock materials in MS Unit 1 are summarized in Table 5.3.

5.5.2 Rock Mass Geomechanical Characteristics

Access for geomechanical mapping of the rock mass beneath the Bruce nuclear site was not available during the Phase 1, 2A and 2B site investigations. Consequently, information regarding the characteristics of the overall rock mass has been derived only from the relatively small diameter, one-dimensional penetrations provided by the vertical DGR boreholes, and the resulting core. As the overall geomechanical characteristics of the rock mass depend in part on the three-dimensional characteristics of the fracture patterns (discontinuities) within the mass, information on the overall rock mass characteristics is limited at the current stage. Because there was neither coring nor borehole geophysical logging completed in MS Unit 1 in inclined boreholes DGR-5 and DGR-6, there is insufficient information on the three-dimensional characteristics of the fracture systems to support detailed assessments of geomechanical characteristics of the rock mass in MS Unit 1.

Table 5.3: MS Unit 1: Estimated Dynamic Properties

Parameter	Estimated Value
P-wave Velocity	20-124 mBGS: 5.1 km/s 124-178 mBGS: 4.3 km/s
S-wave Velocity	20-124 mBGS: 2.7 km/s 124-178 mBGS: 2.2 km/s
Dynamic Modulus of Elasticity	20-124 mBGS: 51 GPa 124-178 mBGS: 36 GPa
Dynamic Shear Modulus	20-124 mBGS: 20 GPa 124-178 mBGS: 13.6 GPa
Dynamic Poisson's Ratio	~ 0.30

5.5.2.1 Rock Quality Designation and Fracture Frequency

Measurements of Rock Mass Quality Designation (RQD) and fracture frequency were conducted routinely throughout the drilling of all DGR boreholes, as reported in Section 3.6. Results of the RQD and natural fracture frequency measurements are summarized in Table 3.4 and Figures 3.3 and 3.4. Overall, for the units comprising MS Unit 1, the RQD and fracture frequency measurements indicate a rock mass that is moderately fractured and of generally poor-to-fair quality. However, RQD results suggest that the lower portion of MS Unit 1 comprising the Bass Islands Formation is of lower overall quality, with a mean RQD of 34% indicating a rock mass of poor quality. Locally, extreme variations in quality are encountered, with RQD values from 0% to 100%. Some of these low RQD values are in part due to difficult drilling conditions where some grinding of core was reported.

5.5.2.2 Bulk Properties from Geophysical Logging

Elastic dynamic properties of a bulk in situ sample of the rock mass are derived from downhole sonic logging. A uniform wet bulk density of 2.63 g/cm^3 (Figure 4.1), was used in all modulus calculations. Downhole sonic logging was not completed within MS Unit 1 in DGR-1, DGR-2 or DGR-3 due to the presence of grouted steel casing. However, such logging was performed in DGR-4 prior to steel casing installation and is the basis for the rock mass dynamic properties listed in Table 5.4. Results are summarized in Table 5.4 for various depth intervals within the MS Unit 1. The depth intervals were selected on the basis that the sonic velocities were relatively constant within the interval.

5.5.2.3 Rock Mass Classification

Rock mass classification systems in common usage for geomechanics purposes include Bieniawski's (1974) Rock Mass Rating (RMR) system, Barton et al. (1974) Tunneling Quality Index (Q-system), and Hoek's (1994) Geological Strength Index (GSI). Subsurface data obtained from the DGR boreholes in the Phase 1 and 2 investigations are not sufficient to provide reliable or complete estimates of all the parameter values required to determine the classification categories under these systems. Preliminary descriptive comments regarding rock mass quality are included under Section 5.5.2.1 above, based on the limited parameters of Rock Quality Designation (RQD) and one-dimensional fracture frequency. As there are no

additional data on inclined fracture mapping in DGR-5 and DGR-6, these preliminary descriptions of rock mass quality in MS Unit 1 have not been carried forward to develop rock mass classification ratings or indices.

Table 5.4: MS Unit 1: Estimated Rock Mass Dynamic Properties

Formation	Depth Range (mBGS)	V_p (m/s)	V_s (m/s)	E_d (GPa)	G_d (GPa)
Lucas	27.00 - 30.39	4863	2263	36.7	13.5
Amherstburg	30.40 – 74.99	4805	2750	33.9	19.9
Bois Blanc	75.00 – 123.99	4376	2674	45.4	18.9
Bass Islands	124.00 – 169.29	4378	2706	46.0	19.3
Salina G Unit	169.30 – 178.59	3666	2040	28.3	11.1

5.6 MS Unit 2: Upper and Middle Silurian Shales, Dolostones and Anhydrite

The MS Unit 2 (178.6 to 411 mBGS in DGR-1) consists primarily of the 189.9- to 198.1-m-thick sequence of evaporite and evaporite-related carbonates and shales of the Salina Formation, underlain by 33.7 to 35.0 m of dolostones.

5.6.1 Rock Material Geomechanical Characteristics

5.6.1.1 Uniaxial Compression

Twenty-five laboratory test specimens were prepared from core in the MS Unit 2 interval, then tested in uniaxial compression. Key results are summarized in Figure 5.8 for each specimen in terms of their peak uniaxial compressive strength (UCS), the percentage of UCS at which crack initiation and crack damage occurred, and the Modulus of Elasticity and Poisson's Ratio measured at 40% of UCS.

As with MS Unit 1, there is one UCS test result in the lower part of the Salina B Unit Carbonate (DGR4-284.91) that shows Poisson's Ratio greater than 0.5 and the crack damage stress less than the crack initiation stress, due to gross specimen dilation during early loading. For this test, the Poisson's Ratio and crack damage stress are unreliable and the test should be interpreted with caution

Figure 5.9 summarizes the Point Load Test (PLT) data from field tests on core recovered in the MS Unit 2, in terms of axially oriented tests (left), and in terms of the ratio of diametral-to-axial PLT (right). The isotropic line defined as equal diametral and axial strength is shown on the right panel of Figure 5.9.

The detailed lithological make-up of the rocks that comprise the 190.3- to 198.2-m-thick Salina Formation F to A0 Units varies substantially, including at the scale of the core samples from which laboratory test samples were prepared. For instance, local layers of anhydrite, gypsum and shale may be interspersed among argillaceous or brecciated dolostones within a single test specimen, giving rise to significant heterogeneity within the test specimen. Consequently, even though the core recovery throughout this formation is generally excellent (Section 3.7.3),

implying only minor in situ fracturing, laboratory and field testing of the core often indicates low compressive strengths due to heterogeneities in the core.

This effect was particularly pronounced in the upper 115 m of the MS Unit 2 (from 178.6 to 293 mBGS in DGR-1; Salina B, C, D, E and F units), and is evident in both the uniaxial compression test results (Figure 5.8) and in the point load test results (Figure 5.9). Within the lower ~118 m of the MS Unit 2, comprising the Salina A1 and A2 Units and the underlying Middle and Lower Silurian dolostones, this effect appears less prevalent, resulting in higher apparent compressive strengths of the tested core samples. Based on these results, the peak compressive strength and modulus of elasticity values for the MS Unit 2 have been grouped into two broad zones, from 178.6 to 293 mBGS, and from 293 to 411 mBGS. Broadly, the upper 115 m of MS Unit 2 consist of weaker and lower modulus materials compared to the lower 118 m of the MS Unit 2. These weaker upper rocks are mostly likely due to collapse caused by paleo-dissolution of the Salina B and D Unit salts.

Poisson's Ratio also shows more variability than might be expected, probably due to the lithological variability noted above, and expert judgement has been used to provide a general estimated value.

Based on the ratio of diametral-to-axial PLT results, rock materials in MS Unit 2 are quite strongly anisotropic with diametral-to-axial ratios of 0.1 to 1.5. While this conclusion should be treated with some caution due to the uncertainties that are inherent in PLT data, the natures of the formations in MS Unit 2 are such that strength anisotropy should be expected.

There are no data available for the rocks in MS Unit 2 regarding possible relationships between short-term strength and the stress threshold at which long-term strength degradation (LSD) may commence.

Results for uniaxial compression parameters are summarized in Table 5.5. With respect to the parameters summarized in Table 5.5, it is important to recognize – particularly for the upper zone (178 to 293 mBGS) – that a single estimated value of any parameter can be used only as a very general guideline, as substantial local variability can be expected to occur.

5.6.1.2 Tension

No data regarding behaviour of MS Unit 2 rock materials under tension were generated during Phase 1 and 2A site investigations.

5.6.1.3 Shear

No data regarding behaviour of MS Unit 2 rock materials under shear were generated during Phase 1 and 2A site investigations.

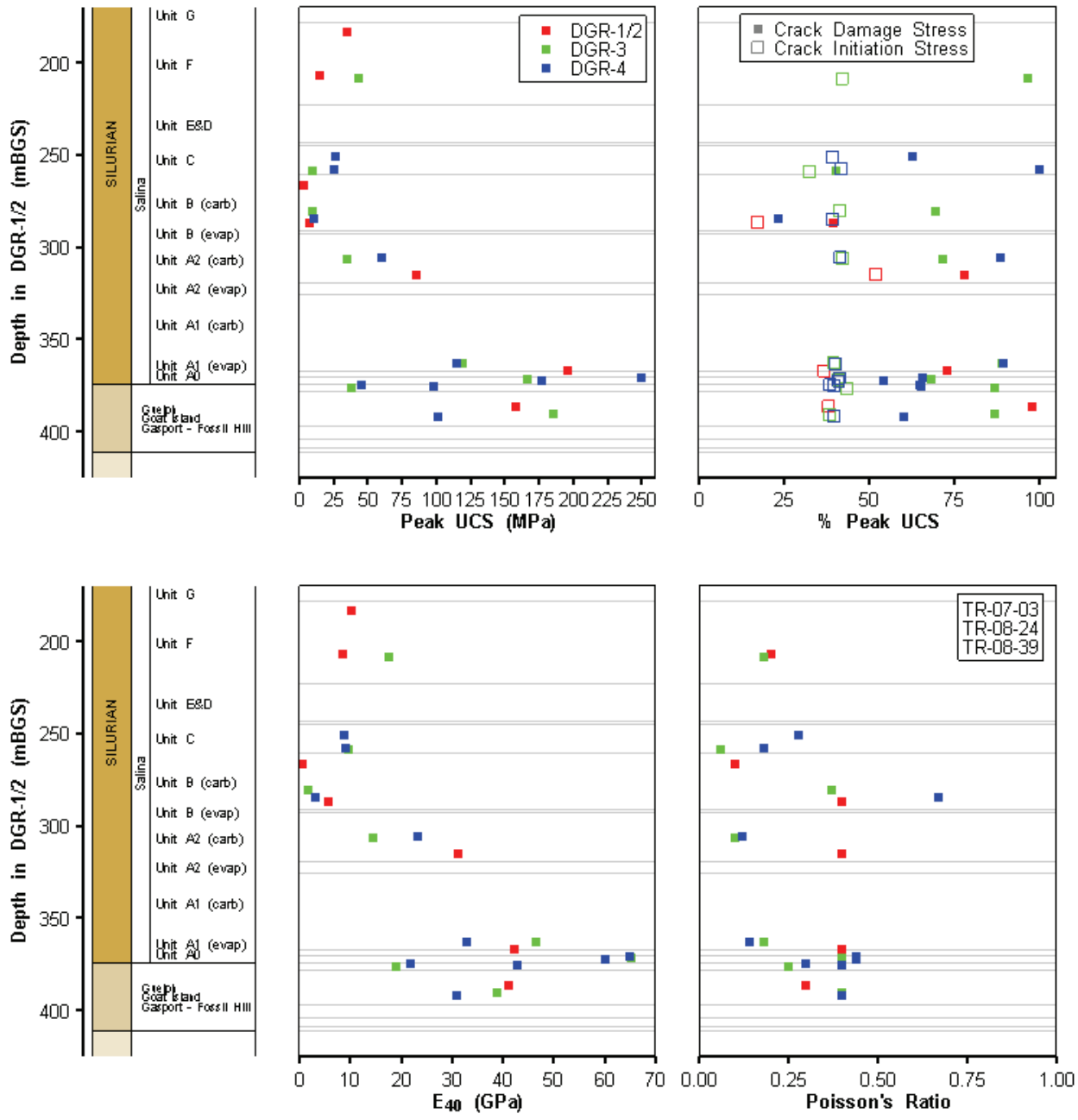

Figure 5.8: MS Unit 2: Uniaxial Compression Test Data

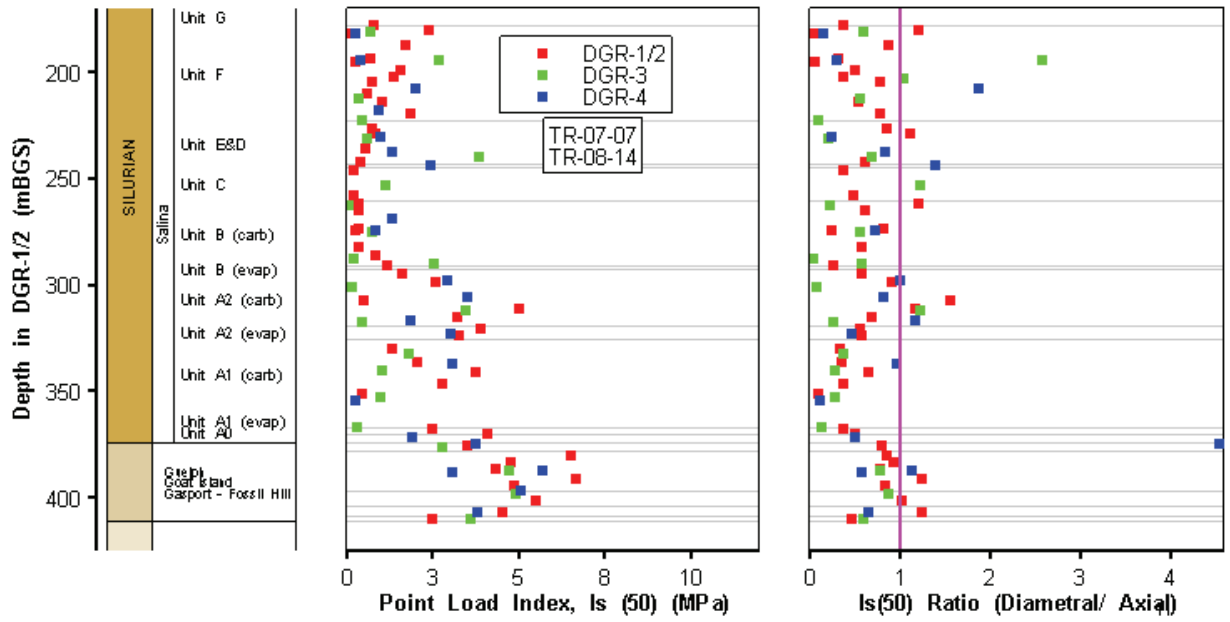

Figure 5.9: MS Unit 2: Point Load Test Data

Table 5.5: MS Unit 2: Estimated Geomechanical Parameters in Uniaxial Compression

Parameter	Mean	Range	Estimate
Peak UCS	178-293 mBGS: 18 MPa 293-411 mBGS: 123 MPa	178-293 mBGS: 3-43 MPa 293-411 mBGS: 35-250 MPa	178-293 mBGS: 20 MPa 293-411mBGS:100 MPa
Crack Initiation	39% (UCS)	17-52% (UCS)	35% (UCS)
Crack Damage	Data inconsistent	23-100% (UCS)	No consistent estimate.
Modulus of Elasticity (E_{40})	178-293 BGS: 6 GPa 293-411 BGS: 38 GPa	178-293 mBGS: 0.5-18 GPa 293-411mBGS: 15-65 GPa	178-293 mBGS: 7 GPa 293-411 mBGS: 35 GPa
Poisson's Ratio	0.31	0.10-0.44	0.30
PLT Strength Anisotropy (Diametral/Axial)	High	Large scatter	~0.5
Long-Term Strength	No data	No data	No data

5.6.1.4 Slake Durability

Slake durability tests were run in the field only on specimens selected from core samples that appeared to contain significant argillaceous (clayey) material, based on visual inspection. In the MS Unit 2 interval, a total of 8 tests were conducted. The results are summarized in Figure 5.10 and indicate that, as expected, some slaking deterioration can be expected to occur in materials with shale content. Slake durability index results range from ~33 to 90% for the 8 samples tested. No general estimated value is given, as the results are highly specific to the clay content of the specimens selected.

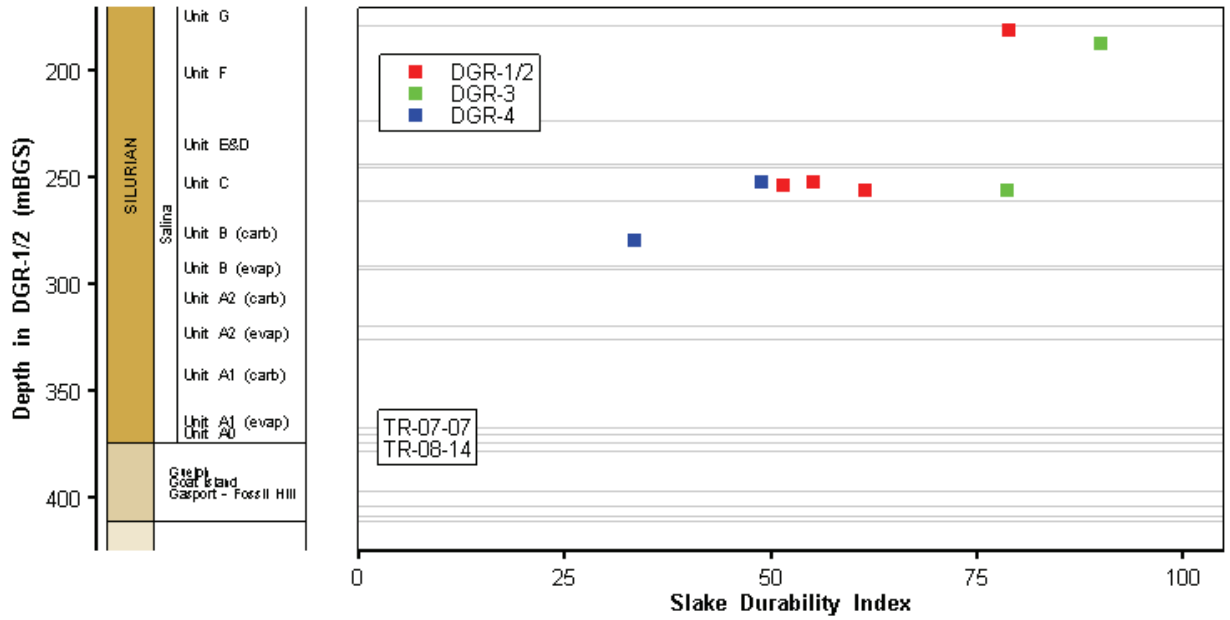

Figure 5.10: MS Unit 2: Slake Durability Index Data

5.6.1.5 Free Swell

Free swell testing of core samples from the Salina Unit of MS Unit 2 was undertaken by K. Y. Lo Inc. (TR-08-26, Figure 5.11). The samples were tested using fresh water to determine swelling potential in the vertical and horizontal directions, respectively. Swelling potential was shown generally to increase with decreasing calcite content. Swelling potential in the horizontal direction was generally low, ranging from 0% per log cycle of time for all samples from DGR-4, to a maximum of 0.9% per log cycle for one DGR-3 sample taken from within the F Unit of the Salina Formation.

In the vertical direction, swelling potential was variable, ranging from 0% to 3.4% per log cycle of time, related to the calcite content of the material, which ranged from 48.6% to a low of 4.6% in the sample with the maximum swell potential.

5.6.1.6 Abrasiveness

No data regarding the abrasive behaviour of MS Unit 2 rock materials were generated during Phase 1, 2A and 2b site investigations.

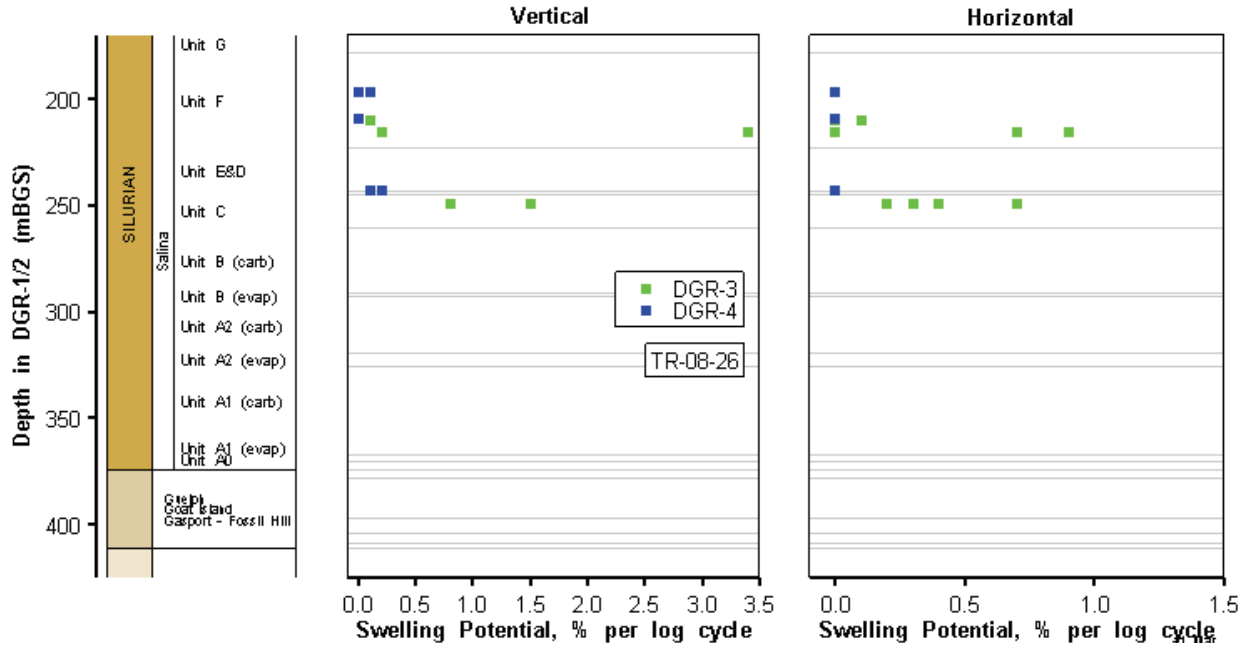

Figure 5.11: MS Unit 2: Swelling Potential In Fresh Water

5.6.1.7 Dynamic Properties

Compression wave (P-wave) and shear wave (S-wave) velocities were measured on core samples both in the field (TR-07-07, TR-08-14) and in the laboratory (TR-07-03, TR-08-24, TR-08-39), from which dynamic elastic constants were calculated for the rock material. Variations between field and laboratory results occur, and this is not unusual. However, as noted in Section 5.6.1.1, there appears to be a distinct change in character between the upper 115-m-thick zone (from 178.6 to 293 mBGS) and the lower 118-m-thick zone (from 293 to 411 mBGS), with the lower zone showing increased compression and shear wave velocities, reflecting the generally stiffer nature of these rocks. Based on review of the test data, estimated values of wave velocities and dynamic elastic constants for the intact rock materials in MS Unit 2 are summarized in Table 5.6.

5.6.2 Rock Mass Geomechanical Characteristics

Access for geomechanical mapping of the rock mass beneath the Bruce nuclear site was not available during the Phase 1, 2A and 2B borehole site investigations. Consequently, information regarding the characteristics of the overall rock mass has been derived only from the relatively small diameter, one-dimensional penetrations provided by the DGR boreholes, and the resulting core. As the overall geomechanical characteristics of the rock mass depend in part on the three-dimensional characteristics of the fracture patterns (discontinuities) within the rock mass, information on the overall rock mass characteristics is limited at the current stage, even with the fracture analysis from inclined boreholes DGR-5 and DGR-6. Total horizontal sampling distances for mapping of inclined fractures in MS Unit 2 was limited to 99.8 m in DGR-5 and 128.4 m in DGR-6.

Table 5.6: MS Unit 2: Estimated Dynamic Properties

Parameter	Estimated Value
P-wave Velocity	178-293 mBGS: 3.7 km/s 293-411mBGS: 5.0 km/s
S-wave Velocity	178-293 mBGS: 2.1 km/s 293-411 mBGS: 2.7 km/s
Dynamic Modulus of Elasticity	178-293 mBGS: 27 GPa 293-411 mBGS: 52 GPa
Dynamic Shear Modulus	178-293 mBGS: 11 GPa 293-411 mBGS: 20 GPa
Dynamic Poisson's Ratio	~ 0.26

5.6.2.1 Rock Quality Designation, Fracture Frequency and Fracture Sets

Measurements of Rock Mass Quality Designation (RQD) and fracture frequency were conducted routinely throughout the drilling of DGR boreholes, as reported in Section 3.6 and summarized in Table 3.4.and Figures 3.3 and 3.4. Core recovery throughout the MS Unit 2 was generally 100%, RQD measurements averaged 90-99% with very little local variation, and fracture spacing was generally greater than 2-3 m. These data indicate a rock mass that is very sparsely fractured and of excellent quality.

Data from the vertical boreholes DGR-1 to DGR-4 provided significant information only on the presence of the horizontal to sub-horizontal discontinuities, and these data indicate clearly the presence of a widely spaced (2-3m) sub-horizontal fracture set. Oriented core logging completed in inclined boreholes DGR-5 and DGR-6 (TR-09-09) provides a preliminary three-dimensional indication of the occurrence and spacing of fractures in MS Unit 2, by providing both vertical and horizontal transects through the Unit. Fracture logging from these holes provides relatively comprehensive or balanced 3-D discontinuity data, and these data have not been combined with data from the vertical holes in order to avoid a major bias towards horizontal fracture data. A total of 216 natural fractures were logged in DGR-5 and DGR-6 core. The contoured equal area plot of all natural fractures logged in DGR-5 and DGR-6 core is shown in Figure 5.12. Figure 5.12 plots the fracture occurrence in MS Unit 2 considering Terzaghi (1965) sampling bias.

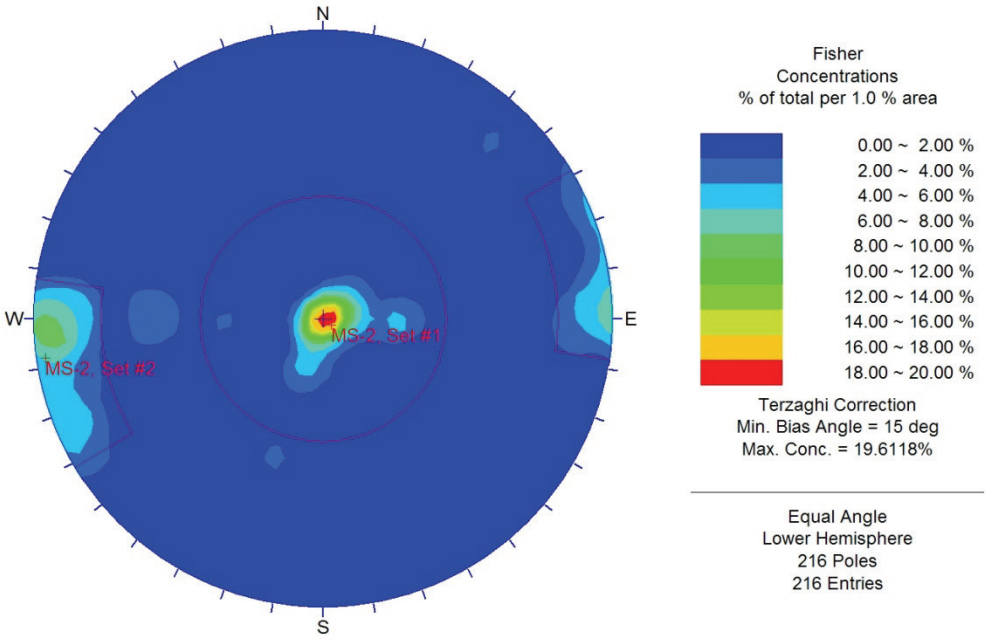

Figure 5.12: Contoured Equal Area Polar Plot of All Natural Fractures in DGR-5 and DGR-6 Core in MS Unit 2

The polar plot from the inclined boreholes data suggests the presence of two major fracture sets. The first, and most pronounced (MS Unit 2, Set #1), is the horizontal fracture set representative of bedding joints, confirming the data from the four vertical boreholes. The other set (MS Unit 2, Set #2) is representative of a near vertical set of fractures, striking north-south. The average weighted fracture set orientation, including number of occurrences and arithmetic average discontinuity spacing for fractures in MS Unit 2 are presented in Table 5.7.

Table 5.7: Natural Fracture Set Orientation and Spacing in MS Unit 2 from DGR-5 and DGR-6 Oriented Core Logging

Fracture Set	Number of Occurrences	Strike	Dip	Average Discontinuity Spacing (m)
MS Unit 2, Set #1	155	N35°E	4°NW	2.8
MS Unit 2, Set #2	24	N8°W	88°E	6.8
Miscellaneous	37	--	--	--

5.6.2.2 Bulk Properties from Geophysical Logging

Elastic dynamic properties of a bulk in situ sample of the rock mass are derived from downhole sonic logging. A uniform wet bulk density of 2.63 g/cm^3 (Figure 4.1), was used in all modulus calculations. Results are summarized in Table 5.7 for various depth intervals within the MS Unit

2 based on logging of DGR-1, DGR-3 and DGR-4. The depth intervals were selected on the basis that the sonic velocities were relatively constant within the interval. The bulk properties shown in Table 5.8 are reasonable and comparable to laboratory data (TR-07-03, TR-08-24).

Table 5.8: MS Unit 2: Estimated Rock Mass Dynamic Properties

Formation	Depth (mBGS)	V_p (m/s)	V_s (m/s)	E_d (GPa)	G_d (GPa)
Salina F Unit	177.00 – 182.99	5031	2754	28.3	11.1
Salina F Unit	183.00 – 218.49	5030	2750	35.3	14.3
Salina F Unit	218.50 – 222.99	4900	2820	35.7	21.4
Salina E Unit	223.00 – 242.99	4890	2640	47.4	18.4
Salina C&D Units	243.00 – 260.29	3820	1930	27.5	16.5
Salina B Unit	260.30 – 283.68	4010	2140	31.4	12.1
Salina B Unit	283.69 – 293.09	5720	2560	31.4	23.2
Salina A2 Unit	293.10 – 327.99	4470	2380	38.7	15.2
Salina A1 Unit	328.00 – 365.97	5110	2810	53.2	20.7
Salina A1 Unit	365.98 – 370.49	5940	3020	54.8	24.0
Salina A0,Guelph, Goat Island	370.50 – 393.37	5113	2750	51.7	19.9
Goat Island, Gasport	393.38 – 404.24	5540	2880	57.3	21.8
Lions Head, Fossil Hill	404.25 – 411.00	5740	2960	60.9	23.1

5.6.2.3 Rock Mass Classification

Subsurface data obtained from DGR boreholes in the Phase 1, 2A and 2B investigations are judged not sufficient to provide complete estimates of all the parameter values required to determine the classification categories under the commonly used rock mass classification systems. Preliminary descriptive comments regarding rock mass quality are included under Section 5.6.2.1 above, based on the limited parameters of Rock Quality Designation (RQD) and one-dimensional fracture frequency. These data indicate a rock mass that is very sparsely fractured and of excellent quality.

Results of oriented core logging in DGR-5 and DGR-6, indicate two fracture sets with average spacings of 2.8 and 6.8 m. These wide fracture spacings, in conjunction with rock material and rock mass geomechanical properties described above, indicate a rock mass of very good to excellent quality. Rock mass classification ratings or indices have not been developed based on the limited horizontal sampling distances available from DGR boreholes.

5.7 MS Unit 3: Lower Silurian and Upper Ordovician Shales and Dolostones

The 246- to 251-m-thick MS Unit 3 (411 to 659.5 mBGS in DGR-1 and DGR-2) was defined as a single mechano-stratigraphic unit in order to group together the thick sequence of shale rocks that directly overlies the repository horizon, although contained within the unit there is one relatively minor (9.5 to 13.2 m thick) layer of dolostone, the Manitoulin Formation. The MS

Unit 3 also includes the Collingwood Shale, which is the Upper Member of the Middle Ordovician Cobourg Formation (Figure 5.1).

5.7.1 Rock Material Geomechanical Characteristics

5.7.1.1 Uniaxial Compression

With the exception of the cherty dolostone of the Manitoulin Formation (434.8 to 447.7 mBGS in DGR-1), the 246- to 251-m-thick MS Unit 3 comprises shale rocks of the Cabot Head, Queenston, Georgian Bay and Blue Mountain formations and the Collingwood Member.

Thirty-nine laboratory specimens for uniaxial compression testing were prepared from core recovered from the MS Unit 3. Key results are summarized in Figure 5.13 for each specimen in terms of their peak uniaxial compressive strength (UCS), the percentage of UCS at which crack initiation and crack damage occurred, and the Modulus of Elasticity and Poisson's Ratio values (measured at 40% of UCS).

Core samples of the Blue Mountain Formation exhibited significant disking of core following core retrieval and during core logging, photography and sample shipment to the testing laboratory. This sample disturbance resulted in several cores being unsuitable for testing upon examination at the laboratory and likely influenced the representativeness of the core rock strengths determined from laboratory testing for the Blue Mountain Formation.

As with MS Unit 1 and MS Unit 2, there is one UCS test result at the top of the Manitoulin Formation (DGR4-436.20) that shows Poisson's Ratio greater than 0.5 and the crack damage stress less than the crack initiation stress, due to gross specimen dilation during early loading. Similarily, for sample DGR2-519.62 at the top of the Georgian Bay Formation, the Poisson's Ratio is greater than 0.5 and the crack damage stress is the same as the crack initiation stress. For these tests, the Poisson's Ratio and crack damage stress are unreliable and the test should be interpreted with caution.

Figure 5.14 summarizes the Point Load Test data from field tests on core recovered from the MS Unit 3 Unit, in terms of axially oriented tests (left), and in terms of the ratio of diametral-to-axial PLT values (right). The isotropic line defined as equal diametral and axial strength is shown on the right panel of Figure 5.14.

In general, and as expected, the peak compressive strength and the modulus of elasticity values for these shale rocks are significantly lower than for the primarily carbonate rocks within the other MS units. Although considerable care was taken to preserve the shale core samples shipped to the laboratory in order to avoid deterioration, some variability in results may be ascribable to the sensitivity of these materials to moisture changes (Sections. 5.7.1.4, 5.7.1.5).

In general, the peak strength, stiffness and Poisson's Ratio values decline in the lower part of the unit (Georgian Bay; Blue Mountain) compared to the upper part (Queenston) and then significantly increase in the Collingwood Member. It is also noted that the Blue Mountain Formation is indicated to be a particularly weak material, with a UCS of ~20 MPa. Despite these variations in the properties of the shale materials (with the exception of the included Manitoulin Formation dolostone) that comprise the MS Unit 3 Unit, the geomechanical properties have been grouped together into a single unit for the purposes of this summary site descriptive report. If required for purposes of detailed design analyses – for instance for shaft

seals at specific elevations - details of the specific test data are available in the reference documents TR-07-03, TR-08-24 and TR-09-07.

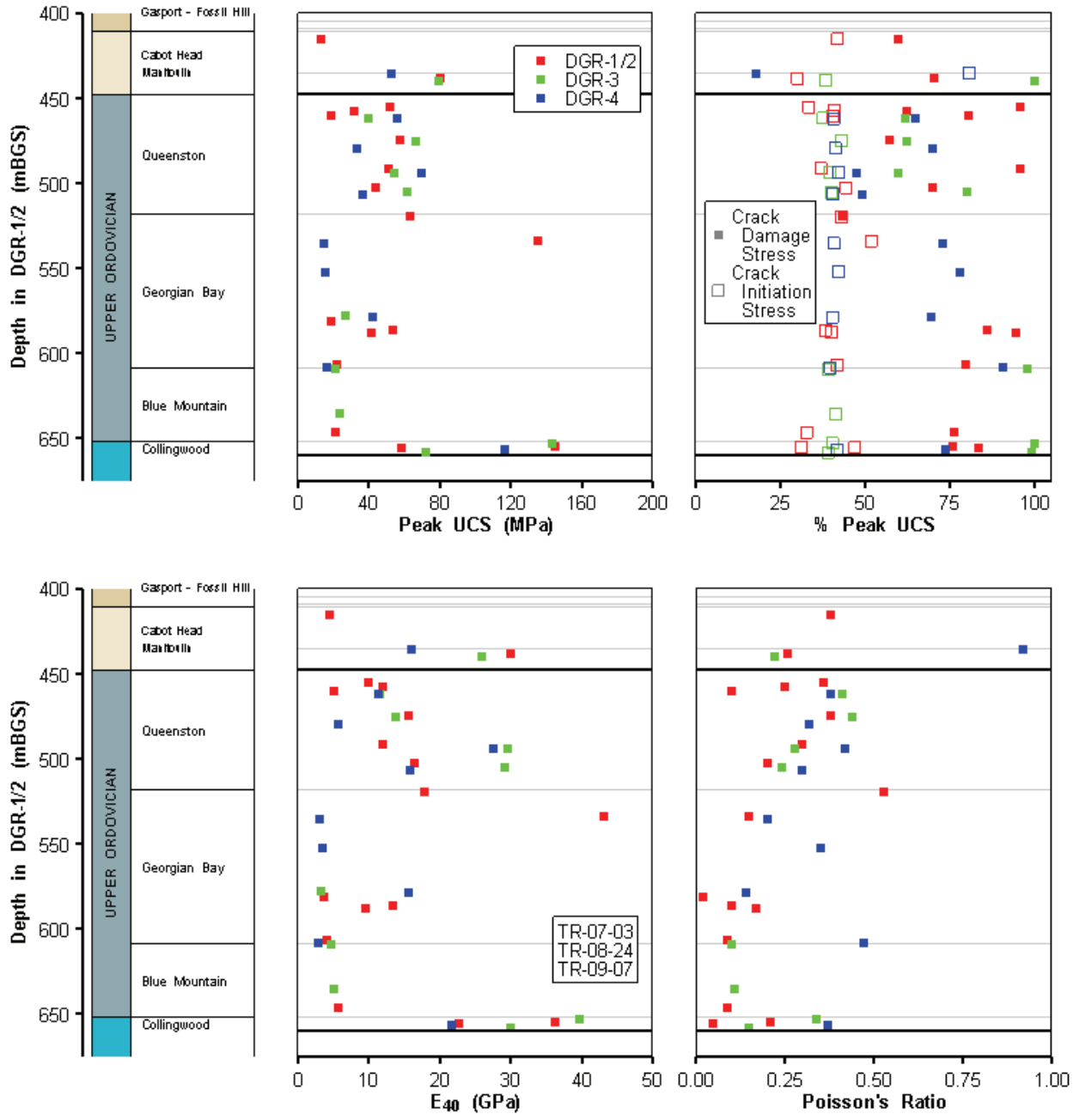

Figure 5.13: MS Unit 3: Uniaxial Compression Test Data

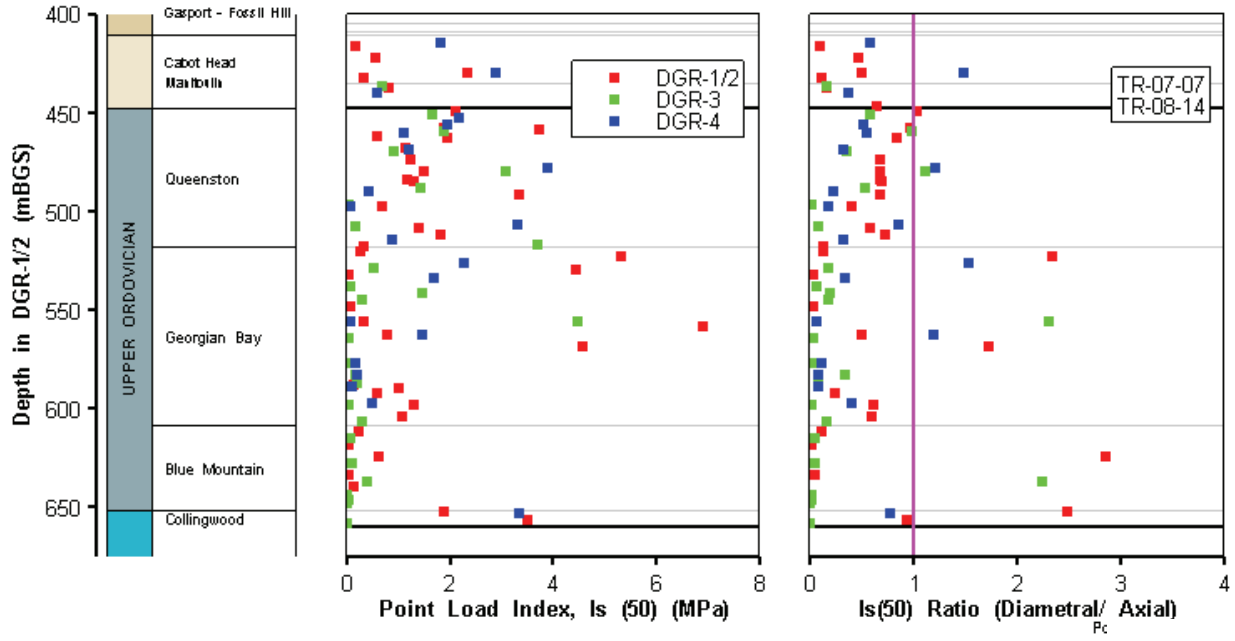

Figure 5.14: MS Unit 3: Point Load Test Data

Based on the ratio of diametral-to-axial PLT results (Figure 5.14), the rock materials in MS Unit 3 are quite strongly anisotropic. While this conclusion should be treated with some caution due to the uncertainties that are inherent in PLT data, the relatively fissile nature of the shale formations in MS Unit 3 is such that strength anisotropy should be expected (see Section 5.7.1.3 below).

There are no data available for the rocks in MS Unit 3 regarding possible relationships between short-term strength and the stress threshold at which long-term strength degradation may commence. However, it has been demonstrated in other units (see MS Unit 4) that no long-term strength degradation is likely to occur at stress levels below crack initiation which consistently occurs at 40% of UCS in the MS Unit 3 units.

Results for uniaxial compression parameters are summarized in Table 5.9, excluding the dolostone of the Manitoulin Formation.

5.7.1.2 Cross-anisotropic Uniaxial Compression

In order to obtain some comparison of compressive strength parallel and perpendicular to bedding, two core samples from the Queenston Shale unit were sub-cored at 90 degrees to the borehole axis (one each from DGR-3 and DGR-4) and tested in uniaxial compression (TR-08-24). Surprisingly, the core from DGR-3 (at 487.1.mBGS) indicated that UCS parallel to bedding was actually greater than perpendicular to bedding (75.2 MPa vs 47.5 MPa). However, the core from DGR-4 (at 477.9 mBGS) indicated that strength parallel to bedding was 42% of strength perpendicular to bedding (19.2 MPa vs 46.2 MPa). The results are inconclusive. Experienced judgement would indicate that the fissile nature of the shale rocks in MS Unit 3 will generally result in reduced compressive strength when loaded parallel to bedding. This

conclusion is supported by the Point Load Test results, which also indicate a high degree of strength anisotropy (Figure 5.14).

Table 5.9: MS Unit 3: Estimated Geomechanical Parameters in Uniaxial Compression

Parameter	Mean	Range	Estimate
Peak UCS	53 MPa	13-145 MPa	50 MPa
Crack Initiation	40% (UCS)	30-52% (UCS)	35% (UCS)
Crack Damage	74% (UCS)	42-100% (UCS)	~75% (UCS)
Modulus of Elasticity (E_{40})	16 GPa	3-43 GPa	15 GPa
Poisson's Ratio	0.25	0.12-0.47	0.25
PLT Strength Anisotropy (Diametral/Axial)	High	Large scatter	~0.5
Long-term Strength	No data	No data	No data

5.7.1.3 Triaxial Compression

Three core samples from the Georgian Bay Formation were tested under triaxial confinement of 5, 10 and 15 MPa (TR-08-24). Four core samples of the Collingwood Member were also tested under triaxial confinement of 5 and 10 MPa (TR-08-24) and triaxial confinement of 8 and 24 MPa (TR-09-07). The results are shown in Figure 5.15, which also shows the best-fit Hoek-Brown envelope for the data separately for the Georgian Bay Formation and for the Collingwood Member of the Cobourg Formation. The best-fit failure envelope indicates the following empirical Hoek-Brown strength parameters for intact Georgian Bay and Collingwood Member rocks:

Georgian Bay Formation	Collingwood Member
σ_c = 44.6 MPa	σ_c = 119.8 MPa
m_i = 13.1	m_i = 6.7
s = 1.0	s = 1.0
a = 0.5	a = 0.5

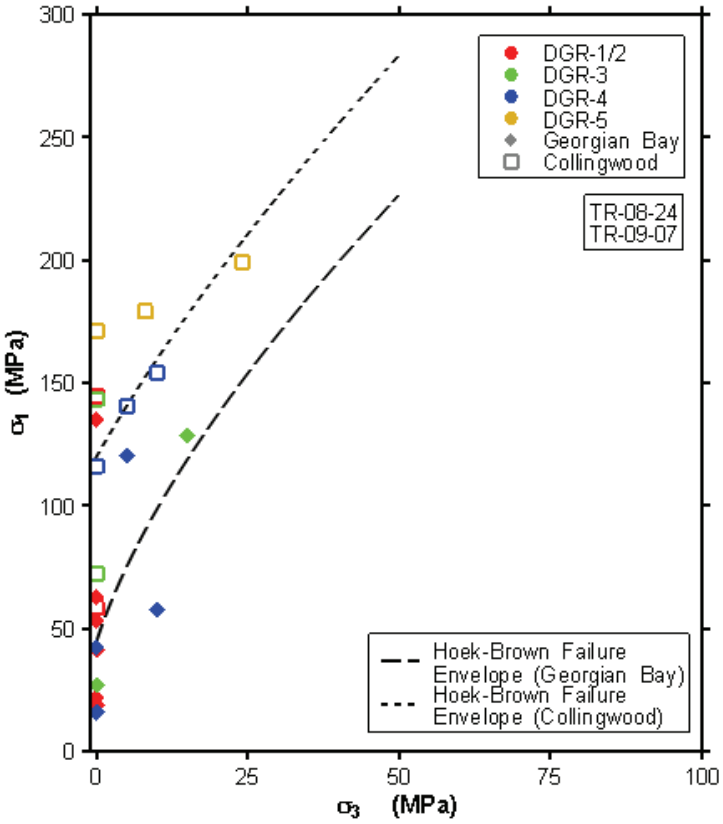

Figure 5.15: MS Unit 3: Triaxial Compression Test Data for Georgian Bay Formation and the Collingwood Member

5.7.1.4 Tension

A limited number of Brazilian tests were conducted to determine indirect tensile strength values for the MS Unit 3 rocks (Figure 5.16). Figure 5.16 shows the results of this tensile strength testing including the style of failure mode recorded by the testing laboratory (TR-07-03, TR-08-24). Failure modes include diametral (Mode 1 - normal to bedding), slabbing (Mode 2- parallel to bedding) or mixed (Mode 3 – normal and parallel to bedding).

While Brazilian test results in rock often display significant variability, it is particularly difficult to obtain valid results in fissile shales, due in part to inconsistency in the modes of failure that occur (e.g., parallel or perpendicular to the core axis, or in combined mode). Estimated values of the indirect tensile strength should be treated with caution. For purposes of this DGSM, a value of 4.0 MPa is considered to a reasonable estimate of the indirect tensile strength. It is noted that values of indirect tensile strength derived from Brazilian tests tend to give results that are 30-40% higher than those from direct tension tests. The ratio of indirect and direct tension test results could be much higher than 30% in interbedded limestone and shale formations like the Georgian Bay. The direct tensile strength is strongly dependent on the presence of weak bedding partings within a specimen.

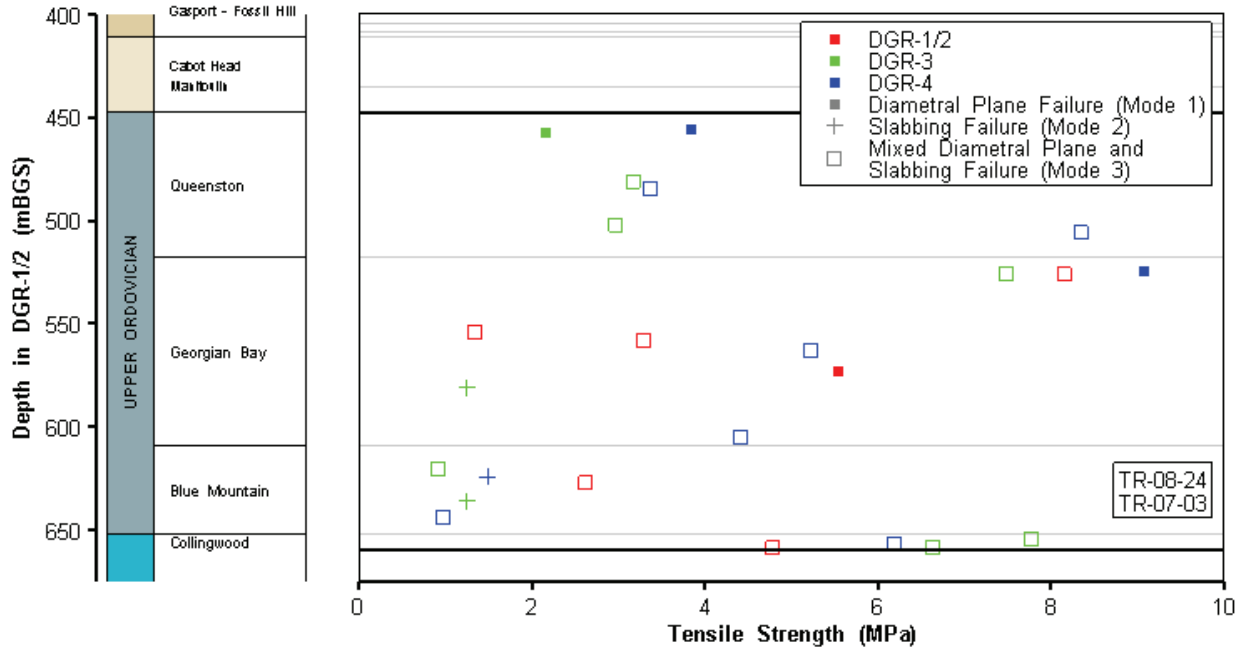

Figure 5.16: MS Unit 3: Brazilian Tests - Indirect Tensile Strength Data

5.7.1.5 Shear

Direct shear tests were conducted on samples from the Georgian Bay, Blue Mountain and Collingwood formations, located in the lower part of the MS Unit 3 Unit. The specimens were sheared along the direction of bedding (i.e., along a horizontal plane). In each case, staged tests were conducted at increasing normal stress in order to define the residual shear strength envelope. In addition, direct shear tests were conducted on one intact core specimen from the Georgian Bay Formation, one from the Blue Mountain Formation, and seven from the Collingwood Formation. Test results are summarized in Figure 5.17.

Residual shear strength parameters appear to be relatively consistent. For purposes of this DGSM, proposed representative values of the residual shear strength parameters are:

- Residual cohesion = 0 MPa, and
- Residual friction angle = 29 degrees.

Residual shear strength envelope: $\tau_r = \sigma_n(\tan 29°)$ MPa, where:

- τ_r = residual shear strength, and
- σ_n = normal stress.

For intact material from MS Unit 3, the data regarding peak shear strength are relatively limited, comprising seven tests conducted at a maximum normal stress of 2 MPa. The best-fit line through these intact shear strength test data implies a very high apparent angle of internal friction at these relatively low normal stresses. This phenomenon is common for direct shear tests of intact rock, and it is generally observed that as the normal stress increases, the

apparent friction declines and the apparent cohesion increases, due to the effect of asperities on the newly formed shear plane (Hoek and Bray 1974).

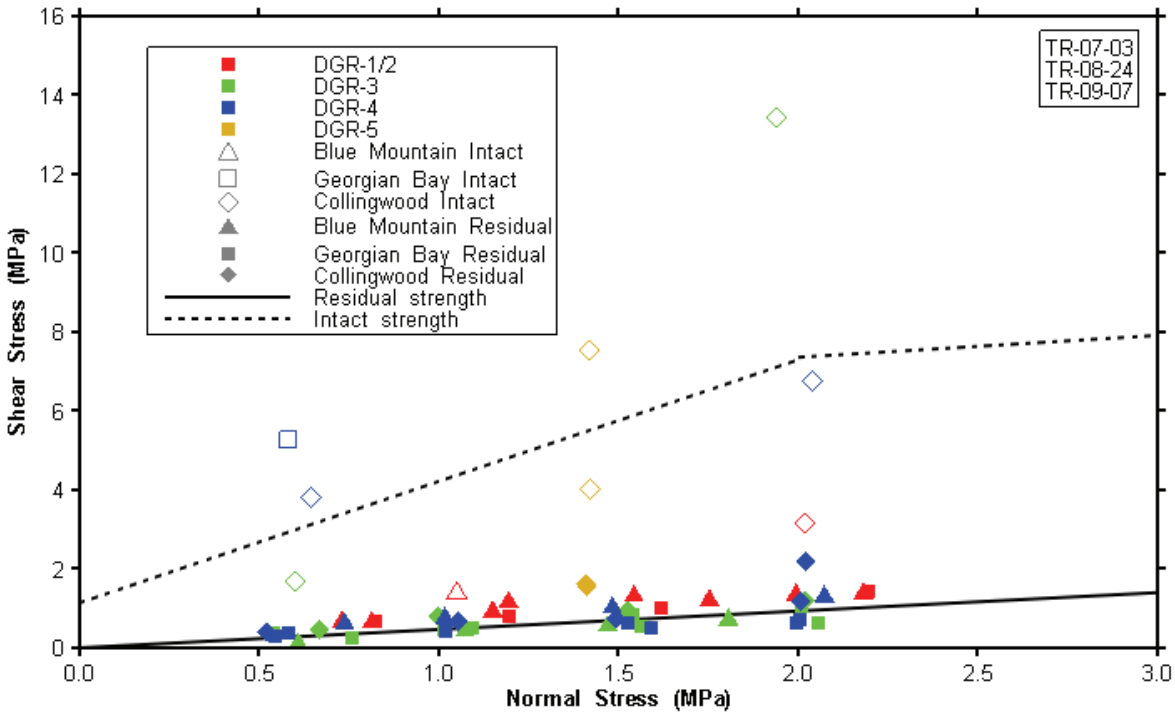

Figure 5.17: MS Unit 3: Direct Shear Test Results for Blue Mountain and Georgian Bay Formations and Collingwood Member

At low normal stresses, the asperities contribute a major geometric effect which effectively increases the apparent friction angle. At high normal stresses, shear occurs through the asperities, increasing the effective cohesion intercept, while the apparent friction angle declines, ultimately reaching the value of the residual friction angle. For this reason, a bi-linear shear strength envelope is proposed for the peak shear strength of these intact materials. At normal stresses below 2 MPa, the best-fit line to the test data is used directly to evaluate apparent cohesion and friction. At normal stresses above 2 MPa, it is conservatively assumed that the friction angle becomes equal to the residual friction angle, as noted above.

For normal stresses (σ_n) in the range: $0<\sigma_n<2$MPa:

- Apparent cohesion intercept = 1.1 MPa;
- Apparent friction angle 72 degrees; and
- Peak shear strength envelope: $\tau_p = 1.1 + \sigma_n(\tan 72°)$, MPa.

For normal stresses (σ_n) greater than 2 MPa:

- Apparent cohesion = 6.3 MPa;

- Apparent friction angle = 29 degrees; and
- Peak shear strength envelope: τ_p =6.3+ σ_n(tan29°), MPa.

5.7.1.6 Slake Durability

The MS Unit 3 consists largely of shaley materials, and a total of 32 slake durability tests were conducted in the field on selected core samples. The results are summarized in Figure 5.18, and show a range of Slake Durability Index (SDI) from 41.5% in the Cabot Head Shale to almost 100% in a sample from the Collingwood Member. In general, it is expected that clay shale units will show some degradation under wetting-drying cycles, and the results indicate that this is the case, with a mean SDI of 80% for the MS unit 3. However, it is noted that the mean SDI value is significantly higher in the Queenston Shale (~90%) than in the underlying Georgian Bay Shale (~76%), indicating that the Queenston Formation will be relatively resistant to slaking degradation compared to the Georgian Bay Formation materials. The Blue Mountain Formation materials are also relatively resistant to slaking degradation, with a mean SDI of ~90%.

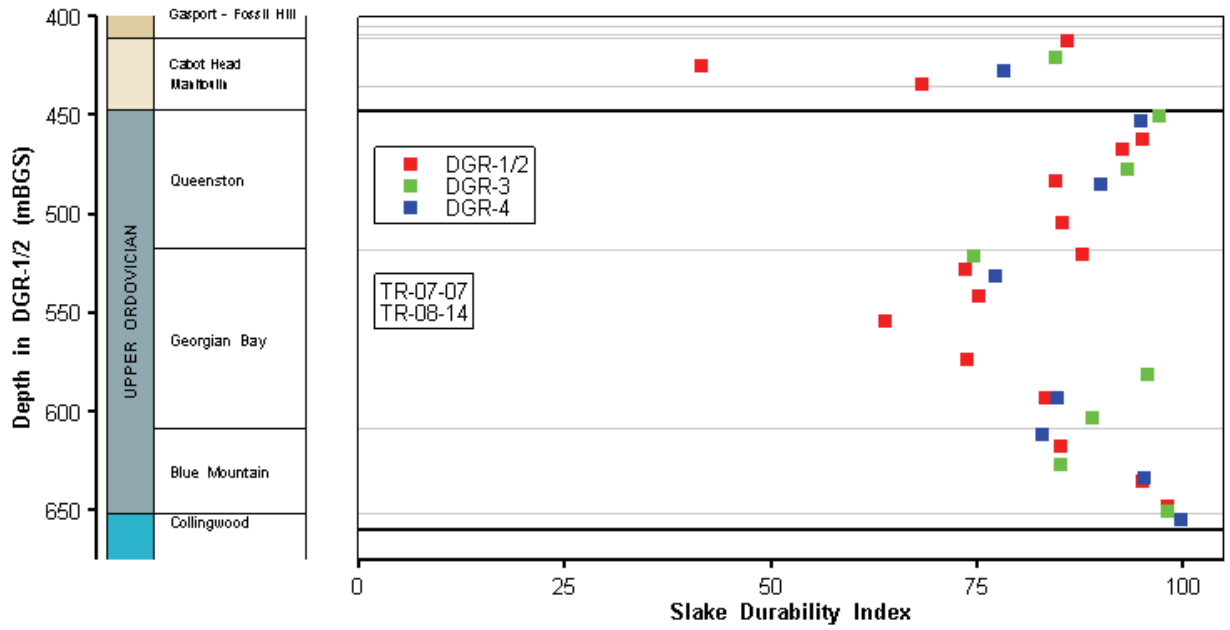

Figure 5.18: MS Unit 3: Slake Durability Index Data

For purposes of this report, the following estimated values of Slake Durability Index are representative for formations and for their corresponding depths in DGR-1 and DGR-2.

- 411 to 447 mBGS (Cabot Head + Manitoulin): SDI~75%.
- 447 to 518 mBGS (Queenston): SDI~90%.
- 518 to 608.9 mBGS (Georgian Bay): SDI~75%.
- 608.9 to 652 mBGS (Blue Mountain): SDI~90%.
- 652 to 659.5 mBGS (Collingwood): SDI ~95%.

5.7.1.7 Free Swell

Time-dependent swelling deformation of several shaley rock formations in Ontario is a well-known phenomenon. The testing methods for determining swelling potential developed by Lo et al. (1978) have become the *de facto* standard methodology for evaluating swelling potential, and these methods were utilized for this project. Swelling potential is expressed as the percent swelling strain that occurs per log cycle of time, in either the vertical (perpendicular to bedding) or horizontal (parallel to bedding) directions.

As the swelling phenomenon appears to be related to ion exchange between the rock porewater and the surrounding water, tests were conducted using both fresh water and artificial (i.e., re-constituted) formation water. A total of 27 swell tests in freshwater and 11 in formation water were run on samples of MS Unit 3 rocks, principally from the Queenston, Georgian Bay and Blue Mountain formations. Where possible, both the Vertical Swelling Potential (VSP) and Horizontal Swelling Potential (HSP) were recorded. Some difficulties regarding sample preparation and preservation were encountered with samples from the Blue Mountain Formation. Details of the testing results are presented in TR-07-16 and TR-08-26, and are summarized below in Figure 5.19 in terms of VSP and HSP.

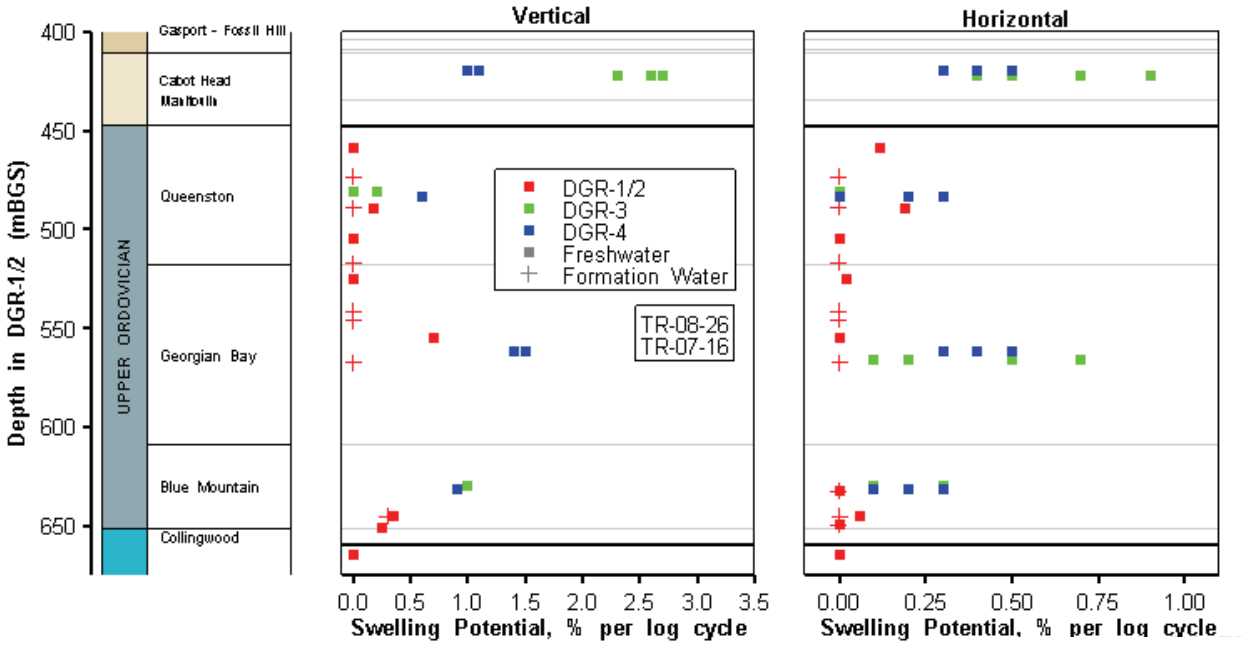

Figure 5.19: MS Unit 3: Swelling Potential in Fresh Water and in Formation Water

In formation water, the swelling potential for MS Unit 3 rocks is essentially zero, as expected. For practical purposes, both the VSP and the HSP can be considered to be zero in formation water.

When exposed to fresh water, the measured swelling potential was found to decrease with increasing calcite content, and higher swelling potential was localized to several low-calcite horizons within MS Unit 3. The vertical swelling potential results were generally consistent with data from precedent projects (TR-07-26), as indicated in Table 5.10 below. However, the Cabot Head Formation – for which no precedent data are available - exhibited significant swelling potential, up to a maximum of 2.7% VSP and up to 0.9% HSP. Except for the Cabot Head, horizontal swelling potential was generally minor.

Table 5.10: MS Unit 3: Vertical and Horizontal Swelling Potential in Fresh Water

Formation	VSP (DGR data)	VSP (precedent)	HSP (DGR data)	HSP (precedent)
Cabot Head	~2%	No data	~0.6%	No data
Queenston	~0.3%	0.02% - 0.54%	~0.1%	0 – 0.34%
Georgian Bay	~1%	0.2% - 1.4%	~0.3%	0 – 0.34%
Blue Mountain	~1%	0.9% - 1.05%	~0.15%	0.15%

5.7.1.8 Abrasiveness

No data regarding the abrasive behaviour of MS Unit 3 rock materials were generated during Phase 1, 2A and 2B site investigations.

5.7.1.9 Dynamic Properties

Compression wave (P-wave) and shear wave (S-wave) velocities were measured on intact core samples both in the field (TR-07-07, TR-08-14) and in the laboratory (TR-07-03, TR-08-24), from which dynamic elastic constants were calculated for the rock material. Variations between field and laboratory results occur, and this is not unusual. Overall, although the Georgian Bay Formation materials appear to have somewhat higher P-wave and S-wave velocities than the other formations in MS Unit 3, these differences are not considered to be significant in practical terms. Based on review of the test data, estimated values of wave velocities and dynamic elastic constants for the intact rock materials in MS Unit 3 are summarized in Table 5.11.

Table 5.11: MS Unit 3: Estimated Rock Material Dynamic Properties

Parameter	Estimated Value
P-wave Velocity	4.0 km/s
S-wave Velocity	2.1 km/s
Dynamic Modulus of Elasticity	34 Pa
Dynamic Shear Modulus	18 GPa
Dynamic Poisson's Ratio	0.31

5.7.2 Rock Mass Geomechanical Characteristics

Access for geomechanical mapping of the rock mass beneath the Bruce nuclear site was not available during the Phase 1, 2A and 2B site investigations. Consequently, information regarding the characteristics of the overall rock mass has been derived only from the relatively small diameter, one-dimensional penetrations provided by the DGR boreholes, and the resulting core. As the overall geomechanical characteristics of the rock mass depend in part on the three-dimensional characteristics of the fracture patterns (discontinuities) within the rock mass, information on the overall rock mass characteristics is limited at the current stage, even with the fracture analysis from inclined boreholes DGR-5 and DGR-6. Total horizontal sampling distances for mapping of inclined fractures in MS Unit 3 was limited to 76.3 m in DGR-5 and 130.6 m in DGR-6.

5.7.2.1 Rock Quality Designation, Fracture Frequency and Fracture Sets

Measurements of Rock Mass Quality Designation (RQD) and fracture frequency were conducted routinely throughout the drilling of DGR boreholes as reported in Section 3.6 and summarized in Table 3.4 and Figures 3.3 and 3.4. Core recovery and RQD values throughout the MS Unit 3 were generally excellent, and fracture frequency measurements indicated a generally very sparsely fractured rock mass. Based on these borehole-derived measurements, and with the exception of a few localized zones located primarily within the Queenston and Georgian Bay formations, the rock mass comprising the MS Unit 3 can be characterized as very sparsely fractured and of excellent quality.

Data from the vertical boreholes DGR-1 to DGR-4 provided significant information only on the presence of the horizontal to sub-horizontal discontinuities, and these data indicate clearly the presence of a widely spaced sub-horizontal fracture set. Oriented core logging completed in inclined boreholes DGR-5 and DGR-6 (TR-09-09) provides a preliminary three-dimensional indication of the occurrence and spacing of fractures in MS Unit 3, by providing both vertical and horizontal transects through the Unit. Fracture logging from these holes provides relatively comprehensive or balanced 3-D discontinuity data, and these data have not been combined with data from the vertical holes in order to avoid a major bias towards horizontal fracture data. A total of 101 natural fractures were logged in DGR-5 and DGR-6 core. The contoured equal area plot of all natural fractures logged in DGR-5 and DGR-6 core is shown in Figure 5.20. Figure 5.20 plots the fracture occurrence in MS Unit 3 considering Terzaghi (1965) sampling bias.

The polar plot from the inclined boreholes data suggests the presence of three major fracture sets in MS Unit 3. The three major fracture sets include a near horizontal bedding plane set (MS Unit 3 Set #1) confirming the data from the four vertical boreholes, an east-west striking near vertical set (MS Unit 3, Set #2), and a northeast-southwest striking sub-vertical set (MS Unit 3, Set #3). The average weighted fracture set orientations, including number of occurrences and arithmetic average discontinuity spacing for MS Unit 3 fracture sets are presented in Table 5.12.

5.7.2.2 Bulk Properties from Geophysical Logging

Elastic dynamic properties of a bulk in situ sample of the rock mass are derived from downhole sonic logging. A uniform bulk density of 2.63 g/cm^3 (Figure 4.1) was used in all modulus calculations. Results are summarized in Table 5.13 for various depth intervals within the MS 3 Unit based on logging in DGR-1, DGR-2, DGR-3 and DGR-4.

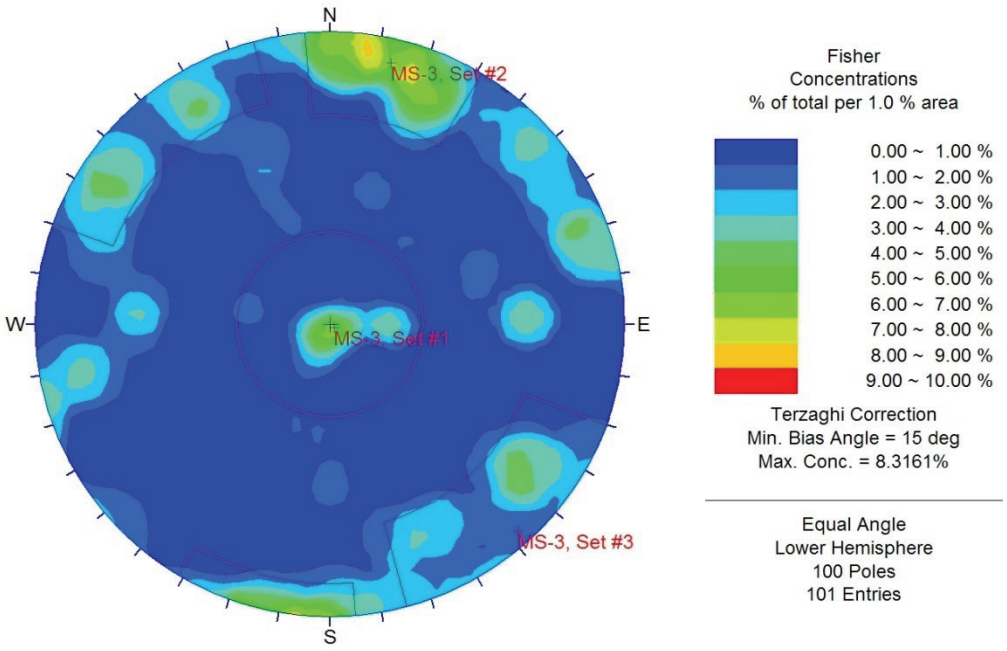

Figure 5.20: Contoured Equal Area Polar Plot of All Natural Fractures in DGR-5 and DGR-6 Core in MS Unit 3

Table 5.12: Natural Fracture Set Orientation and Spacing in MS Unit 3 from Oriented Core Logging in DGR-5 and DGR-6

Fracture Set	Number of Occurrences	Strike	Dip	Average Discontinuity Spacing (m)
MS Unit 3, Set #1	39	N39°E	2°NW	9.6
MS Unit 3, Set #2	15	N77°W	85°S	11.5
MS Unit 3, Set #3	16	N47°E	87°NW	6.8
Miscellaneous	31	--	--	--

5.7.2.3 Rock Mass Classification

Subsurface data obtained from DGR boreholes in the Phase 1, 2A and 2B investigations are judged not sufficient to provide complete estimates of all the parameter values required to determine the classification categories under the commonly used rock mass classification systems. Preliminary descriptive comments regarding rock mass quality are included under Section 5.7.2.1 above, based on the limited parameters of RQD and one-dimensional fracture frequency. These data indicate a rock mass that is very sparsely fractured and of excellent quality.

Results of oriented core logging in DGR-5 and DGR-6, indicate three fracture sets with average spacings of 6.8 to 11.5 m. These wide fracture spacings, in conjunction with rock material and rock mass geomechanical properties described above, indicate a rock mass of excellent quality. Rock mass classification ratings or indices have not been developed based on the limited horizontal sampling distances available from DGR boreholes.

Table 5.13: MS Unit 3: Estimated Rock Mass Dynamic Properties

Formation	Depth Range (mBGS)	V_p (m/s)	V_s (m/s)	E_d (GPa)	G_d (GPa)
Cabot Head	411.00 – 431.49	3810	2170	31.2	12.4
Manitoulin	431.50 – 447.64	5140	2860	54.8	21.5
Queenston	447.65 – 517.99	4170	2220	33.7	12.9
Georgian Bay	518.00 - 579.42	3970	1990	27.6	10.8
Georgian Bay, Blue Mountain	579.43 – 616.49	3670	2000	25.5	10.6
Blue Mountain	616.50 – 649.42	3540	1980	17.5	19.2
Blue Mountain, Collingwood	649.43 – 651.99	4890	2650	17.5	18.9
Collingwood	652.00 – 659.49	4898	2504	44.3	16.7

5.8 MS Unit 4: Middle Ordovician Cobourg Formation

The 27.1- to 28.6-m-thick Lower Member of the Cobourg Formation is MS Unit 4 (659.5 to 688.1 mBGS in DGR-2) and comprises a fossiliferous argillaceous limestone. This is the target horizon to host the DGR (Figure 5.1).

5.8.1 Rock Material Geomechanical Characteristics

5.8.1.1 Uniaxial Compression

A total of 56 laboratory specimens (Figure 5.21) were tested in standard short-term uniaxial compression tests, 45 as part of the initial work by CANMET (TR-07-03, TR-08-24, TR-09-07) and a further 11 samples were tested to provide input data for the Long-term Strength Degradation (LSD) testing (TR-08-11, TR-08-36).

The results of the LSD tests did not indicate that any strength degradation had occurred for samples that had been statically loaded for 100 days to stress levels that averaged 70% (range from 43 to 100%) of the crack initiation stress level or 20 to 57% of UCS (see Figure 5.22). Consequently, these results have been included in the data summary along with the short-term results, giving a total of 67 uniaxial compression strength (UCS) results. Results are summarized in Figure 5.21 for each specimen in terms of peak uniaxial compressive strength (UCS), the percentages of UCS at which crack initiation and crack damage, respectively, occurred, and the Modulus of Elasticity and Poisson's Ratio values measured at 40% of UCS.

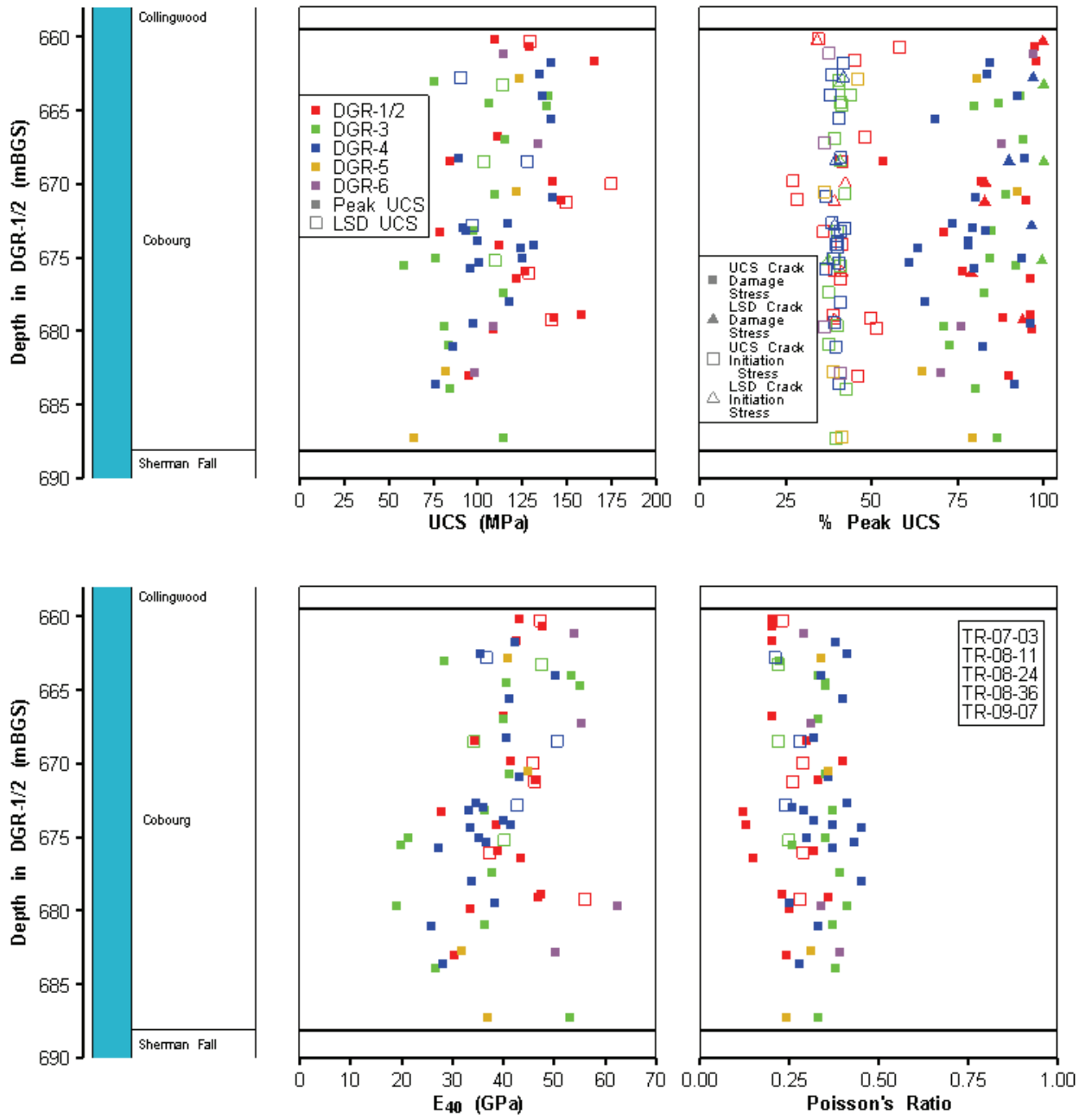

Figure 5.21: MS Unit 4: Uniaxial Compression Test Data

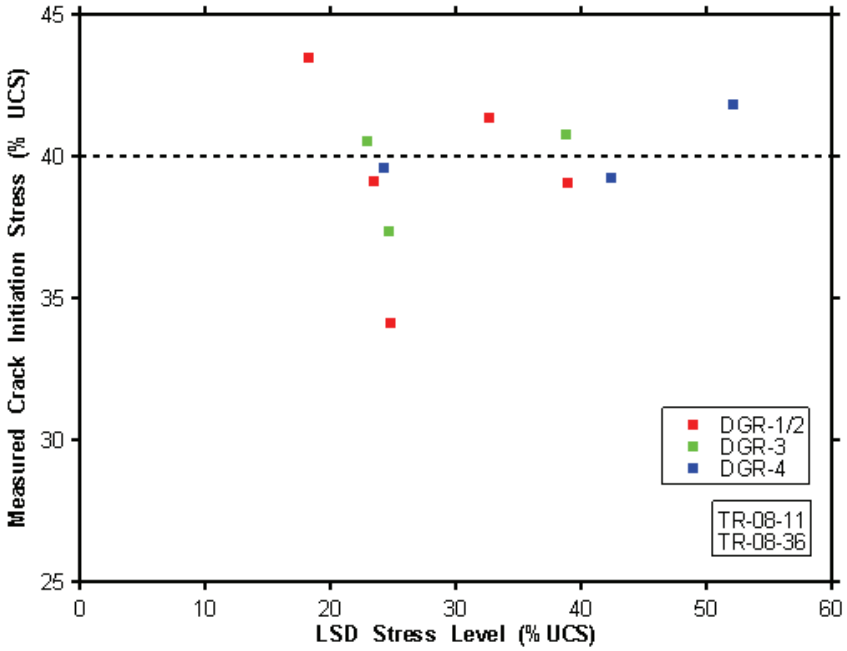

Figure 5.22: Crack Initiation Stresses and Long-term Stress Degradation Testing Levels in % UCS for MS Unit 4

Figure 5.23 summarizes data from the Point Load Tests that were conducted on core recovered from the MS Unit 4. The isotropic line defined as equal diametral and axial strength is shown on the right panel of Figure 5.23. The axial tests gave consistent results with the PLT~3.75 MPa, and the ratio of diametral to axial results indicates a very low degree of anisotropy.

As indicated in Figures 5.21 and 5.23, uniaxial compression test results indicate that the compression parameters display relatively little variability, except for a few outliers. Table 5.14 summarizes the uniaxial compression parameters for the MS Unit 4 rock materials. Due to the large number of compression test results available from the MS Unit 4 (67), the results have been summarized in terms of their mean and standard deviation values.

Figure 5.24 shows the relationship between the peak uniaxial compressive strength data gathered from throughout the region as part of the Phase 1 Regional Geomechanics Report (NWMO and AECOM 2011), and the Phase 1, 2A and 2B data from the Bruce nuclear site. The figure indicates that the site-specific data lie at the upper range of the regional data. In part, this may reflect the rigorous quality control procedures and the state of the art procedures utilized for handling of the core samples from the DGR site, or the fact that most regional data are obtained from shallow depths where weathering and stress relief act to decrease rock strengths.

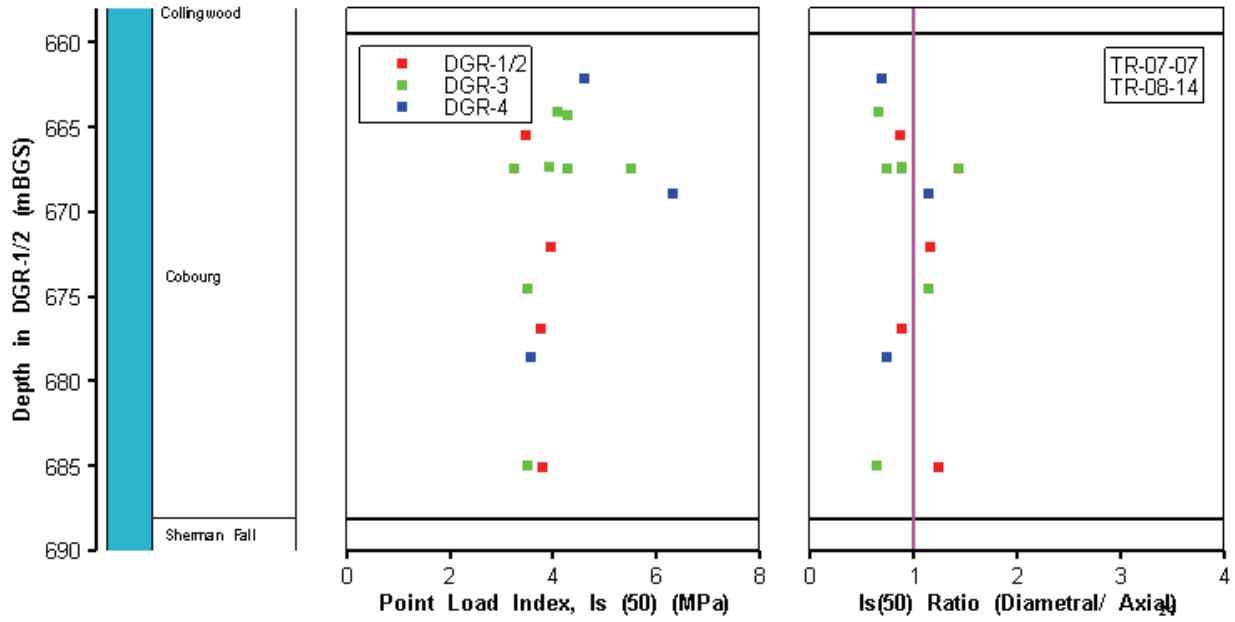

Figure 5.23: MS Unit 4: Point Load Test Data

Table 5.14: MS Unit 4: Geomechanical Parameters in Uniaxial Compression

Parameter	Mean	Std Deviation
Peak UCS (all tests)	113 MPa	25 MPa
Crack Initiation	40% (UCS)	4.4% (UCS)
Crack Damage	85% (UCS)	11% (UCS)
Modulus of Elasticity (E_{40})	40 GPa	9 GPa
Poisson's Ratio	0.31	0.08
PLT Strength Anisotropy (Diametral/Axial)	Low	Minor scatter
Long-term Strength Tests (Peak after 100 days)	124 MPa	-

Note: Includes results from long-term strength degradation tests.

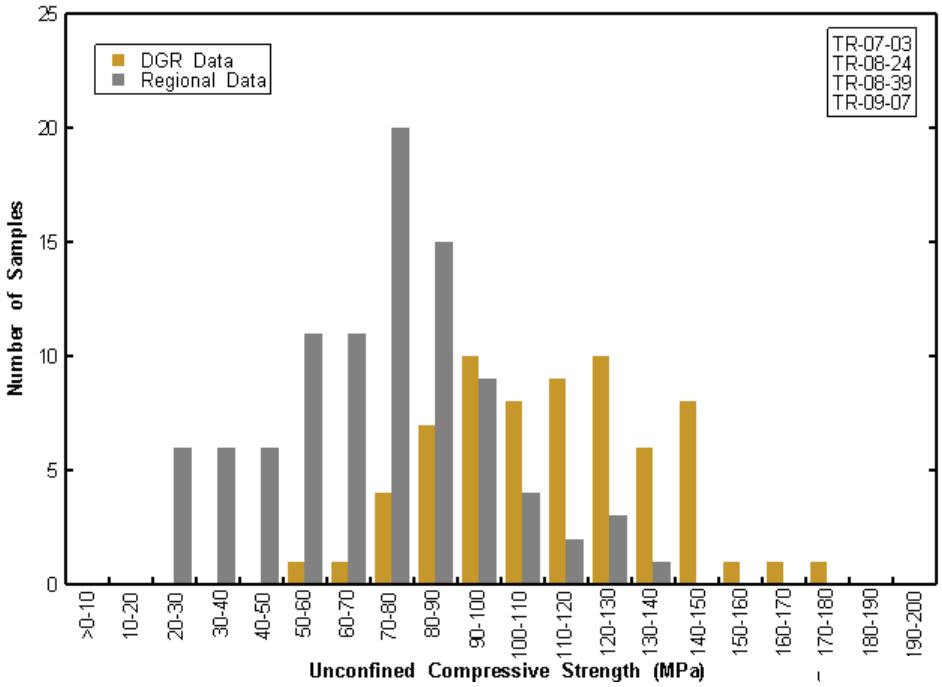

Figure 5.24: MS Unit 4: Peak Uniaxial Compressive Strength (UCS) – Site-specific and Regional Data

5.8.1.2 Cross-anisotropic Uniaxial Compression

In order to obtain some comparison of compressive strength parallel and perpendicular to bedding, two core samples were sub-cored at 90 degrees to the borehole axis (one each from DGR-3 and DGR-4) and tested in uniaxial compression (TR-08-24). The core from DGR-3 (at 678.7.mBGS) indicated that UCS parallel to bedding was 60% of the UCS perpendicular to bedding (87.6 MPa vs 144.0 MPa). However, the core from DGR-4 (at 671.7 mBGS) indicated no change in strength relative to bedding direction (148.9 MPa vs 148.7 MPa). As bedding planes are generally poorly expressed in this unit, it is anticipated that UCS values generally will not be strongly directionally dependent. This conclusion is supported by the Point Load Test results, which also indicate a very low level of strength anisotropy (Figure 5.23).

5.8.1.3 Triaxial Compression

Fourteen core samples from the Lower Member of the Cobourg Formation were tested under triaxial confinement ranging from 7.5 – 30 MPa. The results are shown in Figure 5.25, which includes the best-fit Hoek-Brown envelope for the data, and indicates the following empirical Hoek-Brown strength parameters for the intact rock.

- σ_c = 120 MPa
- m_i = 10.0
- s = 1.0
- a = 0.5

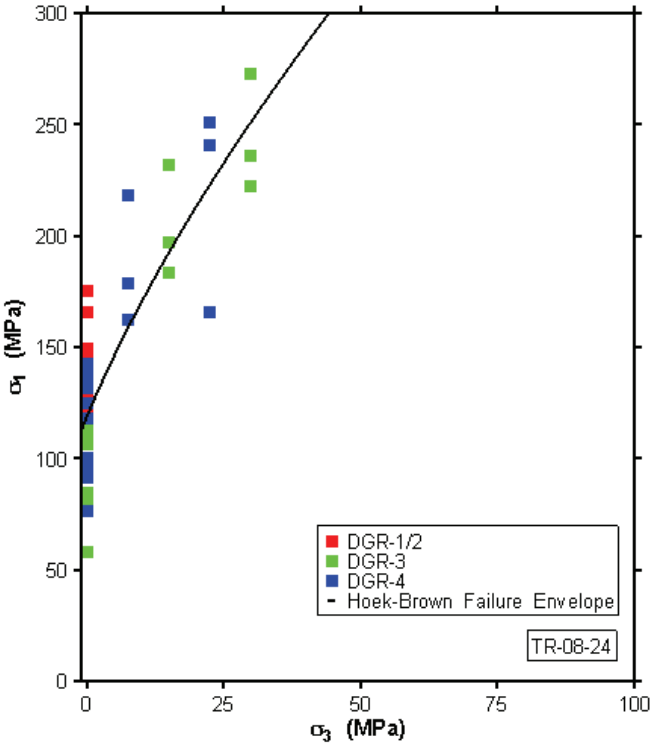

Figure 5.25: MS Unit 4: Triaxial Compression Test Data for Cobourg Formation

5.8.1.4 Tension

Nine valid indirect tension tests (Brazilian tests) were conducted on core from MS Unit 4. The results (Figure 5.26) give a mean value of the estimated tensile strength of ~6.4 MPa.

5.8.1.5 Shear

Direct shear tests were run on 15 samples of intact rock from the Lower Member of the Cobourg Formation. Peak shear strength parallel to bedding was first determined prior to running staged shear tests at increasing normal stress levels to determine the residual strength parameters. Results are summarized in Figure 5.27.

For residual shear strength, based on the best-fit line through the test data, the proposed estimated values of the shear strength parameters are:

- Residual cohesion = 0 MPa; and
- Residual friction angle = 39 degrees.

Residual shear strength envelope: $\tau_r = \sigma_n(\tan 39°)$, MPa, where:

- τ_r = residual shear strength; and
- σ_n = normal stress.

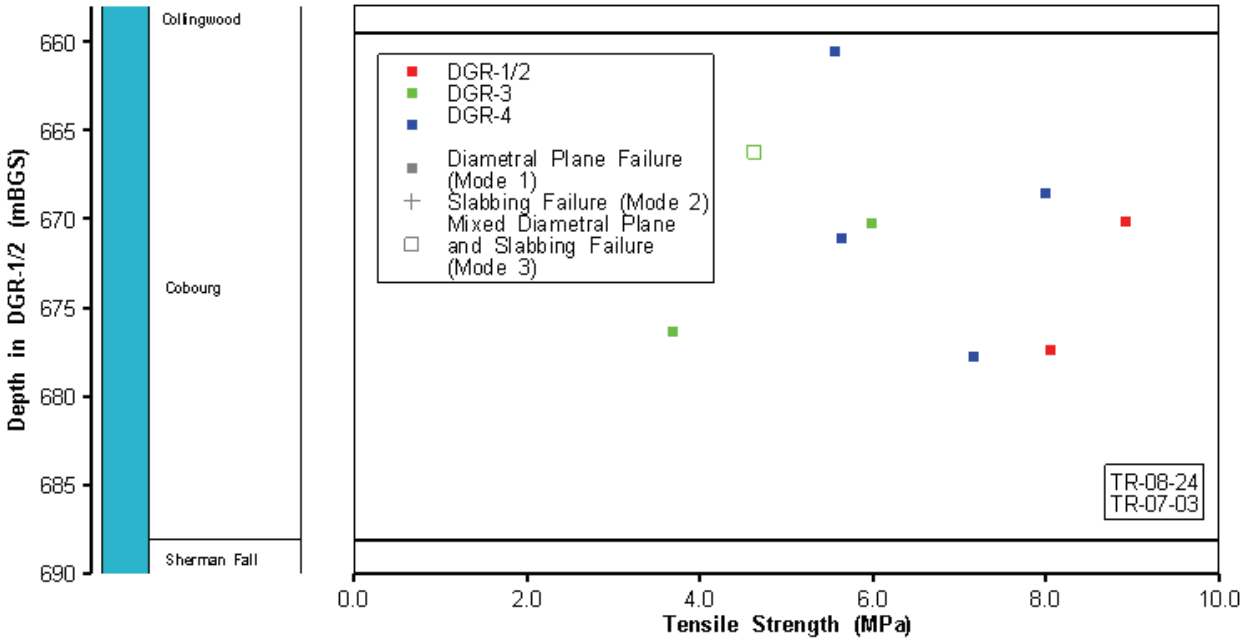

Figure 5.26: MS Unit 4: Brazilian Tests – Indirect Tensile Strength Data

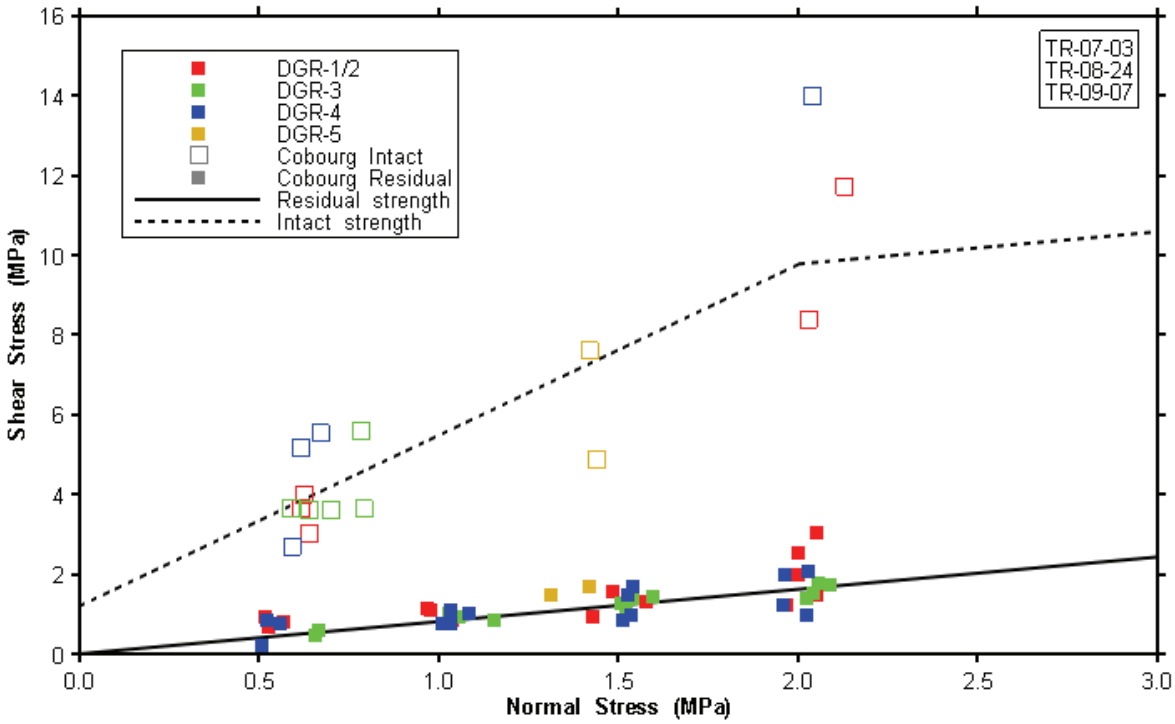

Figure 5.27: MS Unit 4: Direct Shear Test Results for Cobourg Formation

As discussed in Section 5.7.1.5 (MS Unit 3), data regarding peak shear strength of the intact material only extend to normal stresses of approximately 2 MPa. Within this range of relatively low normal stress, the data indicate a high apparent friction angle, due to the geometric effect of asperities along the freshly formed shear plane. As normal stresses increase, apparent friction will decrease and apparent cohesion will increase as the effect of the asperities changes from contributing to apparent friction to adding to apparent cohesion. For this reason, a bi-linear shear strength envelope is proposed for the peak shear strength of these intact materials. At normal stresses below 2 MPa, the best-fit line to the test data is utilized to evaluate apparent cohesion and friction. At normal stresses above 2 MPa, it is conservatively assumed that the friction angle becomes equal to the residual friction angle noted above.

For normal stresses (σ_n) in the range: $0<\sigma_n<2$MPa:

- Apparent cohesion intercept =1.2 MPa;
- Apparent friction angle = 75 degrees; and
- Peak shear strength envelope: $\tau_p = 1.2 + \sigma_n(\tan 75°)$, MPa.

For normal stresses (σ_n) greater than 2 MPa:

- Apparent cohesion = 8.7 MPa;
- Apparent friction angle = 39 degrees; and
- Peak shear strength envelope: $\tau_p = 8.7 + \sigma_n(\tan 39°)$, MPa.

5.8.1.6 Slake Durability

Two slake durability tests were conducted on samples from the MS Unit 4 that appeared to be somewhat argillaceous. Neither sample indicated any significant sensitivity to slaking degradation, as indicated in Figure 5.28.

5.8.1.7 Swelling Potential

Four tests of swelling potential were conducted on MS Unit 4 rocks during the Phase 1 investigation (DGR-2), two in fresh and two in formation water, respectively. The vertical and the horizontal swelling potentials were zero for all tests. No further tests were conducted during Phase 2A (DGR-3 and DGR-4) or Phase 2B (DGR-5 and DGR-6).

5.8.1.8 Abrasiveness

A series of abrasivity tests were performed on samples from the Lower Member of the Cobourg Formation (MS Unit 4) as well as within the lower part of the Collingwood Member of the Cobourg Formation. Details are reported in TR-07-04 and TR-08-25. Testing was based on the standard CERCHAR scratch test (Plinninger et al. 2003) with the results expressed as CERCHAR Abrasivity Index for the smooth surfaces tested (CAI_s). Results, which are shown in Figure 5.29, indicate that the materials would be classified as displaying slight to medium abrasivity with average CERCHAR Abrasivity Index on smooth (saw-cut) surfaces of approximately 0.85. As noted in TR-08-25, these results are consistent with typical values reported in the literature for limestone and marlstone.

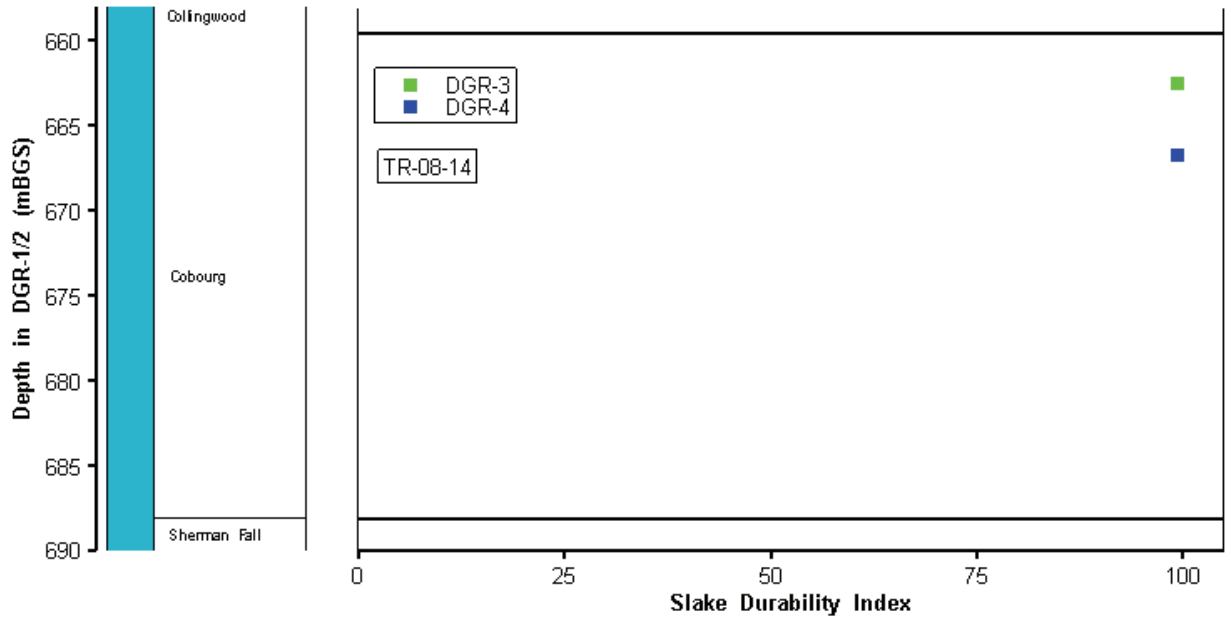

Figure 5.28: MS Unit 4: Slake Durability Index Data

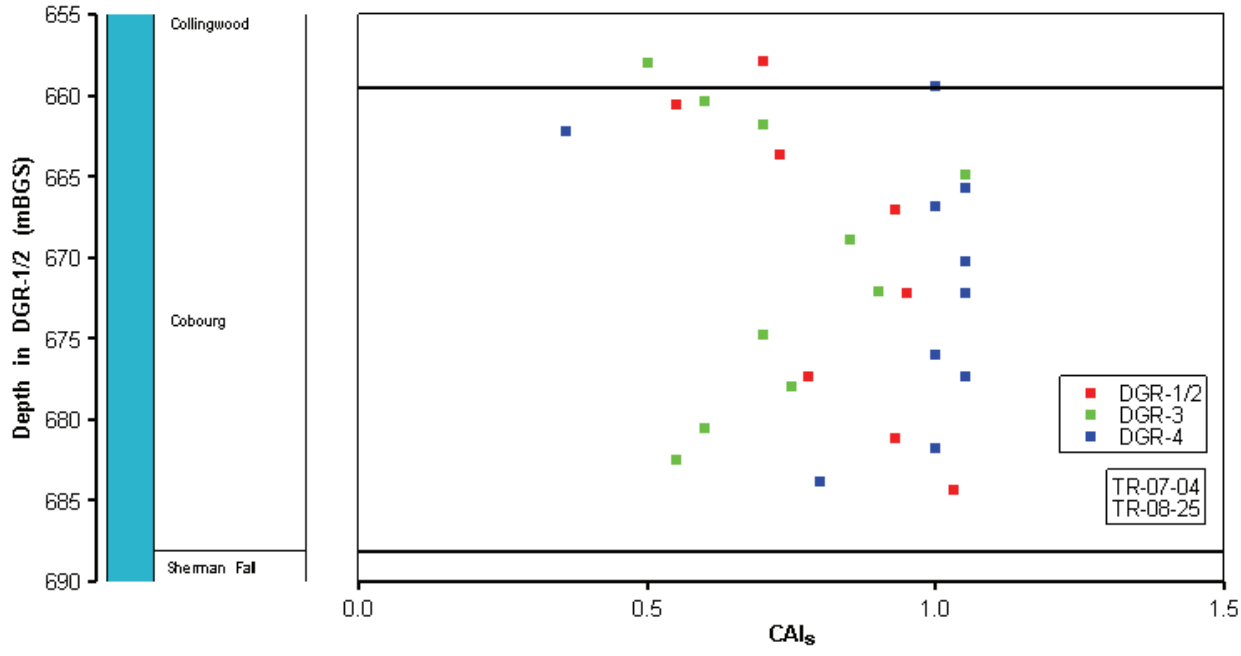

Figure 5.29: MS Unit 4: CERCHAR Abrasivity Index Data

5.8.1.9 Dynamic Properties

Compression wave (P-wave) and shear wave (S-wave) ultrasonic pulse velocities were measured on intact core samples in the field (TR-07-07, TR-08-14) and in the laboratory (TR-07-03, TR-08-24, TR-09-07), from which dynamic elastic constants were calculated for the rock material. As is commonly the case, field and laboratory results show differences, possibly due to factors such as sample disturbance during shipping. Based on overall review of the data, Table 5.15 summarizes estimated values for the dynamic properties.

Table 5.15: MS Unit 4: Estimated Rock Material Dynamic Properties

Parameter	Estimated Value
P-wave Velocity	5.3 km/s
S-wave Velocity	2.7 km/s
Dynamic Modulus of Elasticity	55 GPa
Dynamic Shear Modulus	21 GPa
Dynamic Poisson's Ratio	0.31

5.8.2 Rock Mass Geomechanical Characteristics

Access for geomechanical mapping of the rock mass beneath the Bruce nuclear site was not available during the Phase 1, 2A and 2B site investigations. Consequently, information regarding the characteristics of the overall rock mass has been derived only from the relatively small diameter, one-dimensional penetrations provided by the DGR boreholes, and the resulting core. As the overall geomechanical characteristics of the rock mass depend in part on the three-dimensional characteristics of the fracture patterns (discontinuities) within the rock mass, information on the overall rock mass characteristics is limited at the current stage, even with the fracture analysis from inclined boreholes DGR-5 and DGR-6. Total horizontal sampling distances for mapping of inclined fractures in MS Unit 4 was limited to 6.3 m in DGR-5 and 18.6 m in DGR-6.

5.8.2.1 Rock Quality Designation, Fracture Frequency and Fracture Sets

Measurements of Rock Mass Quality Designation (RQD) and fracture frequency were conducted routinely throughout the drilling of DGR boreholes as reported in Section 3.6 and summarized in Table 3.4 and Figures 3.3 and 3.4. Core recovery and RQD values throughout the MS Unit 4 were excellent, and fracture frequency measurements indicated a very sparsely fractured rock mass. Based on these borehole-derived measurements, and with the exception of a few localized zones located primarily within the Queenston and Georgian Bay formations, the rock mass comprising the MS Unit 3 can be characterized as very sparsely fractured and of excellent quality.

Data from the vertical boreholes DGR-1 to DGR-4 provided significant information only on the presence of the horizontal to sub-horizontal discontinuities, and these data indicate clearly the presence of a widely spaced (2-3m) sub-horizontal fracture set. Oriented core logging completed in inclined boreholes DGR-5 and DGR-6 (TR-09-09) provides a preliminary three-dimensional indication of the occurrence and spacing of fractures in MS Unit 2, by providing

both vertical and horizontal transects through the Unit. Fracture logging from these holes provides relatively comprehensive or balanced 3-D discontinuity data, and these data have not been combined with data from the vertical holes in order to avoid a major bias towards horizontal fracture data. A total of 7 natural fractures were logged in DGR-5 core and no natural fractures were logged in DGR-6 core. The contoured equal area plot of all natural fractures logged in DGR-5 and DGR-6 core is shown in Figure 5.30. Figure 5.30 plots the fracture occurrence in MS Unit 4 considering Terzaghi (1965) sampling bias.

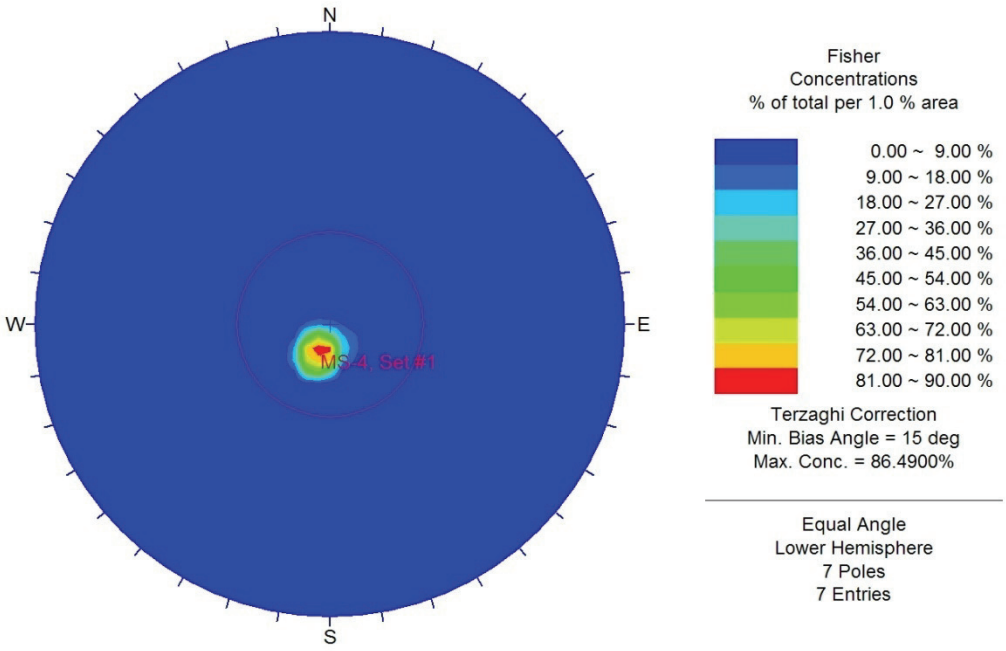

Figure 5.30: Contoured Equal Area Polar Plot of All Natural Fractures in DGR-5 and DGR-6 Core in MS Unit 4

The polar plot from the inclined boreholes data suggests the presence of one fracture set in MS Unit 4. The only fracture set present (MS Unit 4, Set #1) is approximately horizontal and likely represents the discontinuities along the bedding plane. The average weighted fracture set orientation, including number of occurrences and arithmetic average discontinuity spacing for MS Unit 4 are presented in Table 5.16.

Table 5.16: Natural Fracture Set Orientation and Spacing in MS Unit 4 from Oriented Core Logging in DGR-5 and DGR-6

Fracture Set	Number of Occurrences	Strike	Dip	Average Discontinuity Spacing (m)
MS Unit 4, Set #1	7	N71°W	11°NW	2.5
Miscellaneous	0	--	--	--

5.8.2.2 Bulk Properties from Geophysical Logging

Elastic dynamic properties of a bulk in situ sample of the rock mass are derived from downhole sonic logging. A uniform wet bulk density of 2.63 g/cm^3 (Figure 4.1) was used in all modulus calculations. Results are summarized in Table 5.17 for various depth intervals within the MS Unit 4 based on logging of DGR-2, DGR-3 and DGR-4.

Table 5.17: MS Unit 4: Estimated Rock Mass Dynamic Properties

Formation	Depth Range (mBGS)	V_p (m/s)	V_s (m/s)	E_d (GPa)	G_d (GPa)
Cobourg (Lower Member)	659.50 – 686.49	5640	2850	57.9	21.8

5.8.2.3 Rock Mass Classification

Subsurface data obtained from DGR boreholes in the Phase 1, 2A and 2B investigations are judged not sufficient to provide complete estimates of all the parameter values required to determine the classification categories under the commonly used rock mass classification systems. Preliminary descriptive comments regarding rock mass quality are included under Section 5.8.2.1 above, based on the limited parameters of Rock Quality Designation (RQD) and one-dimensional fracture frequency. These data indicate a rock mass that is very sparsely fractured and of excellent quality.

Results of oriented core logging in DGR-5 and DGR-6, indicate one fracture set with average spacing of 2.5 m. These wide fracture spacings, in conjunction with rock material and rock mass geomechanical properties described above, indicate a rock mass of excellent quality. Rock mass classification ratings or indices have not been developed based on the limited horizontal sampling distances available from DGR boreholes

5.9 MS Unit 5: Middle Ordovician Sherman Fall and Deeper Formations

The MS Unit 5 (688.1 to 860.7 mBGS in DGR-2) comprises all rock units lying beneath the repository horizon, to the bottom of each deep exploratory DGR borehole (Figure 5.1). Within MS Unit 5, approximately 150 m of limestone lie immediately below the repository horizon. Of these rocks, the principal units of interest from a geotechnical perspective are the 28.0- to 29.3-m-thick Sherman Fall Formation located directly beneath the repository horizon and the underlying upper part of the Kirkfield Formation that will accommodate the shaft sumps. These two formations have similar geomechanical properties and hence are discussed together in this section. Towards the base of MS Unit 5, Cambrian sandstones lie immediately above the Precambrian granitic gneiss.

Geotechnically, the formations below the upper Kirkfield are of little interest to the design or performance of the DGR. Consequently, the limited laboratory data obtained within MS Unit 5 are focused almost exclusively on the Sherman Fall Formation (688.1 to 716.1 mBGS in DGR-2) and the upper Kirkfield Formation, with some occasional UCS results reported from other deeper Ordovician limestone and Cambrian rocks for purposes of estimating specific storage parameters.

5.9.1 Rock Material Geomechanical Characteristics

5.9.1.1 Uniaxial Compression

Nineteen uniaxial compression tests were conducted on samples recovered from the Sherman Fall to Cambrian rocks. Results are summarized in Figure 5.31.

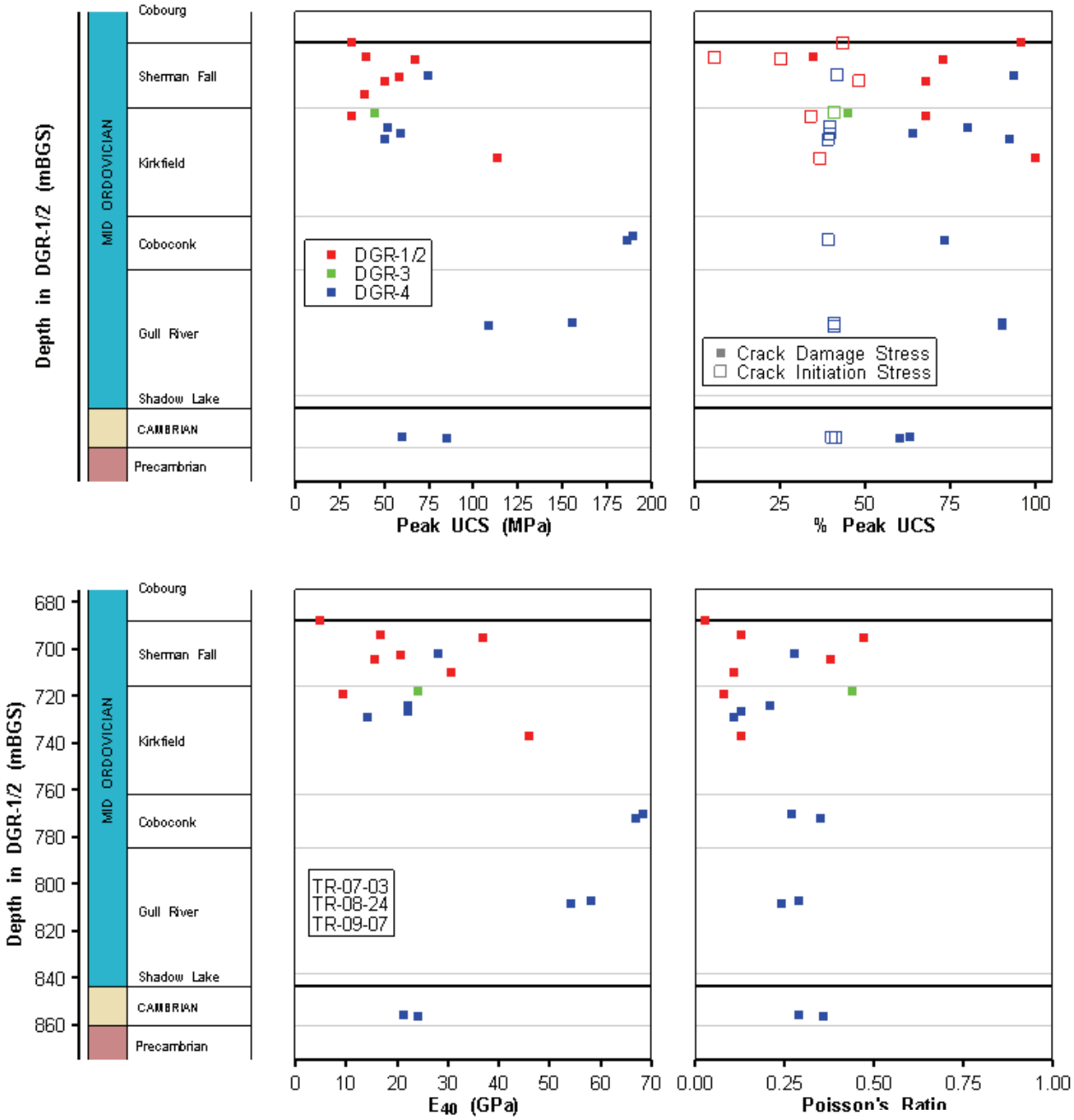

Figure 5.31: MS Unit 5: Uniaxial Compression Test Data

Most of the tests (12) were performed on cores recovered from the Sherman Fall Formation and the upper part of the Kirkfield Formation. Key results are summarized in Figure 5.31 for each specimen in terms of peak uniaxial compressive strength (UCS), the percentage of UCS at which crack initiation and crack damage occurred, and the Modulus of Elasticity and Poisson's Ratio values (measured at 40% of UCS). No significant difference was noted between the properties of the Sherman Fall Formation and the upper Kirkfield Formation.

Figure 5.32 summarizes data from the Point Load Tests that were conducted on core recovered from the MS Unit 5. The isotropic line defined as equal diametral and axial strength is shown on the right panel of Figure 5.32. Table 5.18 summarizes estimated uniaxial compression parameters for only the Sherman Fall and Kirkfield formations of the MS Unit 5, as laboratory data are limited for other formations.

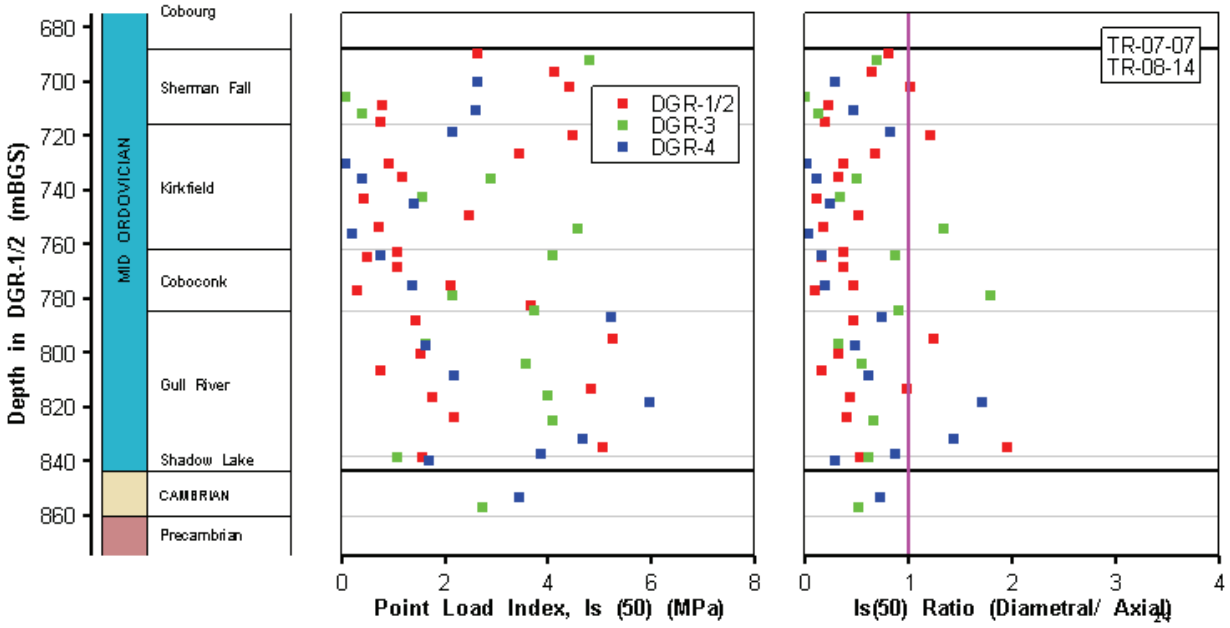

Figure 5.32: MS Unit 5: Point Load Test Data

The data show that the Sherman Fall and Kirkfield Formation materials have a peak (mean) UCS of approximately 45 MPa, and are therefore significantly weaker than the overlying rocks of the Cobourg Formation which hosts the DGR (mean UCS ~125 MPa). The crack initiation stress levels are less predictable in these materials as a percent of UCS than in MS Unit 4 materials, and the elastic modulus shows much greater variation. These measures indicate a relatively weak and variable material in contrast to the limestone in the repository host rock horizon (Lower Cobourg). Throughout the 150 m of limestones in MS Unit 5, the point load test data also show considerable scatter, ranging from 0.3 to 6.0. In general, significant strength anisotropy is indicated, with diametral PLT generally less than 1/3 of the axial PLT.

Table 5.18: MS Unit 5 (Sherman Fall and Kirkfield formations): Estimated Geomechanical Parameters in Uniaxial Compression

Parameter	Mean	Range	Estimate
Peak UCS	55 MPa	32 - 113 MPa	45 MPa
Crack Initiation	35% (UCS)	6 – 48% (UCS)	25% (UCS)
Crack Damage	73% (UCS)	35 - 100% (UCS)	~65% (UCS)
Modulus of Elasticity (E_{40})	24 GPa	5 – 46 GPa	15 GPa
Poisson's Ratio	0.21	0.03 – 0.47	0.25
PLT Strength Anisotropy throughout MS Unit 5. (Diametral/Axial)	High	0.1 – 2.0	~0.4
Long-Term Strength	No data	No data	No data

5.9.1.2 Tension

A total of six indirect (Brazilian) tension tests were conducted on rock cores from the Sherman Fall Formation, five of which resulted in mixed-mode failure as shown in Figure 5.33. With one exception, results were relatively consistent, indicating indirect tensile strength for the intact material of approximately 4 MPa.

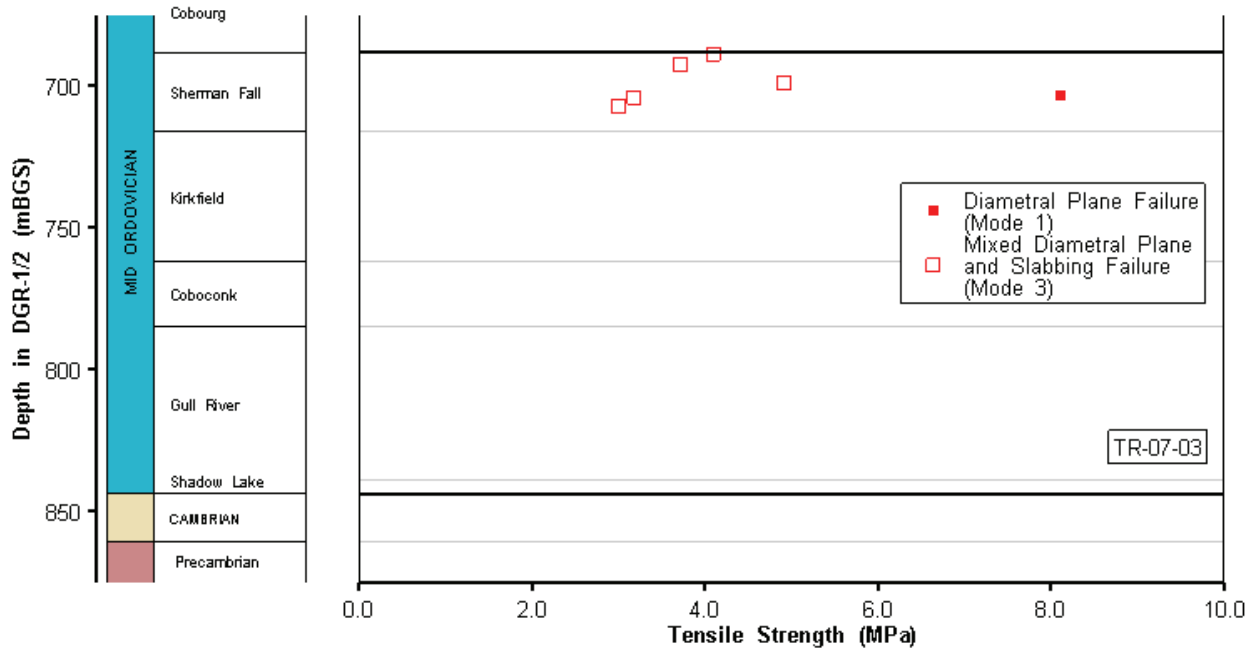

Figure 5.33: MS Unit 5: Brazilian Tests - Indirect Tensile Strength Data

5.9.1.3 Shear

Results from nine sets of direct shear tests on core samples from the Sherman Fall and Kirkfield formations, four of which were intact, are summarized in Figure 5.34. Peak shear strength parallel to bedding was determined for the four intact samples, and staged shear tests were conducted on all samples to evaluate residual shear strength parameters. The best-fit line for the residual shear strength indicates zero apparent cohesion, but a relatively high residual friction angle of ~42 degrees. These data suggest that while there is little or no cohesion along the bedding planes in this argillaceous limestone formation, there may be a significant geometric component to the apparent residual friction angle due to waviness of the bedding planes. Under conditions of higher normal stress, the residual friction angle may decrease, with a related increase in the apparent cohesion. Estimated residual shear strength parameters for normal stresses within the testing range are:

- Apparent cohesion = 0 MPa; and
- Residual friction angle = 40 degrees.

For the intact samples, tested under a normal stress of ~1 MPa, a cohesion value of ~3 MPa appears reasonable. Test data for intact shear strength are too limited to allow a separate best-fit envelope to be determined for peak shear strength. For purposes of this DGSM report, it has been conservatively assumed that the angle of internal friction is equal to the residual angle noted above, with a cohesion intercept of 3 MPa, giving an estimated peak shear strength envelope of:

- $\tau_p = 3.0 + \sigma_n(\tan 40)$, MPa.

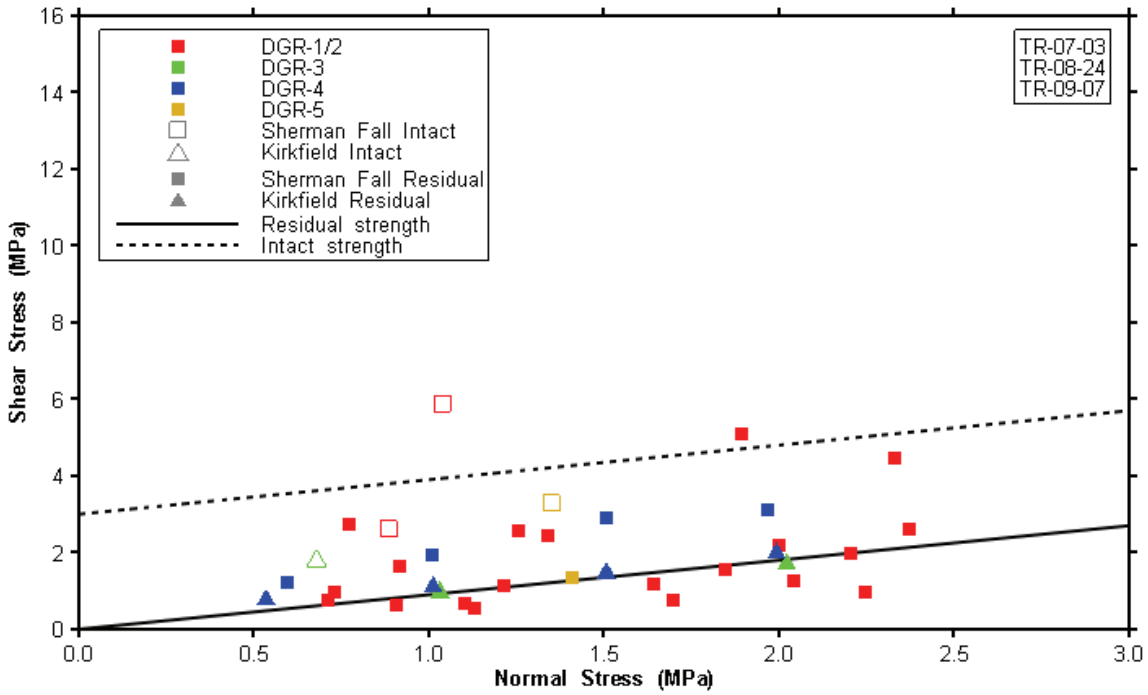

Figure 5.34: MS Unit 5: Direct Shear Test Results for Sherman Fall and Kirkfield Formations

5.9.1.4 Slake Durability

Six samples from within MS Unit 5 were selected for slake durability testing. The results, summarized in Figure 5.35, indicate minor to negligible susceptibility to slaking degradation.

In the Sherman Fall Formation, the slake durability index (SDI) value was approximately 85%, whereas in the lower units beneath the Sherman Fall, the SDI was close to 100%.

5.9.1.5 Swelling Potential

Single swelling potential tests were conducted on Sherman Fall rock material in fresh water and in formation water respectively. Swelling potential was observed to be zero in both cases.

5.9.1.6 Abrasiveness

No data were obtained regarding abrasivity of rock materials in MS Unit 5 as part of Phase 1, 2A and 2B site investigations.

5.9.1.7 Dynamic Properties

There are relatively few data available regarding dynamic elastic properties based on ultrasonic pulse velocity testing of intact core samples from the MS Unit 5. Seven core samples from the Sherman Fall Formation, six from the Kirkfield Formation, two from the Coboconk Formation, two from the Gull River Formation and two from the Cambrian, for a total of 19 samples, were tested in the CANMET laboratory (TR-07-03, TR-08-24, TR-09-07). Additionally ten core samples from the Gull River Formation were tested in the field (TR-07-03). Based on overall review of these data, estimated values are given in Table 5.19 for rock material comprising MS Unit 5.

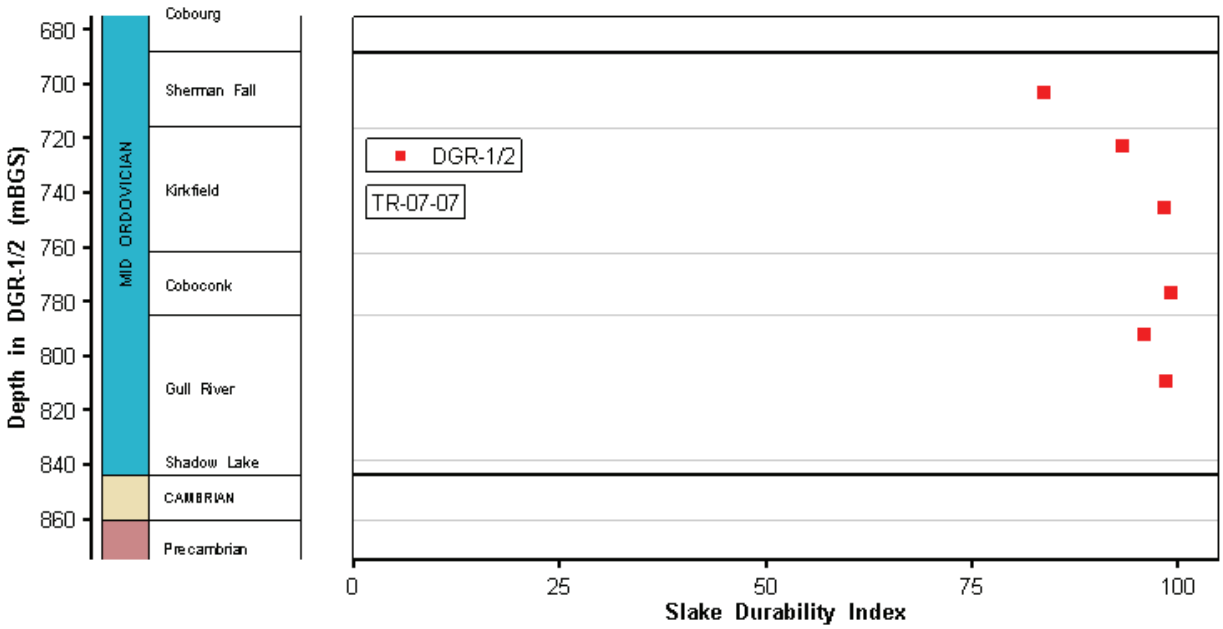

Figure 5.35: MS Unit 5: Slake Durability Index

Table 5.19: MS Unit 5: Estimated Rock Material Dynamic Properties

Parameter	Estimated Value
P-wave Velocity	4.5 km/s
S-wave Velocity	2.3 km/s
Dynamic Modulus of Elasticity	40 GPa
Dynamic Shear Modulus	15 GPa
Dynamic Poisson's Ratio	0.30

5.9.2 Rock Mass Geomechanical Characteristics

Access for geomechanical mapping of the rock mass beneath the Bruce nuclear site was not available during the Phase 1, 2A and 2B site investigations. Consequently, information regarding the characteristics of the overall rock mass has been derived only from the relatively small diameter, one-dimensional penetrations provided by the DGR boreholes, and the resulting core. As the overall geomechanical characteristics of the rock mass depend in part on the three-dimensional characteristics of the fracture patterns (discontinuities) within the rock mass, information on the overall rock mass characteristics is limited at the current stage, even with the fracture analysis from inclined boreholes DGR-5 and DGR-6. Total horizontal sampling distances for mapping of inclined fractures in MS Unit 4 was limited to 15.9 m in DGR-5 and 67.0 m in DGR-6.

5.9.2.1 Rock Quality Designation, Fracture Frequency and Fracture Sets

Measurements of Rock Mass Quality Designation (RQD) and fracture frequency were conducted routinely throughout the drilling of DGR boreholes as reported in Section 3.6 and summarized in Table 3.4 and Figures 3.3 and 3.4. Core recovery and RQD values throughout the MS Unit 5 were generally excellent, with the exception of some local zones in the Kirkfield Formation where the RQD dropped to as low as 28% over a short section in DGR-2 due to core grinding during drilling. Fracture frequency measurements indicated a generally very sparsely fractured rock mass, with the exception of the deep-lying Cambrian sandstone, which appeared to be sparsely to moderately fractured. Based on these borehole-derived measurements, the overall rock mass comprising the MS Unit 5 can be characterized as very sparsely fractured and of excellent quality. However, it is noted that minor local zones of lower quality may occur in the Sherman Fall Formation.

Oriented core logging completed in inclined boreholes DGR-5 and DGR-6 (TR-09-09) provides a preliminary indication of the occurrence and spacing of inclined fractures in MS Unit 5. A total of 10 natural fractures were logged in DGR-5 and DGR-6 core. The contoured equal area plot of all natural fractures logged in DGR-5 and DGR-6 core is shown in Figure 5.36. Figure 5.36 plots the fracture occurrence in MS Unit 5 considering Terzaghi (1965) sampling bias.

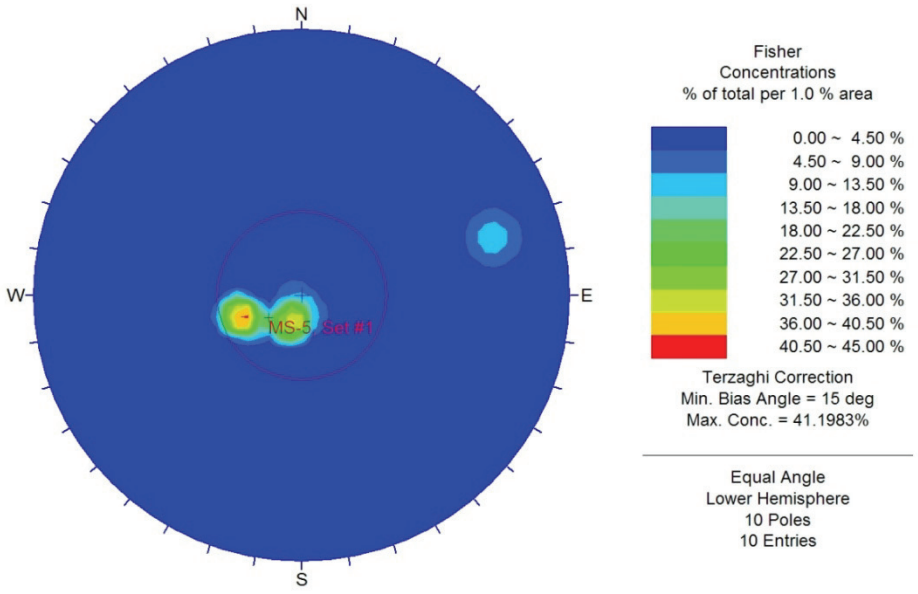

Figure 5.36: Contoured Equal Area Polar Plot of All Natural Fractures in DGR-5 and DGR-6 Core in MS Unit 5

Similar to the results of MS Unit 4, the polar plot shows the presence of only one sub-horizontal fracture set in MS Unit 5 that represents the discontinuities along the bedding planes. The average weighted fracture set orientation, including number of occurrences and arithmetic average discontinuity spacing for MS Unit 5 are presented in Table 5.20.

Table 5.20: Natural Fracture Set Orientation and Spacing in MS Unit 5 from Oriented Core Logging in DGR-5 and DGR-6

Fracture Set	Number of Occurrences	Strike	Dip	Average Discontinuity Spacing (m)
MS Unit 5, Set #1	9	N34°W	17°NE	7.6
Miscellaneous	1	--	--	--

In interpreting the results of oriented core logging it is important to remember that borehole DGR-5 was terminated within the bottom of the Kirkfield Formation, and borehole DGR-6 was terminated within the upper part of the Gull River Formation. Consequently the fracture information presented for MS Unit 5 from boreholes DGR-5 and DGR-6 is most representative of the Sherman Fall and Kirkfield formations and to a lesser extent the Coboconk Formation.

5.9.2.2 Bulk Properties from Geophysical Logging

Elastic dynamic properties of bulk in situ samples of the rock mass are derived from downhole sonic logging. A uniform bulk density of 2.63 g/cm^3 (Figure 4.1) was used in all modulus calculations. Results are summarized in Table 5.21 for various depth intervals within the MS Unit 5 based on logging in DGR-2, DGR-3 and DGR-4.

Table 5.21: MS Unit 5: Estimated Rock Mass Dynamic Properties

Formation	Depth Range (mBGS)	V_p (m/s)	V_s (m/s)	E_d (GPa)	G_d (GPa)
Sherman Fall, Kirkfield	688.10 – 731.99	5280	2760	51.6	19.5
Kirkfield	732.00 – 761.99	5150	2660	49.8	18.9
Coboconk	762.00 – 768.62	5750	3160	68.7	26.8
Coboconk	768.63 – 778.74	6380	3380	69.6	30.7
Coboconk, Gull River	778.75 – 843.69	5740	3080	65.7	25.3

5.9.2.3 Rock Mass Classification

Subsurface data obtained from DGR boreholes in the Phase 1, 2A and 2B investigations are judged not sufficient to provide complete estimates of all the parameter values required to determine the classification categories under the commonly used rock mass classification systems. Preliminary descriptive comments regarding rock mass quality are included under Section 5.9.2.1 above, based on the limited parameters of Rock Quality Designation (RQD) and one-dimensional fracture frequency. These data indicate a rock mass that is very sparsely fractured and of excellent quality.

Results of oriented core logging in DGR-5 and DGR-6, indicate one fracture set with average spacing of 7.6 m. These wide fracture spacings, in conjunction with rock material and rock mass geomechanical properties described above, indicate a rock mass of excellent quality. Rock mass classification ratings or indices have not been developed based on the limited horizontal sampling distances available from DGR boreholes.

5.10 Representative Estimates of Descriptive Geomechanical Model Properties

Tables 5.22, 5.23 and 5.24 summarize the representative estimates of the main geomechanical properties of the 34 layers that comprise the descriptive geomechanical model for the Bruce DGR site. The descriptive geomechanical model includes the 36 model layers that comprise the descriptive geological model minus the overburden and Precambrian layers. However, for some model layers (i.e., those below the Kirkfield Formation), there is very limited to no geomechanical data available as these layers are deeper than planned excavation. Data given in Tables 5.22, 5.23 and 5.24 are consistent with and provide a more detailed summary description of the geomechanical information given in Sections 5.5 to 5.9 on the five mechano-stratigraphic units that represent the Bruce DGR site.

Table 5.22 summarizes the representative estimates of strength properties of intact core from each model layer based on uniaxial compression testing (TR-07-03, TR-08-24, TR-08-39, TR-09-07), including some long-term strength testing results (TR-08-11, TR-08-36). Table 5.22 lists estimates of peak uniaxial compression strength, crack initiation and crack damage stress (as a percentage of peak UCS), modulus of elasticity (E_{40}), Poisson's ratio and estimates of strength anisotropy based on results of diametral and axial point load testing based on arithmetic averages of these parameters. Limited uniaxial strength data are available for model layers below the Kirkfield Formation and no strength data are available for several thin units (Salina E, D, B anhydrite, A2 evaporite and A1 evaporite) and formations (Gasport, Lions Head and Fossil Hill).

Table 5.22: Representative Estimates of Uniaxial Compression Strength Properties of Geomechanical Model Layers

Model Layer	Peak UCS (MPa)	Crack Initiation (% UCS)	Crack Damage (% UCS)	Modulus of Elasticity (GPa)	Poisson's Ratio (-)	PLT Anisotropy (Dia/Axial)
Lucas	98	40	76	50	0.20	1.0
Amherstburg	98	40	76	28	0.20	1.0
Bois Blanc	94	42	87	37	0.20	1.0
Bass Islands	48	39	32	20	0.50	0.95
Salina G Unit	34	40	50	16	0.23	1.0
Salina F Unit	30	42	95	12	0.20	0.70
Salina E Unit	-	-	-	-	-	0.65
Salina D Unit	-	-	-	-	-	1.0
Salina C Unit	20	38	68	9	0.20	0.70
Salina B Unit dolostone	8	32	44	3	0.40	0.55
Salina B Unit anhydrite	-	-	-	-	-	-
Salina A2 Unit dolostone	60	45	80	23	0.20	0.85
Salina A2 Unit evaporite	-	-	-	-	-	0.55
Salina A1 Unit dolostone	117	40	90	40	0.15	0.40
Salina A1 Unit evaporite	-	-	-	-	-	0.35
Salina A0 Unit	198	41	63	63	0.43	1.0
Guelph	60	40	72	28	0.30	0.80
Goat Island	148	39	81	37	0.37	0.90
Gasport	-	-	-	-	-	0.95
Lions Head	-	-	-	-	-	0.95
Fossil Hill	-	-	-	-	-	0.50
Cabot Head	13	42	60	4	0.38	0.55
Manitoulin	71	50	63	24	0.45	0.35
Queenston	48	40	68	15	0.31	0.60
Georgian Bay	41	42	77	11	0.22	0.50
Blue Mountain	22	38	87	5	0.10	0.55
Cobourg – Collingwood Member	107	40	86	30	0.22	1.0
Cobourg - Lower	113	40	85	40	0.31	0.95
Sherman Fall	52	33	73	22	0.23	0.45
Kirkfield	58	38	75	23	0.18	0.45

Note: - Not measured or not determined.

Table 5.23 summarizes the representative estimates of slaking, swelling and abrasivity properties of each model layer, where such data are available. Estimates of slaking potential are presented as slake durability indices based on field testing (TR- 07-07, TR-08-14) of layers with abundant sheet silicates or clays. Estimates of swelling potential are presented as vertical and horizontal swelling in fresh water in % per log cycle (TR-07-16, TR-08-26) for major shale-containing layers. Estimates of rock abrasivity are presented only for the Collingwood Member and the Cobourg Formation as CERCHAR abrasivity indices for smooth surfaces (TR-07-04, TR-08-25).

Table 5.23: Representative Estimates of Slaking, Swelling and Abrasivity Properties of Geomechanical Model Layers

Model Layer	Slake Durability Index (%)	Fresh Water Swelling Potential (% per log cycle)		CERCHAR Abrasivity Index – Smooth Surfaces
		Vertical	Horizontal	
Lucas	-	-	-	-
Amherstburg	100	-	-	-
Bois Blanc	-	-	-	-
Bass Islands	95	-	-	-
Salina G Unit	50	-	-	-
Salina F Unit	80	1.5	0.5	-
Salina E Unit	-	-	-	-
Salina D Unit	55	-	-	-
Salina C Unit	-	1.0	0.4	-
Salina B Unit dolostone	-	-	-	-
Salina B Unit anhydrite	-	-	-	-
Salina A2 Unit dolostone	-	-	-	-
Salina A2 Unit evaporite	-	-	-	-
Salina A1 Unit dolostone	-	-	-	-
Salina A1 Unit evaporite	--	-	-	-
Salina A0 Unit	-	-	-	-
Guelph	-	-		-
Goat Island	-	-	-	-
Gasport	-		-	-
Lions Head	-	-	-	-
Fossil Hill	-	-	-	-
Cabot Head	75	2.0	0.6	-
Manitoulin	-	-	-	-
Queenston	90	0.3	0.1	-

Model Layer	Slake Durability Index (%)	Fresh Water Swelling Potential (% per log cycle)		CERCHAR Abrasivity Index – Smooth Surfaces
		Vertical	Horizontal	
Georgian Bay	75	1.0	0.3	-
Blue Mountain	90	1.0	0.15	-
Cobourg – Collingwood Member	95	-	-	0.6
Cobourg - Lower	100	0	0	0.85
Sherman Fall	85	0	0	-
Kirkfield	90	-	-	-

Note: - Not measured or not determined.

Table 5.24 summarizes the representative estimates of rock mass geomechanical properties for each layer of the geomechanical site model. Table 5.24 provides estimates of rock quality as RQD and natural fracture frequency from Table 3.4 based on core logging (TR-07-06, TR-08-13, TR-09-01). Estimates of in situ rock mass dynamic elastic and shear moduli are given in Table 5.24 based on analysis of P-wave and S-wave velocities measured during borehole geophysical logging of DGR boreholes.

Table 5.24: Representative Estimates of Rock Mass Quality, Natural Fracture Frequency and Dynamic Moduli Properties of Geomechanical Model Layers

Model Layer	RQD (%)	Natural Fracture Frequency (m^{-1})	Dynamic Modulus of Elasticity (GPa)	Dynamic Shear Modulus (GPa)
Lucas	47	5.4	36.7	13.5
Amherstburg	47	5.4	33.9	19.8
Bois Blanc	68	3.6	45.4	18.9
Bass Islands	34	2.7	46.0	19.3
Salina G Unit	54	3.8	28.3	11.1
Salina F Unit	90	0.9	35.3	14.3
Salina E Unit	96	0.8	47.4	18.4
Salina D Unit	98	0.2	27.5	16.5
Salina C Unit	98	0.2	27.5	16.5
Salina B Unit dolostone	97	0.5	31.4	12.1
Salina B Unit anhydrite	97	0.5	31.4	23.2
Salina A2 Unit dolostone	96	0.4	38.7	15.2
Salina A2 Unit evaporite	96	0.4	38.7	15.2
Salina A1 Unit dolostone	99	0.2	53.2	20.7
Salina A1 Unit evaporite	99	0.2	54.8	24.0

Model Layer	RQD (%)	Natural Fracture Frequency (m^{-1})	Dynamic Modulus of Elasticity (GPa)	Dynamic Shear Modulus (GPa)
Salina A0 Unit	99	0.2	51.7	19.9
Guelph	99	0.2	51.7	19.9
Goat Island	99	0.2	51.7	19.9
Gasport	99	0.2	57.3	21.8
Lions Head	99	0.2	60.9	23.1
Fossil Hill	99	0.2	60.9	23.1
Cabot Head	94	0.1	31.2	12.4
Manitoulin	99	0.2	54.8	21.5
Queenston	98	0.2	33.7	12.9
Georgian Bay	97	0.2	27.6	10.8
Blue Mountain	97	0.2	17.5	19.2
Cobourg – Collingwood Member	99	0.4	44.3	16.7
Cobourg - Lower	99	0.1	57.9	21.8
Sherman Fall	99	0.2	51.6	19.5
Kirkfield	98	0.2	49.8	18.9
Coboconk	98	0.3	69.6	30.7
Gull River	99	0.2	65.7	25.3
Shadow Lake	98	0.4	65.7	25.3
Cambrian	96	0.3	-	-

Note: - Not measured or not determined.

5.11 Confidence Assessment of Geomechanical Data and Model

Confidence in the descriptive geomechanical site model presented in Chapter 5 is assessed based on an evaluation of the quality and uncertainty in the key data that comprise the model, consistency of the data sets that comprise the model and consistency of the geomechanical model with other geoscientific models presented in Chapter 3 (descriptive geological site model) and Chapter 4 (descriptive hydrogeological site model).

The following key geomechanical data sets are subject to confidence assessment:

- In situ stresses;
- Rock material strength properties;
- Rock slaking properties;
- Rock swelling properties;
- Rock abrasivity properties; and
- Rock mass geomechanical properties.

5.11.1 In Situ Stresses

Confidence in the reported in situ stresses of the model layers that comprise the descriptive geomechanical model is judged to be moderate to low. This assessment of confidence is due to the fact that in situ stresses have not been directly measured at the depths of interest, rather they have been estimated based on compilation of regional stress measurement data, on geomechanical modeling, and on the observed lack of borehole breakouts in DGR boreholes based on certain assumptions concerning the long-term strength of the borehole walls.

Although confidence in the reported in situ stresses is moderate to low, these stress estimates represent the best available at this time. The fact that no rock failure has been observed in the boreholes, which represent “trial excavations”, provides empirical confidence that the in situ stresses are moderate relative to the in situ strength of the rock materials.

5.11.2 Rock Material Strength Properties

Confidence in the reported strength properties of intact rock material of the model layers that comprise the descriptive geomechanical model is judged to be moderate to high. All laboratory strength testing was completed by CANMET Mining and Mineral Science Laboratories following Standard Operating Procedures based on established ASTM testing procedures.

Strength testing was completed on core samples recovered from all DGR boreholes. Review of the strength data shows that there is no significant variation in strength properties between different DGR boreholes. Consequently, the reported strength properties are judged to representative of conditions at the DGR site. In general, the measured strength properties correlate well with expectations based on precedent data for similar lithologies.

For the majority of model layers where collection of intact rock cores suitable for laboratory testing was easily undertaken, the resulting strength parameters are of high quality. For those formations that were subject to extensive disking of core that influenced the ability to collect intact core samples suitable for testing (e.g., parts of the Georgian Bay Formation, the Blue Mountain Formation and the Collingwood Member), the resultant strength properties may be biased towards stronger materials and hence overall confidence in the strength properties of these model layers is considered moderate.

5.11.3 Rock Slaking Properties

Confidence in the reported slaking properties of intact rock material of the model layers that comprise the descriptive geomechanical model is judged to be high. All slaking tests were completed in the field in accordance with ASTM testing and analysis procedures.

Slake durability testing was completed on samples collected from all DGR boreholes. Review of the slake durability test data shows that there is no discernable variation in slaking properties between different DGR boreholes. Consequently, the reported slaking properties are judged to be representative of conditions at the DGR site. In general, the measured slaking properties correlate well with expectations based on precedent data for rock units with sheet silicate or clay contents.

5.11.4 Rock Swelling Properties

Confidence in the reported swelling properties of intact rock material of the model layers that comprise the descriptive geomechanical model is judged to be moderate to high. All laboratory

swell testing was completed by K.Y. Lo Inc. following standard testing procedures that were pioneered by Dr. Lo in the late 1970s. These testing procedures have been routinely used in assessment of swelling potential of clay-rich rocks throughout Ontario. Swelling potential was originally assessed with both synthetic formation water and fresh water for DGR-2 core and later only in fresh water for DGR-3 and DGR-4 core due to lack of observed swelling with formation water.

Swell testing was completed on samples from all DGR boreholes. Review of the swelling test data shows that there is no discernable variation in swelling properties between different DGR boreholes. Consequently, the reported swelling properties are judged to be representative of conditions at the DGR site. In general, the measured swelling properties correlate well with expectations based on precedent data on the reported calcite contents of different rocks.

Similar to rock strength testing, a high confidence rating is assigned to formations that did not show extensive disking (i.e., Salina F Unit, Salina C Unit, Cabot Head, Queenston, Georgian Bay, Cobourg and Sherman Fall formations) and hence allowed for sample preparation for swell testing. A moderate confidence assessment is provided for the swelling potential of the Blue Mountain shales due to the difficulties in maintaining sample integrity during sample preparation and swell testing.

5.11.5 Rock Abrasivity Properties

Confidence in the reported abrasivity properties of intact rock material of the Collingwood Member and Cobourg Formation is judged to be high. All laboratory abrasivity testing was completed by Mirarco/Geomechanics Research Centre, Laurentian University following the widely accepted and standard CERCHAR testing procedures.

Abrasivity testing was completed on samples from all DGR boreholes. Review of the abrasivity test data shows that there is no discernable variation in abrasivity properties between different DGR boreholes. Consequently, the reported abrasivity properties are judged to representative of conditions at the DGR site.

5.11.6 Rock Mass Geomechanical Properties

Confidence in the reported rock mass geomechanical properties of the model layers that comprise the descriptive geomechanical model is judged to be moderate to high. The rock mass geomechanical properties considered here are rock quality, discontinuity characteristics and bulk elastic properties.

While currently available data on rock quality and discontinuity occurrence as expressed by reported RQD and natural fracture frequency are of high quality, these data have been collected primarily from vertical boreholes. As the overall geomechanical characteristics of the rock mass depend in part on the three-dimensional characteristics of the fracture patterns within the rock mass, information on the characteristics of inclined discontinuities is necessary to improve confidence in the assessment of overall rock mass characteristics from moderate to high. While the results of oriented core logging of DGR-5 and DGR-6 suggest the presence of widely-spaced inclined fractures that would not affect the overall assessment of rock mass geomechanical properties based on data from vertical boreholes, the total horizontal sampling length in DGR-5 and DGR-6 is somewhat limited. Consequently, confidence in the rock mass quality and discontinuity characteristics are judged to be moderate to high.

As described in the descriptive geological site model (Section 3.4.15), confidence in the characterization of minor structural features, such as simple fractures (e.g., joints), is judged to be high for subhorizontal features and moderate for inclined and subvertical features based on current borehole data. These data have been reported for all DGR boreholes and the available data do not show any discernable variability between boreholes. In particular the fracture occurrence and rock quality determined from inclined boreholes DGR-5 and DGR-6 are not noticeably different than from vertical boreholes DGR-1 to DGR-4. Consequently, the reported rock quality and natural fracture frequency based on logging of discontinuity properties in DGR boreholes are judged to be representative of conditions at the DGR site.

Bulk elastic properties of the rock mass are reported based on interpretation of sonic borehole geophysical logging. Although not reported here on an individual borehole basis, the bulk estimates of elastic properties are similar in all DGR boreholes and comparable to estimates reported from P- and S-wave testing of intact cores. As the bulk elastic properties of the rock mass are unlikely to be anisotropic, confidence in the estimates of bulk elastic properties of the layers that comprise the geomechanical site model is judged to be high.

6. SUMMARY

This report describes the Descriptive Geosphere Site Model (DGSM) developed based on the results of Phase 1, 2A and 2B of the GSCP. The GSCP is a three-phase, multi-year program plan designed for iterative development, testing and refinement of site-specific descriptive geosphere models, that was released in April, 2006 and updated in April, 2008. Phase 1, 2A and 2B of GSCP activities were completed in the period August 2006 to June 2010.

The DGSM described in this document summarizes the current understanding of underground geological, hydrogeological and geomechanical conditions of the Bruce nuclear site relevant to DGR repository engineering and safety assessment functions. The geological, hydrogeological and geomechanical site conditions are presented through the development of individual descriptive geological, hydrogeological and geomechanical models of the Bruce nuclear site.

6.1 Descriptive Geological Site Model

The geological site model describes the occurrence and the lithological and structural characteristics of 34 distinct sedimentary bedrock formations, members or units extending from near ground surface to a depth of about 860 metres below ground surface (mBGS) based on drilling, logging and testing of six deep cored boreholes, DGR-1, DGR-2, DGR-3, DGR-4, DGR-5 and DGR-6, and data from several shallow (maximum 200 m depth) Underground Storage (US-) series boreholes. The geological site model provides the framework for hydrogeological and geomechanical models of the Bruce nuclear site. The reference Bruce site stratigraphy from surface to depth at DGR-1 and DGR-2 (see Figure 6.1) comprises: 20 m of recent Pleistocene overburden deposits, 104.0 m of Devonian dolostone, 323.7 m of Silurian dolostone, argillaceous dolostone, shale and evaporite, 211.8 m of Upper Ordovician shale, 179.1 m of Middle Ordovician argillaceous limestone, 5.2 m of Ordovician siltstone and sandstone, 16.9 m of Cambrian sandstone, and Precambrian granitic gneiss.

Logging of boreholes DGR-1 to DGR-6 identified the presence of several important marker beds and 34 distinguishable sedimentary bedrock formations, members or units at the Bruce DGR site. In general, the thickness and orientation of these 34 strata are remarkably uniform between the DGR boreholes separated by up to 1318 m. The thickness and orientation of formations are somewhat variable above the Salina B Unit. This is most likely due to collapse and minor rotation of the overlying bedrock following paleo-dissolution of the Salina B and D Unit salt beds. Below the B Unit the average strike and dip of the deeper Silurian and the Ordovician formations at the Bruce site (N20°W/0.6°SW) is consistent with regional geological mapping of Armstrong and Carter (2006) and with site predictions developed based on the drilling and logging records of the Texaco No. 6 oil and gas exploration well located 2.9 km southeast of the Bruce nuclear site.

Detailed core logging and borehole geophysical logging of DGR- and US-series boreholes show that that Devonian and Upper Silurian dolostones are moderately to highly fractured and of poor to fair rock quality designation (RQD), whereas the deeper Silurian formations below the Salina G Unit and the Ordovician shales (Figure 6.2) that overlie the DGR host formation (Cobourg), the host Cobourg Formation (Figure 6.3) and the argillaceous limestones below the host formation are very sparsely fractured to unfractured with excellent RQD. Many of the low core

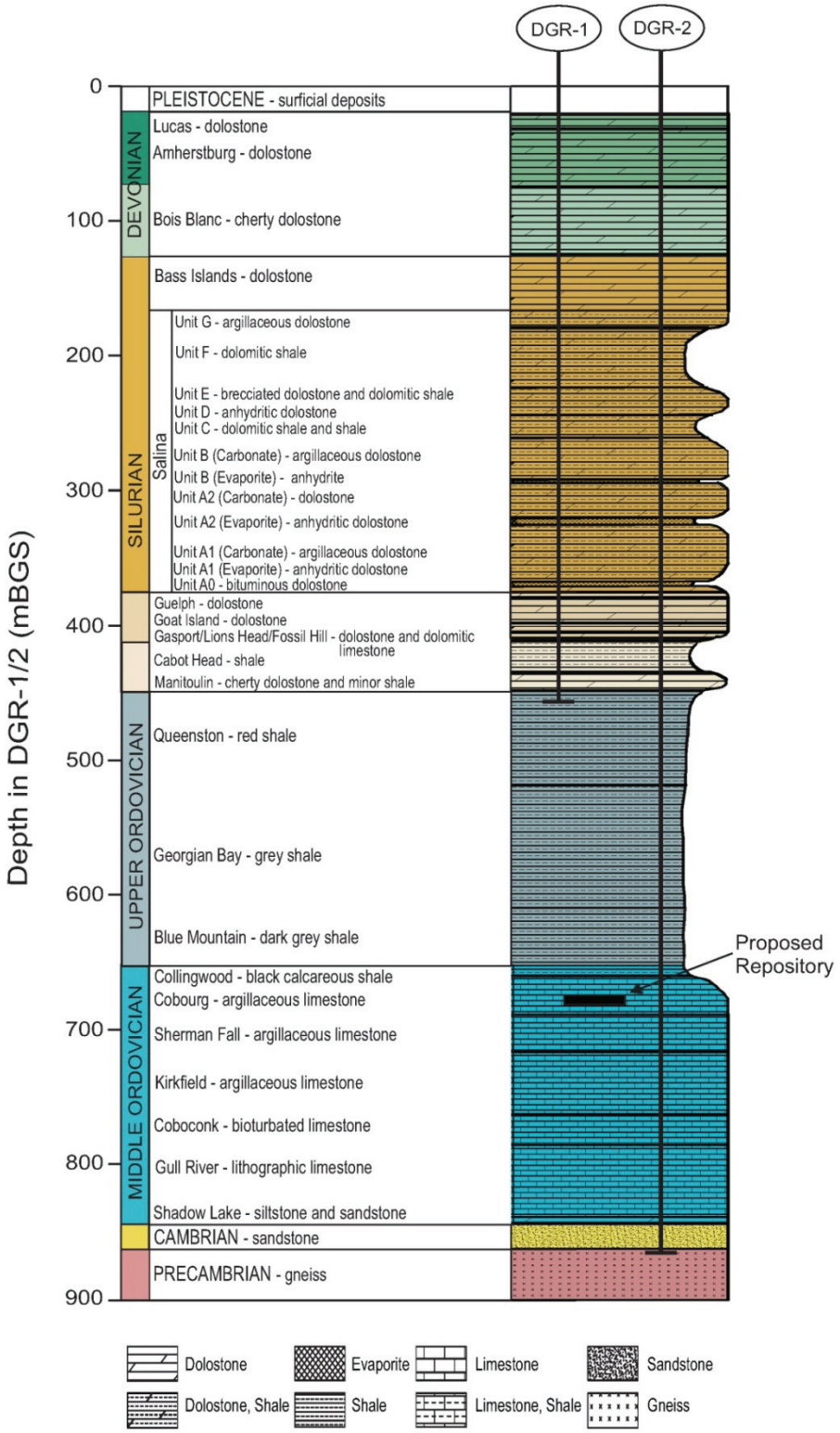

Figure 6.1: Reference Stratigraphic Column at the Bruce Nuclear Site Based on DGR-1 and DGR-2 Borehole Data

recoveries and RQDs recorded for the Lower Devonian and Upper Silurian dolostones were attributed to difficult drilling conditions created, in part, by alternating hard and soft beds within these formations. Occasional natural fractures, that were commonly sealed and tight, were also identified within the deeper Silurian and Ordovician formations. Natural fracture frequency was greater in the Cambrian sandstone. Natural fractures within the Cambrian are open and permeable.

Note: Left: Queenston Formation, 475.73-478.78 mBGS in DGR-3, Right: Blue Mountain Formation, 619.08-622.13 mBGS in DGR-4.

Figure 6.2: Examples of Excellent Quality of Ordovician Shale Barrier Rocks

Logging of recovered core and acoustic imaging of the borehole walls of DGR boreholes identified the presence of inclined fractures. Most of the inclined fractures were found within the Devonian and Upper Silurian dolostones. The total number of inclined fractures identified in boreholes DGR-1 to DGR-6 within the Ordovician shales and limestones ranged from 132 from core logging to 38 from borehole wall imaging. Analysis of the identified inclined fractures in the Ordovician shales and limestones suggests they preferentially strike in east-northeast to northeast and west-northwest directions, somewhat similar to joint strikes reported for outcrops in adjacent Inverhuron Park and the lower Bruce peninsula. A lack of measurable offset along these fractures indicates that they can be classified as joints where unfilled with secondary minerals and veins where filled. Both joints and veins are found at the DGR site.

Intact core samples and a limited number of samples of vein infilling material were analysed for mineralogy and geochemistry using laboratory test methods including thin section petrography with electron microscope analyses, whole rock and clay fraction XRD testing, scanning electron microscope/energy dispersive spectral (SEM/EDS) analyses, trace element inductively coupled plasma (ICP) analyses, elemental oxide analyses by ICP optical emission spectrometry, carbon and sulphur infrared spectroscopy analyses, and chloride by instrumental neutron activation analyses. These detailed analyses generally confirm the strata mineralogy as defined by Armstrong and Carter (2006).

The laboratory testing of intact cores shows that the Devonian and Upper Silurian carbonate sequences are predominately dolostone with some minor limestone-rich layers and minor occurrence of sheet silicates as illite. Parts of the Cabot Head Formation shale are locally calcareous and dolomitized and the Queenston Formation shale is both calcareous and dolomitized particularly in upper parts of the formation. The Georgian Bay, Blue Mountain and Collingwood shales also show dolomite presence. The deepest Paleozoic strata comprising the Cambrian and overlying Shadow Lake Formation and the lower parts of the Gull River Formation, also show presence of stratiform and matrix dolomitization.

Figure 6.3: Intact Core Run from the Approximate Repository Depth in the Cobourg Formation in DGR-3

The clay content of the bedrock sequence in the DGR Paleozoic sequence, as reported by total sheet silicates based on XRD analyses, ranges from zero for the Devonian and Upper Silurian dolostones to 15 wt% to 70 wt% within the Silurian Cabot Head Formation and the Ordovician shales of the Queenston, Georgian Bay and Blue Mountain formations. The clay content of the

Ordovician limestones is typically less than 20%. The total sheet silicates within the Precambrian basement are not clays, but are micaceous minerals including biotite and muscovite. The clay minerals identified in the Ordovician shales are predominately illite and mica (>50% of clay minerals), chlorite (20-45%) with minor interstratified illite/smectite and kaolinite. Figure 6.4 summarizes the calcite and sheet silicate content of DGR rock based on 197 XRD analyses of core collected from DGR-1 to DGR-6.

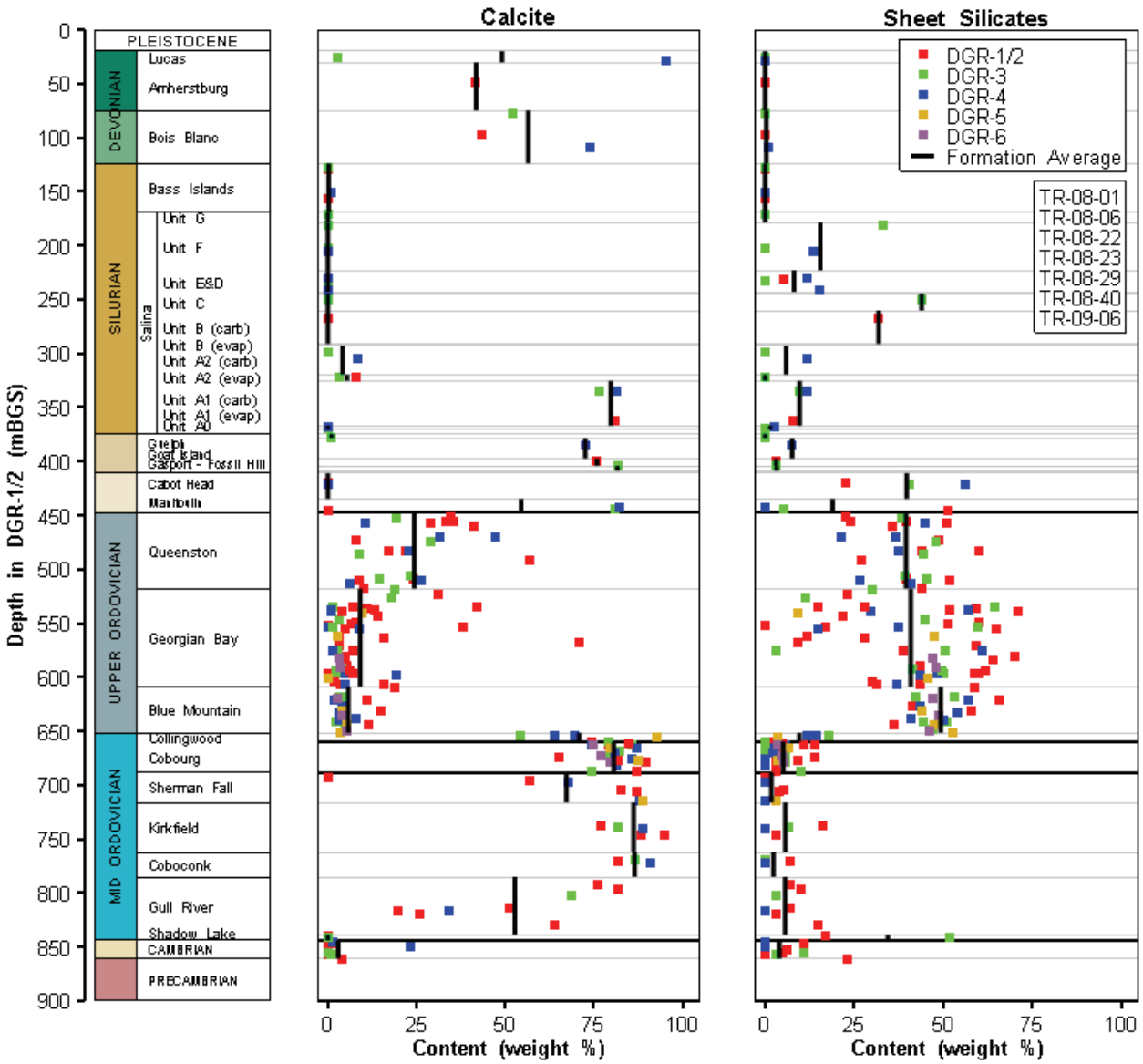

Note: Plots show point data and arithmetic formation averages.

Figure 6.4: Depth Profile of Calcite and Total Sheet Silicates (Clay) Contents Based on XRD Analyses of 197 Core Samples

The organic geochemistry of the Ordovician shales was characterised by standard source rock evaluation methods ('Rock-Eval' pyrolysis) and by measurement of the total organic carbon (TOC as wt %), presumably present as kerogen. TOC concentrations in the Silurian dolostones are <0.25 %, while in the middle Ordovician limestones they are typically ≤ 0.6%. However, in the Ordovician shales TOC increases with depth from 0.1% in the oxidised Queenston to ~ 2.5% in the lower Blue Mountain and Collingwood shales. The pyrolysis data indicate that this deeper organic matter is a Type II kerogen, typical of marine shales, whereas the TOC in the shallower Queenston and Georgian Bay formations suggests a more gas-prone Type III kerogen. The hydrocarbon identified in the lowermost Blue Mountain and Collingwood shales is associated with methane that originates from biogenic acetate fermentation. Thermal maturity values for this organic carbon indicate high in situ temperatures during maturation – probably between 70 and 130°C. The oil that has been observed to bleed from discrete zones within the Coboconk, Gull River and Shadow Lake formations is associated with thermocatalytic methane.

Core logging, laboratory petrography, SEM/EDS and XRD analyses identified the presence of fracture infill, vein and secondary mineralogy in DGR cores. Chert, quartz, calcite, pyrite, anhydrite, gypsum, halite, celestite, illite, chlorite, marcasite and Fe oxide/hydroxide were identified. Several of these minerals (e.g., halite, gypsum, anhydrite and celestite) are soluble and their occurrence is important to interpretation of core porewater analyses and as an indicator of the absence of groundwater flow through these discontinuities. Some Silurian formations are predominately composed of sulphate minerals, e.g., the Salina A1 and A2 Evaporite Units. Anhydrite was frequently found within the Upper Silurian dolostones and appears to be present in trace amounts in the Middle Ordovician limestones. Gypsum was preferentially observed within the Salina G to A2 Units and occasionally within deeper Lower Silurian and Upper Ordovician shales. Halite was frequently detected as fracture-infill and grain-boundary materials in the Ordovician shales (Queenston, Georgian Bay and Blue Mountain formations). It was also detected by SEM/EDS within the rock matrix of the overlying Silurian formations, such as the Salina E and A1 dolostones, the Salina C and Cabot Head shales, the Guelph and Manitoulin formation dolostones, and Gasport dolomitic limestone and in the underlying Ordovician Cobourg and Sherman Fall and Gull River formation limestones.

In addition to carbonate and evaporite minerals, oxides and sulphides are detected throughout the Paleozoic sequence in minor amounts with some notable exceptions. For example, the Cambrian contains quartz at up to 85% of the middle and lower sections of this formation. The quartz identified in the carbonate rocks is mainly chert and can comprise 30-40% of some siltstone layers within the Ordovician shales, i.e., the Queenston and Georgian Bay formations. Quartz as chert was observed in Devonian and Upper Silurian dolostones. Pyrite is the principal iron mineral and is detected throughout the Paleozoic sequence indicating strongly reducing conditions, although hematite is common in the Queenston and Cabot Head formation shales yielding their red colour. The most common oxides are the sheet silicates comprising the clay minerals, which are often coloured by iron oxides.

Surface 2-D seismic reflection surveys completed over 19.7 km on nine survey lines identified the possible presence of five seismic discontinuities that may represent vertical to sub-vertical faults within the Ordovician formations at the Bruce nuclear site. These possible faults trend north-northwest to northwest. Two of these possible structures were investigated through inclined drilling in Phase 2B site characterization work (boreholes DGR-5 and DGR-6). Results of these drilling investigations did not identify faults at the target locations defined by 2-D seismic surveys.

Representative values of key geological properties of the 34 sedimentary bedrock layers that comprise the descriptive geological site model are summarized in tabular form together with a qualitative assessment (low, moderate, high) of the confidence in these layer properties. Representative values are typically arithmetic means based on data from all DGR boreholes. Confidence in layer properties ranges from low to high depending upon the property considered as summarized in Table 6.1 below.

Table 6.1: Summary of Confidence Assessment in Characterization of Descriptive Geological Site Model Properties

Descriptive Geological Site Model Property	Confidence in Property Characterization
Depth, thickness and orientation of model layers	High
Major mineralogy of model layers	High
Occurrence of soluble minerals	Moderate to High
Occurrence of major sub-horizontal structural features	High
Occurrence of major inclined structural features	Moderate
Occurrence of minor sub-horizontal structural features	High
Occurrence of minor inclined structural features	Moderate

6.2 Descriptive Hydrogeological Site Model

The hydrogeological site model describes the hydrogeologic properties and 3-D spatial distribution of all important hydrogeologic units and features within the Paleozoic bedrock units at the Bruce nuclear site. The descriptive hydrogeologic model, based on detailed field and laboratory testing, provides a basis for understanding groundwater flow and radionuclide transport properties of the Paleozoic bedrock that will contain and isolate the proposed DGR. The hydrogeologic site model focuses on description of the physical properties (rock density, porosity, fluid saturations, surface area, permeability, hydraulic head and diffusivity) of the bedrock, and the geochemical and isotopic properties of the groundwater and porewater of the Bruce nuclear site.

Laboratory testing of DGR cores was undertaken to quantify intact rock physical properties including bulk and grain density, physical and water loss porosity, residual fluid saturations, rock permeability to gas, mercury injection pore-size distribution, gas entry pressure, specific surface area, gas-brine flow properties, effective diffusion coefficients and diffusion accessible porosity. Bulk and grain densities were measured by three different laboratories and showed comparable results that were in accordance with expectations based on formation mineralogy and porosity.

Total and liquid porosities were also measured on 592 DGR cores by four independent laboratories. Total porosity was measured by helium gas expansion and from bulk dry and grain density data. Liquid porosity was measured by vacuum distillation and oven drying. The mean total and liquid porosities ranged from 8.9% and 9.8%, respectively in the Silurian and Devonian strata, to 1.9% and 1.7% respectively, in Ordovician limestones, to 1.7% and 1.0% respectively, for limestone/siltstone hard beds within Ordovician shales, to 7.3% and 8.0% respectively, for Ordovician shales, to 9.5% and 8.1% respectively, in the Shadow Lake siltstone

and Cambrian sandstone. The very low porosities of the Ordovician limestones including the host DGR Cobourg Formation contribute to the very low hydraulic and diffusive properties of these rocks.

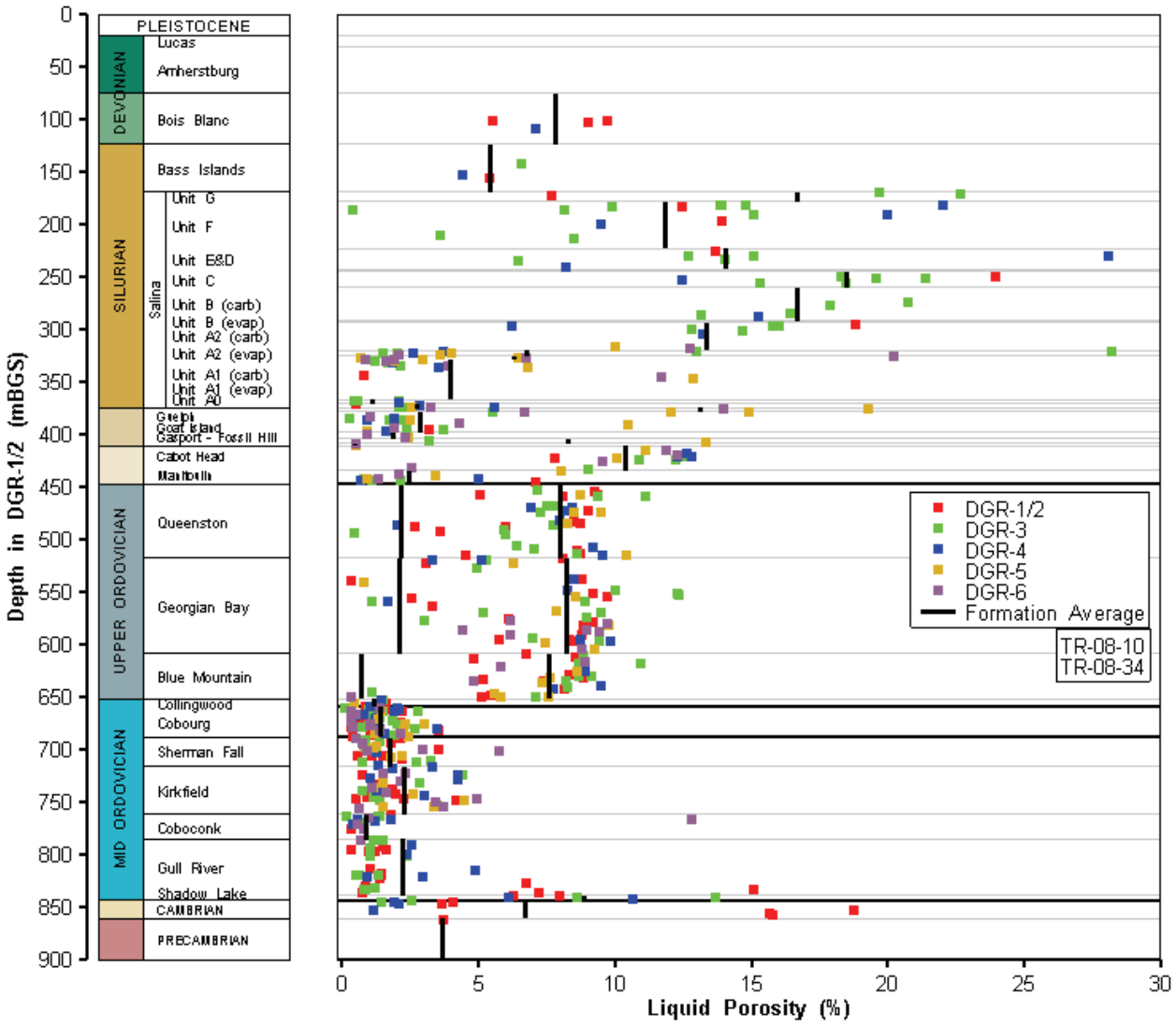

Note:. Plot shows point data and arithmetic formation averages.

Figure 6.5: Depth Profile of Liquid Porosity from Testing of 454 DGR Core Samples

The fluid saturations or fractions of brine, oil and gas within rock pore volumes were determined for DGR cores. Saturations of oil of up to 11.8% of the pore space were detected in 24% of tested samples from petrophysical testing of DGR cores. The brine or water saturations typically range from 60% to 100% and the gas saturations, which are calculated by difference,

range from 0% to 40% of the pore space. Although there are some uncertainties in these gas saturations related to sample dehydration, core relaxation and test equipment sensitivity, particularly in the very low porosity Ordovician limestones, analysis of the available data, including calculations of methane supersaturation, suggest that a discontinuous gas phase is present within the pore space of the Ordovician shales and limestones.

Mercury injection porosimetry data were used to estimate gas entry or displacement pressures for the DGR host formation (Cobourg) and the overlying Ordovician shales and Silurian strata, as well as for the deeper sections of the Gull River Formation and the Cambrian sandstone. The gas entry pressures for the porous deeper parts of the Gull River Formation and Cambrian sandstone are quite low at 40 to 150 kPa, whereas the values for the Cobourg Formation, overlying Ordovician shales, and most of the Middle to Lower Silurian dolostones and shales are typically greater than 10 MPa.

Mercury injection porosimetry data, fluid saturation data and gas pulse permeability data were used to calculate van Genuchten characteristic gas-brine flow parameters. The fitted relative permeability-saturation curves indicate that the measured gas saturations could result in reductions of brine permeability by upwards of one order of magnitude.

Diffusion properties of intact DGR cores collected from Silurian and Ordovician formations were measured using conventional laboratory through diffusion methods using iodide, tritium and ^{125}I as tracers to estimate vertical properties, and X-ray radiography using iodide as a tracer to estimate vertical and horizontal properties. The iodide effective diffusion coefficients for the Ordovician shales and limestones were found to be proportional to the porosity of the formations with values of about $1x10^{-12}$ m^2/s for Queenston and Georgian Bay Formation shales and $4x10^{-13}$ m^2/s for the Cobourg Formation limestone. The experimental program also observed iodide diffusion coefficient anisotropy with values parallel to bedding being larger than normal to bedding by factors of 1 to 4. Diffusion coefficients for iodide were less than those for tritium, particularly in shale, and iodide diffusion-accessible porosity was typically 50% of liquid porosity, suggesting commonly reported anion exclusion effects in the iodide diffusion testing of DGR shale cores. The effective diffusion coefficients measured on DGR cores are the lowest of those known from international data sets for sedimentary rocks (see Figure 6.6).

Groundwater and porewater in the Paleozoic bedrock sequence at the Bruce nuclear site were characterized for master variables of pH and Eh, major and trace ions, environmental isotopes, radioisotopes and some gases. Groundwater samples were collected from multi-level monitoring systems established in three US-series boreholes to maximum 200 m depth and as opportunistic samples collected from permeable packer-isolated intervals during drilling of DGR-boreholes. Groundwater samples were collected during drilling from the Salina Upper A1 Unit, the Guelph Formation and the Cambrian sandstone aquifers. Initial groundwater sampling of the upper 190 m of the bedrock shows that the groundwater transitions from fresh Ca:Mg-HCO_3 water (TDS ~500 mg/L) near the top of the bedrock to brackish Ca-SO_4 water (TDS ~5,000 mg/L) at depth. The depleted $\delta^{18}O$ and δD signatures at depths of 100 to 180 m and within the Salina Upper A1 Unit aquifer at reference depth of 325.5 - 328.5 mBGS in DGR-1 suggest the presence of a glacial meltwater component. Groundwater collected from the Guelph Formation at reference depths of 374.5 - 378.6 mBGS is a Na-Cl brine with the highest TDS (375,000 mg/L) of any water samples tested at the Bruce DGR site. Groundwater collected from the Cambrian sandstone at a reference depth of 843.8 – 860.7 is a Na:Ca-Cl brine (TDS ~230,000 mg/L).

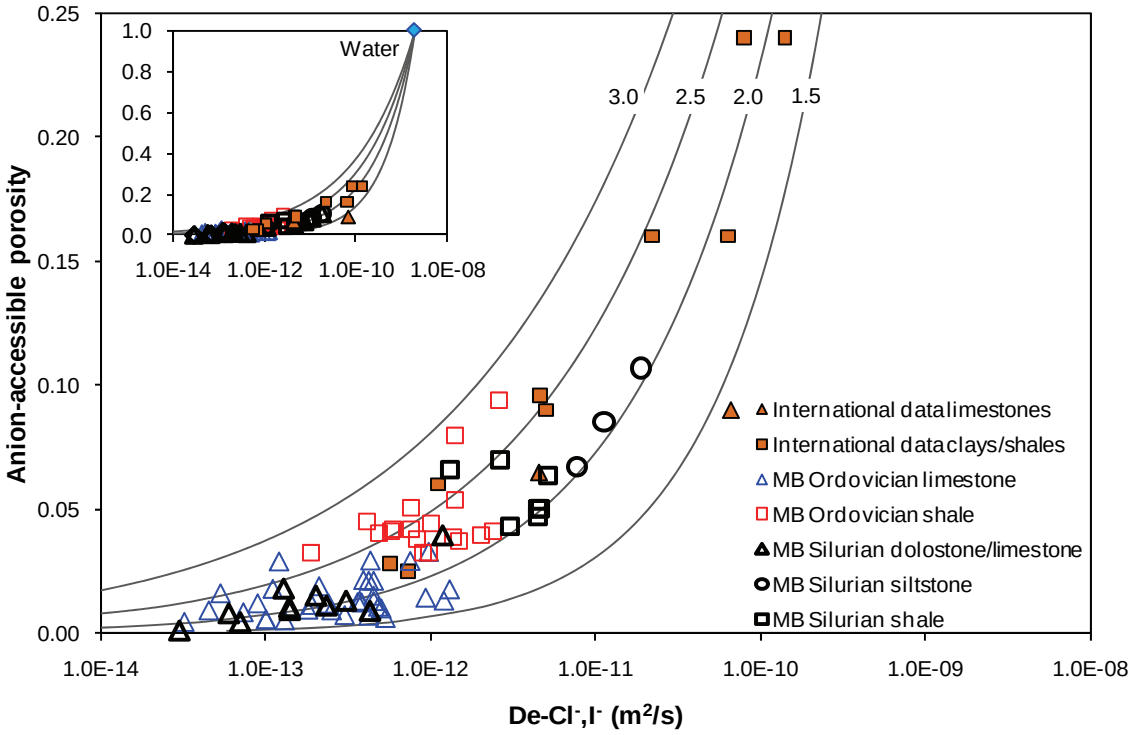

Figure 6.6: Comparison of Bruce DGR Effective Diffusion Coefficients (Labelled MB – Michigan Basin) for Cl^- and I^- with International Data from OCED/NEA Claytrac Project

Porewater was extracted from crushed DGR cores at the University of Ottawa by high-temperature vacuum distillation (150°C) for dissolved gases and isotopes followed by deionized water leaching of crushed (2-4 mm grain size) rock samples for major dissolved ions. These porewater analyses, supported by the available shallow and deep groundwater analyses and corroborating porewater analyses for chloride, bromide, sodium completed by the University of Bern, Switzerland and the University of New Brunswick using crush and leach methods, were used to generate water chemistry profiles for the Paleozoic bedrock at the Bruce nuclear site.

The porewater and groundwater data (Figure 6.7) show gradual increasing salinity and major ion concentration profiles from near surface to the depths of about 350 to 400 mBGS where a Na-Cl basin brine occurs (TDS=350,000 mg/L). Below this depth, salinity and major ion profiles decrease gradually through the Ordovician shales and the Ordovician limestones of the Trenton Group (Cobourg, Sherman Fall and Kirkfield formations), to the top/middle of the Gull River Formation limestone (TDS=200,000 mg/L). Salinity and major ion concentrations in the lower Gull River Formation then increase toward those observed in Cambrian groundwater and porewater (TDS=230,000 mg/L).

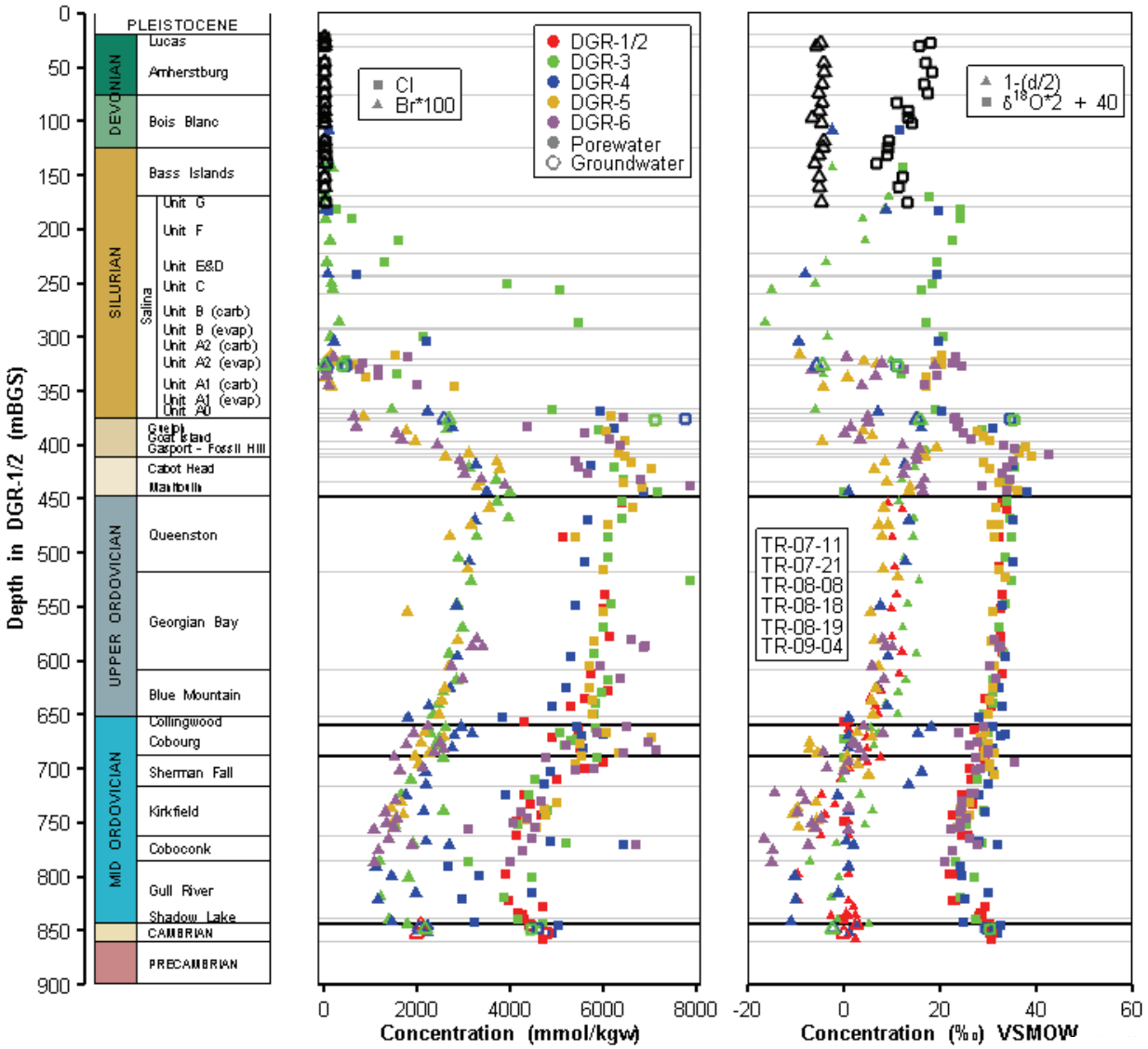

Figure 6.7: Major Ion (Cl, Br) and Environmental Isotope (^{18}O and Deuterium Excess) Tracer Profiles in DGR Porewater and Groundwater

The environmental isotope data (including deuterium excess) and the major ion data (e.g., Cl, Br, Sr,) suggest the deeper Ordovician limestone porewaters are mixtures of different basin fluids particularly within the Gull River Formation.

Figure 6.7 shows the major ion and environmental isotope tracer profile in DGR rocks based on porewater and groundwater analyses. Figure 6.7 shows the chloride, bromide, ^{18}O and deuterium excess depth profiles. For ease of plotting and comparison of trends in depth profiles, bromide values have been multiplied by 100, ^{18}O data have been multiplied by 2 and added to 40, and deuterium excess data have divided by 2 and subtracted from 1.

Historical hydraulic testing of the upper 100 m of bedrock in combination with the results of pulse, slug and drill-stem hydraulic testing of DGR boreholes using a custom-built straddle-packer testing tool, were used to quantify formation horizontal hydraulic conductivity. Borehole straddle-packer tests were analyzed using the Sandia National Laboratories numerical hydraulic-test simulator - nSIGHTS. Measured horizontal hydraulic conductivities ranged from 10^{-15} m/s in the Kirkfield Formation to $3x10^{-6}$ m/s in the Cambrian sandstone. A summary of all DGR borehole field hydraulic testing results is shown in Figure 6.8.

Considering field and lab permeability testing, core observations and other hydraulic test data, the average estimates of horizontal hydraulic conductivity of the Ordovician shale and Trenton Group limestone formations range from $4x10^{-15}$ to $3x10^{-14}$ m/s, with vertical hydraulic conductivity estimated as a factor of 10 less than horizontal hydraulic conductivity. The formation average estimates of horizontal hydraulic conductivity in the Black River limestones are greater ranging from $2x10^{-12}$ to $2x10^{-11}$ m/s, with vertical hydraulic conductivity potentially being a factor of 10 to 1000 less than horizontal hydraulic conductivity.

Following the completion of borehole geophysical logging and straddle-packer testing, boreholes US-3, US-7, US-8, DGR-1, DGR-2, DGR-3 and DGR-4 were equipped with Westbay multiport groundwater monitoring systems. Stable pressure profiles measured in US-3, US-7 and US-8 show slight upward hydraulic gradients in the upper 200 m of dolostone bedrock with lateral flow toward Lake Huron. Monitoring of formation pressures in 42 (DGR-3 and DGR-4) to 46 (DGR-1 and DGR-2) packer-isolated intervals in DGR boreholes over monitoring periods of months to a year shows the presence of moderate overpressures in Salina A1 and A0 Units, Goat Island, Gasport and Fossil Hill formations, significant stable overpressure in the Cambrian sandstone, and significant transient underpressures throughout most of the Ordovician shale and limestone (see Figure 6.8).

Environmental water heads calculated from formation pressures and the porewater/groundwater fluid density profile range from 165 m above ground surface (350 mASL) for the Cambrian sandstone to less than 300 mBGS (-115 mASL) in the Blue Mountain shale. The exact cause or causes of the observed overpressures and underpressures in DGR boreholes are not evident at this time, although glacial/erosional unloading and presence of a separate gas phase are suggested as possible explanations. Regardless of the exact cause, the occurrence of such significant underpressures implies that the formations in which they are measured must be of extremely low permeability in order for them to persist.

Initial measurements of formation pressures in DGR boreholes were used to determine horizontal groundwater flow directions in the three deep permeable aquifers at the Bruce nuclear site. Groundwater flow directions in the Upper A1 Unit aquifer are the same as those in the shallow dolostones, being to the northwest toward Lake Huron. In contrast, the calculated groundwater flow directions for the Guelph Formation and the Cambrian sandstone are outward from the middle of the Michigan Basin toward the northeast (Guelph Formation) and to the east (Cambrian sandstone). Calculated hydraulic gradients in all three deep permeable aquifers are in the range of $2x10^{-3}$ to $9x10^{-3}$ m/m. These initial assessments of groundwater flows need to be confirmed with additional formation pressure measurements.

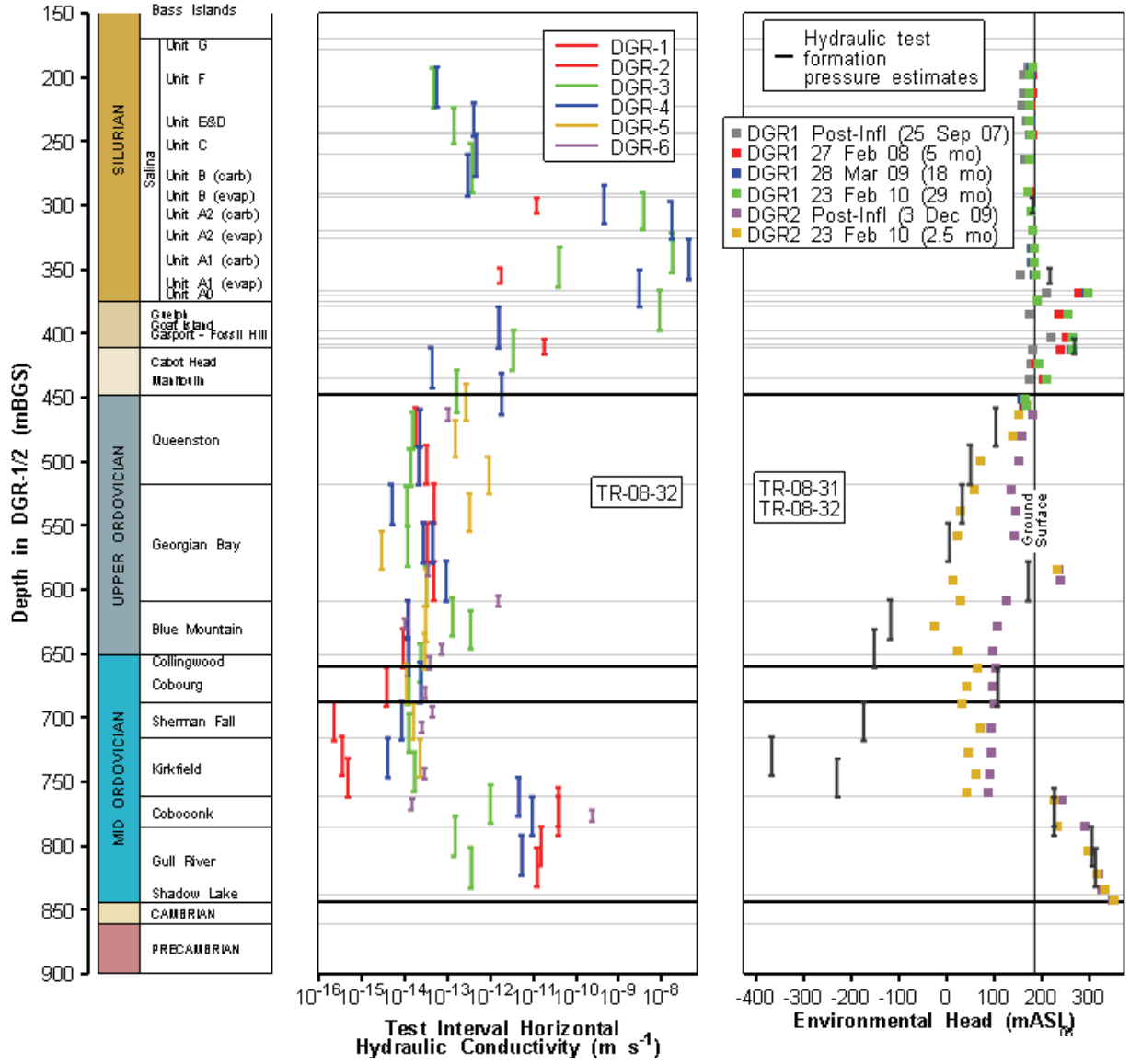

Figure 6.8: Summary of Measurements of Hydraulic Conductivity (DGR-1 to DGR-6) and Environmental Head Data (DGR-1 and DGR-2) at the Bruce Site

Considering all of the available Phase 1, 2A and 2B hydrogeological site characterization data, the overburden and bedrock formations were categorized and grouped in hydrostratigraphic units that have similar hydrogeologic characteristics. Based on DGR-1 and DGR-2 reference depths, the nine hydrostratigraphic (HS) units include:

- HS Unit 1: Overburden aquitard; 0 to 20 mBGS;
- HS Unit 2: Devonian and Upper Silurian Dolostone aquifer, 20 to 169.3 mBGS;
- HS Unit 3: Silurian shale, dolostone & anhydrite aquitards, 169.3 to 447.7 mBGS, excluding Unit 4.
- HS Unit 4: Silurian dolostone aquifers, 325.5 to 328.5 mBGS and 374.5 to 378.6 mBGS

- HS Unit 5: Ordovician shale aquiclude, 447.7 to 659.5 mBGS;
- HS Unit 6: Ordovician limestone aquiclude, 659.5 to 762.0 mBGS;
- HS Unit 7: Ordovician limestone aquitard, 762.0 to 838.6 mBGS;
- HS Unit 8: Cambrian sandstone aquifer, 838.6 to 860.7 mBGS; and
- HS Unit 9: Precambrian aquitard, >860.7 mBGS.

Estimates of vertical and horizontal hydraulic conductivity, specific storage, total porosity, hydraulic gradients, vertical and horizontal effective diffusion coefficient, diffusion porosity and groundwater/porewater properties of these Bruce DGR hydrostratigraphic units are summarized in this report.

Hydrostratigraphic units and hydrogeological data are further interpreted and consolidated into three major hydrogeologic systems at the Bruce nuclear site – shallow, intermediate and deep.

The shallow hydrogeological system includes HS Units 1 and 2. It extends from ground surface to depths of 169.3 mBGS in DGR-1 and contains fresh to brackish water with evidence of glacial meltwater. Solute migration within this permeable groundwater system is principally by advection. The intermediate system comprises HS Units 3 and 4 and extends to depths of 447.7 mBGS in DGR-1. Groundwater and porewater within this predominantly low-permeability system, transitions from saline Ca-SO_4 water near the top of the system to a Na-Cl brine at the bottom of the system. Tracer profiles indicate solute transport within most of the intermediate system is by diffusion with advective transport likely occurring laterally within the two thin permeable Upper A1 Unit and Guelph non-potable aquifers. The deep system occurs at depths of 447.7 to 860.7 mBGS and includes HS Units 5, 6, 7 and 8. It comprises an exceptionally low permeability Ordovician shale and Trenton Group limestone aquiclude ($K_h = 10^{-15}$ to 10^{-14} m/s), a low permeability Black River Group aquitard ($K_h = 10^{-12}$ to 10^{-11} m/s) and a non-potable Cambrian aquifer ($K_h = 10^{-9}$ to 10^{-6} m/s). Groundwater and porewater within the deep system is Na-Cl to Na:Ca-Cl brine. Tracer profiles suggest diffusion-controlled solute transport within the bulk of the deep system, with the possible exception of the permeable Cambrian aquifer.

Representative values of key hydrogeological properties of the 39 layers that comprise the descriptive hydrogeological site model are also summarized in tabular form together with a qualitative assessment (low, moderate, high) of the confidence in these layer properties. Representative values are typically arithmetic or geometric means based on data from all DGR boreholes. Confidence in layer properties ranges from low to high depending upon the property considered as summarized in Table 6.2.

6.3 Descriptive Geomechanical Site Model

The geomechanical site model describes and summarizes the current understanding of the principal geomechanical properties of the rock materials and rock mass beneath the Bruce nuclear site. The geomechanical site model focuses on presentation of quantitative estimated physical properties that will control the geomechanical behaviour of the rock mass beneath the site during and after construction of the subsurface infrastructure required for development of the DGR. Representative values are based on combining the specific quantitative values of various parameters derived from field and laboratory testing with expert judgement, where appropriate.

Table 6.2: Summary of Confidence Assessment in Characterization of Descriptive Hydrogeological Site Model Properties

Descriptive Hydrogeological Site Model Property	Confidence in Property Characterization
Rock densities	High
Liquid and total porosities	Moderate
Gas saturations	Low
Gas-brine flow properties	Low to Moderate
Diffusion properties	High
Porewater characterization – Na, B, Cl, Br, TDS	Moderate
Porewater characterization – Ca, Mg, K, Sr, SO_4	Low
Porewater characterization – $\delta^{18}O$, δD, d	High
Porewater characterization – CH_4, Sr and CH_4 isotopes	Moderate to High
Porewater characterization – CO_2 and CO_2 isotopes	Low
Porewater characterization – He and He isotopes	Low to Moderate
Porewater characterization – radioisotopes – ^{14}C	High
Porewater characterization – radioisotopes – ^{36}Cl, ^{129}I	Low to Moderate
Formation hydraulic properties – K horizontal, K vertical	High, Moderate
Formation hydraulic properties – specific storage	Moderate
Formation pressures and environmental heads – underpressured	Low and High
Formation pressures and environmental heads – normal and overpressured	High
Groundwater flow directions and gradients in bedrock aquifers - Devonian	High
Groundwater flow directions and gradients in bedrock aquifers – Salina Upper A1 Unit, Guelph and Cambrian	Low to Moderate

Seismic monitoring at and in the vicinity of the Bruce nuclear site is being undertaken from an expanded seismic monitoring network installed in 2007 to obtain understanding of the contemporary microseismic activity within 50 km of the Bruce nuclear site. This monitoring, in addition to other information, will be used to conduct a seismic hazard evaluation for the DGR and to provide information on the contemporary seismicity and microseismicity that can be used in identification of seismogenic features in the region surrounding the Bruce nuclear site. The current and historical monitoring data show that the Bruce nuclear site is located in a seismically quiet area.

The in situ state of stress below the DGR site, and particularly at the repository elevation, is a key geomechanical parameter affecting the design of the repository facilities. Although the vertical stress magnitude and orientation will closely match the gravitational stress caused by the weight of rock above any elevation of interest, the challenge lies in trying to evaluate the

magnitudes and orientations of the horizontal stress components at depth. Unfortunately, there are no reliable direct measurement methods for quantifying in situ horizontal stresses at the depths of interest from a surface-based exploratory borehole. Based on a review of the regional stress measurements and the observation of a lack of borehole breakouts in DGR boreholes up to 2 years following completion of drilling, the representative in situ stress levels at the elevation of the DGR (~680 mBGS) are:

- Vertical stress (σ_v) ~ gravity load of super-incumbent materials, ~ 18 MPa;
- Maximum horizontal stress (σ_H): $1.5<\sigma_H/\sigma_v<2.0$; and
- Minimum horizontal stress (σ_h): $1.0<\sigma_h/\sigma_v<1.2$.

Similar to the development of hydrostratigraphic units for the hydrogeological site model, mechano-stratigraphic (MS) units are developed for describing the geomechanical properties of the bedrock formations at the Bruce nuclear site. Considering all of the available Phase 1, 2A and 2B geomechanical site characterization data, five MS units have been defined based on DGR-1 and DGR-2 reference depths:

- MS Unit 1; Devonian and Upper Silurian dolostones, including the Salina G Unit dolostone, 20 to 178.6 mBGS;
- MS Unit 2; Silurian shales, dolostones and anhydrites, 178.6 to 411 mBGS;
- MS Unit 3; Lower Silurian and Upper Ordovician shales (with minor Lower Silurian dolostone and Middle Ordovician shale), 411 to 659.5 mBGS;
- MS Unit 4; Middle Ordovician Cobourg Formation argillaceous limestone (repository horizon), 659.5 to 688.1 mBGS; and
- MS Unit 5; all deeper Ordovician, Cambrian and Precambrian units, 688.1 to >860.7 mBGS.

The geomechanical site model describes both the rock material geomechanical characteristics and the rock mass geomechanical characteristics for each of the MS units based on Phase 1, 2A and 2B data generated from drilling and testing of DGR-1, DGR-2, DGR-3, DGR-4, DGR-5 and DGR-6. Rock material geomechanical characteristics include, where available, information on short and long-term uniaxial compression strengths, triaxial compression strength, indirect tensile strength, direct shear strength, slake durability, free swell behaviour, abrasiveness, and dynamic properties (elastic and shear moduli, Poisson's ratio) based on the testing of intact cores. Rock mass geomechanical characteristics include, where available, information on rock quality designation (RQD), natural fracture frequency, and bulk properties from borehole geophysical logging (dynamic elastic and shear moduli). Figure 6.9 shows the depth profile of uniaxial compression test data for the Cobourg Formation (DGR host horizon) generated from testing of 67 cores collected from DGR-1 through DGR-6.

The available data on rock material and rock mass geomechanical characteristics generated from Phase 1, 2A and 2B site characterization work demonstrate that the geomechanical properties of the Bruce DGR rocks are better than expected results based on precedent projects and regional data summaries. For example, Figure 6.10 shows a comparison of the strength of the Cobourg Formation - proposed to host the DGR, from testing in DGR boreholes at the Bruce site and from regional data.

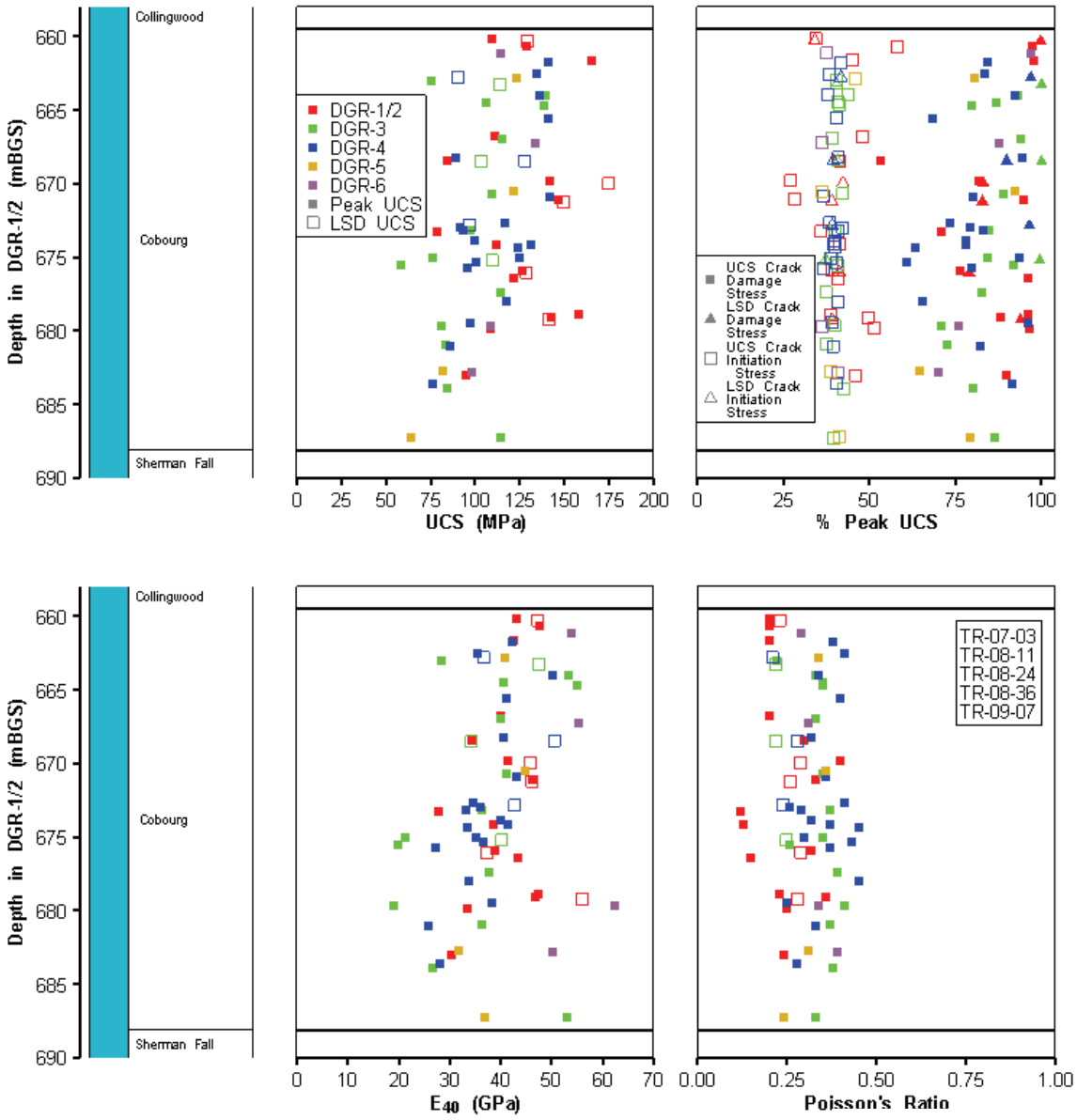

Figure 6.9: Uniaxial Compression Test Data for MS Unit 4 Consisting of the Cobourg Formation

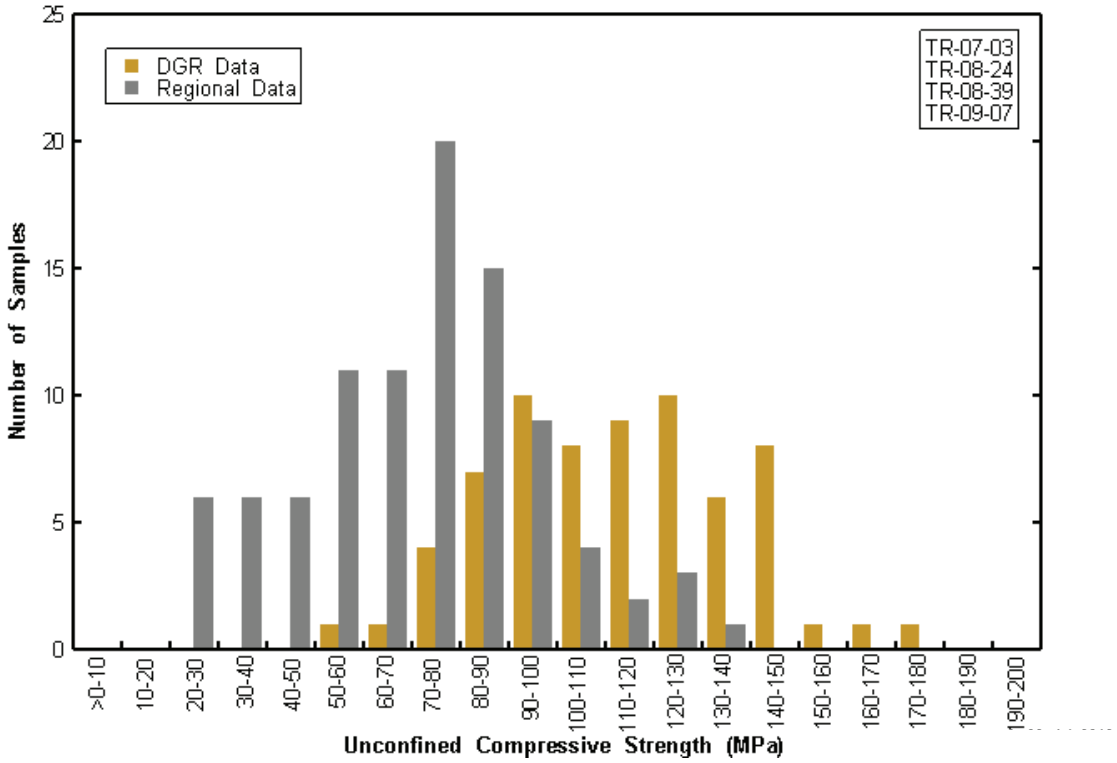

Figure 6.10: Comparison of DGR Uniaxial Compressive Strength of the Cobourg Formation from DGR Boreholes and Regional Data

Representative values of key geomechanical properties of the 34 layers that comprise the descriptive geomechanical site model are summarized in tabular form together with a qualitative assessment (low, moderate, high) of the confidence in these layer properties. Representative values are typically based on professional judgment or where data is sufficient based arithmetic means considering data from all DGR boreholes. Confidence in layer properties ranges from low to high depending upon the property considered as summarized in Table 6.3 below.

Table 6.3: Summary of Confidence Assessment in Characterization of Descriptive Geomechanical Site Model Properties

Descriptive Geological Model Site Property	Confidence in Property Characterization
In situ stresses	Low to Moderate
Rock material strength properties	Moderate to High
Rock slaking properties	High
Rock swelling properties	Moderate to High
Rock abrasivity properties	High
Rock mass geomechanical properties	Moderate to High

7. REFERENCES

AECOM and ITASCA CANADA. 2011. Regional Geology – Southern Ontario. AECOM Canada Ltd. and Itasca Consulting Canada, Inc. report for the Nuclear Waste Management Organization NWMO DGR-TR-2011-15 R000. Toronto, Canada.

Al, T., Y. Xiang and L. Cavé. 2010a. Measurement of Diffusion Properties by X-Ray Radiography and by Through-Diffusion Techniques Using Iodide and Tritium Tracers: Core Samples from OS-1 and DGR-2. Intera Engineering Ltd. Report TR-07-17 Rev.3. University of New Brunswick, Fredericton, Canada.

Al, T., Y. Xiang, D. Loomer and L. Cavé. 2010b. Measurement of Diffusion Properties by X-Ray Radiography and by Through-Diffusion Techniques Using Iodide and Tritium Tracers: Core Samples from DGR-3 and DGR-4. Intera Engineering Ltd. Report TR-08-27 Rev.0. University of New Brunswick, Fredericton, Canada.

Altinier, M.V., S. Savoye, J.-L. Michelot, C. Beaucaire, M. Massault, D. Tessier and H.N. Waber. 2007. The isotopic composition of pore-water from Tournemire argillite (France): An inter-comparison study. Physics and Chemistry of the Earth, Parts A/B/C 32,1-7, 209-218.

Andrews, J.N., J.-Ch. Fontes, J-L. Michelot and D. Elmore. 1986. In-situ neutron flux, ^{36}Cl production and groundwater evolution in crystalline rocks at Stripa, Sweden. Earth and Planetary Science Letters 77, 49-58.

Appelo, C.A.J. and D. Postma. 1996. Geochemistry, Groundwater and Pollution. A.A. Balkema, Rotterdam, Netherlands.

Aravena, R., L.I. Wassenaar and L.N. Plummer. 1995. Estimating ^{14}C ages in a methanogenic aquifer. Water Resources Research 31 (9), 2307-2317.

Armstrong, D.K. and T.R. Carter. 2010. The Subsurface Paleozoic Stratigraphy of Southern Ontario. Ontario Geological Survey, Special Volume 7.

Armstrong, D.K. and T.R. Carter. 2006. An Updated Guide to the Subsurface Paleozoic Stratigraphy of Southern Ontario. Ontario Geological Survey, Open File Report 6191.

Armstrong, D.K. and W.R. Goodman. 1990. Stratigraphy and depositional environments of Niagaran carbonates, Bruce Peninsula, Ontario. Field Trip No. 4 Guidebook. American Association of Petroleum Geologists, 1990 Eastern Section Meeting, hosted by the Ontario Petroleum Institute. London, Ontario.

Bahr, J.M., G.R. Moline and G.C. Nadon. 1994. Anomalous pressures in the deep Michigan Basin. In: Basin Compartments and Seals. Ortoleva, P. (Ed.), AAPG Memoir 61,153-165.

Ballentine, C.J. and P.G., Burnard. 2002. Production, release and transport of noble gases in the continental crust. Reviews in Mineralogy and Geochemistry 47 (1), 481-538.

Barton, N.R., R. Lien and J. Lunde. 1974. Engineering classification of rock masses for the design of tunnel support. Rock Mechanics 6 (4), 189-239.

Beauheim, R.L. 2009. Evaluation of Possible Hydraulic Communication Between Boreholes DGR-1 and DGR-2 at the Bruce Site. Intera Engineering Ltd. Report TR-08-07 Rev.0. Sandia National Laboratories, USA.

Beauheim, R.L. and W.H. Pedler. 2009. Fluid Electrical Conductivity Logging in Borehole DGR-1. Intera Engineering Ltd. Report TR-07-14 Rev.2. Sandia National Laboratories, USA.

Bense, V.F. and M.A. Person. 2008. Transient hydrodynamics within intercratonic sedimentary basins during glacial cycles. Journal of Geophysical Research 113, F04005.

Bentley, H.W., F.M. Philips, S.N. Davis, M.A. Habermehl, P.L. Airey, G.E. Calf, D. Elmore, H.E. Gove and T. Torgersen. 1986. Chlorine 36 dating of very old groundwater 1. The Great Artesian Basin, Australia. Water Resources Research 22, 1991-2001.

Berner, R.A. 1981. A new geochemical classification of sedimentary environments. J. Sedimentary Petrology 51, 359-365.

Bieniawski, Z.T. 1974. Geomechanics classification of rock masses and its application in tunnelling. In: Advances in Rock Mechanics 2, part A: 27-32, Washington D.C. National Academy of Sciences.

Boisson, J.-Y., L. Betrand, J.-F. Heitz and Y. Moreau-Le Golvan. 2001. In-situ and laboratory investigations of fluid flow through an argillaceous formation at different scales of space and time, Tournemire tunnel, southern France. Hydrogeology Journal 9, 108-123.

Bottomley, D.J., R. Renaud, T. Kotzer and I.D. Clark. 2002. Iodine-129 constraints on residence times of deep marine brines in the Canadian Shield. Geology 30 (7), 587-590.

Boving, T.B. and P. Grathwohl. 2001. Tracer diffusion coefficients in sedimentary rocks: correlation to porosity and hydraulic conductivity. Journal of Contaminant Hydrology 53, 85-100.

Brace, W.F., J.B. Walsh and W.T. Frangos. 1968. Permeability of granite under high pressure. Journal of Geophysical Research 73 (6), 2225-2236.

Brand, U. 2004. Carbon, oxygen and strontium isotopes in Paleozoic carbonate components: an evaluation of original seawater-chemistry proxies. Chemical Geology 204, 23-44.

Brett, C.E., D.H. Tepper, W.M. Goodman, S.T. LoDuca and B.-Y. Eckert. 1995. Revised Stratigraphy and Correlation of the Niagaran Provincial Series (Medina, Clinton and Lockport Groups) in the Type Area of Western New York. United States Geological Survey, Bulletin 2086.

Briscoe, G., A. Wigston and M. Melaney. 2010a. Drilling, Logging and Sampling of DGR-3 and DGR-4. Intera Engineering Report TR-08-13 Rev.1. Ottawa, Canada.

Briscoe, G. 2009. Drilling and Logging of US-8. Intera Engineering Ltd. Report TR-07-19 Rev.0. Ottawa, Canada.

Bruce Power. 2008. Annual Summary & Assessment of Environmental Radiological Data for 2007. Bruce Power Report B-REP-03419-00008 R000. Tiverton, Canada.

Brunauer, S., P.H. Emmett and E. Teller. 1938. Adsorption of Gases in Multimolecular Layers. Journal of the American Chemical Society 60, 309-319.

Calder, N. 2011. Two-Phase Flow Parameters from DGR-2, DGR-3 and DGR-4 Petrophysics Data. Intera Engineering Ltd. Report TR-08-33 Rev.0. Ottawa, Canada.

Carter, T. 2002. The stratigraphic setting, hydrocarbon exploration plays and production in southern Ontario. Abstract, Annual Convention, Canadian Society of Petroleum Geologists.

Carter, T.R., R.A. Trevail and R.M. Easton. 1996. Basement controls on some hydrocarbon traps in southern Ontario. In: van der Pluijm, B.A. and P.A. Catacosinos (Eds.), Basement and Basins of Eastern North America. Geological Society of America Special Paper 308, 95-107.

Carter, T.R., R.A. Trevail and L. Smith. 1994. Core Workshop: Niagaran Reef and Inter-reef Relationships in the Subsurface of Southwestern Ontario. Geological Association of Canada/Mineralogical Association of Canada Joint Annual Meeting. Waterloo, Ontario.

Cavé, L., T. Al, Y. Xiang and D. Loomer. 2010. Investigations of Diffusive Transport Processes in Sedimentary Rock. University of New Brunswick Report prepared for Nuclear Waste Management Organization NWMO TR-2010-04. Toronto, Canada.

Cavé, L., T. Al, Y. Xiang and P. Vilks. 2009. A technique for estimating one-dimensional diffusion coefficient in low-permeability sedimentary rock using X-ray radiography: Comparison with through-diffusion measurements, Journal of Contaminant Hydrology 35, 41-53.

Clark, I. and M. Herod. 2011. Radioisotopes in DGR Groundwater and Porewater. Intera Engineering Ltd. Report TR-08-38 Rev.0. University of Ottawa, Ottawa, Canada.

Clark, I., V. Scharf, J. Zuliani and M. Herod. 2011. Pore Water Analysis in DGR-5 and DGR-6 Core. Intera Engineering Ltd. Report TR-09-04 Rev.0. University of Ottawa, Ottawa, Canada.

Clark, I., R. Mohapatra, H. Mohammadzadeh and T. Kotzer. 2010a. Pore Water and Gas Analysis in DGR-1 and DGR-2 Core. Intera Engineering Ltd. Report TR-07-21 Rev.1. University of Ottawa, Ottawa, Canada.

Clark, I., I. Liu, H. Mohammadzadeh, P. Zhang, R. Mohapatra, and M. Wilk. 2010b. Pore Water and Gas Analysis in DGR-3 and DGR-4 Core. Intera Engineering Ltd. Report TR-08-19 Rev.0. University of Ottawa, Ottawa, Canada.

Clark, I., R. Jackson, I. Lui and D. Heagle. 2010c. Vacuum Distillation Experiments on DGR Core. Intera Engineering Ltd. Report TR-08-37 Rev.0. University of Ottawa, Ottawa, Canada.

Clark, I.D. and P. Fritz. 1997. Environmental Isotopes in Hydrogeology. Lewis Publishers, New York, USA.

Clayton, R.N., I. Friedman, D.L. Graff, T.K. Mayeda, W.F. Meents and N.F. Shimp. 1966. The origin of saline formation waters, 1. Isotopic composition. Journal of Geophysical Research 71, 3869-3882.

Coniglio, M. and A.E. Williams-Jones. 1992. Diagenesis of Ordovician carbonates from the north-east Michigan Basin, Manitoulin Island area, Ontario: evidence from petrography, stable isotopes and fluid inclusions. Sedimentology 39, 813-836.

Corbet, T.F. and C.M. Bethke. 1992. Disequilibrium fluid pressures and groundwater flow in the western Canada sedimentary basin. Journal of Geophysical Research B97, 7203-7217.

Cruden, A. 2011. Outcrop Fracture Mapping. Nuclear Waste Management Organization Report NWMO DGR-TR-2011-43 R000. Toronto, Canada.

Dacy, J. and P. Martin. 2006. Practical advances in core-based water saturation analysis of shaly tight gas sands. International Symposium of the Society of Core Analysts, Paper no. SCA2006-29. Trondheim, Norway.

Dansgaard, W. 1964. Stable isotopes in precipitation. Tellus 16, 436-468.

Desaulniers, D.E., J.A. Cherry and P. Fritz. 1981. Origin, age and movement of pore water in argillaceous Quaternary deposits at four sites in southwestern Ontario. Journal of Hydrology 50, 231-257.

Drever, J.I. 1988. The Geochemistry of Natural Waters, 2nd Edition. Prentice Hall, Englewood Cliffs, New Jersey, USA.

Duan, Z. and S. Mao. 2006. A thermodynamic model for calculating methane solubility, density and gas phase composition of methane-bearing aqueous fluids from 273 to 523°K and from 1 to 2000 bar. Geochimica et Cosmochimica Acta. 70, 3369–3386.

Duan, Z. and R. Sun. 2003. An improved model calculating CO2 solubility in pure water and aqueous NaCl solutions from 273 to 533 K and from 0 to 2000 bar. Chemical Geology, 193 (3-4), 257-271.

Dullien, F.A.L. 1979. Porous Media: Fluid Transport and Pore Structure. Academic Press, New York, USA.

Fabryka-Martin, J. 1999. Iodine-129 as a Groundwater Tracer. In: Cook P.G. and A.L. Herczeg (Eds.). Environmental Tracers in Subsurface Hydrology. Kluwer Academic Press, Boston, 504-510.

Faure, G. 1998. Principles and Applications of Geochemistry, Second Edition. ISBN: 0023364505, Prentice Hall, New Jersey.

Finsterle, S. and P. Persoff, 1997. Determining permeability of tight rock samples using inverse modeling. Water Resources Research, 33 (8), 1803-1811.

Frape, S.K. and P. Fritz. 1987. Geochemical trends for groundwater from the Canadian Shield, In: Saline Water and Gases in Crystalline Rocks. GAC Special Paper 33, 19-38.

Frape, S.K., P. Fritz and R.H. McNutt. 1984. The role of water-rock interaction in the chemical evolution of groundwaters from the Canadian Shield. Geochimica et Cosmochimica Act. 48, 1617-1627.

Freeze, R.A. and J.A Cherry. 1979. Groundwater. Prentice-Hall Inc., Englewood Cliffs, New Jersey, USA.

Fritz, P., R.J. Drimmie, S.K. Frape and O. O'Shea. 1987. The isotopic composition of precipitation and groundwater in Canada, In: Isotope Techniques in Water Resources Development, IAEA Symposium 299, Vienna, 539-550.

Gaines, S., K.G. Raven and M. Melaney. 2011a. Oriented Core Logging of DGR-5 and DGR-6 Core. Intera Engineering Ltd. Report TR-09-09 Rev.0. Ottawa, Canada.

Gaines, S., S. Sterling and D. Heagle. 2011b. Temporary Sealing of Boreholes DGR-5 and DGR-6. Intera Engineering Ltd. Report TR-09-10 Rev.0. Ottawa, Canada.

Gaines, S. and S. Sterling. 2009a. Field Geomechanical Testing of DGR-1 and DGR-2 Core. Intera Engineering Ltd. Report TR-07-07 Rev. 1. Ottawa, Canada.

Gaines, S. and S. Sterling. 2009b. Field Geomechanical Testing of DGR-3 and DGR-4 Core. Intera Engineering Ltd. Report TR-08-14 Rev.0. Ottawa, Canada.

Gascoyne, M., C.C. Davison, J.D. Ross and R. Pearson. 1987. Saline groundwaters and brine in plutons in the Canadian Shield. In: Saline Water and Gases in Crystalline Rocks. GAC Special Paper 33, 53-68.

Geological Survey of Canada. 1981. Bedrock Geology, Map 1335A, Southern Ontario, Ontario Sheet 305, Scale 1:1,000,000. Compilation by Sanford, B.V. and A.J. Bear.

Gimmi, T., H.N. Waber, A. Gautschi and A. Rübel. 2007. Stable water isotopes in pore water of Jurassic argillaceous rocks as tracers for solute transport over large spatial and temporal scales. Water Resources Research 43, 1-16.

Gimmi, T. and H.N. Waber. 2004. Modeling of Tracer Profiles in Pore Water of Argillaceous Rocks in the Benken Borehole: Stable Water Isotopes, Chloride, and Chlorine Isotopes. NAGRA Technical Report 04-05.

GOLDER. 2003. LLW Geotechnical Feasibility Study, Western Waste Management Facility, Bruce Site, Tiverton, Ontario. Golder Associates Ltd. report to Municipality of Kincardine and Ontario Power Generation. Toronto, Canada.

Gorski, B., D. Rogers and B. Conlon. 2011. Laboratory Geomechanical Strength Testing of DGR-2 to DGR-6 Core. Intera Engineering Ltd. Report TR-09-07 Rev.0. CANMET Mining and Mineral Sciences Laboratories. Ottawa, Canada.

Gorski, B., T. Anderson and B. Conlon. 2010a. Laboratory Geomechanical Strength Testing of DGR-3 & DGR-4 Core. Intera Engineering Ltd. Report TR-08-24 Rev.1. CANMET Mining and Mineral Sciences Laboratories. Ottawa, Canada.

Gorski, B., T. Anderson and B. Conlon. 2010b. Long-Term Strength Degredation Testing of DGR-3 & DGR-4 Core. Intera Engineering Ltd. Report TR-08-36 Rev.1. CANMET Mining and Mineral Sciences Laboratories. Ottawa, Canada.

Gorski, B., T. Anderson and D. Rogers. 2010c. Supplementary Uniaxial Compressive Strength Testing of DGR-3 and DGR-4 Core. Intera Engineering Ltd. Report TR-08-39 Rev.1. CANMET Mining and Mineral Sciences Laboratories. Ottawa, Canada.

Gorski, B., T. Anderson and B. Conlon. 2009a. Laboratory Geomechanical Strength Testing of DGR-1 & DGR-2 Core. Intera Engineering Ltd. Report TR-07-03 Rev.3. CANMET Mining and Mineral Sciences Laboratories. Ottawa, Canada.

Gorski, B., T. Anderson and B. Conlon. 2009b. Long-Term Strength Degradation Testing of DGR-2 Core. Intera Engineering Ltd. Report TR-08-11 Rev.0. CANMET Mining and Mineral Sciences Laboratories. Ottawa, Canada.

Guéguen, Y. and V. Palciauskas. 1994. Introduction to the Physics of Rocks. Princeton University Press, Princeton, New Jersey, USA.

Hart, D.J. and H.F. Wang. 2001. A single method for determination of poroelastic constants and flow parameters in rocks with low hydraulic conductivities. International Journal of Rock Mechanics & Mining Sciences 38, 577-583.

Heagle, D. 2010. Initial Groundwater Monitoring, US-3, US-7 and US-8. Intera Engineering Ltd. Report TR-08-08 Rev.1. Ottawa, Canada.

Heagle, D. and L. Pinder. 2010. Opportunistic Groundwater Sampling in DGR-3 and DGR-4. Intera Engineering Ltd. Report TR-08-18 Rev.1. Ottawa, Canada.

Heaman, L.M. and B.A. Kjarsgaard. 2000. Timing of eastern North American kimberlite magmatism: Continental extension of the Great Meteor hotspot track? Earth and Planetary Science Letters 178, 253-268.

Hendry, M.J., L.I. Wassenaar and T.Kotzer. 2000. Chloride and chlorine isotopes (36Cl and δ37Cl) as tracers of solute migration in a thick, clay-rich aquitard system. Water Resources Research 36 (1), 285-296.

Hendry, M.J., T.G. Kotzer and D.K. Solomon. 2005. Sources of radiogenic helium in a clay till aquitard and its use to evaluate the timing of geologic events. Geochimica et Cosmochimica Acta 69, 475-483.

Herwegh, M. and M. Mazurek. 2008. Feasibility SEM Study: Primary and Secondary Salts and Sulfates in the Paleozoic of the DGR-2 Borehole, Bruce, Southwestern Ontario, Progress Report PR 08-03. Institute of Geological Sciences, University of Bern, Switzerland.

Hobbs, M.Y., A. de Haller, M. Koroleva, M. Mazurek, J. Spangenberg, U. Mäder and D. Meier, 2011a. Boreholes DGR-3 and DGR-4 Porewater Investigations. Intera Engineering Ltd. Report TR-08-40 Rev.0. Rock Water Interaction (RWI). Institute of Geological Sciences, University of Bern, Bern, Switzerland.

Hobbs, M.Y., S.K. Frape, O. Shouakar-Stash and L.R. Kennell. 2011b. Regional Hydrogeochemistry – Southern Ontario. Nuclear Waste Management Organization Report NWMO DGR-TR-2011-12 R000. Toronto, Canada.

Hoek, E. 1994. Strength of rock and rock masses. ISRM News Journal 2 (2), 4-16.

Hoek, E. and J. Bray. 1974. Rock Slope Engineering. The Institution of Mining and Metallurgy, London.

Hayek, S.J., J.A. Drysdale, J. Adams, V. Peci, S. Halchuk and P. Street. 2010. Seismic Monitoring near the DGR - Annual Report 2009. Nuclear Waste Management Organization Report DGR-TR-2010-03. Toronto, Canada.

INTERA. 2004. Waterborne Tritium Impact Assessment, Bruce Site Conventional and #3 Construction Landfills. Intera Engineering Ltd. Final Report 03-227-1 prepared for Ontario Power Generation. Ottawa, Canada.

INTERA. 2006. Geoscientific Site Characterization Plan, OPG's Deep Geologic Repository for Low and Intermediate Level Waste. Intera Engineering Ltd. document prepared for Ontario Power Generation INTERA 05-220-1, OPG 00216-REP-03902-00002-R00. Ottawa, Canada.

INTERA. 2007. OPG Conventional and #3 Construction Landfills, Two Year Groundwater and Surface Water Monitoring Study, 2005-2007. Intera Engineering Ltd. Final Report 05-208 prepared for Ontario Power Generation. Ottawa, Canada.

INTERA. 2008. Phase 2 Geoscientific Site Characterization Plan, OPG's Deep Geologic Repository for Low and Intermediate Level Waste, Intera Engineering Ltd. document prepared for Ontario Power Generation INTERA 06-219.50-Phase 2 GSCP-R0, OPG 00216-REP-03902-00006-R00. Ottawa, Canada.

INTERA. 2009. Project Quality Plan, DGR Site Characterization. Intera Engineering Ltd. Report 06-219/08-200 PQP_R4. Ottawa, Canada.

Intera Technologies Ltd. 1988. Inventory and Assessment of Hydrogeologic Conditions of Underground Openings in Sedimentary Rock, Final Report H87-040 prepared for Ontario Hydro. Ottawa, Canada.

International Society for Rock Mechanics. 1977. Suggested Methods for the Quantitative Description of Discontinuities in Rock Masses, Commission on Standardization of Laboratory and Field Tests, Int. J. Rock Mech. Min. Sci. & Geomech. Abstract 15, 319-368.

ITASCA. 2011. Long-Term Geomechanical Stability Analysis. Itasca Consulting Group, Inc. report for the Nuclear Waste Management Organization NWMO DGR-TR-2011-17 R000. Toronto, Canada.

Jackson, R.E. and D. Heagle. 2010. Opportunistic Groundwater Sampling in DGR-1 and DGR-2. Intera Engineering Ltd. Report TR-07-11 Rev.2. Ottawa, Canada.

Jackson, R.E. and S. Murphy. 2011. Mineralogical and Lithogeochemical Analyses of DGR-5 and DGR-6 Core. Intera Engineering Ltd. Report TR-09-06 Rev.0. Ottawa, Canada.

Jackson, R.E and A. Wigston. 2010. Laboratory Petrophysical Testing of DGR-3 and DGR-4 Core. Intera Engineering Ltd. Report TR-08-28 Rev.0. Ottawa, Canada.

Jackson, R.E. 2009. Organic Geochemistry and Clay Mineralogy of DGR-3 and DGR-4 Core . Intera Engineering Ltd. Report TR-08-29. Rev.0. Ottawa, Canada.

Jackson, R.E. and S. Sterling. 2008. Summary of Surrogate Core Analyses. Intera Engineering Ltd. Report TR-07-02 Rev.1. Ottawa, Canada.

Jensen, M.R. and R.J. Heystee. 1989. Bruce NPD Conventional Landfill Site, Investigation of Hydrogeological Conditions. Ontario Hydro Report No. 89206. Toronto, Canada.

Jensen, M.R. and R.J. Heystee. 1987. BNPD Radioactive Waste Operations Sites 1 and 2 Survey of Local Geologic and Hydrogeologic Conditions. Ontario Hydro Report No. 87126. Toronto, Canada.

Jensen, M.R. and J.F. Sykes. 1995. Numerical Simulation of a Shallow Ground Water Flow System, Southwestern Ontario Reference Site. Report COG-95-254. Toronto, Canada.

Jensen, M.R. and J.F. Sykes. 1993. Bruce NPD Radioactive Waste Operations Site 1 Analysis of Ground Water Flow and Tritium Migration. Ontario Hydro Report No. 938025. Toronto, Canada.

Johnson, M.D., D.K. Armstrong, B.V. Sanford, P.G. Telford and M.A. Rutka. 1992. Paleozoic and Mesozoic geology of Ontario: In Geology of Ontario, Ontario Geological Survey 4 (2), 907-1008.

Jones, S.C. 1997. A technique for faster pulse-decay permeability measurements in tight rocks. SPE Formation Evaluation 12 (1), 19-26.

Jorgensen, D.G., T. Gogel and D.C. Signor. 1982. Determination of flow in aquifers containing variable-density water. Groundwater Monitoring Review 2 (2), 40-45.

Keelan, D.K. and V.J. Pugh. 1975. Trapped-gas saturations in carbonate formations. SPE Journal 15 (2), 149-160.

Kolata, R., W.D. Huff and S.M. Bergstrom. 1998. Nature and regional significance of unconformities associated with Middle Ordovician Hagan K-bentonite complex in the North American midcontinent. Geological Society of America Bulletin 110, 723-739.

Koroleva, M., A. de Haller, U. Mader, H.N. Waber and M. Mazurek. 2009. Borehole DGR-2: Pore-Water Investigations, Intera Engineering Ltd. Report TR-08-06 Rev.0. Rock Water Interaction (RWI), Institute of Geological Sciences, University of Bern, Bern, Switzerland.

Kotzer, T., M. Gascoyne, M. Mukai, J. Ross, G. Waite, G. Milton, G. and R.J. Cornett. 1998. ^{36}Cl, ^{129}I and noble gas isotope systematics in groundwaters from the Lac du Bonnet Batholith, Manitoba, Canada. Radiochimica Acta 82, 313–318.

Lake, L.W. 1989. Enhanced Oil Recovery, Prentice Hall, Englewood Cliffs, New Jersey.

Langmuir, D. 1997. Aqueous Environmental Geochemistry. Prentice Hall, Upper Saddle River, New Jersey.

Lee, D., T. Kotzer and K. King. 1995. Preliminary Assessment of Low- and Intermediate-Level Waste Disposal in the Michigan Basin: Isotopic and Geochemical Measurements. Report COG-95-248-I. Chalk River, Canada.

Lerman, A. 1979. Geochemical Processes: Water and Sediment Environments. Wiley-Interscience, New York, NY USA.

Lo, K.Y., R.S.C. Wai, J.H.L. Palmer and R.M. Quigley. 1978. Time-dependent deformation of shaly rocks in Southern Ontario. Canadian Geotechnical Journal 15, 537-547.

Lowenstein, T.K. and M.N. Timofeeff. 2008. Secular variations in seawater chemistry as a control on the chemistry of basinal brines: test of hypothesis. Geofluids 8, 77-92.

Lowenstein, T.K., M.N. Timofeeff, S.T. Srennan, L.A. Hardie and R.V. Demicco. 2001. Oscillations in Phanerozoic Seawater Chemistry: Evidence from Fluid Inclusions. Science 294, 1086-1088.

Lucia, F.J. 1999. Carbonate Reservoir Characterization. Springer, Berlin, Germany.

Lukajic, B.J. 1988. Preliminary Results of the 1986-87 Geological Investigations, BNPD Proposed Underground Irradiated Fuel Storage Facility. Ontario Hydro Report GHED-DR-8801. Toronto, Canada.

Lukajic, B.J., I. Azis and L. Mansson. 1986. Seepage control during tunnel driving under Lake Huron. Proceedings, International Symposium on Large Rock Caverns, August 25-29. Helsinki, Finland.

Lukajic, B.J. and D.D. Dupak. 1986. Summary of Ontario Hydro's Tunnelling Experience at Bruce, Darlington and Wesleyville. Ontario Hydro Report No. 86009. Toronto, Canada.

Lusczynski, N. J. 1961. Head and flow of groundwater of variable density. Journal of Geophysical Research 66, 4247-4256.

Ma, L., M.C. Castro and C. M. Hall. 2009. Crustal noble gases in deep brines as natural tracers of vertical transport processes in the Michigan Basin. Geochemistry. Geophysics. Geosystems. 10.

Maloney, S. 2010. CERCHAR Abrasivity Testing of Argillaceous Limestone of the Cobourg Formation. Intera Engineering Ltd. Report TR-07-04 Rev.2. MIRARCO/Geomechanics Research Centre, Laurentian University. Sudbury, Canada.

Maloney, S. and N. Bahrani. 2009. CERCHAR Abrasivity Testing of Argillaceous Limestone of the Cobourg Formation from DGR-3 and DGR-4. Intera Engineering Ltd. Report TR-08-25 Rev.0. MIRARCO/Geomechanics Research Centre, Laurentian University. Sudbury, Canada.

Martin, C.D. and G.W. Lanyon. 2003. EDZ in Clay Shale. Mont Terri, Mont Terri TR2001-01, Geoscience Ltd. Falmouth, United Kingdom.

Martin, C. D. and B. Stimpson. 1994. The effect of sample disturbance on laboratory properties of Lac du Bonnet granite. Canadian Geotechnical Journal 31, (5), 692-702.

Mazurek, M. 2004. Long-term Used Nuclear Fuel Waste Management – Geoscientific Review of the Sedimentary Sequence in Southern Ontario. Institute of Geological Sciences, University of Bern Technical Report TR 04-01, Switzerland.

Mazurek, M., P. Alt-Epping, A. Bath, T. Gimmi and H.N. Waber. 2009. Natural Tracer Profiles Across Argillaceous Formations: The CLAYTRAC Project. OECD/NEA Report No. 6253.

McIntosh, J.C. and L.M. Walter. 2006. Paleowaters in Silurian-Devonian carbonate aquifers: Geochemical evolution of groundwater in the Great Lakes region since the Late Pleistocene. Geochimica et Cosmochimica Acta 70, 2454-2479.

McIntosh, J.C. and L.M. Walter. 2005. Volumetrically significant recharge of Pleistocene glacial meltwaters into epicratonic basins: Constraints imposed by solute mass balances. Chemical Geology 222, 292-309.

McKay, D.A. 1989. Bruce NGS, "B" Stress Measurements, Co-operative Pilot Project - Final Report. Ontario Hydro Research Report 89-156-K. Toronto, Canada.

Melaney, M. 2009. Borehole Geophysical Logging of US-3 and US-7. Intera Engineering Ltd. Report TR-08-03 Rev.1. Ottawa, Canada.

Micic, S. and K.Y. Lo. 2009. Laboratory Free Swell Testing of DGR-3 and DGR-4 Core. Intera Engineering Ltd. Report TR-08-26 Rev.0. K.Y. Lo Inc. London, Canada.

Micic, S. and K.Y. Lo. 2010. Laboratory Swell Testing of DGR-2 Core. Intera Engineering Ltd. Report TR-07-16 Rev.2. K.Y. Lo Inc. London, Canada.

Murphy, S. and D. Heagle. 2011. Phase 2 Groundwater Monitoring: US-3, US-7 and US-8. Intera Engineering Ltd. Report TR-08-30 Rev.0. Ottawa, Canada.

Neuzil, C.E. 2000. Osmotic generation of 'anomalous' fluid pressures in geological environments. Nature 13, 182-184.

Neuzil, C.E. 1995. Abnormal pressures as hydrodynamic phenomena. American Journal of Science 295, 742-786.

Neuzil, C.E. 1994. How permeable are clays and shales? Water Resources Research 30, (2), 145-150.

Neuzil, C.E. 1993. Low fluid pressure within the Pierre Shale: A transient response to erosion, Water Resources Research 29 (7), 2007-2020.

Nightingale, E.R. 1959. Phenomenological theory of ion salvation. Effective radii of hydrated ions. Journal of Physical Chemistry 63, 1381-1387.

NWMO 2009. L&ILW Deep Geologic Repository Project Quality Plan. Nuclear Waste Management Organization Document 00216N-PLAN-00120-0002-R002. Toronto, Canada.

NWMO. 2011. Geosynthesis. Nuclear Waste Management Organization Report NWMO DGR-TR-2011-11 R000. Toronto, Canada.

NWMO and AECOM. 2011. Regional Geomechanics – Southern Ontario. AECOM Canada Ltd. and Nuclear Waste Management Organization Report NWMO DGR-TR-2011-13 R000. Toronto, Canada.

Obermajer, M., M.G. Fowler and L.R. Snowdon. 2002. Petroleum systems in southern Ontario: A geochemical perspective. Abstract, Annual Convention, Canadian Society of Petroleum Geologists.

Obermajer, M., M.G. Fowler, Goodarzi, F. and L.R. Snowdon. 1996. Assessing thermal maturity of Paleozoic rocks from reflectance of chitinozoa as constrained by geochemical indicators: an example from southern Ontario, Canada. Marine & Petroleum Geology 13 (8), 907-919.

Obermajer, M., M.G. Fowler and L.R. Snowdon. 1999. Depositional environment and oil generation in Ordovician source rocks from southwestern Ontario, Canada: Organic geochemical and petrological approach. AAPG Bulletin 83 (9), 1426-1453.

Ontario Geological Survey. 1991. Bedrock Geology of Ontario, Southern Sheet. Ontario Geological Survey, Map 2544, Scale 1:1,000,000.

Parkhurst, D.L. and C.A.J. Appelo. 1999. User's guide to PHREEQC (Version 2) – A computer program for speciation, batch-reaction, one-dimensional transport, and inverse geochemical calculations. U.S. Geological Survey, Water-Resources Investigations Report, 99-4259.

Pearson, F.J. 1987. Models of mineral controls on the composition of saline groundwaters of the Canadian Shield. In: Saline Water and Gases in Crystalline Rocks. Fritz, P. and S.K. Frape (Eds.). Geological Association of Canada Special Paper 33, 39-51.

Pearson, F.J. 1965. Use of C-13/C-12 ratios to correct radiocarbon ages of material initially diluted by limestone. In: Proceedings of the 6th International Conference on Radiocarbon and Tritium Dating, Pulman, Washington DC, 357-366.

Pearson, F.J. and B.B. Hanshaw. 1970. Sources of dissolved carbonate species in groundwater and their effects on carbon-14 dating. In: Isotope Hydrology 1970, IAEA Symposium 129/18, March 1970, Vienna, 271-286.

Pehme, P. and M. Melaney. 2010a. Borehole Geophysical Logging in DGR-1 and DGR-2. Intera Engineering Ltd. Report TR-07-08 Rev.3. Ottawa, Canada.

Pehme, P. and M. Melaney. 2010b. Borehole Geophysical Logging in DGR-3 and DGR-4. Intera Engineering Ltd. Report TR-08-15 Rev.1. Ottawa, Canada.

Pehme, P. and M. Melaney. 2011. Borehole Geophysical Logging of DGR-5 and DGR-6. Intera Engineering Ltd. Report TR-09-03 Rev.0. Ottawa, Canada.

Petrychenko, O.Y., T.M. Peryt and E.I. Chechel. 2005. Early Cambrian seawater chemistry from fluid inclusions in halite from Siberian evaporates. Chemical Geology 219,149-161.

Pinder, L. 2009. Drilling Fluid Management and Testing in DGR-3 and DGR-4. Intera Engineering Ltd. Report TR-08-16 Rev.0. Ottawa, Canada.

Pittman, E.D. 1992. Relationship of porosity and permeability to various parameters derived from the mercury injection-capillary pressure curves for sandstone. AAPG Bulletin 76 (2), 191-198.

Plinninger, R., H. Kasling, K. Thuro and G. Spaun. 2003. Technical note – Testing conditions and geomechanical properties influencing the CERCHAR abrasiveness index (CAI) value. International Journal of Rock Mechanics & Mining Sciences 40 (2), 259-263.

Pusch, R. 2008. Geological Storage of Radioactive Waste. Springer, Berlin, Germany.

Rao, U. and U. Fehn, 1999. Sources and reservoirs of anthropogenic iodine-129 in western New York. Geochimica et Cosmochimica Acta 63, 1927-1938.

Raven, K.G. and S. Gaines. 2010. Westbay MP55 Casing Completions in DGR-1 and DGR-2. Intera Engineering Ltd. Report TR-07-10 Rev.3. Ottawa, Canada.

Raven, K.G. and R.E. Jackson. 2011. Laboratory Petrophysical Testing of DGR-5 and DGR-6 Core. Intera Engineering Ltd. Report TR-09-08 Rev.0. Ottawa, Canada.

Raven, K.G. and S. Sterling. 2010. Westbay MP38 Casing Completions in US-3, US-7 and US-8. Intera Engineering Ltd. Report TR-07-20 Rev.2. Ottawa, Canada.

Raven, K. E. and S. Sterling. 2011. Drilling Fluid Management and Testing in DGR-5 and DGR-6. Intera Engineering Ltd. Report TR-09-02 Rev.0. Ottawa, Canada.

Raven, K. E. and S. Sterling. 2009. Drilling Fluid Management and Testing in DGR-1 and DGR-2. Intera Engineering Ltd. Report TR-07-09 Rev.0. Ottawa, Canada.

Raven, K.G., S. Sterling, S. Gaines and A. Wigston. 2009. Regional and site geological frameworks – proposed Deep Geologic Repository, Bruce County, Ontario. Proceedings, 62nd Canadian Geotechnical Conference and 10th Joint CGS/IAH-CNC Groundwater Conference, Halifax, 1348-1355.

Raven, K.G., K.S. Novakowski, R.M. Yager and R.J. Heystee. 1992a. Supernormal fluid pressures in sedimentary rocks of southern Ontario – western New York State. Canadian Geotechnical Journal 29, 80-93.

Raven, K.G., J.L. Smith and R.A. Freeze. 1992b. Hydrogeologic Scoping Calculations on Radionuclide Transport to the Biosphere. Technical Report prepared by Subsurface Advisory Committee to Nuclear Programs Division, Environment Canada.

Remenda, V., G. van der Kamp and J.A. Cherry. 1996. Use of vertical profiles of δ18O to constrain estimates of hydraulic conductivity in a thick, unfractured aquitard. Water Resources Research 32 (10), 2979-2987.

Renaud, R., I.D., Clark, T.G Kotzer, G.M Milton and D.J. Bottomley. 2005. The mobility of anthropogenic 129I in a shallow sand aquifer at Sturgeon Falls, Ontario, Canada, Radiochimica Acta 93, 363-371.

Roberts, R., D. Chace, R.L. Beauheim and J. Avis. 2011. Analysis of Borehole Straddle-Packer Tests in DGR Boreholes. Intera Engineering Ltd. Report TR-08-32 Rev.0. HydroResolutions LLC, Albuquerque, New Mexico, USA.

Rübel, A.P., C. Sonntag, J. Lippmann, F.J. Pearson and A. Gautschi. 2002. Solute transport in formations of very low permeability: Profiles of stable isotope and dissolved noble gas contents of pore water in the Opalinus Clay, Mont Terri, Switzerland. Geochimica et Cosmochimica Acta 66 (8), 1311-1321.

Santarelli, F.J. and M.B. Dusseault. 1991. Core quality control in petroleum engineering, Proceedings 32nd U.S. Symposium on Rock Mechanics. A.A. Balkema, Rotterdam.

Schandl, E. 2011. Petrographic Analyses of DGR-5 and DGR-6 Core. Intera Engineering Ltd. Report TR-09-05 Rev.0. GeoConsult, Toronto, Canada.

Schandl, E. 2010a. Petrographic Analysis of DGR-3 Core. Intera Engineering Ltd. Report TR-08-20 Rev.0. GeoConsult, Toronto, Canada.

Schandl, E. 2010b. Petrographic Analysis of DGR-4 Core. Intera Engineering Ltd. Report TR-08-21 Rev.0. GeoConsult, Toronto, Canada.

Schandl, E. 2009. Petrography of DGR-1 and DGR-2 Core. Intera Engineering Ltd. Report TR-07-12 Rev.0. GeoConsult, Toronto, Canada.

Sharpe, D.R. and W.A.D. Edwards. 1979. Quaternary Geology of the Chesley-Tiverton Area, Southern Ontario. Ontario Geological Survey Preliminary Map p.2314, Geological Series, Scale 1:50,000.

Sherwood Lollar, B., S.M. Weise, S.K. Frape and J.F. Barker. 1994. Isotopic constraints on the migration of hydrocarbon and helium gases of southwestern Ontario. Bulletin of Canadian Petroleum Geology 42 (3), 283-295.

Shouakar-Stash, O. 2008. Evaluation of Stable Chlorine and Bromine Isotopes in Sedimentary Formation Fluids. Ph.D. Thesis, University of Waterloo. Waterloo, Canada.

Skowron, A. and E. Hoffman. 2009a. XRD Mineralogical Analysis of DGR-1 and DGR-2 Core. Intera Engineering Ltd. Report TR-08-01 Rev.0. Activation Laboratories, Ancaster, Canada.

Skowron, A. and E. Hoffman. 2009b. Geochemical and SEM/EDS Analysis of DGR-1 and DGR-2 Core. Intera Engineering Ltd. Report TR-08-02 Rev.0. Activation Laboratories, Ancaster, Canada.

Sterling, S. 2010a. Bedrock Formations in DGR-1 and DGR-2. Intera Engineering Ltd. ReportTR-07-05 Rev.3. Ottawa, Canada.

Sterling, S. 2010b. Drilling Logging and Sampling of DGR-1 and DGR-2. Intera Engineering Ltd. Report TR-07-06 Rev.1. Ottawa, Canada.

Sterling, S. and K.G. Raven. 2011. Pressure and Head Monitoring in MP55 Casing Systems in DGR-1 to DGR-4. Intera Engineering Ltd. Report TR-08-31 Rev.0. Ottawa, Canada.

Sterling, S. and M. Melaney. 2011. Bedrock Formations in DGR-1 to DGR-6. Intera Engineering Ltd. Report TR-09-11 Rev.0. Ottawa, Canada.

Sterling, S., S. Gaines and K.E. Raven. 2011a. Westbay MP55 Casing Completions in DGR-2, DGR-3 and DGR-4. Intera Engineering Ltd. Report TR-08-17 Rev.0. Ottawa, Canada.

Sterling, S., R.E. Jackson, R. Walsh, D. Heagle and I. Clark. 2011b. Assessment of Porosity Data and Gas Phase Presence in DGR Cores. Intera Engineering Ltd. Report TR-08-34 Rev.0. Ottawa, Canada.

Sterling, S., G. Briscoe and M. Melaney. 2011c. Drilling, Logging and Sampling of DGR-5 and DGR-6. Intera Engineering Ltd. Report TR-09-01 Rev.0. Ottawa, Canada.

Stoessell, R.K. and P.A. Byrne. 1982. Salting-out of methane in single-salt solutions at 25°C and below 800 psia. Geochimica et Cosmochimica Acta 46, 1327–1332.

Stumm, W. 1992. Chemistry of the Solid-Water Interface. Wiley-Interscience, New York, USA.

Stumm, W. and J.J. Morgan. 1981. Aquatic Chemistry. John Wiley & Sons Inc., New York, USA.

Sykes, J. F., S. D. Normani and Y. Yin. 2011. Hydrogeologic Modelling. Nuclear Waste Management Organization Report NWMO DGR-TR-2011-16 R000. Toronto, Canada.

Terzaghi, R. D. 1965. Sources of error in joint surveys. Geotechnique 15, 287-304.

Tiab, D. and E.C. Donaldson. 2004. Petrophysics: Theory and Practice of Measuring Reservoir Rock and Fluid Transport Properties. Elsevier Publishers.

Tidwell, V.C., L.C. Meigs, T. Christian-Frear and C.M. Boney. 2000. Effects of spatially heterogeneous porosity on matrix diffusion as investigated by X-ray absorption imaging. Journal of Contaminant Hydrology 42, 285-302.

US EPA. 2002. EPA Guidance for Quality Assurance Project Plans, EPA QA/G-5. United States Environmental Protection Agency Report EPA/660/R-98/018. Washington, D.C., USA.

Valley, B. and S. Maloney. 2010. Analysis of DGR-1, DGR-2, DGR-3 and DGR-4 Borehole Images for Stress Characterization. Intera Engineering Ltd. Report TR-08-35 Rev.1. MIRARCO/ Geomechanics Research Centre, Laurentian University. Sudbury, Canada.

Valley, B. and S. Maloney. 2009. Analysis of DGR-1 and DGR-2 Borehole Images for Stress Characterization. Intera Engineering Ltd. Report TR-08-04 Rev.0. MIRARCO/ Geomechanics Research Centre, Laurentian University. Sudbury, Canada.

Van Loon, L.R. 2010. Diffusion of ^{125}I- in Limestone and Red Shale Samples from DGR-2. Intera Engineering Ltd. Report TR-07-22 Rev.1. Paul Scherrer Institute, Switzerland.

Van Loon, L.R., J.M. Soler and M.H. Bradbury. 2003. Diffusion of HTO, ^{36}Cl- and ^{125}I- in Opalinus Clay samples from Mont Terri: Effect of confining pressure. Journal of Contaminant Hydrology 61, 73-83.

Vavra, C.L., J.G. Kaldi and R.M. Schneider. 1992. Geological applications of capillary pressure: A review. AAPG Bulletin 76, (2), 840-850.

Veizer, J. 1989. Strontium isotopes in seawater through time. Annual Review of Earth and Planetary Science 17, 141-167.

Vilks, P. and N.H. Miller. 2007. Evaluation of Experimental Protocols for Characterizing Diffusion in Sedimentary Rocks. Nuclear Waste Management Organization Report TR-2007-11. Toronto, Canada.

Vinard, P. 1988. Generation and Evolution of Hydraulic Underpressures in a Marl-Shale Aquitard at Wellenberg, Central Switzerland. Ph.D. Thesis, Université de Neuchâtel, Switzerland.

Waber, H.N., U.K. Mader, M. Koroleva and A. de Haller. 2007. Testing Methods for the Characterization of Saline Pore Water in an Ordovician Limestone (Cobourg Formation, St. Mary's Quarry, Ontario), Feasibility Study. Intera Engineering Ltd. Report TR-07-01. Rock Water Interaction, University of Bern, Switzerland.

Walsh, R. 2011. Compilation and Consolidation of Field and Laboratory Data for Hydrogeological Properties. Intera Engineering Ltd. Report TR-08-10 Rev.0. Ottawa, Canada.

Wang, H.F., Crowley, K.D. and G.C. Nadon. 1994. Chapter 12: Thermal History of the Michigan Basin from Apatite Fission-Track Analysis and Vitrinite Reflectance. In: Ortoleva, P.J. (Ed.). Basin Compartments and Seals. American Association of Petroleum Geologists Memoir 61.

Watts, M., D. Schieck and M. Coniglio. 2009. 2D Seismic Survey of the Bruce Site. Intera Engineering Ltd. Report TR-07-15 Rev.0. Ottawa, Canada.

Weaver, T.R., S.K. Frape and J.A. Cherry. 1995. Recent cross-formational flow and mixing in the shallow Michigan Basin. GSA Bulletin 107 (6), 697-707.

Whiticar, M.J. 1999. Carbon and hydrogen isotope systematic of bacterial formation and oxidation of methane. Chemical Geology 161, 291-314.

Whitney, C. and R. Lee. 2010. Laboratory Petrophysical Testing of DGR-2 Core. Intera Engineering Ltd. Report TR-07-18 Rev.2. Core Laboratories, Houston, USA.

Wigston, A. and D. Heagle. 2009. Bedrock Formations in DGR-1, DGR-2, DGR-3 and DGR-4. Intera Engineering Ltd. Report TR-08-12 Rev.1. Ottawa, Canada.

Wigston, A. and R.E. Jackson. 2010a. Mineralogy and Geochemistry of DGR-3 Core. Intera Engineering Ltd. Report TR-08-22 Rev.0. Ottawa, Canada.

Wigston, A. and R.E. Jackson. 2010b. Mineralogy and Geochemistry of DGR-4 Core. Intera Engineering Ltd. Report TR-08-23 Rev.0. Ottawa, Canada.

8. UNITS

kPa	kilo Pascal
mASL	metres Above Sea Level
mAGS	metres Above Ground Surface
mBGS	metres Below Ground Surface
mLBGS	metres Length Below Ground Surface
MPa	Mega Pascal
TU	Tritium Units

9. ABBREVIATIONS AND ACRONYMS

AEM	Acoustic Emission Monitoring
ANDRA	Agence Nationale pour la Gestion des Déchets Radioactifs
ATV	Acoustic Televiewer
BGS	Below Ground Surface
BP	Before Present
CHIS	Canadian Hazard Information Service
CNSC	Canadian Nuclear Safety Commission
D	Deuterium
D_e	Effective Diffusion Coefficient
D_p	Pore Diffusion Coefficient
DGR	Deep Geologic Repository
DGSM	Descriptive Geosphere Site Model
DO	Dissolved Oxygen
DST	Drill Stem Test
EC	Electrical Conductivity
EDS	Energy Dispersive Spectral
EDZ	Excavation Damage Zone
GMWL	Global Meteoric Water Line
GSCP	Geoscientific Site Characterization Plan
GSI	Geological Strength Index
GW	Groundwater
HS	Hydrostratigraphic Unit
HTO	Tritiated Water
ICP/MS	Inductively Coupled Plasma Mass Spectrometry
K	Hydraulic Conductivity
k	Permeability
m_N	Earthquake Magnitude Nuttli scale
M	Earthquake Magnitude
MNR	Ontario Ministry of National Resources
MS	Mechanostratigraphic Unit
MP	Multi-Port
NWMO	Nuclear Waste Management Organization
OGW	Opportunistic Groundwater

OPG	Ontario Power Generation Inc.
pCO_2	Partial Pressure of CO_2
ρ	Density
σ	Compressive stress
P_c	Capillary Pressure
PIP	Production Injection Packer
PLT	Point Load Test
PDP	Pulse Decay Permeability
PQP	Project Quality Plan
PW	Porewater
QMS	Quality Management System
RMR	Rock Mass Rating
RQD	Rock Quality Designation
S	Saturation
SDI	Slake Durability Index
SI	Saturation Index
SEM	Scanning Electron Microscope
SCP	Site Characterization Plan
TDS	Total Dissolved Solids
TP	Test Plan
TR	Technical Report
UCS	Uniaxial Compressive Strength
V	Linear Groundwater Velocity
VSMOW	Vienna Standard Mean Ocean Water
XRD	X-Ray Diffraction

APPENDICES

THIS PAGE HAS BEEN LEFT BLANK INTENTIONALLY

APPENDIX A: COMPARISON OF HYDROGEOLOGICAL PARAMETERS USED IN MODELLING AND IN DGSM

The tables in this appendix compare interim values of modelling parameters calculated from DGR-1 through DGR-4 data to the final values calculated from data sourced from DGR-1 through DGR-6. Most changes are as a result of recalculating formation averages with additional data from DGR-5 and DGR-6. The interim data were used in Postclosure Safety Assessment modelling (QUINTESSA 2011, QUINTESSA and SENES 2011, INTERA 2011, and INTERA and QUINTESSA 2011) and regional groundwater modeling performed for Geosynthesis (Sykes et al 2011). Compilations of interim data are also presented in QUINTESSA and INTERA (2011). For the most part, interim data were sourced from the April 2010 Revision C version of the current DGSM report and the July 2010 Revision D report.

In the tables below, cells are shaded if a difference in property values is apparent. Column titles show the report revision: V1 is the current, final version, while V1C and V1D are the interim versions. Even though a number of values did change for each parameter, the changes were largely inconsequential, and are anticipated to have no significant impact on modelling results.

Table A1: Comparison of Hydraulic Conductivity Values

Formation	V1 K_h (m/s)	V1D K_h (m/s)	V1 K_h:K_v (−)	V1D K_h:K_v (−)
Clay till overburden	$8x10^{-10}$	$8x10^{-10}$	2:1	2:1
Lucas	$1x10^{-6}$	$1x10^{-6}$	10:1	10:1
Amherstburg (top 20 m)	$1x10^{-6}$	$1x10^{-6}$	10:1	10:1
Amherstburg (lower 25 m)	$1x10^{-7}$	$1x10^{-7}$	10:1	10:1
Bois Blanc	$1x10^{-7}$	$1x10^{-7}$	10:1	10:1
Bass Islands (upper 20m)	$1x10^{-4}$	$1x10^{-4}$	10:1	10:1
Bass Islands (lower 25 m)	$1x10^{-5}$	$1x10^{-5}$	10:1	10:1
Salina G Unit	$1x10^{-11}$	$1x10^{-11}$	10:1	10:1
Salina F Unit	$5x10^{-14}$	$5x10^{-14}$	10:1	10:1
Salina E Unit	$2x10^{-13}$	$2x10^{-13}$	10:1	10:1
Salina D Unit	$2x10^{-13}$	$2x10^{-13}$	10:1	10:1
Salina C Unit	$4x10^{-13}$	$4x10^{-13}$	10:1	10:1
Salina B Unit − Carbonate	$4x10^{-13}$	$4x10^{-13}$	10:1	10:1
Salina B Unit − Evaporite	$3x10^{-13}$	$3x10^{-13}$	10:1	10:1
Salina A2 Unit − Carbonate	$3x10^{-10}$	$3x10^{-10}$	10:1	10:1
Salina A2 Unit − Evaporite	$3x10^{-13}$	$3x10^{-13}$	10:1	10:1
Salina A1 Unit – Upper Carbonate	$2x10^{-7}$	$2x10^{-7}$	1:1	1:1
Salina A1 Unit − Lower Carbonate	$9x10^{-12}$	$9x10^{-12}$	10:1	10:1
Salina A1 Unit − Evaporite	$3x10^{-13}$	$3x10^{-13}$	10:1	10:1
Salina A0 Unit	$3x10^{-13}$	$3x10^{-13}$	10:1	10:1
Guelph	$3x10^{-8}$	$3x10^{-8}$	1:1	1:1
Goat Island	$2x10^{-12}$	$2x10^{-12}$	10:1	10:1
Gasport	$2x10^{-12}$	$2x10^{-12}$	10:1	10:1
Lions Head	$5x10^{-12}$	$5x10^{-12}$	10:1	10:1
Fossil Hill	$5x10^{-12}$	$5x10^{-12}$	10:1	10:1
Cabot Head	$9x10^{-14}$	$9x10^{-14}$	10:1	10:1
Manitoulin	$1x10^{-13}$	$9x10^{-14}$	10:1	10:1
Queenston	$3x10^{-14}$	$2x10^{-14}$	10:1	10:1
Georgian Bay	$3x10^{-14}$	$3x10^{-14}$	10:1	10:1
Blue Mountain	$3x10^{-14}$	$5x10^{-14}$	10:1	10:1
Cobourg – Collingwood Member	$2x10^{-14}$	$2x10^{-14}$	10:1	10:1
Cobourg − Lower	$1x10^{-14}$	$2x10^{-14}$	10:1	10:1
Sherman Fall	$9x10^{-15}$	$1x10^{-14}$	10:1	10:1
Kirkfield	$4x10^{-15}$	$8x10^{-15}$	10:1	10:1
Coboconk	$2x10^{-11}$	$4x10^{-12}$	10−1000:1	10−100:1
Gull River	$2x10^{-12}$	$7x10^{-13}$	10−1000:1	10:1
Shadow Lake	$1x10^{-9}$	$1x10^{-9}$	10:1	10:1
Cambrian	$3x10^{-6}$	$3x10^{-6}$	1:1	1:1
Upper Precambrian	$1x10^{-10}$	$1x10^{-10}$	1:1	1:1

Table A2: Comparison of Liquid Porosity Values

Formation	V1 Liquid Porosity (%)	V1D Liquid Porosity (%)	V1C Liquid Porosity (%)
Clay till overburden	20	20	20
Lucas	7.8	7.7	7.0
Amherstburg (top 20 m)	7.8	7.7	7.0
Amherstburg (lower 25 m)	7.8	7.7	7.0
Bois Blanc	7.8	7.7	7.7
Bass Islands (upper 20m)	5.5	5.6	5.7
Bass Islands (lower 25 m)	5.5	5.6	5.7
Salina G Unit	16.7	17.2	17.2
Salina F Unit	10.7	10.0	12.8
Salina E Unit	11.9	10.0	13.5
Salina D Unit	6.7	8.9	9.8
Salina C Unit	18.5	20.5	20.5
Salina B Unit − Carbonate	15.8	14.5	16.5
Salina B Unit − Evaporite	6.7	8.9	9.8
Salina A2 Unit − Carbonate	12.4	12.0	14.5
Salina A2 Unit − Evaporite	6.7	8.9	9.8
Salina A1 Unit – Upper Carbonate	6.3	7.0	7.0
Salina A1 Unit − Lower Carbonate	4.0	1.9	1.9
Salina A1 Unit − Evaporite	1.1	0.7	0.7
Salina A0 Unit	2.7	3.2	2.7
Guelph	13.1	5.7	5.7
Goat Island	2.8	2.0	2.0
Gasport	1.9	2.0	2.0
Lions Head	8.3	3.1	3.1
Fossil Hill	0.5	3.1	3.1
Cabot Head	10.4	11.6	11.6
Manitoulin	2.4	2.8	2.8
Queenston	7.5	7.3	7.3
Georgian Bay	7.1	7.1	7.1
Blue Mountain	7.1	7.8	7.8
Cobourg – Collingwood Member	1.1	1.2	1.2
Cobourg − Lower	1.4	1.5	1.5
Sherman Fall	1.7	1.6	1.6
Kirkfield	2.3	2.1	2.1
Coboconk	0.9	0.9	0.9
Gull River	2.2	2.2	2.2
Shadow Lake	8.9	9.7	9.7
Cambrian	6.7	7.1	7.1
Upper Precambrian	3.7	3.8	3.8

Table A3: Comparison of Diffusion Porosity Values

Formation	V1 Diffusion Porosity (%)	V1D Diffusion Porosity (%)	V1C Diffusion Porosity (%)
Clay till overburden	20	20	20
Lucas	7.8	7.0	7.0
Amherstburg (top 20 m)	7.8	7.0	7.0
Amherstburg (lower 25 m)	7.8	7.0	7.0
Bois Blanc	7.8	7.0	7.0
Bass Islands (upper 20m)	5.5	5.6	5.7
Bass Islands (lower 25 m)	5.5	5.6	5.7
Salina G Unit	0.9	0.9	0.9
Salina F Unit	4.8	4.8	4.8
Salina E Unit	5.5	5.5	5.5
Salina D Unit	0.7	0.7	0.7
Salina C Unit	8.5	8.5	8.5
Salina B Unit − Carbonate	8.7	8.7	8.7
Salina B Unit − Evaporite	0.7	0.7	0.7
Salina A2 Unit − Carbonate	3.9	3.9	3.9
Salina A2 Unit − Evaporite	0.7	0.7	0.7
Salina A1 Unit – Upper Carbonate	6.3	7.0	7.0
Salina A1 Unit − Lower Carbonate	1.1	1.1	1.1
Salina A1 Unit − Evaporite	0.1	0.1	0.1
Salina A0 Unit	1.8	1.8	1.8
Guelph	13.1	5.7	5.7
Goat Island	1.2	1.2	1.2
Gasport	1.2	1.2	1.2
Lions Head	8.3	1.3	1.3
Fossil Hill	0.5	1.3	1.3
Cabot Head	6.8	6.8	6.8
Manitoulin	1.2	1.3	1.3
Queenston	3.7	3.7	3.7
Georgian Bay	3.4	3.4	3.4
Blue Mountain	4.3	4.3	4.3
Cobourg – Collingwood Member	1.7	1.7	1.7
Cobourg − Lower	1.3	1.3	1.3
Sherman Fall	0.45	0.45	0.45
Kirkfield	2.1	2.1	2.1
Coboconk	1.1	1.1	1.1
Gull River	1.4	1.4	1.4
Shadow Lake	8.9	9.7	9.7
Cambrian	6.7	7.1	7.1
Upper Precambrian	3.7	3.8	3.8

Table A4: Comparison of Total Porosity Values

Formation	V1 Total Porosity (%)	V1D Total Porosity (%)	V1C Total Porosity (%)
Clay till overburden	20	20	20
Lucas	7.8	7.7	7.0
Amherstburg (top 20 m)	7.8	7.7	7.0
Amherstburg (lower 25 m)	7.8	7.7	7.0
Bois Blanc	7.8	7.7	7.7
Bass Islands (upper 20m)	5.5	5.6	5.7
Bass Islands (lower 25 m)	5.5	5.6	5.7
Salina G Unit	16.7	17.2	17.2
Salina F Unit	10.7	10.7	10.7
Salina E Unit	11.9	11.9	11.9
Salina D Unit	8.9	8.9	8.8
Salina C Unit	19.4	19.4	19.4
Salina B Unit − Carbonate	15.8	15.7	15.7
Salina B Unit − Evaporite	8.9	8.9	8.8
Salina A2 Unit − Carbonate	12.4	12.4	12.4
Salina A2 Unit − Evaporite	8.9	8.9	8.9
Salina A1 Unit – Upper Carbonate	6.3	7.0	7.0
Salina A1 Unit − Lower Carbonate	4.0	2.9	2.9
Salina A1 Unit − Evaporite	1.2	1.2	1.2
Salina A0 Unit	5.4	5.4	5.4
Guelph	13.1	7.5	7.5
Goat Island	2.8	2.1	2.1
Gasport	1.9	2.1	2.1
Lions Head	8.3	3.1	3.1
Fossil Hill	0.5	3.1	3.1
Cabot Head	10.4	7.6	7.6
Manitoulin	3.1	3.1	3.1
Queenston	7.5	6.9	6.7
Georgian Bay	7.1	7.6	5.3
Blue Mountain	7.1	7.2	6.5
Cobourg – Collingwood Member	2.3	2.9	2.9
Cobourg − Lower	1.9	1.8	1.7
Sherman Fall	2.9	3.0	1.7
Kirkfield	2.3	2.1	2.1
Coboconk	0.9	0.7	0.7
Gull River	2.2	1.8	1.8
Shadow Lake	8.9	8.3	8.3
Cambrian	10.1	10.1	10.1
Upper Precambrian	3.8	3.8	3.8

Table A5: Comparison of Specific Storage Values

Formation	V1 S_s (m^{-1})	V1D S_s (m^{-1})	Sykes et al. 2011 S_s (m^{-1})
Clay till overburden	$1x10^{-3}$	$1x10^{-3}$	$9.90x10^{-5}$
Lucas	$5x10^{-7}$ – $7x10^{-7}$	$8x10^{-7}$	$1.40x10^{-6}$
Amherstburg (top 20 m)	$7x10^{-7}$ – $2x10^{-6}$	$2x10^{-6}$	$1.40x10^{-6}$
Amherstburg (lower 25 m)	$7x10^{-7}$ – $2x10^{-6}$	$2x10^{-6}$	$1.40x10^{-6}$
Bois Blanc	$6x10^{-7}$ – $1x10^{-6}$	$1x10^{-6}$	$1.40x10^{-6}$
Bass Islands (upper 20m)	$1x10^{-6}$ – $2x10^{-6}$	$2x10^{-6}$	$2.00x10^{-6}$
Bass Islands (lower 25 m)	$1x10^{-6}$ – $2x10^{-6}$	$2x10^{-6}$	$2.00x10^{-6}$
Salina G Unit	$1x10^{-6}$ – $2x10^{-6}$	$5x10^{-6}$	$1.10x10^{-6}$
Salina F Unit	$1x10^{-6}$ – $7x10^{-6}$	$3x10^{-6}$	$9.50x10^{-7}$
Salina E Unit	$1x10^{-6}$ – $7x10^{-6}$	$3x10^{-6}$	$6.50x10^{-7}$
Salina D Unit	$5x10^{-7}$ – $7x10^{-7}$	$8x10^{-7}$	$6.40x10^{-7}$
Salina C Unit	$2x10^{-6}$ – $1x10^{-5}$	$5x10^{-6}$	$9.50x10^{-7}$
Salina B Unit − Carbonate	$5x10^{-6}$ – $2x10^{-5}$	$3x10^{-5}$	$9.50x10^{-7}$
Salina B Unit − Evaporite	$5x10^{-7}$ – $7x10^{-7}$	$9x10^{-7}$	$6.90x10^{-7}$
Salina A2 Unit − Carbonate	$1x10^{-6}$ – $2x10^{-6}$	$2x10^{-6}$	$7.20x10^{-7}$
Salina A2 Unit − Evaporite	$5x10^{-7}$ – $6x10^{-7}$	$7x10^{-7}$	$5.80x10^{-7}$
Salina A1 Unit – Upper Carbonate	$5x10^{-7}$ – $1x10^{-6}$	$1x10^{-6}$	$4.10x10^{-7}$
Salina A1 Unit − Lower Carbonate	$5x10^{-7}$ – $1x10^{-6}$	$1x10^{-6}$	$4.10x10^{-7}$
Salina A1 Unit − Evaporite	$3x10^{-7}$ – $4x10^{-7}$	$4x10^{-7}$	$4.50x10^{-7}$
Salina A0 Unit	$3x10^{-7}$ – $3x10^{-7}$	$2x10^{-7}$	
Guelph	$9x10^{-7}$ – $1x10^{-6}$	$1x10^{-6}$	$2.70x10^{-7}$
Goat Island	$3x10^{-7}$ – $5x10^{-7}$	$5x10^{-7}$	
Gasport	$3x10^{-7}$ – $5x10^{-7}$	$5x10^{-7}$	
Lions Head	$5x10^{-7}$ – $7x10^{-7}$	$7x10^{-7}$	
Fossil Hill	$3x10^{-7}$ – $4x10^{-7}$	$9x10^{-7}$	$2.90x10^{-7}$
Cabot Head	$4x10^{-6}$ – $3x10^{-5}$	$3x10^{-5}$	$1.10x10^{-6}$
Manitoulin	$7x10^{-7}$ – $1x10^{-6}$	$2x10^{-6}$	$7.50x10^{-7}$
Queenston	$1x10^{-6}$ – $5x10^{-6}$	$4x10^{-6}$	$9.00x10^{-7}$
Georgian Bay	$2x10^{-6}$ – $1x10^{-5}$	$1x10^{-5}$	$1.20x10^{-6}$
Blue Mountain	$3x10^{-6}$ – $3x10^{-5}$	$1x10^{-5}$	$1.20x10^{-6}$
Cobourg – Collingwood Member	$5x10^{-7}$ – $1x10^{-6}$	$1x10^{-6}$	
Cobourg − Lower	$3x10^{-7}$ – $6x10^{-7}$	$7x10^{-7}$	$2.60x10^{-7}$
Sherman Fall	$8x10^{-7}$ – $2x10^{-6}$	$3x10^{-6}$	$4.90x10^{-7}$
Kirkfield	$7x10^{-7}$ – $2x10^{-6}$	$2x10^{-6}$	$4.90x10^{-7}$
Coboconk	$2x10^{-7}$ – $4x10^{-7}$	$2x10^{-6}$	$4.60x10^{-7}$
Gull River	$3x10^{-7}$ – $6x10^{-7}$	$2x10^{-6}$	$4.90x10^{-7}$
Shadow Lake	$8x10^{-7}$ – $1x10^{-6}$	$1x10^{-6}$	$7.40x10^{-7}$
Cambrian	$8x10^{-7}$ – $1x10^{-6}$	$1x10^{-6}$	$3.70x10^{-7}$
Upper Precambrian	$1x10^{-6}$	$1x10^{-6}$	$2.60x10^{-7}$

Table A6: Comparison of Effective Diffusion Values

Formation	V1 D_e NaI (m^2/s)	V1D D_e NaI (m^2/s)	V1C D_e NaI (m^2/s)
Clay till overburden	$6.0x10^{-10}$	$6.0x10^{-10}$	$6.0x10^{-10}$
Lucas	$1.0x10^{-11}$	$6.0x10^{-12}$	$6.0x10^{-12}$
Amherstburg (top 20 m)	$1.0x10^{-11}$	$6.0x10^{-12}$	$6.0x10^{-12}$
Amherstburg (lower 25 m)	$1.0x10^{-11}$	$6.0x10^{-12}$	$6.0x10^{-12}$
Bois Blanc	$1.0x10^{-11}$	$6.0x10^{-12}$	$6.0x10^{-12}$
Bass Islands (upper 20m)	$5.0x10^{-12}$	$1.3x10^{-11}$	$1.3x10^{-11}$
Bass Islands (lower 25 m)	$5.0x10^{-12}$	$1.3x10^{-11}$	$1.3x10^{-11}$
Salina G Unit	$4.3x10^{-13}$	$4.3x10^{-13}$	$4.3x10^{-13}$
Salina F Unit	$4.1x10^{-12}$	$4.1x10^{-12}$	$4.1x10^{-12}$
Salina E Unit	$4.7x10^{-12}$	$4.7x10^{-12}$	$4.7x10^{-12}$
Salina D Unit	$4.7x10^{-12}$	$4.7x10^{-12}$	$4.7x10^{-12}$
Salina C Unit	$1.1x10^{-11}$	$1.1x10^{-11}$	$1.1x10^{-11}$
Salina B Unit − Carbonate	$1.2x10^{-11}$	$1.2x10^{-11}$	$1.2x10^{-11}$
Salina B Unit − Evaporite	$7.7x10^{-14}$	$7.7x10^{-14}$	$7.7x10^{-14}$
Salina A2 Unit − Carbonate	$1.2x10^{-12}$	$1.2x10^{-12}$	$1.2x10^{-12}$
Salina A2 Unit − Evaporite	$7.7x10^{-14}$	$7.7x10^{-14}$	$7.7x10^{-14}$
Salina A1 Unit – Upper Carbonate	$6.8x10^{-12}$	$4.9x10^{-12}$	$4.9x10^{-12}$
Salina A1 Unit − Lower Carbonate	$1.8x10^{-13}$	$1.8x10^{-13}$	$1.8x10^{-13}$
Salina A1 Unit − Evaporite	$3.0x10^{-14}$	$3.0x10^{-14}$	$3.0x10^{-14}$
Salina A0 Unit	$3.0x10^{-14}$	$3.0x10^{-14}$	$3.0x10^{-14}$
Guelph	$2.9x10^{-11}$	$3.2x10^{-12}$	$3.2x10^{-12}$
Goat Island	$1.5x10^{-13}$	$1.5x10^{-13}$	$1.5x10^{-13}$
Gasport	$1.5x10^{-13}$	$1.5x10^{-13}$	$1.5x10^{-13}$
Lions Head	$1.2x10^{-11}$	$6.2x10^{-12}$	$6.2x10^{-12}$
Fossil Hill	$4.3x10^{-14}$	$1.6x10^{-11}$	$1.6x10^{-11}$
Cabot Head	$3.1x10^{-12}$	$3.1x10^{-12}$	$3.1x10^{-12}$
Manitoulin	$1.5x10^{-13}$	$1.5x10^{-13}$	$1.5x10^{-13}$
Queenston	$1.0x10^{-12}$	$1.0x10^{-12}$	$1.0x10^{-12}$
Georgian Bay	$4.3x10^{-13}$	$4.3x10^{-13}$	$6.8x10^{-13}$
Blue Mountain	$8.2x10^{-13}$	$8.2x10^{-13}$	$8.2x10^{-13}$
Cobourg – Collingwood Member	$4.9x10^{-13}$	$4.9x10^{-13}$	$4.9x10^{-13}$
Cobourg − Lower	$3.7x10^{-13}$	$3.7x10^{-13}$	$3.7x10^{-13}$
Sherman Fall	$2.2x10^{-13}$	$2.2x10^{-13}$	$2.2x10^{-13}$
Kirkfield	$4.2x10^{-13}$	$4.2x10^{-13}$	$4.2x10^{-13}$
Coboconk	$2.7x10^{-13}$	$2.7x10^{-13}$	$2.7x10^{-13}$
Gull River	$2.6x10^{-13}$	$2.6x10^{-13}$	$2.6x10^{-13}$
Shadow Lake	$1.3x10^{-12}$	$6.1x10^{-12}$	$6.1x10^{-12}$
Cambrian	$1.7x10^{-11}$	$7.7x10^{-12}$	$7.7x10^{-12}$
Upper Precambrian	$3.0x10^{-13}$	$3.0x10^{-13}$	$3.0x10^{-13}$

Table A6: Comparison of Effective Diffusion Ratios

Formation	V1 D_{e-h}:D_{e-v} (−)	V1D D_{e-h}:D_{e-v} (−)	V1C D_{e-h}:D_{e-v} (−)
Clay till overburden	1:1	1:1	1:1
Lucas	1:1	1:1	1:1
Amherstburg (top 20 m)	1:1	1:1	1:1
Amherstburg (lower 25 m)	1:1	1:1	1:1
Bois Blanc	1:1	1:1	1:1
Bass Islands (upper 20m)	1:1	1:1	1:1
Bass Islands (lower 25 m)	1:1	1:1	1:1
Salina G Unit	2:1	2:1	2:1
Salina F Unit	2:1	2:1	2:1
Salina E Unit	2:1	2:1	2:1
Salina D Unit	2:1	2:1	2:1
Salina C Unit	2:1	2:1	2:1
Salina B Unit − Carbonate	2:1	2:1	2:1
Salina B Unit − Evaporite	2:1	2:1	2:1
Salina A2 Unit − Carbonate	2:1	2:1	2:1
Salina A2 Unit − Evaporite	2:1	2:1	2:1
Salina A1 Unit – Upper Carbonate	1:1	1:1	1:1
Salina A1 Unit − Lower Carbonate	2:1	2:1	2:1
Salina A1 Unit − Evaporite	2:1	2:1	2:1
Salina A0 Unit	2:1	2:1	2:1
Guelph	1:1	1:1	2:1
Goat Island	2:1	2:1	1:1
Gasport	2:1	2:1	2:1
Lions Head	2:1	2:1	2:1
Fossil Hill	2:1	2:1	2:1
Cabot Head	2:1	2:1	2:1
Manitoulin	2:1	2:1	2:1
Queenston	2:1	2:1	2:1
Georgian Bay	7:1	7:1	2:1
Blue Mountain	2:1	2:1	2:1
Cobourg – Collingwood Member	2:1	2:1	2:1
Cobourg − Lower	2:1	2:1	2:1
Sherman Fall	2:1	2:1	2:1
Kirkfield	2:1	2:1	2:1
Coboconk	2:1	2:1	2:1
Gull River	2:1	2:1	2:1
Shadow Lake	2:1	2:1	2:1
Cambrian	1:1	1:1	1:1
Upper Precambrian	1:1	1:1	1:1

Table A7: Comparison of Fluid TDS and Gas Saturation

Formation	V1 Fluid TDS (g/l)	V1D Fluid TDS (g/l)	V1 Gas Saturation (%PV)	V1D Gas Saturation (% PV)
Clay till overburden	0.5	0.5	–	–
Lucas	0.5	0.5	–	–
Amherstburg (top 20 m)	0.5	1.0	–	–
Amherstburg (lower 25 m)	0.5	2.0	–	–
Bois Blanc	3.2	3.2	–	–
Bass Islands (upper 20m)	6.0	6.0	–	–
Bass Islands (lower 25 m)	6.0	6.0	–	–
Salina G Unit	14.8	14.8	–	–
Salina F Unit	59.6	59.6	15.8	16.0
Salina E Unit	124	124	17.8	21.7
Salina D Unit	200	200	–	–
Salina C Unit	249	249	18.0	18.0
Salina B Unit − Carbonate	321	321	0	0
Salina B Unit − Evaporite	321	321	–	–
Salina A2 Unit − Carbonate	120	136	0.7	0.3
Salina A2 Unit − Evaporite	45.6	45.6	15.7	14.7
Salina A1 Unit – Upper Carbonate	22.4	28.6	–	–
Salina A1 Unit − Lower Carbonate	118	192	–	–
Salina A1 Unit − Evaporite	325	325	0	0.3
Salina A0 Unit	318	360	16.9	16.5
Guelph	370	370	–	–
Goat Island	290	300	0.1	0
Gasport	307	300	–	–
Lions Head	306	300	–	–
Fossil Hill	327	300	–	–
Cabot Head	301	306	–	–
Manitoulin	349	350	0	0
Queenston	304	310	6.7	6.6
Georgian Bay	302	308	6.6	7.6
Blue Mountain	294	295	14.5	14.0
Cobourg – Collingwood Member	225	225	18.3	24.1
Cobourg − Lower	286	272	11.9	12.1
Sherman Fall	269	270	15.2	15.1
Kirkfield	230	234	19.9	20.3
Coboconk	255	255	4.0	3.7
Gull River	204	203	20.0	21.3
Shadow Lake	201	200	–	–
Cambrian	235	235	3.3	3.5
Upper Precambrian	–	-	–	–

REFERENCES FOR APPENDIX A

INTERA and QUINTESSA. 2011. Postclosure Safety Assessment: Gas Modelling. Intera Engineering Ltd. and Quintessa Ltd. report for the Nuclear Waste Management Organization NWMO DGR-TR-2011-31 R000. Toronto, Canada.

INTERA. 2011. Postclosure Safety Assessment: Groundwater Modelling. Intera Engineering Ltd. report for the Nuclear Waste Management Organization NWMO DGR-TR-2011-31 R000. Toronto, Canada.

QUINTESSA. 2011a. Postclosure Safety Assessment: Analysis of the Normal Evolution Scenario. Quintessa Ltd. report for the Nuclear Waste Management Organization NWMO DGR-TR-2011-26 R000. Toronto, Canada.

QUINTESSA and INTERA. 2011. Postclosure Safety Assessment: Data. Quintessa Ltd. and Intera Engineering Ltd. report for the Nuclear Waste Management Organization NWMO DGR-TR-2011-32 R000. Toronto, Canada.

QUINTESSA and SENES. 2011. Postclosure Safety Assessment: Analysis of Human Intrusion and Other Disruptive Scenarios. Quintessa Ltd. and SENES Consultants Ltd. report for the Nuclear Waste Management Organization NWMO DGR-TR-2011-27 R000. Toronto, Canada.

Sykes, J.F., S.D. Normani and Y. Yin. 2011. Hydrogeologic Modelling. Nuclear Waste Management Organization Report NWMO DGR-TR-2011-16 R000. Toronto, Canada.

APPENDIX B: COMPOSITE GEOPHYSICAL LOGS OF DGR BOREHOLES

(on enclosed CD)

Figure B.1: DGR-1 Borehole Geophysical Logs – April, May, August 2007

Figure B.2: DGR-2 Borehole Geophysical Logs – June 2007, August 2007

Figure B.3: DGR-2 ATV Comparison Logs – June 2007, August 2007, June 2009

Figure B.4: DGR-3 Borehole Geophysical Logs – July, August 2008

Figure B.5: DGR-3 Relog Borehole Geophysics – July, August 2008, November 2008

Figure B.6: DGR-4 Upper Borehole Geophysical Logs – August 2008

Figure B.7: DGR-4 Lower Borehole Geophysical Logs – November 2008

Figure B.8: DGR-5 Borehole Geophysical Logs – November 2009

Figure B.9: DGR-6 Borehole Geophysical Logs – February, March 2010